

NIST Special Publication 1402

Second Edition

RadCal
Improvements to the Narrow-Band Model
for Radiation Calculations
in a Combustion Environment

Vivien R. Lecoustre



NIST Special Publication 1402
Second Edition

RadCal
Improvements to the Narrow-Band Model
for Radiation Calculations
in a Combustion Environment

Vivien R. Lecoustre

Fire Research Division
Engineering Laboratory
Gaithersburg, Maryland, USA

June 16, 2014
RadCal
SVN Repository Revision : 28



U.S. Department of Commerce
Rebecca Blank, Acting Secretary

National Institute of Standards and Technology
Patrick D. Gallagher, Under Secretary of Commerce for Standards and Technology and Director

Certain commercial entities, equipment, or materials may be identified in this document in order to describe an experimental procedure or concept adequately. Such identification is not intended to imply recommendation or endorsement by the National Institute of Standards and Technology, nor is it intended to imply that the entities, materials, or equipment are necessarily the best available for the purpose.

National Institute of Standards and Technology Special Publication 1402
Natl. Inst. Stand. Technol. Spec. Publ. 1402, 281 pages (July 2014)

Authors

Principal Developers (in alphabetical order)

Vivien Lecoustre, University of Maryland, USA

About the Authors

Principal Developers

Vivien Lecoustre is a Research Associate at the University of Maryland. He received a master of science in aerospace engineering from ENSMA (France) in 2005 and a doctorate in Mechanical Engineering from the University of Maryland in 2009. His research interests include radiation properties of fuels and numerical turbulent combustion.

Preface

The report compiles the improvements that have been brought to RadCal, initially developed by William L. Grosshandler. It aims to provide a complete description of the models used, a presentation of the different species already present in the prior version and presents the radiative coefficients prepared from the experimental characterization of several fuels that was conducted at the National Institute of Standard and Technology. This report also features a description of the new input file and a throughout presentation of the code structure, along with verification tests and some validations tests.

Disclaimer

The US Department of Commerce makes no warranty, expressed or implied, to users of RadCal, and accepts no responsibility for its use. Users of RadCal assume sole responsibility under Federal law for determining the appropriateness of its use in any particular application; for any conclusions drawn from the results of its use; and for any actions taken or not taken as a result of analysis performed using these tools.

Users are warned that RadCal is intended for use only by those competent in the fields of heat transfer and fire science, and is intended only to supplement the informed judgment of the qualified user. The software package is a computer model that may or may not have predictive capability when applied to a specific set of factual circumstances. Lack of accurate predictions by the model could lead to erroneous conclusions with regard to fire safety. All results should be evaluated by an informed user.

Throughout this document, the mention of computer hardware or commercial software does not constitute endorsement by NIST, nor does it indicate that the products are necessarily those best suited for the intended purpose.

Contents

Authors	i
About the Authors	iii
Preface	v
Disclaimer	vii
1 Introduction	1
2 Narrow Band Models and Approximations	3
2.1 Introduction	3
2.1.1 Radiative Transfer Equation (RTE)	3
2.1.2 Planck blackbody distribution law	6
2.2 Single line emission	8
2.2.1 Lorentz lines	8
2.2.2 Doppler lines	9
2.2.3 Emission from an isolated line	10
2.3 Narrow band models	11
2.3.1 Elsasser model	11
2.3.2 Generalities on statistical narrow band models	14
2.3.3 Goody model	14
2.3.4 Malkmus model	15
2.4 Treatment of the RTE in the scope of narrow band model	17
2.4.1 Treatment of Homogeneous pressure-path	18
2.4.2 Treatment of non-Homogeneous pressure-path - Curtis-Godson approximation	19
2.5 Output quantities: effective coefficients and integrated quantities	19
2.5.1 Effective absorption coefficient	20
2.5.2 Planck mean absorption coefficient	20
2.5.3 Total transmissivity	21
2.5.4 Total emissivity	21
2.5.5 Received flux	21
3 Presentation of the Old Species in RADCAL	23
3.1 Water vapor: H ₂ O	23
3.2 Carbon dioxide: CO ₂	27
3.3 Carbon monoxide: CO	31
3.4 Methane: CH ₄	32

3.5 Soot	35
4 Presentation of the New Species in RADCAL	37
4.1 Integrated band intensity	37
4.2 Fitting procedure	37
4.3 Ethylene: C ₂ H ₄	39
4.3.1 Integrated Band Intensity	39
4.3.2 Malkmus Narrow Band Parameters	40
4.3.3 Verification SNB Parameters	45
4.4 Ethane: C ₂ H ₆	53
4.4.1 Integrated Band Intensity	53
4.4.2 Malkmus Narrow Band Parameters	53
4.4.3 Verification SNB Parameters	57
4.5 Propylene: C ₃ H ₆	65
4.5.1 Integrated Band Intensity	65
4.5.2 Malkmus Narrow Band Parameters	65
4.5.3 Verification SNB Parameters	69
4.6 Propane: C ₃ H ₈	77
4.6.1 Integrated Band Intensity	77
4.6.2 Malkmus Narrow Band Parameters	77
4.6.3 Verification SNB Parameters	80
4.7 Toluene: C ₇ H ₈	88
4.7.1 Integrated Band Intensity	88
4.7.2 Malkmus Narrow Band Parameters	88
4.7.3 Verification SNB Parameters	94
4.8 <i>n</i> -Heptane: C ₇ H ₁₆	102
4.8.1 Integrated Band Intensity	102
4.8.2 Malkmus Narrow Band Parameters	102
4.8.3 Verification SNB Parameters	105
4.9 Methanol: CH ₃ OH	113
4.9.1 Integrated Band Intensity	113
4.9.2 Malkmus Narrow Band Parameters	113
4.9.3 Verification SNB Parameters	118
4.10 Methyl Methacrylate: C ₅ H ₈ O ₂	126
4.10.1 Integrated Band Intensity	126
4.10.2 Malkmus Narrow Band Parameters	126
4.10.3 Verification SNB Parameters	133
5 Using RadCal	141
5.1 Compiling RadCal	141
5.2 Input file	141
5.2.1 Example	142
5.2.2 Input file structure	143
5.2.3 Naming the case: the HEADER namelist group	143
5.2.4 Defining the integration bounds: the BAND namelist group	143
5.2.5 Defining the surrounding blackbody temperature: the WALL namelist group	143
5.2.6 Characterizing the homogeneous pathlength segment: the Path_Segment namelist group	144

5.3	Output files	144
5.4	Python script	145
6	Structure of the Code	147
6.1	RadCal Module	148
6.1.1	RadCal Variables	148
6.1.2	Subroutine init_radcal	151
6.1.3	Subroutine sub_radcal	151
6.1.4	Function collision_broadening	152
6.1.5	Subroutine species_optical_depth	153
6.1.6	Function growth_doppler	154
6.1.7	Function combined_lines	155
6.1.8	Function Goody	155
6.1.9	Function Malkmus	156
6.1.10	Function Elsasser	156
6.1.11	Function partition_function	157
6.1.12	Function approx_vib_rot	157
6.1.13	Subroutine co2	158
6.1.14	Subroutine h2o	159
6.1.15	Subroutine co	160
6.1.16	Subroutine pod	160
6.1.17	Subroutine ch4_old	161
6.1.18	Subroutine ch4	161
6.1.19	Subroutine c3h6	162
6.1.20	Subroutine c3h8	163
6.1.21	Subroutine c7h16	164
6.1.22	Subroutine c7h8	165
6.1.23	Subroutine ch3oh	166
6.1.24	Subroutine c5h8o2	167
6.1.25	Subroutine c2h6	168
6.1.26	Subroutine c2h4	169
6.1.27	Function get_spectral_absorption	169
6.1.28	Function planck	170
6.1.29	Function planck_wn	171
6.1.30	Function integration	171
6.1.31	Subroutine rcalloc	172
6.1.32	Subroutine populate_species	172
6.1.33	Function index_species	172
6.1.34	Subroutine rcdealloc	173
6.1.35	Subroutine termination	173
6.1.36	Subroutine write_input	174
6.1.37	Subroutine read_input	174
6.1.38	Subroutine read_point	175
6.1.39	Subroutine read_band	176
6.1.40	Subroutine read_wall	176
6.1.41	Subroutine read_header	176
6.2	Driver (main) Program	177
6.2.1	Program driver	177

6.2.2 Subroutine tau_print	177
7 Verification Tests	179
7.1 Ethylene: C ₂ H ₄	180
7.2 Ethane: C ₂ H ₆	188
7.3 Propylene: C ₃ H ₆	196
7.4 Propane: C ₃ H ₈	204
7.5 Toluene: C ₇ H ₈	212
7.6 <i>n</i> -Heptane: C ₇ H ₁₆	220
7.7 Methanol: CH ₃ OH	228
7.8 Methyl Methacrylate: C ₅ H ₈ O ₂	236
8 Validations Tests	245
8.1 Test 1: isothermal CO ₂	245
8.2 Test 2: fixed pressure path-length CO ₂	247
8.3 Test 3: isothermal H ₂ O	249
8.4 Test 4: fixed pressure path-length H ₂ O	251
8.5 Test 5: simulated one meter diameter pool fire	253
8.6 Test 6: methane premixed flame	255
8.7 Test 7: methanol pool fire	258

Chapter 1

Introduction

Thermal radiation in fire plays a preponderant role in most fire. Thermal radiation are responsible to fire spread, fire growth due to thermal feedback from the hot upper layer or the hot plume, or controls the mass loss rate in large scale pool fire. In all the aforementioned cases, it is crucial to determinate accurately the radiative heat transfer between the different regions. The use of the Wien's displacement law informs us of the frequency of the maximum radiative energy emitted by a blackbody. This law is expressed by

$$\lambda_m T = 2897 \mu\text{m.K} \quad (1.1)$$

with λ_m being the wavelength, in units of m, corresponding to the peak of a blackbody emittance; T represents the temperature, in units of Kelvin, of the blackbody emitting the thermal radiation. Equation 1.1 tells us that in typical fire configurations, where the temperature ranges from 300 K to about 2500 K, the peak emittance location in the wavelength ranges varies from $10 \mu\text{m}$ to $1.1 \mu\text{m}$: almost all the radiative exchanges happen in the near to mid infrared range. Most of the components involved in fire are present in gas phase. The infrared spectrum of the gases is very discontinuous, with few narrow spectral ranges that participate to the radiative exchanges. The rest of the spectrum is transparent. The participation propensity varies with the amount of the species present and with the local temperature.

These intrinsics aspects of the radiative exchange between medium with important gradients of temperature, species amount, and non-homogeneity in species render this problem quite complex and some levels of sophistication is needed in its treatment. The radiative properties of a gas species are dictated by the quantum mechanic and originates from the composition and the geometry of the component considered. The discrete nature of the energy levels (mostly vibrational and rotational modes) allowed for a given molecule generates its infrared “fingerprint”. While a throughout consideration of all the energy levels will give an exact assessment of the radiative exchanges – this is often referred to as line-by-line calculation in the literature – this operating mode is still too computationally expensive for engineering applications and is only used for simple configurations. Moreover, the lack of data for both elevated temperatures and for most hydrocarbon species further restricts its applicability to fire scenarii. The development of narrow-band models constitutes a valid compromise between accuracy and efficiency. Narrow band models divide the spectrum of interest into small spectral segments of uniform spectral properties and use statical representations of the energy level over these segments. Narrow band models are computationally fast and accurate. In particular, they do not require the detailed knowledge of all the energy levels activated in a given molecule. They are easier to implement and use than the Line-by-Line techniques.

RadCal has previously been developed by Grosshandler [1] to predict radiative heat transfer from gases at elevated temperature using narrow band models. RadCal is a computer program, originally written in FORTRAN 77, that computes the directional spectral intensity from a non-isothermal, non-uniform mixture of gases and soot, by spectrally solving the radiative transfer equation. In addition, RadCal returns the Planck

mean absorption coefficient, an effective absorption coefficient, and other integrated quantities. Details about the different models used and the quantities printed by RadCal are provided in Chapter 2.

The first version of RadCal was developed to predict the enhancement in radiation caused by the addition of pulverized coal to a 60 kW methanol-fired furnace. This has been documented in Ref. [2]. This first version considered the contributions of CO, CO₂, H₂O, and soot. Validation of first version of RadCal was documented in 1979 and can be found in Ref. [3]. Predictions from RadCal for CO₂, CO, and H₂O in individual or in mixtures were compared against published data. Good agreement was found except for some data. As Grosshandler states in Ref. [1]: “...The spectrum between 1.25 and 12.5 μm was satisfactory reproduced, although some of the data at particular wavelengths differed from the prediction by as much as 17%. Considerable disagreement occurred between the integrated emittance of CO₂ as predicted from RADCAL and that computed from the charts of Hottel [4]. No one source for this disagreement was identified, but it was thought to be a combination of the difficulty in obtaining high accuracy spectral measurements under the full range of conditions investigated, the uncertainty associated with extrapolating total transmittance results beyond the measured temperature and pressure-pathlengths, and the approximations associated with the narrow-band models.”

Methane was added to RadCal in 1985 [5], along with an extension to 200 μm of the considered spectrum. The added methane data originates mostly from experiments performed by Brosmer *et al.* [6] and Lee *et al.* [7]. At this time, the code structure was updated and a new input file was created.

This second edition of the NIST Special Publication 1402 presents the enhancements brought lately to RadCal and aims to provide an exhaustive list of the mathematical and physical models used in RadCal, which was missing from the first edition. Chapter 2 presents the fundamental mathematical models used in radiative heat transfer and presents the different narrow band models used in RadCal. Chapter 3 recalls the characteristics of the species that were present in the 1993 version of RadCal: H₂O, CO₂, CO, CH₄, and soot. Additional hydrocarbons have been implemented into RadCal and the code has been rewritten, for its most part, into Fortran 2008. FTIR transmission measurements at the National Institute of Standards and Technology (NIST) were undertaken to provide highly resolved spectral absorption coefficients in the mid-IR and NIR as a function of temperature for many fuel species [8, 9, 10]. These measurements were performed over a range of temperatures from 300 K up to 1000 K for several fuel species, including paraffins (methane, ethane, propane, and n-heptane), olefins (ethylene and propylene), and other fuel-related species (methanol, toluene, and methyl-methacrylate). The uniform set of conditions and spectral resolution of these measurements have provided a set of data for developing calculation methodologies for absorption coefficients of these species in flame environments. New species and their associated narrow band parameters are described in Chapter 4. The syntax of the input file was modified to make good use of native Fortran namelist that offers a more flexible way to input data. Chapter 5 describes the new input file syntax, and how to compile and use RadCal. The code was modified following a modular approach and was translated into Fortran 2008 to benefit from the recent advances in Fortran. The list of the RadCal functions and subroutines is detailed in Chapter 6. The code has also been modified to account for any type of fuel mixture. Verifications of the new fuels data has been performed and results from these tests are reported in this report in Chapter 7. Finally, Chapter 8 compares the new version of RadCal with the 1993 one for the various validation tests presented in the first edition of this report. This chapter also presents predicted quantities from an experimentally characterized small methanol pool fire.

Chapter 2

Narrow Band Models and Approximations

This chapter briefly presents the models and their formulations that are used in RadCal. The reader seeking further details on the rather complex theory behind these models is invited to read the exhaustive monographs from Penner [11], Tien [12], and Modest [13], the review from Viskanta and Menguc [14], and the report from Ludwig *et al.* [15]. Most of the equations used in RadCal can be found in the latter.

RadCal was designed for uses at moderate gas pressure (near atmospheric pressure) and for ambient to high gas temperature (typically from around 300 K to 2500 K). As such, collision broadening is the main broadening mechanism considered. However, the effects of Doppler line broadening, which are preponderant at low pressure (typically less than 0.01 atm) and/or at high temperature, are still accounted for in the overall expression of the narrow band transmissivity. The Doppler broadening effect is accounted using the method presented in Ludwig *et al.* [15]. The Voigt profile, commonly used in atmospheric sciences [16], is not considered here. The reason behind is unlike the Lorentz profile the Voigt profile does not have a close analytical expression. Effects of scattering or reflection are not included in RadCal; as such, RadCal considers only absorption and emission.

RadCal can be used to model homogeneous and non-homogeneous conditions. Following Ludwig [15], the Curtis-Godson approximation is then used with the assumption of Single Line Group. In the case of a mixture of different radiative participating gases, the contribution for each species is calculated independently and their contribution on the total spectral optical depth is assumed to be additive. Finally, it is important to recall the important assumption of local thermodynamic equilibrium used in establishing the Radiative Transfer Equation as solved by RadCal. This justifies the consideration of the Planck blackbody distribution law as the emission term.

2.1 Introduction

2.1.1 Radiative Transfer Equation (RTE)

The expression of the equation of transfer in non-scattering, participating media in local thermodynamic equilibrium is recalled. This equation is the mathematical foundation of RadCal. The Eulerian point of view is adopted here. The assumption of local thermodynamic equilibrium has for consequences that the spectral blackbody emission can be modeled with the Planck blackbody distribution - denoted from here and in the rest of this manuscript I_b , and that the Kirchoff law applies at the spectral level, *i.e.* for a monochromatic light the absorption and emission coefficients are equal. The amount of radiative energy emitted by a participating medium of local thermodynamic temperature T , over an infinitesimal spectrum dv , in an arbitrary direction \hat{s} , and along an infinitesimal length ds , is expressed by:

$$j_{e,v} ds dv = \kappa_v I_{b,v}(T) dv ds \quad (2.1)$$

where $j_{e,v}$ is the emission at the frequency v , κ_v is the absorption coefficient at the considered frequency, $I_{b,v}$ denotes the spectral intensity emitted by a blackbody of temperature T . Naturally, the absorption coefficient κ_v is proportional to the amount of local participating molecule.

Note: it is common in spectroscopy to use B_b and \tilde{v} as the Planck function and wavenumber, respectively. However in the continuation of the previous work on RadCal, we keep the previously used nomenclature. In the rest of the manuscript, ω denotes the wavenumber. A common units employs to characterize radiative spectrum is the wavelength, denoted λ . Wavelength λ represents the distance traveled during one cycle when propagating at the speed of light in vacuum. When dealing with infrared radiation, its units are commonly expressed in μm . Wavenumber ω is the reciprocal of the wavelength. It represents the number of cycles per unit of length. It is expressed in units of cm^{-1} . It is convenient to use wavelength λ or wavenumber ω instead of frequency v when dealing with thermal radiation. Wavenumber and wavelength are related to frequency through:

$$\lambda = c/v \text{ and } \omega = v/c, \quad (2.2)$$

and one can easily switch from wavenumber in units of cm^{-1} to wavelength in units of μm with:

$$\lambda \mu\text{m} = 10000/\omega \text{ cm}^{-1}. \quad (2.3)$$

Similarly to Eq. 2.1, an expression characterizing the amount of energy of an incident beam, of propagating direction \hat{s} absorbed by local participating molecules over an infinitesimal spectrum dv and along an infinitesimal length ds can be derived:

$$j_{a,v} dv ds = -\kappa_v I_v dv ds \quad (2.4)$$

where I_v is the spectral intensity at frequency v of the incident beam of direction \hat{s} .

Using Eqs. 2.1 and 2.4, the change in the spectral intensity of an incident beam of direction \hat{s} penetrating a participating medium over a distance ds is then expressed by:

$$dI_v dv = (j_{e,v} + j_{a,v}) ds dv. \quad (2.5)$$

The local Radiative Transfer Equation (neglecting scattering) is then expressed as:

$$\frac{dI_v}{ds} dv = \kappa_v (I_{b,v}(T) - I_v) dv. \quad (2.6)$$

Equation 2.6 is a first-order ordinary differential equation; it is assumed here that the speed of light is very large compared to local time and length scales involved. The functional form of the spectral intensity $I_v(s)$ at an arbitrary depth s within the participating medium, assuming that the participating medium starts at $s = 0$, is expressed as:

$$I_v(s) = I_v(0) \exp \left(- \int_0^s \kappa_v ds' \right) + \int_0^s I_{b,v}(T(s')) \exp \left(- \int_{s'}^s \kappa_v ds'' \right) \kappa_v ds'. \quad (2.7)$$

Note that κ_v is a function of the local thermodynamic conditions and hence is an implicit function of s .

The first right-hand side term of Eq. 2.7 represents the fraction of the incident spectral intensity that is transmitted unto the depth s . The second right-hand side term corresponds to the contribution of the local emission and accounts for self-absorption. The spectral transmissivity, denoted $\tau(v; 0 \rightarrow s)$, is defined as the fraction of the spectral energy of frequency v incident upon a participating medium which is transmitted by it. It can be seen from Eq. 2.7, that an explicit formulation of the spectral transmissivity is:

$$\tau(v; 0 \rightarrow s) = \exp \left(- \int_0^s \kappa_v ds' \right). \quad (2.8)$$

It can be shown that:

$$\exp\left(-\int_{s'}^s \kappa_v ds''\right) \kappa_v = \frac{\partial \tau}{\partial s'}(v; s' \rightarrow s). \quad (2.9)$$

Therefore, the RTE can be rewritten as:

$$I_v(s) = I_v(0)\tau(v; 0 \rightarrow s) + \int_0^s I_{b,v}(T(s')) \frac{\partial \tau}{\partial s'}(v; s' \rightarrow s) ds'. \quad (2.10)$$

Equation 2.10 represents the fundamental governing equation for the radiative transfer into a non-scattering, non-reflective participating medium at local thermodynamic equilibrium. This equation is valid regardless whether the model is homogeneous or not. It is of course assumed here that the spectral distribution of the incident intensity, $I_v(s=0)$, is known. In RadCal, $I_v(0)$ is the spectral distribution of a blackbody at a temperature defined by the user. This temperature is referred to as the *wall* temperature, denoted T_w .

Equation 2.10 can be used to calculate the incident energy at the location s comprised in a spectral range Δv :

$$\int_{\Delta v} I_v(s) dv = \int_{\Delta v} I_v(0)\tau(v; 0 \rightarrow s) dv + \int_{\Delta v} \int_0^s I_{b,v}(T(s')) \frac{\partial \tau}{\partial s'}(v; s' \rightarrow s) ds' dv. \quad (2.11)$$

Some simplifications can be made if one assumes that Δv is small enough so that I_v and $I_{b,v}$ can satisfactorily be assumed constant over Δv . In this case, Eq. 2.11 can be written as:

$$I_{v_0}(s) = I_{v_0}(0)\bar{\tau}(v_0; 0 \rightarrow s) + \int_0^s I_{b,v_0}(T(s')) \frac{\partial \bar{\tau}}{\partial s'}(v_0; s' \rightarrow s) ds', \quad (2.12)$$

where v_0 is the center of the narrow band Δv and with

$$\bar{\tau} = \frac{1}{\Delta v} \int_{\Delta v} \tau dv = \frac{1}{\Delta v} \int_{\Delta v} \exp\left(-\int \kappa_v ds'\right) dv. \quad (2.13)$$

It is very important, in the narrow band framework, to note that in general:

$$\bar{\tau} \neq \exp\left(-\int \bar{\kappa}_v ds'\right), \quad (2.14)$$

where the mean absorption coefficient $\bar{\kappa}_v$ is defined as the average of the spectral absorption coefficient over the spectral range Δv :

$$\bar{\kappa}_v = \frac{1}{\Delta v} \int_{\Delta v} \kappa_v dv. \quad (2.15)$$

Equation 2.14 arises from:

$$\int_{\Delta} \exp f(x) dx \neq \exp\left(\int_{\Delta} f(x) dx\right), \quad (2.16)$$

where the equality is only verified for some particular functions and integration domain.

One of the main difficulties in calculating the incident radiative intensity over a given spectral range is the rapid variation of κ_v with v for all gas phase species. Indeed, the spectroscopic study of participating species in gas-phase shows that their infrared spectrum consists of millions of narrow peaks. The discrete nature of the infrared spectrum is a direct consequence of the quantification of the energy associated with a species molecular vibration and rotation motions. Figure 2.1 below plots the spectral absorption coefficient for H_2O in the spectral range $1050 - 1100 \text{ cm}^{-1}$. This spectrum was generated using H_2O line specifications from the HITRAN 2012 database [17].

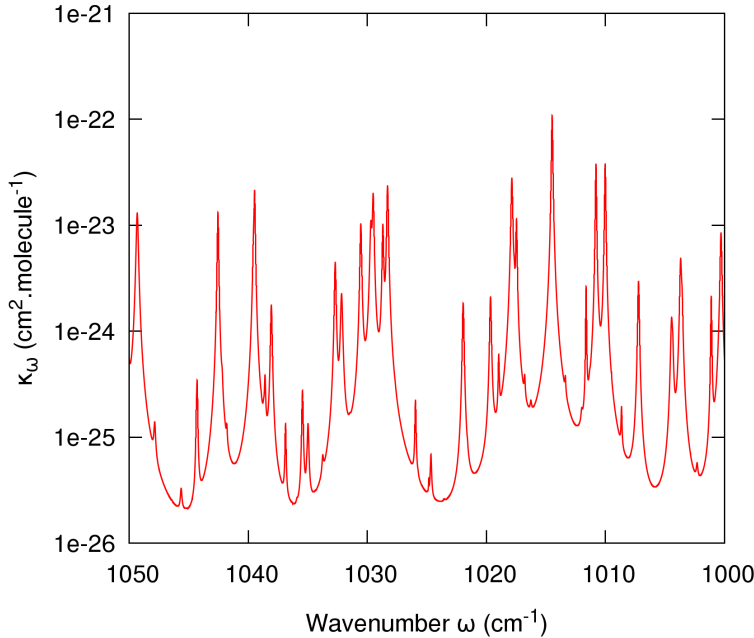


Figure 2.1: Spectral H_2O absorption coefficient κ_ω for the spectral range $1000 - 1050 \text{ cm}^{-1}$. This synthetic spectrum calculated using HITRAN 2012 line specifications assumes a temperature of 296 K and 10% of water in a total pressure of 1 atm.

2.1.2 Planck blackbody distribution law

The Planck blackbody distribution law, sometime called the Planck function, but the term is misleading as it is a distribution, describes the spectral distribution of the equilibrium rate of radiant energy emitted from a blackbody at temperature T . Its expression is given, as a function of frequency ν and for an unit of solid angle, by:

$$I_{b,\nu}(T) = \frac{2h\nu^3}{c^2} \frac{1}{\exp\left(\frac{h\nu}{k_B T}\right) - 1}. \quad (2.17)$$

Here, h is the Planck constant ($6.626 \times 10^{-34} \text{ J}\cdot\text{s}$), and k_B is the Boltzmann constant ($1.381 \times 10^{-23} \text{ J/K}$). $I_{b,\nu}(T)$ is in units of $\text{W/m}^2/\text{str/s}^{-1}$.

In terms of wavenumber, the Planck blackbody distribution law, $I_{b,\omega}$, is written:

$$I_{b,\omega}(T) = \frac{2hc^2\omega^3}{\exp\left(\frac{hc\omega}{k_B T}\right) - 1}. \quad (2.18)$$

$I_{b,\omega}(T)$ is in units of $\text{W/m}^2/\text{str/m}^{-1}$; the wavenumber ω in Eq. 2.18 is in units of m^{-1} .

The user who wishes to express the Planck blackbody distribution law as a function of wavelength should take caution when performing the change of variables. One should start by expressing that the radiant energy emitted at a wavelength λ over an infinitesimal spectral range $d\lambda$ is the same as the radiant energy emitted at the corresponding wavenumber ω over an infinitesimal spectral range $d\omega$:

$$I_{b,\lambda}(T)d\lambda = -I_{b,\omega}(T)d\omega, \quad (2.19)$$

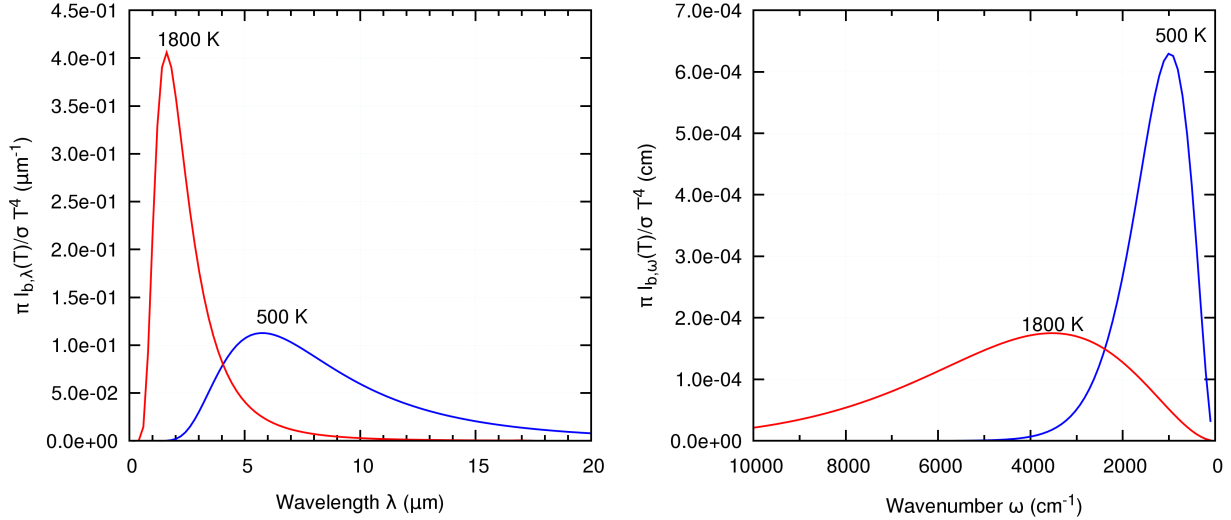


Figure 2.2: Normalized spectral Blackbody distributions at $T = 500$ K (blue line) and $T = 1800$ K (red line) with the wavelength in units of μm (left) and with the wavenumber in units of cm^{-1} (right).

the negative sign is introduced because ω is the reciprocal of λ . Since $\lambda = 1/\omega$, it comes:

$$\frac{d\lambda}{d\omega} = -\frac{1}{\omega^2}. \quad (2.20)$$

Equation 2.19 can be rewritten, after the appropriate change of variables:

$$I_{b,\lambda}(T) = \frac{2hc^2}{\lambda^5} \frac{1}{\exp\left(\frac{hc}{\lambda k_B T}\right) - 1}, \quad (2.21)$$

where $I_{b,\lambda}$ is in units of $\text{W}/\text{m}^2/\text{str}/\text{m}$; the wavelength λ in Eq. 2.21 is in unit of m.

Figure 2.2 plots profiles of normalized spectral Blackbody distribution for temperatures of 500 K and 1800 K using wavelength and wavenumber. It can be seen that an increase of temperature will shift the mode of the distribution toward lower wavelength and higher wavenumber. Figure 2.2 indicates that the shape of the distribution is not invariant with the units chosen to characterize the spectrum. Indeed, while an elevation of blackbody temperature corresponds to a narrowing of the normalized distribution when using wavelength, the same elevation of blackbody temperature leads to a spreading of the profile when using wavenumber. Finally, an important remark is that the location of the distribution mode (corresponding to the location of maximum emission) does not relate between wavelength and wavenumber. This location can be calculated using the Wien's displacement law. Using wavelength, the Wien's displacement law is expressed by:

$$\lambda_{\max} T = 2898 \text{ } \mu\text{m.K}, \quad (2.22)$$

while using wavenumber, the Wien's displacement law is expressed by:

$$\frac{\omega_{\max}}{T} = 1.961 \text{ } \text{cm}^{-1} \cdot \text{K}^{-1}. \quad (2.23)$$

Using Eq. 2.22, the maximum of emission at 500 K is located at $\lambda_{\max} = 5.8 \text{ } \mu\text{m}$. The same calculation using Eq. 2.23 gives $\omega_{\max} = 980 \text{ } \text{cm}^{-1}$. It is crucial to note that $10000/\lambda_{\max} = 1725 \text{ } \text{cm}^{-1} \neq \omega_{\max}$. Hence caution must be taken when converting spectral variable from wavenumber to wavelength and vice versa. In RadCal, the wavenumber is the variable of choice for spectral quantities.

2.2 Single line emission

This section briefly recalls the characteristics of a single line emission. The expression for an isolated line with pressure broadening mechanism (also called Lorentz lines) is recalled along with the expression of lines broadened by Doppler effects. Note that RadCal mixes both lines expression in the calculation of the RTE. Hence, it is important to recall some of their properties. The underlying mechanisms responsible for the emission and/or absorption of electromagnetic radiation by a molecule or atom are not recalled here as they are out of the scope of this work. It is just recalled here that the discrete nature of a species spectrum in the infrared region is a direct consequence of the discretization of the vibrational and rotational energy level admissible for a given species. The location and intensity of these lines can be obtained from the solution of the time-dependent Schrödinger wave equation of a molecule with an incident radiation field. The lines location and intensity depend on the molecule geometry, mass, and its electric dipole moments. For further details, see Chapter 7 of Penner, Ref. [11]; Herzberg Ref. [18]; Chapter 11 of Modest, Ref. [13]; and Tien monograph Ref. [12].

2.2.1 Lorentz lines

A spectral line is never truly monochromatic as different line broadening mechanisms are present. The most fundamental one is the natural line broadening which is a consequence of the Heisenberg's uncertainty principle. While this effect is always present, it is usually omitted in engineering applications as the collision broadening and the Doppler broadening mechanisms are much more important.

The collision broadening mechanism originates from disruptions during the emission or absorption of energy due to the collision between molecules. The broadening of the line increases as the collision frequency increases, hence as the local pressure is increased. The shape of such broadened lines can be calculated using the electron theory of Lorentz or from quantum mechanism. The shape of the line is given by:

$$\kappa_\omega = \frac{S}{\pi} \frac{\gamma_c}{(\omega - \omega_0)^2 + \gamma_c^2}, \quad (2.24)$$

where γ_c is the collision broadening half-width at half the maximum (HWHM), ω_0 is the wavenumber at the line center, and S is called the line intensity or line strength and is defined as:

$$S = \int \kappa_\omega d\omega. \quad (2.25)$$

Note that S is a function of the temperature alone while γ_c is a function of the temperature, pressure, and mixture composition. Because the effects of collision depend on the molecular diameters of the colliding species, the quantity γ_c varies with the collisional partner. Among the collision broadening, distinction is made between the foreign gas broadening, *i.e.* due to collisions among dissimilar species, and self-broadening, *i.e.* due to collisions among like species. The self-broadening collisions can be further differentiated between resonant and non-resonant collisions. Resonant collisions are more effective than non-resonant collisions but they have a different temperature dependence than non-resonant collisions. Non-resonant collisions are similar to collisions with a foreign gas. In RadCal, when not tabulated, the Lorentz HWHM $\gamma_{c,i}$ of a given species i belonging to a mixture, is calculated according to:

$$\gamma_{c,i} = \sum_j \gamma_{c0,(i,j)} \left(\frac{P_j}{P_0} \right) \sqrt{\frac{T_0}{T}} + \gamma_{c0,i}^* \frac{P_i}{P_0} \left(\frac{T_0}{T} \right), \quad (2.26)$$

where $\gamma_{c0,(i,j)}$ denotes the value of non-resonant collision broadening HWHM with species j at conditions of standard pressure (denoted P_0) and temperature (denoted T_0), and $\gamma_{c0,i}^*$ denotes the value of resonant self-collision broadening HWHM at conditions of standard pressure and temperature. Note that Eq. 2.26 first right-hand side term includes the effects of foreign gas collision and non-resonant self-collision.

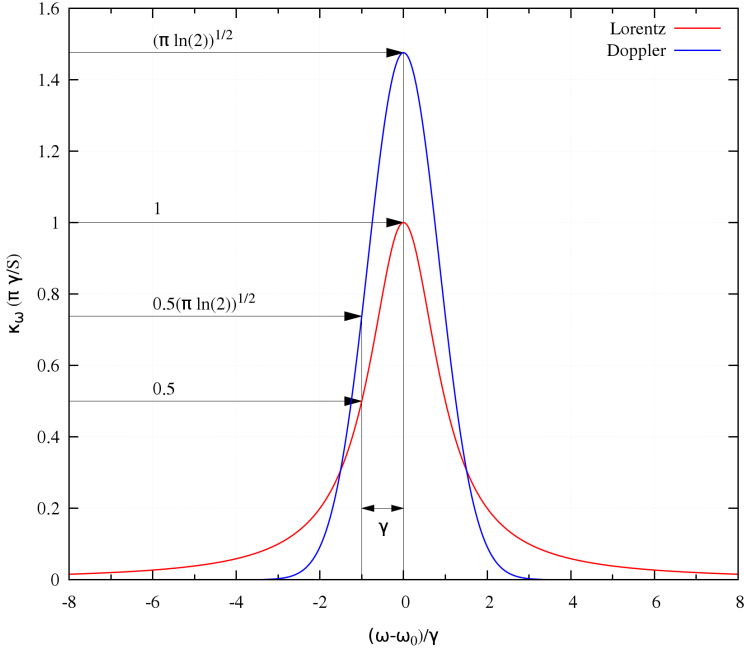


Figure 2.3: Profiles of a normalized Lorentz line (in red) and a normalized Doppler line (in blue).

Profile of a normalized Lorentz line ($\kappa_\omega(\pi\gamma_c)/S$) as a function of $(\omega - \omega_0)/\gamma_c$ is plotted in Fig. 2.3 together with the profile of a normalized Doppler line.

2.2.2 Doppler lines

The motion of radiating particles in the line of sight may change the apparent frequency due to the Doppler effect. The apparent frequency increases when the particle moves toward the observer and decreases when it moves away. The Doppler line profile is calculated considering the Maxwell velocity distribution (which is a consequence of the local thermodynamic equilibrium assumption). The absorption coefficient is then expressed as:

$$\kappa_\omega = S \frac{\sqrt{\ln(2)}}{\gamma_D \sqrt{\pi}} \exp \left[-\ln(2) \left(\frac{\omega - \omega_0}{\gamma_D} \right)^2 \right], \quad (2.27)$$

where S and ω_0 are the line strength and the wavenumber at the line center, respectively. The quantity γ_D is the Doppler HWHM. It is calculated from:

$$\gamma_D = \frac{\omega_0}{c} \sqrt{\ln(2) \frac{2k_B T}{m}}, \quad (2.28)$$

where m is the mass of the radiating species. Note that the Doppler HWHM depends linearly on the wavenumber; it increases with elevated wavenumber. The Doppler broadening mechanism is important at high temperature ($T > 2000 K$) [13] and/or low pressure, typically lower than 0.01 atm. In RadCal both broadening mechanisms are included in the calculation of the RTE; see Section 2.4.

2.2.3 Emission from an isolated line

This subsection recalls the results of the emission and absorption of radiation for an isolated Lorentz line. This ideal case helps to bring an understanding of a single line absorption variation with the pressure path length as it is a very fundamental concept.

The spectral variation of the absorption coefficient κ_ω of a single line centered in ω_0 , of line strength S , and of HWHM γ_c with the wavenumber ω is recalled:

$$\kappa_\omega = \frac{S}{\pi} \frac{\gamma_c}{(\omega - \omega_0)^2 + \gamma_c^2}. \quad (2.24)$$

The shape of the line is plotted in Fig. 2.3.

Assuming a path going through an isothermal gas, of temperature T_g , and homogeneous layer of participating species of partial pressure P_i , and of physical thickness L , the RTE, Eq. 2.10, can be simplified as:

$$I_\omega(L) = I_\omega(0) \exp(-\kappa_\omega P_i L) + I_{b,\omega}(T_g) (1 - \exp(-\kappa_\omega P_i L)). \quad (2.29)$$

Note that in this equation, the local amount of participating species is expressed by the partial pressure P_i ; hence in the equation above, κ_ω has the dimension of an inverse pressure times an inverse length. In RadCal, κ_ω is expressed in $(\text{cm}^{-1} \cdot \text{atm}^{-1})$, while P_i is in atm and the path physical length L is in cm. The product $P_i L$, the pressure path length, is referred to in RadCal as a species optical thickness and is also denoted U , and the product $\kappa_\omega P_i L$ is referred to as the optical depth.

Considering only the emission term (*i.e.* $I_\omega(0) = 0$), the exiting intensity integrated over the whole spectrum, emitted by a single line, denoted $I(L)$, is expressed as:

$$I(L) = I_{b,\omega}(T_g) \int_{\Delta\omega} (1 - \exp(-\kappa_{\omega'} P_i L) d\omega'), \quad (2.30)$$

this assumes that $I_{b,\omega}$ does not vary much over the $\Delta\omega$ range. The integrand is often called the equivalent line width [13] and is usually denoted W ,

$$W = \int_{\Delta\omega} (1 - \exp(-\kappa_{\omega'} P_i L) d\omega'). \quad (2.31)$$

The analytical expression of W for a Lorentz line can be derived, see for example Penner, [11]:

$$W(P_i L) = 2\pi\gamma_c L(x) = 2\pi\gamma_c x \exp(-x) (I_0(x) + I_1(x)), \quad x = \frac{SP_i L}{2\pi\gamma_c}. \quad (2.32)$$

The function $L(x)$ is named the Ladenburg-Reiche function, and I_0 and I_1 are the modified Bessel functions of the first kind. The graph of the Ladenburg-Reiche function is given in Fig. 2.4. Note that for small and large values of x , the equivalent line has the following asymptotic forms:

$$W(x) \sim SP_i L, \text{ for } x \ll 1 \quad (2.33)$$

$$W(x) \sim 2\sqrt{S\gamma_c P_i L}, \text{ for } x \gg 1. \quad (2.34)$$

It is worth noting that the parameter x gives an indication of the optical thickness of the gas layer for a single line. When x is small, this indicates that the medium is weakly participating (either S or the product $P_i L$ is small) and the absorption and emission of a single line is linear with the product $P_i L$. On the contrary, when x is much greater than unity, the absorption or emission of a single line is not linear anymore but has a square-root dependency.

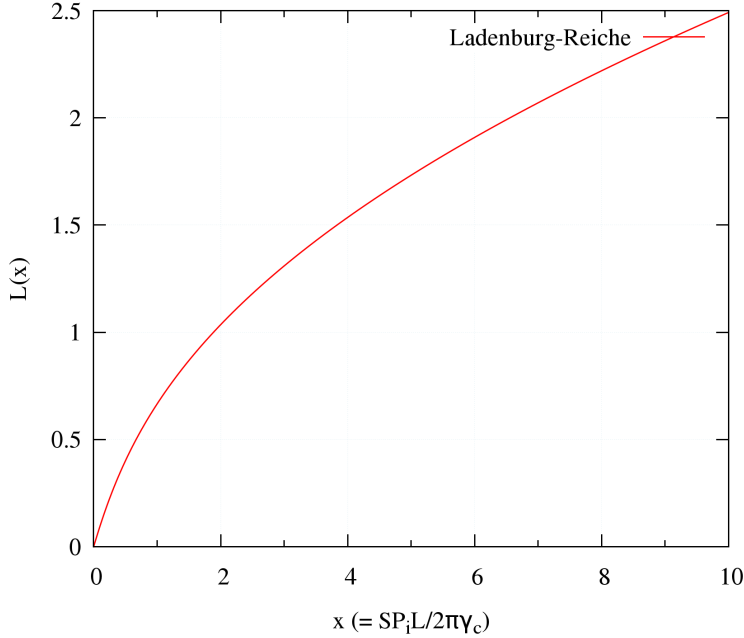


Figure 2.4: Profile the Ladenburg-Reiche function.

2.3 Narrow band models

This section briefly describes the different models used to obtain most of the tabulated species IR spectral mean absorption coefficients at different temperatures, $\bar{\kappa}_i(\omega, T)$. Narrow band models are used in lieu of line-by-line models to represent the IR spectra of radiating species in engineering applications. In the narrow band approach, the whole spectrum is divided into small spectral bands (typically several cm^{-1}), and different statistical approaches are used to compute the average radiative properties over these narrow bands. What is of interest is to give functional expression of the integrand:

$$\bar{\tau}_\omega = \int_{\Delta\omega} (\exp(-\kappa_\omega P_i L) d\omega'), \quad (2.35)$$

when $\Delta\omega$ is large enough so it includes hundreds, even thousands, of single lines, but small enough to assume $I_{b,\omega}(T_g)$ and the incident spectral intensity $I_\omega(0)$ constant over it. It is important to state that generally:

$$\bar{\tau}_\omega \neq \int_{\Delta\omega} (\exp(-\bar{\kappa}_\omega P_i L) d\omega'). \quad (2.36)$$

Equality is verified only in some specific situations (*e.g.* $P_i L \ll 1$). An important assumption to recall is that it is assumed that the Kirchoff law, *i.e.* $\bar{\alpha} = \bar{\varepsilon}$, holds over a narrow band.

Three main narrow band models are presented below: the Elsasser model, the Goody model, and the Malkmus model. All assume Lorentz lines.

2.3.1 Elsasser model

The Elsasser model assumes all the lines to have the same HWHM γ_c , the same line strength S , and to be equally spaced every d wavenumber from each other. As a consequence, the absorption coefficient can be

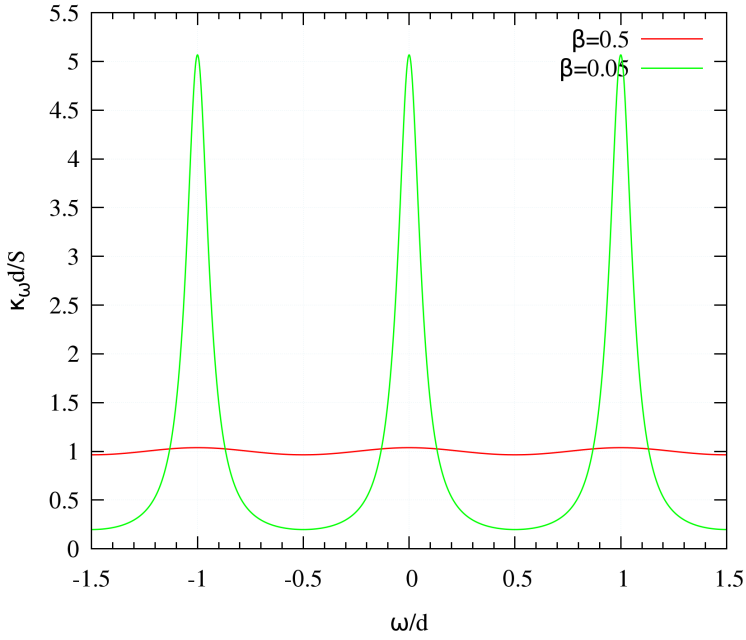


Figure 2.5: Variations of the Elsasser absorption coefficient normalized by $\bar{\kappa}$ plotted as a function of the ratio ω/d for two different values of the overlap parameter $\beta = 0.05$ (in green) and $\beta = 0.5$ (in red).

expressed by the infinite sequence:

$$\kappa_\omega = \sum_{n=-\infty}^{\infty} \frac{S}{\pi} \frac{\gamma_c}{(\omega - (\omega_0 + nd))^2 + \gamma_c^2}. \quad (2.37)$$

This function is periodic, with a period d . Following Elsasser derivation (see Ref. [11]), Eq. 2.37 can be expressed as:

$$\kappa_\omega = \frac{S}{d} \frac{\sinh(8\beta)}{\cosh(8\beta) - \cos(\frac{2\pi}{d}(\omega - \omega_0))}, \quad (2.38)$$

where the overlap parameter β , which is also called the (Lorentz) fine structure parameter and denoted a_c in Ref. [15] and in the code, is defined here as:

$$\beta = \frac{\pi}{4} \frac{\gamma_c}{d}. \quad (2.39)$$

The mean absorption coefficient $\bar{\kappa}$ over the narrow band centered in ω is:

$$\bar{\kappa}_\omega = \frac{S}{d}. \quad (2.40)$$

Figure 2.5 plots the variations of the Elsasser absorption coefficient κ_ω normalized by $\bar{\kappa}$ as a function of the ratio ω/d for two different values of the overlap parameter β . Strong overlap effects are seen for the largest value of β .

The mean transmissivity $\bar{\tau}_\omega$ of the narrow band centered in ω can be calculated using Eq. 2.38, averaging over one period d :

$$\bar{\tau}_\omega = \frac{1}{d} \int_{-\frac{d}{2}}^{\frac{d}{2}} \exp \left(-\bar{\kappa}_\omega P_i L \frac{\sinh(8\beta)}{\cosh(8\beta) - \cos(\frac{2\pi}{d}(\omega' - \omega))} \right) d\omega'. \quad (2.41)$$

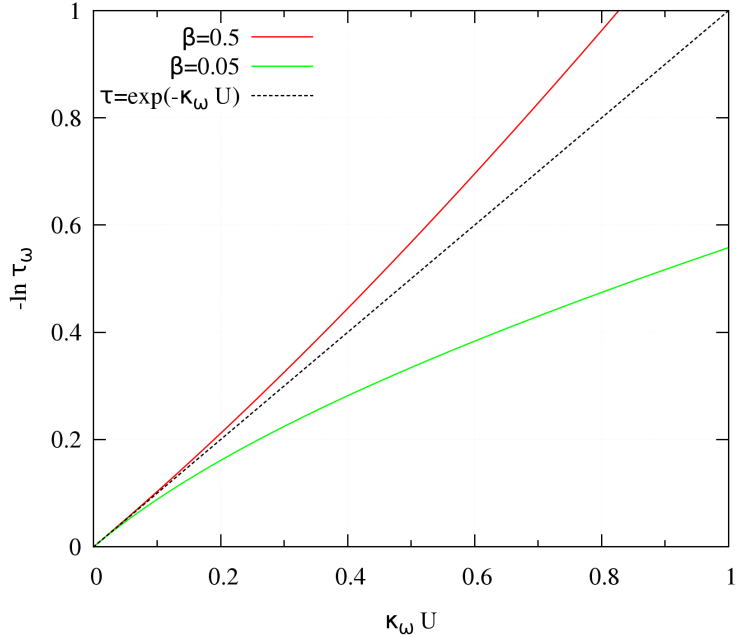


Figure 2.6: Elsasser model curve of growth ($\ln \bar{\tau}$) as a function of the product $\bar{\kappa}_\omega U$. Two different values of the overlap parameter are plotted: $\beta = 0.05$ (in green) and $\beta = 0.5$ (in red). The curve of growth for the “weak line regime” is plotted in the back dashed curve.

This expression can be assessed using the Godson and Tien approximations [19, 20]:

$$\bar{\tau}_\omega = 1 - \text{erf} \left(\frac{\sqrt{\pi}}{2} \frac{\bar{\kappa}_\omega U}{\sqrt{1 + \frac{\pi \bar{\kappa}_\omega U}{16\beta}}} \right), \quad (2.42)$$

where $U = P_t L$ is the optical thickness. Equation 2.42 is used in RadCal to compute $\bar{\tau}_\omega$ when using the Elsasser narrow band model, which is only used for Methane. Note that the Godson and Tien approximation is reasonably accurate for values of the overlap parameter lower or of the order of unity, *i.e.* $\beta < 1$. Figure 2.6 plots the quantity $-\ln(\bar{\tau}_\omega)$ (this quantity is also referred to as the curve of growth) versus the product $\bar{\kappa}_\omega U$ for two different values of the overlap parameter: $\beta = 0.05$ (in green) and $\beta = 0.5$ (in red). The back dashed curve corresponds to the “linear” behavior, *i.e.* $\bar{\tau}_\omega = \exp(-\bar{\kappa}U)$. It is noteworthy that this linear behavior corresponds to either “weak lines regimes” (situations with small product $\bar{\kappa}U$) or to situations with a strong overlap, $\beta > 1$). Outside of these regimes, assuming linear behavior might lead to overestimation of the curve of growth. Figure 2.6 also illustrates a case where the Godson and Tien approximation loses its accuracy and leads to unphysical results, as seen for the case $\beta = 0.5$, which overestimates the absorption.

It can be seen from Eq. 2.42 that $\bar{\tau}_\omega$ is fully characterized once the narrow band parameters $\bar{\kappa}_\omega$ and β are known. Note that these two parameters are by construction independent of the physical length of radiation propagation but depend on the local temperature, pressure, and local mixture composition.

2.3.2 Generalities on statistical narrow band models

The Goody and Malkmus models have been developed to provide a better modeling of the narrow band spectral properties than that predicted by the Elsasser model, which is based on strong assumptions: uniformity of the line strength and of line spacing. While the Elsasser model works fine for some light, diatomic species (*i.e.* HCl), most of the more complex polyatomic species cannot be modeled appropriately with the Elsasser model, since the very detailed experimental characterization of their spectral lines does not exhibit regularity [13].

The Goody and Malkmus models are statistical narrow band models, the former preceding the latter by a couple of decades and was first developed by Mayer and Goody [11]. Statistical narrow band models are based on two main assumptions: first, there is no correlation between lines position and line intensities, and the location of the line can be modeled by any random arrangement [11, 21]; second, while all the lines have the same shape, their line strength within the narrow band of spectral range $\Delta\nu$ is a random variable assigned to a continuous probability density function $P(\bar{S}, S)$, with \bar{S} the mean value of the line strength, *i.e.*

$$\bar{S} = \int_0^{+\infty} SP(\bar{S}, S) dS.$$

A consequence of these assumptions for a very large number of lines contained within the narrow band is that the transmissivity of a narrow band $\bar{\tau}_\omega$, and of optical thickness U , is expressed by:

$$\bar{\tau}_\omega(U) = \exp\left(-\frac{\bar{W}(U)}{d}\right), \quad (2.43)$$

where d is the average line spacing and $\bar{W}(U)$ is the average equivalent line width of the narrow band considered and is calculated as:

$$\begin{aligned} \bar{W}(U) &= \int_0^{+\infty} P(\bar{S}, S) W(S, U) dS \\ &= \int_0^{+\infty} P(\bar{S}, S) \int_{-\infty}^{+\infty} 1 - \exp(-\kappa_\omega P_i L) d\omega dS \end{aligned} \quad (2.44)$$

where κ_ω is the absorption coefficient of a Lorentz line, given by Eq. 2.24. An example of the derivation of Eq. 2.44 is presented in Penner's book [11]. By their different choice of the probability density function $P(\bar{S}, S)$, the Goody and Malkmus models provide an explicit and simple evaluation of the average equivalent line width of a narrow band, $\frac{\bar{W}}{d}$.

2.3.3 Goody model

The Goody model assumes an exponential distribution of the line strength:

$$P(\bar{S}, S) = \frac{1}{\bar{S}} \exp\left(-\frac{S}{\bar{S}}\right) \quad (2.45)$$

$$= \frac{4}{\pi S_E} \exp\left(-\frac{4S}{\pi S_E}\right), \quad (2.46)$$

where S_E is an effective equivalent line strength which relates to the average line strength \bar{S} with [22, 15]:

$$\bar{S} = \frac{\pi}{4} S_E. \quad (2.47)$$

Solving Eq. 2.43 and introducing the effective average lines spacing $d_E = \frac{4}{\pi}d$, Ref. [22], it comes:

$$\begin{aligned}\bar{\tau}_\omega &= \exp \left(-\frac{S_E}{d_E} \frac{U}{\sqrt{1 + \frac{S_E U}{4 \gamma_c}}} \right) \\ \bar{\tau}_\omega &= \exp \left(-\frac{\bar{\kappa}_\omega U}{\sqrt{1 + \frac{\bar{\kappa}_\omega U}{4 \beta}}} \right)\end{aligned}\quad (2.48)$$

where the band overlap parameter β is here defined as:

$$\beta = \frac{\gamma}{d_E} = \frac{\pi}{4} \frac{\gamma}{d}. \quad (2.49)$$

It is important to remark that the band overlap parameter β , while constant over a narrow band, varies with the wavenumber. In addition, it has a strong dependence on the total pressure. This dependence varies from species to species. The mean absorption coefficient $\bar{\kappa}$ in Eq. 2.48 keeps the same definition as given in Eq. 2.40. It is noteworthy to realize that:

$$\bar{\kappa} = \frac{S}{d} = \frac{S_E}{d_E}, \quad (2.50)$$

from the definition of d_E and S_E . The effective parameter has been introduced to be consistent with the definition from Ludwig *et al.*, Ref. [15], from which most of RadCal is formulated after.

Figure 2.7 plots the curve of growth, $-\ln(\bar{\tau}_\omega)$, versus the product $\bar{\kappa}_\omega U$ for two different values of the overlap parameter: $\beta = 0.05$ (in green) and $\beta = 0.5$ (in red) using the Goody model. The back dashed curve corresponds to the “linear” behavior, *i.e.* $\bar{\tau}_\omega = \exp(\bar{\kappa}U)$.

Again, it can be seen from Eq. 2.48 that $\bar{\tau}_\omega$ is fully characterized once the narrow band parameters $\bar{\kappa}_\omega$ and β are known.

2.3.4 Malkmus model

Like the Goody model, the Malkmus model assumes the line strength of all the lines in a given narrow band model follows a particular distribution. This model was developed because the exponential distribution assumed in the Goody model substantially underestimates the number of low-intensity lines. The Malkmus model is based on a more physical approach that assumes that the line strength distribution $P(S)$ varies proportionally to S^{-1} . This assumption is based on physical arguments and is empirically verified for some molecules, see Malkmus [22] for more details.

The problem of non-normalization of the S^{-1} distribution is circumvented by cutting-off the S^{-1} distribution below some very small and above some very large values of S . A continuous distribution can then be constructed based on some assumptions relating the energy of a transition with the line strength and assuming that the ratio between the maximum and the minimum line strengths considered is very large. The line strength probability distribution used in the Malkmus model is expressed by an exponential-tailed S^{-1} distribution [22, 21]:

$$P(S_E, S) = \frac{1}{S} \exp \left(-\frac{4}{\pi} \frac{S}{S_E} \right), \quad (2.51)$$

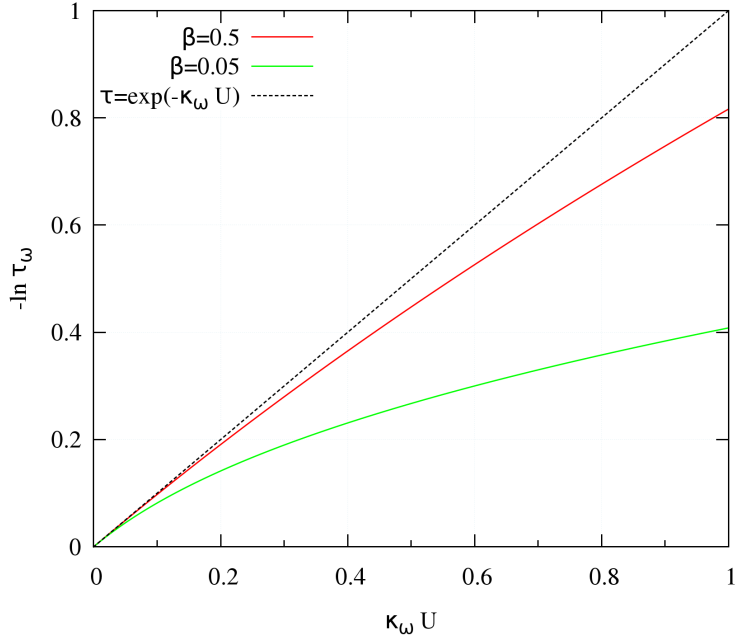


Figure 2.7: Goody model curve of growth ($\ln \bar{\tau}$) as a function of the product $\bar{\kappa}_\omega U$. Two different values of the overlap parameter are plotted: $\beta = 0.05$ (in green) and $\beta = 0.5$ (in red). The curve of growth for the “weak line regime” is also plotted (dashed curve).

where the effective line strength S_E relates to the average line strength \bar{S} through Eq. 2.47. Solving Eq. 2.43, and using the same definition for the effective average lines spacing d_E as given in the above section, it comes:

$$\begin{aligned}\bar{\tau}_\omega &= \exp \left(-2 \frac{\gamma_c}{d_E} \sqrt{1 + \frac{S_E U}{\gamma_c}} - 1 \right) \\ \bar{\tau}_\omega &= \exp \left(-2\beta \left[\sqrt{1 + \frac{\bar{\kappa}_\omega U}{\beta}} - 1 \right] \right)\end{aligned}\quad (2.52)$$

where the band overlap parameter β is here again defined as:

$$\beta = \frac{\gamma}{d_E} = \frac{\pi \gamma}{4 d}. \quad (2.53)$$

The Malkmus band model is recognized as the most suitable statistical narrow-band model for polyatomic gases [13]. In this new version of RadCal, this model has been introduced to model the newly implemented fuel species. Note that the Malkmus and Goody models do not differ when considering the extreme cases of optically thin and optically thick medium. In such cases, both models asymptote to:

$$\lim_{U \rightarrow 0} \frac{\bar{W}}{d} / U = \bar{\kappa} \quad (2.54)$$

$$\lim_{U \rightarrow +\infty} \frac{\bar{W}}{d} / \sqrt{U} = 2\sqrt{\bar{\kappa}\beta} \quad (2.55)$$

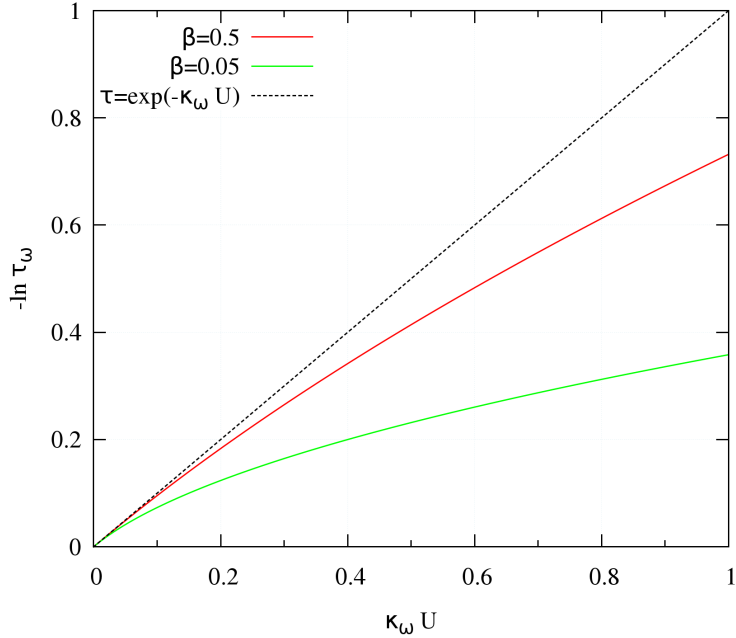


Figure 2.8: Malkmus model curve of growth ($-\ln \bar{\tau}$) as a function of the product $\bar{\kappa}_\omega U$. Two different values of the overlap parameter are plotted: $\beta = 0.05$ (in green) and $\beta = 0.5$ (in red). The curve of growth for the “weak line regime” is also plotted (dashed curve).

Figure 2.8 plots the curve of growth, $-\ln(\bar{\tau}_\omega)$, versus the product $\bar{\kappa}_\omega U$ for two different values of the overlap parameter: $\beta = 0.05$ (in green) and $\beta = 0.5$ (in red) using the Malkmus model. The back dashed curve corresponds to the “linear” behavior, *i.e.* $\bar{\tau}_\omega = \exp(-\bar{\kappa}U)$.

Again, it can be seen from Eq. 2.52 that $\bar{\tau}_\omega$ is fully characterized once the narrow band parameters $\bar{\kappa}_\omega$ and β are known. These two narrow band spectral quantities can be obtained either from line-by-line calculations, by fitting experimental data, or by physical considerations.

Note: For all the tabulated data, a linear interpolation of $\bar{\kappa}_\omega$ and β_ω in temperature and/or in wavenumber is performed by RadCal when necessary. If the temperature sought is out of the tabulated data range, then the data at the nearest temperature are used.

2.4 Treatment of the RTE in the scope of narrow band model

This section presents the expression of the different calculations performed by RadCal to numerically solve the Radiative Transfer Equation for a narrow band. The Radiative Transfer Equation for a narrow band is recalled below using wavenumbers:

$$\underbrace{I_{\omega_0}(s)}_{\text{Received intensity in } s} = \underbrace{I_{b,\omega_0}(T_w)\bar{\tau}(\omega_0; 0 \rightarrow s)}_{\text{transmitted incident intensity}} + \underbrace{\int_0^s I_{b,\omega_0}(T(s')) \frac{\partial \bar{\tau}}{\partial s'}(\omega_0; s' \rightarrow s) ds'}_{\text{intensity emitted by the medium between 0 and } s}. \quad (2.56)$$

where $\Delta\omega$ is the narrow band centered in ω_0 , $I_{\omega_0}(s)$ is the received flux at the location s , $I_{b,\omega_0}(T_w)$ is the incident flux penetrating the participating medium and which is modeled in RadCal as a flux from a blackbody of temperature T_w (T_w is an user input). The second term of the equation right-hand side accounts for the medium radiative emission and self-absorption.

2.4.1 Treatment of Homogeneous pressure-path

If the participating medium is homogeneous – *i.e.* of constant composition, temperature T , and total pressure P_T – Eq. 2.56 can be simplified as:

$$I_{\omega_0}(s) = I_{b,\omega_0}(T_w)\bar{\tau}(\omega_0; 0 \rightarrow s) + I_{b,\omega_0}(T)(1 - \bar{\tau}(\omega_0; 0 \rightarrow s)). \quad (2.57)$$

RadCal computes the value of $\bar{\tau}(\omega_0; 0 \rightarrow s)$ combining Lorentz and Doppler lines. While usually for cases at atmospheric pressure and at moderate temperature the Doppler lines are not important, they are however included for the sake of completeness. The different steps of the calculation of $\bar{\tau}(\omega_0; 0 \rightarrow s)$ are presented below.

For each participating species present in the medium, RadCal first retrieve the band mean absorption coefficient $\bar{\kappa}_\omega$, the band overlap parameter β (for Lorentz lines), and the Doppler fine structure parameter, denoted a_D , which is defined as the ratio of the Doppler HWHM γ_D , given by Eq. 2.28, over the mean line spacing d .

Then RadCal computes the optical depth from Lorentz lines, denoted X_C , using Eqs. 2.42, 2.48, and 2.52, depending on the species appropriate model, using $\bar{\kappa}_\omega$ and β . Note that:

$$X_C = \frac{\bar{W}}{d} \quad (2.58)$$

RadCal computes the optical depth from Doppler lines, denoted X_D . The expression of X_D depends of the model chosen to compute X_C . If the Elsasser or Goody model is used to compute X_C , then the optical depth from Doppler lines is calculated by [15]:

$$X_D = \sqrt{\frac{2}{\ln 2}} a_D \sqrt{\ln \left(1 + \frac{\ln 2}{2} \left(\frac{\bar{\kappa}_{\omega_0} U}{a_D} \right)^2 \right)}, \quad (2.59)$$

where U is the optical thickness defined by $U = P_i s$, with P_i the partial pressure (in atm) of the participating species considered and s is the distance given in cm. If the Malkmus model is used to compute X_C , then the optical depth from Doppler lines is calculated by [15]:

$$X_D = \sqrt{\frac{3}{2 \ln 2}} a_D \left[\ln \left(1 + \left(\sqrt{\frac{2 \ln 2}{3}} \frac{\bar{\kappa}_{\omega_0} U}{a_D} \right)^{2/3} \right) \right]^{3/2}. \quad (2.60)$$

The combined optical depth, Y , is then calculated:

$$Y = \left(1 - \left(\frac{X_C}{\bar{\kappa}_{\omega_0} U} \right)^2 \right)^{-2} + \left(1 - \left(\frac{X_D}{\bar{\kappa}_{\omega_0} U} \right)^2 \right)^{-2} - 1. \quad (2.61)$$

Finally, the narrow band transmissivity, $\bar{\tau}(\omega_0; 0 \rightarrow s)$, is obtained by:

$$\bar{\tau}(\omega_0; 0 \rightarrow s) = \exp \left(-\bar{\kappa}_{\omega_0} U \sqrt{1 - \frac{1}{\sqrt{Y}}} \right). \quad (2.62)$$

If there are more than one participating species, then $\bar{\tau}(\omega_0; 0 \rightarrow s)$ is calculated from:

$$\bar{\tau}(\omega_0; 0 \rightarrow s) = \exp \left(-\sum_i \bar{\kappa}_{i,\omega_0} U \sqrt{1 - \frac{1}{\sqrt{Y_i}}} \right), \quad (2.63)$$

the optical depth for each species i is first calculated separately, and then summed altogether.

2.4.2 Treatment of non-Homogeneous pressure-path - Curtis-Godson approximation

The treatment of the RTE in the case of non-homogeneous medium (where gradients of species, temperature, or pressure are present) is explicitly detailed below. The non-homogeneous case is first treated by discretizing the depth of penetration of the incident beam of direction \hat{s} into a set of n smaller segments $\{[s_{i-1}; s_i]\}_n$ over which the local composition, temperature, and pressure can reasonably be assumed constant. Hence, the expression of the RTE over a narrow band $\Delta\omega$, centered in ω_0 and given by Eq. 2.56 can be simplified as:

$$I_{\omega_0}(s) = I_{b,\omega_0}(T_w)\bar{\tau}(\omega_0; 0 \rightarrow s) + \sum_{i=1}^n I_{b,\omega_0}(T_i)(\bar{\tau}(\omega_0; s_i \rightarrow s) - \bar{\tau}(\omega_0; s_{i-1} \rightarrow s)). \quad (2.64)$$

In the expression, it assumed that $s_0 = 0$, which is coincided with the location of the blackbody wall of temperature T_w , and $s_n = s$. The temperature T_i is the temperature of the small segment $\{[s_{i-1}; s_i]\}_n$. The difficulty in solving Eq. 2.56 lies in evaluating $\bar{\tau}(\omega_0; s_i \rightarrow s)$ as it is correlated with the cells crossed by the beam \widehat{sis} .

To circumvent this difficulty, the Curtis-Godson approach is used. In this approach, it is assumed that each $\bar{\tau}(\omega_0; s_i \rightarrow s)$ for a given species can still be calculated using Eqs. 2.59, 2.60, 2.61, 2.62, and the models presented in Section 2.3 but their parameters $\bar{\kappa}$, β , and a_D are replaced by some effective parameters, $\bar{\kappa}^*$, β^* , a_D^* , respectively. See Young [21] and Ludwig *et al.* [15] for additional details on the Curtis-Godson approach. It was found that using path-averaged parameters as effective parameters work best [21] to calculate the transmissivity of non-homogeneous medium. These parameters are defined as:

$$\bar{\kappa}^* = \frac{\int_{s_i}^s \bar{\kappa}(s') P_i(s') ds'}{\int_{s_i}^s P_i(s') ds'}, \quad (2.65)$$

$$\beta^* = \frac{\int_{s_i}^s \beta(s') \bar{\kappa}(s') P_i(s') ds'}{\int_{s_i}^s \bar{\kappa}(s') P_i(s') ds'}, \quad (2.66)$$

$$a_D^* = \frac{\int_{s_i}^s a_D(s') \bar{\kappa}(s') P_i(s') ds'}{\int_{s_i}^s \bar{\kappa}(s') P_i(s') ds'}, \quad (2.67)$$

with P_i is the partial pressure of the participating gas considered. The quantity:

$$U = \int_{s_i}^s P_i(s') ds', \quad (2.68)$$

is the optical thickness, in atm.cm, between the points s_i and s .

2.5 Output quantities: effective coefficients and integrated quantities

RadCal solves the RTE based on the input parameters found in the input file `RADCAL.in` and returns in a Tecplot file (`<CASE ID>.tec`, where `<CASE ID>` is an user input defined in the input file) the spectral profile of the spectral transmissivity of the medium $\bar{\tau}(\omega_0; 0 \rightarrow s)$ and the incident spectral intensity $I_{\omega_0}(s)$ calculated using either Eq. 2.57 or 2.64.

In addition to the Tecplot file, RadCal also generates an output file `RADCAL.out`, that contains several effective coefficients and integrated quantities. Some of these integrated quantities were already included

in the previous version of RadCal. This is the case of the effective absorption coefficient, the Planck mean absorption coefficient, and the received total directional radiative energy flux (or received total intensity). Two new integrated quantities have been added: the total emissivity, and the total transmissivity. These effective coefficients and integrated quantities are described formally in this section. Note that the integration is performed using a Simpson rule over non regular abscissa using a 3-point Lagrangian interpolation (quadratic interpolation).

2.5.1 Effective absorption coefficient

The path-averaged or effective absorption coefficient, denoted here κ_e and denoted `Amean` in the output file, is defined such that the received total intensity in $s = L$ can be expressed as a sum of a transmitted total intensity coming from the blackbody wall, set at temperature T_w , and a total intensity emitted by the gas at the local temperature T_g :

$$\int_{\omega_{\min}}^{\omega_{\max}} I_{\omega}(L) d\omega = \exp(-\kappa_e L) \int_{\omega_{\min}}^{\omega_{\max}} I_{b,\omega}(T_w) d\omega + (1 - \exp(-\kappa_e L)) \int_{\omega_{\min}}^{\omega_{\max}} I_{b,\omega}(T_g) d\omega \quad (2.69)$$

where L is the total path length given in cm. The bounds of integration in Eq. 2.69 are fixed, with $\omega_{\min} = 5 \text{ cm}^{-1}$, and $\omega_{\max} = 25000 \text{ cm}^{-1}$. However, the bounds of the integration for the gas-phase species are specified by the user. The remain outside spectral domain is integrated then considering only the contribution of soot (if present). See Eq. 2.78. The large bounds of integration ($5 - 25000 \text{ cm}^{-1}$) is large enough such that:

$$\int_{\omega_{\min}}^{\omega_{\max}} I_{b,\omega}(T) d\omega \approx \frac{\sigma}{\pi} T^4. \quad (2.70)$$

Formally, κ_e is calculated from:

$$\kappa_e = -\frac{1}{L} \ln \left(\frac{\int_{\omega_{\min}}^{\omega_{\max}} I_{\omega}(L) - I_{b,\omega}(T_g) d\omega}{\int_{\omega_{\min}}^{\omega_{\max}} I_{b,\omega}(T_w) - I_{b,\omega}(T_w) d\omega} \right). \quad (2.71)$$

Note that κ_e has the units of cm^{-1} . The effective absorption coefficient is calculated for homogeneous and non-homogeneous cases. For the latter, the gas temperature T_g used in Eq. 2.71 is the path-average temperature:

$$T_g = \frac{\int_0^L T(s) ds}{L}. \quad (2.72)$$

While the effective absorption coefficient works well for a given length L , one has to be careful when using it to estimate the received total intensity from a similar homogeneous isothermal medium but with a different thickness as the calculated results using Eq. 2.71 might deviate significantly from the actual results unless the medium considered is gray (no spectral variation of the absorption coefficient).

2.5.2 Planck mean absorption coefficient

The Planck mean coefficient, denoted here κ_{Planck} , is calculated by:

$$\kappa_{\text{Planck}} = \frac{\pi}{\sigma T_g^4} \int_{\omega_{\min}}^{\omega_{\max}} I_{b,\omega}(T_g) \sum_i \bar{\kappa}_{i,\omega} P_i d\omega \quad (2.73)$$

where P_i is the partial pressure of participating species i , in units of atm; and $\bar{\kappa}_{i,\omega}$ is the narrow band mean absorption coefficient of participating species i , in units of $\text{atm}^{-1} \cdot \text{cm}^{-1}$. Note that the temperature used in

this expression is the local gas temperature; thus, κ_{Planck} is a function of the gas phase temperature and of the species partial pressure. It is independent of the path physical length. Its units are in cm^{-1} . The integration bounds, ω_{\min} , and ω_{\max} are defined by the user in the input file.

The Planck mean absorption coefficient is calculated for homogeneous and non-homogeneous cases. For the latter, the gas temperature used to calculate $I_{b,\omega}(T_g)$ is the path-average temperature as defined by Eq. 2.72. The term T_g^4 is also calculated using a path-average value:

$$T_g^4 = \frac{\int_0^L T(s)^4 ds}{L}, \quad (2.74)$$

where L is the total path length given in cm.

For non-homogeneous cases, the mean absorption coefficient used in Eq. 2.73, $\bar{\kappa}_{i,\omega}$, corresponds to the effective mean absorption coefficient $\bar{\kappa}^*$ defined by Eq. 2.65. The partial pressure used is a path-average partial pressure:

$$P_i = \frac{\int_0^L P_i(s) ds}{L}. \quad (2.75)$$

2.5.3 Total transmissivity

Radcal returns the total transmissivity, denoted τ_T , of the spectral range bounded between the user defined ω_{\min} and ω_{\max} . The total transmissivity is calculated as:

$$\tau_T = \frac{\int_{\omega_{\min}}^{\omega_{\max}} \tau(0 \rightarrow s; \omega) I_{b,\omega}(T_w) d\omega}{\int_{\omega_{\min}}^{\omega_{\max}} I_{b,\omega}(T_w) d\omega}. \quad (2.76)$$

This quantity is dimensionless. It represents the fraction of transmitted incident intensity from the blackbody wall set at temperature T_w . It is worth noting that since it depends on T_w , changing T_w while keeping constant all the other simulation parameters will yield different values of τ_T .

2.5.4 Total emissivity

Radcal returns the total emissivity, denoted ε_T , for the spectral range bounded by the user defined ω_{\min} and ω_{\max} . It is derived from the effective absorption coefficient κ_e through:

$$\varepsilon_T = 1 - \exp(-\kappa_e L), \quad (2.77)$$

where L is the total physical length of the participating layer, given in cm. The total emissivity is dimensionless.

2.5.5 Received flux

RadCal returns the integrated value of the received total directional radiative energy flux (or received total intensity), denoted Received Flux in RADCAL.out file. The integration is performed between the user defined bounds ω_{\min} and ω_{\max} . Note that contribution of soot (if present) is added in the ranges 5 cm^{-1} to ω_{\min} and ω_{\max} to $25,000 \text{ cm}^{-1}$. Its units are in $\text{W.m}^{-2}.\text{str}^{-1}$. The received total intensity, denoted $I(L)$, is calculated by:

$$I(L) = \underbrace{\int_{\omega_{\min}}^{\omega_{\max}} I_{\omega}(L) d\omega}_{\text{All species}} + \underbrace{\int_5^{\omega_{\min}} I_{\omega}(L) d\omega}_{\text{Soot only}} + \underbrace{\int_{\omega_{\max}}^{25,000} I_{\omega}(L) d\omega}_{\text{Soot only}}, \quad (2.78)$$

where $I_\omega(L)$ is obtained from Eq. 2.57 for homogeneous cases, and Eq. 2.64 for non-homogeneous cases.

Chapter 3

Presentation of the Old Species in RADCAL

The characteristics of the “old” RadCal species, *i.e.* the species present in the 1993 RadCal version are presented in this chapter. These species are gas phase H₂O, CO₂, CO, and CH₄. The data pertaining to these species have not been changed since the 1993 RadCal version.

3.1 Water vapor: H₂O

The water molecule is an asymmetric top molecule with the oxygen atom in the middle. The bound length is 0.958 Å and the bond angle is 104.45°. Because of its large permanent electric dipole moment (6.16×10^{-30} Coulomb-meters) in its equilibrium configuration, it has strong rotational bands. In addition, its three moments of inertia differ greatly: the rotational constants are A = 27.877 cm⁻¹, B = 14.512 cm⁻¹, and C = 9.285 cm⁻¹ (values from Ref. [23]). Recall that the rotational constant relates to the molecule principal moment of inertia with:

$$A = \frac{h}{8\pi^2 c I_A}, \quad (3.1)$$

where I_A is one of the principal moment of inertia, h is the Planck constant (6.626×10^{-34} J·s), and c is the speed of light in vacuum, $c = 299,792,458$ m/s.

Because the three moments of inertia are greatly different from each other and are small, they give rise to a widespread and apparently disorderly array of rotation lines. This makes the infrared spectrum of H₂O very complex. H₂O has three fundamental vibration modes, which are reported in Table 3.1.

Table 3.1: Observed wavenumbers associated with fundamental vibration modes of H₂O.

Band	Upper State	H ¹⁶ OH
v ₁	100	3657.05
v ₂	010	1594.75
v ₃	001	3755.93

The important bands of water vapor fall into a number of distinct classes: rotation band from 0 to 900 cm⁻¹, v₂ bands from 900 to 2400 cm⁻¹ (6.3 μm region), v₁, v₃, and 2v₂ bands from 2800 to 4400 cm⁻¹ (2.7 μm region), 6 distinguishable groups of lines between 4500 and 11,000 cm⁻¹: Ω, Ψ, Φ, τ^c, σ^c, ρ^c; these are combined vibrational modes and overtones.

The strongest bands at atmospheric temperature are the rotational (0 – 900 cm⁻¹) and the 6.3 μm band. In fire application, the shift of the dominant region of the Planck distribution toward higher wavenumber renders the 2.7 μm very important for high temperature emission purposes.

In Radcal, the H_2O mean absorption coefficient $\bar{\kappa}$ has been tabulated for the wavenumbers between 50 to 9300 cm^{-1} , and for the following temperatures: 300 K, 600 K, 1000 K, 1500 K, 2000 K, 2500 K. Figures 3.1 to 3.6 plot the spectral mean absorption coefficient, in units of $\text{atm}^{-1} \cdot \text{cm}^{-1}$, at these different temperatures. The data originate from Ludwig *et al.* [15]. Experimental data have been fitted using the statistical Goody narrow band model.

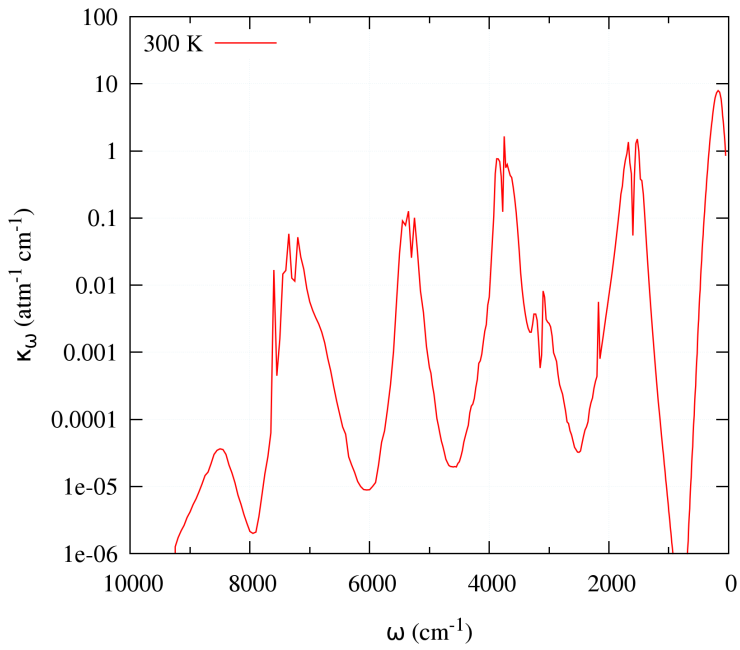


Figure 3.1: Spectral variations of the H_2O mean absorption coefficient $\bar{\kappa}_\omega$, in $\text{atm}^{-1} \cdot \text{cm}^{-1}$, at 300 K as tabulated in RadCal.

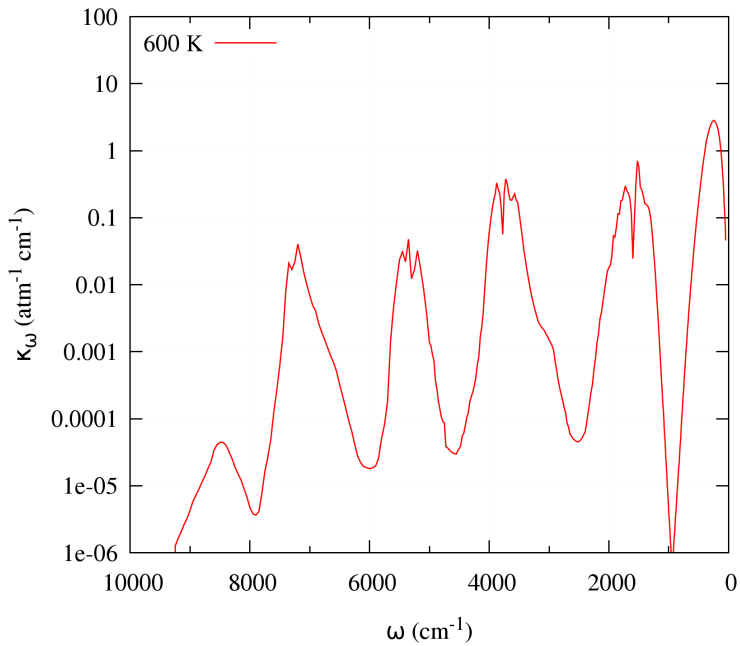


Figure 3.2: Spectral variations of the H_2O mean absorption coefficient $\bar{\kappa}_\omega$, in $\text{atm}^{-1} \cdot \text{cm}^{-1}$, at 600 K as tabulated in RadCal.

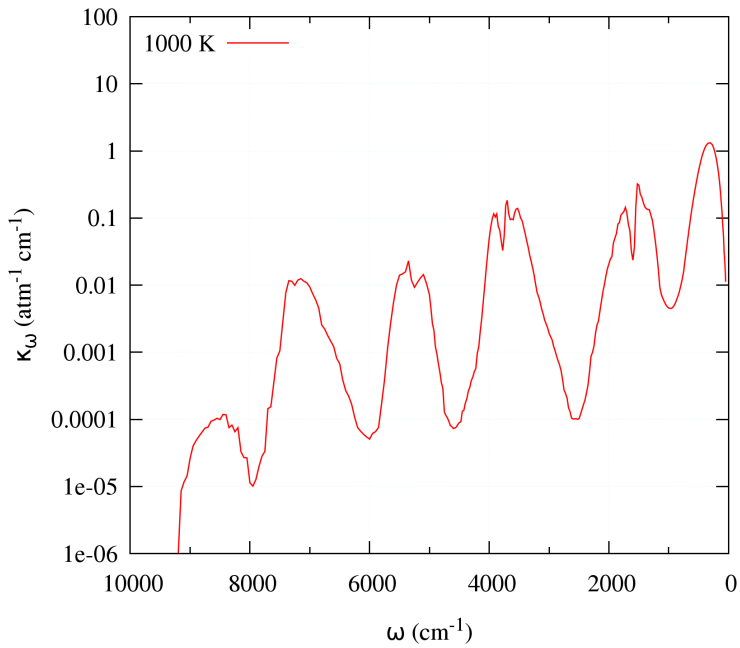


Figure 3.3: Spectral variations of the H_2O mean absorption coefficient $\bar{\kappa}_\omega$, in $\text{atm}^{-1} \cdot \text{cm}^{-1}$, at 1000 K as tabulated in RadCal.

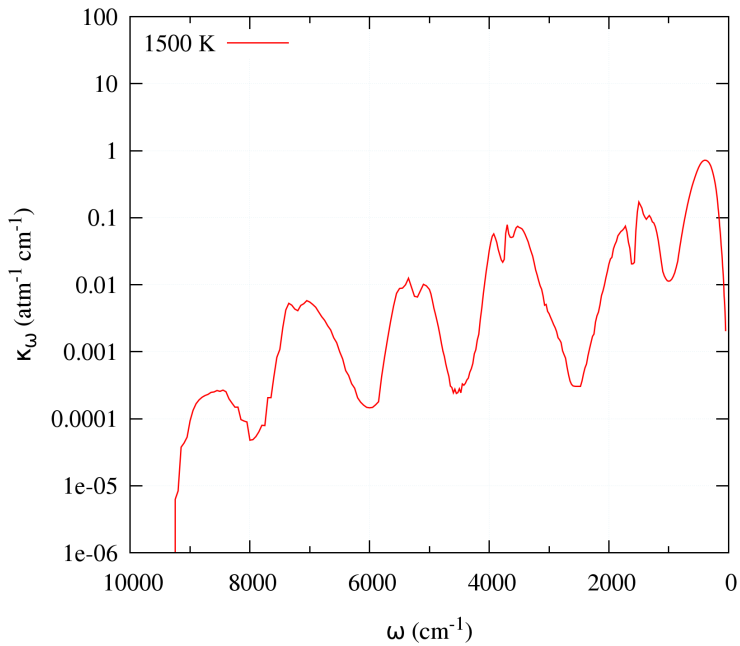


Figure 3.4: Spectral variations of the H_2O mean absorption coefficient $\bar{\kappa}_\omega$, in $\text{atm}^{-1} \cdot \text{cm}^{-1}$, at 1500 K as tabulated in RadCal.

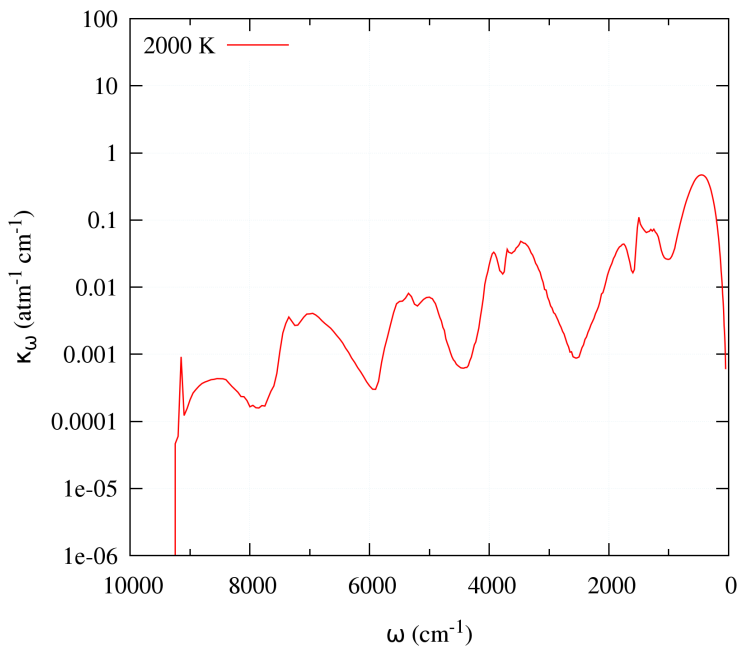


Figure 3.5: Spectral variations of the H_2O mean absorption coefficient $\bar{\kappa}_\omega$, in $\text{atm}^{-1} \cdot \text{cm}^{-1}$, at 2000 K as tabulated in RadCal.

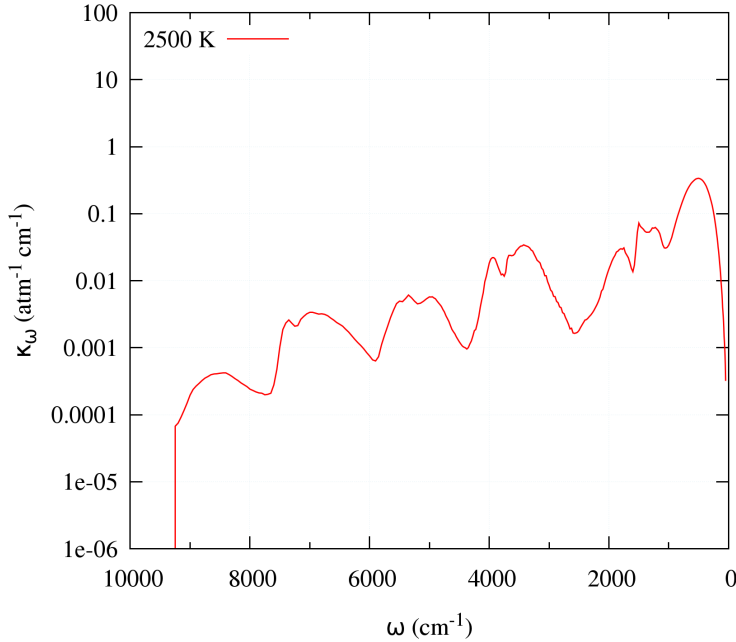


Figure 3.6: Spectral variations of the H_2O mean absorption coefficient $\bar{\kappa}_\omega$, in $\text{atm}^{-1}.\text{cm}^{-1}$, at 2500 K as tabulated in RadCal.

To calculate the band overlap parameter β , the Lorentz HWHM is considered constant over the spectrum and is calculated using Eq. 2.26, while the effective line spacing is given by [15]:

$$d = \exp(0.7941 \sin(0.036\omega - 8.043) + 2.294 + 0.3004 \times 10^{-2}T - 0.366 \times 10^{-6}T^2), \quad (3.2)$$

where T is the local temperature.

3.2 Carbon dioxide: CO_2

Carbon dioxide is a linear, symmetric molecule. Its bond length is 115.98 pm in ground state, and its rotational constant is 0.3906 cm^{-1} . Because of the symmetry, CO_2 has no permanent dipole moment. It has four vibrational modes, but only two fundamental IR vibration modes. Five distinct bands are included in RadCal (four are calculated, one is tabulated), see Table 3.2. All the bands are modeled after the Goody model.

Table 3.2: Spectral bands of CO_2 included in RADCAL.

Band #	Bounds (cm^{-1})		Method	Notes:
1	500	880	tabulated	$15 \mu\text{m}$ region - strong (for atmospheric application)
2	880	1100	modeled	$10 \mu\text{m}$ region
3	1975	2475	modeled	4.9 and $4.3 \mu\text{m}$ region - very strong
4	3050	3800	modeled	$2.7 \mu\text{m}$ region - important for fire application
5	4550	5275	modeled	$2.0 \mu\text{m}$ region

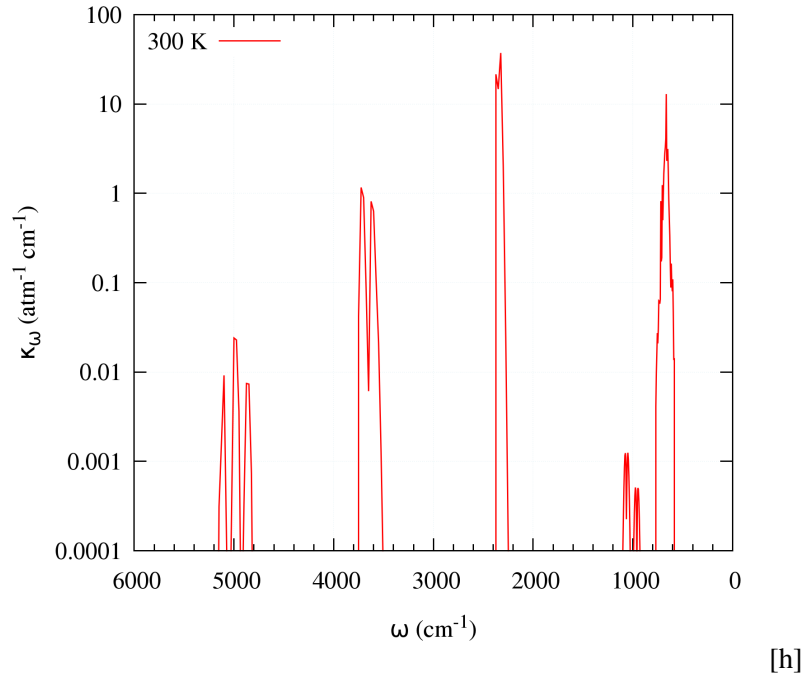


Figure 3.7: Spectral variations of the CO_2 mean absorption coefficient $\bar{\kappa}_\omega$, in $\text{atm}^{-1} \cdot \text{cm}^{-1}$, at 300 K as tabulated and modeled in RadCal.

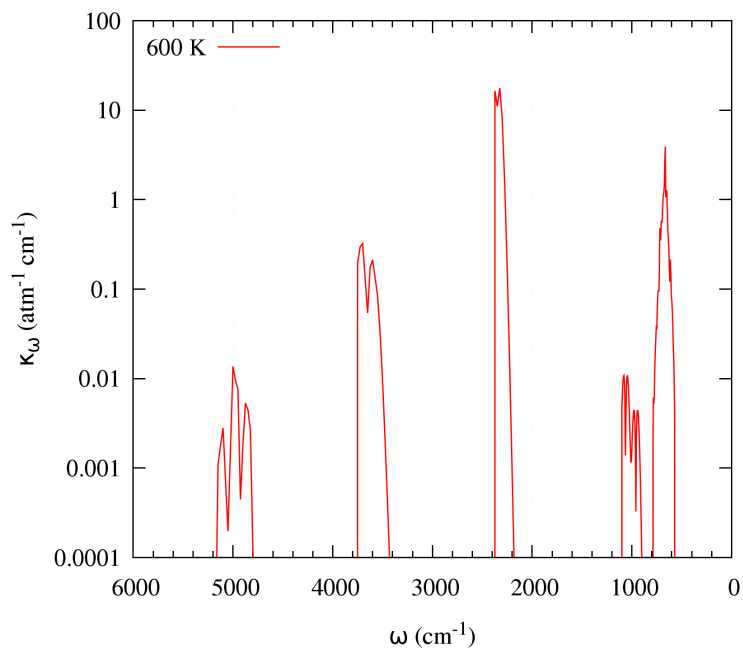


Figure 3.8: Spectral variations of the CO_2 mean absorption coefficient $\bar{\kappa}_\omega$, in $\text{atm}^{-1} \cdot \text{cm}^{-1}$, at 600 K as tabulated and modeled in RadCal.

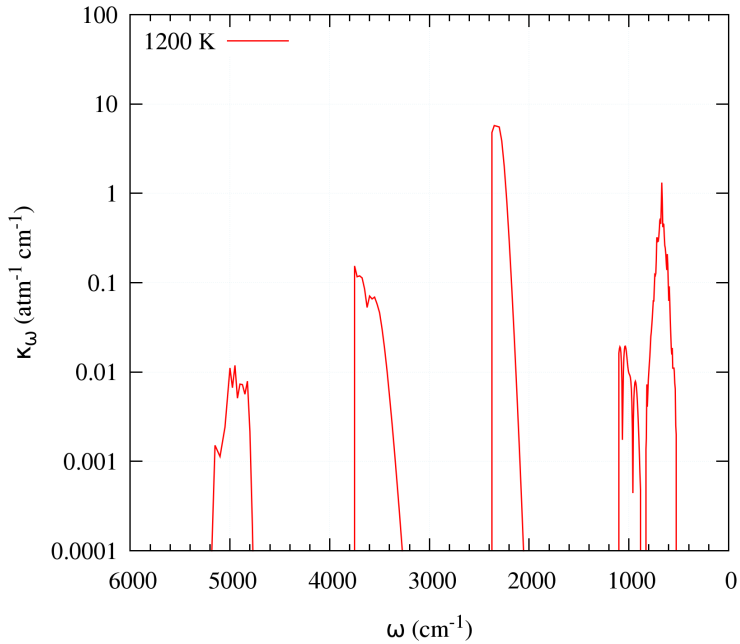


Figure 3.9: Spectral variations of the CO_2 mean absorption coefficient $\bar{\kappa}_\omega$, in $\text{atm}^{-1}.\text{cm}^{-1}$, at 1200 K as tabulated and modeled in RadCal.

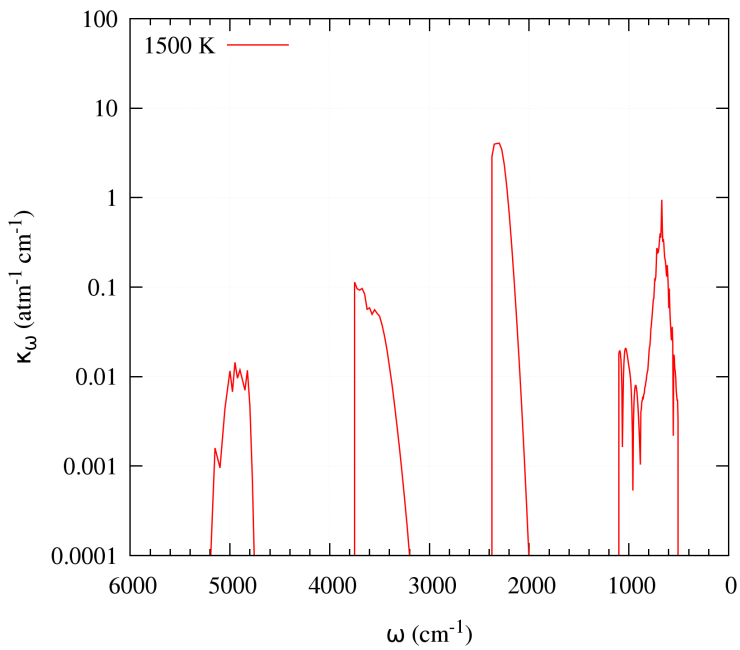


Figure 3.10: Spectral variations of the CO_2 mean absorption coefficient $\bar{\kappa}_\omega$, in $\text{atm}^{-1}.\text{cm}^{-1}$, at 1500 K as tabulated and modeled in RadCal.

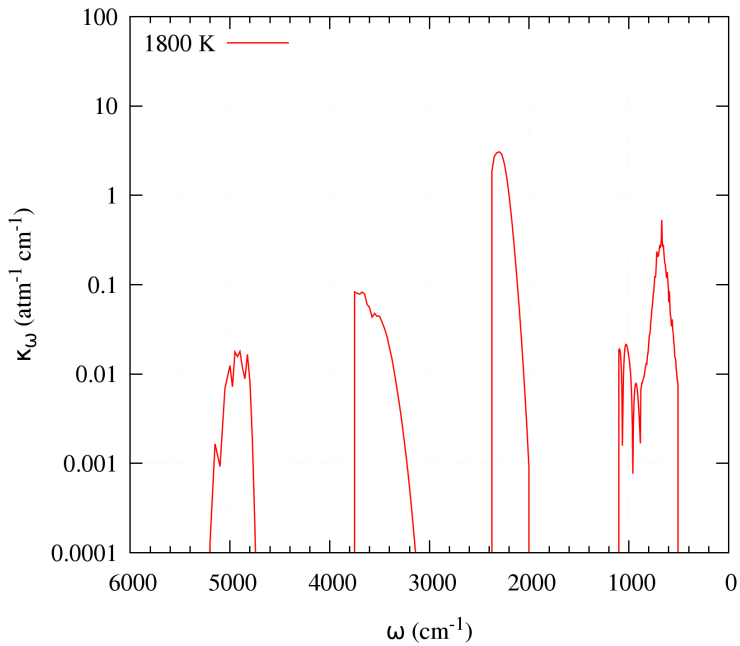


Figure 3.11: Spectral variations of the CO_2 mean absorption coefficient $\bar{\kappa}_\omega$, in $\text{atm}^{-1} \cdot \text{cm}^{-1}$, at 1800 K as tabulated and modeled in RadCal.

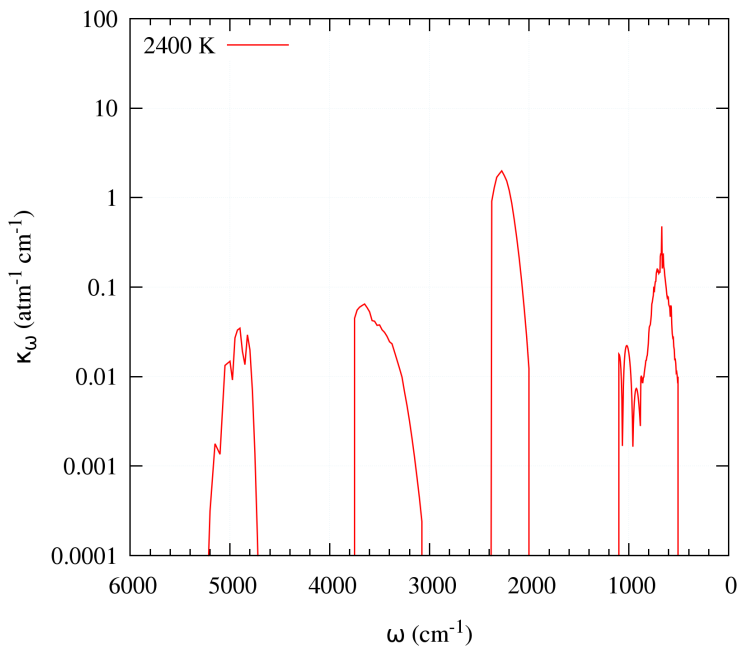


Figure 3.12: Spectral variations of the CO_2 mean absorption coefficient $\bar{\kappa}_\omega$, in $\text{atm}^{-1} \cdot \text{cm}^{-1}$, at 2400 K as tabulated and modeled in RadCal.

The strongest band in the CO₂ spectrum is Band 3. At 300 K, it has an integrated band intensity (see Section 4.1 for a definition of this quantity) of 2963 atm⁻¹cm⁻². The tabulated data (mean absorption coefficient $\bar{\kappa}_\omega$) were obtained from experiments for the following temperatures: 300, 600, 1200, 1500, 1800, 2400 K. The modeled bands use the harmonic oscillator approximation. All the bands uses the Goody statistical narrow band model. Figures 3.7 to 3.12 plot the mean absorption coefficient at 300, 600, 1200, 1500, 1800, 2400 K, as tabulated (Band 1) and modeled in RadCal (Bands 2 to 5).

3.3 Carbon monoxide: CO

Carbon Monoxide is a diatomic molecule and as such, it has only one fundamental vibrational mode. RAD-CAL includes one distinct band, the 1600–2400 band. It corresponds to the stretching of the triple bond C ≡ O. This band is modeled and it uses the model from Malkmus and Thompson [?]. It is based on the anharmonic oscillator model and uses band integrated intensity measurements. Figures 3.13 to 3.14 plot the spectral mean absorption coefficient of CO at 300 K and 2500 K, respectively.

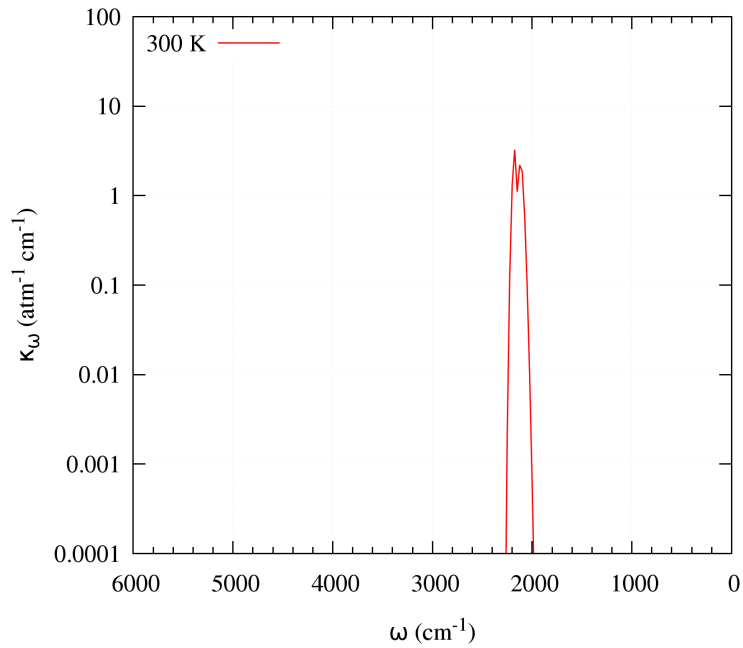


Figure 3.13: Spectral variations of the CO mean absorption coefficient $\bar{\kappa}_\omega$, in atm⁻¹.cm⁻¹, at 300 K as modeled in RadCal.

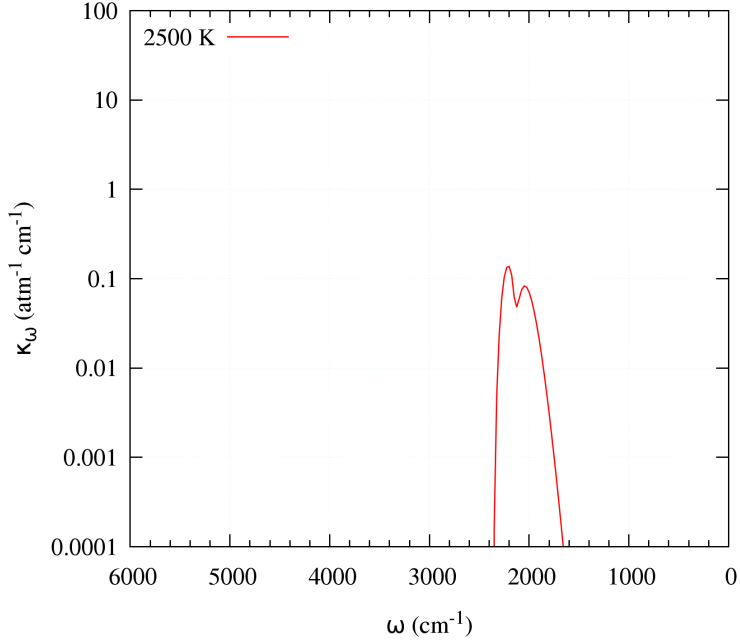


Figure 3.14: Spectral variations of the CO mean absorption coefficient $\bar{\kappa}_\omega$, in $\text{atm}^{-1} \cdot \text{cm}^{-1}$, at 2500 K as modeled in RadCal.

The first overtone (centered at $\omega \approx 4260 \text{ cm}^{-1}$) is not accounted for as its integrated band intensity is negligible at standard temperature and pressure. See Table 3.3.

Table 3.3: Spectral bands of CO included in RADCAL.

Band #	Bounds (cm^{-1})	Method	Assignment	$\alpha(T = 296 \text{ K}) (\text{atm}^{-1} \text{cm}^{-2})$
1	1600 2400	modeled	C \equiv O stretching	260

At 295 K, the integrated band intensity of Band 1 is $260 \text{ atm}^{-1} \text{cm}^{-2}$. The statistical narrow band model associated with CO is the Goody model. Recommended temperatures of use range from 295 K to 2500 K.

3.4 Methane: CH_4

Methane is a spherical top molecule of tetrahedral shape with the carbon atom occupying the center of the tetrahedron. It belongs to the point group T_d . The methane IR spectrum is the result of the vibration-rotation modes of the C – H groups. It has nine vibrational modes, but due to its symmetry, this translates into only two distinct IR active fundamental vibration frequencies. In RadCal, the methane IR spectrum is divided into three distinct bands, which include the fundamentals plus degenerate (overtone) vibration modes. Bands 1 and 2 are calculated using tabulated mean absorption coefficient data which were obtained by Brosmer and Tien, [6] for temperatures of 290, 600, 850 K. Band 3 is modeled, using a just-overlapping line model; the integrated intensities are computed in the harmonic-oscillator, rigid-rotator approximation. See Penner and Gray, Ref. [24], for more details. In RadCal, the Elsasser model is used to calculate the collision optical depth. Table 3.4 tabulates the different characteristics of the CH_4 bands.

Table 3.4: Spectral bands of CH_4 included in RADCAL.

Band #	Bounds (cm^{-1})		Method	Assignment	$\alpha(T = 296 \text{ K}) (\text{atm}^{-1}\text{cm}^{-2})$
1	1150	1600	tabulated	C – H Bend	237
2	2700	3250	tabulated	C – H Stretch	212
3	3400	5000	modeled	C – H Stretch	35

The strongest bands are Bands 1 and 2 which at standard temperature and pressure have an integrated band intensity of $237 \text{ atm}^{-1}\text{cm}^{-2}$ and $212 \text{ atm}^{-1}\text{cm}^{-2}$, respectively. Figures 3.15, 3.16, and 3.17 plot the spectral mean absorption coefficient $\bar{\kappa}$ for CH_4 at 290 K, 600 K, and 850 K, respectively.

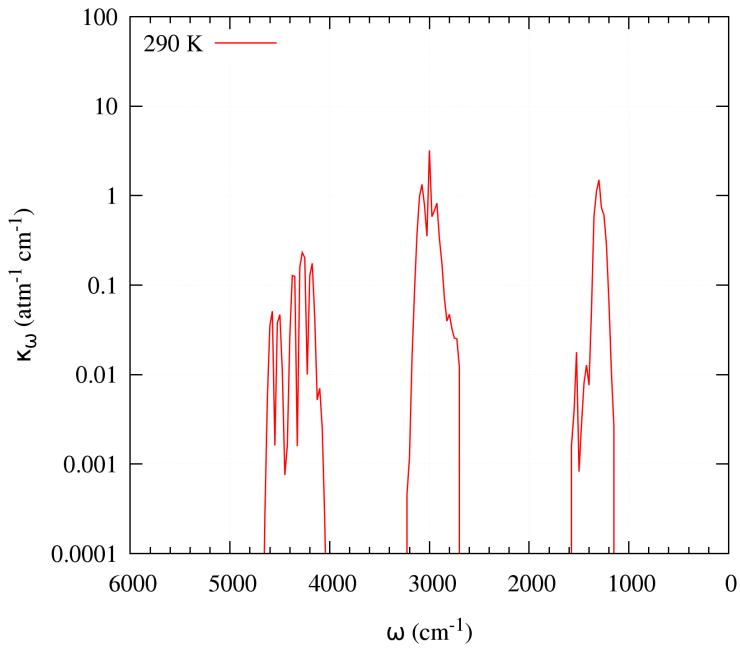


Figure 3.15: Spectral variations of the CH_4 mean absorption coefficient $\bar{\kappa}_\omega$, in $\text{atm}^{-1}\cdot\text{cm}^{-1}$, at 290 K as tabulated and modeled in RadCal.

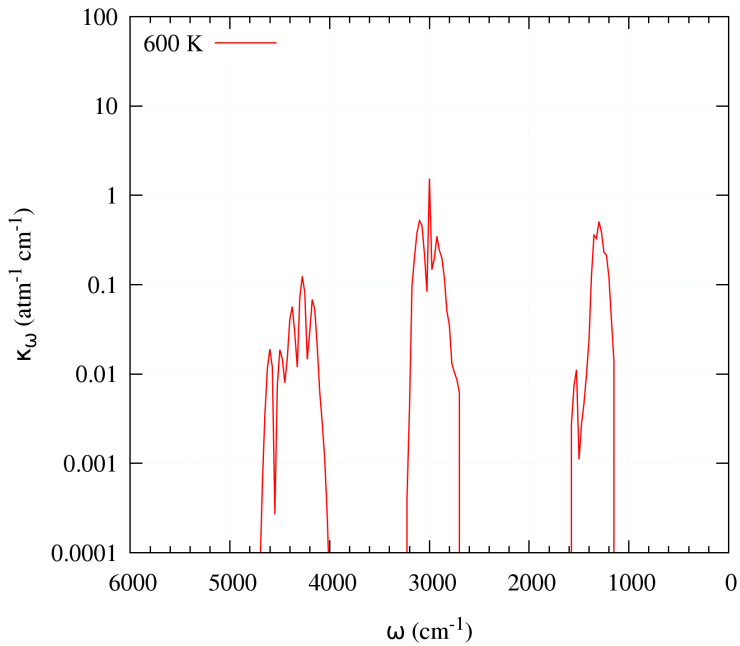


Figure 3.16: Spectral variations of the CH_4 mean absorption coefficient $\bar{\kappa}_\omega$, in $\text{atm}^{-1}.\text{cm}^{-1}$, at 600 K as tabulated and modeled in RadCal.

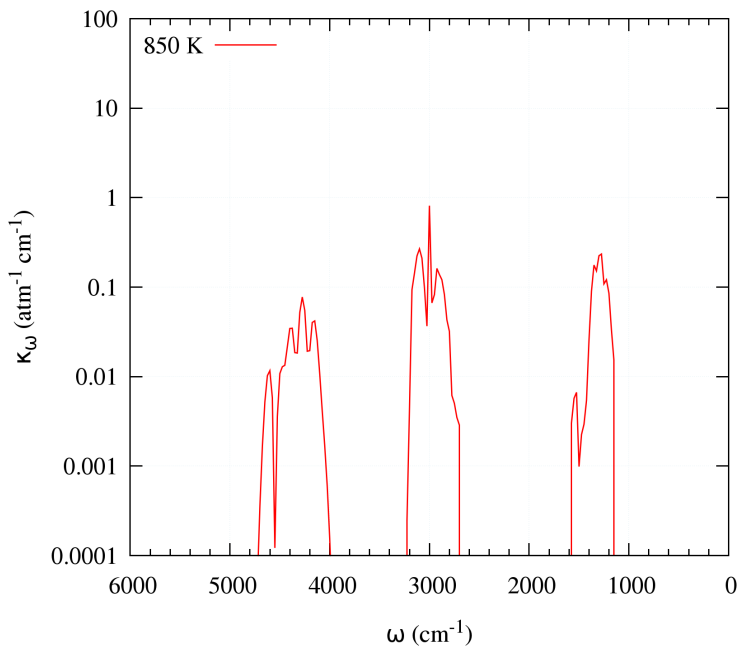


Figure 3.17: Spectral variations of the CH_4 mean absorption coefficient $\bar{\kappa}_\omega$, in $\text{atm}^{-1}.\text{cm}^{-1}$, at 850 K as tabulated and modeled in RadCal.

3.5 Soot

The soot spectral absorption coefficient is calculated using the below formulation:

$$\bar{\kappa} = 7.0\omega f_v \quad (3.3)$$

where f_v is the soot volume fraction and is unitless. The narrow band transmissivity of soot is calculated as:

$$\bar{\tau}(0 \rightarrow s) = \exp(-\bar{\kappa}s). \quad (3.4)$$

From Eq. 3.3, it can be seen that particulate matters tend to absorb soot in the high wavenumber part of the spectrum. Figure 3.18 plots the spectral transmissivity of a homogeneous layer of soot at 300 K with a soot volume fraction value of 5 ppm (5×10^{-6}) and a thickness of 20 cm.

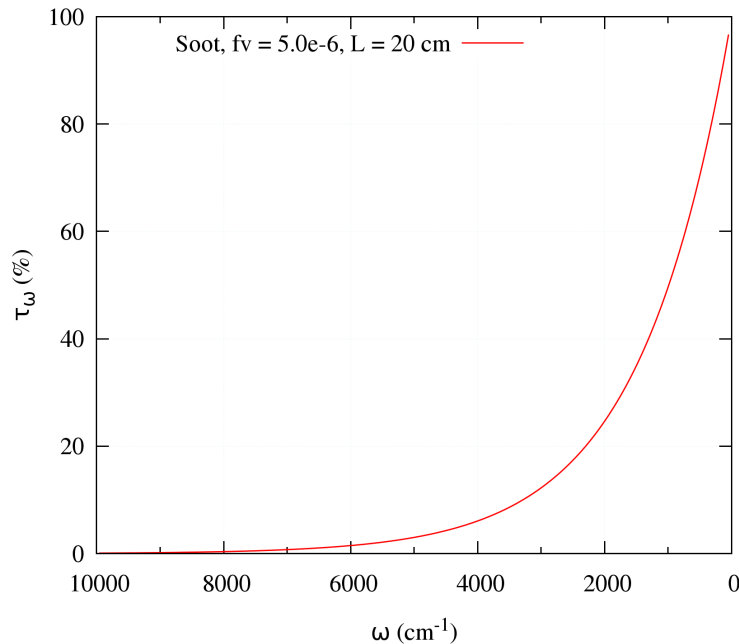


Figure 3.18: Predicted spectral transmissivity of a homogeneous layer of soot at 300 K, of thickness 20 cm, and with a soot volume fraction of 5 ppm ($f_v = 5 \times 10^{-6}$).

Chapter 4

Presentation of the New Species in RADCAL

The original RADCAL data have been supplemented with new tabulated experimental data for the following fuels: Ethylene (C_2H_4), Ethane (C_2H_6), Propylene (C_3H_6), Propane (C_3H_8), Toluene (C_7H_8), *n*-Heptane (C_7H_{16}), Methanol (CH_3OH), Methyl Methacrylate ($C_5H_8O_2$). These new data have been obtained through Wakatsuki Fourier Transform Infra-Red (FTIR) measurements for wavenumbers between $700\text{--}4000\text{ cm}^{-1}$. See Ref. [25] for a detailed description of the experimental methodology.

The sections below briefly describe the molecules and their IR active molecular bands. Bands bounds used in RADCAL are tabulated with a brief description of the band assignment and their integrated band intensity (see definition below) at the lowest temperature is also included. Unlike the data previously included in RadCal that contained a mix of tabulated and modeled data, the species data presented here in the chapter are all tabulated.

4.1 Integrated band intensity

A useful quantity to compare the relative importance of the different IR bands is provided by the integrated band intensity, α_i , defined for the i th participating species as:

$$\alpha_i(T) = \int_{\omega_{\min}}^{\omega_{\max}} \bar{\kappa}_i(\omega', T) d\omega' \quad (4.1)$$

whose units are $\text{atm}^{-1}\text{cm}^{-2}$. The integrated band intensity is an intrinsic property of a molecule directly related to its geometry, its elements, and the nature of the chemical bonds. It is proportional to the amplitude of the electric moment variations for a vibration-rotation transition [26]. It is usually referred to as the coefficient C_1 in the exponential wide-band model.

The value of the spectral absorption coefficient, $\bar{\kappa}_i$, is averaged over a narrow band whose spectral width, $\Delta\omega$, varies from 5 cm^{-1} for $\omega < 1100\text{ cm}^{-1}$, to 25 cm^{-1} for $1100\text{ cm}^{-1} \leq \omega < 5000\text{ cm}^{-1}$, and to 50 cm^{-1} for $5000\text{ cm}^{-1} \leq \omega$. In the sections below, value were obtained by integrated the narrow band absorption coefficients over the band of interest.

4.2 Fitting procedure

In Section 2.3, expressions for the Elsasser, Goody, and Malkmus narrow band models were presented, see Eqs. 2.42, 2.48, and 2.52. Each gives a functional expression of the spectral transmissivity over narrow

bands in the form:

$$\bar{\tau}_\omega = f(\bar{\kappa}_\omega, \beta_\omega, U), \quad (4.2)$$

where the expression of f depends on the model chosen; the pressure-path $U = P_i L$ is known from the experimental configuration; the experimental spectral transmissivity $\bar{\tau}_\omega$ is obtained by FTIR measurements; and the couple $\bar{\kappa}_\omega, \beta_\omega$ are the sought parameters. In the following, the subscript ω denoting the spectral dependence of the quantities is omitted for ease of reading.

To find the optimal narrow band model parameters for each model, at a given temperature and at a given wavenumber, a fitting objective function was minimized using a least-square fitting approach. The objective function \mathcal{F} was defined as:

$$\mathcal{F}_i = \frac{|\bar{\tau}_{exp,i} - f(\bar{\kappa}, \beta, U_i)|}{\bar{\tau}_{exp,i}}, \quad (4.3)$$

where the subscript exp denotes experimentally measured values, and i denotes an experimental condition of pressure-path. The experimental transmissivity relative to the i^{th} pressure-path is denoted $\bar{\tau}_{exp,i}$. This is an averaged value over the narrow band interval at the desired resolution. Typically three different pressure-paths were used for each temperature and fuel. The narrow band parameters $(\bar{\kappa}, \beta)$ hence found minimize the square of the l^2 -norm of the objective function \mathcal{F} :

$$\min_{(\bar{\kappa}, \beta)} \|\mathcal{F}\|_2^2 = \min_{(\bar{\kappa}, \beta)} \left(\sum_i \left(\frac{\bar{\tau}_{exp,i} - f(\bar{\kappa}, \beta, U_i)}{\bar{\tau}_{exp,i}} \right)^2 \right). \quad (4.4)$$

The spectral narrow band parameters were obtained for all the fuels presented in this section, for the three aforementioned narrow band models. As a verification test, the experimental transmissivities obtained were reconstructed using the narrow band models and compared with the measured values. For each experimental condition, very good agreements were observed between the synthetic and the experimental transmissivity profiles regardless of the narrow band model. No model stands out nor performs better than the other two.

The similar accuracy of three different narrow band models is likely a result of the small number of pressure-paths used to fit the data; the fitted narrow-band parameters were obtained by fitting only three experimental pressure-paths. In previous works, the appropriate band narrow band model was selected based on the value of the model deviation from the experimental data, see Ref. [20]. This is a valid method as long as the experimental data has lower error than that associated with any narrow band models. Here, the experimental error associated with the mean absorption coefficient is 5% [9], which is higher than the difference between experimental and synthetic data for each model.

It is customary to validate the choice of the assumed narrow band model or to derive its parameters from the knowledge of the integrated band intensities, α , defined by Eq. 4.1. Experimentally, α is computed from the extrapolation technique first proposed by Wilson and Wells [27, 28] and further explained in Penner [11]. The technique is briefly recalled. A parameter B is defined as:

$$B = \frac{1}{P_i L} \int_{band} -\ln(\tau_\omega) d\omega. \quad (4.5)$$

The apparent integrated band intensity, \mathcal{A} , defined as:

$$\mathcal{A} = \int_{band} -\ln \tau_\omega d\omega \quad (4.6)$$

relates with B through the relation:

$$\mathcal{A} = P_i L B. \quad (4.7)$$

The work by Wilson and Wells [27, 28] showed that the α relates with the parameter B through:

$$\alpha = \lim_{P_i L \rightarrow 0} B \quad (4.8)$$

Hence, the experimental value for α can be obtained through extrapolation of A to the origin and measuring the slope at the origin. While a direct extrapolation is not recommended as it may be subject to significant error as mentioned by Kaplan *et al.*, [29], a extrapolation using an educated curve-of-growth procedure [29] can help alleviate this problem. The functional relation between the absorption and the pressure-path can be assumed to be a function of the unknown α and some characteristic line width. Fitting the experimental data is required to obtain the unknown parameters and it provides a more rigorous evaluation of α .

While a representative functional relation can be derived for a fundamental band, *i.e.* a band associated with only one vibration transition mode, it is more difficult to do so for bands that are the results of multiple vibration modes. This is the case for all the species presented here. Hence, no extrapolation was performed as they could lead to bias depending on the extrapolation method used. Instead, following comments presented in Modest [13], the Malkmus model was chosen as it is recognized as the best for polyatomic molecules. Verification tests for each species are presented in Section 7. Some of the data, ethane, ethylene, and propane, have been carefully examined and some species were compared with the HITRAN 2012 edition. See Lecoustre *et al.* [30] for more details.

4.3 Ethylene: C₂H₄

4.3.1 Integrated Band Intensity

Ethylene, C₂H₄, is a plane symmetrical molecule and belongs to the point group D_{2h} . It has 12 vibrational modes. In RADCAL, its IR spectrum is divided into four distinct bands that are associated with different vibrational modes, see Table 4.1. The bands from 750 - 1250 cm⁻¹ and 1300 - 1600 cm⁻¹ are associated with the bending motion of the CH₂ groups. The band between 1750 and 2075 cm⁻¹ is associated with the stretching motion of the carbon double bond, C=C. The fourth band from 2800 - 3400 cm⁻¹ is associated with the stretching of the CH groups. The strongest absorption band is located at lower wavenumbers, between 780 and 1250 cm⁻¹. This indicates the propensity of ethylene to strong participation to the radiative heat exchange corresponding to low to moderate temperatures. This spectral range corresponds to the highest blackbody spectral emittance at temperatures ranging between 400 to 700 K which are characteristic of cooler regions of the fuel rich cores for liquid and solid fires. Band 1 is the strongest absorbing band. All

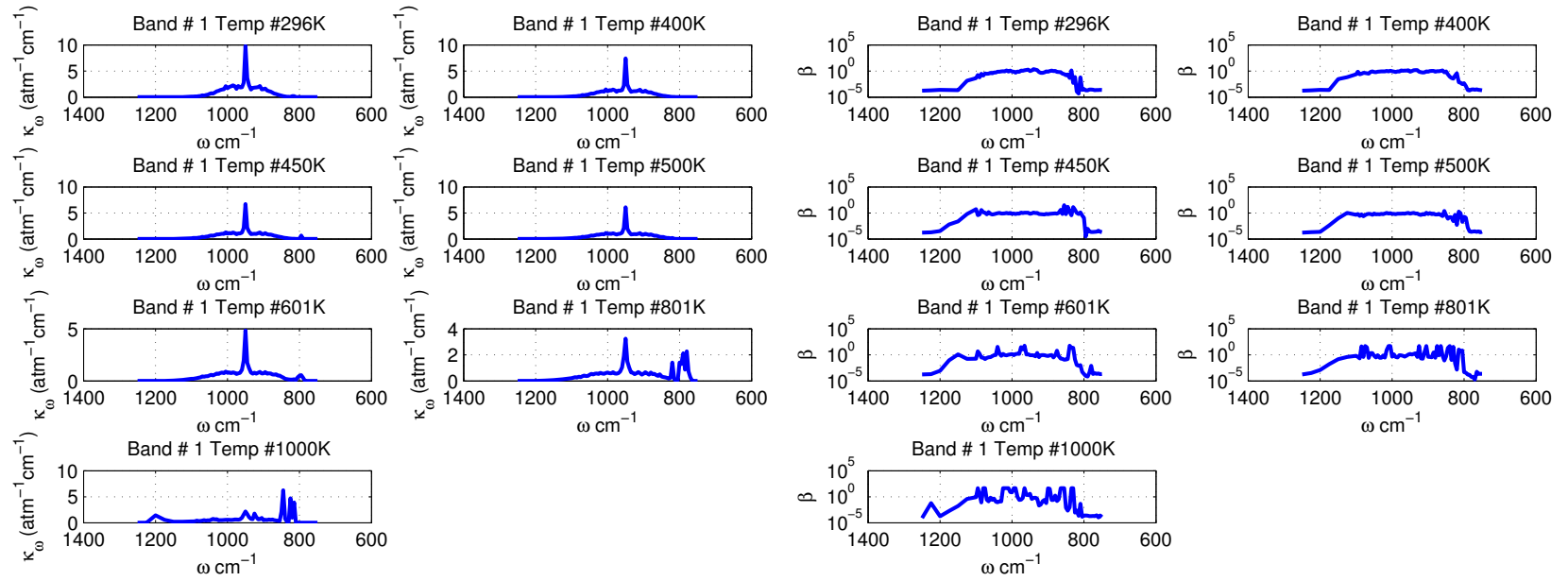
Table 4.1: Spectral bands of C₂H₄ included in RADCAL.

Band #	Bounds (cm ⁻¹)	Assignment	$\alpha(T = 296 \text{ K}) (\text{atm}^{-1}\text{cm}^{-2})$
1	750	1250	CH ₂ Bend
2	1300	1600	CH ₂ Bend
3	1750	2075	C = C Stretch
4	2800	3400	C – H Stretch

the ethylene IR spectral absorption data were obtained from high resolution FTIR experiments with temperatures varying from 296 K to 1000 K. See Wakatsuki [25] for more details about the experimental process followed to obtain the experimental data.

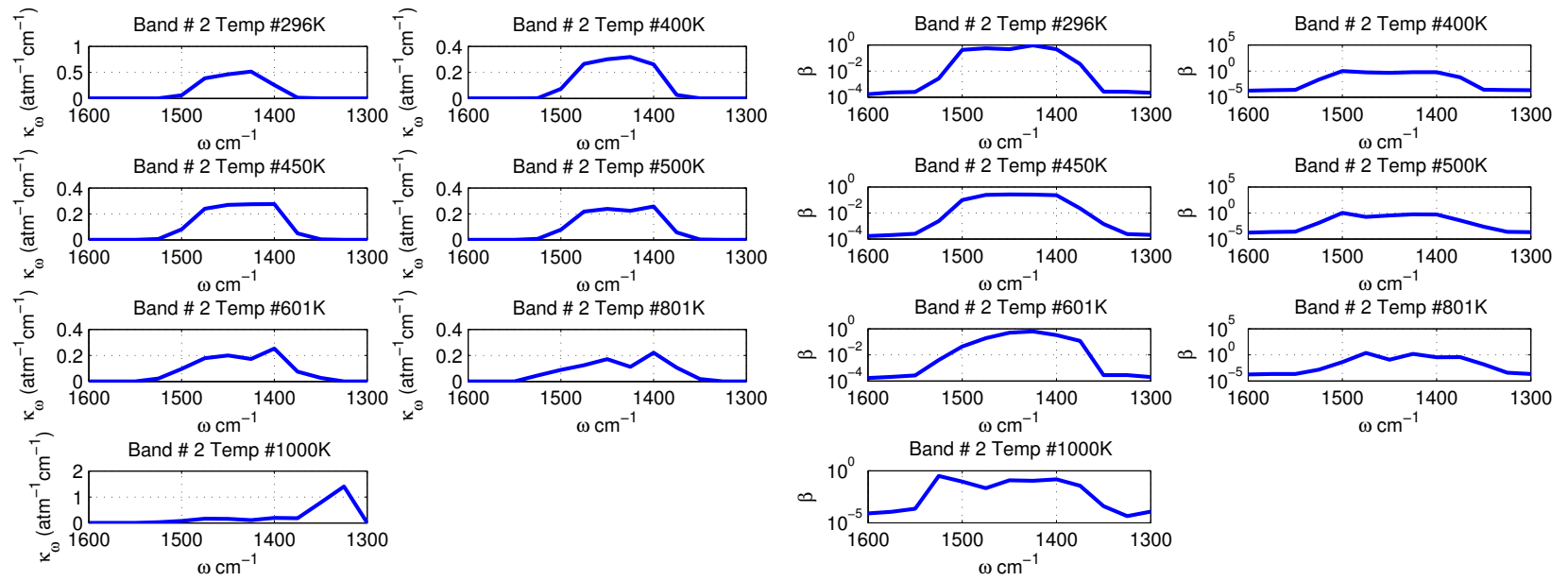
4.3.2 Malkmus Narrow Band Parameters

The spectral absorption coefficients were obtained by least square fitting of the experimental transmissivity using the Malkmus model. The ethylene narrow band parameters, $\bar{\kappa}$ and β , for temperatures ranging from 296 K to 1000 K are plotted in Figures 4.1–4.4 for Bands 1 to 4.



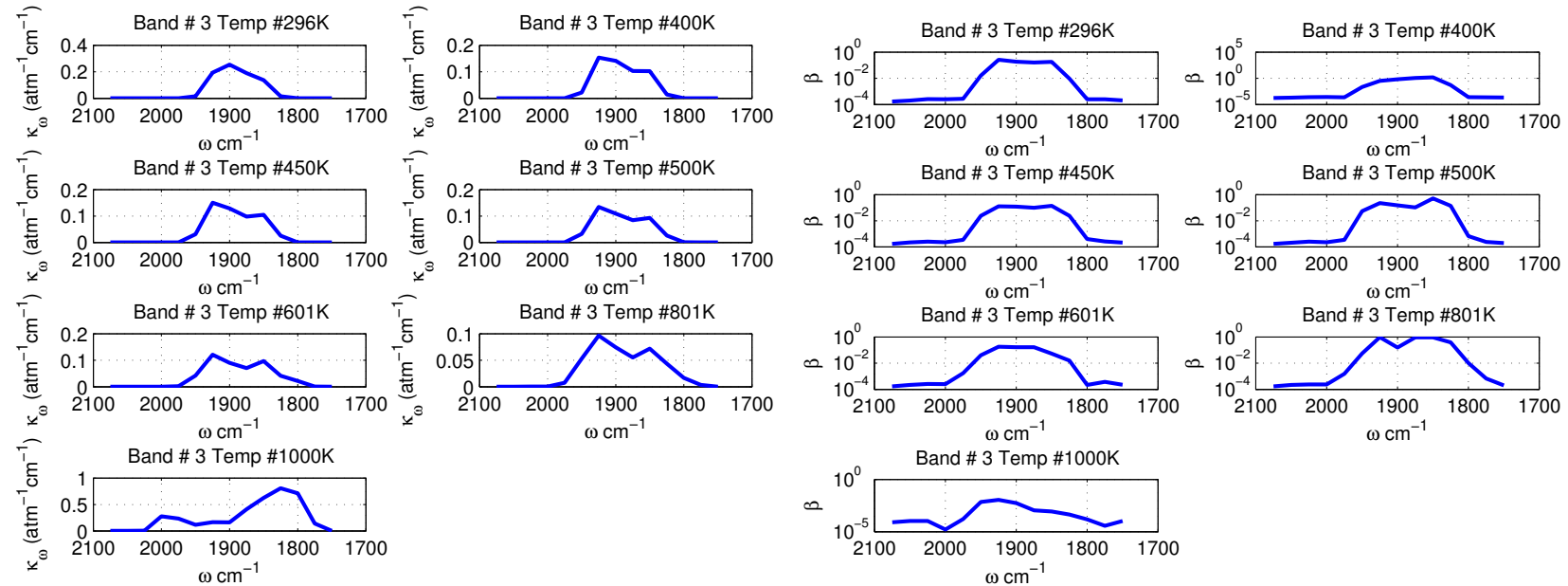
(a) Narrow band spectral absorption coefficient $\bar{\kappa}$ (in $\text{atm}^{-1}\text{cm}^{-1}$) for the 750–1250 cm^{-1} band.
(b) Narrow band spectral fine structure parameter β (in atm^{-1}) for the 750–1250 cm^{-1} band.

Figure 4.1: Ethylene narrow band parameters $\bar{\kappa}$ and β obtained for the 750–1250 cm^{-1} band corresponding to the bending motion of the CH_2 chemical group. Temperatures plotted are: 296, 400, 450, 500, 601, 801, and 1000 K. The narrow band resolution $\Delta\omega$ is 5 cm^{-1} .



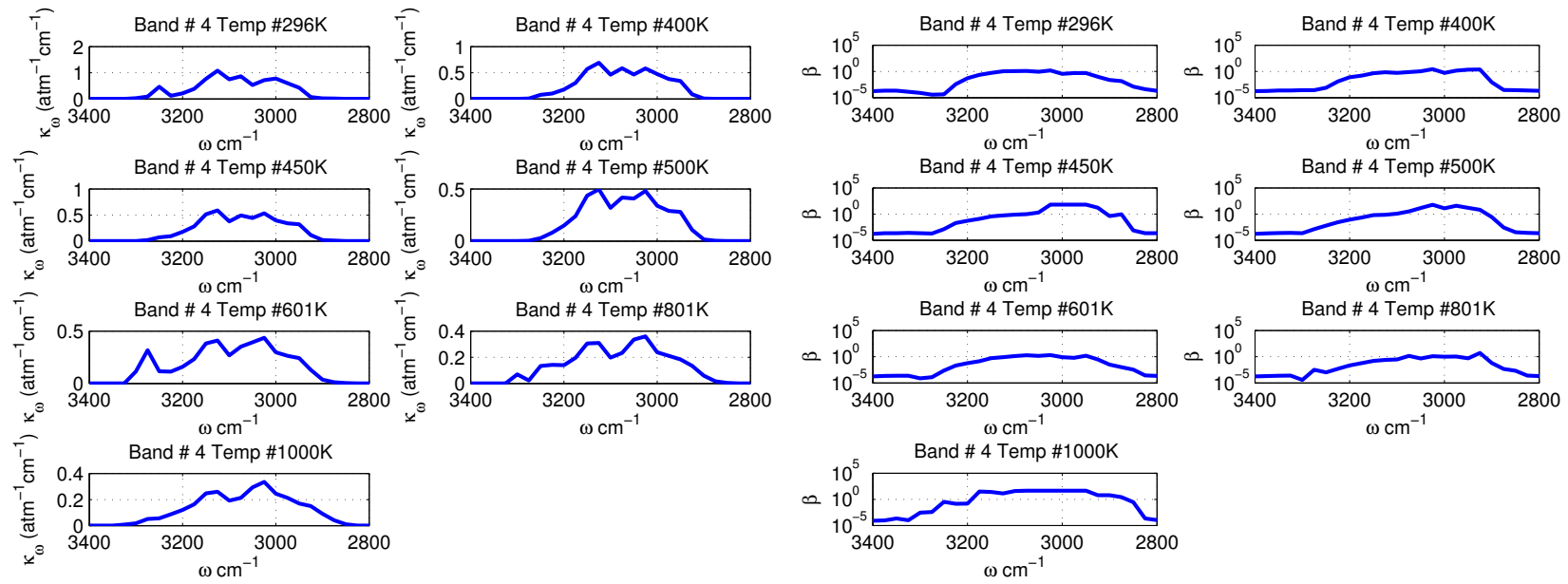
(a) Narrow band spectral absorption coefficient $\bar{\kappa}$ (in $\text{atm}^{-1}\text{cm}^{-1}$) for the 1300–1600 cm^{-1} band.
(b) Narrow band spectral fine structure parameter β (in atm^{-1}) for the 1300–1600 cm^{-1} band.

Figure 4.2: Ethylene narrow band parameters $\bar{\kappa}$ and β obtained for the 1300–1600 cm^{-1} band corresponding to the bending motion of the CH_2 chemical group. Temperatures plotted are: 296, 400, 450, 500, 601, 801, and 1000 K. The narrow band resolution $\Delta\omega$ is 25 cm^{-1} .



(a) Narrow band spectral absorption coefficient $\bar{\kappa}$ (in $\text{atm}^{-1}\text{cm}^{-1}$) for the 1750–2075 cm^{-1} band.
(b) Narrow band spectral fine structure parameter β (in atm^{-1}) for the 1750–2075 cm^{-1} band.

Figure 4.3: Ethylene narrow band parameters $\bar{\kappa}$ and β obtained for the 1750–2075 cm^{-1} band corresponding to the stretching motion of the C = C chemical group. Temperatures plotted are: 296, 400, 450, 500, 601, 801, and 1000 K. The narrow band resolution $\Delta\omega$ is 25 cm^{-1} .



(a) Narrow band spectral absorption coefficient $\bar{\kappa}$ (in $\text{atm}^{-1}\text{cm}^{-1}$) for the 2800–3400 cm^{-1} band.
(b) Narrow band spectral fine structure parameter β (in atm^{-1}) for the 2800–3400 cm^{-1} band.

Figure 4.4: Ethylene narrow band parameters $\bar{\kappa}$ and β obtained for the 2800–3400 cm^{-1} band corresponding to the stretching motion of the C – H chemical group. Temperatures plotted are: 296, 400, 450, 500, 601, 801, and 1000 K. The narrow band resolution $\Delta\omega$ is 25 cm^{-1} .

4.3.3 Verification SNB Parameters

To assess the accuracy of the narrow band parameters $\bar{\kappa}$ and β , synthetic transmissivities were constructed for the same experimental conditions as the FTIR data and compare with it. This subsection plots the comparison and the relative error in transmissivity (relative to FTIR measurements) using the ethylene parameters presented in Figs. 4.1 to 4.4.

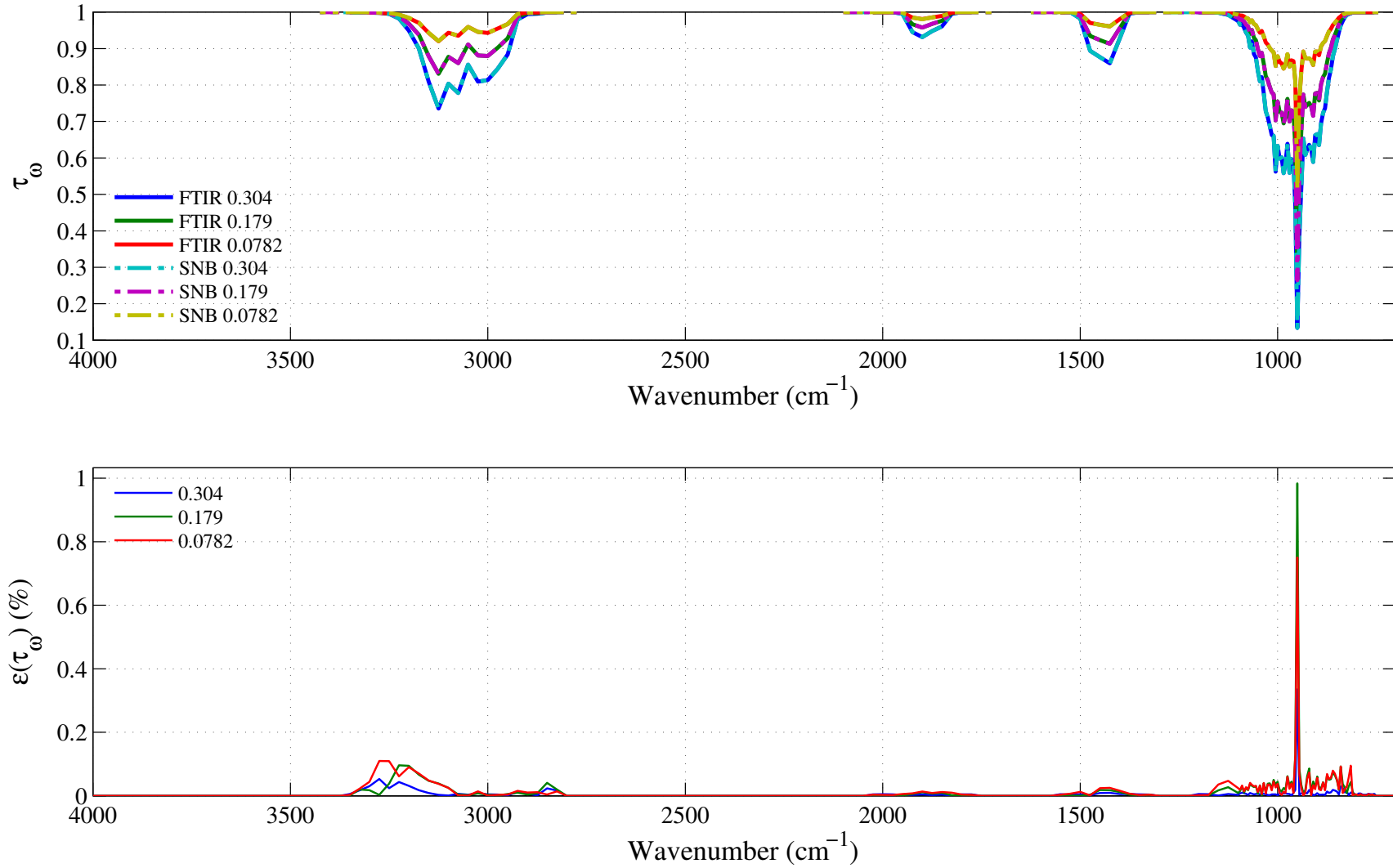


Figure 4.5: Top: comparison between the experimental (FTIR, in solid lines) and the synthetic (dashed lines) spectral transmissivity profiles, denoted τ_ω , of an isothermal homogeneous column of ethylene. The synthetic profiles were generated using the Malkmus narrow band parameters presented in Figs. 4.1 to 4.4. Bottom: relative transmissivity error, denoted $\varepsilon(\tau_\omega)$, between the experiment and the synthetic profiles presented on the top figure. Three different pressure-paths are considered: 0.304, 0.179 and 0.0782 atm.cm. The gas temperature is set at 296 K and the total pressure is 101 kPa. Note: the experimental data resolution has been changed to match that of the narrow band model.

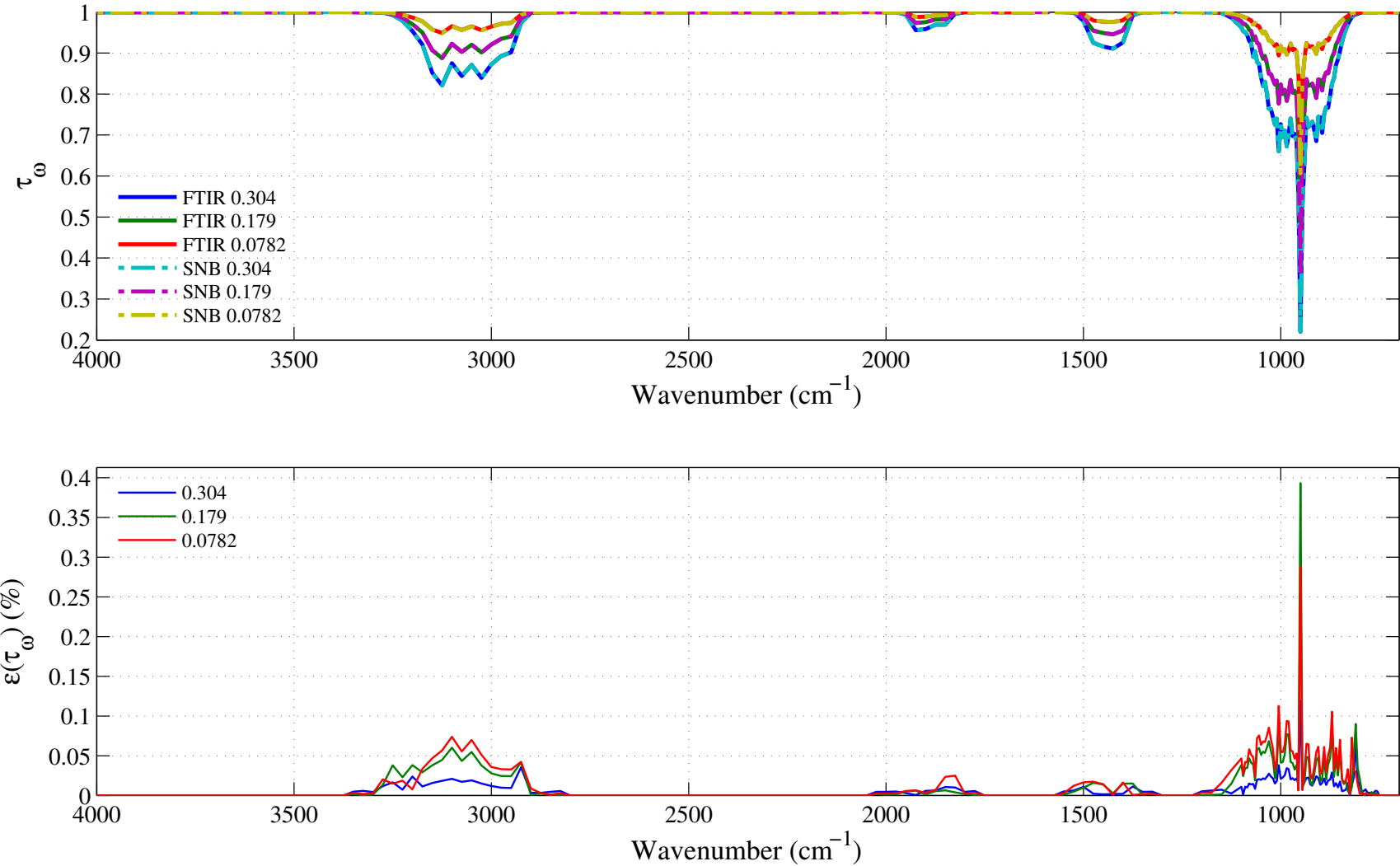


Figure 4.6: Top: comparison between the experimental (FTIR, in solid lines) and the synthetic (dashed lines) spectral transmissivity profiles, denoted τ_ω , of an isothermal homogeneous column of ethylene. The synthetic profiles was generated using the Malkmus narrow band parameters presented in Figs. 4.1 to 4.4. Bottom: relative transmissivity error, denoted $\varepsilon(\tau_\omega)$, between the experiment and the synthetic profiles presented on the top figure. Three different pressure-paths are considered: 0.304, 0.179 and 0.0782 atm.cm. The gas temperature is set at 400 K and the total pressure is 101 kPa. Note: the experimental data resolution has been changed to match that of the narrow band model.

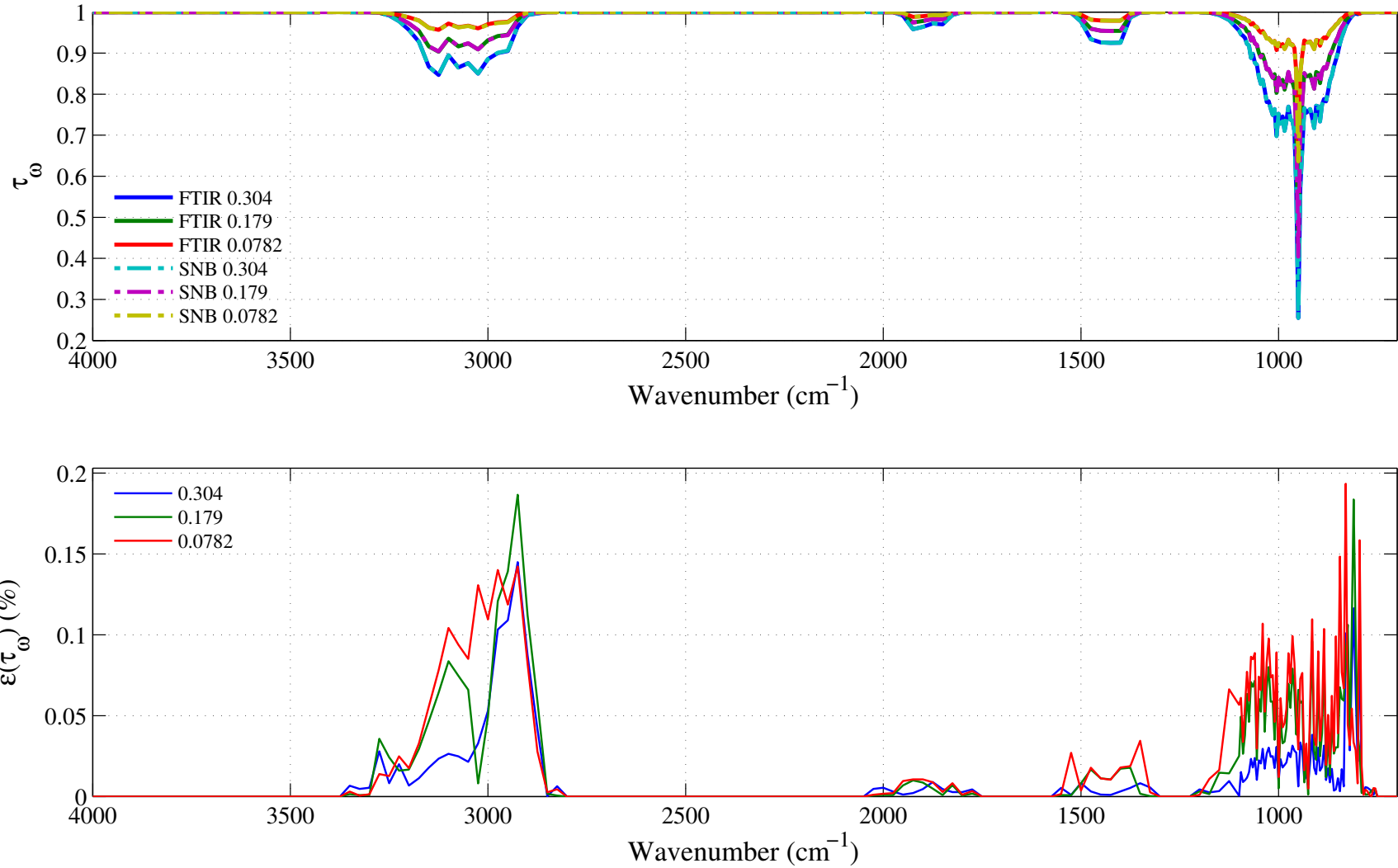


Figure 4.7: Top: comparison between the experimental (FTIR, in solid lines) and the synthetic (dashed lines) spectral transmissivity profiles, denoted τ_ω , of an isothermal homogeneous column of ethylene. The synthetic profiles was generated using the Malkmus narrow band parameters presented in Figs. 4.1 to 4.4. Bottom: relative transmissivity error, denoted $\varepsilon(\tau_\omega)$, between the experiment and the synthetic profiles presented on the top figure. Three different pressure-paths are considered: 0.304, 0.179 and 0.0782 atm.cm. The gas temperature is set at 450 K and the total pressure is 101 kPa. Note: the experimental data resolution has been changed to match that of the narrow band model.

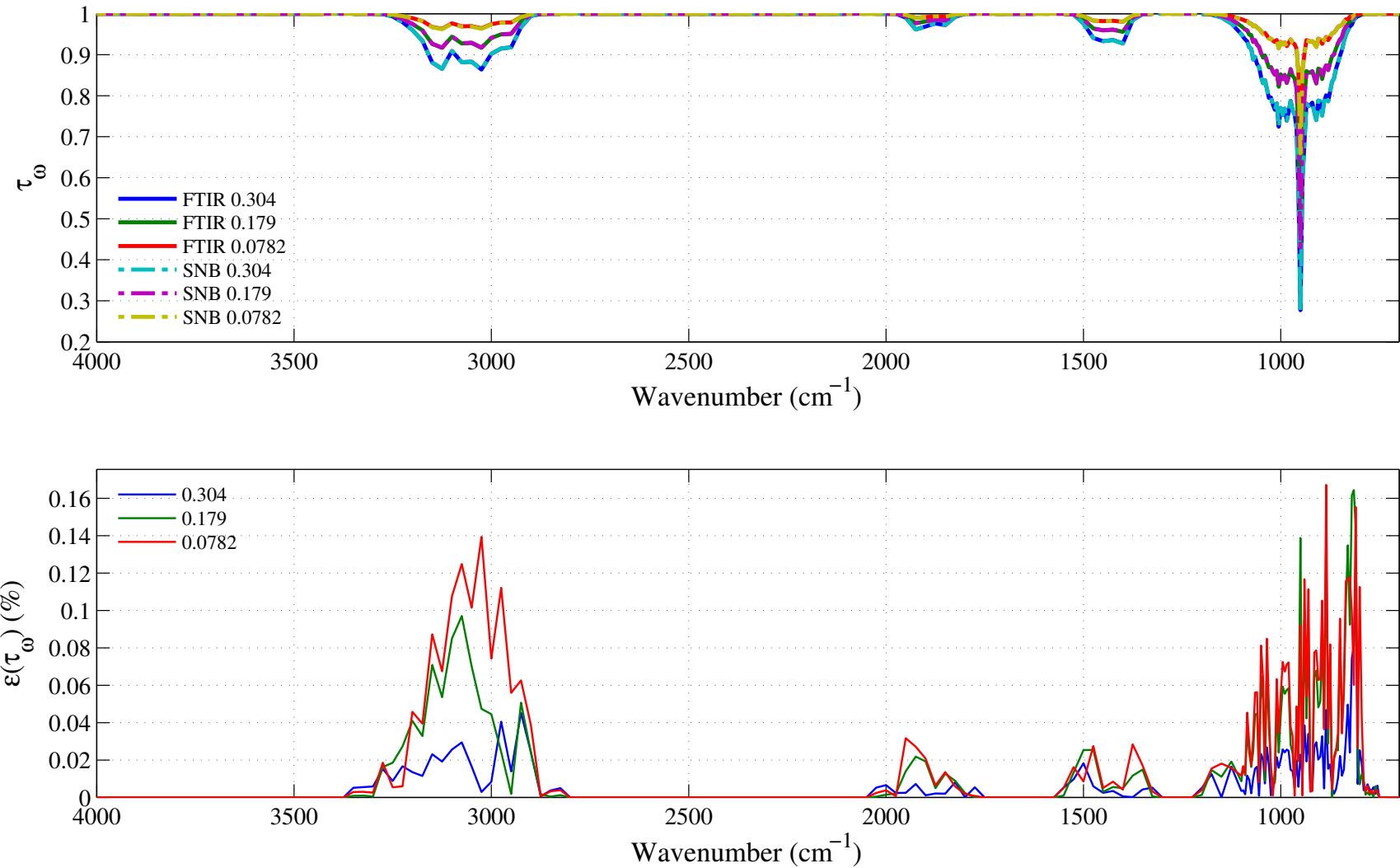


Figure 4.8: Top: comparison between the experimental (FTIR, in solid lines) and the synthetic (dashed lines) spectral transmissivity profiles, denoted τ_ω , of an isothermal homogeneous column of ethylene. The synthetic profiles was generated using the Malkmus narrow band parameters presented in Figs. 4.1 to 4.4. Bottom: relative transmissivity error, denoted $\varepsilon(\tau_\omega)$, between the experiment and the synthetic profiles presented on the top figure. Three different pressure-paths are considered: 0.304, 0.179 and 0.0782 atm.cm. The gas temperature is set at 500 K and the total pressure is 101 kPa. Note: the experimental data resolution has been changed to match that of the narrow band model.

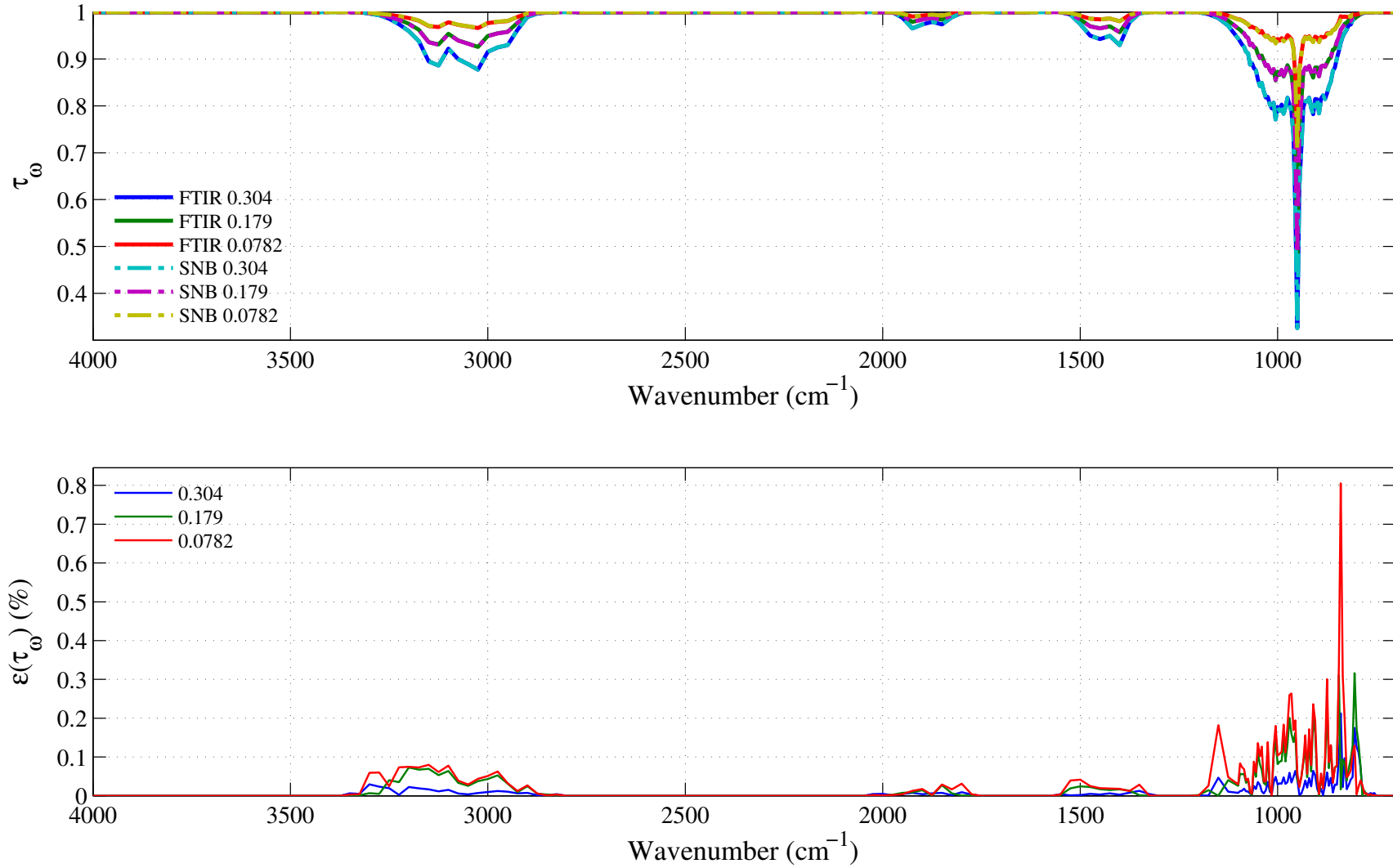


Figure 4.9: Top: comparison between the experimental (FTIR, in solid lines) and the synthetic (dashed lines) spectral transmissivity profiles, denoted τ_ω , of an isothermal homogeneous column of ethylene. The synthetic profiles were generated using the Malkmus narrow band parameters presented in Figs. 4.1 to 4.4. Bottom: relative transmissivity error, denoted $\varepsilon(\tau_\omega)$, between the experiment and the synthetic profiles presented on the top figure. Three different pressure-paths are considered: 0.304, 0.179 and 0.0782 atm.cm. The gas temperature is set at 601 K and the total pressure is 101 kPa. Note: the experimental data resolution has been changed to match that of the narrow band model.

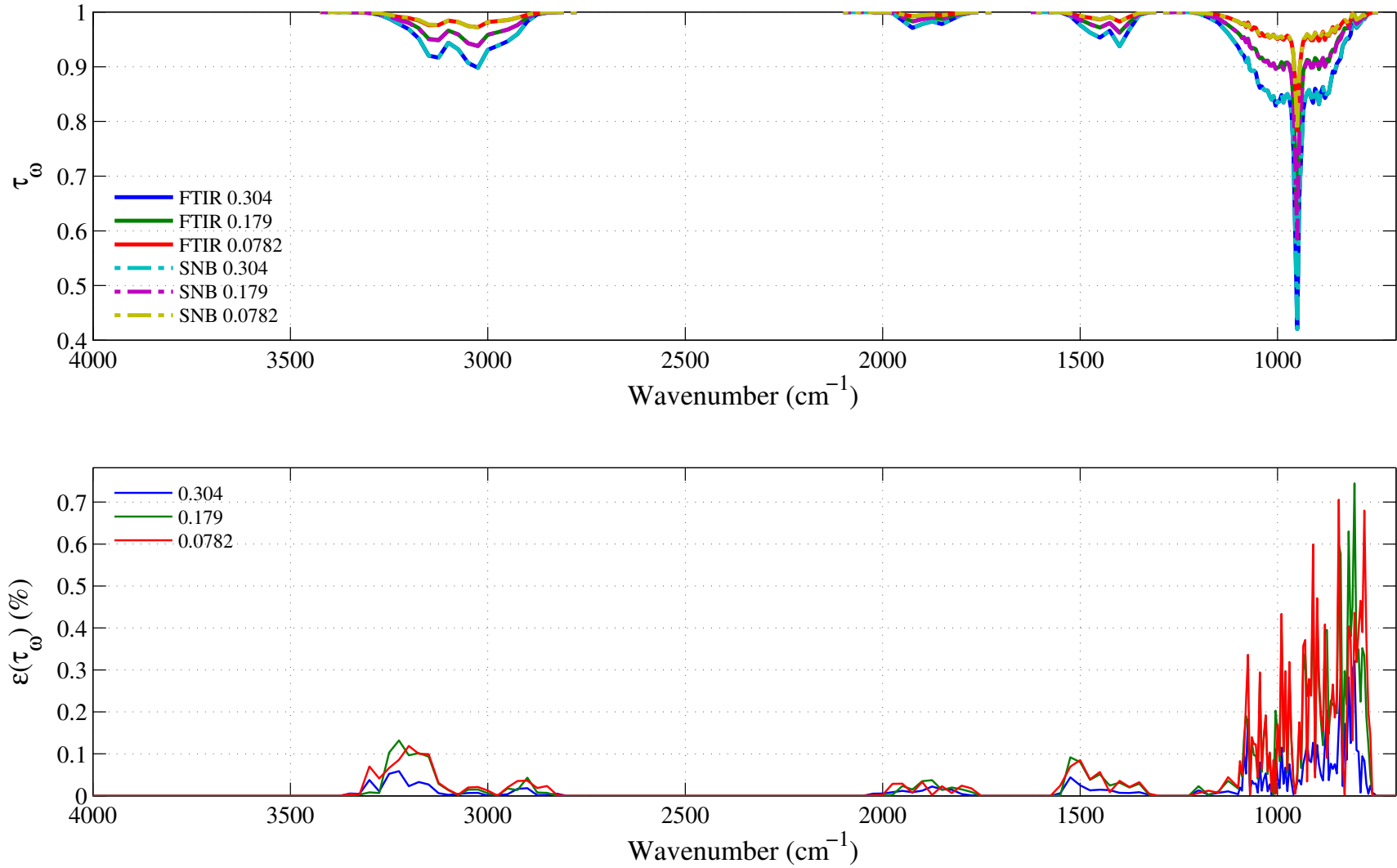


Figure 4.10: Top: comparison between the experimental (FTIR, in solid lines) and the synthetic (dashed lines) spectral transmissivity profiles, denoted τ_{ω} , of an isothermal homogeneous column of ethylene. The synthetic profiles were generated using the Malkmus narrow band parameters presented in Figs. 4.1 to 4.4. Bottom: relative transmissivity error, denoted $\varepsilon(\tau_{\omega})$, between the experiment and the synthetic profiles presented on the top figure. Three different pressure-paths are considered: 0.304, 0.179 and 0.0782 atm.cm. The gas temperature is set at 801 K and the total pressure is 101 kPa. Note: the experimental data resolution has been changed to match that of the narrow band model.

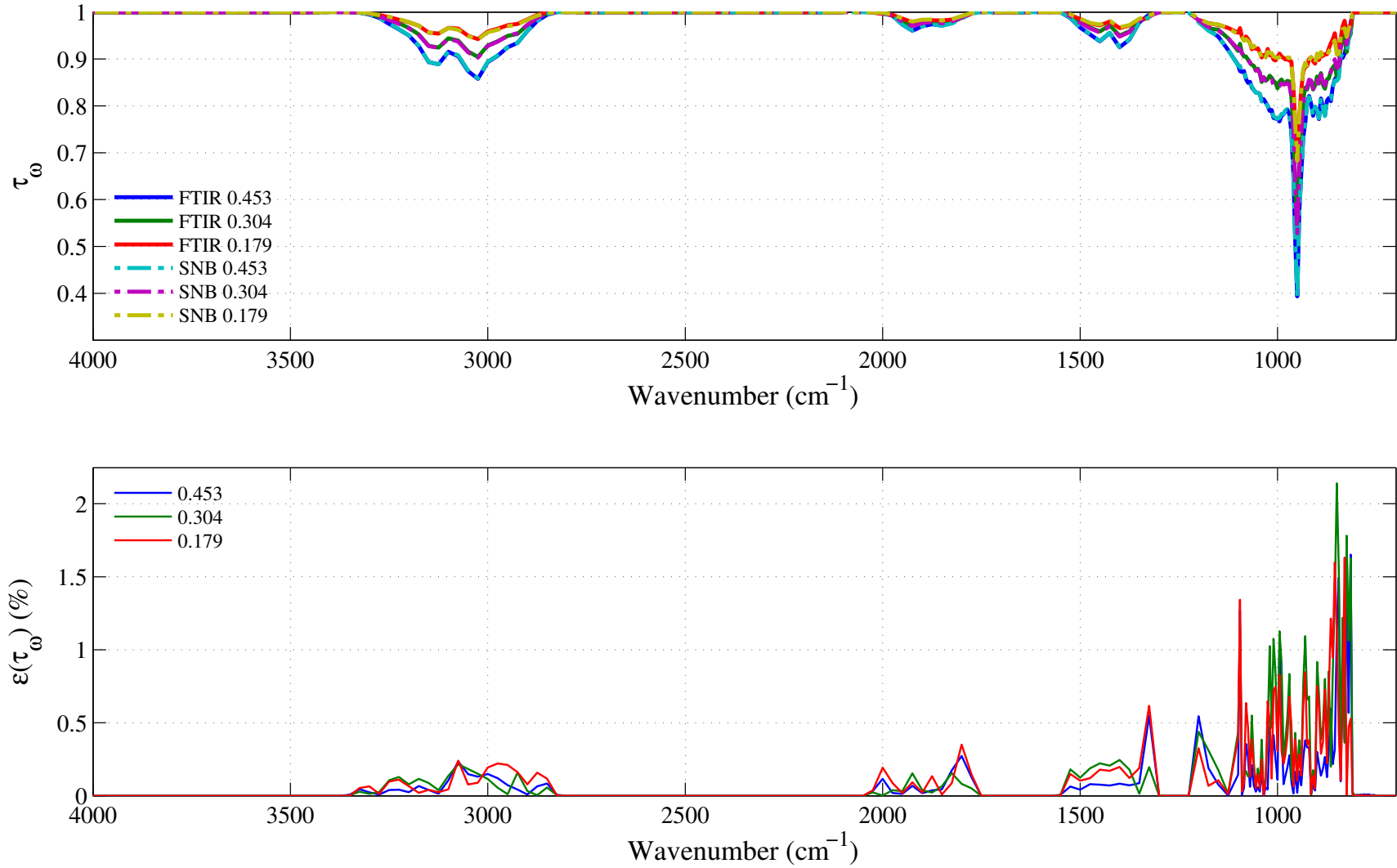


Figure 4.11: Top: comparison between the experimental (FTIR, in solid lines) and the synthetic (dashed lines) spectral transmissivity profiles, denoted τ_ω , of an isothermal homogeneous column of ethylene. The synthetic profiles were generated using the Malkmus narrow band parameters presented in Figs. 4.1 to 4.4. Bottom: relative transmissivity error, denoted $\varepsilon(\tau_\omega)$, between the experiment and the synthetic profiles presented on the top figure. Three different pressure-paths are considered: 0.304, 0.179 and 0.0782 atm.cm. The gas temperature is set at 1000 K and the total pressure is 101 kPa. Note: the experimental data resolution has been changed to match that of the narrow band model.

4.4 Ethane: C₂H₆

4.4.1 Integrated Band Intensity

Ethane, C₂H₆, has a three-fold axis of symmetry and belongs to the point group D_{3d} , [18]. Being a non-linear molecule, it has 18 vibrational modes, but due to its symmetry, some modes are identical, and the number of distinct vibrational modes is reduced to 12. In RADCAL, its spectra are defined by 3 distinct bands associated with different vibrational modes, see Table 4.2. The band from 730–1095 cm⁻¹ is associated with the rocking motion of the CH₃ groups, the band from 1250–1700 cm⁻¹ is associated with the bending motion of the CH groups, and the main band between 2550–3375 cm⁻¹ is associated with the stretching of the CH groups.

The CH stretching band located from 2550–3375 cm⁻¹ has the lowest transmissivity, *i.e.* highest absorption, and dominates absorption due to ethane for blackbody emissions at typical combustion temperatures between 1300 K and 1800 K, characteristic of sooting flames. At standard temperature and pressure, its integrated band intensity is more than 10 times the value of Band 2, and more than 20 times the value of Band 1.

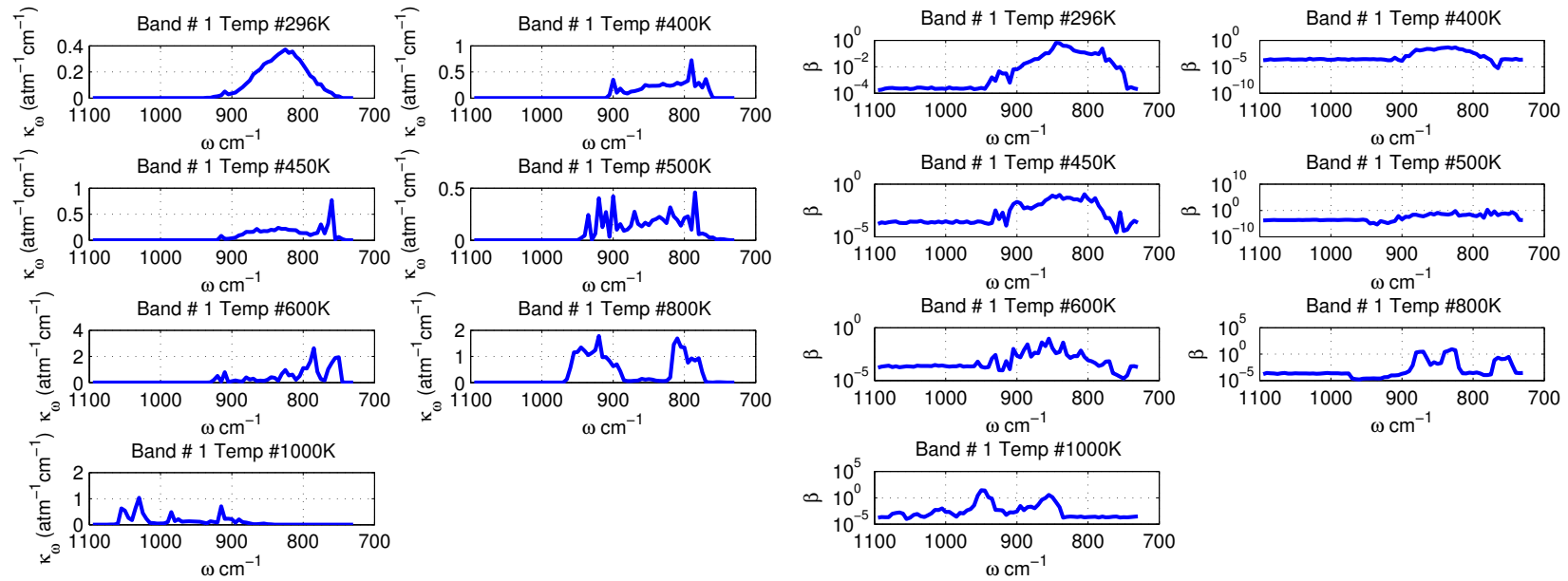
Table 4.2: Spectral bands of C₂H₆ included in RADCAL.

Band #	Bounds (cm ⁻¹)		Assignment	$\alpha(T = 296 \text{ K}) (\text{atm}^{-1}\text{cm}^{-2})$
1	730	1095	CH ₃ Rock	30
2	1250	1700	CH Bend	64
3	2550	3375	CH Stretch	774

4.4.2 Malkmus Narrow Band Parameters

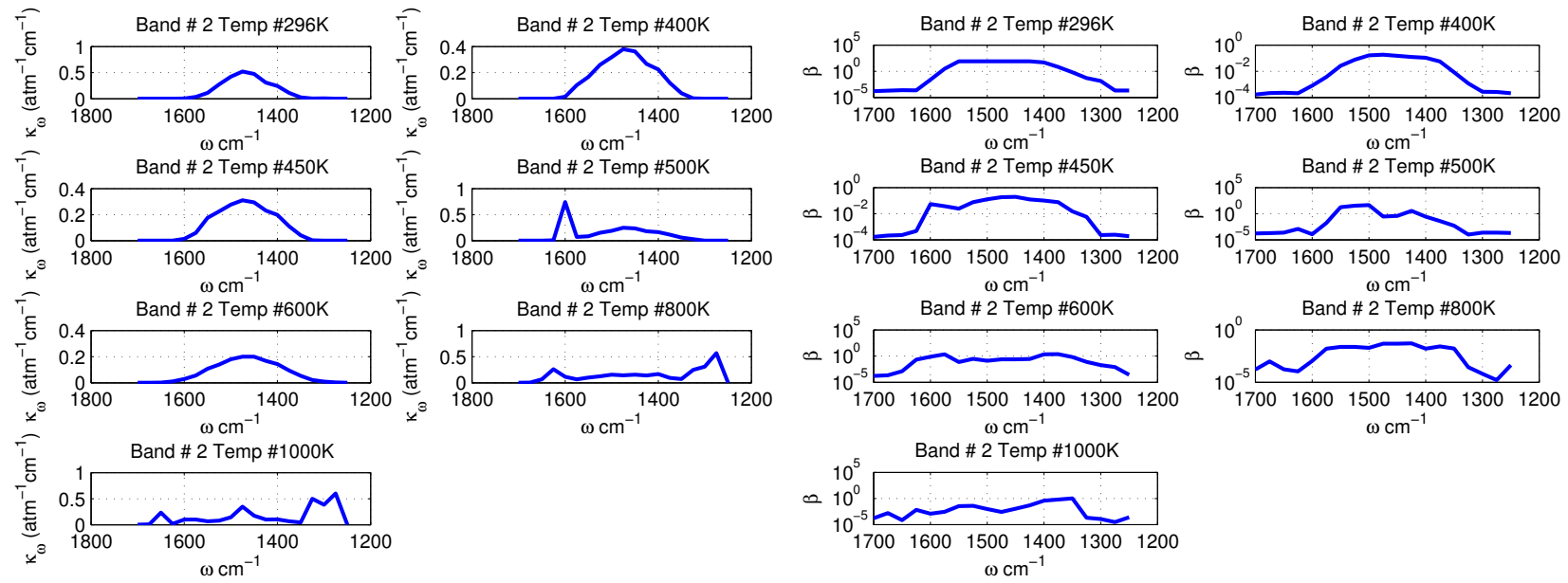
All the ethane IR spectral absorption data were obtained from high resolution FTIR experiments with temperatures varying from 296 K to 1000 K. The spectral absorption coefficients were obtained by fitting the experimental spectral transmissivity of a homogeneous column of isothermal ethane with a total pressure of 1 atm using the Malkmus model.

The ethane narrow band parameters, $\bar{\kappa}$ and β , for temperatures ranging from 296 K to 1000 K are plotted in Figures 4.12–4.14 for Bands 1 to 3.



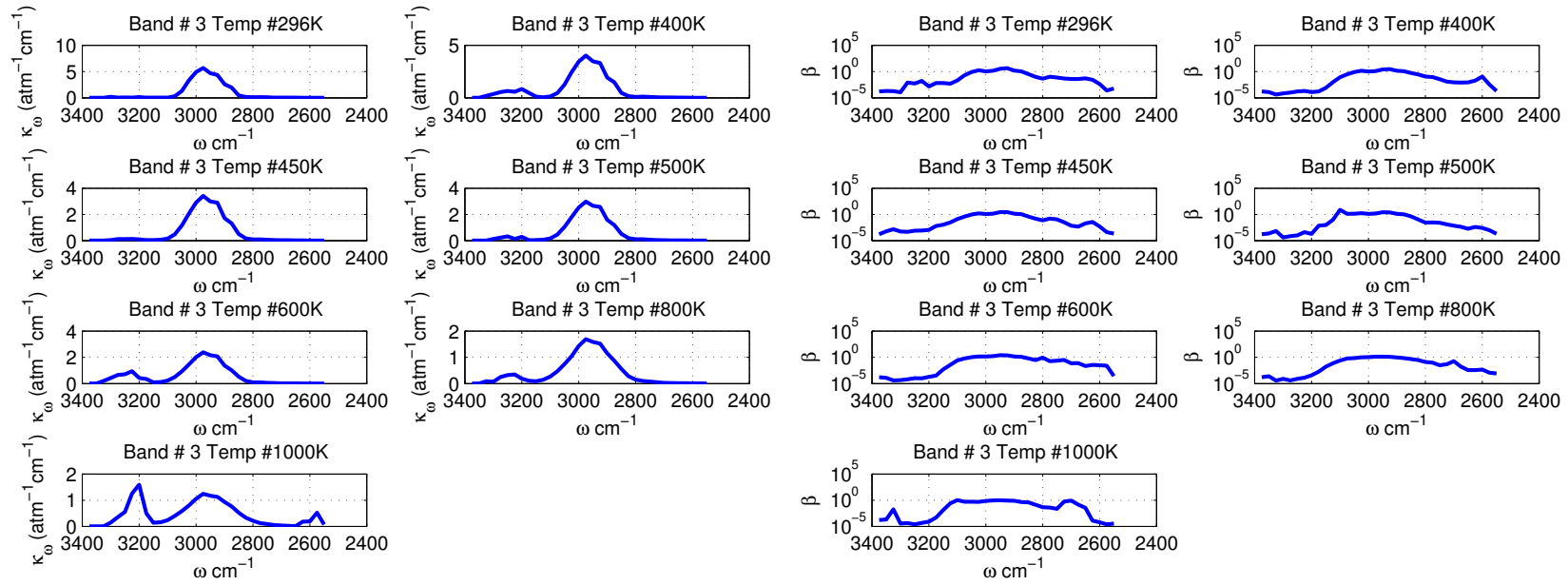
(a) Narrow band spectral absorption coefficient $\bar{\kappa}$ (in $\text{atm}^{-1}\text{cm}^{-1}$) for the 730–1095 cm^{-1} band.
(b) Narrow band spectral fine structure parameter β (in atm^{-1}) for the 730–1095 cm^{-1} band.

Figure 4.12: Ethane narrow band parameters $\bar{\kappa}$ and β obtained for the 730–1095 cm^{-1} band corresponding to the rocking motion of the CH_3 chemical group. Temperatures plotted are: 296, 400, 450, 500, 600, 800, and 1000 K. The narrow band resolution $\Delta\omega$ is 5 cm^{-1} .



(a) Narrow band spectral absorption coefficient $\bar{\kappa}$ (in $\text{atm}^{-1}\text{cm}^{-1}$) for the 1250–1700 cm^{-1} band.
(b) Narrow band spectral fine structure parameter β (in atm^{-1}) for the 1250–1700 cm^{-1} band.

Figure 4.13: Ethane narrow band parameters $\bar{\kappa}$ and β obtained for the 1250–1700 cm^{-1} band corresponding to the bending motion of the CH chemical group. Temperatures plotted are: 296, 400, 450, 500, 600, 800, and 1000 K. The narrow band resolution $\Delta\omega$ is 25 cm^{-1} .



(a) Narrow band spectral absorption coefficient $\bar{\kappa}$ (in atm⁻¹cm⁻¹) for the 2550–3375 cm⁻¹ band.
(b) Narrow band spectral fine structure parameter β (in atm⁻¹) for the 2550–3375 cm⁻¹ band.

Figure 4.14: Ethane narrow band parameters $\bar{\kappa}$ and β obtained for the 2550–3375 cm⁻¹ band corresponding to the stretching motion of the C – H chemical group. Temperatures plotted are: 296, 400, 450, 500, 600, 800, and 1000 K. The narrow band resolution $\Delta\omega$ is 25 cm⁻¹.

4.4.3 Verification SNB Parameters

To assess the accuracy of the narrow band parameters $\bar{\kappa}$ and β , synthetic transmissivities were constructed for the same experimental conditions as the FTIR data and compare with it. This subsection plots the comparison and the relative error in transmissivity (relative to FTIR measurements) using the ethane parameters presented in Figs. 4.12 to 4.14.

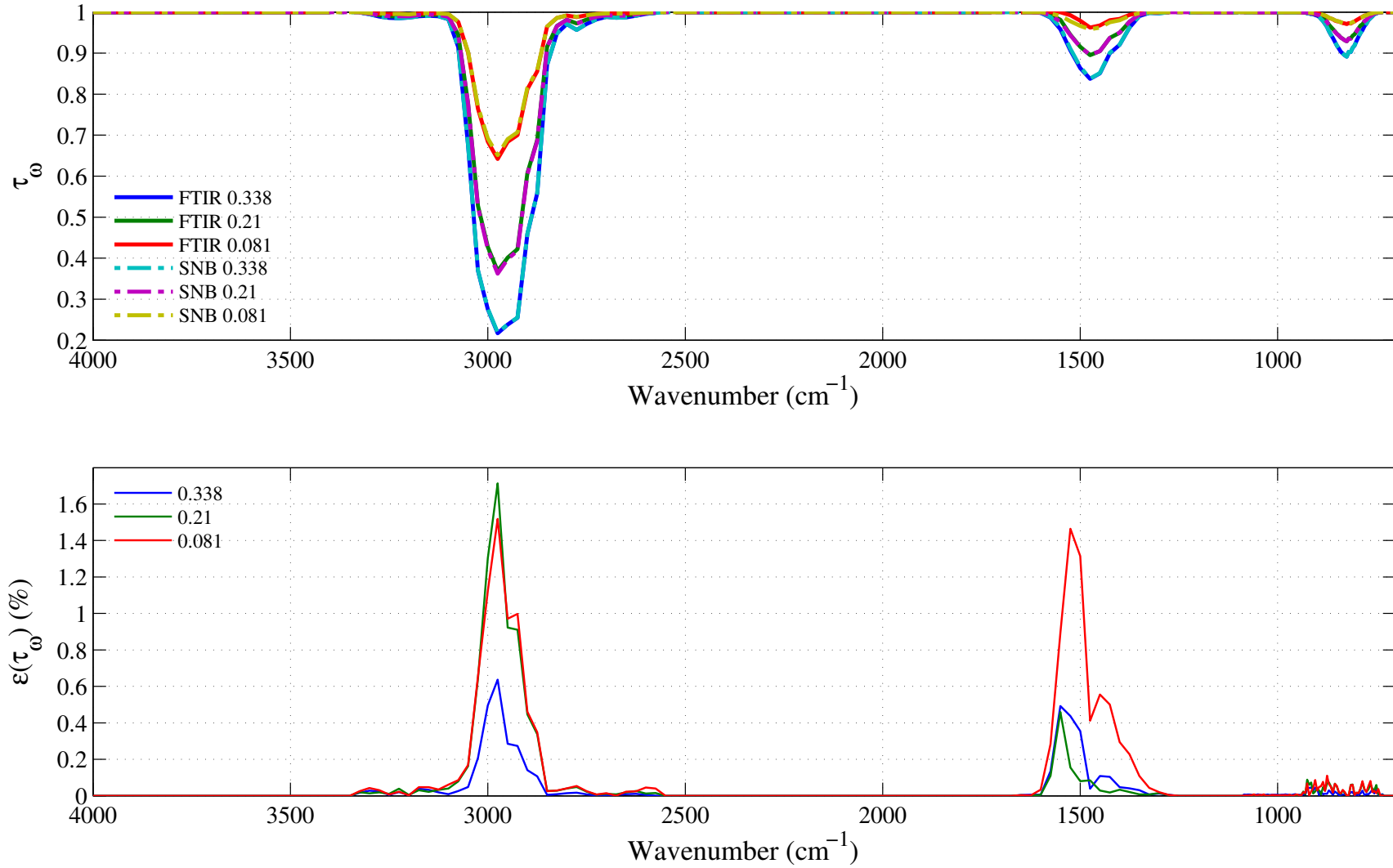


Figure 4.15: Top: comparison between the experimental (FTIR, in solid lines) and the synthetic (dashed lines) spectral transmissivity profiles, denoted τ_{ω} , of an isothermal homogeneous column of ethane. The synthetic profiles were generated using the Malkmus narrow band parameters presented in Figs. 4.12 to 4.14. Bottom: relative transmissivity error, denoted $\varepsilon(\tau_{\omega})$, between the experiment and the synthetic profiles presented on the top figure. Three different pressure-paths are considered: 0.338, 0.21 and 0.081 atm.cm. The gas temperature is set at 296 K and the total pressure is 101 kPa. Note: the experimental data resolution has been changed to match that of the narrow band model.

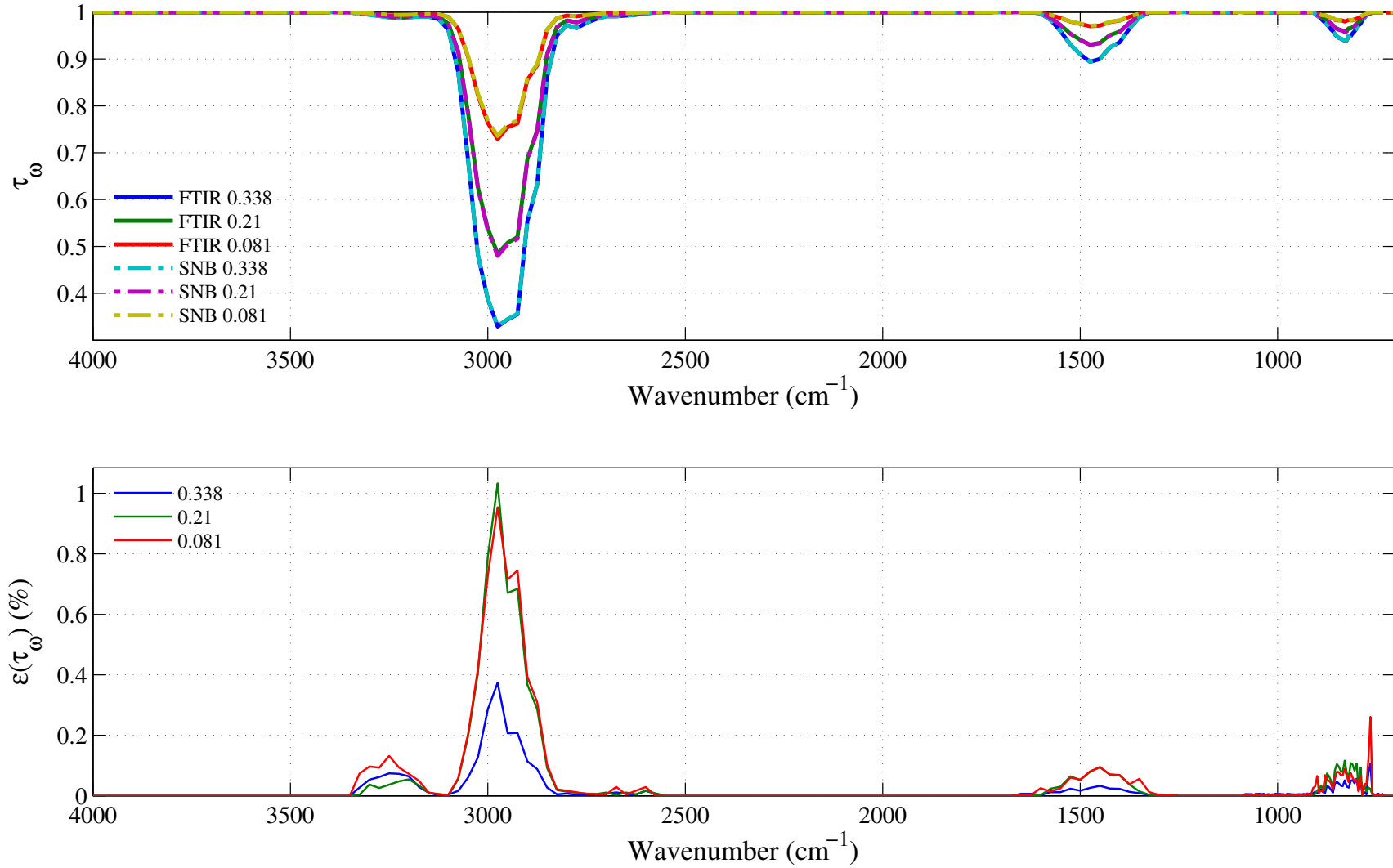


Figure 4.16: Top: comparison between the experimental (FTIR, in solid lines) and the synthetic (dashed lines) spectral transmissivity profiles, denoted τ_ω , of an isothermal homogeneous column of ethane. The synthetic profiles were generated using the Malkmus narrow band parameters presented in Figs. 4.12 to 4.14. Bottom: relative transmissivity error, denoted $\varepsilon(\tau_\omega)$, between the experiment and the synthetic profiles presented on the top figure. Three different pressure-paths are considered: 0.338, 0.21 and 0.081 atm.cm . The gas temperature is set at 400 K and the total pressure is 101 kPa. Note: the experimental data resolution has been changed to match that of the narrow band model.

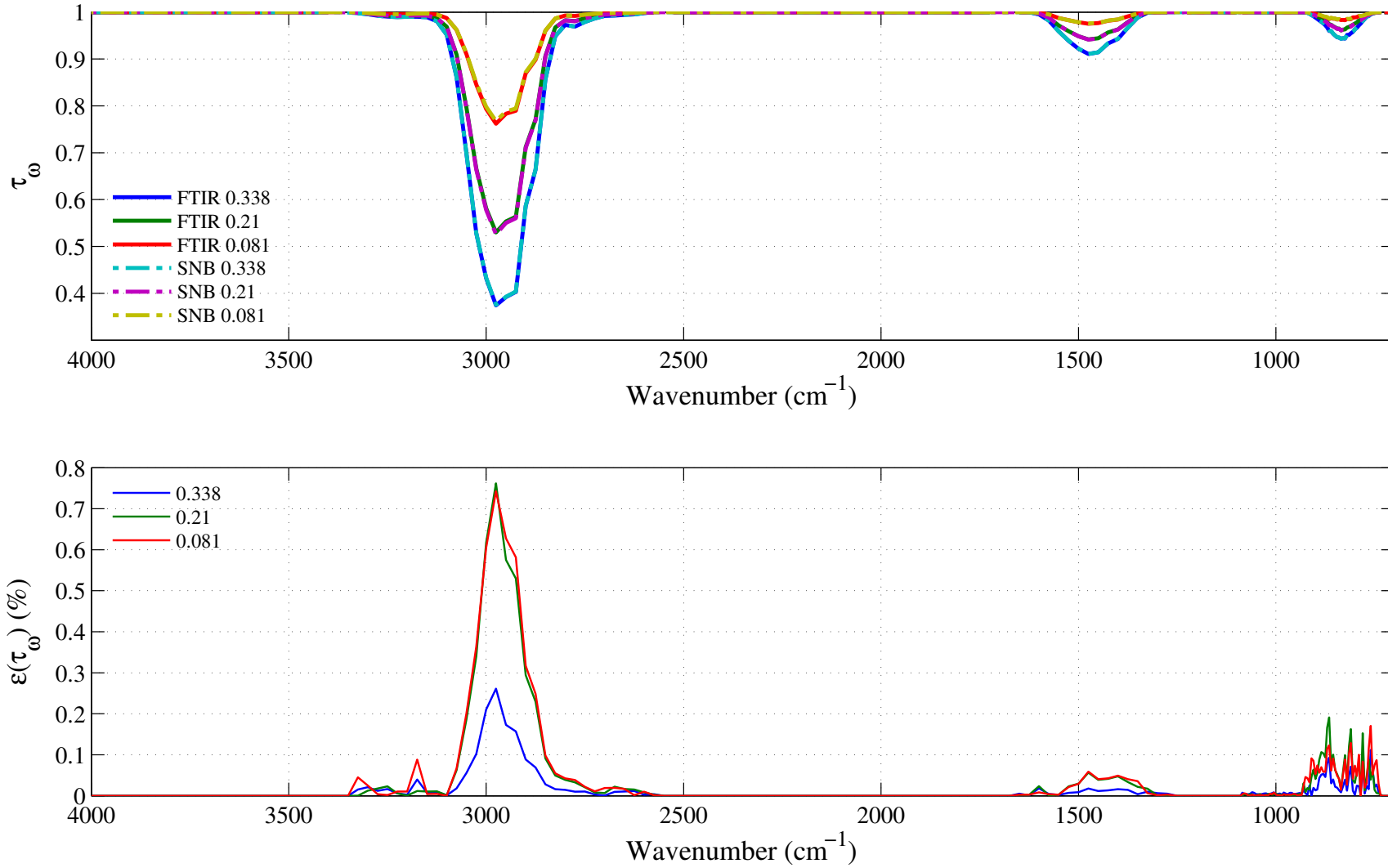


Figure 4.17: Top: comparison between the experimental (FTIR, in solid lines) and the synthetic (dashed lines) spectral transmissivity profiles, denoted τ_ω , of an isothermal homogeneous column of ethane. The synthetic profiles was generated using the Malkmus narrow band parameters presented in Figs. 4.12 to 4.14. Bottom: relative transmissivity error, denoted $\varepsilon(\tau_\omega)$, between the experiment and the synthetic profiles presented on the top figure. Three different pressure-paths are considered: 0.338, 0.21 and 0.081 atm.cm. The gas temperature is set at 450 K and the total pressure is 101 kPa. Note: the experimental data resolution has been changed to match that of the narrow band model.

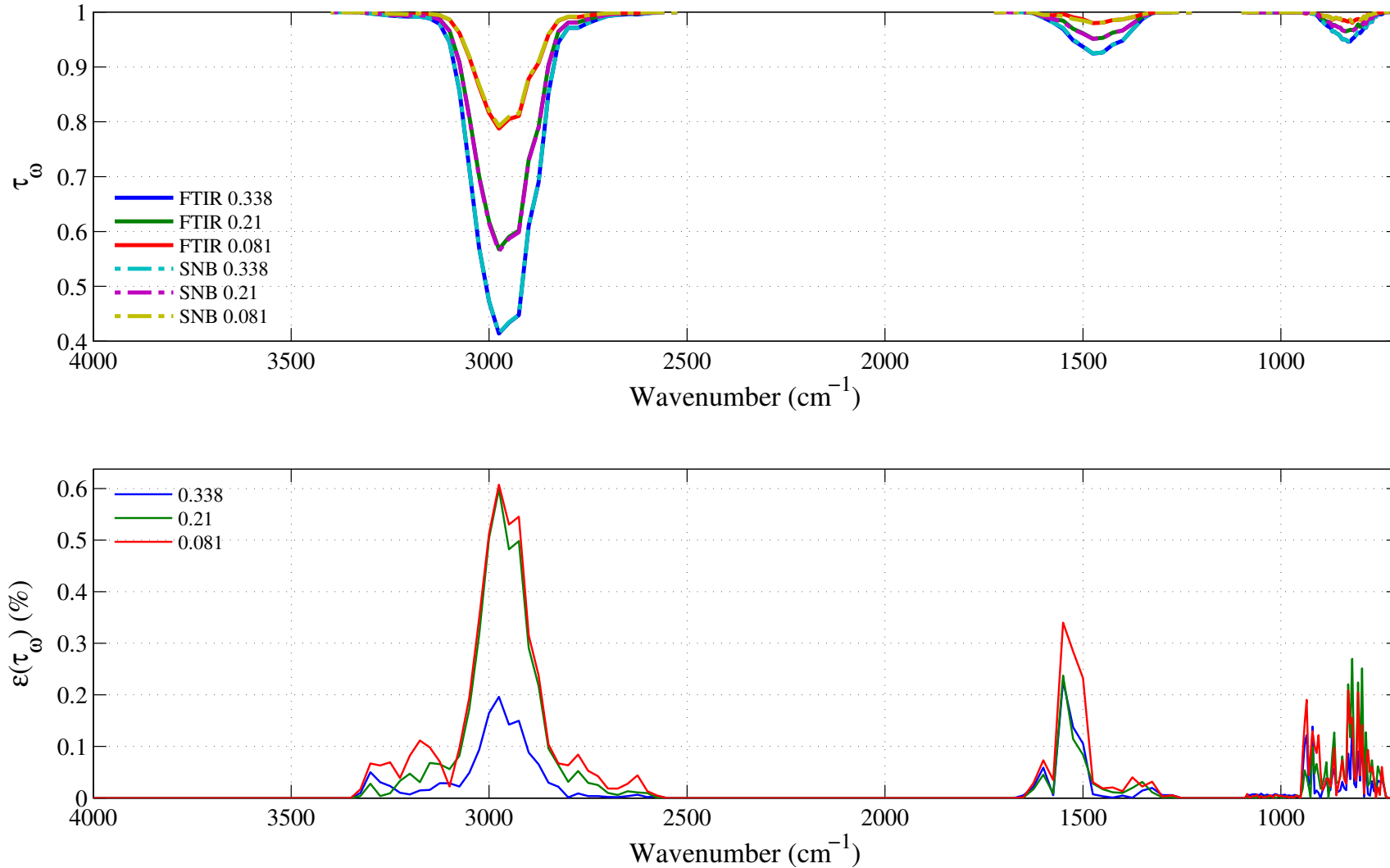


Figure 4.18: Top: comparison between the experimental (FTIR, in solid lines) and the synthetic (dashed lines) spectral transmissivity profiles, denoted τ_{ω} , of an isothermal homogeneous column of ethane. The synthetic profiles was generated using the Malkmus narrow band parameters presented in Figs. 4.12 to 4.14. Bottom: relative transmissivity error, denoted $\varepsilon(\tau_{\omega})$, between the experiment and the synthetic profiles presented on the top figure. Three different pressure-paths are considered: 0.338, 0.21 and 0.081 atm.cm. The gas temperature is set at 500 K and the total pressure is 101 kPa. Note: the experimental data resolution has been changed to match that of the narrow band model.

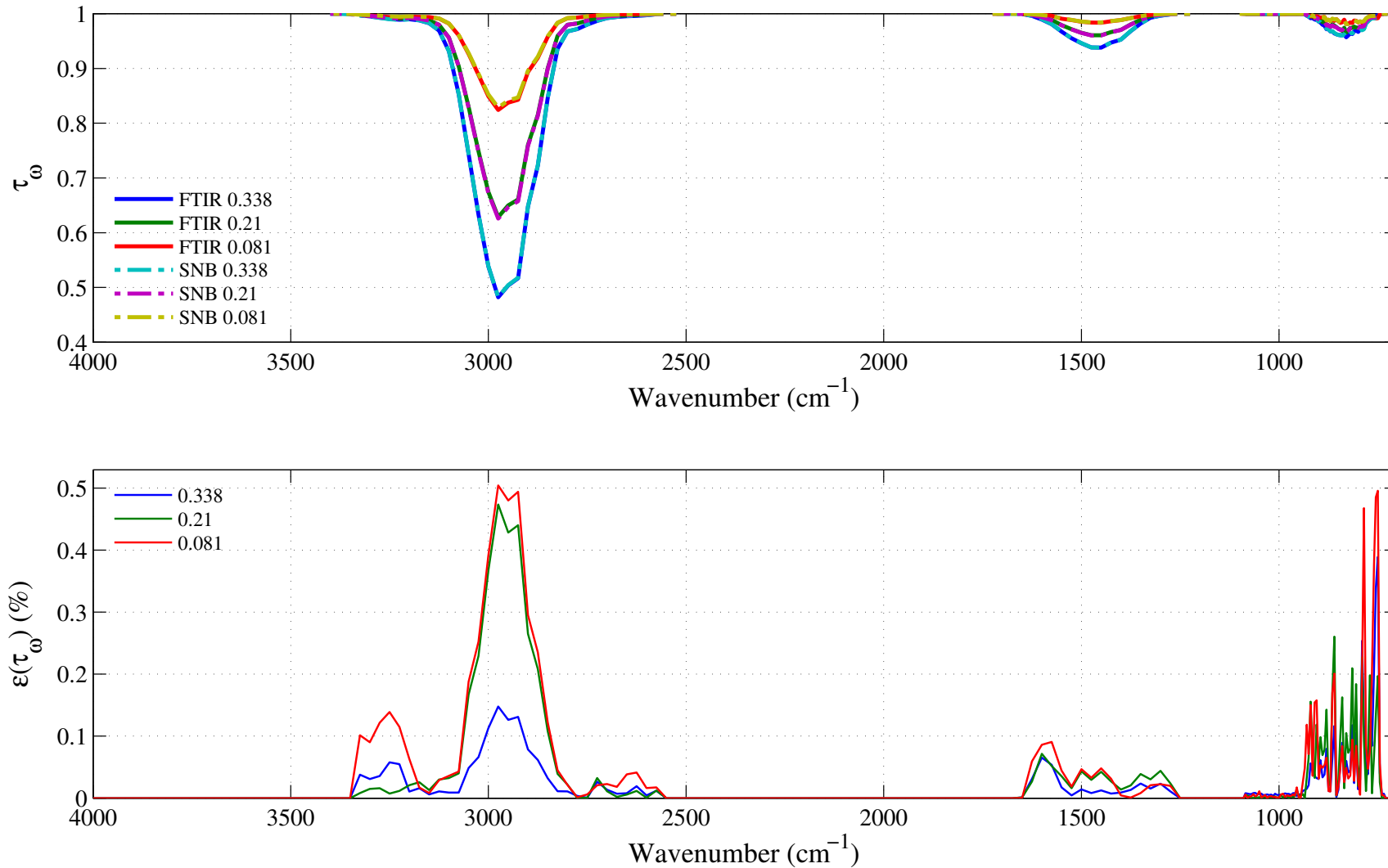


Figure 4.19: Top: comparison between the experimental (FTIR, in solid lines) and the synthetic (dashed lines) spectral transmissivity profiles, denoted τ_{ω} , of an isothermal homogeneous column of ethane. The synthetic profiles were generated using the Malkmus narrow band parameters presented in Figs. 4.12 to 4.14. Bottom: relative transmissivity error, denoted $\varepsilon(\tau_{\omega})$, between the experiment and the synthetic profiles presented on the top figure. Three different pressure-paths are considered: 0.338, 0.21 and 0.081 atm.cm. The gas temperature is set at 600 K and the total pressure is 101 kPa. Note: the experimental data resolution has been changed to match that of the narrow band model.

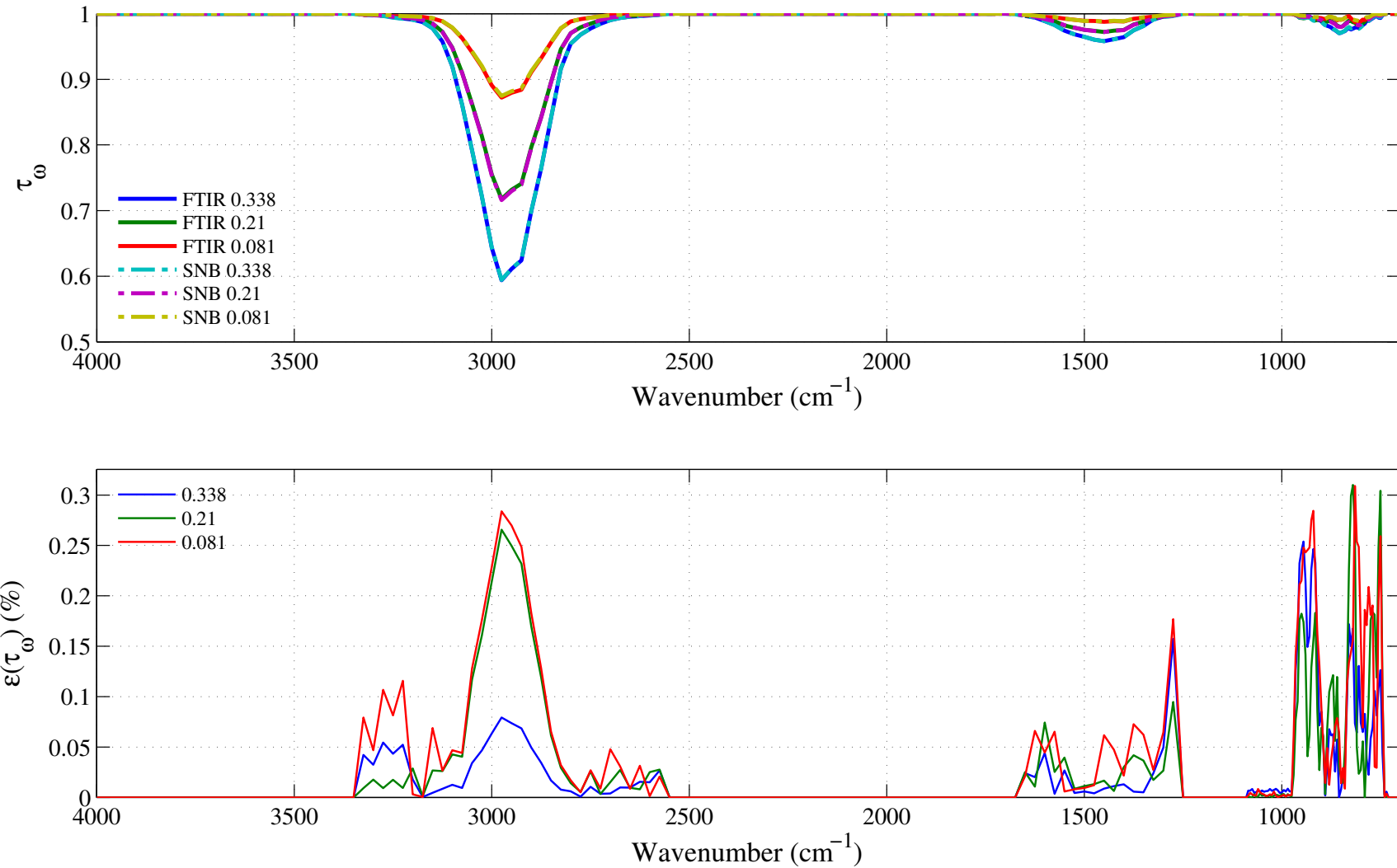


Figure 4.20: Top: comparison between the experimental (FTIR, in solid lines) and the synthetic (dashed lines) spectral transmissivity profiles, denoted τ_ω , of an isothermal homogeneous column of ethane. The synthetic profiles were generated using the Malkmus narrow band parameters presented in Figs. 4.12 to 4.14. Bottom: relative transmissivity error, denoted $\varepsilon(\tau_\omega)$, between the experiment and the synthetic profiles presented on the top figure. Three different pressure-paths are considered: 0.338, 0.21 and 0.081 atm.cm. The gas temperature is set at 800 K and the total pressure is 101 kPa. Note: the experimental data resolution has been changed to match that of the narrow band model.

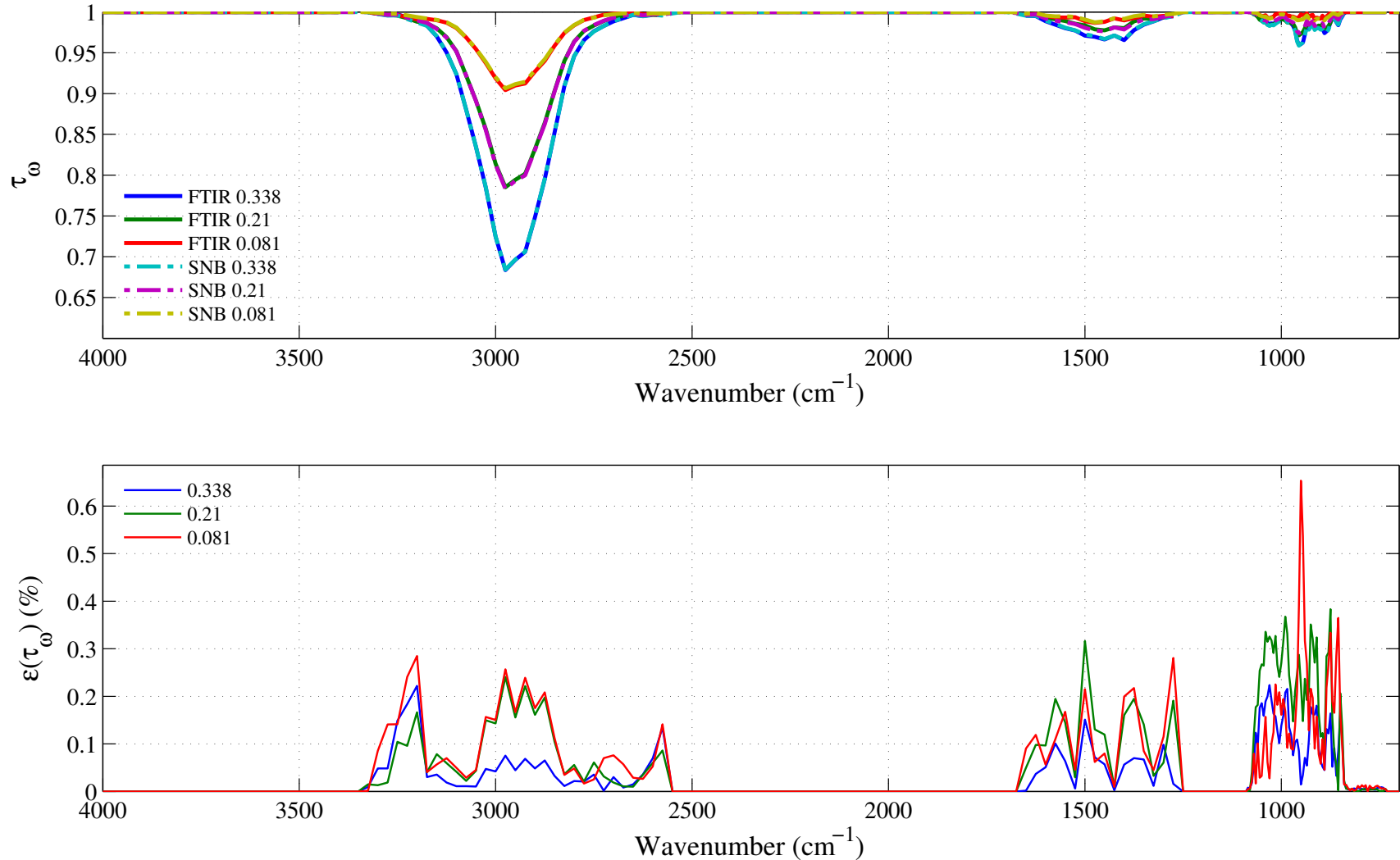


Figure 4.21: Top: comparison between the experimental (FTIR, in solid lines) and the synthetic (dashed lines) spectral transmissivity profiles, denoted τ_ω , of an isothermal homogeneous column of ethane. The synthetic profiles were generated using the Malkmus narrow band parameters presented in Figs. 4.12 to 4.14. Bottom: relative transmissivity error, denoted $\varepsilon(\tau_\omega)$, between the experiment and the synthetic profiles presented on the top figure. Three different pressure-paths are considered: 0.338, 0.21 and 0.081 atm.cm. The gas temperature is set at 1000 K and the total pressure is 101 kPa. Note: the experimental data resolution has been changed to match that of the narrow band model.

4.5 Propylene: C₃H₆

4.5.1 Integrated Band Intensity

Propylene, C₃H₆, has only one plane of symmetry and belongs to the point group C_s , [18]. It has 21 vibrational modes. In RADCAL, its spectrum is divided into three distinct bands, associated with different vibrational modes, see Table 4.3. The first band from 775–1150 cm⁻¹ is associated with the stretching motion of the carbon simple bond C–C, the rocking motion of the CH₃ group, and the out-of-plane bending motion of the =CH₂ group. The second band from 1225–1975 cm⁻¹ is derived from the stretching motion of the carbon double bond C=C and the bending motion of the CH group. Finally, the third band from 2650–3275 cm⁻¹ is due to the stretching motion of the CH and =CH₂ groups.

The strongest absorption bands for propylene are the 775–1150 cm⁻¹ (Band 1) and the 2650–3275 cm⁻¹ bands (Band 3). The 775–1150 cm⁻¹ band corresponds to radiation absorption and emission at near ambient temperature. The 2650–3275 cm⁻¹ band gives propylene strong absorption of radiation emitted by blackbody at high temperatures characteristic of sooting flames.

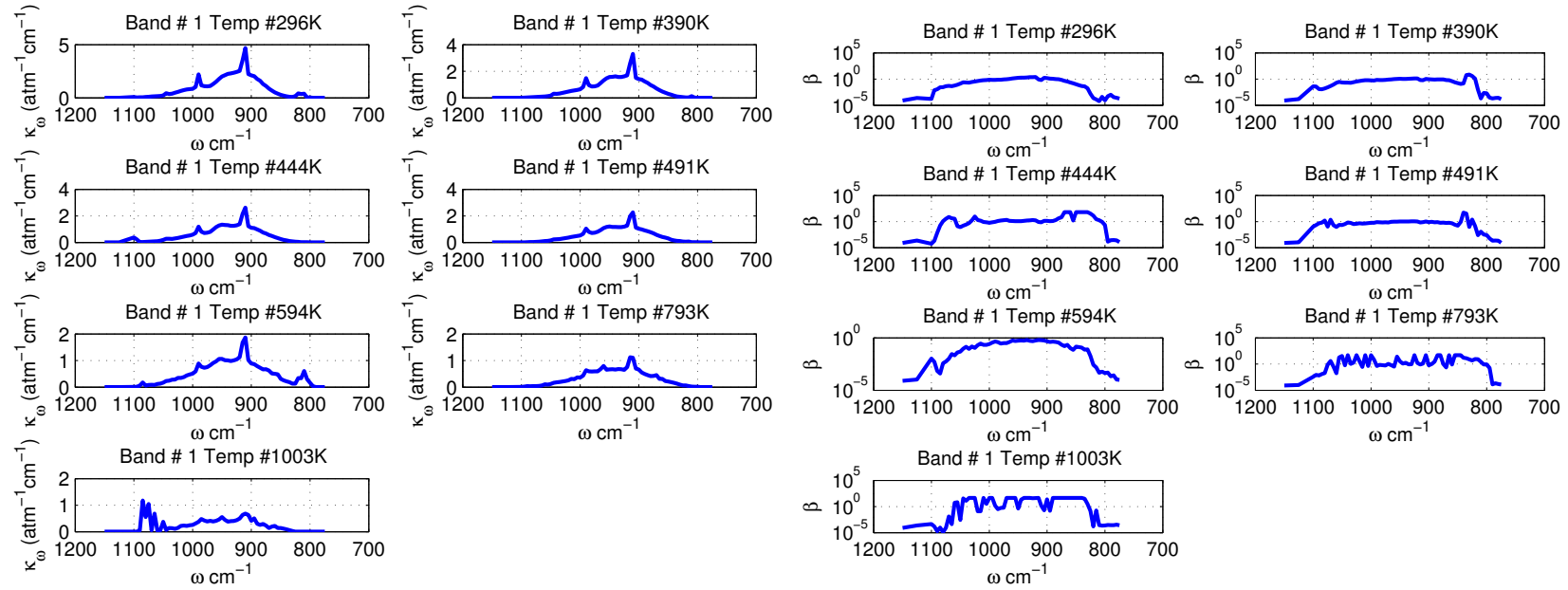
Table 4.3: Spectral bands of C₃H₆ included in RADCAL.

Band #	Bounds (cm ⁻¹)		Assignment	$\alpha(T = 296 \text{ K}) (\text{atm}^{-1}\text{cm}^{-2})$
1	775	1150	C–C Stretch, CH ₃ Rock	296
2	1225	1975	C = C Stretch, CH Bend	271
3	2650	3275	CH & CH ₂ Stretch	509

4.5.2 Malkmus Narrow Band Parameters

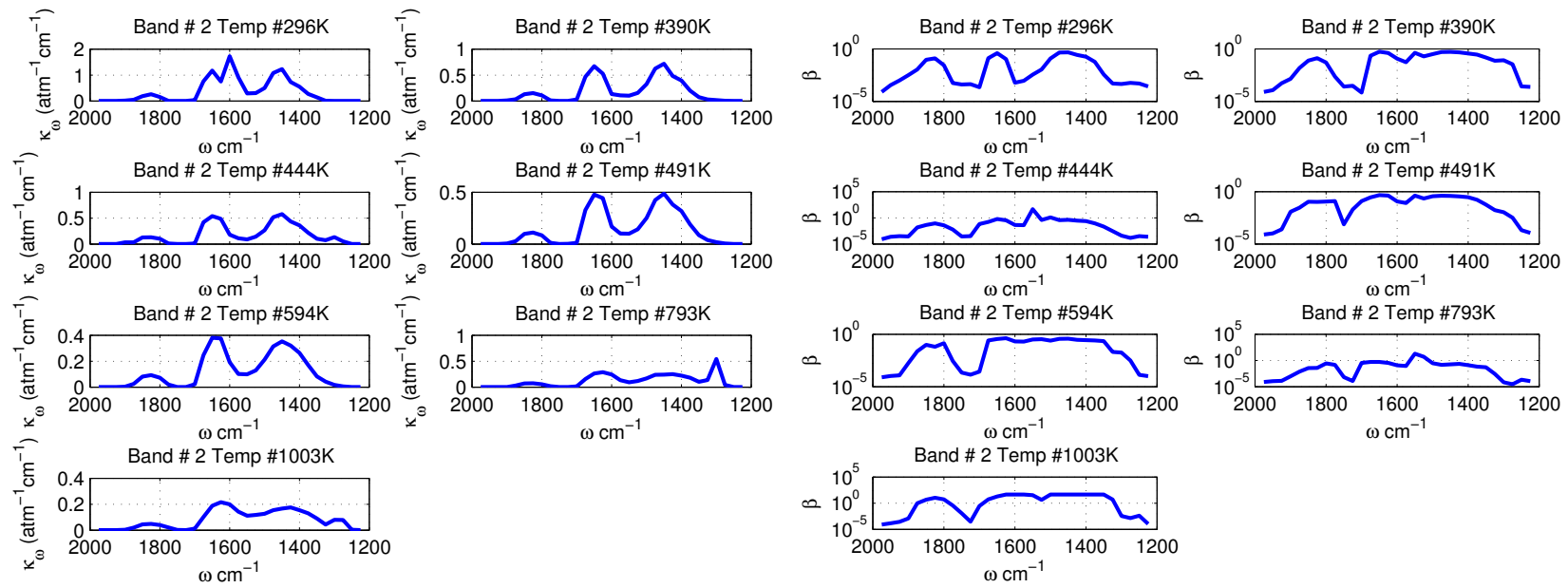
All the propylene IR spectral absorption data were obtained from high resolution FTIR experiments with temperatures varying from 296 K to 1003 K. The spectral absorption coefficients were obtained by fitting the experimental spectral transmissivity of a homogeneous column of isothermal propylene with a total pressure of 1 atm using the Malkmus model.

The propylene narrow band parameters, $\bar{\kappa}$ and β , for temperatures ranging from 296 K to 1003 K are plotted in Figures 4.22–4.24 for Bands 1 to 3.



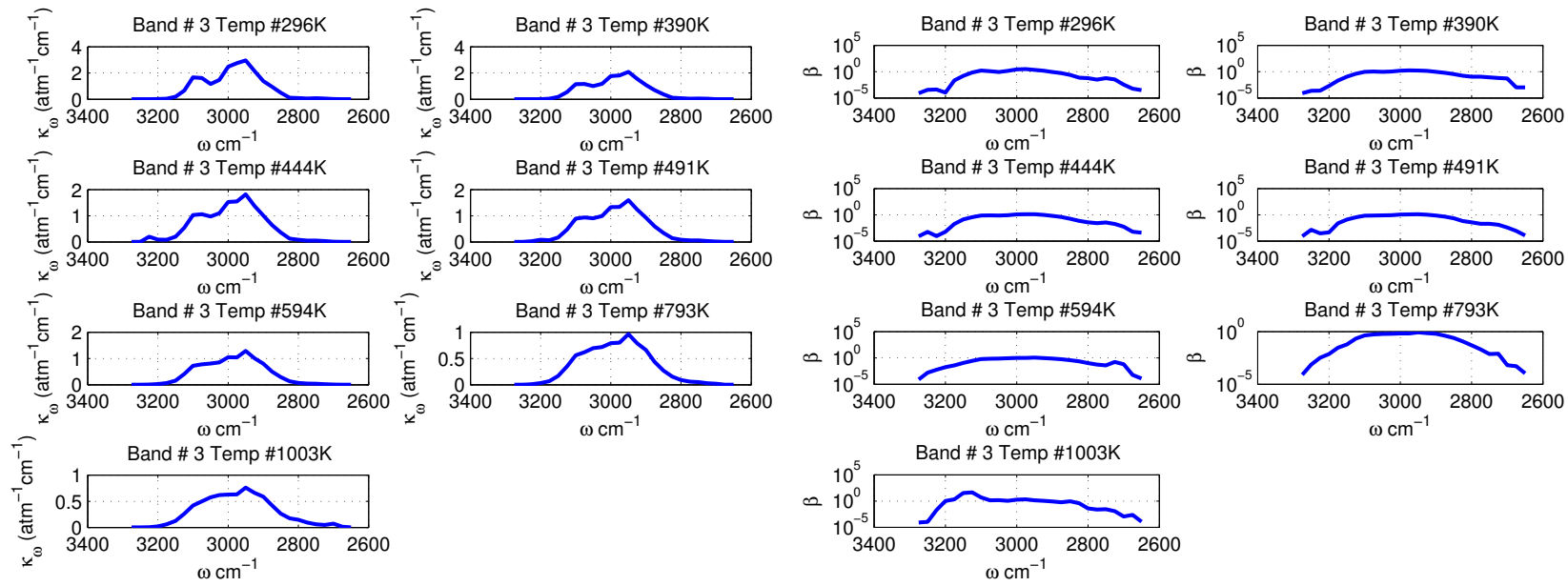
(a) Narrow band spectral absorption coefficient $\bar{\kappa}$ (in atm⁻¹cm⁻¹) for the 775–1150 cm⁻¹ band.
(b) Narrow band spectral fine structure parameter β (in atm⁻¹) for the 775–1150 cm⁻¹ band.

Figure 4.22: Propylene narrow band parameters $\bar{\kappa}$ and β obtained for the 775–1150 cm⁻¹ band corresponding to the rocking motion of the CH₃ chemical group. Temperatures plotted are: 296, 390, 444, 491, 594, 793, and 1003 K. The narrow band resolution $\Delta\omega$ is 5 cm⁻¹.



(a) Narrow band spectral absorption coefficient $\bar{\kappa}$ (in $\text{atm}^{-1}\text{cm}^{-1}$) for the 1225–1975 cm^{-1} band.
(b) Narrow band spectral fine structure parameter β (in atm^{-1}) for the 1225–1975 cm^{-1} band.

Figure 4.23: Propylene narrow band parameters $\bar{\kappa}$ and β obtained for the 1225–1975 cm^{-1} band corresponding to the bending motion of the CH chemical group. Temperatures plotted are: 296, 390, 444, 491, 594, 793, and 1003 K. The narrow band resolution $\Delta\omega$ is 25 cm^{-1} .



(a) Narrow band spectral absorption coefficient $\bar{\kappa}$ (in $\text{atm}^{-1}\text{cm}^{-1}$) for the 2650–3275 cm^{-1} band.
(b) Narrow band spectral fine structure parameter β (in atm^{-1}) for the 2650–3275 cm^{-1} band.

Figure 4.24: Propylene narrow band parameters $\bar{\kappa}$ and β obtained for the 2650–3275 cm^{-1} band corresponding to the stretching motion of the C – H chemical group. Temperatures plotted are: 296, 390, 444, 491, 594, 793, and 1003 K. The narrow band resolution $\Delta\omega$ is 25 cm^{-1} .

4.5.3 Verification SNB Parameters

To assess the accuracy of the narrow band parameters $\bar{\kappa}$ and β , synthetic transmissivities were constructed for the same experimental conditions as the FTIR data and compare with it. This subsection plots the comparison and the relative error in transmissivity (relative to FTIR measurements) using the propylene parameters presented in Figs. 4.22 to 4.24.

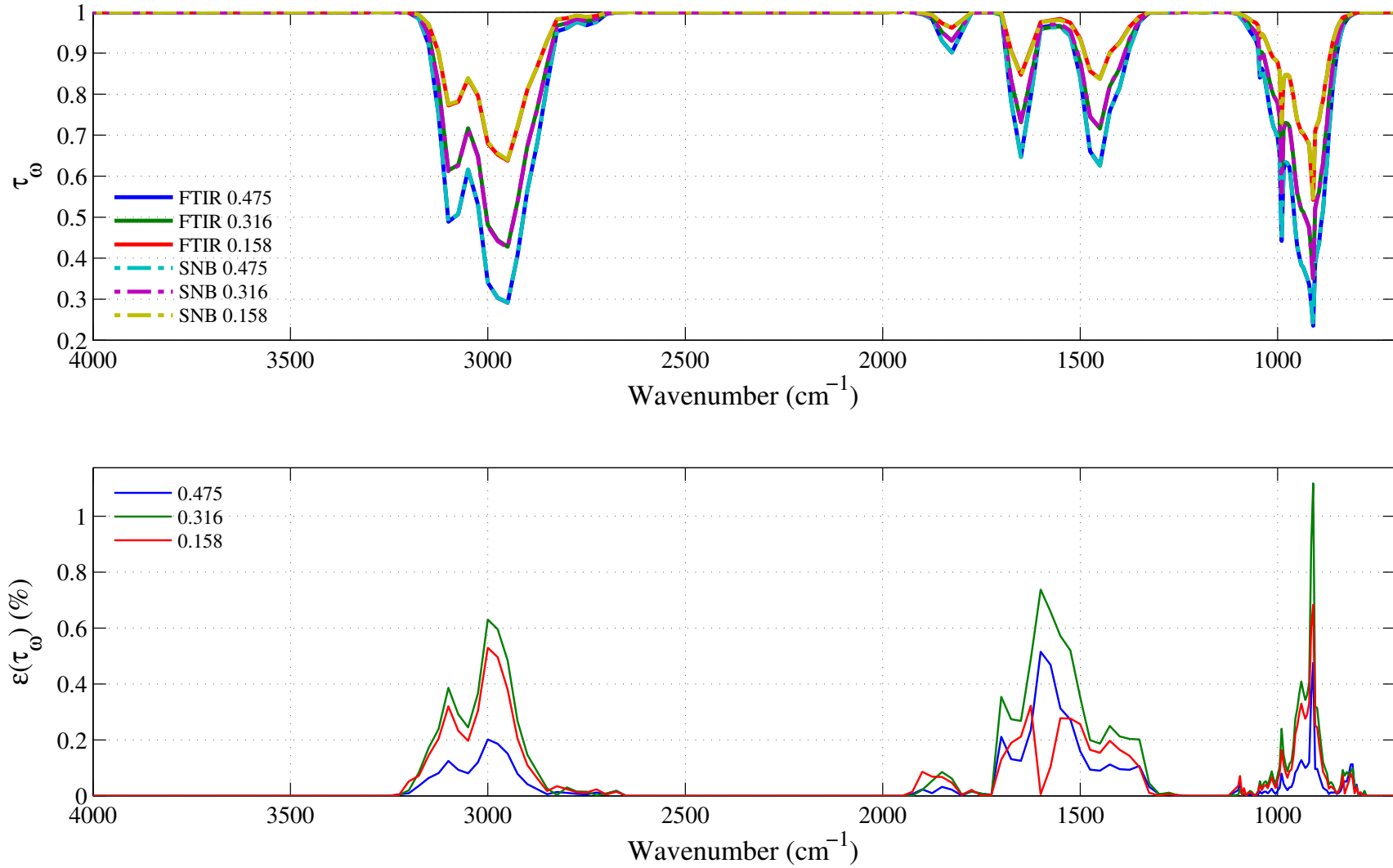


Figure 4.25: Top: comparison between the experimental (FTIR, in solid lines) and the synthetic (dashed lines) spectral transmissivity profiles, denoted τ_{ω} , of an isothermal homogeneous column of propylene. The synthetic profiles were generated using the Malkmus narrow band parameters presented in Figs. 4.22 to 4.24. Bottom: relative transmissivity error, denoted $\varepsilon(\tau_{\omega})$, between the experiment and the synthetic profiles presented on the top figure. Three different pressure-paths are considered: 0.475, 0.316 and 0.158 atm.cm. The gas temperature is set at 296 K and the total pressure is 101 kPa. Note: the experimental data resolution has been changed to match that of the narrow band model.

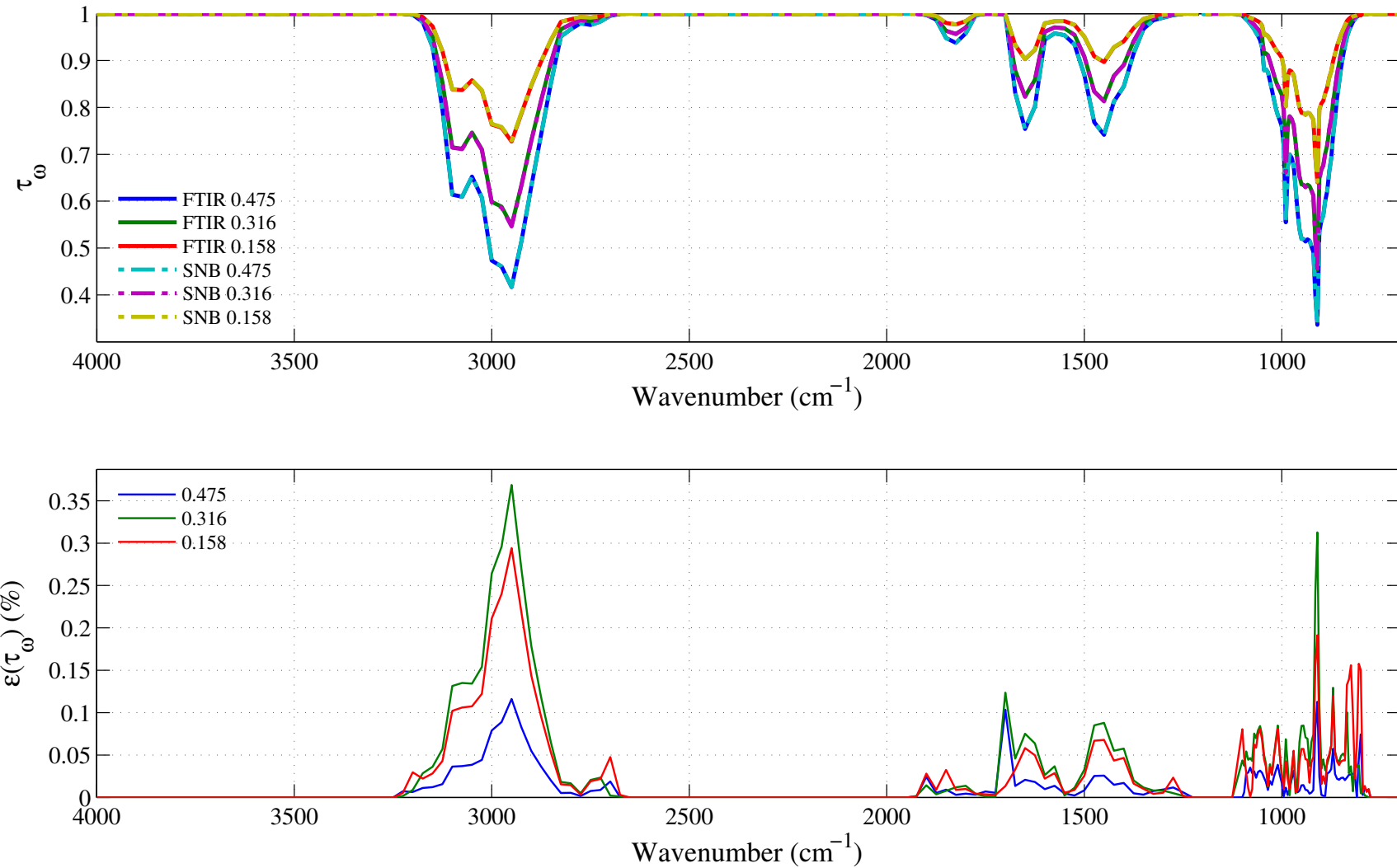


Figure 4.26: Top: comparison between the experimental (FTIR, in solid lines) and the synthetic (dashed lines) spectral transmissivity profiles, denoted τ_ω , of an isothermal homogeneous column of propylene. The synthetic profiles was generated using the Malkmus narrow band parameters presented in Figs. 4.22 to 4.24. Bottom: relative transmissivity error, denoted $\varepsilon(\tau_\omega)$, between the experiment and the synthetic profiles presented on the top figure. Three different pressure-paths are considered: 0.475, 0.316 and 0.158 atm.cm. The gas temperature is set at 390 K and the total pressure is 101 kPa. Note: the experimental data resolution has been changed to match that of the narrow band model.

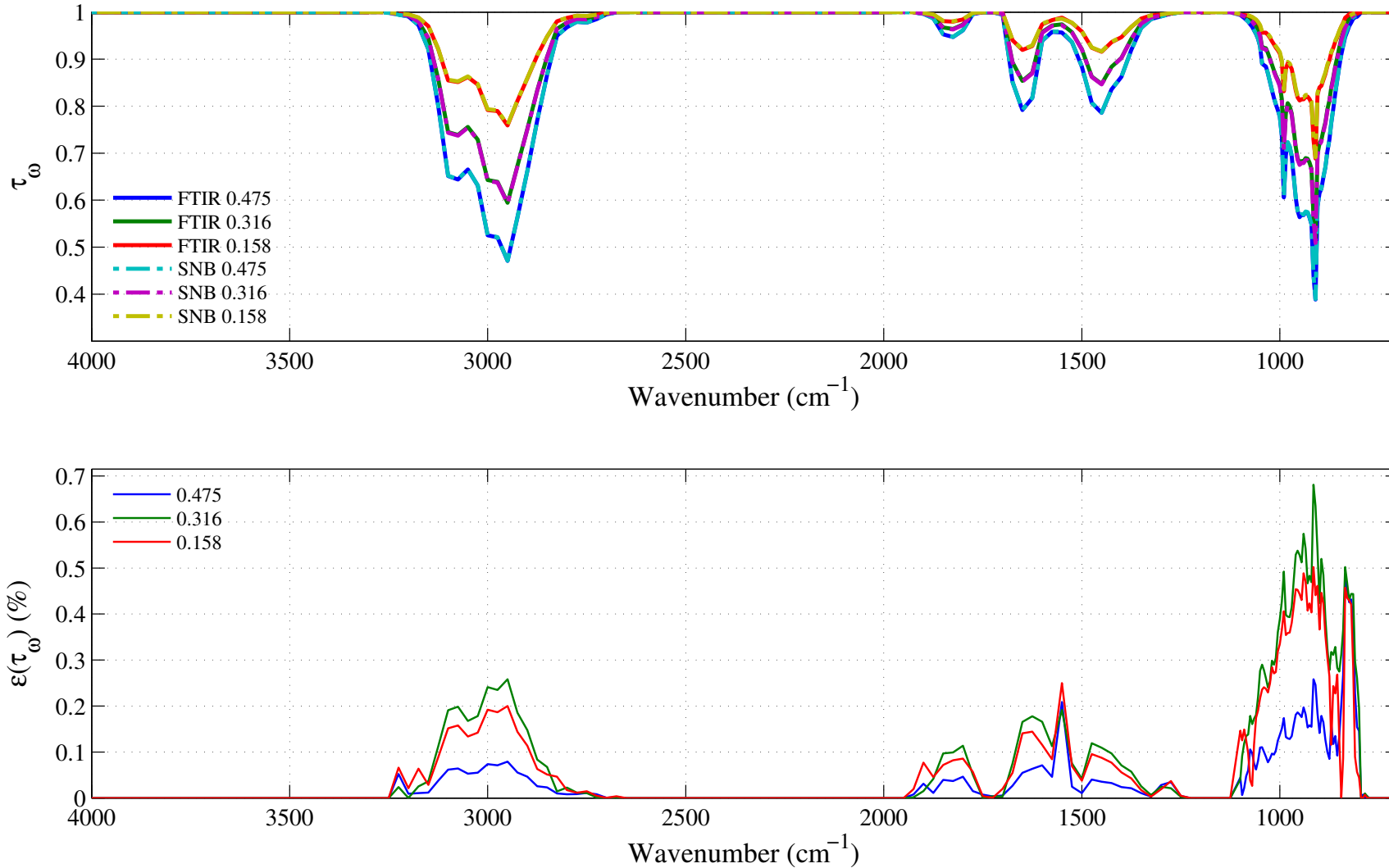


Figure 4.27: Top: comparison between the experimental (FTIR, in solid lines) and the synthetic (dashed lines) spectral transmissivity profiles, denoted τ_ω , of an isothermal homogeneous column of propylene. The synthetic profiles were generated using the Malkmus narrow band parameters presented in Figs. 4.22 to 4.24. Bottom: relative transmissivity error, denoted $\varepsilon(\tau_\omega)$, between the experiment and the synthetic profiles presented on the top figure. Three different pressure-paths are considered: 0.475, 0.316 and 0.158 atm.cm. The gas temperature is set at 444 K and the total pressure is 101 kPa. Note: the experimental data resolution has been changed to match that of the narrow band model.

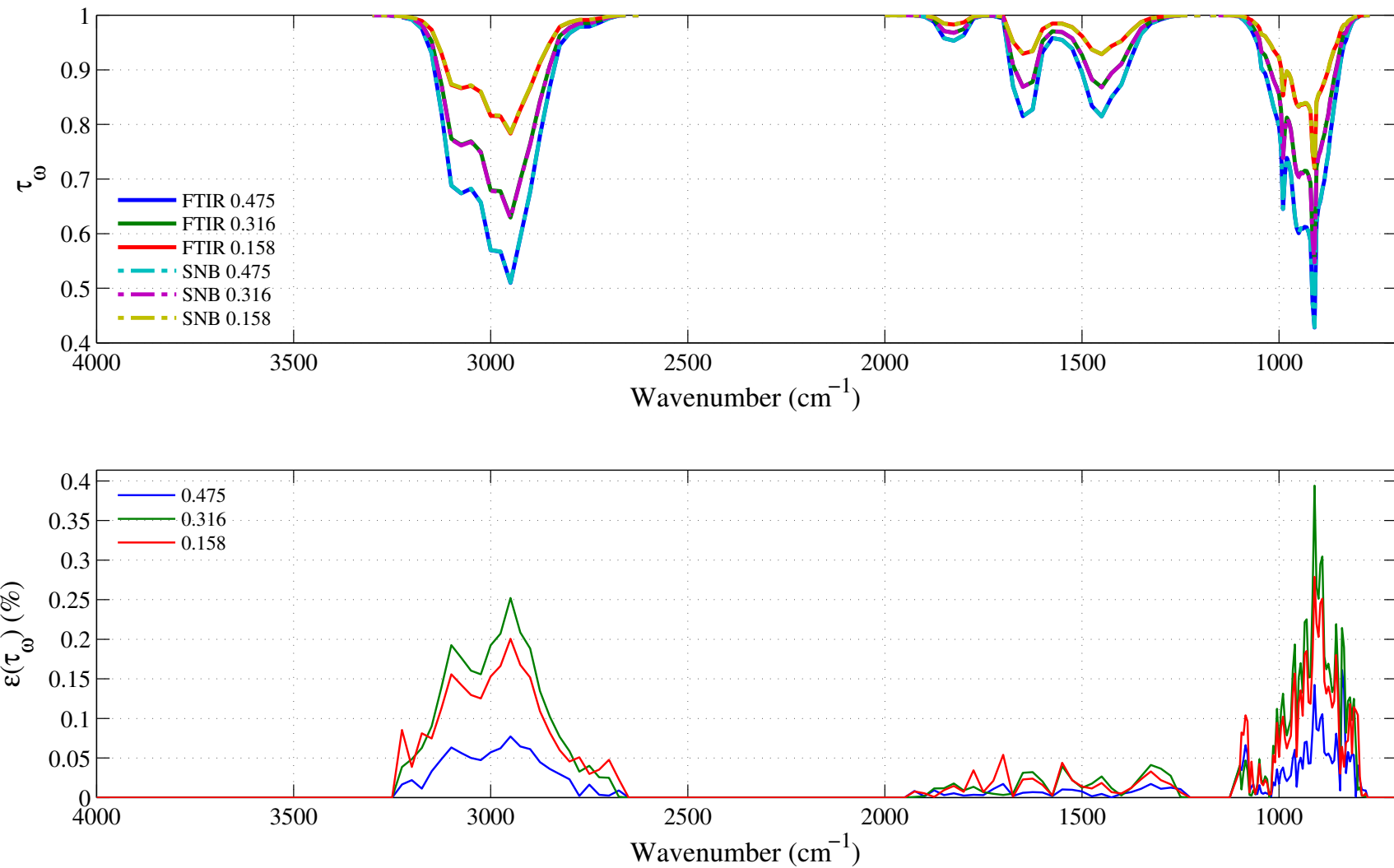


Figure 4.28: Top: comparison between the experimental (FTIR, in solid lines) and the synthetic (dashed lines) spectral transmissivity profiles, denoted τ_ω , of an isothermal homogeneous column of propylene. The synthetic profiles were generated using the Malkmus narrow band parameters presented in Figs. 4.22 to 4.24. Bottom: relative transmissivity error, denoted $\varepsilon(\tau_\omega)$, between the experiment and the synthetic profiles presented on the top figure. Three different pressure-paths are considered: 0.475, 0.316 and 0.158 atm.cm. The gas temperature is set at 491 K and the total pressure is 101 kPa. Note: the experimental data resolution has been changed to match that of the narrow band model.

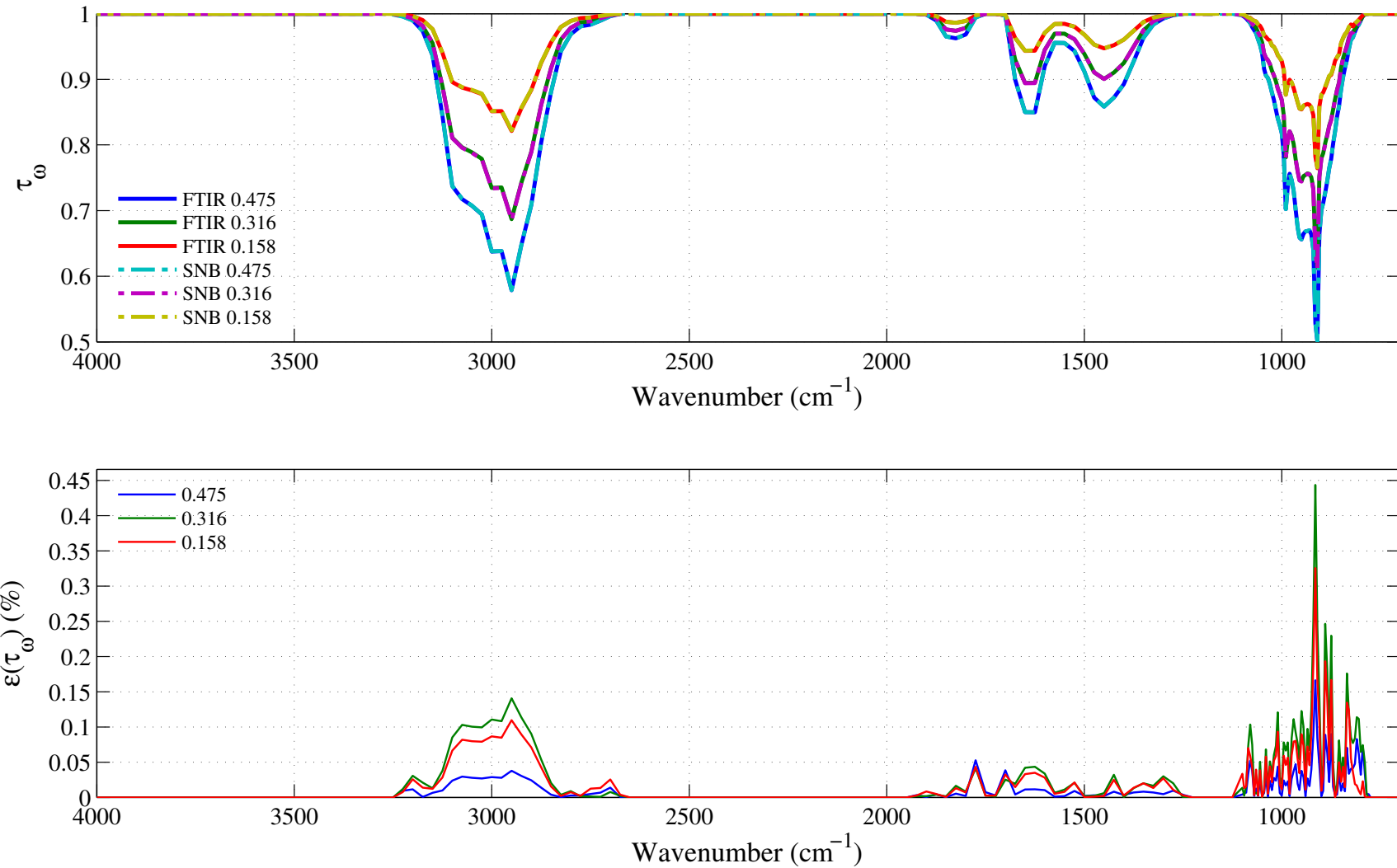


Figure 4.29: Top: comparison between the experimental (FTIR, in solid lines) and the synthetic (dashed lines) spectral transmissivity profiles, denoted τ_ω , of an isothermal homogeneous column of propylene. The synthetic profiles were generated using the Malkmus narrow band parameters presented in Figs. 4.22 to 4.24. Bottom: relative transmissivity error, denoted $\varepsilon(\tau_\omega)$, between the experiment and the synthetic profiles presented on the top figure. Three different pressure-paths are considered: 0.475, 0.316 and 0.158 atm.cm. The gas temperature is set at 594 K and the total pressure is 101 kPa. Note: the experimental data resolution has been changed to match that of the narrow band model.

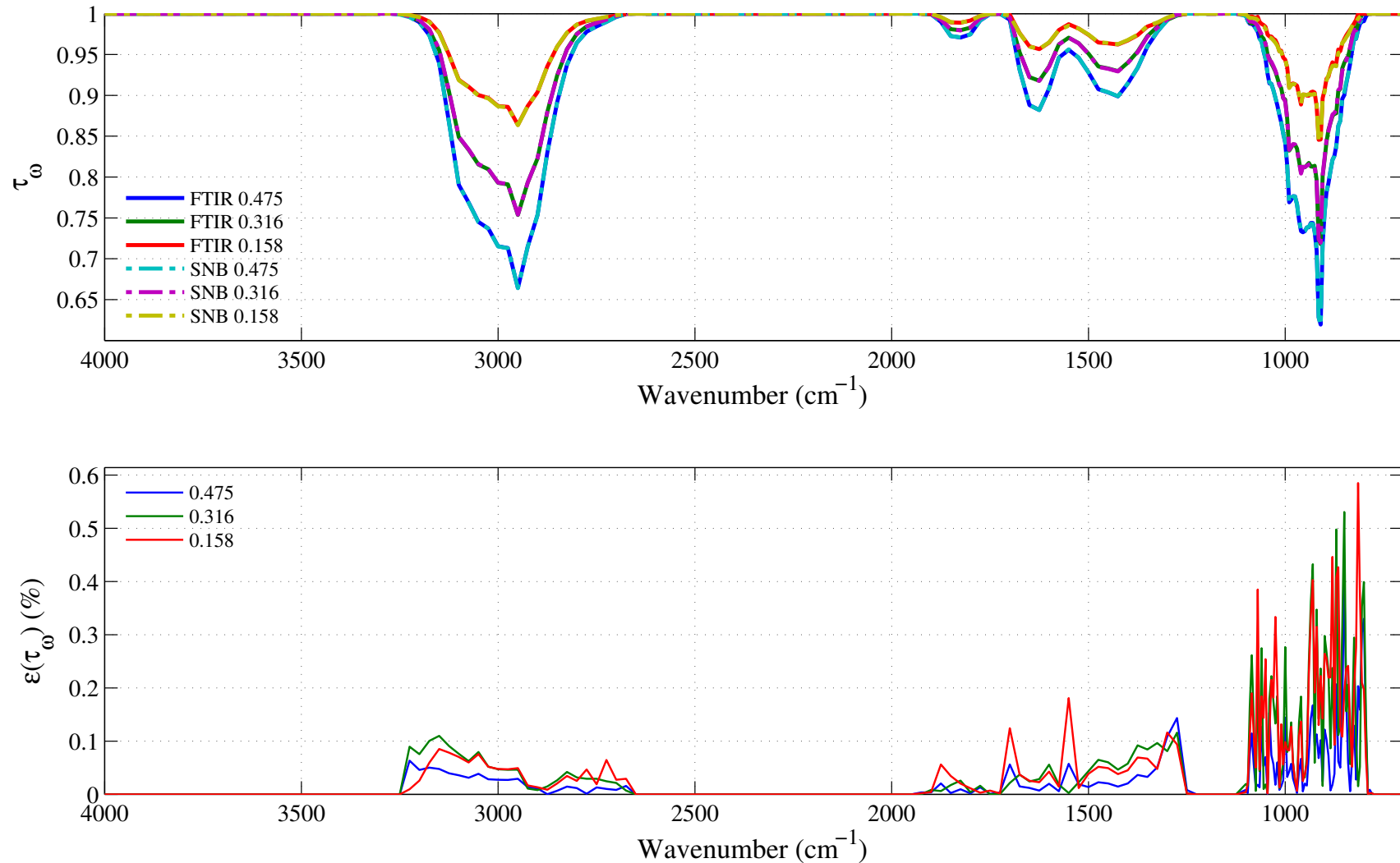


Figure 4.30: Top: comparison between the experimental (FTIR, in solid lines) and the synthetic (dashed lines) spectral transmissivity profiles, denoted τ_ω , of an isothermal homogeneous column of propylene. The synthetic profiles were generated using the Malkmus narrow band parameters presented in Figs. 4.22 to 4.24. Bottom: relative transmissivity error, denoted $\varepsilon(\tau_\omega)$, between the experiment and the synthetic profiles presented on the top figure. Three different pressure-paths are considered: 0.475, 0.316 and 0.158 atm.cm. The gas temperature is set at 793 K and the total pressure is 101 kPa. Note: the experimental data resolution has been changed to match that of the narrow band model.

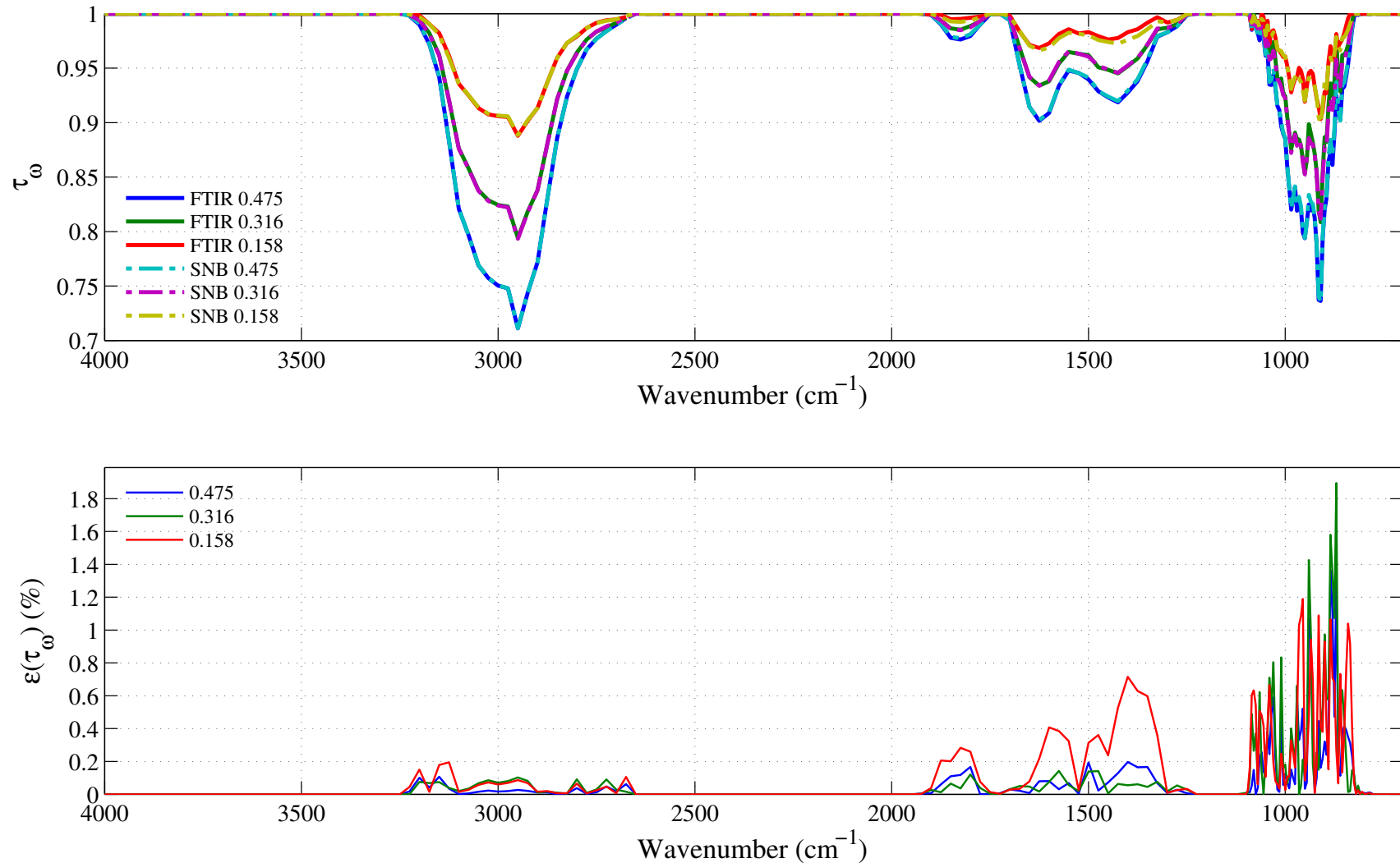


Figure 4.31: Top: comparison between the experimental (FTIR, in solid lines) and the synthetic (dashed lines) spectral transmissivity profiles, denoted τ_ω , of an isothermal homogeneous column of propylene. The synthetic profiles were generated using the Malkmus narrow band parameters presented in Figs. 4.22 to 4.24. Bottom: relative transmissivity error, denoted $\varepsilon(\tau_\omega)$, between the experiment and the synthetic profiles presented on the top figure. Three different pressure-paths are considered: 0.475, 0.316 and 0.158 atm.cm. The gas temperature is set at 1003 K and the total pressure is 101 kPa. Note: the experimental data resolution has been changed to match that of the narrow band model.

4.6 Propane: C₃H₈

4.6.1 Integrated Band Intensity

Propane, C₃H₈, has two planes of symmetry and two axes of rotation and belongs to the point group C_{2v} [18]. It has 27 vibrational modes. In RADCAL, its spectrum is divided into two distinct bands, associated with different vibrational modes, see Table 4.4. The propane IR spectrum is the result of the vibration-rotation modes of the C – C, CH₂, CH₃ groups. The first band from 1175–1675 cm⁻¹ is associated with the bending motion of the CH₃ chemical group. The second band from 2550–3375 cm⁻¹ is associated with the stretching motion of the chemical groups CH₃ and CH₂. It is the strongest band; its integrated band intensity is about 10 times that of the 1175–1675 cm⁻¹ band.

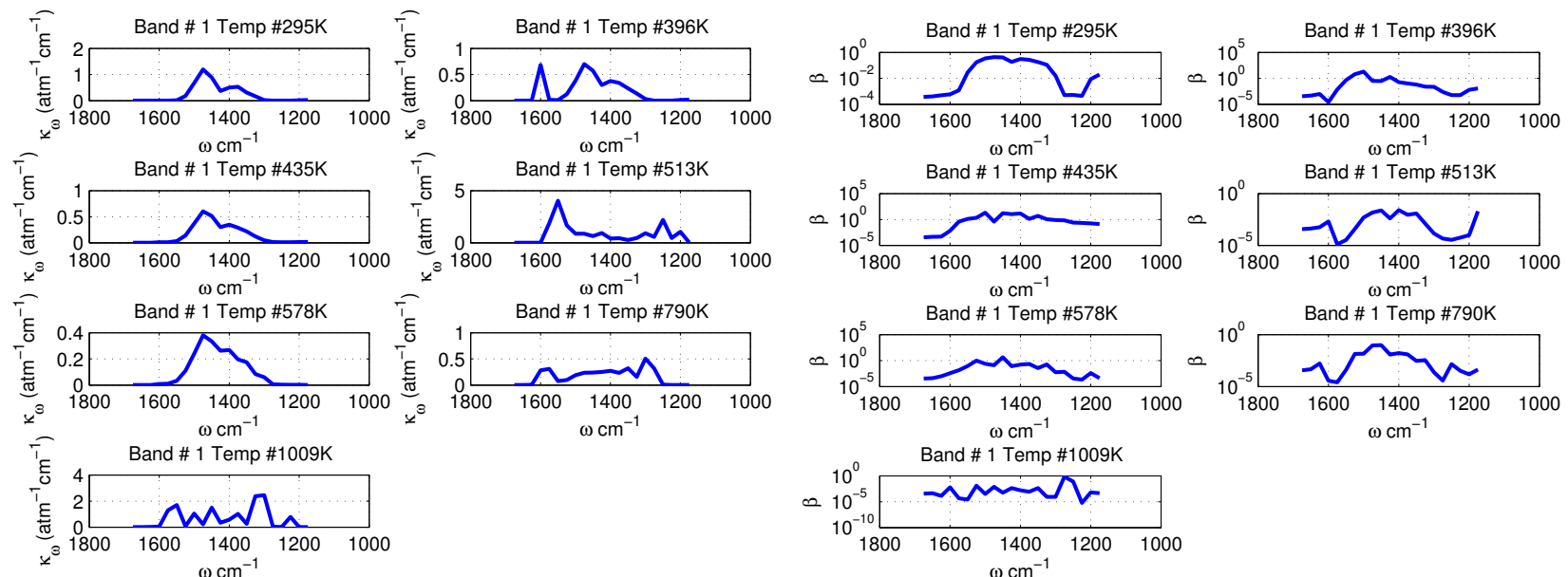
Table 4.4: Spectral bands of C₃H₈ included in RADCAL.

Band #	Bounds (cm ⁻¹)		Assignment	$\alpha(T = 295 \text{ K}) (\text{atm}^{-1}\text{cm}^{-2})$
1	1175	1675	CH ₃ Bending	122
2	2550	3375	CH ₃ , CH ₂ Stretch	1191

4.6.2 Malkmus Narrow Band Parameters

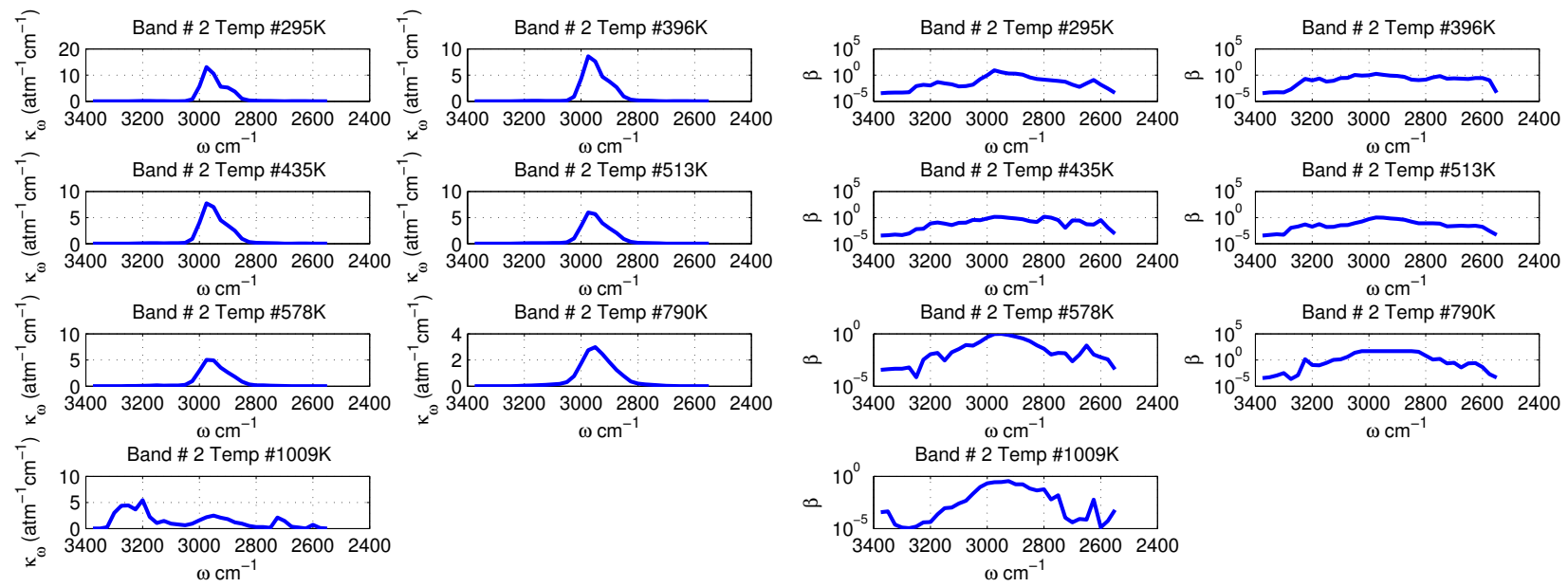
All the propane IR spectral absorption data were obtained from high resolution FTIR experiments with temperatures varying from 295 K to 1009 K. The spectral absorption coefficients were obtained by fitting the experimental spectral transmissivity of a homogeneous column of isothermal propane with a total pressure of 1 atm using the Malkmus model.

The propane narrow band parameters, $\bar{\kappa}$ and β , for temperatures ranging from 295 K to 1009 K are plotted in Figures 4.32–4.33 for Bands 1 to 2.



(a) Narrow band spectral absorption coefficient $\bar{\kappa}$ (in $\text{atm}^{-1}\text{cm}^{-1}$) for the 1175–1675 cm^{-1} band.
(b) Narrow band spectral fine structure parameter β (in atm^{-1}) for the 1175–1675 cm^{-1} band.

Figure 4.32: Propane narrow band parameters $\bar{\kappa}$ and β obtained for the 1175–1675 cm^{-1} band corresponding to the bending motion of the CH_3 chemical group. Temperatures plotted are: 295, 396, 435, 513, 578, 790, and 1009 K. The narrow band resolution $\Delta\omega$ is 5 cm^{-1} .



(a) Narrow band spectral absorption coefficient $\bar{\kappa}$ (in $\text{atm}^{-1}\text{cm}^{-1}$) for the 2550–3375 cm^{-1} band.
(b) Narrow band spectral fine structure parameter β (in atm^{-1}) for the 2550–3375 cm^{-1} band.

Figure 4.33: Propane narrow band parameters $\bar{\kappa}$ and β obtained for the 2550–3375 cm^{-1} band corresponding to the bending motion of the CH chemical group. Temperatures plotted are: 295, 396, 435, 513, 578, 790, and 1009 K. The narrow band resolution $\Delta\omega$ is 25 cm^{-1} .

4.6.3 Verification SNB Parameters

To assess the accuracy of the narrow band parameters $\bar{\kappa}$ and β , synthetic transmissivities were constructed for the same experimental conditions as the FTIR data and compare with it. This subsection plots the comparison and the relative error in transmissivity (relative to FTIR measurements) using the propane parameters presented in Figs. 4.32 to 4.33.

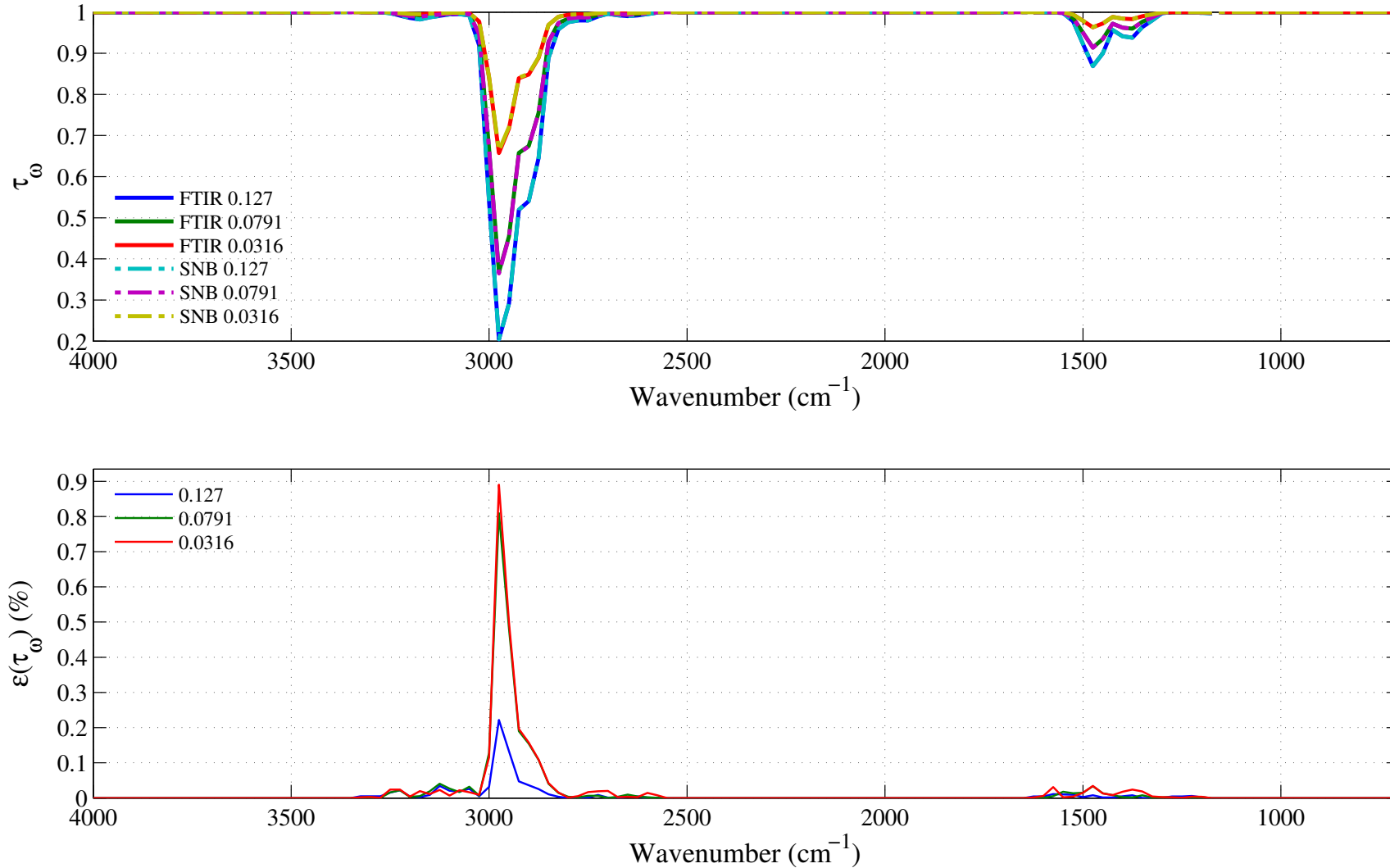


Figure 4.34: Top: comparison between the experimental (FTIR, in solid lines) and the synthetic (dashed lines) spectral transmissivity profiles, denoted τ_{ω} , of an isothermal homogeneous column of propane. The synthetic profiles was generated using the Malkmus narrow band parameters presented in Figs. 4.32 to ???. Bottom: relative transmissivity error, denoted $\varepsilon(\tau_{\omega})$, between the experiment and the synthetic profiles presented on the top figure. Three different pressure-paths are considered: 0.127, 0.0791 and 0.0316 atm.cm. The gas temperature is set at 295 K and the total pressure is 101 kPa. Note: the experimental data resolution has been changed to match that of the narrow band model.

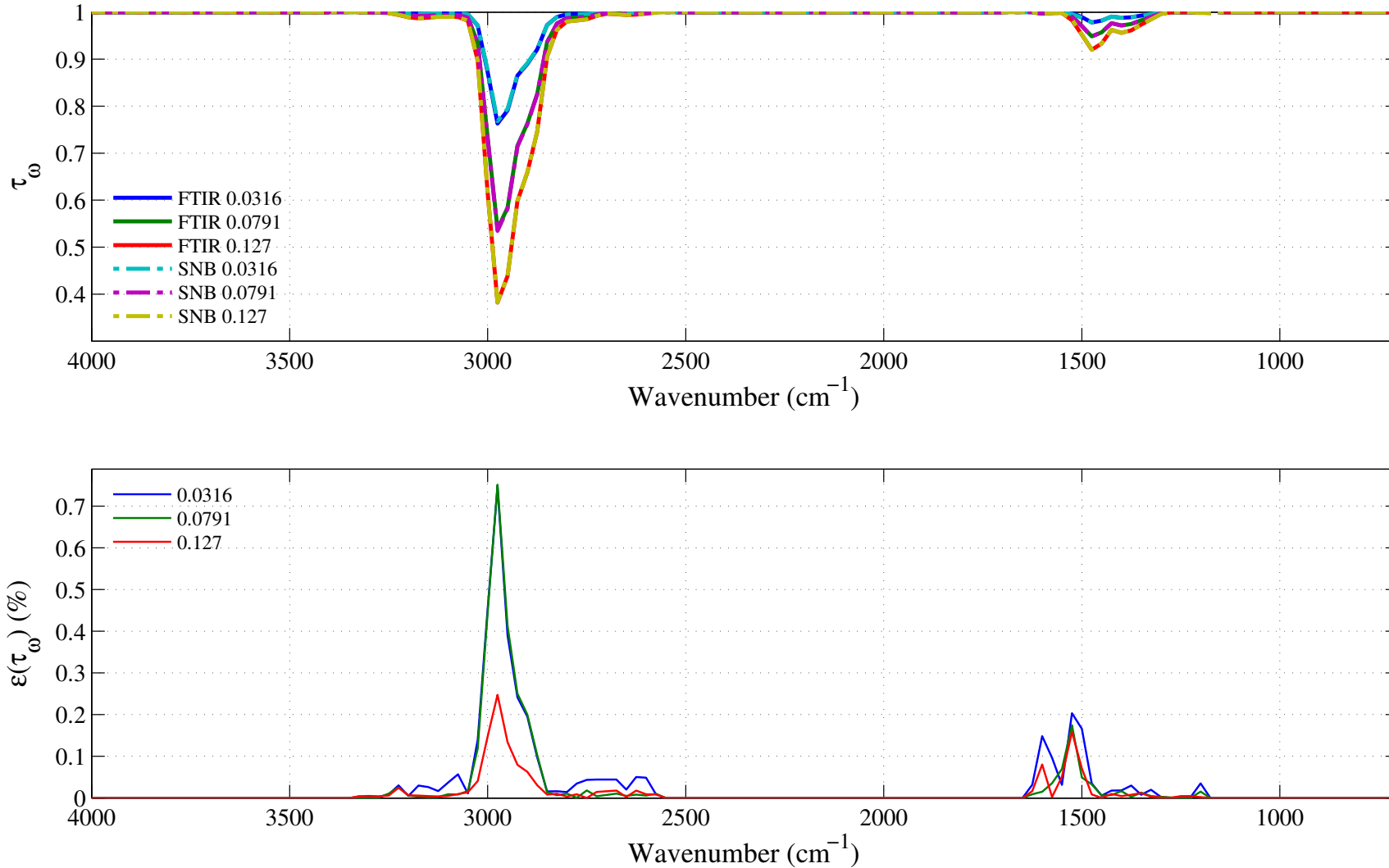


Figure 4.35: Top: comparison between the experimental (FTIR, in solid lines) and the synthetic (dashed lines) spectral transmissivity profiles, denoted τ_ω , of an isothermal homogeneous column of propane. The synthetic profiles was generated using the Malkmus narrow band parameters presented in Figs. 4.32 to ???. Bottom: relative transmissivity error, denoted $\varepsilon(\tau_\omega)$, between the experiment and the synthetic profiles presented on the top figure. Three different pressure-paths are considered: 0.127, 0.0791 and 0.0316 atm.cm. The gas temperature is set at 396 K and the total pressure is 101 kPa. Note: the experimental data resolution has been changed to match that of the narrow band model.

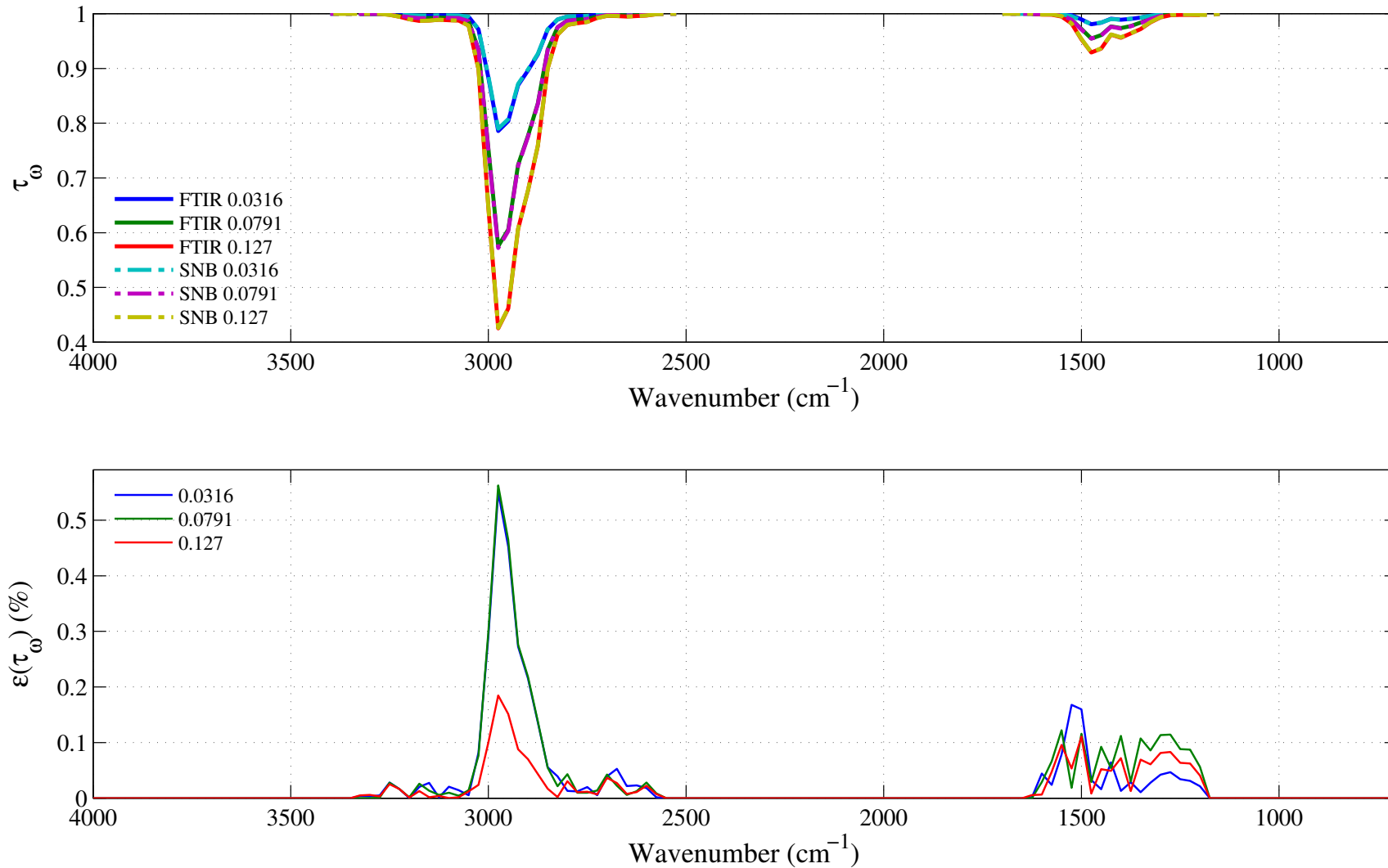


Figure 4.36: Top: comparison between the experimental (FTIR, in solid lines) and the synthetic (dashed lines) spectral transmissivity profiles, denoted τ_{ω} , of an isothermal homogeneous column of propane. The synthetic profiles was generated using the Malkmus narrow band parameters presented in Figs. 4.32 to ???. Bottom: relative transmissivity error, denoted $\varepsilon(\tau_{\omega})$, between the experiment and the synthetic profiles presented on the top figure. Three different pressure-paths are considered: 0.127, 0.0791 and 0.0316 atm.cm. The gas temperature is set at 435 K and the total pressure is 101 kPa. Note: the experimental data resolution has been changed to match that of the narrow band model.

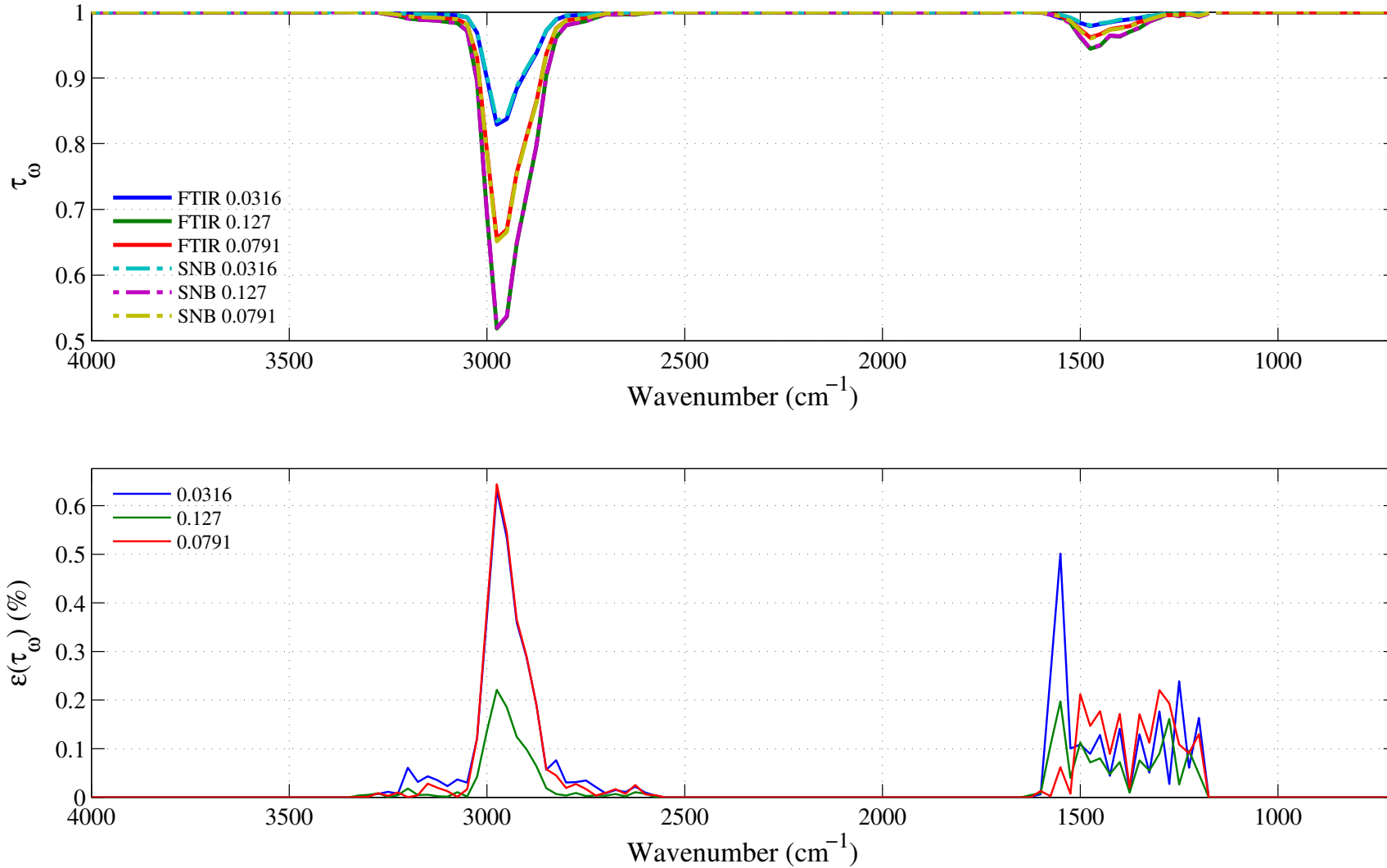


Figure 4.37: Top: comparison between the experimental (FTIR, in solid lines) and the synthetic (dashed lines) spectral transmissivity profiles, denoted τ_ω , of an isothermal homogeneous column of propane. The synthetic profiles was generated using the Malkmus narrow band parameters presented in Figs. 4.32 to ???. Bottom: relative transmissivity error, denoted $\varepsilon(\tau_\omega)$, between the experiment and the synthetic profiles presented on the top figure. Three different pressure-paths are considered: 0.127, 0.0791 and 0.0316 atm.cm. The gas temperature is set at 513 K and the total pressure is 101 kPa. Note: the experimental data resolution has been changed to match that of the narrow band model.

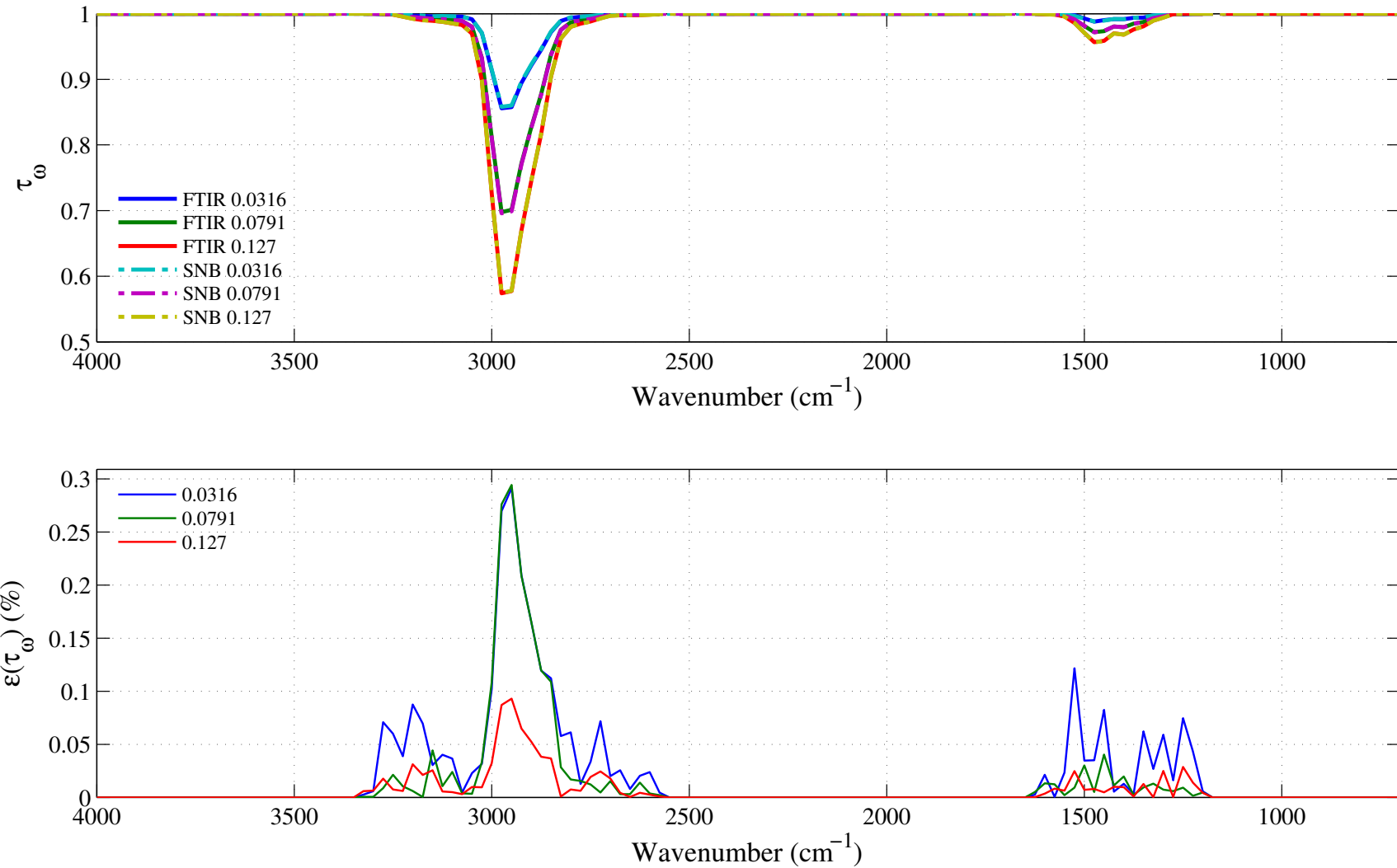


Figure 4.38: Top: comparison between the experimental (FTIR, in solid lines) and the synthetic (dashed lines) spectral transmissivity profiles, denoted τ_ω , of an isothermal homogeneous column of propane. The synthetic profiles was generated using the Malkmus narrow band parameters presented in Figs. 4.32 to ???. Bottom: relative transmissivity error, denoted $\varepsilon(\tau_\omega)$, between the experiment and the synthetic profiles presented on the top figure. Three different pressure-paths are considered: 0.127, 0.0791 and 0.0316 atm.cm. The gas temperature is set at 578 K and the total pressure is 101 kPa. Note: the experimental data resolution has been changed to match that of the narrow band model.

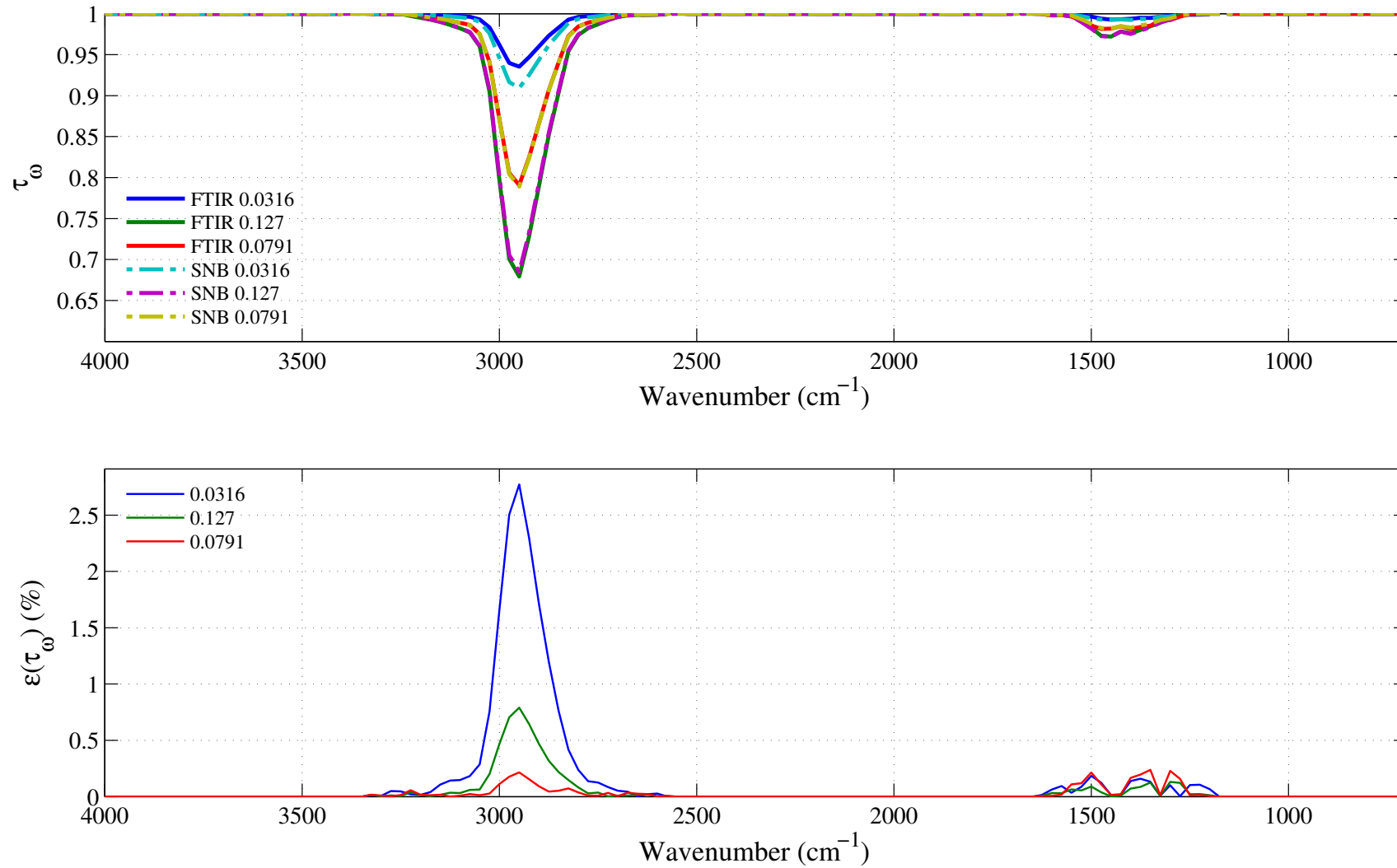


Figure 4.39: Top: comparison between the experimental (FTIR, in solid lines) and the synthetic (dashed lines) spectral transmissivity profiles, denoted τ_ω , of an isothermal homogeneous column of propane. The synthetic profiles was generated using the Malkmus narrow band parameters presented in Figs. 4.32 to ???. Bottom: relative transmissivity error, denoted $\varepsilon(\tau_\omega)$, between the experiment and the synthetic profiles presented on the top figure. Three different pressure-paths are considered: 0.127, 0.0791 and 0.0316 atm.cm. The gas temperature is set at 790 K and the total pressure is 101 kPa. Note: the experimental data resolution has been changed to match that of the narrow band model.

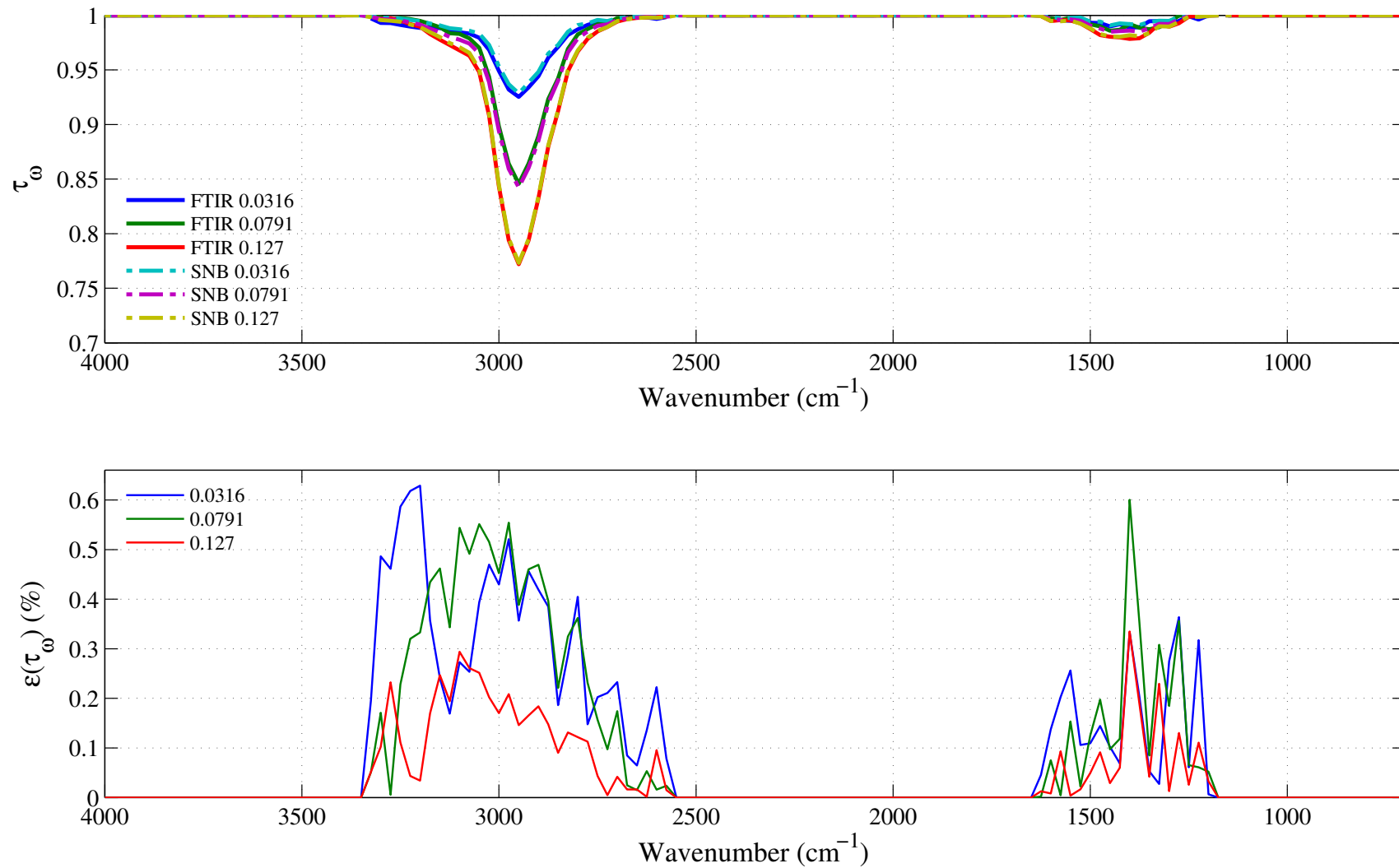


Figure 4.40: Top: comparison between the experimental (FTIR, in solid lines) and the synthetic (dashed lines) spectral transmissivity profiles, denoted τ_ω , of an isothermal homogeneous column of propane. The synthetic profiles was generated using the Malkmus narrow band parameters presented in Figs. 4.32 to ???. Bottom: relative transmissivity error, denoted $\varepsilon(\tau_\omega)$, between the experiment and the synthetic profiles presented on the top figure. Three different pressure-paths are considered: 0.127, 0.0791 and 0.0316 atm.cm. The gas temperature is set at 1009 K and the total pressure is 101 kPa. Note: the experimental data resolution has been changed to match that of the narrow band model.

4.7 Toluene: C₇H₈

4.7.1 Integrated Band Intensity

Toluene, C₇H₈, has only one plane of symmetry; it belongs to the point group C_s [18]. Its IR spectrum is the result of the vibration-rotation modes of the C = C, CH, and CH₃ groups. It has 39 vibrational modes. In RADCAL, its IR spectrum has been divided into five distinct bands. The first band from 700–805 cm⁻¹ is associated with the bending motion of the CH chemical group. The second band from 975–1175 cm⁻¹ is associated with the bending motion of the CH chemical group. The third band from 1275–1650 cm⁻¹ is associated with the bending motion of the CH₃ chemical group. The fourth band from 1650–2075 cm⁻¹ is associated with the stretching motion of the C = C chemical group. The fifth band from 2675–3225 cm⁻¹ is associated with the stretching motion of the CH₃ and CH chemical groups. The first and fifth bands have the highest integrated band intensity. See Table 4.5.

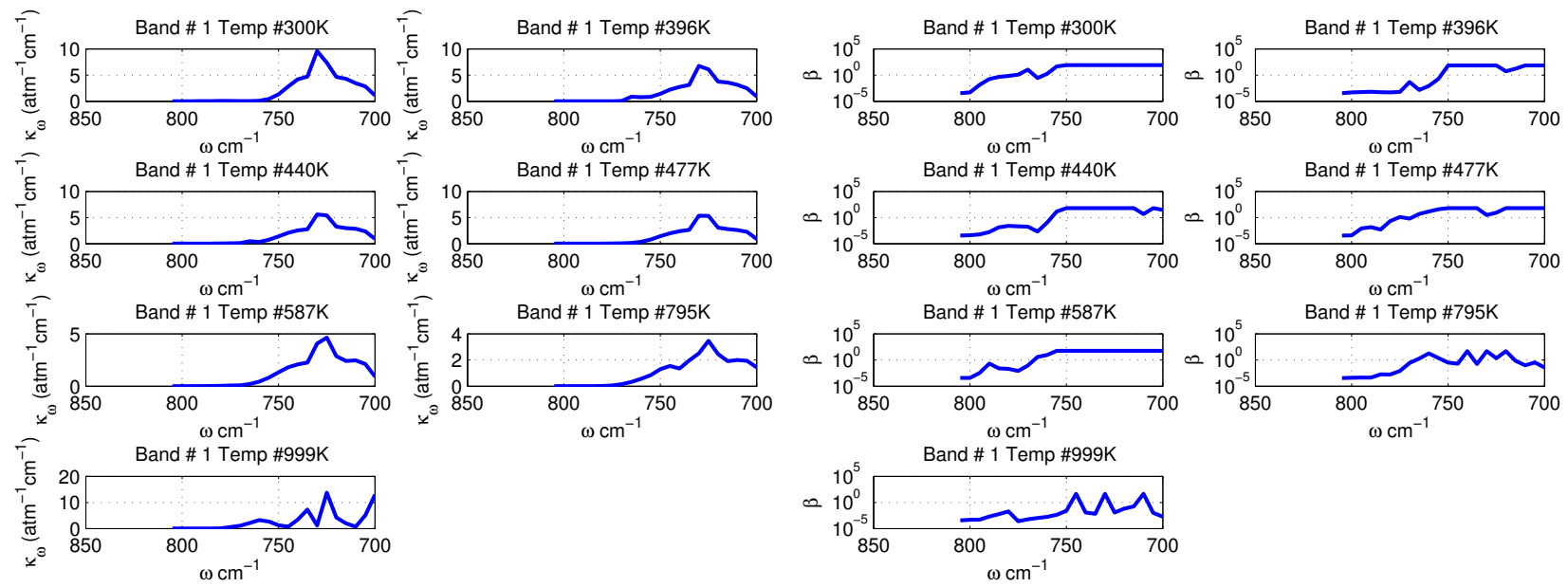
Table 4.5: Spectral bands of C₇H₈ included in RADCAL.

Band #	Bounds (cm ⁻¹)		Assignment	$\alpha(T = 300 \text{ K}) (\text{atm}^{-1}\text{cm}^{-2})$
1	700	805	CH Bending	234
2	975	1175	CH Bending	40
3	1275	1650	CH ₃ Bending	166
4	1650	2075	C = C Stretching	205
5	2675	3225	CH ₃ , CH Stretching	507

4.7.2 Malkmus Narrow Band Parameters

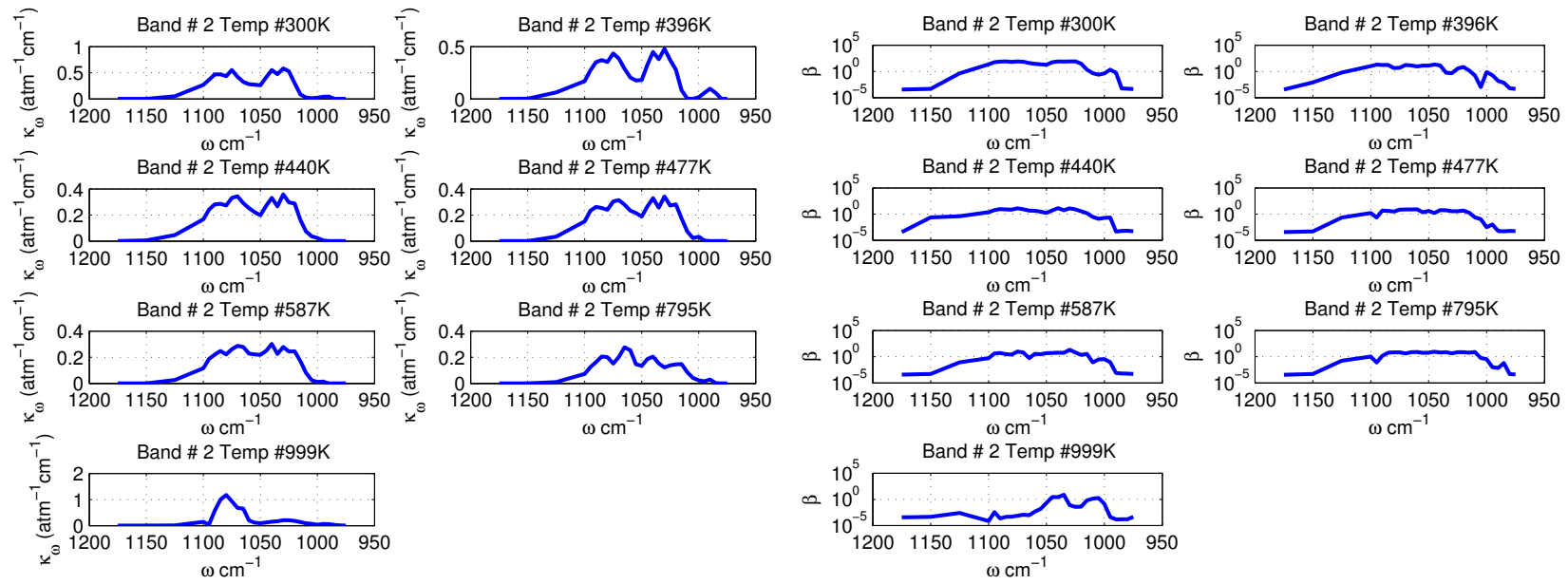
All the toluene IR spectral absorption data were obtained from high resolution FTIR experiments with temperatures varying from 300 K to 999 K. The spectral absorption coefficients were obtained by fitting the experimental spectral transmissivity of a homogeneous column of isothermal toluene with a total pressure of 1 atm using the Malkmus model.

The toluene narrow band parameters, $\bar{\kappa}$ and β , for temperatures ranging from 300 K to 999 K are plotted in Figures 4.41–4.45 for Bands 1 to 5.



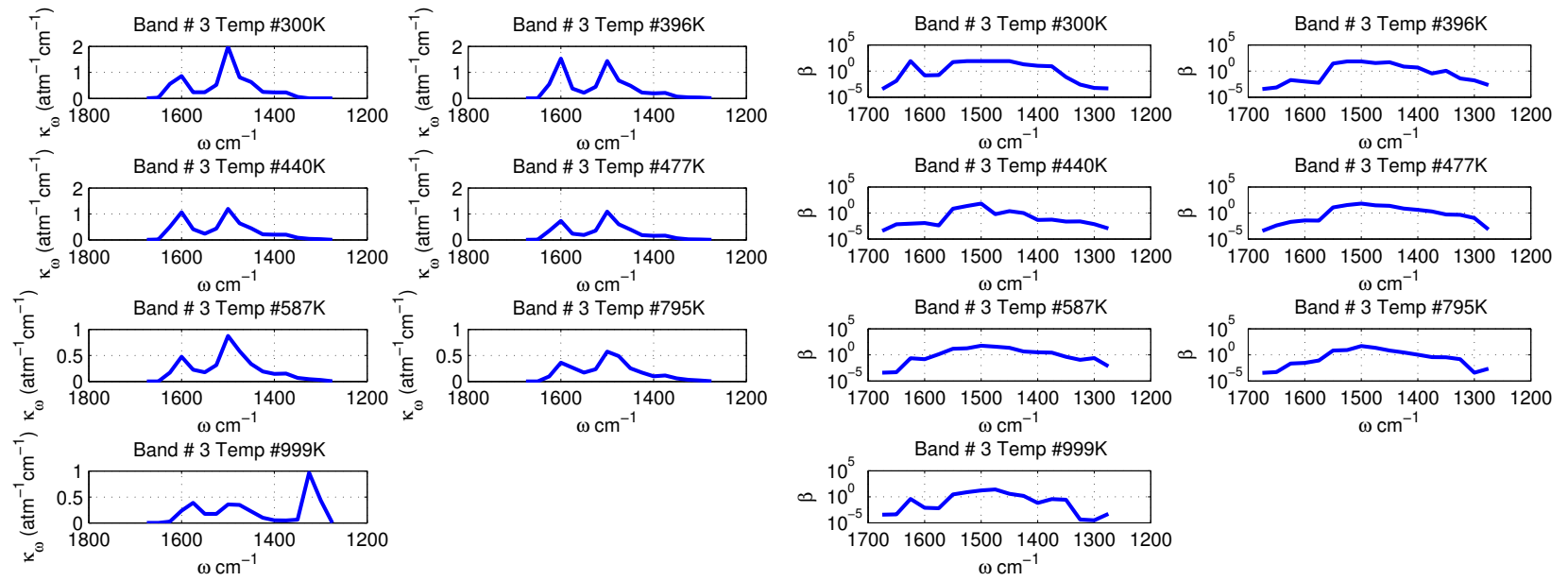
(a) Narrow band spectral absorption coefficient $\bar{\kappa}$ (in $\text{atm}^{-1}\text{cm}^{-1}$) for the 700–805 cm^{-1} band.
(b) Narrow band spectral fine structure parameter β (in atm^{-1}) for the 700–805 cm^{-1} band.

Figure 4.41: Toluene narrow band parameters $\bar{\kappa}$ and β obtained for the 700–805 cm^{-1} band corresponding to the bending motion of the CH chemical group. Temperatures plotted are: 300, 396, 440, 477, 587, 795, and 999 K. The narrow band resolution $\Delta\omega$ is 5 cm^{-1} .



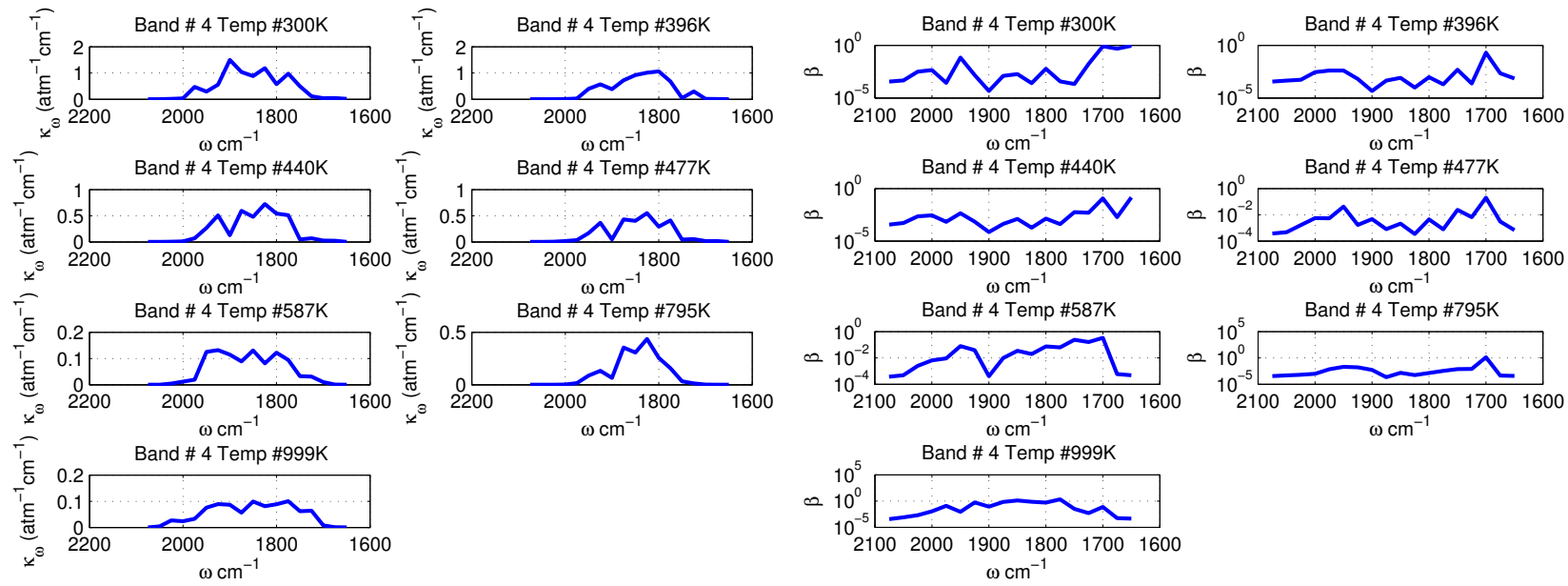
(a) Narrow band spectral absorption coefficient $\bar{\kappa}$ (in $\text{atm}^{-1}\text{cm}^{-1}$) for the 975–1175 cm^{-1} band.
(b) Narrow band spectral fine structure parameter β (in atm^{-1}) for the 975–1175 cm^{-1} band.

Figure 4.42: Toluene narrow band parameters $\bar{\kappa}$ and β obtained for the 975–1175 cm^{-1} band corresponding to the bending motion of the CH chemical group. Temperatures plotted are: 300, 396, 440, 477, 587, 795, and 999 K. The narrow band resolution $\Delta\omega$ is 5 cm^{-1} .



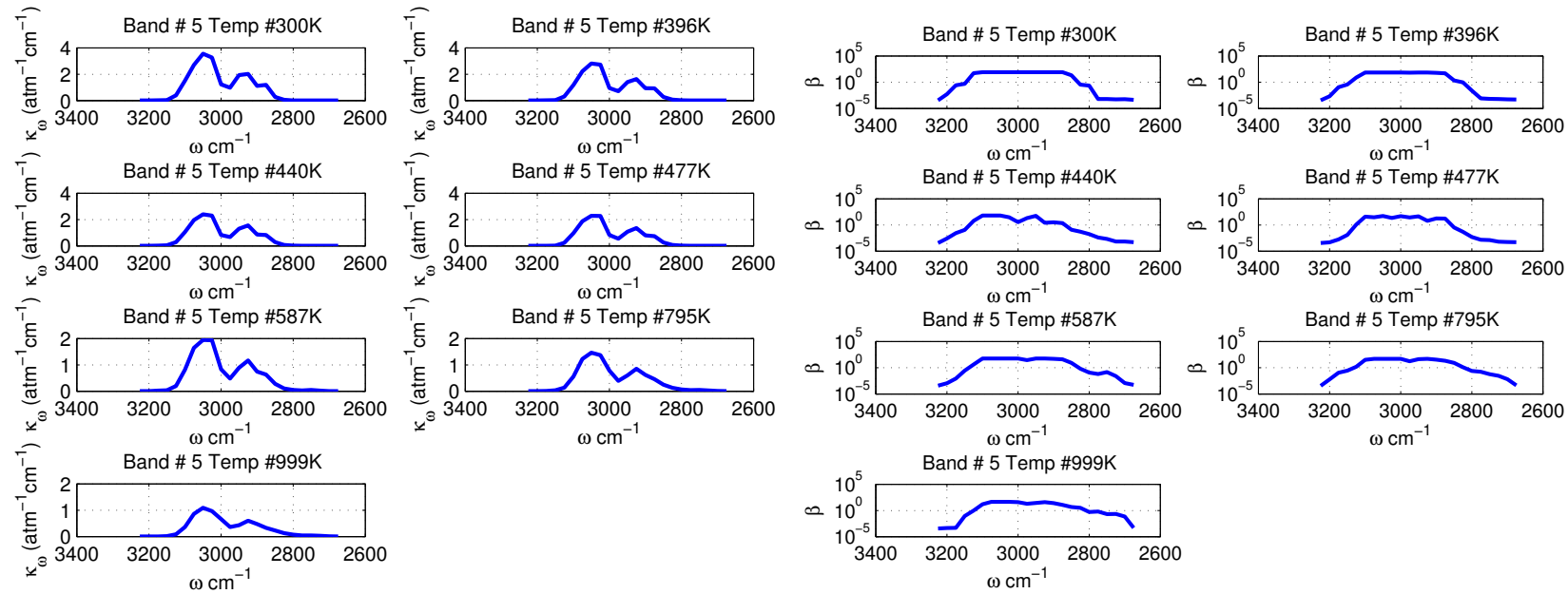
(a) Narrow band spectral absorption coefficient $\bar{\kappa}$ (in atm $^{-1}$ cm $^{-1}$) for the 1275–1650 cm $^{-1}$ band.
(b) Narrow band spectral fine structure parameter β (in atm $^{-1}$) for the 1275–1650 cm $^{-1}$ band.

Figure 4.43: Toluene narrow band parameters $\bar{\kappa}$ and β obtained for the 1275–1650 cm $^{-1}$ band corresponding to the bending motion of the CH₃ chemical group. Temperatures plotted are: 300, 396, 440, 477, 587, 795, and 999 K. The narrow band resolution $\Delta\omega$ is 25 cm $^{-1}$.



(a) Narrow band spectral absorption coefficient $\bar{\kappa}$ (in $\text{atm}^{-1}\text{cm}^{-1}$) for the 1650–2075 cm^{-1} band.
(b) Narrow band spectral fine structure parameter β (in atm^{-1}) for the 1650–2075 cm^{-1} band.

Figure 4.44: Toluene narrow band parameters $\bar{\kappa}$ and β obtained for the 1650–2075 cm^{-1} band corresponding to the stretching motion of the C = C chemical group. Temperatures plotted are: 300, 396, 440, 477, 587, 795, and 999 K. The narrow band resolution $\Delta\omega$ is 25 cm^{-1} .



(a) Narrow band spectral absorption coefficient $\bar{\kappa}$ (in $\text{atm}^{-1}\text{cm}^{-1}$) for the 2675–3225 cm^{-1} band.
(b) Narrow band spectral fine structure parameter β (in atm^{-1}) for the 2675–3225 cm^{-1} band.

Figure 4.45: Toluene narrow band parameters $\bar{\kappa}$ and β obtained for the 2675–3225 cm^{-1} band corresponding to the bending motion of the CH_3 and CH chemical groups. Temperatures plotted are: 300, 396, 440, 477, 587, 795, and 999 K. The narrow band resolution $\Delta\omega$ is 25 cm^{-1} .

4.7.3 Verification SNB Parameters

To assess the accuracy of the narrow band parameters $\bar{\kappa}$ and β , synthetic transmissivities were constructed for the same experimental conditions as the FTIR data and compare with it. This subsection plots the comparison and the relative error in transmissivity (relative to FTIR measurements) using the toluene parameters presented in Figs. 4.41 to 4.45.

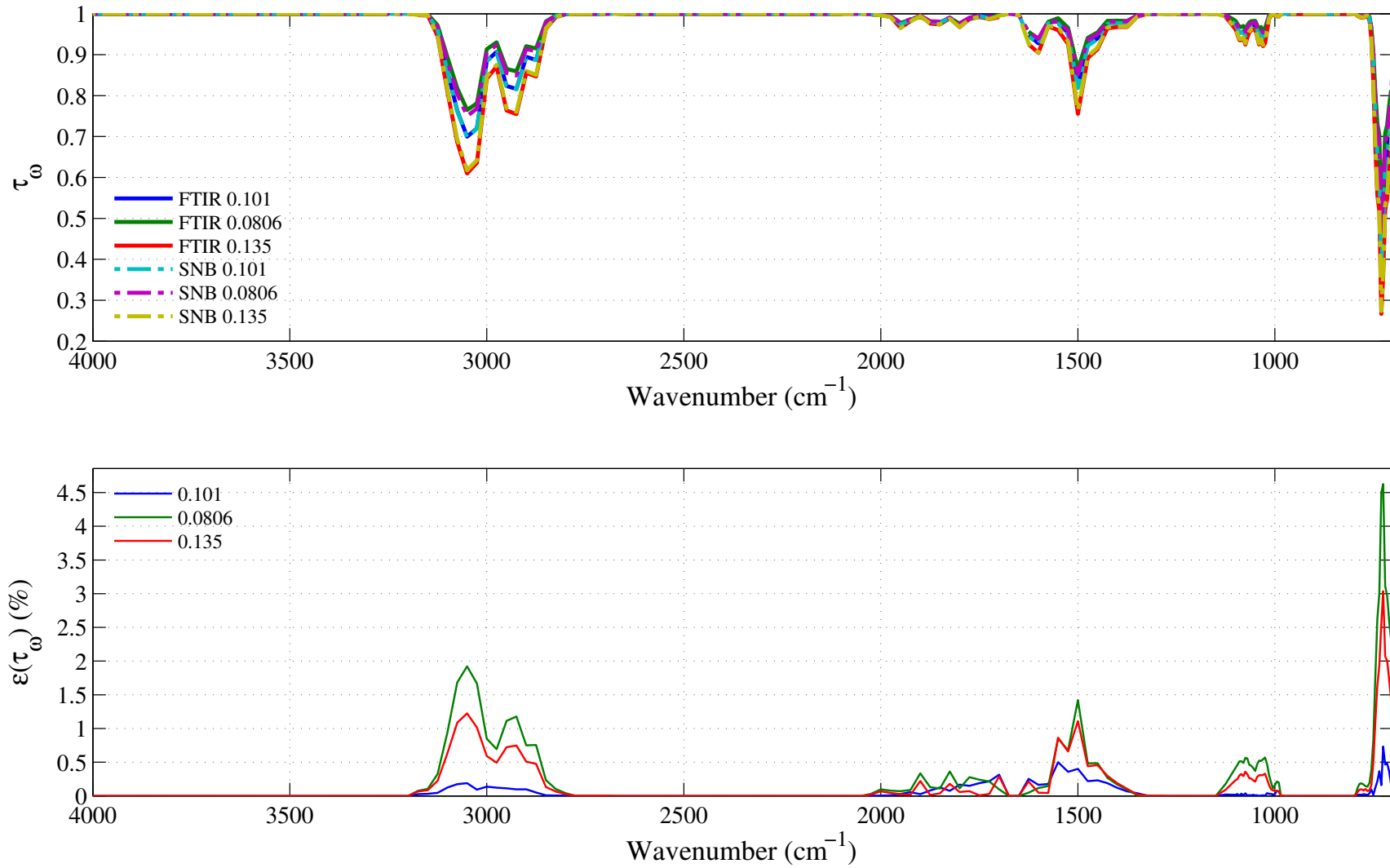


Figure 4.46: Top: comparison between the experimental (FTIR, in solid lines) and the synthetic (dashed lines) spectral transmissivity profiles, denoted τ_{ω} , of an isothermal homogeneous column of toluene. The synthetic profiles was generated using the Malkmus narrow band parameters presented in Figs. 4.41 to 4.45. Bottom: relative transmissivity error, denoted $\varepsilon(\tau_{\omega})$, between the experiment and the synthetic profiles presented on the top figure. Three different pressure-paths are considered: 0.135, 0.101 and 0.0806 atm.cm. The gas temperature is set at 300 K and the total pressure is 101 kPa. Note: the experimental data resolution has been changed to match that of the narrow band model.

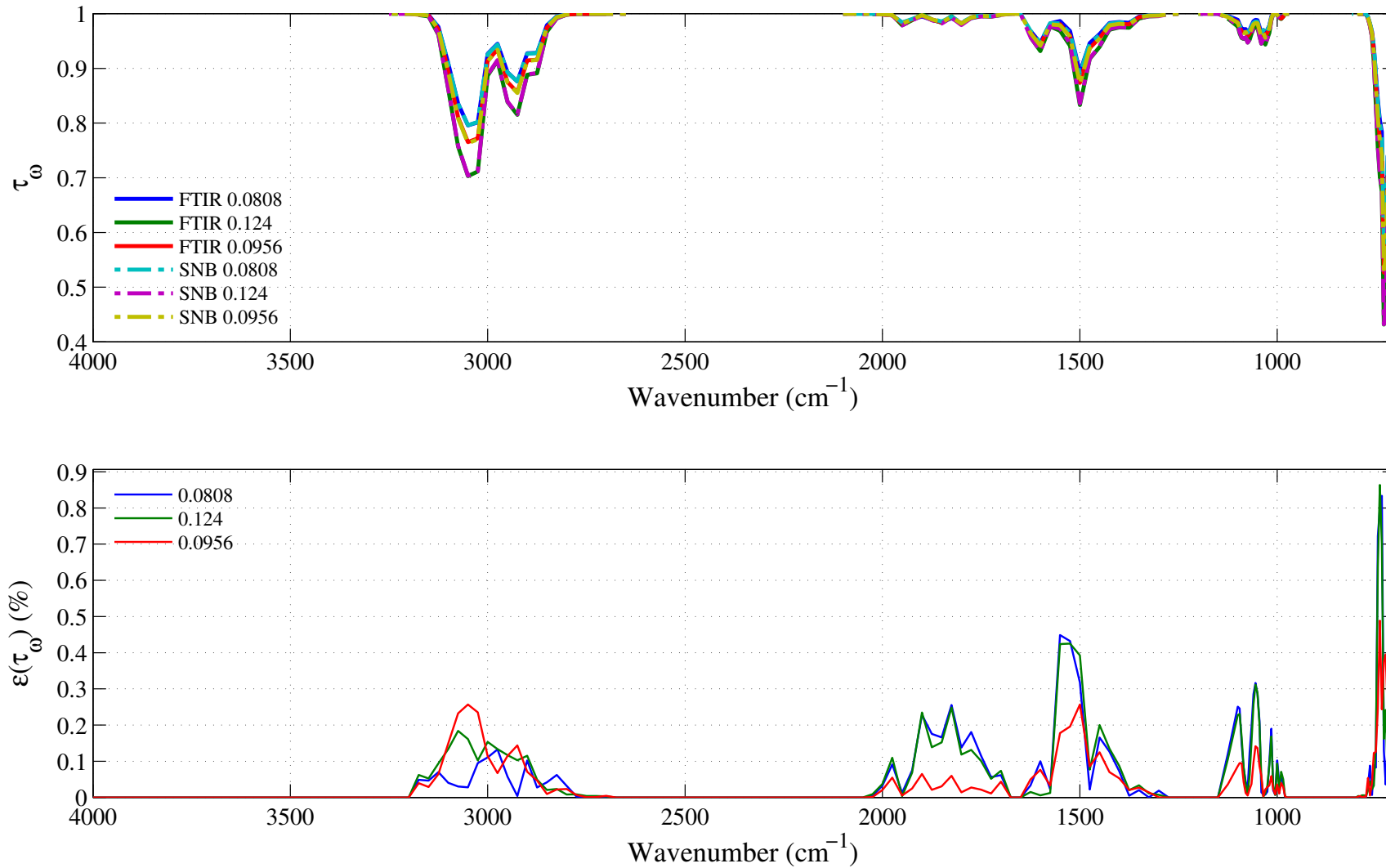


Figure 4.47: Top: comparison between the experimental (FTIR, in solid lines) and the synthetic (dashed lines) spectral transmissivity profiles, denoted τ_{ω} , of an isothermal homogeneous column of toluene. The synthetic profiles was generated using the Malkmus narrow band parameters presented in Figs. 4.41 to 4.45. Bottom: relative transmissivity error, denoted $\varepsilon(\tau_{\omega})$, between the experiment and the synthetic profiles presented on the top figure. Three different pressure-paths are considered: 0.124, 0.0956 and 0.0808 atm.cm. The gas temperature is set at 396 K and the total pressure is 101 kPa. Note: the experimental data resolution has been changed to match that of the narrow band model.

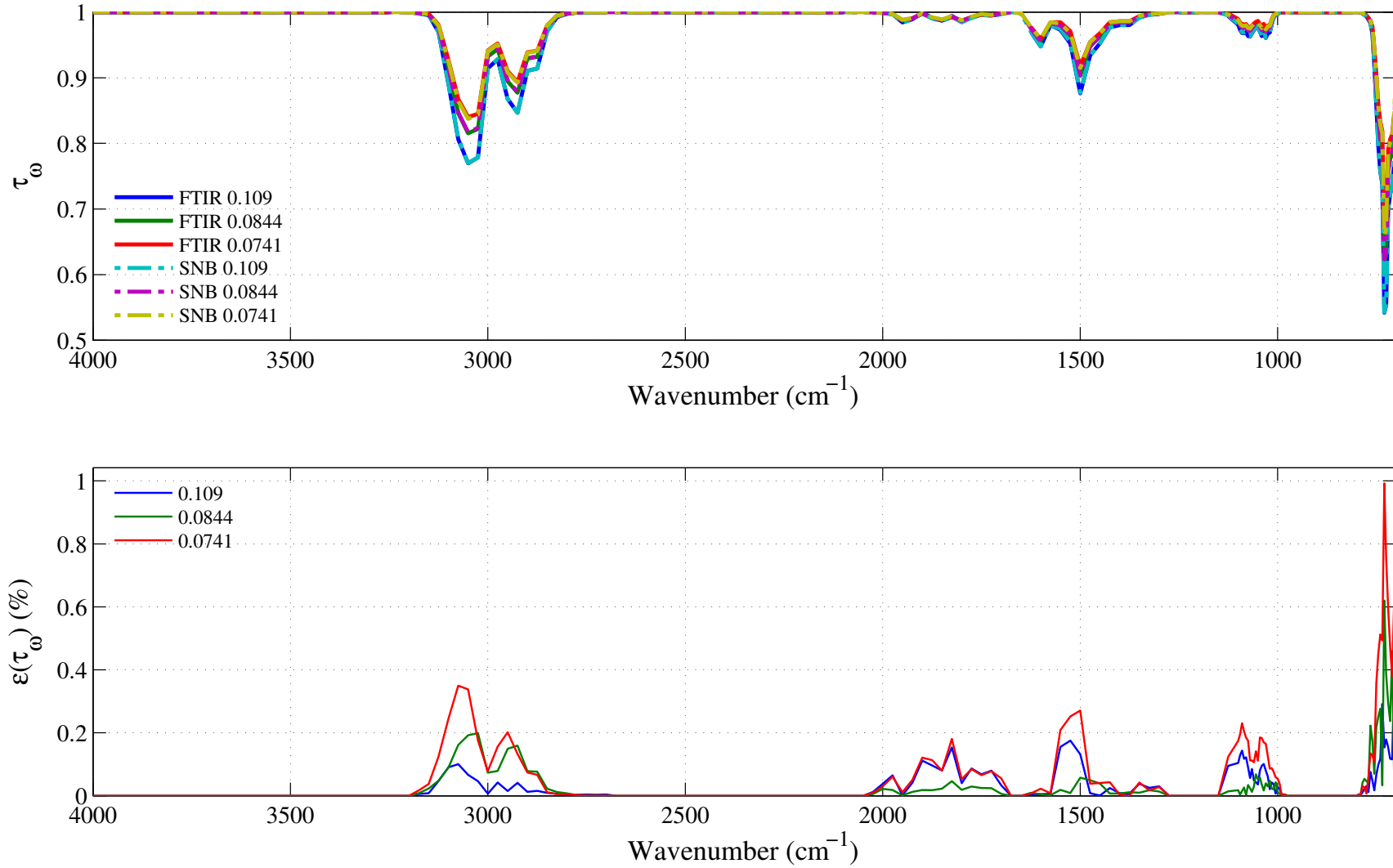


Figure 4.48: Top: comparison between the experimental (FTIR, in solid lines) and the synthetic (dashed lines) spectral transmissivity profiles, denoted τ_ω , of an isothermal homogeneous column of toluene. The synthetic profiles was generated using the Malkmus narrow band parameters presented in Figs. 4.41 to 4.45. Bottom: relative transmissivity error, denoted $\varepsilon(\tau_\omega)$, between the experiment and the synthetic profiles presented on the top figure. Three different pressure-paths are considered: 0.109, 0.0844 and 0.0741. The gas temperature is set at 440 K and the total pressure is 101 kPa. Note: the experimental data resolution has been changed to match that of the narrow band model.

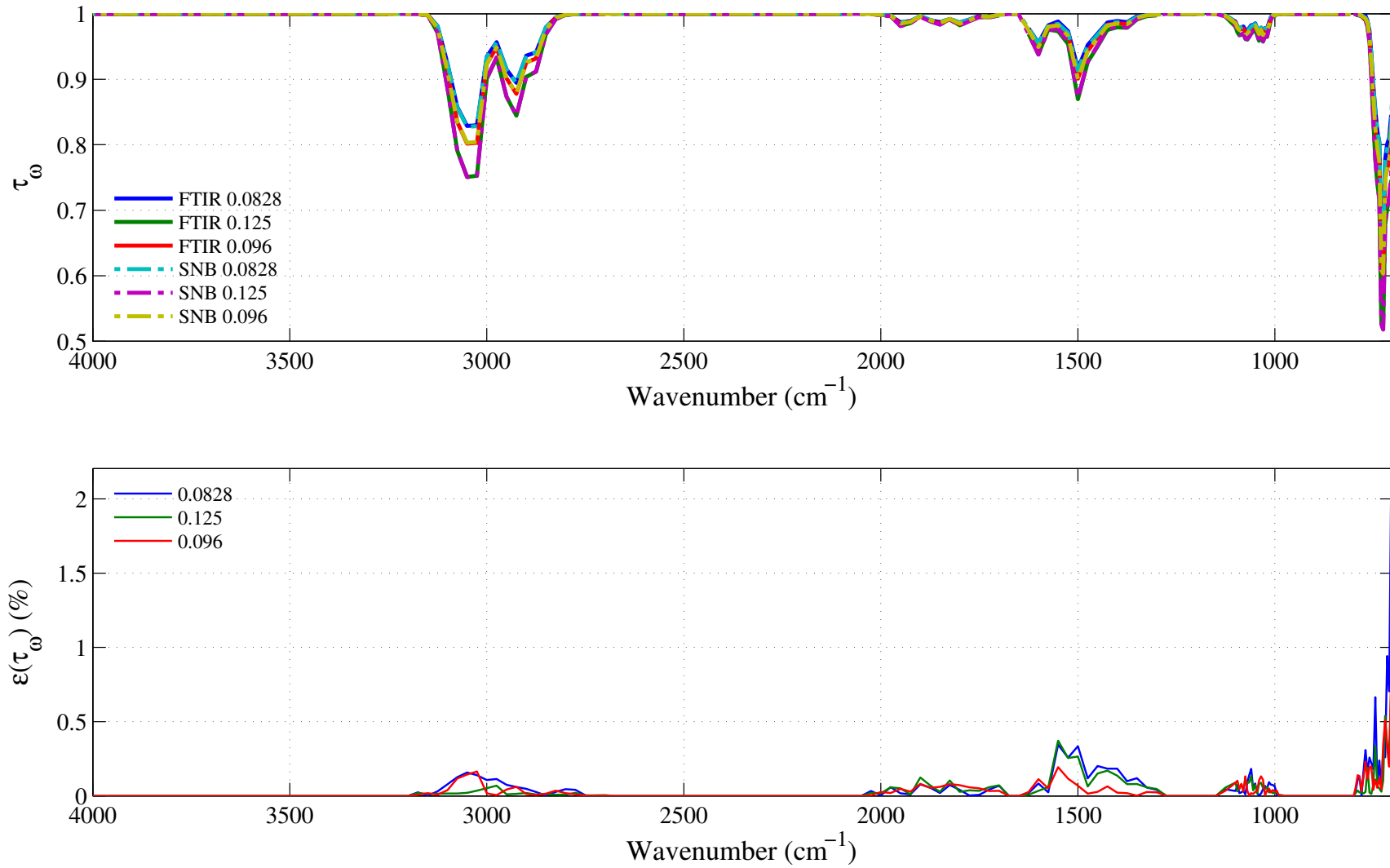


Figure 4.49: Top: comparison between the experimental (FTIR, in solid lines) and the synthetic (dashed lines) spectral transmissivity profiles, denoted τ_ω , of an isothermal homogeneous column of toluene. The synthetic profiles was generated using the Malkmus narrow band parameters presented in Figs. 4.41 to 4.45. Bottom: relative transmissivity error, denoted $\varepsilon(\tau_\omega)$, between the experiment and the synthetic profiles presented on the top figure. Three different pressure-paths are considered: 0.125, 0.096 and 0.0828 atm.cm. The gas temperature is set at 477 K and the total pressure is 101 kPa. Note: the experimental data resolution has been changed to match that of the narrow band model.

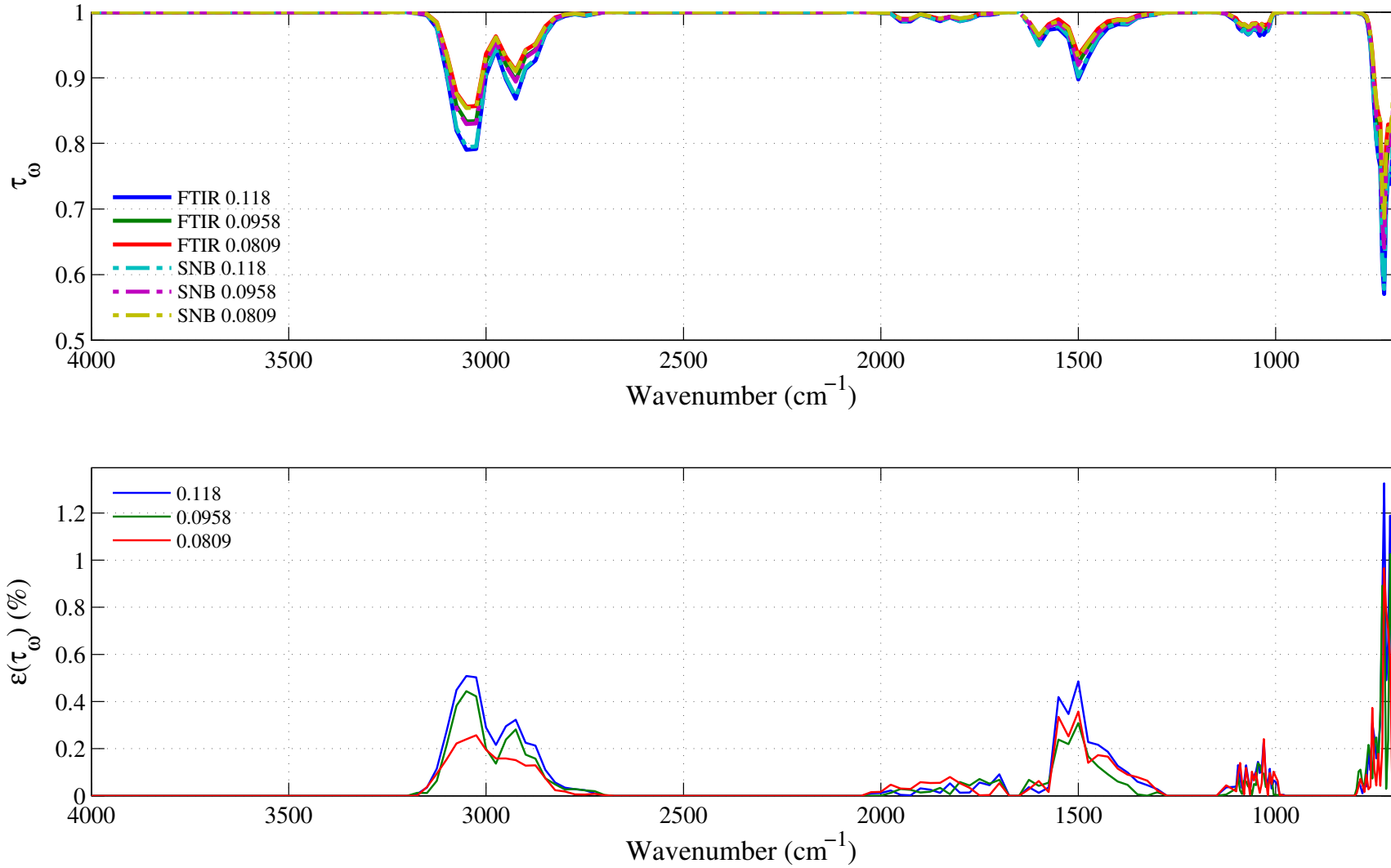


Figure 4.50: Top: comparison between the experimental (FTIR, in solid lines) and the synthetic (dashed lines) spectral transmissivity profiles, denoted τ_ω , of an isothermal homogeneous column of toluene. The synthetic profiles was generated using the Malkmus narrow band parameters presented in Figs. 4.41 to 4.45. Bottom: relative transmissivity error, denoted $\varepsilon(\tau_\omega)$, between the experiment and the synthetic profiles presented on the top figure. Three different pressure-paths are considered: 0.118, 0.0958 and 0.0809 atm.cm. The gas temperature is set at 587 K and the total pressure is 101 kPa. Note: the experimental data resolution has been changed to match that of the narrow band model.

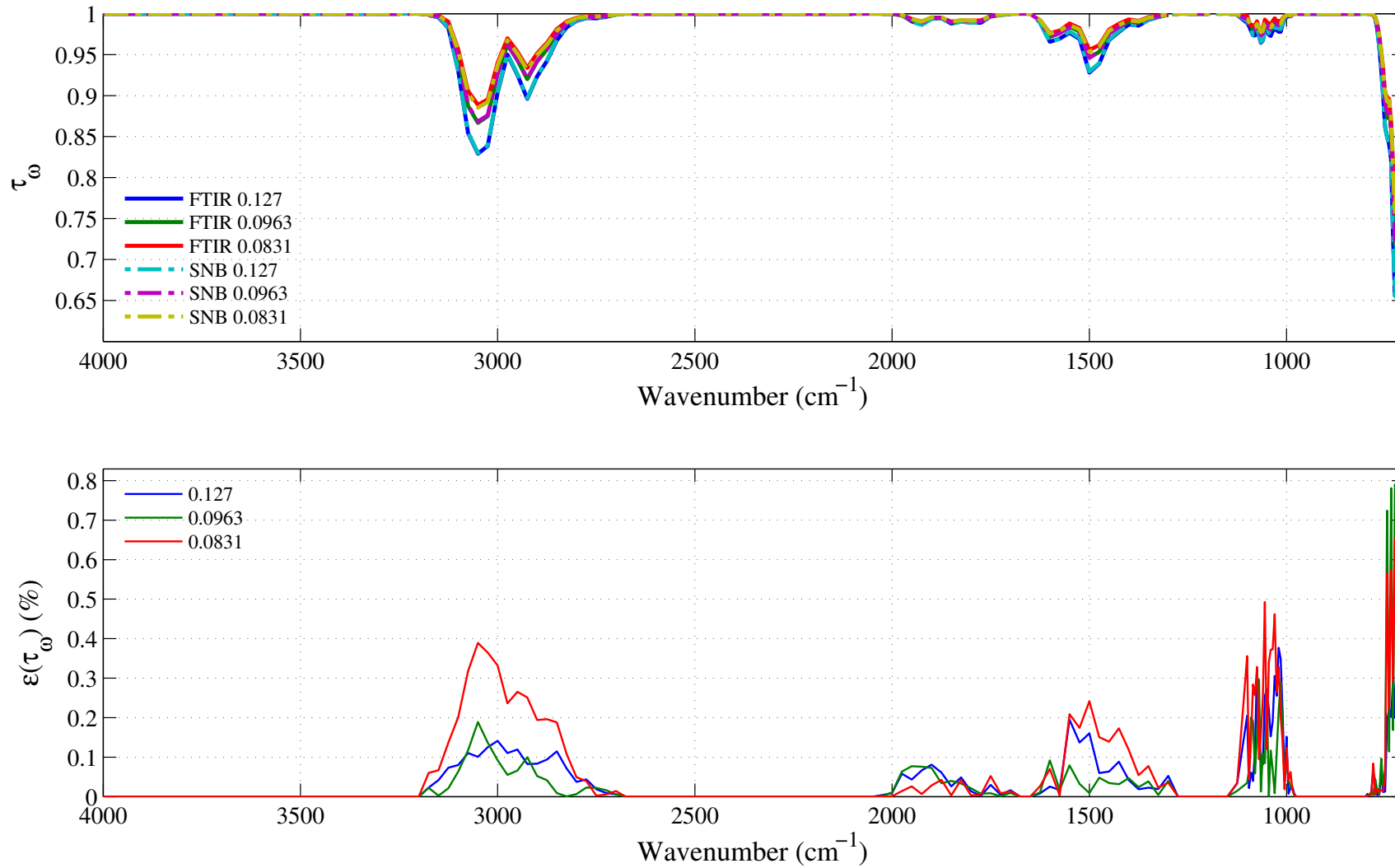


Figure 4.51: Top: comparison between the experimental (FTIR, in solid lines) and the synthetic (dashed lines) spectral transmissivity profiles, denoted τ_ω , of an isothermal homogeneous column of toluene. The synthetic profiles was generated using the Malkmus narrow band parameters presented in Figs. 4.41 to 4.45. Bottom: relative transmissivity error, denoted $\varepsilon(\tau_\omega)$, between the experiment and the synthetic profiles presented on the top figure. Three different pressure-paths are considered: 0.127, 0.0963 and 0.0831 atm.cm. The gas temperature is set at 795 K and the total pressure is 101 kPa. Note: the experimental data resolution has been changed to match that of the narrow band model.

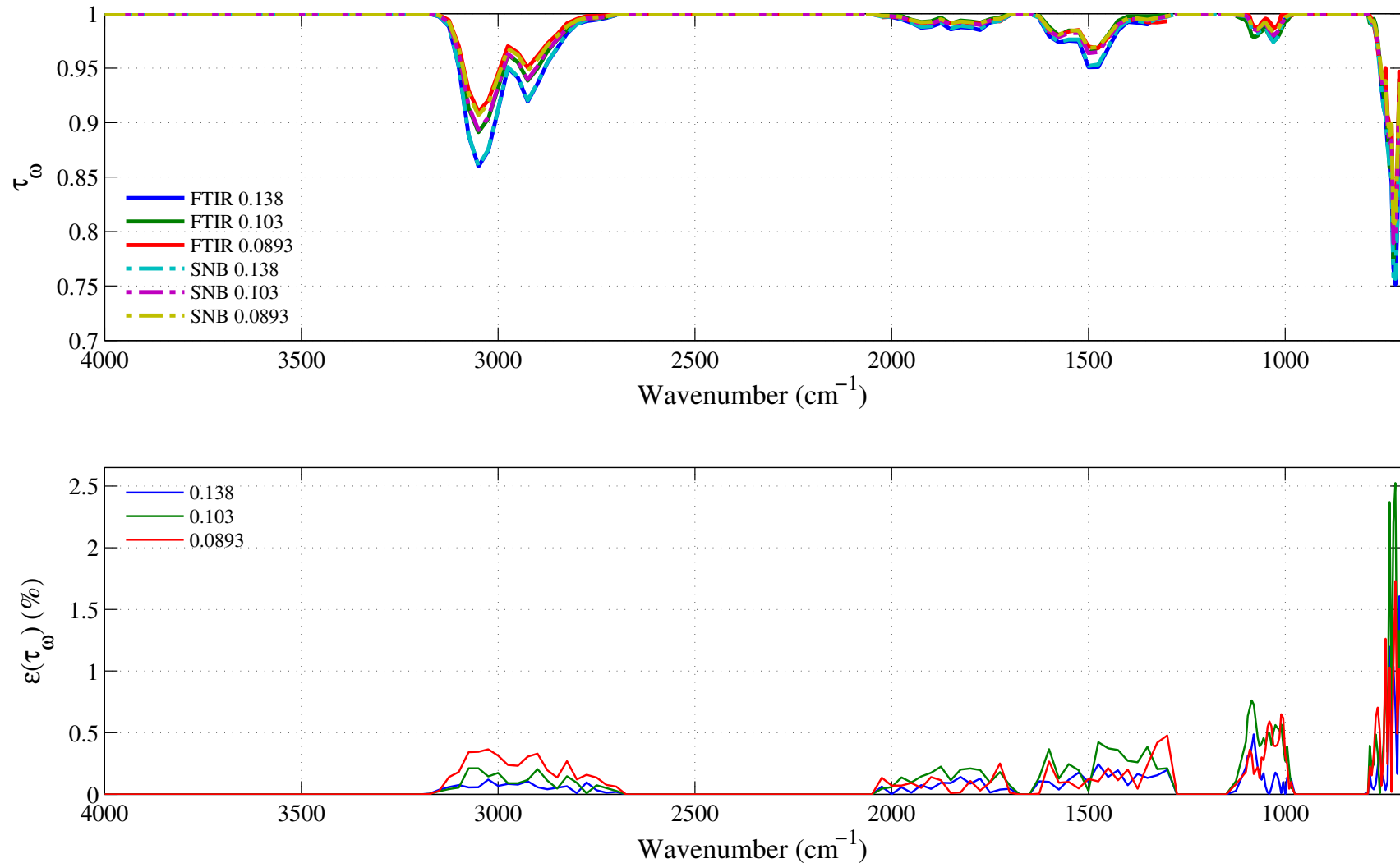


Figure 4.52: Top: comparison between the experimental (FTIR, in solid lines) and the synthetic (dashed lines) spectral transmissivity profiles, denoted τ_ω , of an isothermal homogeneous column of toluene. The synthetic profiles were generated using the Malkmus narrow band parameters presented in Figs. 4.41 to 4.45. Bottom: relative transmissivity error, denoted $\varepsilon(\tau_\omega)$, between the experiment and the synthetic profiles presented on the top figure. Three different pressure-paths are considered: 0.138, 0.103 and 0.0893 atm.cm. The gas temperature is set at 999 K and the total pressure is 101 kPa. Note: the experimental data resolution has been changed to match that of the narrow band model.

4.8 *n*-Heptane: C₇H₁₆

4.8.1 Integrated Band Intensity

n-heptane, C₇H₁₆, has two planes of symmetry and two axes of rotation. It belongs to the point group C_{2v} [18]. The *n*-heptane IR spectrum results from the vibration-rotation modes of the C – C, CH₂, and CH₃ groups. It has 63 vibrational modes. In RADCAL, its IR spectrum has been divided into two distinct bands. The first band from 1100–1800 cm^{−1} is associated with the bending motion of the CH₂ and CH₃ chemical groups. The second band from 2250–3275 cm^{−1} is associated with the stretching motion of the CH₂ and CH₃ chemical groups. This band has the highest integrated band intensity. Its value is more than 10 times that of the first band, see Table 4.6.

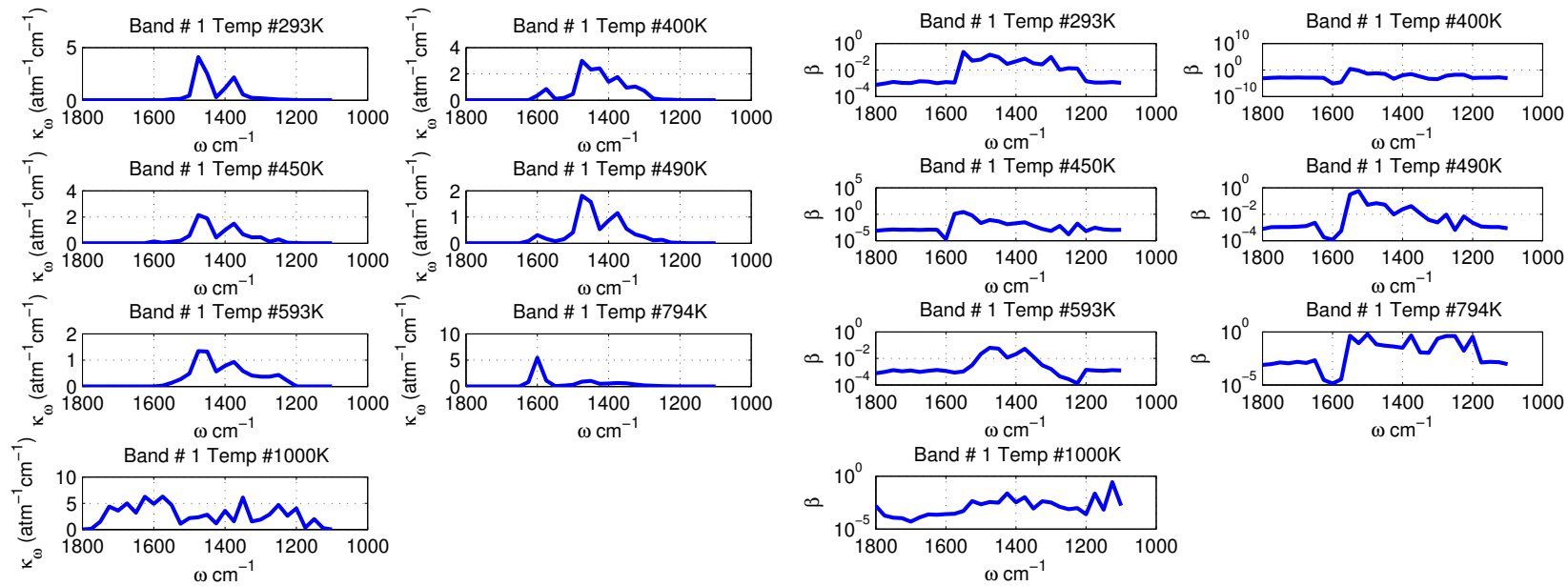
Table 4.6: Spectral bands of C₇H₁₆ included in RADCAL.

Band #	Bounds (cm ^{−1})		Assignment	$\alpha(T = 293 \text{ K}) (\text{atm}^{-1}\text{cm}^{-2})$
1	1100	1800	CH ₂ , CH ₃ Bending	304
2	2250	3275	CH ₂ , CH ₃ Stretching	3165

4.8.2 Malkmus Narrow Band Parameters

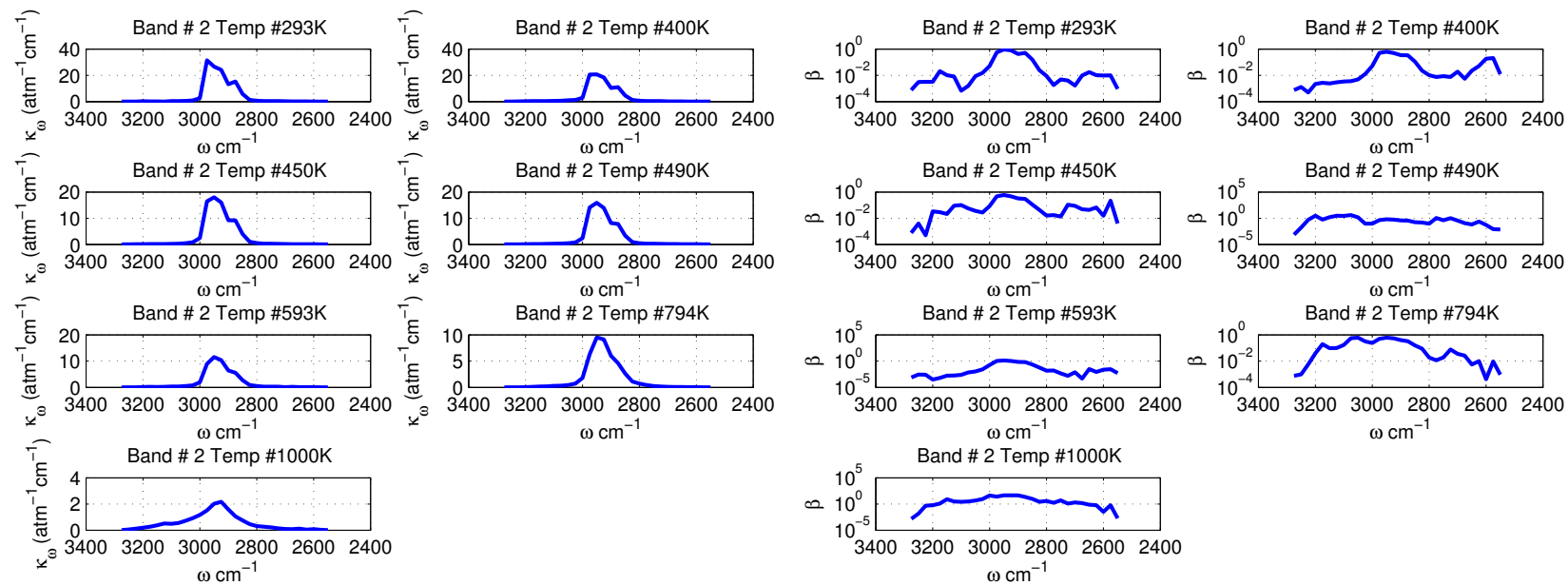
All the *n*-heptane IR spectral absorption data were obtained from high resolution FTIR experiments with temperatures varying from 293 K to 794 K. The spectral absorption coefficients were obtained by fitting the experimental spectral transmissivity of a homogeneous column of isothermal *n*-heptane with a total pressure of 1 atm using the Malkmus model.

The *n*-heptane narrow band parameters, $\bar{\kappa}$ and β , for temperatures ranging from 293 K to 1000 K are plotted in Figures 4.53–4.54 for Bands 1 and 2.



(a) Narrow band spectral absorption coefficient $\bar{\kappa}$ (in $\text{atm}^{-1}\text{cm}^{-1}$) for the 1100–1800 cm^{-1} band.
(b) Narrow band spectral fine structure parameter β (in atm^{-1}) for the 1100–1800 cm^{-1} band.

Figure 4.53: *n*-heptane narrow band parameters $\bar{\kappa}$ and β obtained for the 1100–1800 cm^{-1} band corresponding to the bending motion of the CH_2 and CH_3 chemical groups. Temperatures plotted are: 293, 400, 450, 490, 593, 794, and 1000 K. The narrow band resolution $\Delta\omega$ is 25 cm^{-1} .



(a) Narrow band spectral absorption coefficient $\bar{\kappa}$ (in $\text{atm}^{-1}\text{cm}^{-1}$) for the 2250–3275 cm^{-1} band.
(b) Narrow band spectral fine structure parameter β (in atm^{-1}) for the 2250–3275 cm^{-1} band.

Figure 4.54: *n*-heptane narrow band parameters $\bar{\kappa}$ and β obtained for the 2250–3275 cm^{-1} band corresponding to the stretching motion of the CH_2 and CH_3 chemical groups. Temperatures plotted are: 293, 400, 450, 490, 593, 794, and 1000 K. The narrow band resolution $\Delta\omega$ is 25 cm^{-1} .

4.8.3 Verification SNB Parameters

To assess the accuracy of the narrow band parameters $\bar{\kappa}$ and β , synthetic transmissivities were constructed for the same experimental conditions as the FTIR data and compare with it. This subsection plots the comparison and the relative error in transmissivity (relative to FTIR measurements) using the *n*-heptane parameters presented in Figs. 4.53 to 4.54.

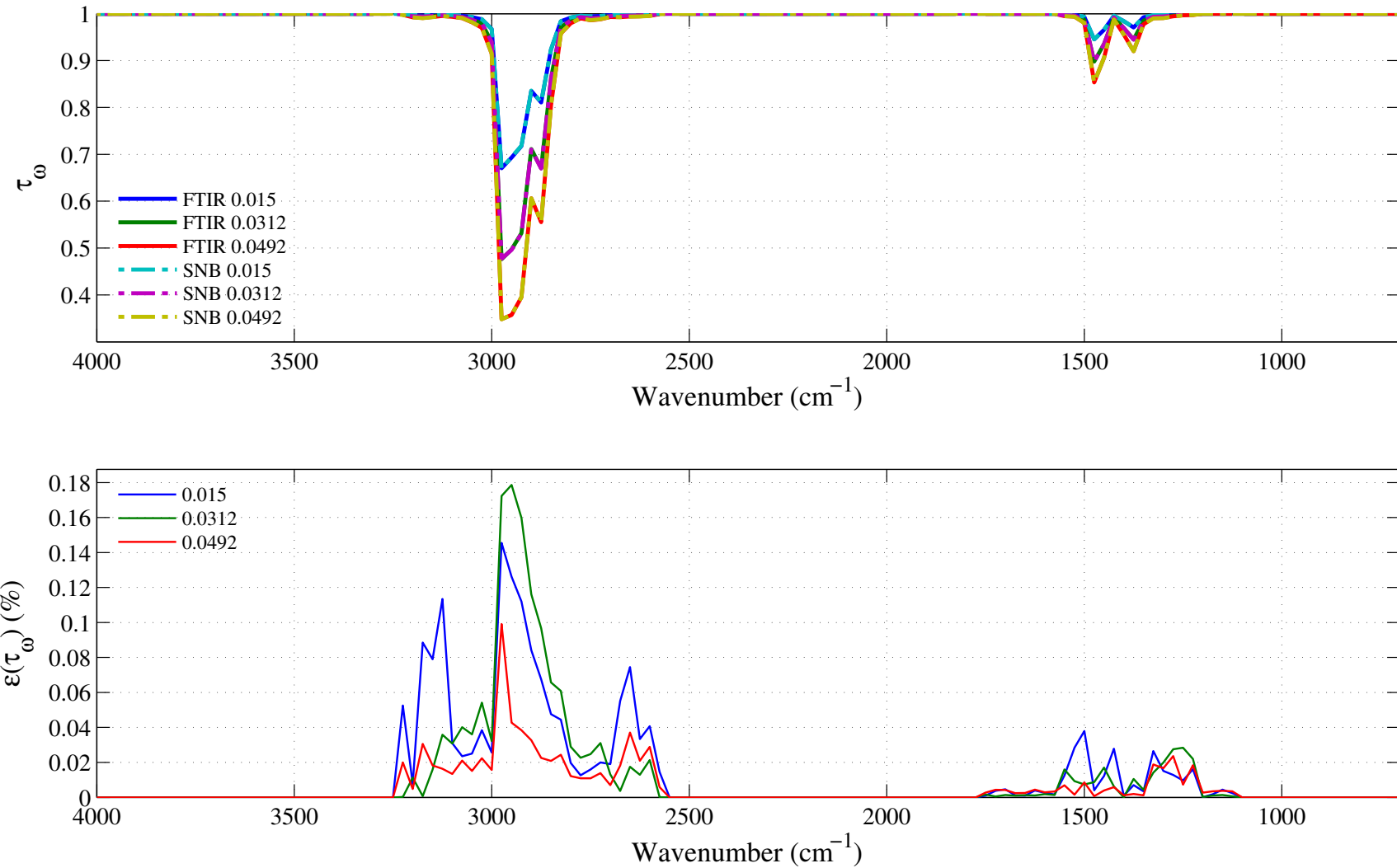


Figure 4.55: Top: comparison between the experimental (FTIR, in solid lines) and the synthetic (dashed lines) spectral transmissivity profiles, denoted τ_ω , of an isothermal homogeneous column of *n*-heptane. The synthetic profiles was generated using the Malkmus narrow band parameters presented in Figs. 4.53 to 4.54. Bottom: relative transmissivity error, denoted $\varepsilon(\tau_\omega)$, between the experiment and the synthetic profiles presented on the top figure. Three different pressure-paths are considered: 0.0492, 0.0312 and 0.015 atm.cm. The gas temperature is set at 293 K and the total pressure is 101 kPa. Note: the experimental data resolution has been changed to match that of the narrow band model.

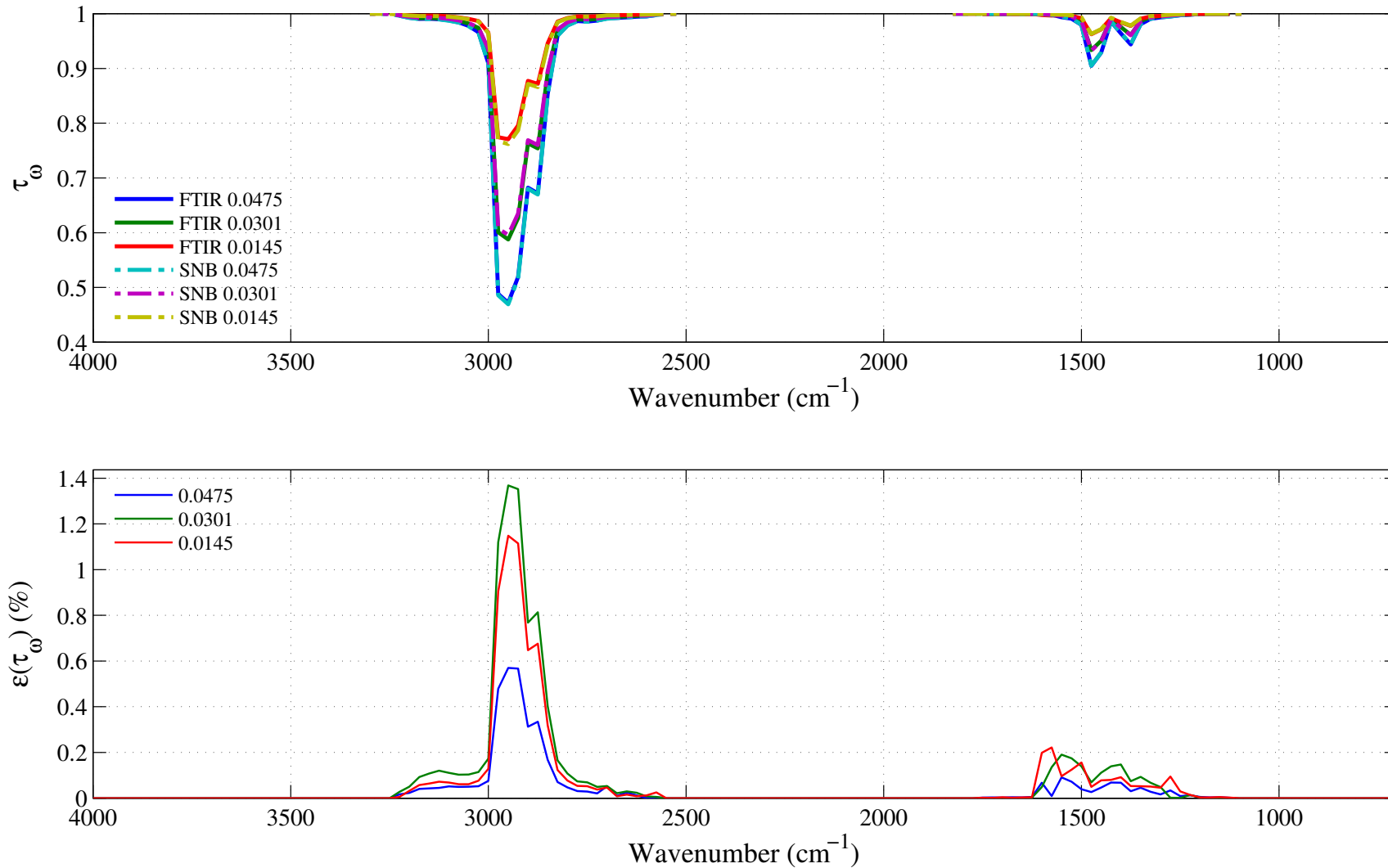


Figure 4.56: Top: comparison between the experimental (FTIR, in solid lines) and the synthetic (dashed lines) spectral transmissivity profiles, denoted τ_{ω} , of an isothermal homogeneous column of *n*-heptane. The synthetic profiles was generated using the Malkmus narrow band parameters presented in Figs. 4.53 to 4.54. Bottom: relative transmissivity error, denoted $\varepsilon(\tau_{\omega})$, between the experiment and the synthetic profiles presented on the top figure. Three different pressure-paths are considered: 0.0475, 0.0301 and 0.0145 atm.cm. The gas temperature is set at 400 K and the total pressure is 101 kPa. Note: the experimental data resolution has been changed to match that of the narrow band model.

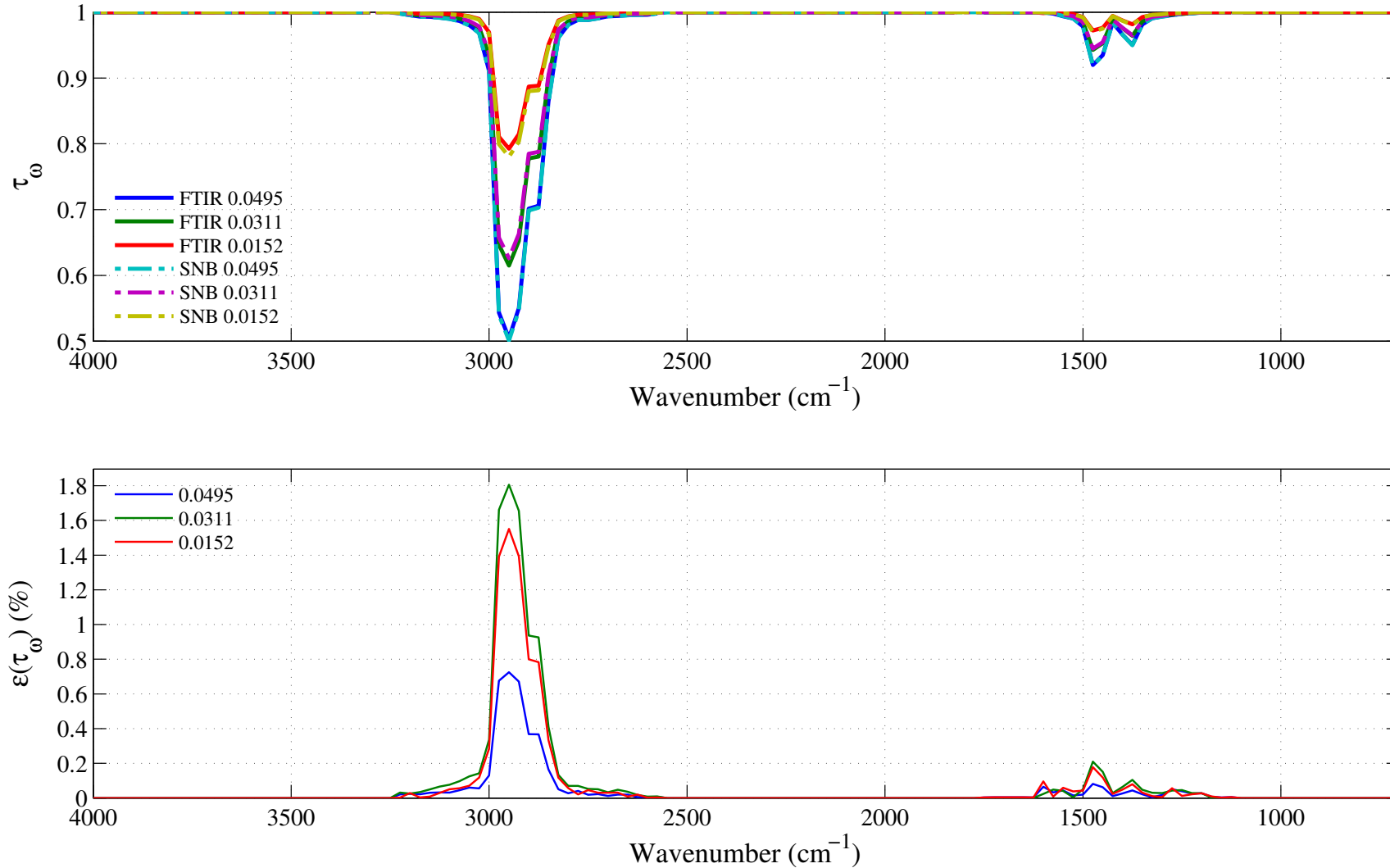


Figure 4.57: Top: comparison between the experimental (FTIR, in solid lines) and the synthetic (dashed lines) spectral transmissivity profiles, denoted τ_ω , of an isothermal homogeneous column of *n*-heptane. The synthetic profiles were generated using the Malkmus narrow band parameters presented in Figs. 4.53 to 4.54. Bottom: relative transmissivity error, denoted $\varepsilon(\tau_\omega)$, between the experiment and the synthetic profiles presented on the top figure. Three different pressure-paths are considered: 0.0495, 0.0311 and 0.0152. The gas temperature is set at 450 K and the total pressure is 101 kPa. Note: the experimental data resolution has been changed to match that of the narrow band model.

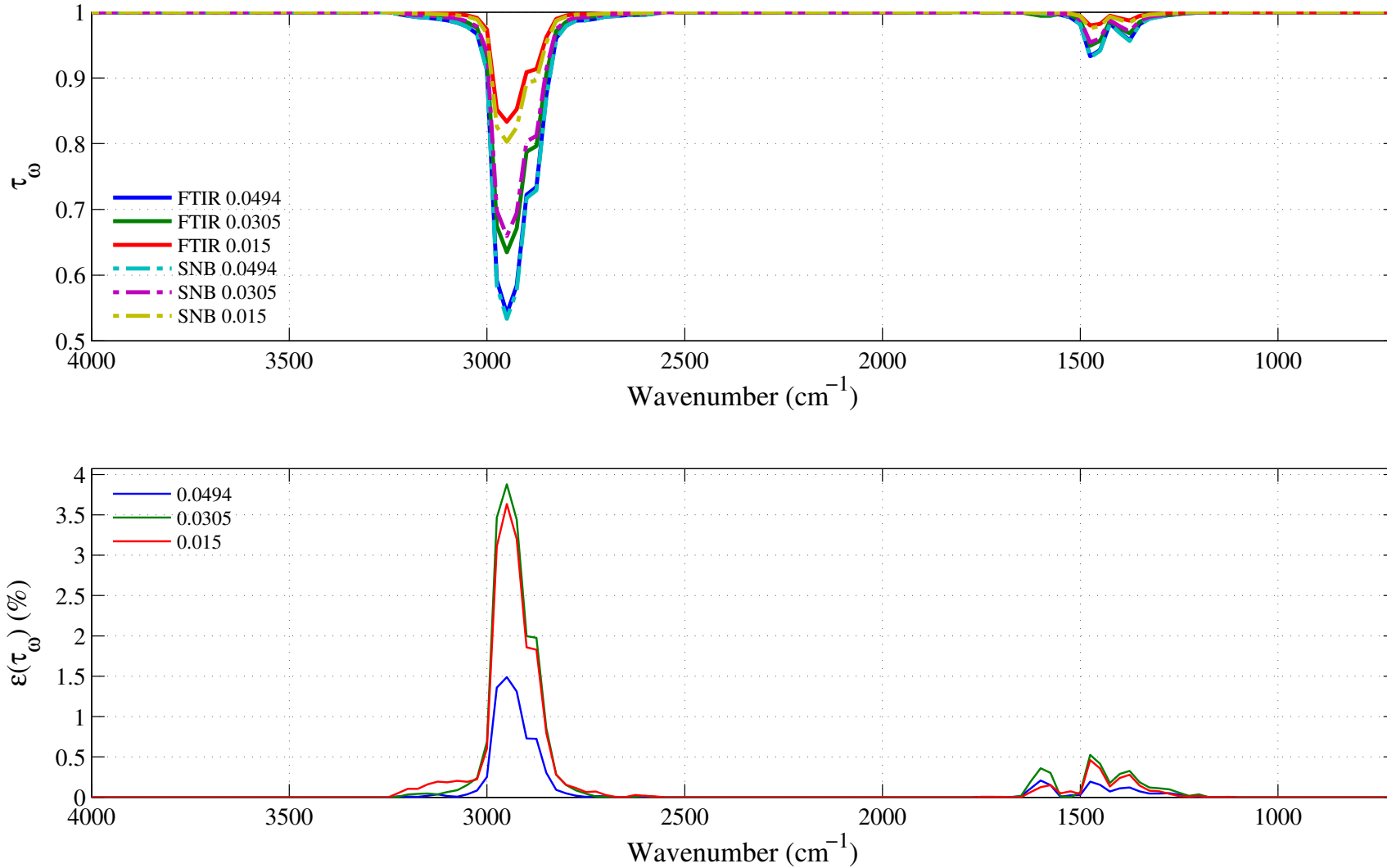


Figure 4.58: Top: comparison between the experimental (FTIR, in solid lines) and the synthetic (dashed lines) spectral transmissivity profiles, denoted τ_ω , of an isothermal homogeneous column of *n*-heptane. The synthetic profiles was generated using the Malkmus narrow band parameters presented in Figs. 4.53 to 4.54. Bottom: relative transmissivity error, denoted $\varepsilon(\tau_\omega)$, between the experiment and the synthetic profiles presented on the top figure. Three different pressure-paths are considered: 0.0494, 0.0305 and 0.015 atm.cm. The gas temperature is set at 490 K and the total pressure is 101 kPa. Note: the experimental data resolution has been changed to match that of the narrow band model.

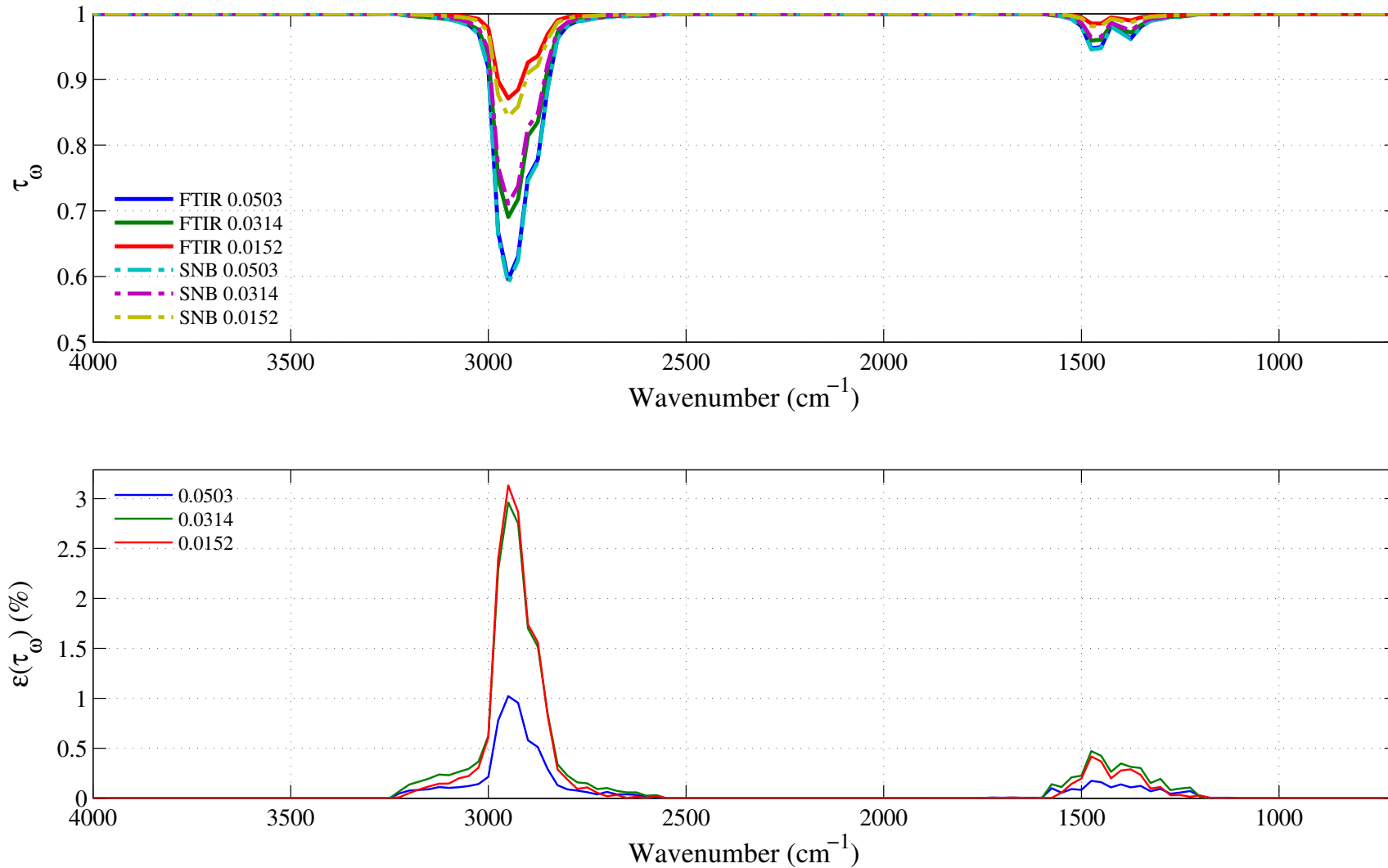


Figure 4.59: Top: comparison between the experimental (FTIR, in solid lines) and the synthetic (dashed lines) spectral transmissivity profiles, denoted τ_ω , of an isothermal homogeneous column of *n*-heptane. The synthetic profiles was generated using the Malkmus narrow band parameters presented in Figs. 4.53 to 4.54. Bottom: relative transmissivity error, denoted $\varepsilon(\tau_\omega)$, between the experiment and the synthetic profiles presented on the top figure. Three different pressure-paths are considered: 0.0503, 0.0314 and 0.0152 atm.cm. The gas temperature is set at 593 K and the total pressure is 101 kPa. Note: the experimental data resolution has been changed to match that of the narrow band model.

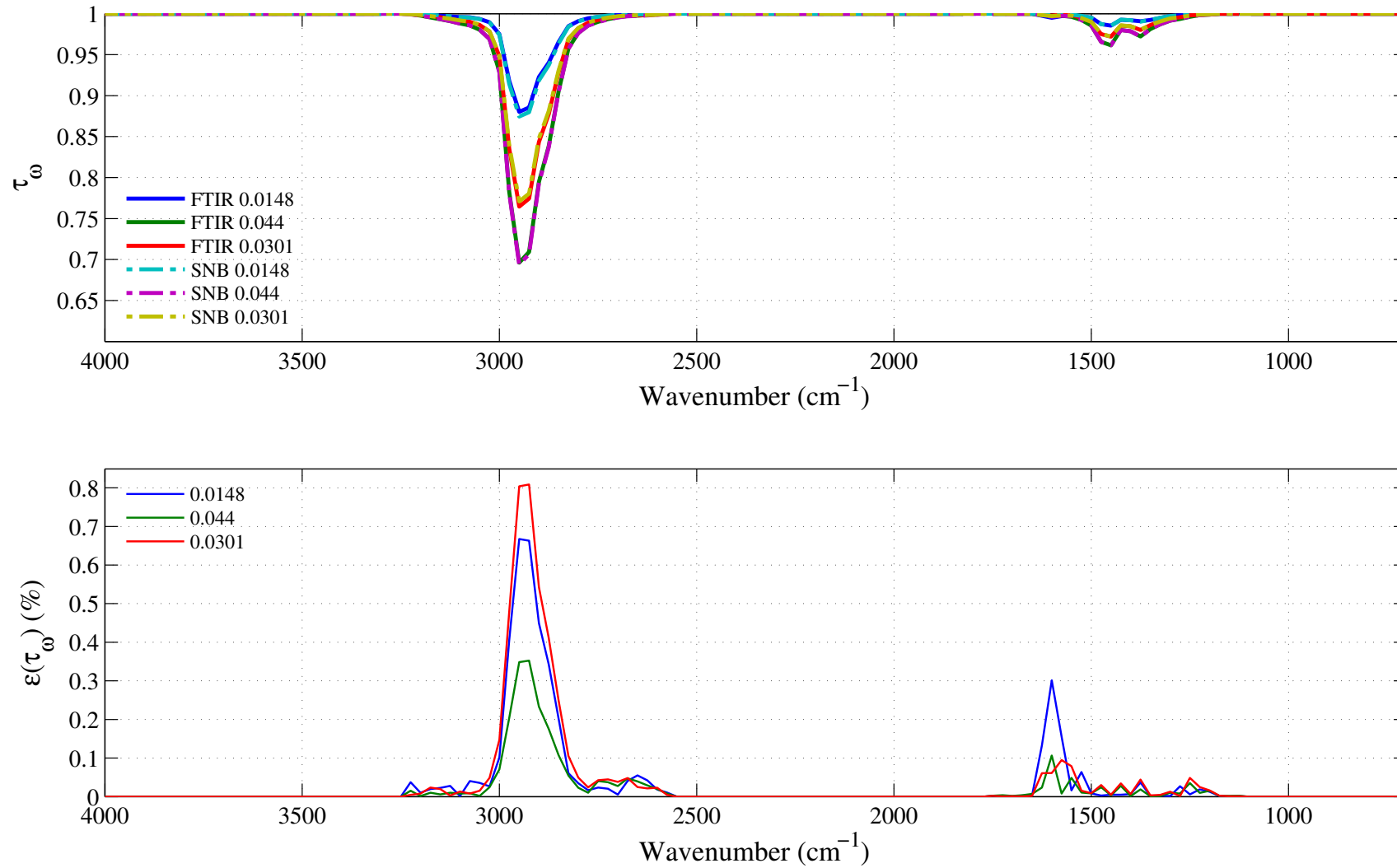


Figure 4.60: Top: comparison between the experimental (FTIR, in solid lines) and the synthetic (dashed lines) spectral transmissivity profiles, denoted τ_ω , of an isothermal homogeneous column of *n*-heptane. The synthetic profiles was generated using the Malkmus narrow band parameters presented in Figs. 4.53 to 4.54. Bottom: relative transmissivity error, denoted $\varepsilon(\tau_\omega)$, between the experiment and the synthetic profiles presented on the top figure. Three different pressure-paths are considered: 0.044, 0.0301, and 0.0148 atm.cm. The gas temperature is set at 794 K and the total pressure is 101 kPa. Note: the experimental data resolution has been changed to match that of the narrow band model.

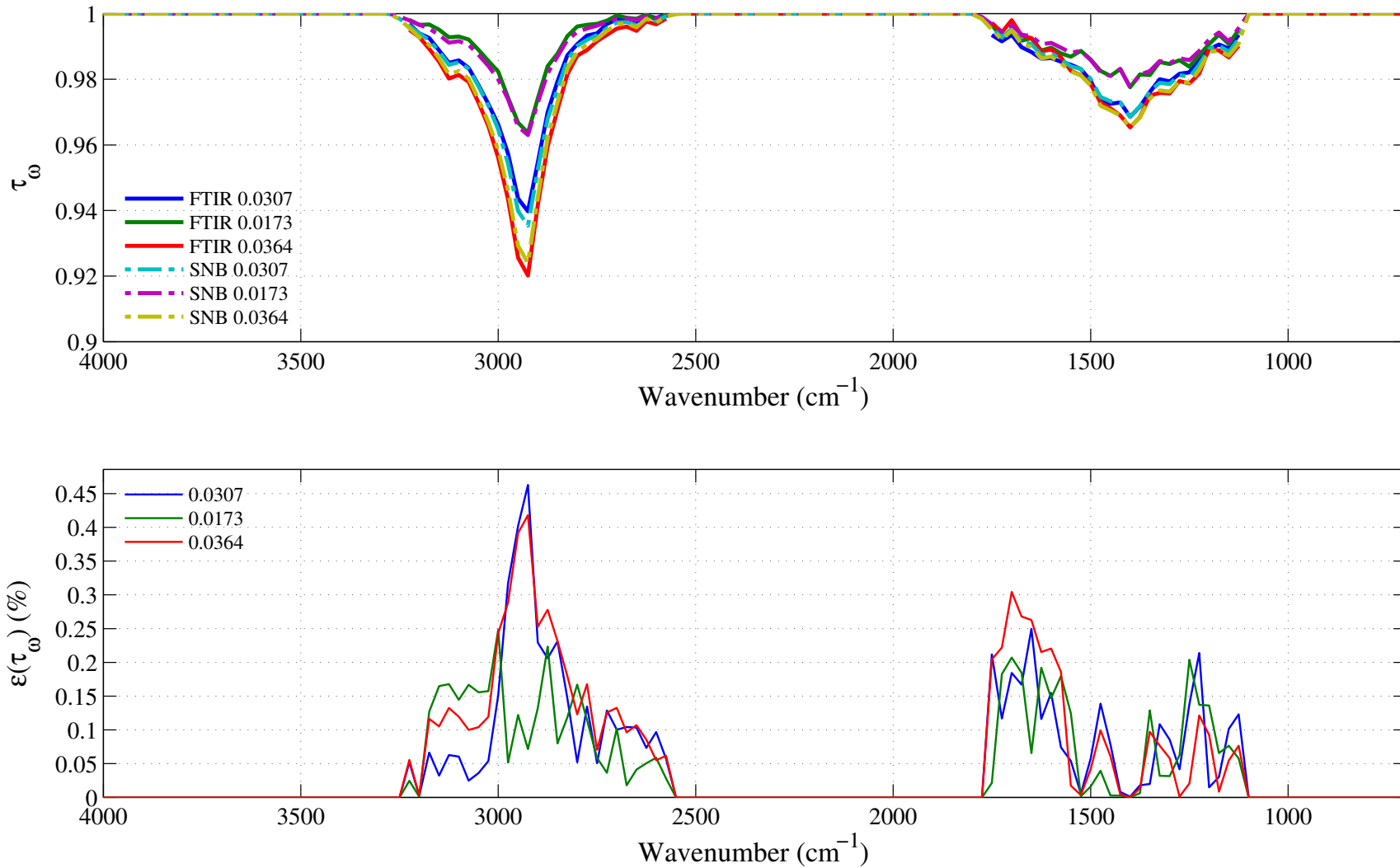


Figure 4.61: Top: comparison between the experimental (FTIR, in solid lines) and the synthetic (dashed lines) spectral transmissivity profiles, denoted τ_ω , of an isothermal homogeneous column of *n*-heptane. The synthetic profiles was generated using the Malkmus narrow band parameters presented in Figs. 4.53 to 4.54. Bottom: relative transmissivity error, denoted $\varepsilon(\tau_\omega)$, between the experiment and the synthetic profiles presented on the top figure. Three different pressure-paths are considered: 0.0364, 0.0307 and 0.0173 atm.cm. The gas temperature is set at 1000 K and the total pressure is 101 kPa. Note: the experimental data resolution has been changed to match that of the narrow band model.

4.9 Methanol: CH₃OH

4.9.1 Integrated Band Intensity

Methanol, CH₃OH, has only one plane of symmetry. It belongs to the point group C_s [18]. Its IR spectrum results from the vibration-rotation modes of the C – O, OH, and CH₃ groups. It has 12 vibrational modes. In RADCAL, its IR spectrum has been divided into four distinct bands. The first band from 825–1125 cm⁻¹ is associated with the stretching motion of the C – O chemical group. The second band from 1125–1700 cm⁻¹ is associated with the bending motion of the CH₃ and OH chemical groups. The third band from 2600–3225 cm⁻¹ is associated with the stretching motion of the CH₃ chemical group. The fourth and last band from 3525–3850 cm⁻¹ is associated with the stretching motion of the OH chemical group. The strongest absorbing bands are the third band (2600–3225 cm⁻¹) and the first band (825–1125 cm⁻¹). See Table 4.7.

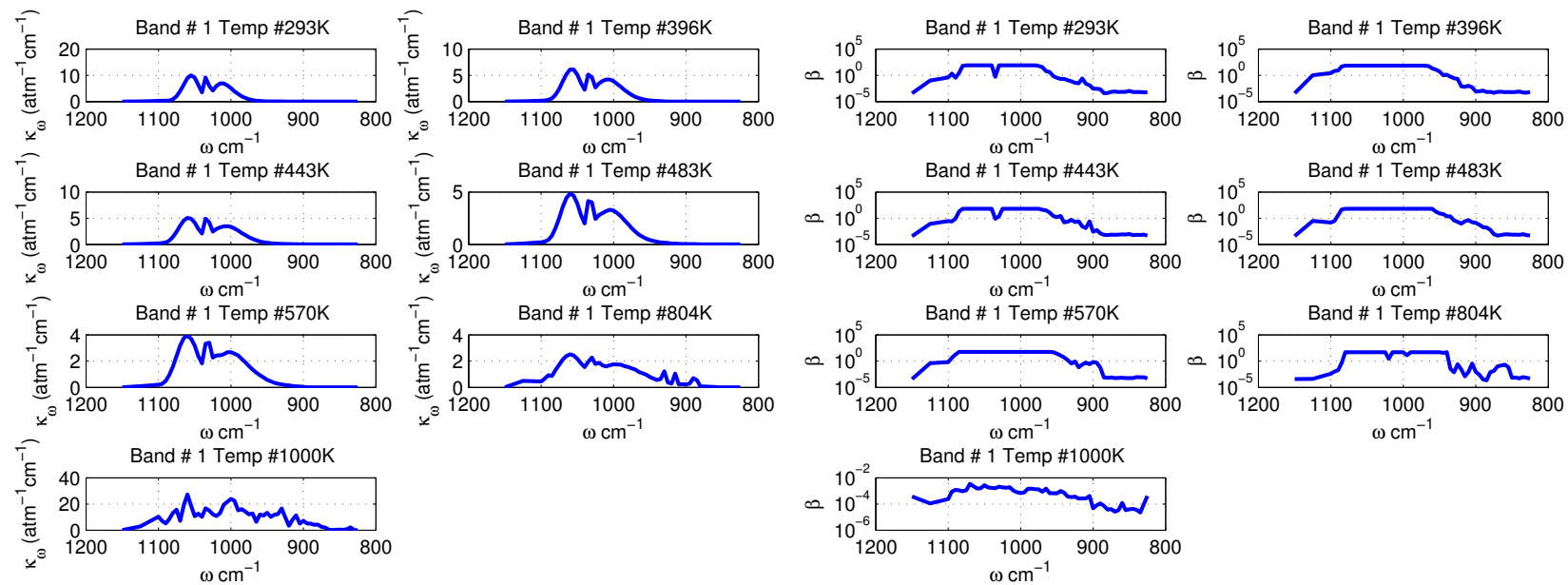
Table 4.7: Spectral bands of CH₃OH included in RADCAL.

Band #	Bounds (cm ⁻¹)		Assignment	$\alpha(T = 293 \text{ K}) (\text{atm}^{-1}\text{cm}^{-2})$
1	825	1125	C – O Stretching	598
2	1125	1700	CH ₃ , OH Bending	199
3	2600	3225	CH ₃ Stretching	680
4	3525	3850	OH Stretching	112

4.9.2 Malkmus Narrow Band Parameters

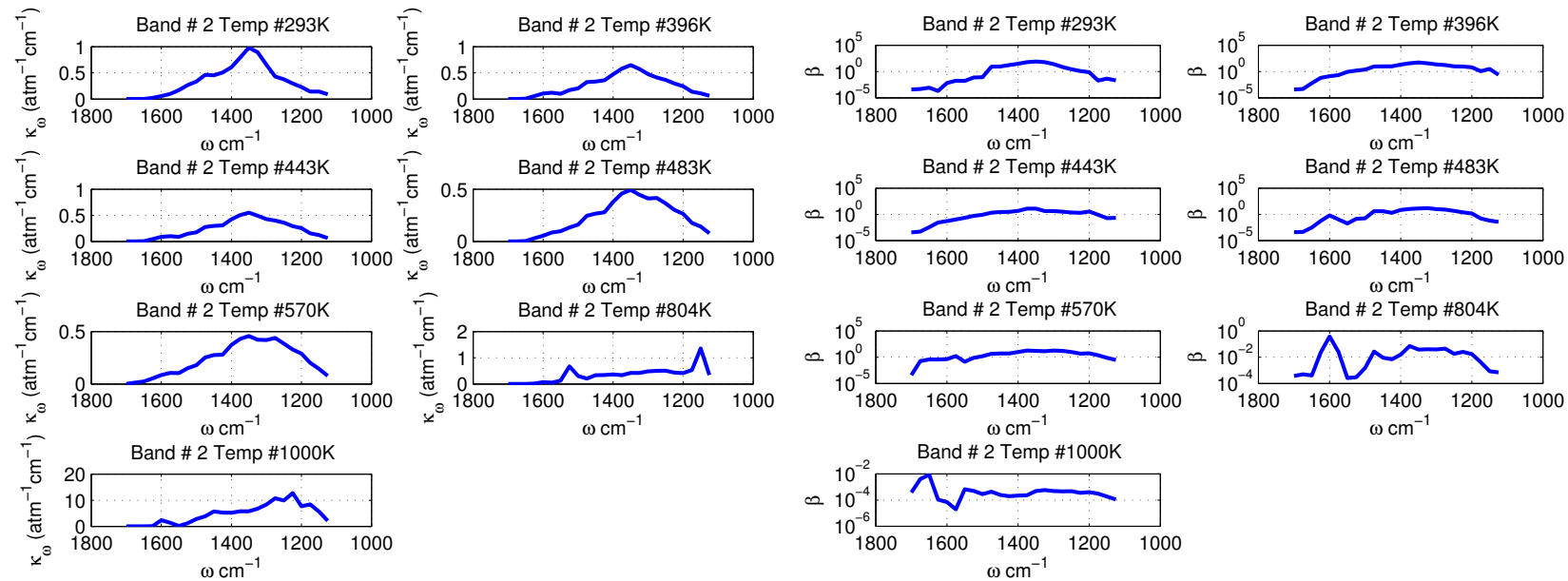
All the methanol IR spectral absorption data were obtained from high resolution FTIR experiments with temperatures varying from 293 K to 804 K. The spectral absorption coefficients were obtained by fitting the experimental spectral transmissivity of a homogeneous column of isothermal methanol with a total pressure of 1 atm using the Malkmus model.

The methanol narrow band parameters, $\bar{\kappa}$ and β , for temperatures ranging from 293 K to 1000 K are plotted in Figures 4.62–4.65 for Bands 1 to 4.



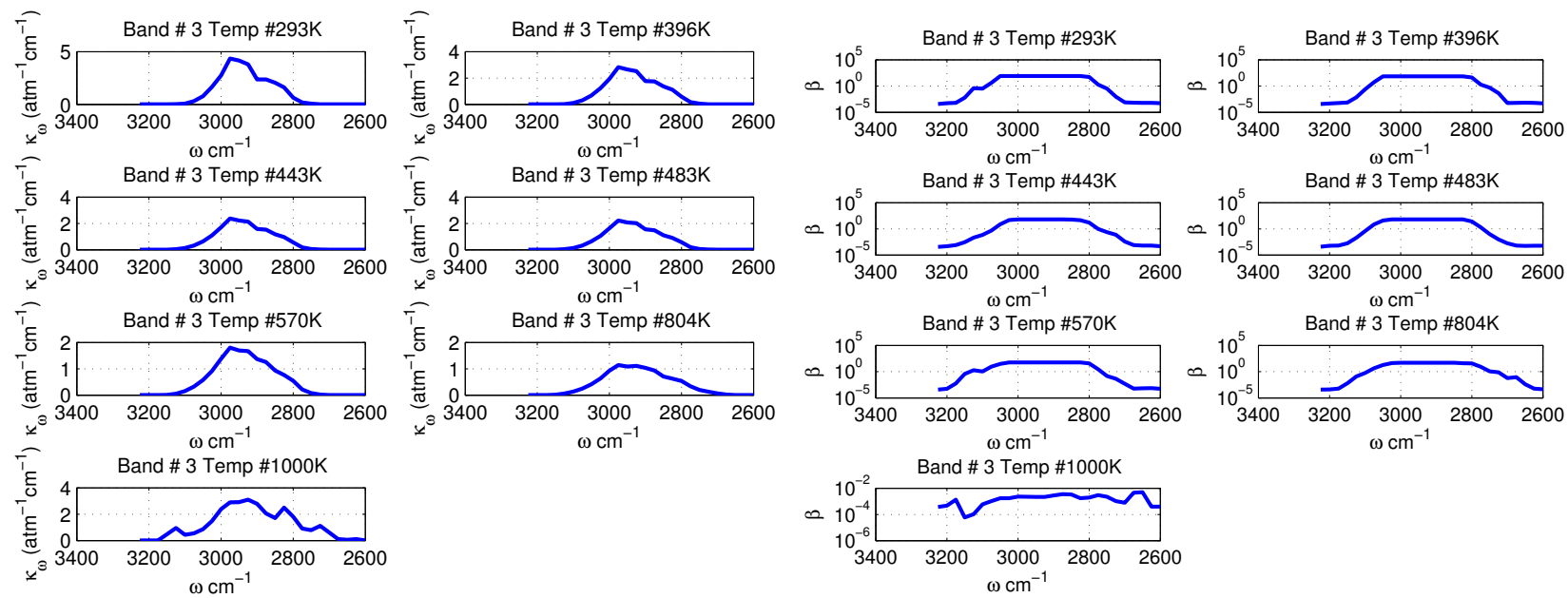
(a) Narrow band spectral absorption coefficient $\bar{\kappa}$ (in $\text{atm}^{-1}\text{cm}^{-1}$) for the 825–1125 cm^{-1} band.
(b) Narrow band spectral fine structure parameter β (in atm^{-1}) for the 825–1125 cm^{-1} band.

Figure 4.62: Methanol narrow band parameters $\bar{\kappa}$ and β obtained for the 825–1125 cm^{-1} band corresponding to the stretching motion of the C – O chemical group. Temperatures plotted are: 293, 396, 443, 483, 570, 804, and 1000 K. The narrow band resolution $\Delta\omega$ is 5 cm^{-1} .



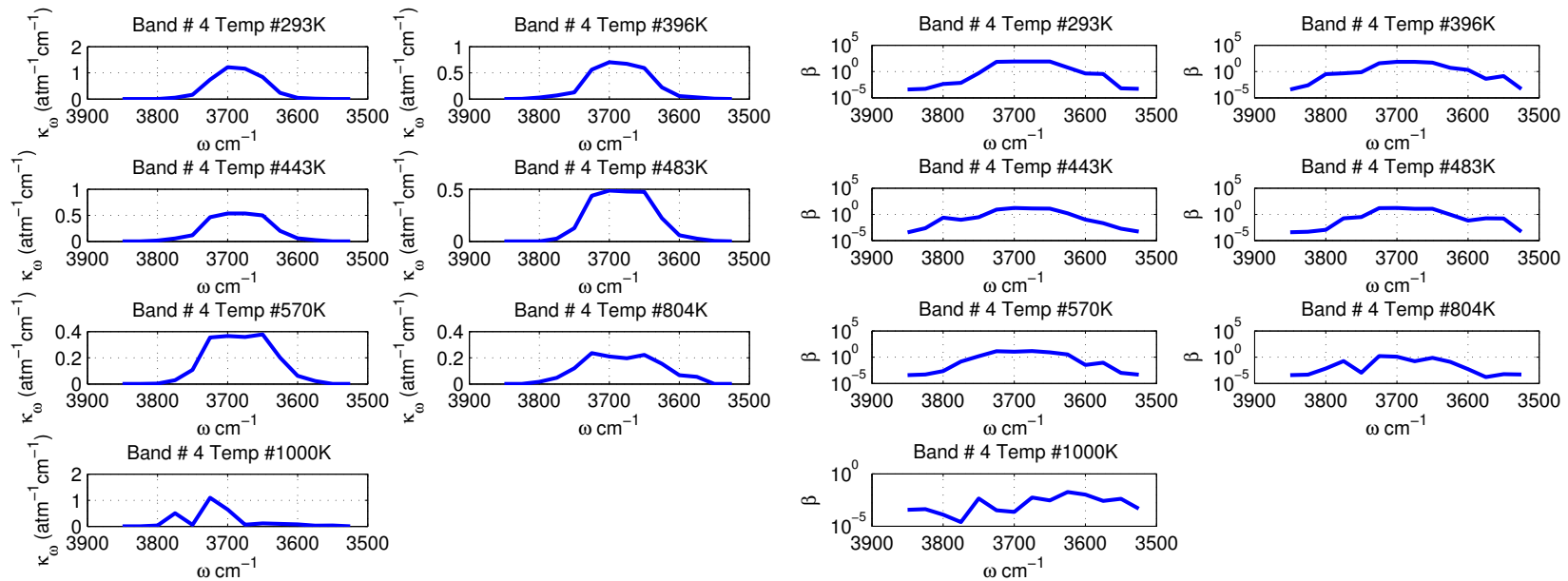
(a) Narrow band spectral absorption coefficient $\bar{\kappa}$ (in $\text{atm}^{-1}\text{cm}^{-1}$) for the 1125–1700 cm^{-1} band.
(b) Narrow band spectral fine structure parameter β (in atm^{-1}) for the 1125–1700 cm^{-1} band.

Figure 4.63: Methanol narrow band parameters $\bar{\kappa}$ and β obtained for the 1125–1700 cm^{-1} band corresponding to the bending motion of the CH_3 and OH chemical groups. Temperatures plotted are: 293, 396, 443, 483, 570, 804, and 1000 K. The narrow band resolution $\Delta\omega$ is 25 cm^{-1} .



(a) Narrow band spectral absorption coefficient $\bar{\kappa}$ (in $\text{atm}^{-1}\text{cm}^{-1}$) for the 2600–3225 cm^{-1} band.
(b) Narrow band spectral fine structure parameter β (in atm^{-1}) for the 2600–3225 cm^{-1} band.

Figure 4.64: Methanol narrow band parameters $\bar{\kappa}$ and β obtained for the 2600–3225 cm^{-1} band corresponding to the stretching motion of the CH_3 chemical groups. Temperatures plotted are: 293, 396, 443, 483, 570, 804, and 1000 K. The narrow band resolution $\Delta\omega$ is 25 cm^{-1} .



(a) Narrow band spectral absorption coefficient $\bar{\kappa}$ (in atm $^{-1}$ cm $^{-1}$) for the 3525–3850 cm $^{-1}$ band.
(b) Narrow band spectral fine structure parameter β (in atm $^{-1}$) for the 3525–3850 cm $^{-1}$ band.

Figure 4.65: Methanol narrow band parameters $\bar{\kappa}$ and β obtained for the 3525–3850 cm $^{-1}$ band corresponding to the stretching motion of the OH chemical groups. Temperatures plotted are: 293, 396, 443, 483, 570, 804, and 1000 K. The narrow band resolution $\Delta\omega$ is 25 cm $^{-1}$.

4.9.3 Verification SNB Parameters

To assess the accuracy of the narrow band parameters $\bar{\kappa}$ and β , synthetic transmissivities were constructed for the same experimental conditions as the FTIR data and compare with it. This subsection plots the comparison and the relative error in transmissivity (relative to FTIR measurements) using the methanol parameters presented in Figs. 4.62 to 4.65.

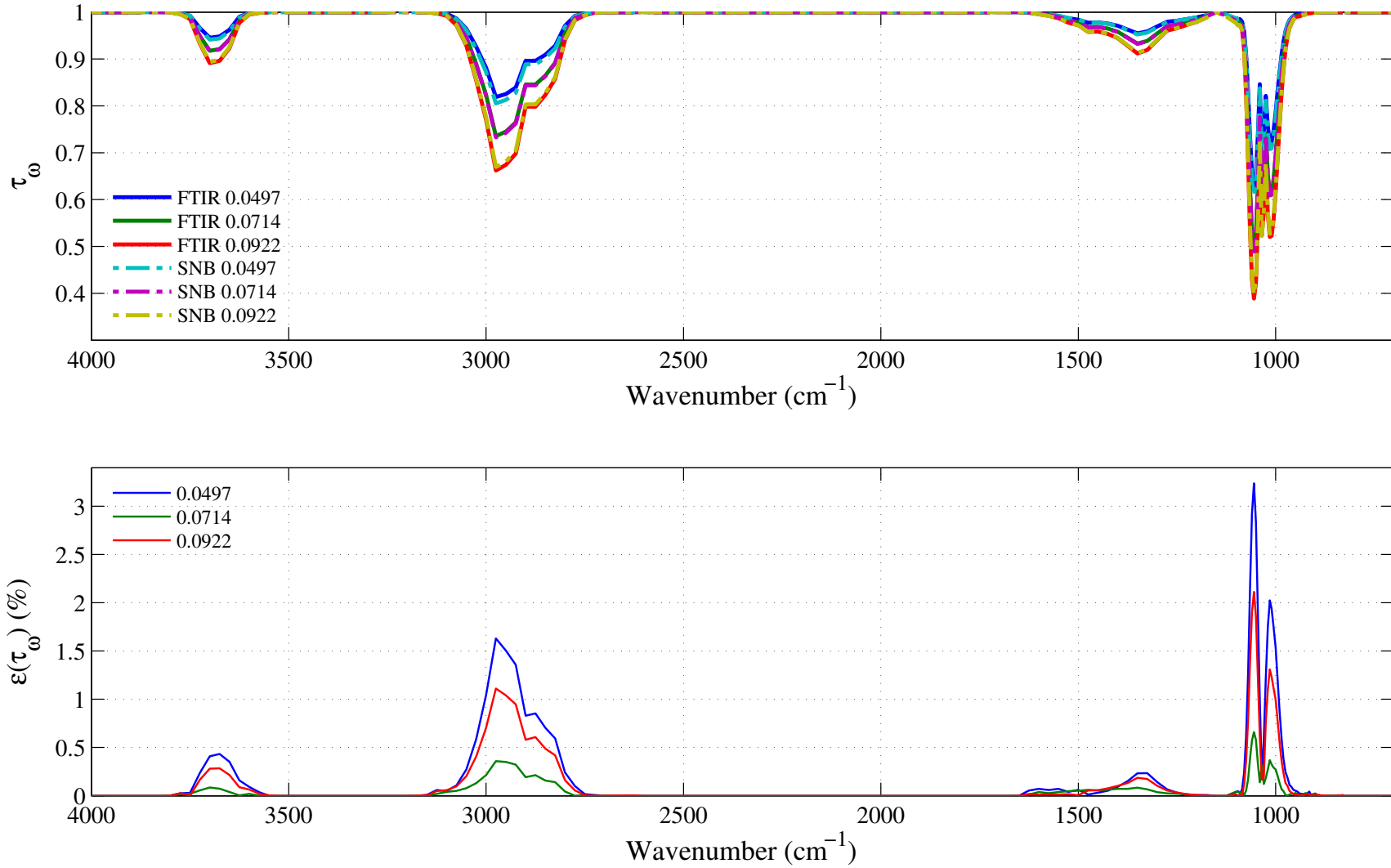


Figure 4.66: Top: comparison between the experimental (FTIR, in solid lines) and the synthetic (dashed lines) spectral transmissivity profiles, denoted τ_ω , of an isothermal homogeneous column of methanol. The synthetic profiles were generated using the Malkmus narrow band parameters presented in Figs. 4.62 to 4.65. Bottom: relative transmissivity error, denoted $\varepsilon(\tau_\omega)$, between the experiment and the synthetic profiles presented on the top figure. Three different pressure-paths are considered: 0.0922, 0.0714 and 0.0497 $\text{atm}\cdot\text{cm}$. The gas temperature is set at 293 K and the total pressure is 101 kPa. Note: the experimental data resolution has been changed to match that of the narrow band model.

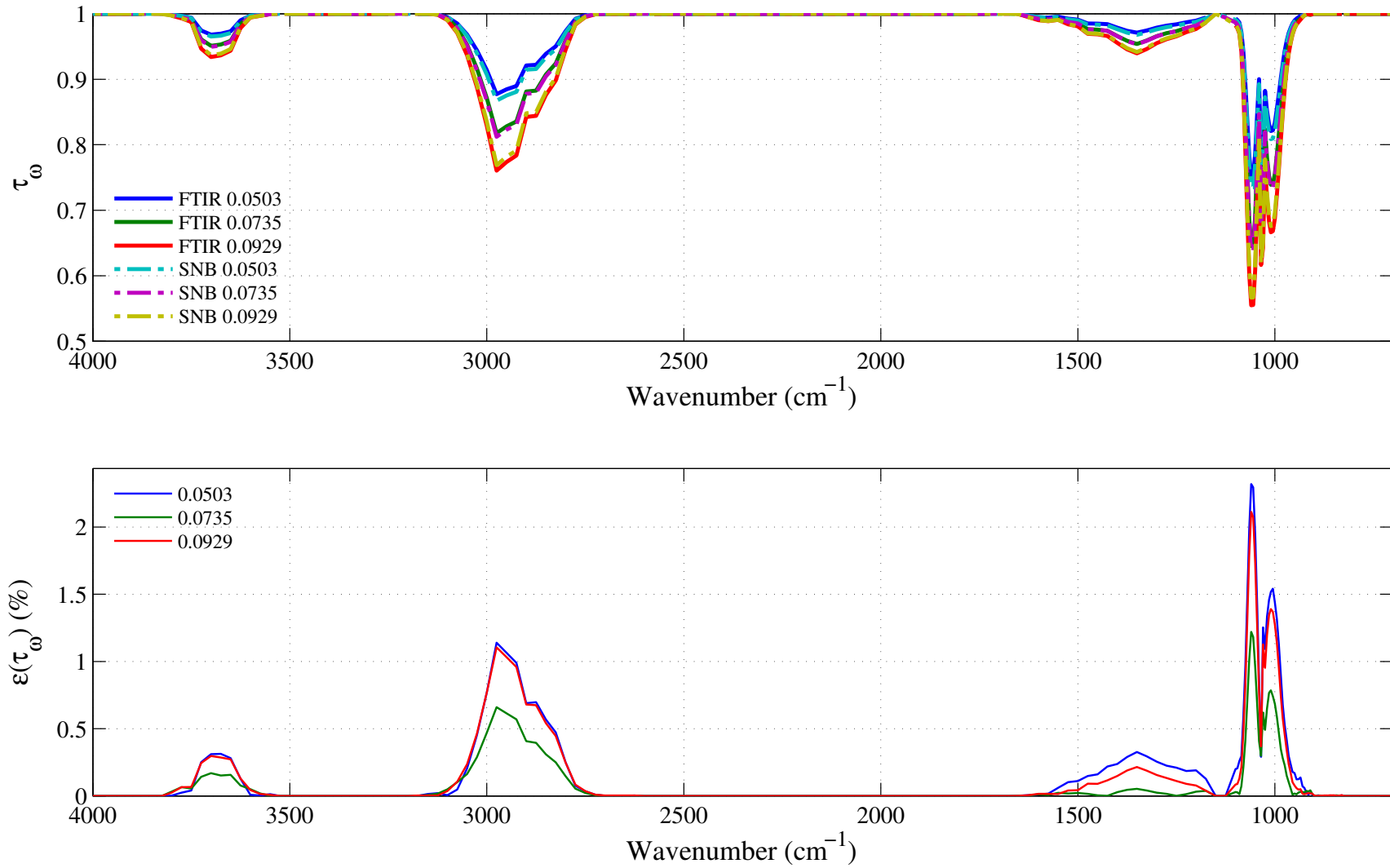


Figure 4.67: Top: comparison between the experimental (FTIR, in solid lines) and the synthetic (dashed lines) spectral transmissivity profiles, denoted τ_ω , of an isothermal homogeneous column of methanol. The synthetic profiles was generated using the Malkmus narrow band parameters presented in Figs. 4.62 to 4.65. Bottom: relative transmissivity error, denoted $\varepsilon(\tau_\omega)$, between the experiment and the synthetic profiles presented on the top figure. Three different pressure-paths are considered: 0.0929, 0.0735 and 0.0503 atm.cm. The gas temperature is set at 396 K and the total pressure is 101 kPa. Note: the experimental data resolution has been changed to match that of the narrow band model.

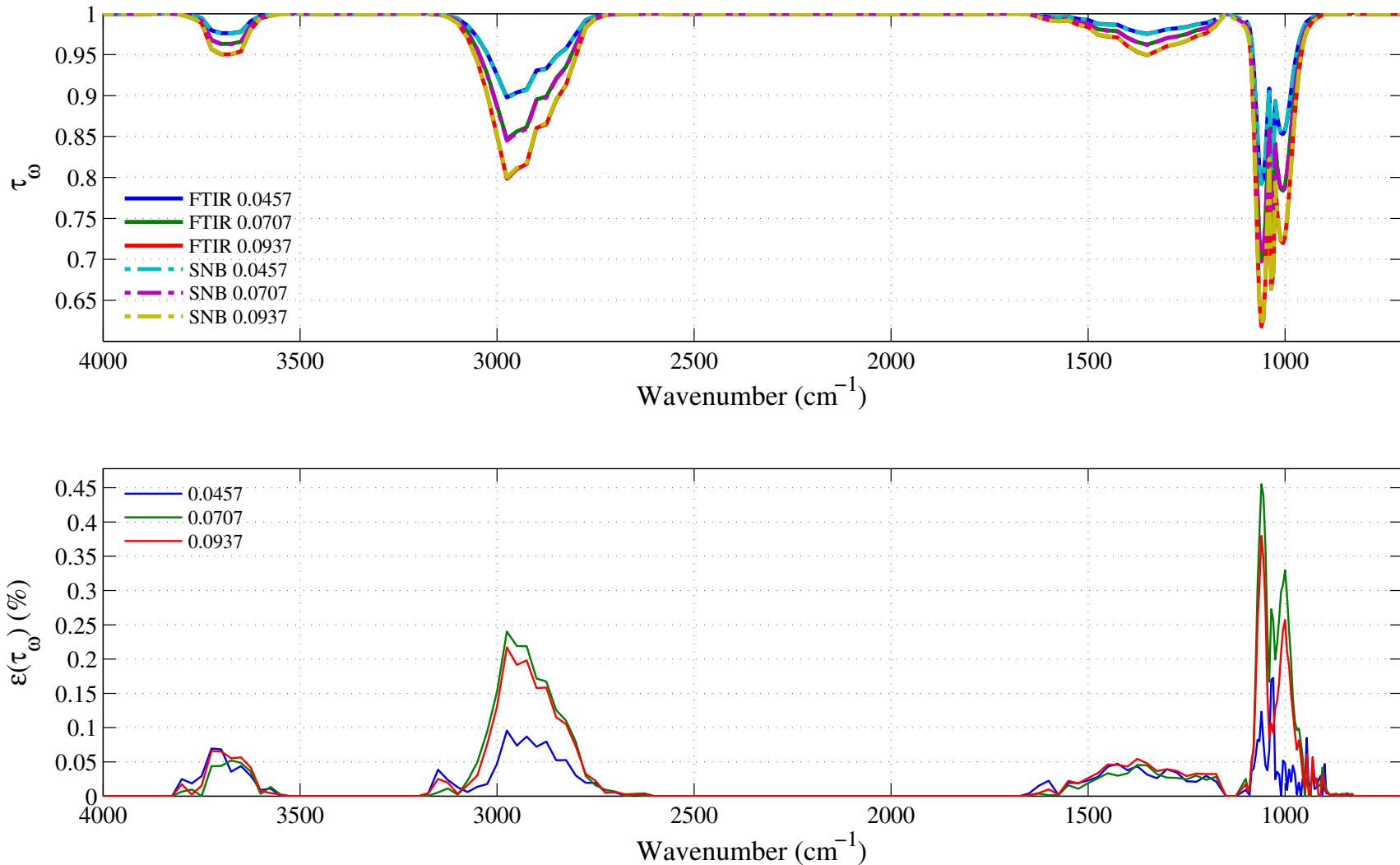


Figure 4.68: Top: comparison between the experimental (FTIR, in solid lines) and the synthetic (dashed lines) spectral transmissivity profiles, denoted τ_ω , of an isothermal homogeneous column of methanol. The synthetic profiles were generated using the Malkmus narrow band parameters presented in Figs. 4.62 to 4.65. Bottom: relative transmissivity error, denoted $\varepsilon(\tau_\omega)$, between the experiment and the synthetic profiles presented on the top figure. Three different pressure-paths are considered: 0.0937, 0.0707 and 0.0457. The gas temperature is set at 443 K and the total pressure is 101 kPa. Note: the experimental data resolution has been changed to match that of the narrow band model.

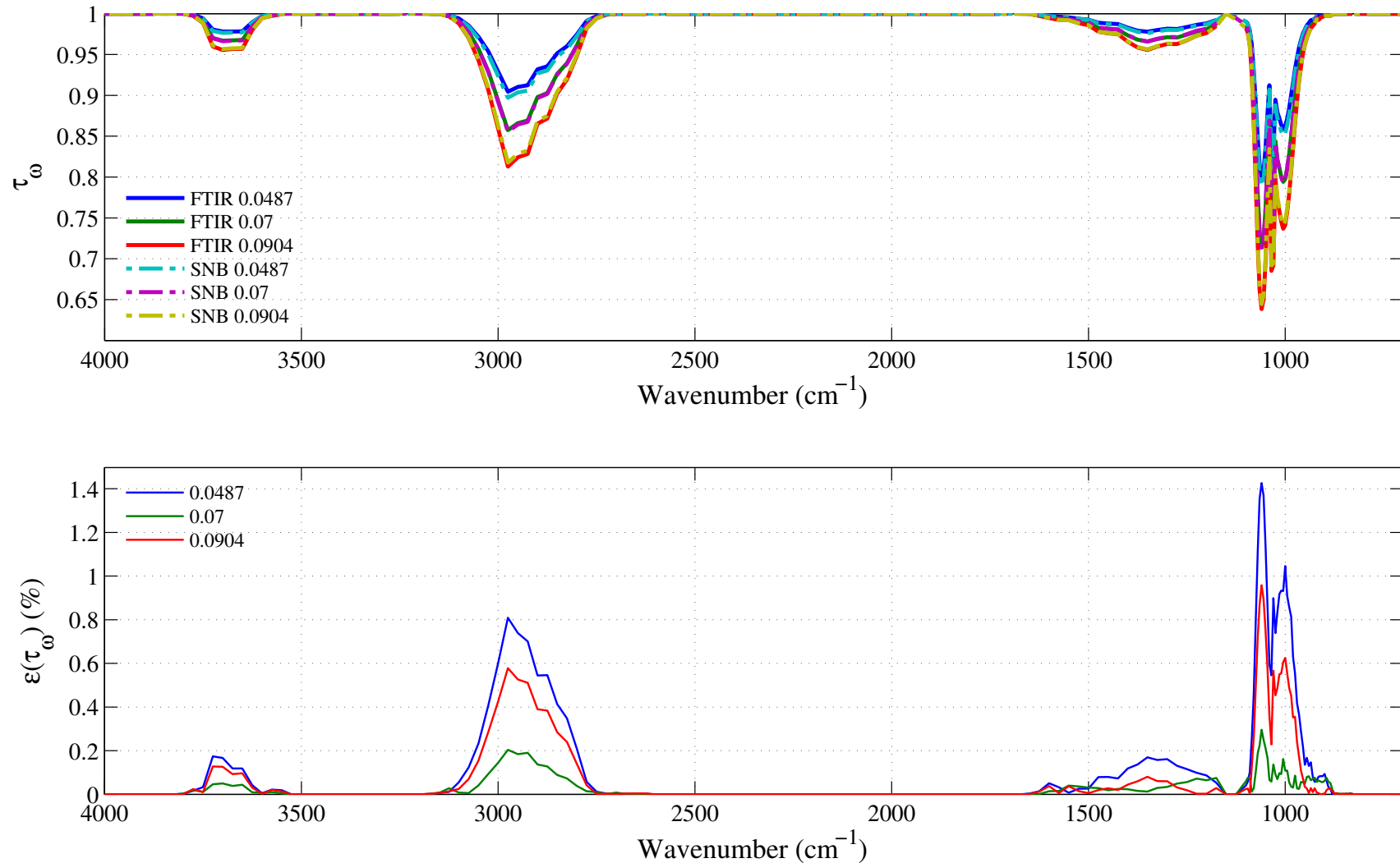


Figure 4.69: Top: comparison between the experimental (FTIR, in solid lines) and the synthetic (dashed lines) spectral transmissivity profiles, denoted τ_ω , of an isothermal homogeneous column of methanol. The synthetic profiles was generated using the Malkmus narrow band parameters presented in Figs. 4.62 to 4.65. Bottom: relative transmissivity error, denoted $\varepsilon(\tau_\omega)$, between the experiment and the synthetic profiles presented on the top figure. Three different pressure-paths are considered: 0.0904, 0.07 and 0.0487 atm.cm. The gas temperature is set at 483 K and the total pressure is 101 kPa. Note: the experimental data resolution has been changed to match that of the narrow band model.

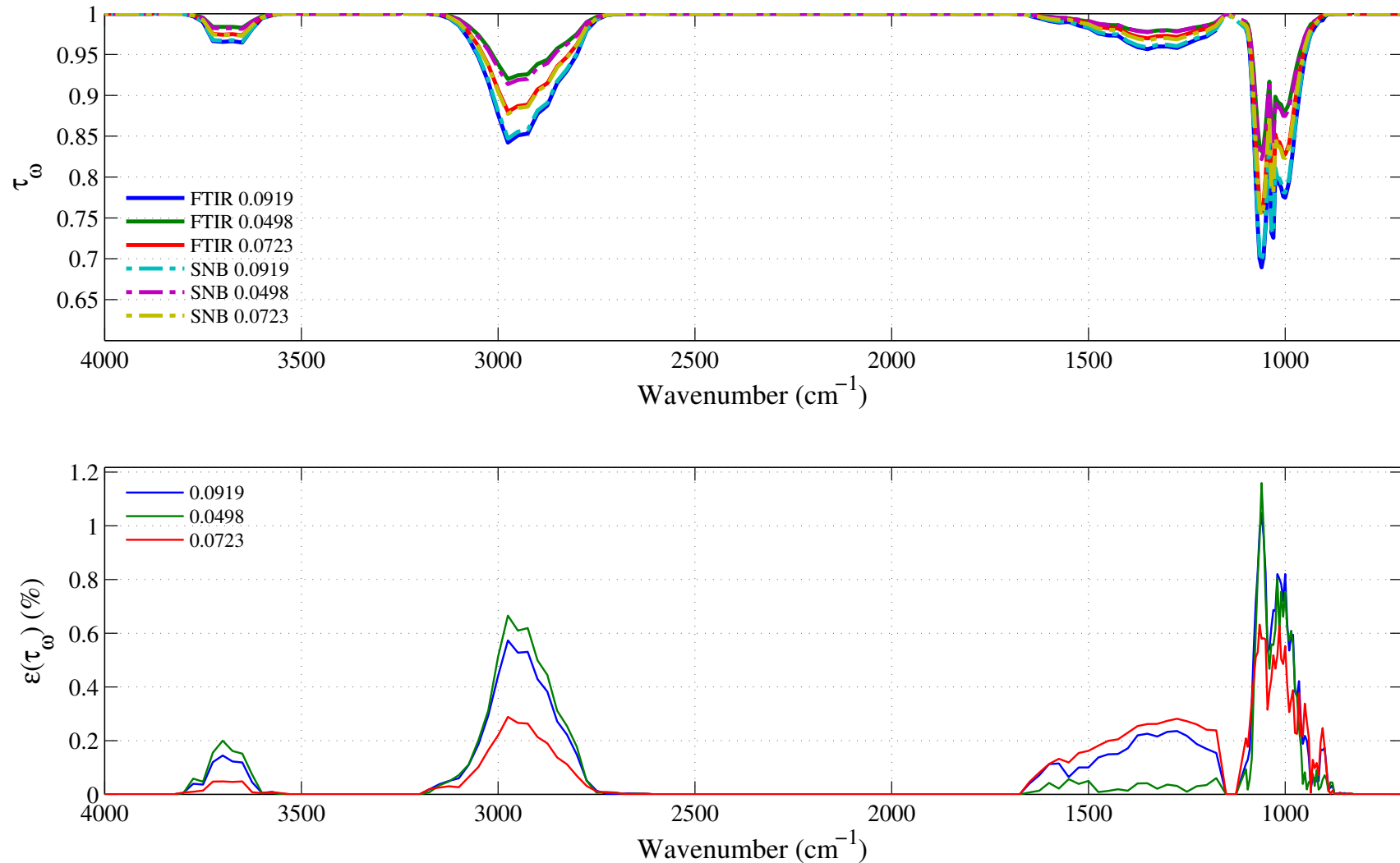


Figure 4.70: Top: comparison between the experimental (FTIR, in solid lines) and the synthetic (dashed lines) spectral transmissivity profiles, denoted τ_ω , of an isothermal homogeneous column of methanol. The synthetic profiles was generated using the Malkmus narrow band parameters presented in Figs. 4.62 to 4.65. Bottom: relative transmissivity error, denoted $\varepsilon(\tau_\omega)$, between the experiment and the synthetic profiles presented on the top figure. Three different pressure-paths are considered: 0.0919, 0.0498 and 0.0723 atm.cm. The gas temperature is set at 570 K and the total pressure is 101 kPa. Note: the experimental data resolution has been changed to match that of the narrow band model.

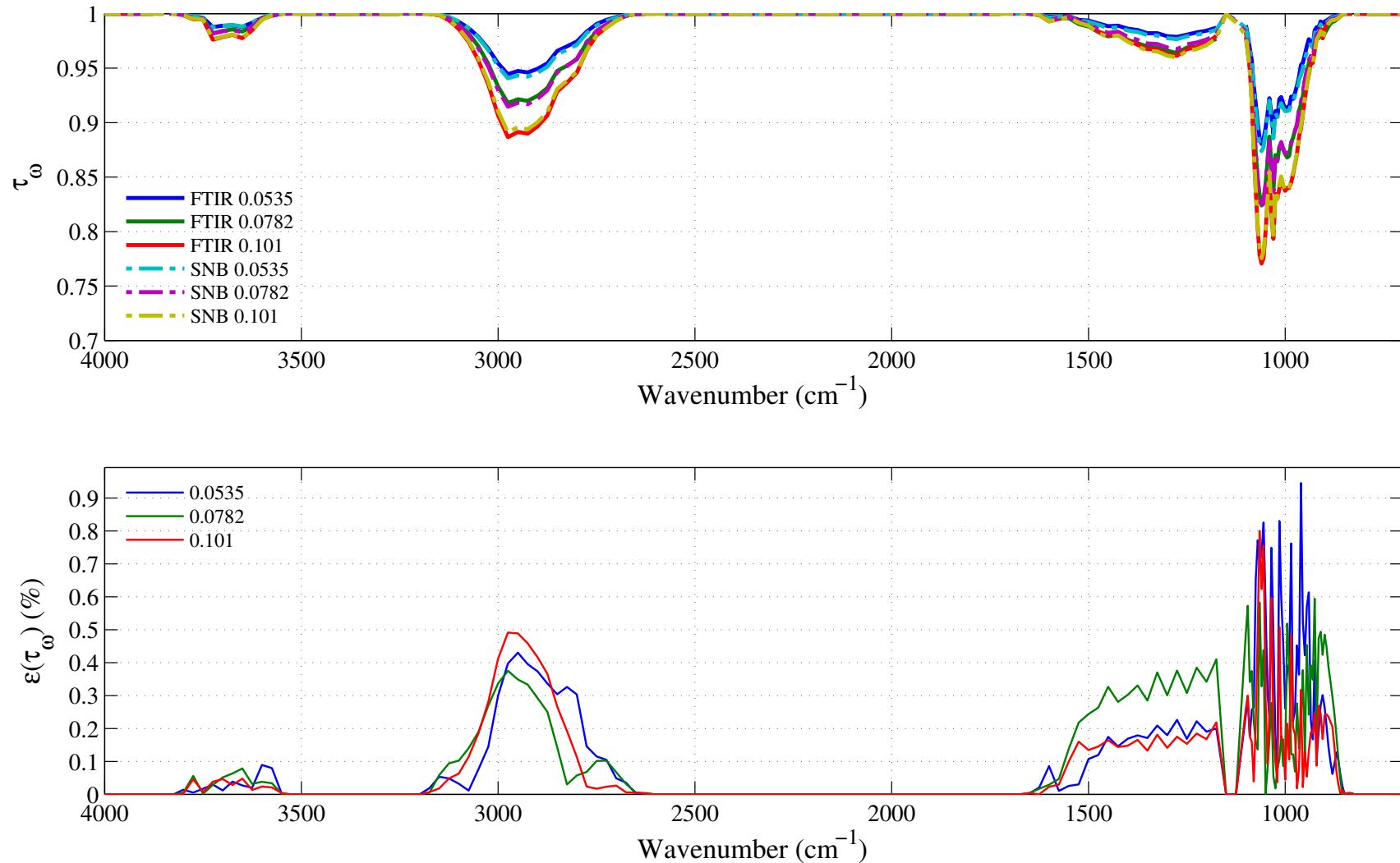


Figure 4.71: Top: comparison between the experimental (FTIR, in solid lines) and the synthetic (dashed lines) spectral transmissivity profiles, denoted τ_ω , of an isothermal homogeneous column of methanol. The synthetic profiles was generated using the Malkmus narrow band parameters presented in Figs. 4.62 to 4.65. Bottom: relative transmissivity error, denoted $\varepsilon(\tau_\omega)$, between the experiment and the synthetic profiles presented on the top figure. Three different pressure-paths are considered: 0.101, 0.0782 and 0.0535 atm.cm. The gas temperature is set at 804 K and the total pressure is 101 kPa. Note: the experimental data resolution has been changed to match that of the narrow band model.

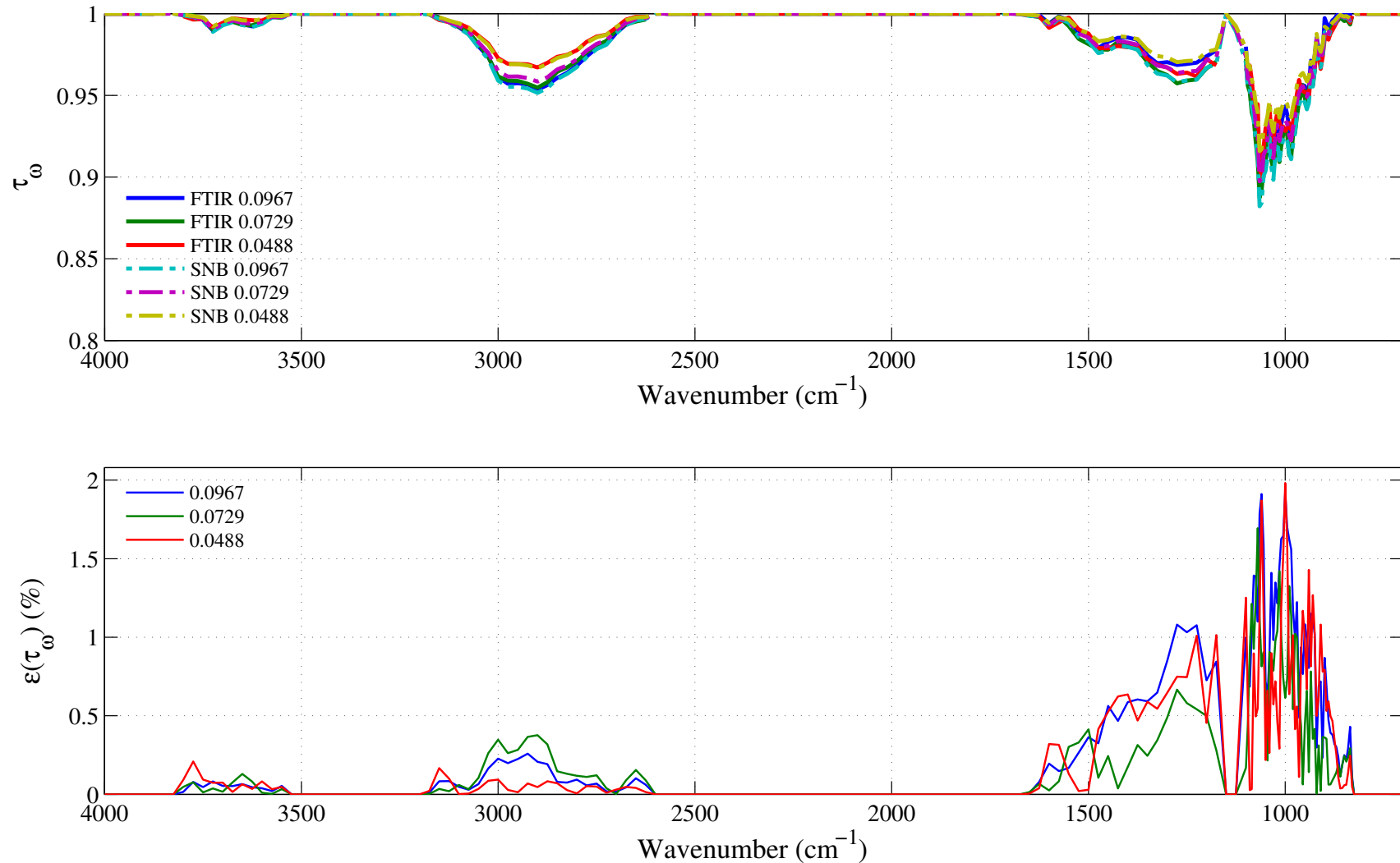


Figure 4.72: Top: comparison between the experimental (FTIR, in solid lines) and the synthetic (dashed lines) spectral transmissivity profiles, denoted τ_ω , of an isothermal homogeneous column of methanol. The synthetic profiles was generated using the Malkmus narrow band parameters presented in Figs. 4.62 to 4.65. Bottom: relative transmissivity error, denoted $\varepsilon(\tau_\omega)$, between the experiment and the synthetic profiles presented on the top figure. Three different pressure-paths are considered: 0.0967, 0.0729 and 0.0488 atm.cm. The gas temperature is set at 1000 K and the total pressure is 101 kPa. Note: the experimental data resolution has been changed to match that of the narrow band model.

4.10 Methyl Methacrylate: C₅H₈O₂

4.10.1 Integrated Band Intensity

Methyl Methacrylate, C₅H₈O₂, or MMA, has the most complex IR spectrum of all the fuels presented above. With 15 atoms, it has 39 vibrational modes. The MMA IR spectrum results from the vibration-rotation modes of the C – O, C = O, C = C, CH₂, and CH₃ groups. In RADCAL, its IR spectrum has been divided into six distinct bands. The first band from 750–875 cm⁻¹ is associated with the bending motion of the CH₂ chemical group. The second band from 875–1050 cm⁻¹ is associated with the bending motion of the CH₂ chemical group. The third band from 1050–1250 cm⁻¹ is associated with the stretching motion of the C – O chemical group. The fourth band from 1250–1550 cm⁻¹ is associated with the bending motion of the CH₃ chemical group. The fifth band from 1550–1975 cm⁻¹ is associated with the stretching motion of the C = C and C = O chemical groups. Finally, the sixth and last band from 2650–3275 cm⁻¹ is associated with the stretching motion of the CH₂ and CH₃ chemical groups. The band with the strongest absorption is the third band (1050–1250 cm⁻¹), see Table 4.8.

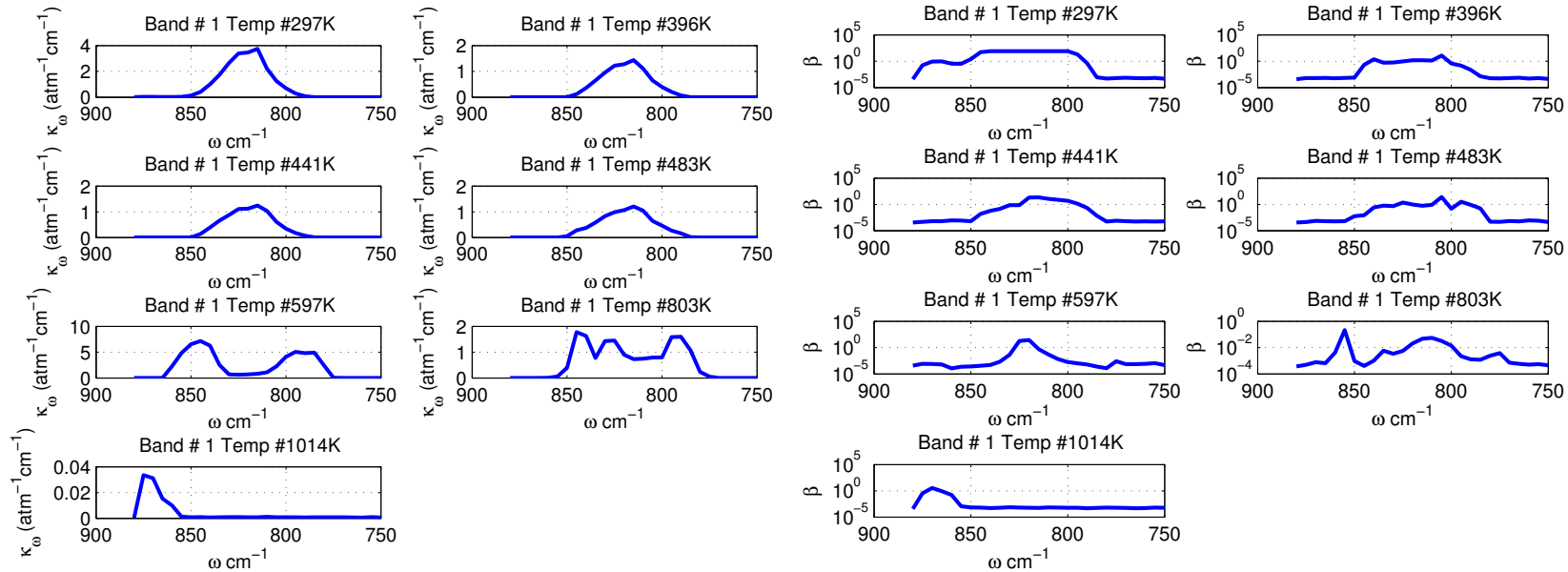
Table 4.8: Spectral bands of C₅H₈O₂ included in RADCAL.

Band #	Bounds (cm ⁻¹)		Assignment	$\alpha(T = 396 \text{ K}) (\text{atm}^{-1}\text{cm}^{-2})$
1	750	875	CH ₂ Bending	42
2	875	1050	CH ₂ Bending	134
3	1050	1250	C – O Stretching	805
4	1250	1550	CH ₃ Bending	492
5	1550	1975	C = C, C = O Stretching	542
6	2650	3275	CH ₂ , CH ₃ Stretching	295

4.10.2 Malkmus Narrow Band Parameters

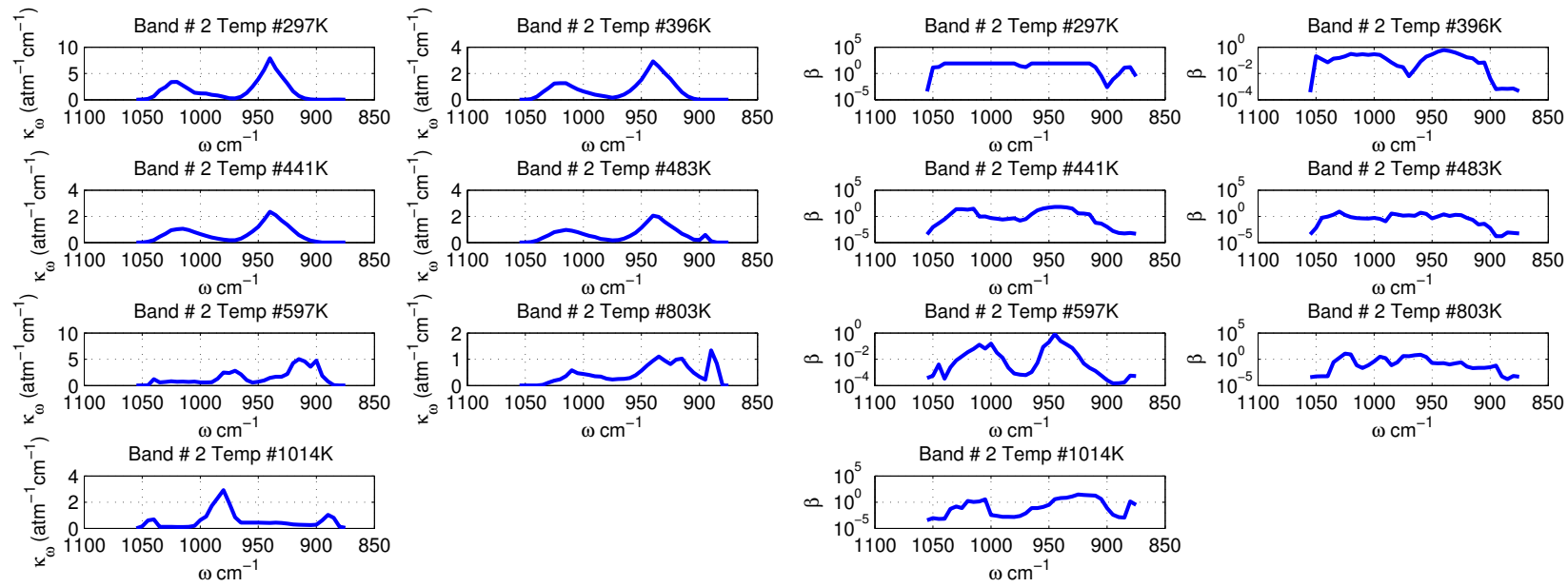
All the MMA IR spectral absorption data were obtained from high resolution FTIR experiments with temperatures varying from 297 K to 1014 K. The spectral absorption coefficients were obtained by fitting the experimental spectral transmissivity of a homogeneous column of isothermal MMA with a total pressure of 1 atm using the Malkmus model.

The MMA narrow band parameters, $\bar{\kappa}$ and β , for temperatures ranging from 297 K to 1014 K are plotted in Figures 4.73–4.78 for Bands 1 to 6. Note, while we have included data for temperatures up to 1014 K, it is recommended to use caution when interpreting data for temperatures higher than 803 K as the stability of the component at high temperature is questionable.



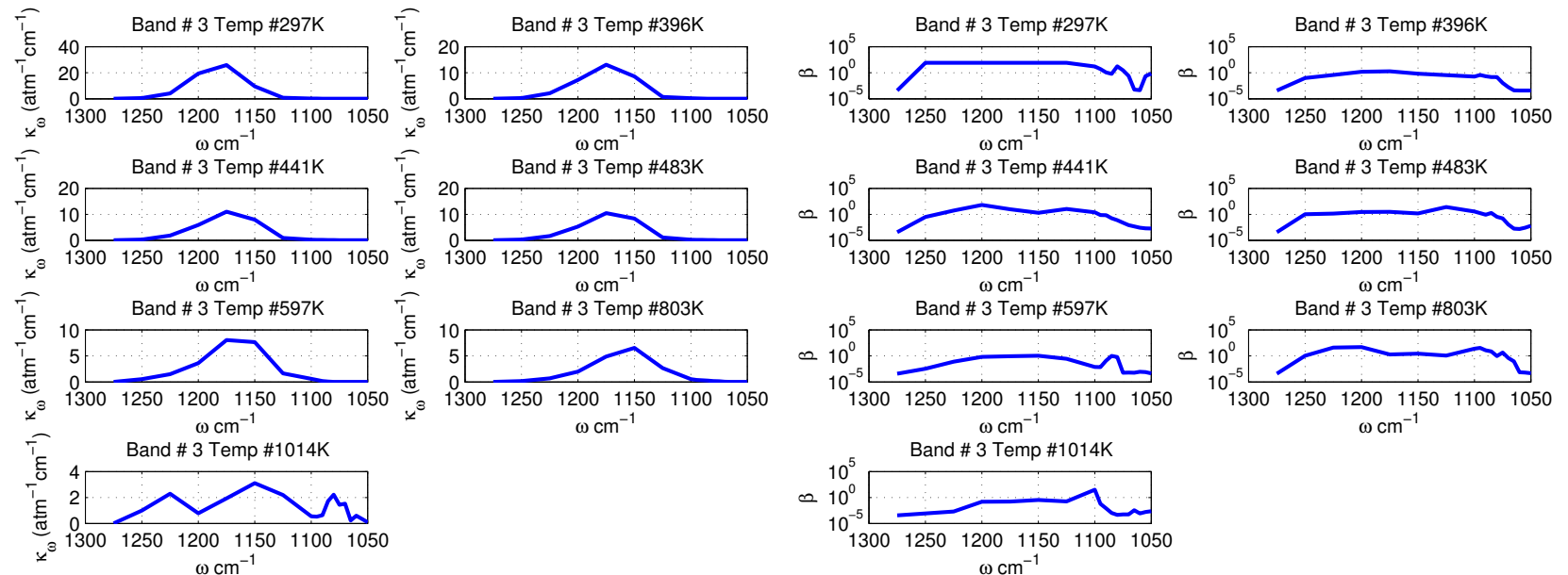
(a) Narrow band spectral absorption coefficient $\bar{\kappa}$ (in $\text{atm}^{-1}\text{cm}^{-1}$) for the 750–875 cm^{-1} band.
(b) Narrow band spectral fine structure parameter β (in atm^{-1}) for the 750–875 cm^{-1} band.

Figure 4.73: MMA narrow band parameters $\bar{\kappa}$ and β obtained for the 750–875 cm^{-1} band corresponding to the bending motion of the CH_2 chemical group. Temperatures plotted are: 297, 396, 441, 483, 597, 803, and 1014 K. The narrow band resolution $\Delta\omega$ is 5 cm^{-1} .



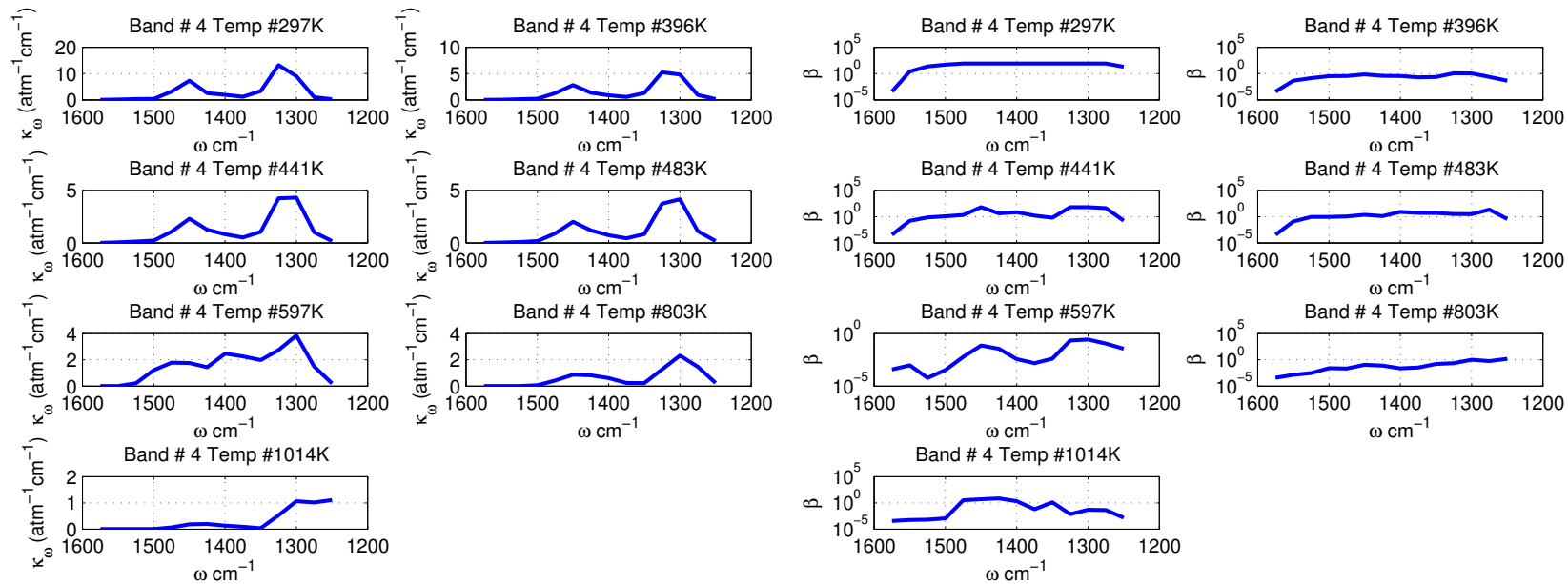
(a) Narrow band spectral absorption coefficient $\bar{\kappa}$ (in $\text{atm}^{-1}\text{cm}^{-1}$) for the $875\text{--}1050\text{ cm}^{-1}$ band.
(b) Narrow band spectral fine structure parameter β (in atm^{-1}) for the $875\text{--}1050\text{ cm}^{-1}$ band.

Figure 4.74: MMA narrow band parameters $\bar{\kappa}$ and β obtained for the $875\text{--}1050\text{ cm}^{-1}$ band corresponding to the bending motion of the CH_2 chemical group. Temperatures plotted are: 297, 396, 441, 483, 597, 803, and 1014 K. The narrow band resolution $\Delta\omega$ is 5 cm^{-1} .



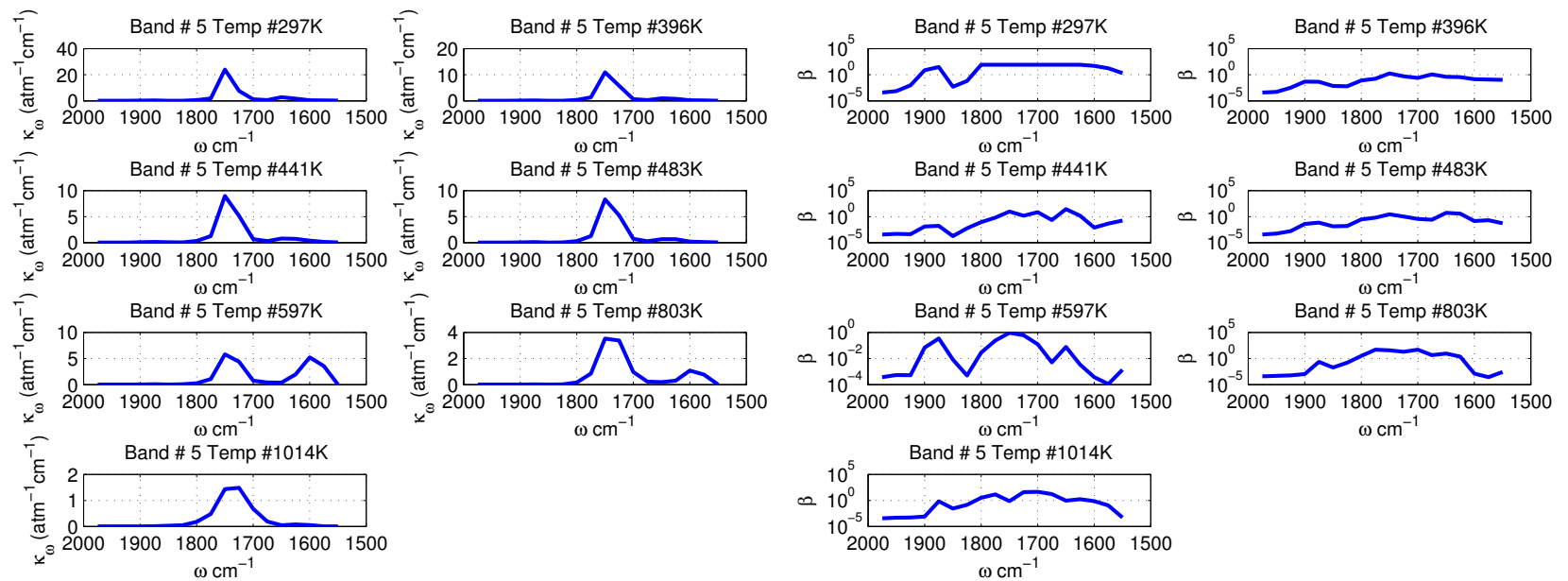
(a) Narrow band spectral absorption coefficient $\bar{\kappa}$ (in atm⁻¹cm⁻¹) for the 1050–1250 cm⁻¹ band.
(b) Narrow band spectral fine structure parameter β (in atm⁻¹) for the 1050–1250 cm⁻¹ band.

Figure 4.75: MMA narrow band parameters $\bar{\kappa}$ and β obtained for the 1050–1250 cm⁻¹ band corresponding to the stretching motion of the C – O chemical group. Temperatures plotted are: 297, 396, 441, 483, 597, 803, and 1014 K. The narrow band resolution $\Delta\omega$ is 25 cm⁻¹ below 1100 cm⁻¹ and 25 cm⁻¹ above.



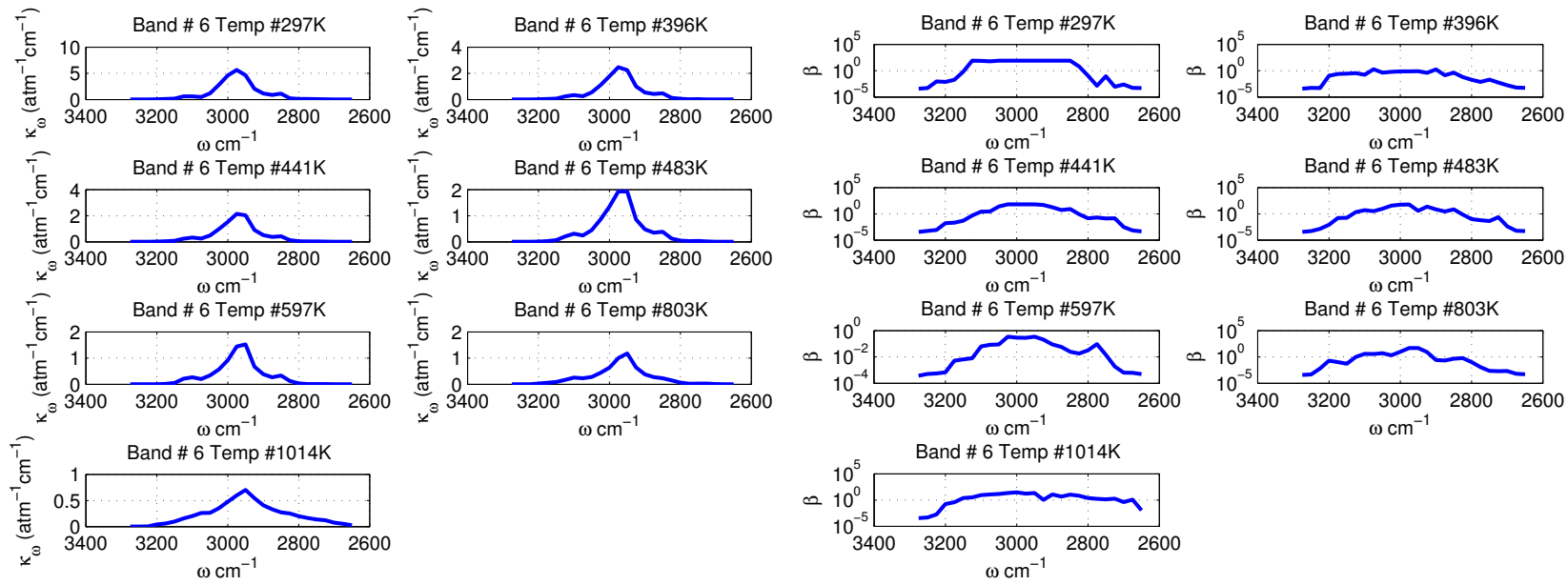
(a) Narrow band spectral absorption coefficient $\bar{\kappa}$ (in $\text{atm}^{-1}\text{cm}^{-1}$) for the 1250–1550 cm^{-1} band.
(b) Narrow band spectral fine structure parameter β (in atm^{-1}) for the 1250–1550 cm^{-1} band.

Figure 4.76: MMA narrow band parameters $\bar{\kappa}$ and β obtained for the 1250–1550 cm^{-1} band corresponding to the bending motion of the CH_3 chemical group. Temperatures plotted are: 297, 396, 441, 483, 597, 803, and 1014 K. The narrow band resolution $\Delta\omega$ is 25 cm^{-1} .



(a) Narrow band spectral absorption coefficient $\bar{\kappa}$ (in $\text{atm}^{-1}\text{cm}^{-1}$) for the 1550-1975 cm^{-1} band.
(b) Narrow band spectral fine structure parameter β (in atm^{-1}) for the 1550-1975 cm^{-1} band.

Figure 4.77: MMA narrow band parameters $\bar{\kappa}$ and β obtained for the 1550-1975 cm^{-1} band corresponding to the stretching motion of the C = C and C = O chemical groups. Temperatures plotted are: 297, 396, 441, 483, 597, 803, and 1014 K. The narrow band resolution $\Delta\omega$ is 25 cm^{-1} .



(a) Narrow band spectral absorption coefficient $\bar{\kappa}$ (in $\text{atm}^{-1}\text{cm}^{-1}$) for the 2650–3275 cm^{-1} band.
(b) Narrow band spectral fine structure parameter β (in atm^{-1}) for the 2650–3275 cm^{-1} band.

Figure 4.78: MMA narrow band parameters $\bar{\kappa}$ and β obtained for the 2650–3275 cm^{-1} band corresponding to the stretching motion of the CH_2 and CH_3 chemical groups. Temperatures plotted are: 297, 396, 441, 483, 597, 803, and 1014 K. The narrow band resolution $\Delta\omega$ is 25 cm^{-1} .

4.10.3 Verification SNB Parameters

To assess the accuracy of the narrow band parameters $\bar{\kappa}$ and β , synthetic transmissivities were constructed for the same experimental conditions as the FTIR data and compare with it. This subsection plots the comparison and the relative error in transmissivity (relative to FTIR measurements) using the MMA parameters presented in Figs. 4.73 to 4.78.

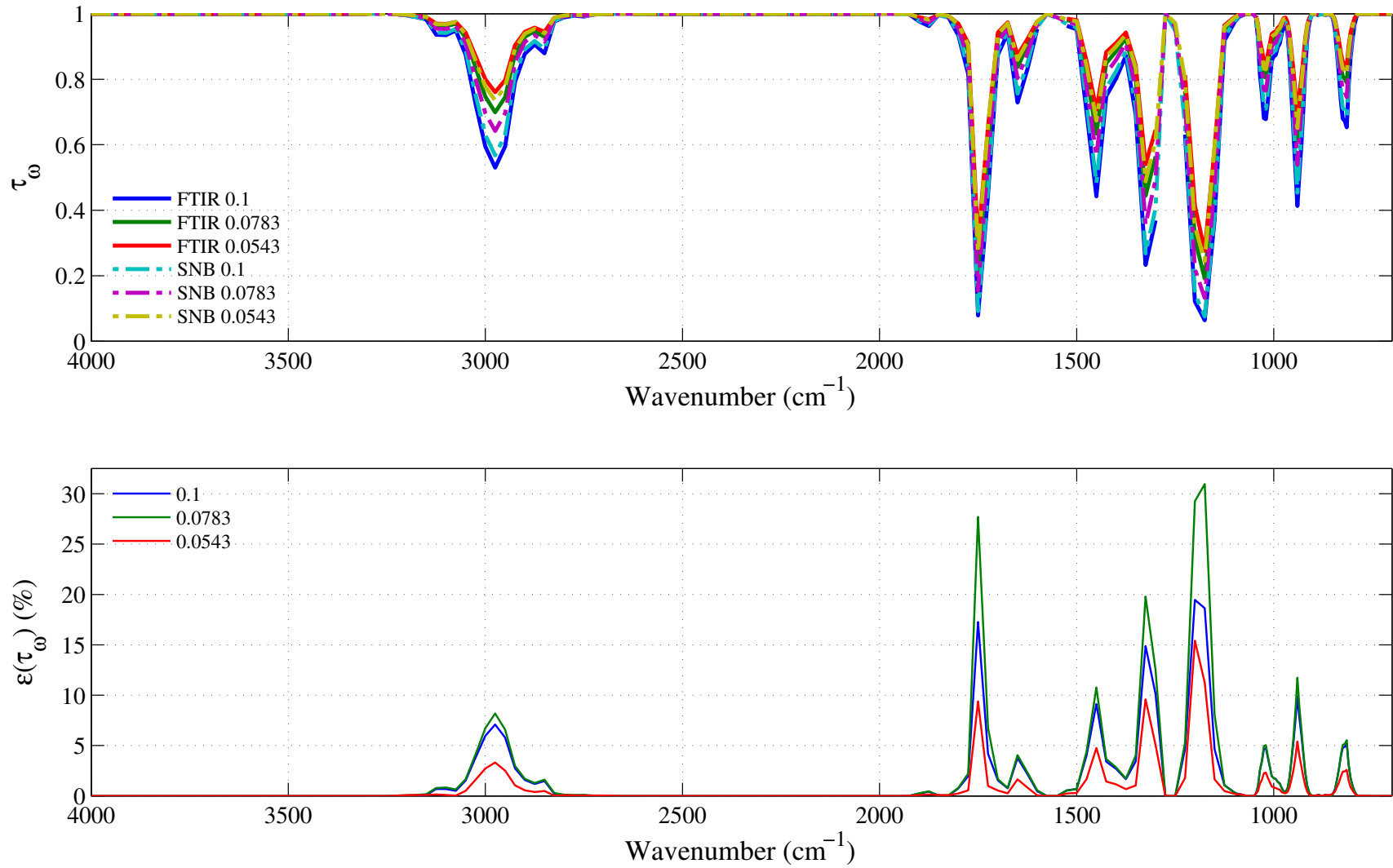


Figure 4.79: Top: comparison between the experimental (FTIR, in solid lines) and the synthetic (dashed lines) spectral transmissivity profiles, denoted τ_ω , of an isothermal homogeneous column of MMA. The synthetic profiles were generated using the Malkmus narrow band parameters presented in Figs. 4.73 to 4.78. Bottom: relative transmissivity error, denoted $\varepsilon(\tau_\omega)$, between the experiment and the synthetic profiles presented on the top figure. Three different pressure-paths are considered: 0.1, 0.0783 and 0.0543 atm.cm. The gas temperature is set at 297 K and the total pressure is 101 kPa. Note: the experimental data resolution has been changed to match that of the narrow band model.

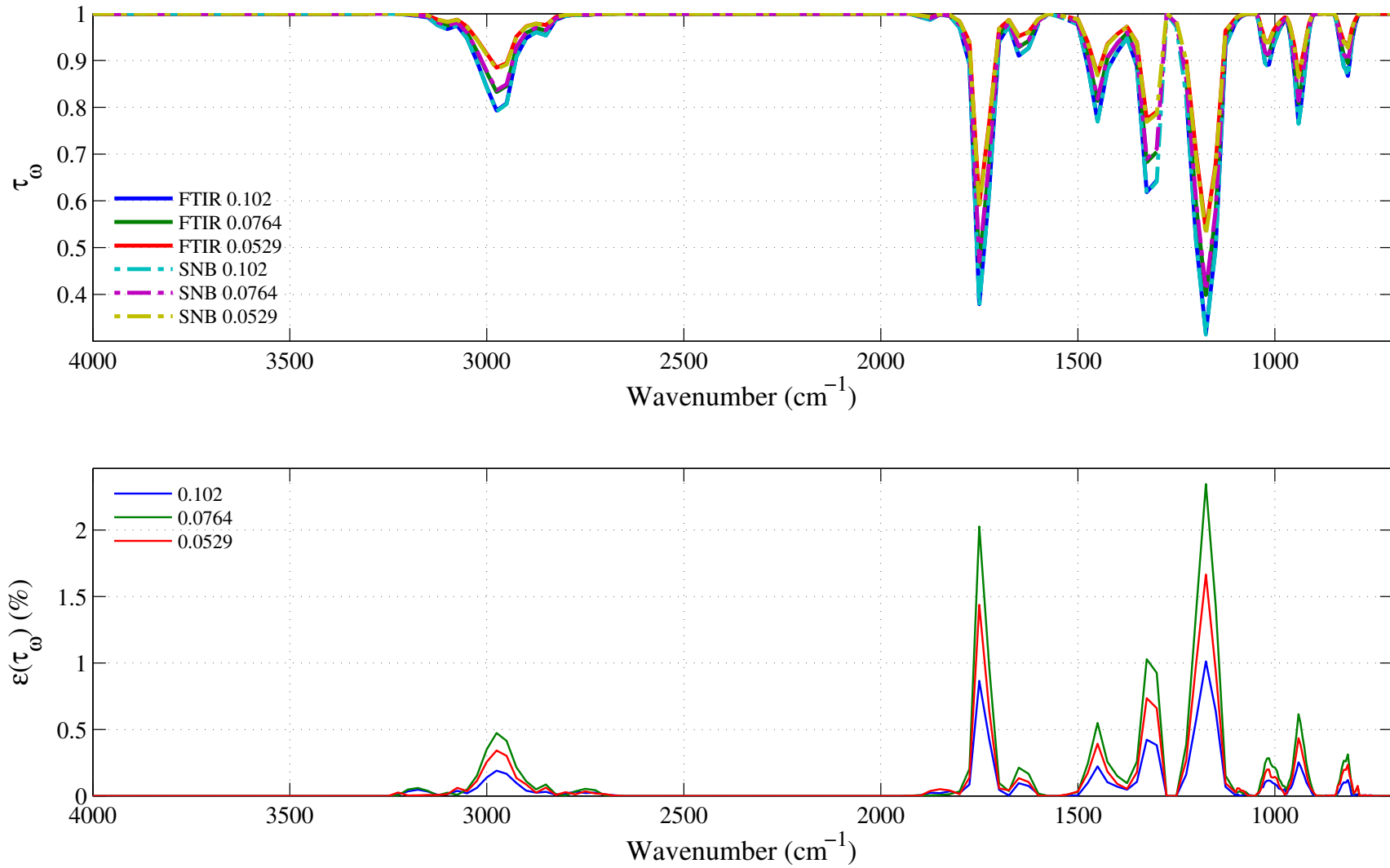


Figure 4.80: Top: comparison between the experimental (FTIR, in solid lines) and the synthetic (dashed lines) spectral transmissivity profiles, denoted τ_ω , of an isothermal homogeneous column of MMA. The synthetic profiles were generated using the Malkmus narrow band parameters presented in Figs. 4.73 to 4.78. Bottom: relative transmissivity error, denoted $\varepsilon(\tau_\omega)$, between the experiment and the synthetic profiles presented on the top figure. Three different pressure-paths are considered: 0.102, 0.0764 and 0.0529 atm.cm. The gas temperature is set at 396 K and the total pressure is 101 kPa. Note: the experimental data resolution has been changed to match that of the narrow band model.

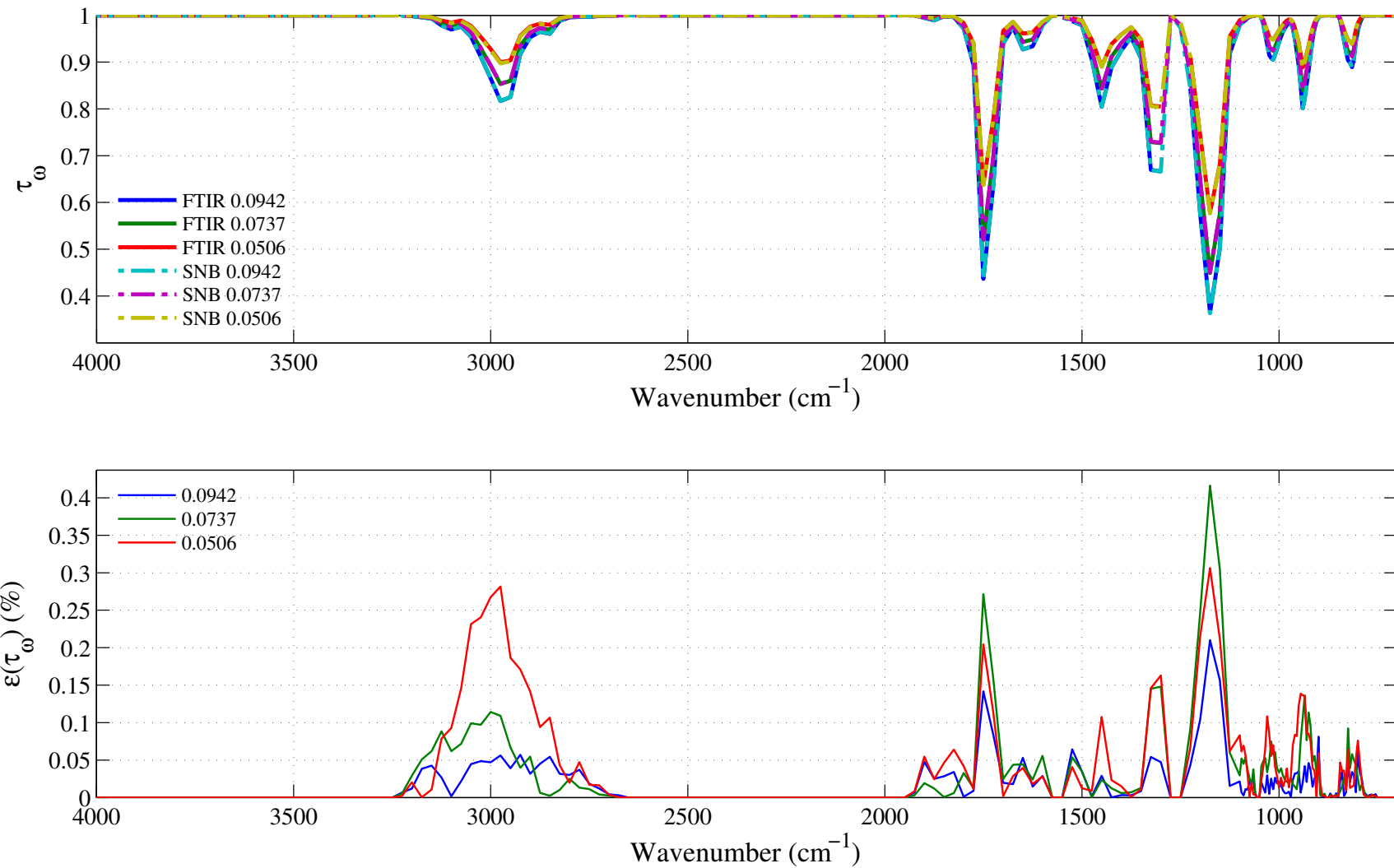


Figure 4.81: Top: comparison between the experimental (FTIR, in solid lines) and the synthetic (dashed lines) spectral transmissivity profiles, denoted τ_ω , of an isothermal homogeneous column of MMA. The synthetic profiles was generated using the Malkmus narrow band parameters presented in Figs. 4.73 to 4.78. Bottom: relative transmissivity error, denoted $\varepsilon(\tau_\omega)$, between the experiment and the synthetic profiles presented on the top figure. Three different pressure-paths are considered: 0.0942, 0.0737 and 0.0506. The gas temperature is set at 441 K and the total pressure is 101 kPa. Note: the experimental data resolution has been changed to match that of the narrow band model.

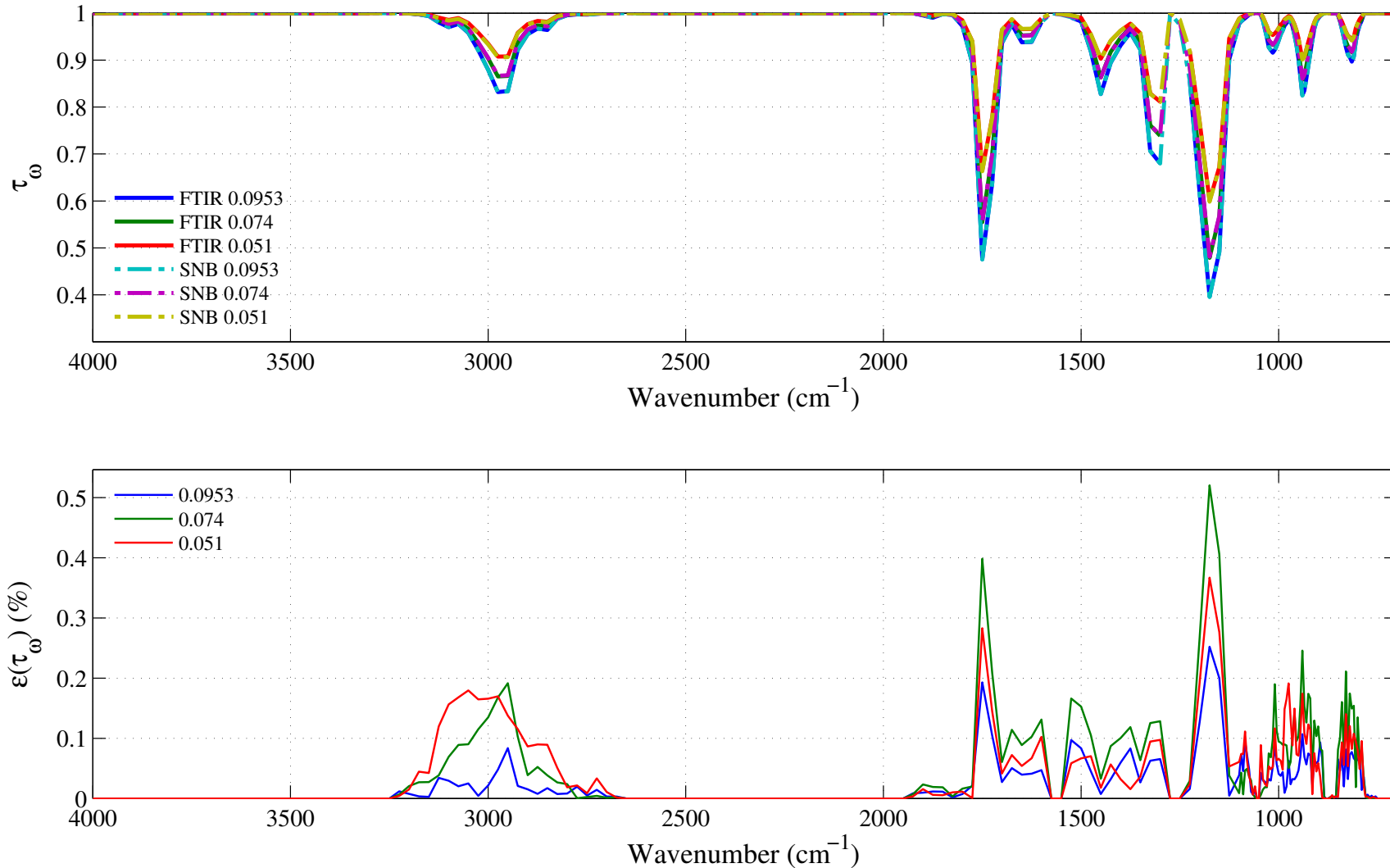


Figure 4.82: Top: comparison between the experimental (FTIR, in solid lines) and the synthetic (dashed lines) spectral transmissivity profiles, denoted τ_ω , of an isothermal homogeneous column of MMA. The synthetic profiles were generated using the Malkmus narrow band parameters presented in Figs. 4.73 to 4.78. Bottom: relative transmissivity error, denoted $\varepsilon(\tau_\omega)$, between the experiment and the synthetic profiles presented on the top figure. Three different pressure-paths are considered: 0.0953, 0.074 and 0.051 atm.cm. The gas temperature is set at 483 K and the total pressure is 101 kPa. Note: the experimental data resolution has been changed to match that of the narrow band model.

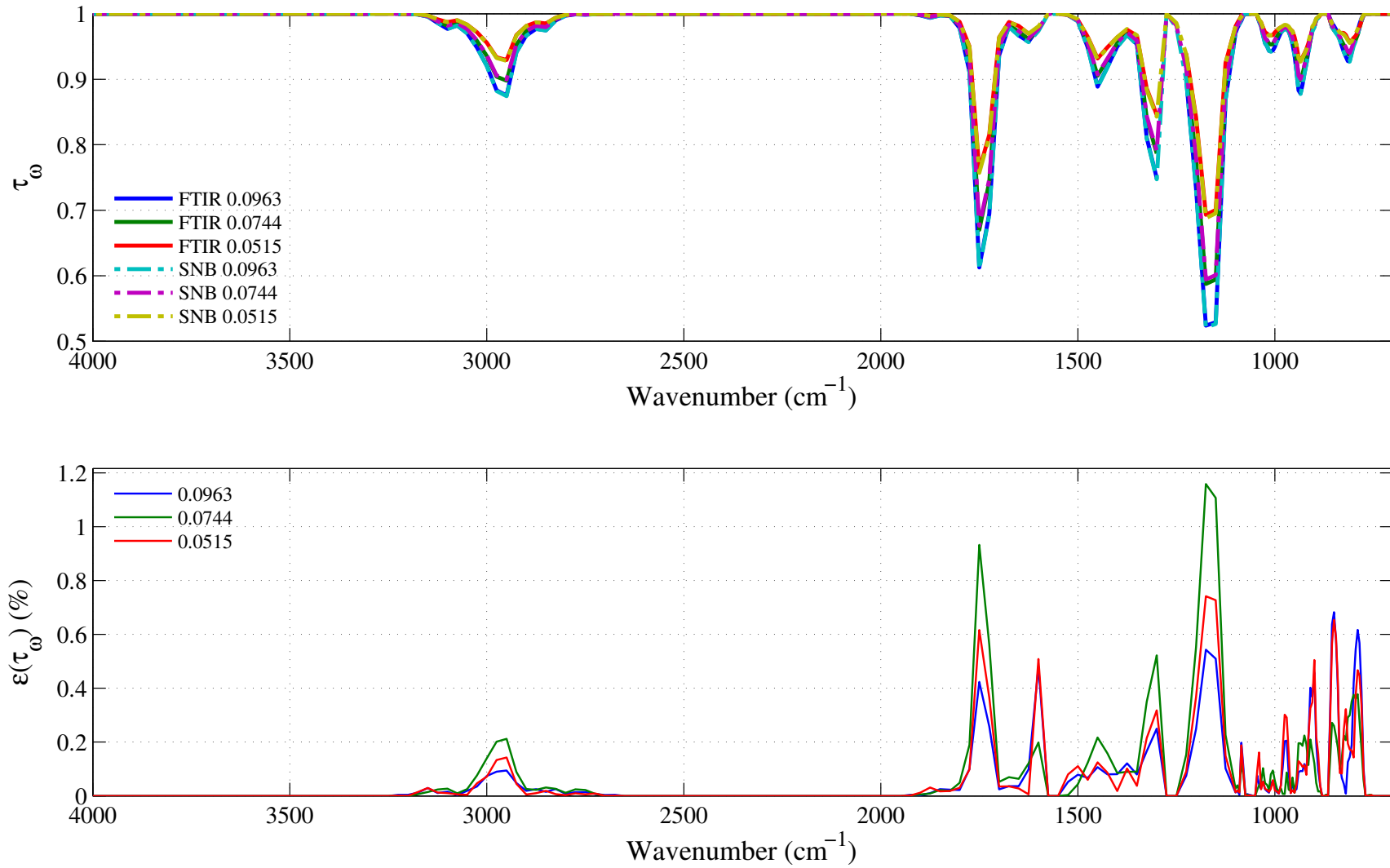


Figure 4.83: Top: comparison between the experimental (FTIR, in solid lines) and the synthetic (dashed lines) spectral transmissivity profiles, denoted τ_ω , of an isothermal homogeneous column of MMA. The synthetic profiles were generated using the Malkmus narrow band parameters presented in Figs. 4.73 to 4.78. Bottom: relative transmissivity error, denoted $\varepsilon(\tau_\omega)$, between the experiment and the synthetic profiles presented on the top figure. Three different pressure-paths are considered: 0.0963, 0.0744 and 0.0515 $\text{atm}\cdot\text{cm}$. The gas temperature is set at 597 K and the total pressure is 101 kPa. Note: the experimental data resolution has been changed to match that of the narrow band model.

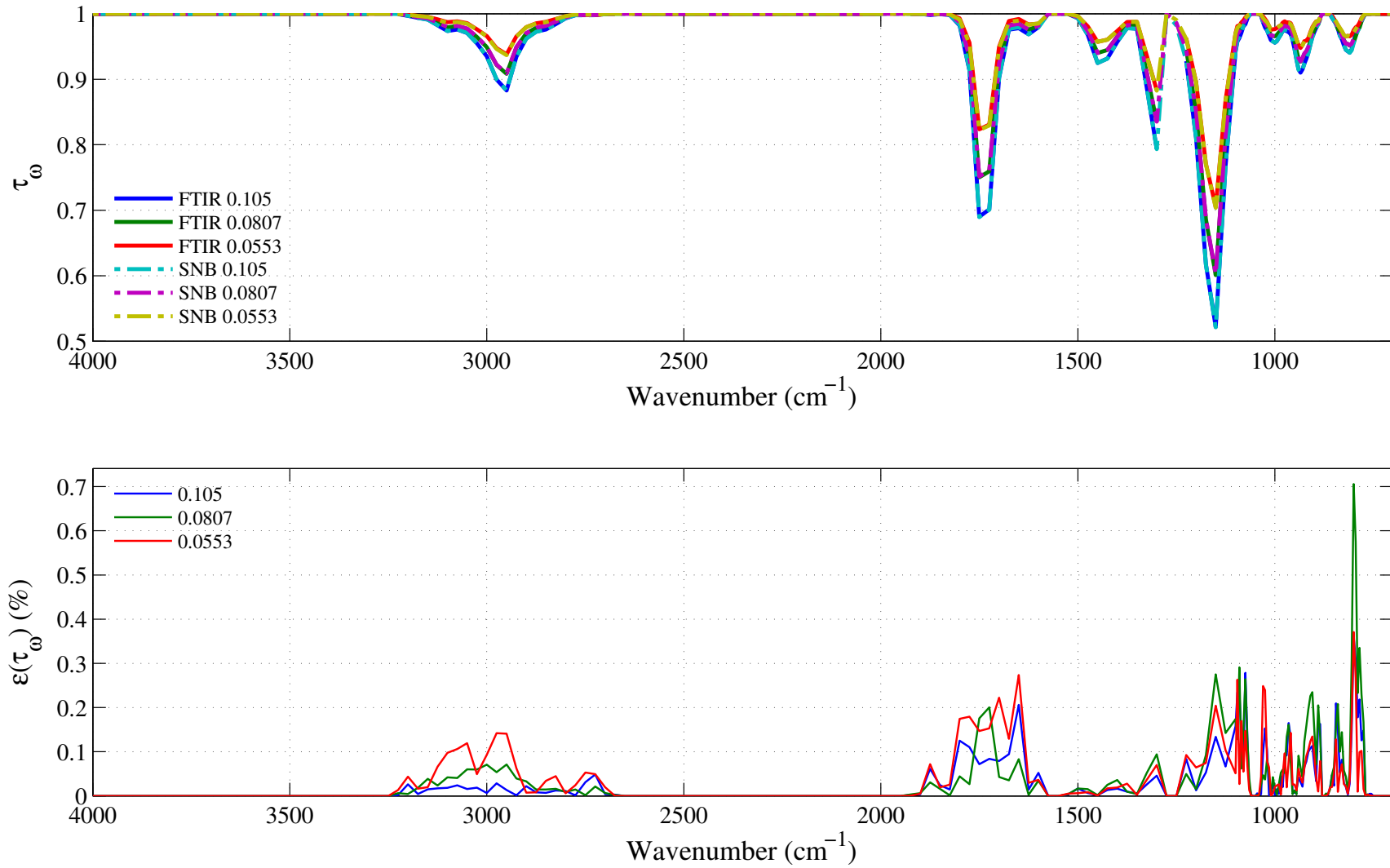


Figure 4.84: Top: comparison between the experimental (FTIR, in solid lines) and the synthetic (dashed lines) spectral transmissivity profiles, denoted τ_ω , of an isothermal homogeneous column of MMA. The synthetic profiles were generated using the Malkmus narrow band parameters presented in Figs. 4.73 to 4.78. Bottom: relative transmissivity error, denoted $\varepsilon(\tau_\omega)$, between the experiment and the synthetic profiles presented on the top figure. Three different pressure-paths are considered: 0.105, 0.0807 and 0.0553 atm.cm. The gas temperature is set at 803 K and the total pressure is 101 kPa. Note: the experimental data resolution has been changed to match that of the narrow band model.

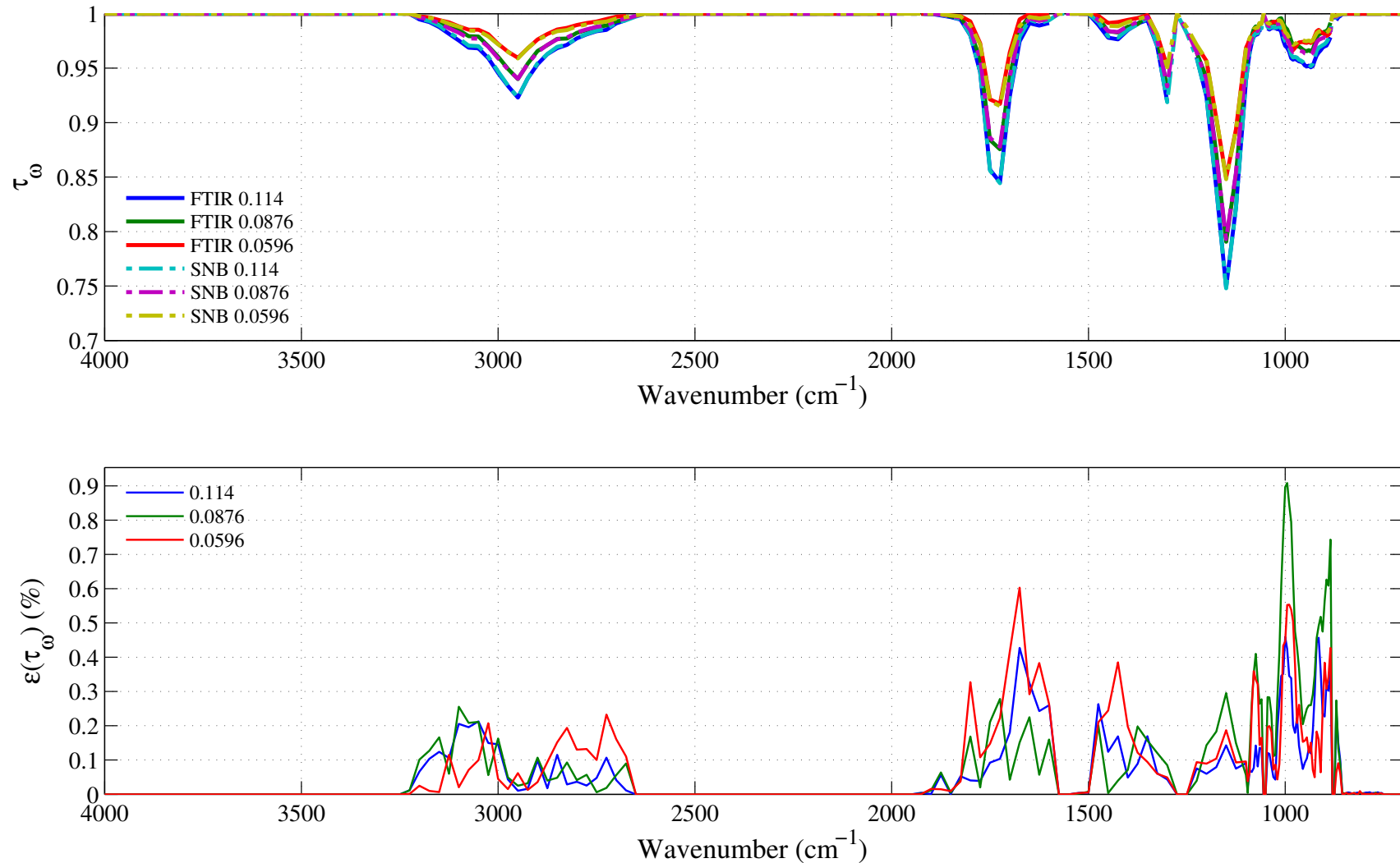


Figure 4.85: Top: comparison between the experimental (FTIR, in solid lines) and the synthetic (dashed lines) spectral transmissivity profiles, denoted τ_ω , of an isothermal homogeneous column of MMA. The synthetic profiles was generated using the Malkmus narrow band parameters presented in Figs. 4.73 to 4.78. Bottom: relative transmissivity error, denoted $\varepsilon(\tau_\omega)$, between the experiment and the synthetic profiles presented on the top figure. Three different pressure-paths are considered: 0.114, 0.0876 and 0.0596 atm.cm. The gas temperature is set at 1014 K and the total pressure is 101 kPa. Note: the experimental data resolution has been changed to match that of the narrow band model.

Chapter 5

Using RadCal

This chapter describes in details how to compile RadCal, how to write an input file using the namelist formalism, how to run RadCal, and describes the output files. Important modifications were brought to the code since its last release in 1993 [1]. In particular, the input file has been completely upgraded and the user who wishes to use this new version of the code must rewrite the old RadCal input file to comply with the new syntax.

5.1 Compiling RadCal

This new version of RadCal is a Fortran 2008 written software, written following modular paradigm. A complete description of the code is presented in Chapter 6. The source code is contained in the file RADCAL.f90. It includes the RADCAL module and the main program.

The file `Makefile` is the make file to compile RADCAL.f90 and to generate the executable RADCAL.x. It is made for Linux machine using the Intel Fortran compiler (`ifort`). It has a couple of flags. Typing `make DEBUG=0` will compile RADCAL using the compiler optimization flags. Typing `make DEBUG=1` will compile the code in debugging mode. This is useful to detect any error or bug when the source file is modified. In debug mode, the code displays additional data on the screen. It prints the pressure (in atm), physical length (in cm), the temperature (in K) of each segment that composes the domain. It also prints on screen the values contained of the Lorentz half-width at half-maximum γ_c vector for each species included in RadCal. Furthermore, it also prints characteristics pertaining to CO₂ if this species is included in the calculation and if the wavenumber 3600 cm⁻¹ is included in the user defined spectrum. It is recommended to use RadCal with the optimizing flag as it is slightly faster than the debugging mode.

In addition to the optimization flag, a second flag enabling the compilation of the code with OpenMP (for loop parallelization) has been implemented. To compile the code with OpenMP, just type `make DEBUG=0 PARALL=1` (for optimization version) or `make DEBUG=1 PARALL=1` for the debugging OpenMP version. Note that the OpenMP version does not improve much the performances, but it was included there for experimentation.

5.2 Input file

The input file is named RADCAL.in. The input file format has changed since the last RADCAL version. It now uses the Fortran namelist formalism, which is more convenient. What is needed is the knowledge, for each segment along the line of sight, of the local temperature (T), distance (LENGTH), pressure (PRESSURE), soot volume fraction (Fv), and species mole fraction, (X<species name>). **It is very**

important that the sum of all the species mole fraction over a given segment is equal to 1. Otherwise the code will not compute and will return an error message in the output file RADCAL.out.

A list of all the RadCal available species is included in the code and is printed in a automatically generated RADCAL.in in the case the user did not provide any input file. Unlike the old version, you can now solve the radiative Transfer Equation for any mixture of fuels and products of combustion.

5.2.1 Example

Below is an example of input file RADCAL.in, automatically generated by RadCal in the case that RadCal is started without an existing input file. The header prints automatically the list of species present in RadCal.

```
#-----
# Generic RADCAL input file
# Created automatically
# List of species currently available:
#-----
# <species name>      ! <phase> <comments>
# CO2      ! (gas) Carbon dioxide
# H2O      ! (gas) Water
# CO       ! (gas) Carbon monoxide
# CH4      ! (gas) Methane
# C2H4     ! (gas) Ethylene
# C2H6     ! (gas) Ethane
# C3H6     ! (gas) Propylene
# C3H8     ! (gas) Propane
# C7H8     ! (gas) Toluene
# C7H16    ! (gas) n-Heptane
# CH3OH    ! (gas) Methanol
# MMA      ! (gas) MMA, C5H8O2
# Fv       ! (solid) Soot. Defined by its soot volume fraction, Fv
# N2       ! (gas) Nitrogen does not participate to the radiative transfer
#           but is needed for collision broadening
# CH4_OLD   ! (gas) Former Methane data
# O2       ! (gas) Oxygen does not participate to the radiative transfer
#           but is needed for collision broadening
#-----
#
# How to use:
#   1) Discretize the line of sight into isothermal, homogeneous
#      segments
#   2) Define each segment temperature (variable "T", in Kelvin) and
#      length (variable "LENGTH", in meters)
#   3) Enter the pressure of each segment (variable "PRESSURE", in
#      atmosphere)
#   4) Enter the composition of the mixture, in mole fraction for
#      gas phase species (variable "X<name of species>")
#      Important: make sure the sum of species mole fraction is
#      equal to 1
#   5) Define bounds of the spectrum OMMIN/OMMAX in wavenumber
#      (1/cm)
#   6) Do not forget to enter the temperature of the surrounding,
#      which is represented by a wall at an infinite distance at its
#      blackbody temperature (variable "TWALL" in Kelvin)
#-----
Example:
&HEADER TITLE="Example" CHID="Example" /
```

```

&BAND
    OMMIN = 50.0
    OMMAX = 10000.0 /
&WALL TWALL = 500.0 /

&Path_Segment ! Define a homogeneous segment
    T      = 300.0 ! Temperature in Kelvin
    LENGTH = 0.3175 ! Length of the segment in meters
    PRESSURE = 1.0 ! Pressure in atm
    XC2H4   = 0.01 ! Mole fraction of Ethylene
    XCO2    = 0.0033 ! Mole fraction of CO2
    XH2O    = 0.01 ! Mole fraction of H2O
    XO2     = 0.21 ! Mole fraction of O2
    XN2     = 0.7667 ! Mole fraction of N2
    Fv     = 1.0e-7!/! Soot volume fraction
#-----

```

5.2.2 Input file structure

Each line starting with a character # is a comment. The comments on the header in the above input file are generated automatically.

Each namelist name is preceded by a & character. The needed namelist are: HEADER, BAND, WALL, Path_Segment. These namelist names are not case-sensitive.

Each namelist has a set of parameters you may provide. Parameters not provided have their values taken by default. They are presented below and in the input file. A "slash" character '/' is needed after providing the parameters of each namelist.

The name of the case is defined by assigning a value to &HEADER TITLE="*<value here>*" and CHID="*<value here>*".

The band limit, in cm^{-1} , is defined with the keyword OMMIN and OMMAX.

5.2.3 Naming the case: the HEADER namelist group

the namelist HEADER defines the case title with the parameter TITLE and the CASEID with the parameter CHID. This parameter are of type string. The title of the case TITLE is just used for the user own organization. The parameter CHID is used to name the Tecplot output file: *<CHID>.tec*.

5.2.4 Defining the integration bounds: the BAND namelist group

The namelist BAND defines the lower bound wavenumber, ω_{min} of the spectrum with the parameter OMMIN and the upper bound wavenumber, ω_{max} of the spectrum with the parameter OMMAX. Units are in cm^{-1} .

5.2.5 Defining the surrounding blackbody temperature: the WALL namelist group

The surrounding temperature is given by TWALL (given in Kelvin). This defines the temperature of an emitting blackbody located at one extremity of the path (the observer is located on the other side). This corresponds to the temperature of T_w in the Eq. 2.56.

5.2.6 Characterizing the homogeneous pathlength segment: the Path_Segment namelist group

Any homogeneous segment can be defined by using the keyword &Path_Segment. For each path segment, the user needs to define the local temperature (in Kelvin) using the parameter T, the length of the segment (in meters) with LENGTH, the segment total pressure (in atm) with PRESSURE, the mole fraction of any species present in the segment with the parameter X<name of species>, and the volume fraction of soot (if any) with the parameter Fv. Values omitted are set internally to zero. The user does not need to enter a value for a species not present in the segment.

It is very important that the sum of mole fraction X<name of species> is equal to 1 otherwise the segment will be dismissed.

Each segment definition is terminated with a "slash" character /.

If there is more than one segment, the user should add other segments by adding and defining extra &Path_Segment keywords. There is no restriction on the number of segment considered. The segments are to be entered from the closest to the observer, *i.e.* closest to where the incident intensity is calculated (variable s in Eq. 2.56), to the furthest (defined as s = 0 in Eq. 2.56). It is assumed that the furthest point is bounded by an emitting blackbody wall of temperature specified by TWALL.

5.3 Output files

RadCal generates two output files: RADCAL.out which contains a summary of the case run and the integrated quantities presented in Section 2.5, and a Tecplot file of name <CHID>.tec, where CHID is the value entered by the user. The Tecplot file prints the spectral transmissivity along the whole line of sight (quantity $\bar{\tau}(\omega_0; 0 \rightarrow s)$ in Eq. 2.56) expressed in %, and the incident spectral intensity $I_{\omega_0}(s)$, given in $\text{W/m}^2/\text{str/cm}^{-1}$, as calculated using either Eq. 2.57, against the wavenumber, given in cm^{-1} .

If RADCAL.in was not provided, the code will print in RADCAL.out the following message:

```
WARNING ! RADCAL.in was NOT provided.  
Creating Default RADCAL.in for illustration purposes.
```

The output file generated by RadCal using the input file RADCAL.in presented in Subsection 5.2.1 is given below as an example:

```
CASEID: Example TITLE: Example  
-----  
Calculation completed.  
Total path length (m): 0.317500000000000  
Amean (cm-1): 4.079920581529569E-003  
Planck mean absorption (cm-1): 9.468434716110452E-003  
Total Emissivity: 0.121498337093312  
Received Flux (W/m2/str): 1008.60961294274  
Total Transmissivity: 0.878725505722343  
-----  
Version: $Revision: 51 $  
Version created on: $Date: 2014-06-05 14:56:35 -0400 (Thu, 05 Jun 2014) $  
Version built on: Thu Jun 12 18:08:23 EDT 2014  
Execution time (ms): 1.85840E+01
```

The first line recalls the case title and the caseid. On the fourth line, RadCal recalls the total length of the line of sight (*i.e.* the sum of all the segments LENGTH). The value is given in meters. The fifth line prints the effective absorption coefficient as calculated by Eq. 2.71. The sixth line prints the Planck mean

absorption coefficient as defined by Eq. 2.73. The seventh line prints the total emissivity, as calculated from Eq. 2.77. The total received flux as calculated by Eq. 2.78 is given on the eighth line. Finally, the ninth line prints the value of the total transmissivity, calculated using Eq. 2.76. The last four lines of RADCAL.out recall the version of the code, the date at which this version was created, the date and time at which the code was compiled. The last line indicates the duration of code execution.

5.4 Python script

A Python script has been written to facilitate the visualization of the data present in the Tecplot file. The Python script, named Start_Radcal.py, executes RadCal, reads the output Tecplot file and RADCAL.out, and displays the plots of $\bar{\tau}(\omega_0; 0 \rightarrow s)$ against the wavenumber ω on the top window, and the spectral evolution of the incident intensity $I_{\omega_0}(s)$ against the wavenumber ω on the bottom window. The script also prints some integrated quantities and generates automatically a pdf file. In order to use this script, beside Python, the matplotlib library, Ref. [31], is needed. Figure 5.1 plots the spectral transmissivity and the incident spectral intensity for the case given as an example in Subsection 5.2.1 as generated by the Start_Radcal.py script.

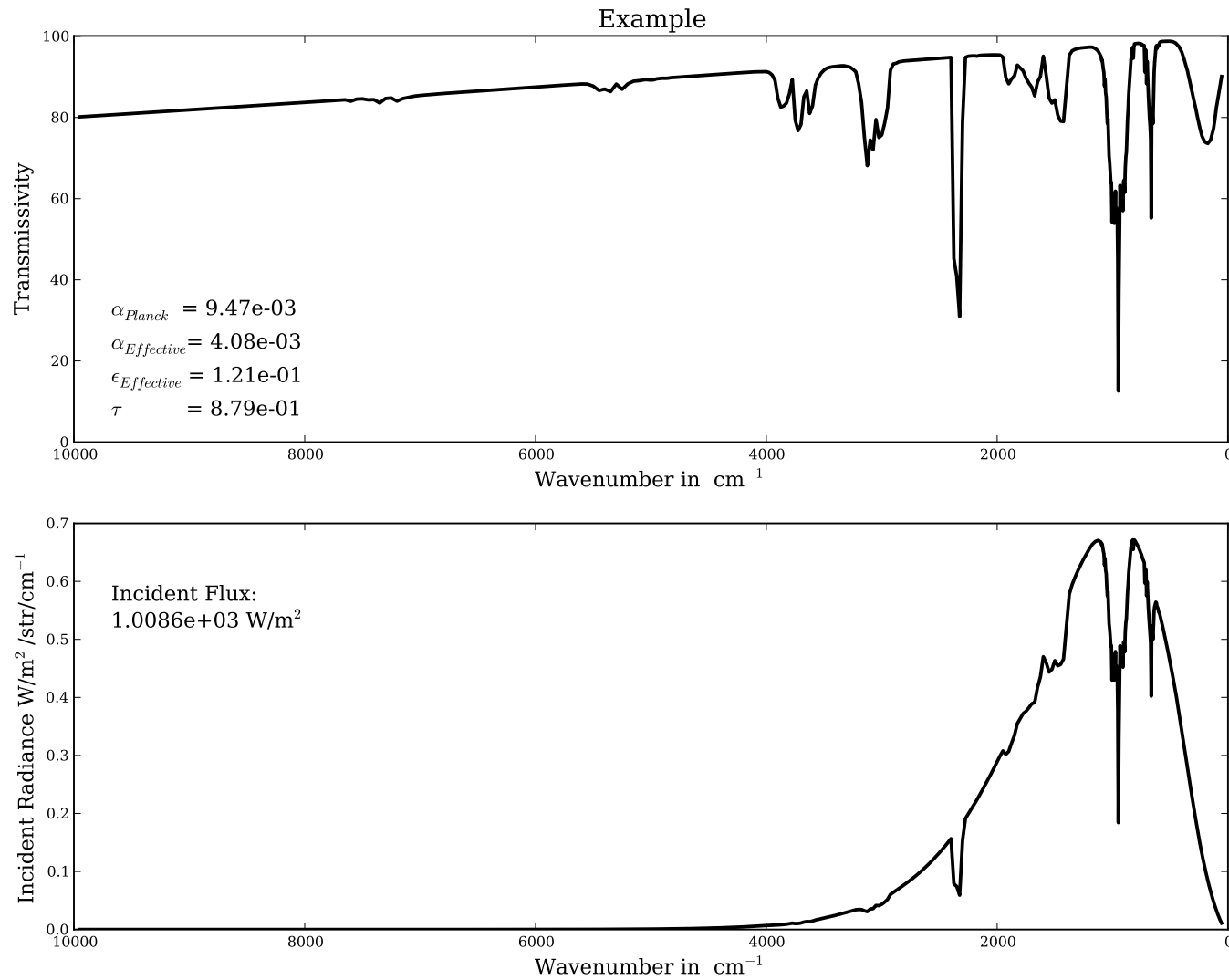


Figure 5.1: Top: Spectral transmissivity of the medium, in %, using the input file given in Subsection 5.2.1. Bottom: Associated incident spectral intensity, $I_{\omega_0}(s)$, given in $\text{W/m}^2/\text{str}/\text{cm}^{-1}$.

Chapter 6

Structure of the Code

This chapter presents the structure of the code and the diverse subroutines and functions that comprise it. Originally written in FORTRAN 77, RadCal has been rewritten in Fortran 2008 to benefit from the recent language updates. Furthermore, the code has been divided into modules, subroutine, and functions for ease of code maintenance and understanding.

RadCal source file, RADCAL.f90, contains one main module, named `radcal`, and one main program or driver, named `driver`, which uses the `radcal` module. The `radcal` module contains about 40 functions and subroutines that initialize the different species spectral data (mean absorption coefficient $\bar{\kappa}$ and for some species the overlap parameter β), discretize the spectral range, solve the radiative transfer equation (RTE) for homogeneous and/or non-homogeneous paths, extract the adequate spectral data, interpolate the data when needed, read the input file `RADCAL.in`, deallocate memory prior to exiting RadCal, print some error messages whenever some errors are raised. The `radcal` module is self-consistent. The only dependence is OpenMP which is only required when the code is compiled using the makefile `PARALL=1` flag.

The program `driver` contains also one subroutine that creates the TECPLOT file named `<CASEID>.tec`, and plots in ASCII format the wavenumber, the spectral transmissivity, and the incidents spectral intensity. The `driver` program starts by a call to the intrinsic routine `cpu_time` to initialize the system chronometer (it is used to assess the execution time of RadCal) and opens or creates the output file `RADCAL.out`. It then calls the subroutine `read_input` from the `radcal` module to read the input file `RADCAL.in` and populates the needed variables. Then `driver` calls `init_radcal` to initialize the species spectral variables; the scope of these variables is limited to the entire module, they cannot be accessed from the `driver` program as they have the `private` attribute.

Once the data are initialized, the `driver` program calls `sub_radcal` which solves the RTE over the user defined spectral range, calculates and returns the integrated quantities presented in Section 2.5. The main program then writes in the output file `RADCAL.out` the appropriate data, and calls `tau_print` to print the wavenumber in cm^{-1} , the spectral transmissivity in %, and the incident spectral intensity in $\text{W}/\text{m}^2/\text{str}/\text{cm}^{-1}$. Finally the `driver` program calls `rcdealloc` to deallocate the variables allocated in `init_radcal` and calls `cpu_time` to returns the execution time. If the code was compiled using the makefile `DEBUG=1` flag, then RadCal prints the execution time in *ms*, along with the `svn` version of RadCal used, the date at which this version of RadCal has been committed into the `svn` system, and the date at which the code has been compiled. RadCal then stops.

6.1 RadCal Module

6.1.1 RadCal Variables

RADCAL VARIABLES

```
character(255), parameter, private :: Radcalid='$Id: RADCAL.f90 51 2014-06-05 18:56:35Z
vlecoust $'
character(255), parameter, public  :: Radcalrev='$Revision: 51 $'
character(255), parameter, public  :: Radcaldate='$Date: 2014-06-05 14:56:35 -0400 (Thu, 05
Jun 2014) $'

character(255), parameter, public :: date_compile = date

integer, parameter :: fb = selected_real_kind(6)
integer, parameter :: eb = selected_real_kind(12)

integer, public :: n_threads

character(len=32)          :: radcal_id
character(len=32)          :: id
character(len=2048)         :: comments
real(eb), pointer, dimension(:) :: bands
real(eb), pointer, dimension(:) :: temp_exp

integer, parameter :: n_species = 16           ! number of radcal species (including soot) plus nitrogen and oxygen
integer, parameter :: n_species_gas = n_species-1 ! number of radcal gaseous species

type(elements), dimension(n_species) :: species !

character(len=255) :: chid   ! radcal case id
character(len=255) :: title   ! radcal case title

real(eb), allocatable, dimension(:, :) :: gamma, sd15, sd, sd7, sd3

integer :: n_temp_c3h6,    n_band_c3h6
integer :: n_temp_c3h8,    n_band_c3h8
integer :: n_temp_c7h16,   n_band_c7h16
integer :: n_temp_c7h8,    n_band_c7h8
integer :: n_temp_ch4,     n_band_ch4
integer :: n_temp_ch3oh,   n_band_ch3oh
integer :: n_temp_c5h8o2,   n_band_c5h8o2
integer :: n_temp_c2h6,    n_band_c2h6
integer :: n_temp_c2h4,    n_band_c2h4

integer :: i_model_c3h6   ! 1: goody, 2: malkmus, 3: elsasser
integer :: i_model_c3h8   ! 1: goody, 2: malkmus, 3: elsasser
integer :: i_model_c7h16   ! 1: goody, 2: malkmus, 3: elsasser
integer :: i_model_c7h8   ! 1: goody, 2: malkmus, 3: elsasser
integer :: i_model_ch3oh   ! 1: goody, 2: malkmus, 3: elsasser
integer :: i_model_c5h8o2   ! 1: goody, 2: malkmus, 3: elsasser
integer :: i_model_c2h6   ! 1: goody, 2: malkmus, 3: elsasser
integer :: i_model_c2h4   ! 1: goody, 2: malkmus, 3: elsasser

integer :: i_model_co2    ! 1: goody, 2: malkmus, 3: elsasser
integer :: i_model_h2o    ! 1: goody, 2: malkmus, 3: elsasser
integer :: i_model_co      ! 1: goody, 2: malkmus, 3: elsasser
integer :: i_model_ch4    ! 1: goody, 2: malkmus, 3: elsasser

real(eb), allocatable, dimension(:) :: sd_c3h6_temp
real(eb), allocatable, dimension(:) :: sd_c3h8_temp
real(eb), allocatable, dimension(:) :: sd_c7h16_temp
real(eb), allocatable, dimension(:) :: sd_c7h8_temp
real(eb), allocatable, dimension(:) :: sd_ch3oh_temp
```

```

real(eb), allocatable , dimension(:)      :: sd_c5h8o2_temp
real(eb), allocatable , dimension(:)      :: sd_c2h6_temp
real(eb), allocatable , dimension(:)      :: sd_ch4_temp
real(eb), allocatable , dimension(:)      :: sd_c2h4_temp

real(eb), allocatable , dimension(:)      :: be_c3h6
real(eb), allocatable , dimension(:)      :: be_c3h8
real(eb), allocatable , dimension(:)      :: be_c7h16
real(eb), allocatable , dimension(:)      :: be_c7h8
real(eb), allocatable , dimension(:)      :: be_ch3oh
real(eb), allocatable , dimension(:)      :: be_c5h8o2
real(eb), allocatable , dimension(:)      :: be_c2h6
real(eb), allocatable , dimension(:)      :: be_c2h4

real(eb), allocatable , target , dimension(:,:)  :: om_bnd_ch4
real(eb), allocatable , target , dimension(:,:)  :: om_bnd_c3h6
real(eb), allocatable , target , dimension(:,:)  :: om_bnd_c3h8
real(eb), allocatable , target , dimension(:,:)  :: om_bnd_c7h16
real(eb), allocatable , target , dimension(:,:)  :: om_bnd_c7h8
real(eb), allocatable , target , dimension(:,:)  :: om_bnd_ch3oh
real(eb), allocatable , target , dimension(:,:)  :: om_bnd_c5h8o2
real(eb), allocatable , target , dimension(:,:)  :: om_bnd_c2h6
real(eb), allocatable , target , dimension(:,:)  :: om_bnd_c2h4

real(eb), allocatable , target , dimension(:,:)  :: sd1_ch4
real(eb), allocatable , target , dimension(:,:)  :: sd2_ch4

real(eb), allocatable , target , dimension(:,:)  :: sd1_c3h6
real(eb), allocatable , target , dimension(:,:)  :: sd2_c3h6
real(eb), allocatable , target , dimension(:,:)  :: sd3_c3h6

real(eb), allocatable , target , dimension(:,:)  :: sd1_c3h8
real(eb), allocatable , target , dimension(:,:)  :: sd2_c3h8

real(eb), allocatable , target , dimension(:,:)  :: sd1_c7h16
real(eb), allocatable , target , dimension(:,:)  :: sd2_c7h16

real(eb), allocatable , target , dimension(:,:)  :: sd1_c7h8
real(eb), allocatable , target , dimension(:,:)  :: sd2_c7h8
real(eb), allocatable , target , dimension(:,:)  :: sd3_c7h8
real(eb), allocatable , target , dimension(:,:)  :: sd4_c7h8
real(eb), allocatable , target , dimension(:,:)  :: sd5_c7h8

real(eb), allocatable , target , dimension(:,:)  :: sd1_ch3oh
real(eb), allocatable , target , dimension(:,:)  :: sd2_ch3oh
real(eb), allocatable , target , dimension(:,:)  :: sd3_ch3oh
real(eb), allocatable , target , dimension(:,:)  :: sd4_ch3oh

real(eb), allocatable , target , dimension(:,:)  :: sd1_c5h8o2
real(eb), allocatable , target , dimension(:,:)  :: sd2_c5h8o2
real(eb), allocatable , target , dimension(:,:)  :: sd3_c5h8o2
real(eb), allocatable , target , dimension(:,:)  :: sd4_c5h8o2
real(eb), allocatable , target , dimension(:,:)  :: sd5_c5h8o2
real(eb), allocatable , target , dimension(:,:)  :: sd6_c5h8o2

real(eb), allocatable , target , dimension(:,:)  :: sd1_c2h6
real(eb), allocatable , target , dimension(:,:)  :: sd2_c2h6
real(eb), allocatable , target , dimension(:,:)  :: sd3_c2h6

real(eb), allocatable , target , dimension(:,:)  :: sd1_c2h4
real(eb), allocatable , target , dimension(:,:)  :: sd2_c2h4
real(eb), allocatable , target , dimension(:,:)  :: sd3_c2h4
real(eb), allocatable , target , dimension(:,:)  :: sd4_c2h4

real(eb), allocatable , target , dimension(:,:)  :: gammad1_c3h6
real(eb), allocatable , target , dimension(:,:)  :: gammad2_c3h6
real(eb), allocatable , target , dimension(:,:)  :: gammad3_c3h6

```

```

real(eb), allocatable , target , dimension(:,:) :: gammad1_c3h8
real(eb), allocatable , target , dimension(:,:) :: gammad2_c3h8

real(eb), allocatable , target , dimension(:,:) :: gammad1_c7h16
real(eb), allocatable , target , dimension(:,:) :: gammad2_c7h16

real(eb), allocatable , target , dimension(:,:) :: gammad1_c7h8
real(eb), allocatable , target , dimension(:,:) :: gammad2_c7h8
real(eb), allocatable , target , dimension(:,:) :: gammad3_c7h8
real(eb), allocatable , target , dimension(:,:) :: gammad4_c7h8
real(eb), allocatable , target , dimension(:,:) :: gammad5_c7h8

real(eb), allocatable , target , dimension(:,:) :: gammad1_ch3oh
real(eb), allocatable , target , dimension(:,:) :: gammad2_ch3oh
real(eb), allocatable , target , dimension(:,:) :: gammad3_ch3oh
real(eb), allocatable , target , dimension(:,:) :: gammad4_ch3oh

real(eb), allocatable , target , dimension(:,:) :: gammad1_c5h8o2
real(eb), allocatable , target , dimension(:,:) :: gammad2_c5h8o2
real(eb), allocatable , target , dimension(:,:) :: gammad3_c5h8o2
real(eb), allocatable , target , dimension(:,:) :: gammad4_c5h8o2
real(eb), allocatable , target , dimension(:,:) :: gammad5_c5h8o2
real(eb), allocatable , target , dimension(:,:) :: gammad6_c5h8o2

real(eb), allocatable , target , dimension(:,:) :: gammad1_c2h6
real(eb), allocatable , target , dimension(:,:) :: gammad2_c2h6
real(eb), allocatable , target , dimension(:,:) :: gammad3_c2h6

real(eb), allocatable , target , dimension(:,:) :: gammad1_c2h4
real(eb), allocatable , target , dimension(:,:) :: gammad2_c2h4
real(eb), allocatable , target , dimension(:,:) :: gammad3_c2h4
real(eb), allocatable , target , dimension(:,:) :: gammad4_c2h4

real(eb), dimension(:,:), pointer , private :: kappa_d , gamma_d
real(eb), dimension(:), pointer , private :: band_omega

real(eb), allocatable , dimension(:) :: ab , wave_number , lambda
real(eb), allocatable , dimension(:) :: incident_radiance

real(eb), allocatable , dimension(:,:) :: ttau

real(eb), allocatable , dimension(:,:) :: partial_pressures_atm
real(eb), allocatable , dimension(:) :: temp_gas
real(eb), allocatable , dimension(:) :: segment_length_m
real(eb), allocatable , dimension(:) :: total_pressure_atm

real(eb) :: ommin, ommax, lambdamin, lambdamax
real(eb) :: twall, tau, xtot, fv

integer :: nom, npt

real(eb), parameter :: sigma = 5.670400e-8_eb
real(eb), parameter :: m_to_cm = 100.0_eb ! conversion factor meters->centimeters
real(eb), parameter :: cm_to_m = 0.01_eb ! conversion factor centimeters->meters

character(30) :: radcal_id
real(eb) :: pfuel

real(eb), parameter :: zero_p = tiny(sigma)
real(eb), parameter :: pi = acos(-1.0)
real(eb), parameter :: sqrt(pi) = sqrt(pi)
real(eb), parameter :: rpi_sigma = sigma/pi

integer :: i_co, i_co2, i_h2o, i_n2, i_o2, i_fv, i_c2h4, i_c2h6, i_c3h6, i_c3h8
integer :: i_c7h8, i_c7h16, i_ch3oh, i_ch4, i_ch4_old, i_mma

```

Note: variables `sd_<species>_temp` contain the temperature corresponding to the experimental conditions at which the mean absorption coefficient `sd<band index>_<species>` (example: `sd1_ch4`) and the band overlap parameter `gammad<band index>_<species>` (example: `gammad1_c7h8`) were obtained from. The variables `om_bnd_<species>` contain the lower, the upper bounds, and the narrow band size (in wavenumber) of a species main band.

6.1.2 Subroutine init_radcal

INIT_RADCAL SIGNATURE

```
subroutine init_radcal(io)
```

Initializes variables `nom`, vectors `wave_number` and `lambda`, and calls `rcalloc` based on parameters present in input file `radcal.in`.

INIT_RADCAL VARIABLES

```
integer, intent(in) :: io
real(eb) :: dom, omega
integer :: i_wavenumb
```

6.1.3 Subroutine sub_radcal

SUB_RADCAL SIGNATURE

```
subroutine sub_radcal(effective_absorption, planck_mean_absorption, radiance,
total_transmissivity, io)
```

input variables:

- `io`: (integer) output file unit

output variables:

- `effective_absorption` : (real) effective absorption coefficient, in cm^{-1} , as defined by Eq. 2.71
- `planck_mean_absorption` : (real) planck mean absorption coefficient, in cm^{-1} , as defined by Eq. 2.73
- `radiance` : (real) incident power per unit of area per unit of solid angle, units: $\text{W}/\text{m}^2/\text{str}/\text{cm}^{-1}$, as defined by Eq. 2.78

- `total_transmissivity` : (real) total transmissivity, as defined by Eq. 2.76, computed only when `TWALL` (blackbody wall temperature T_w) is strictly greater than 0. Dimensionless number

Local variables:

- `a_collision` : (real) collision broadened fine structure parameter, as defined by Eq. 2.39
- `a_doppler` : (real) doppler broadened fine structure parameter, as defined by Eq. 2.39
- `azotemp` : (real) ratio reference temperature (273 K) over local temperature, $= 273/T$
- `omega` : (real) wavenumber
- `optical_thickness`: (real) optical thickness of the i th species, units: cmstp
- `ptot` : (real) total pressure in atm
- `temp4` : (real) local temperature raised to the power 4
- `x_collision` : (real) optical depth for a pure collision curve of growth, as defined by Eq. 2.58
- `x_doppler` : (real) optical depth for a pure doppler curve of growth, as defined by Eqs. 2.59 and 2.60
- `x_particle` : (real) optical depth for particle, as defined by Eq. 3.4

This is the most important subroutine of the RadCal module. This function solves the RTE as defined by Eqs. 2.57 and 2.64 and returns the effective absorption coefficient, the Planck mean absorption coefficient, the total transmissivity, and populates the global variables `incident_radiance` (spectral incident intensity as defined by Eq. 2.78) and `ttau` (spectral transmissivities used in Eq. 2.64).

SUB_RADCAL VARIABLES

```
integer , intent(in) :: io
real(eb), intent(out) :: effective_absorption , planck_mean_absorption , radiance ,
    total_transmissivity

real(eb), allocatable , dimension(:) :: path_length_cm , azotemp
real(eb), allocatable , dimension(:) :: taus , taul , x_particle , ab_planck , ab_tau , bb_spect ,
    bb_gas , bb_wall
real(eb), allocatable , dimension(:, :) :: curtis_xstar , curtis_acollision , curtis_adoppler ,
    gc , optical_thickness , optical_depth
real(eb) :: rsl , rss , omega , wave_length , dambda , lterm , temp4 , avg_temp , total_length_cm ,
    int_bb_gas , int_bb_wall
integer :: i_wavenumb , kmax , kmin , i_path , i_species
```

6.1.4 Function `collision_broadening`

COLLISION_BROADENING SIGNATURE

```
function collision_broadening(species_pressure_atm,ptot,azotemp) result(gc)
```

This function computes the collision broadening half-width at half-maximum (HWHM). Calculation proceeded in accordance with the SLG model, Table 5-18, in nasa sp-3080, based on eq 5-34 from Ref. [15], also presented in Eq. 2.26. It returns vector g_c that contains the collision broadening HWHM including foreign and self-broadening collision coefficients. g_c units in cm^{-1} .

COLLISION_BROADENING VARIABLES

```

real(eb), dimension(:), intent(in) :: species_pressure_atm ! species partial pressure, units: atm
real(eb), intent(in) :: ptot           ! total pressure, units: atm
real(eb), intent(in) :: azotemp       ! recall azotemp = 273/T, units: none

real(eb), allocatable, dimension(:) :: gc ! units in cm-1
real(eb) :: p_fuel
integer, dimension(6) :: i_indices
integer :: i, ii, i_fuel

```

6.1.5 Subroutine species_optical_depth

SPECIES_OPTICAL_DEPTH SIGNATURE

```

subroutine
    species_optical_depth(path_length_cm,p_atm,ptot,gc,temp,omega,optical_thickness,
    curtis_xstar,curtis_acollision, curtis_adoppler,optical_depth)

```

This subroutine computes the species optical depth for all the species given a wavenumber ω and species optical thickness. It returns the optical depth for each species using the Curtis Godson approximation. Follows method presented in Sections 2.4.1 and 2.4.2.

Arguments in:

- path_length_cm : scalar, physical length, in cm
- p_atm : vector, (dimension nspecies) species partial pressure, in atm
- ptot : scalar, total pressure, in atm
- gc : vector, collision-broadened half-width values, in cm^{-1}
- temp : scalar, local temperature, in K
- omega : scalar, wavenumber, in cm^{-1}
- optical_thickness: vector (dimension nspecies) elements, units in stp.cm.atm

Arguments inout: variables used to compute the Curtis-Godson approximation parameters. The first value (*i.e.*) (nspecies, 1) was either computed previously or is equal to 0 (for the first point).

- curtis_xstar : array of values of $\bar{\kappa}U$. Dimension: (nspecies, 2)

- `curtis_acollision`: array of values of β . Dimension: `(nspecies, 2)`
- `curtis_adoppler`: array of values of γ_D/d . Dimension: `(nspecies, 2)`
- `optical_depth`: array of values of elements optical depth, dimensionless, dimension: `(nspecies, 2)`.

SPECIES_OPTICAL_DEPTH VARIABLES

```

real(eb), dimension(:), intent(in) :: p_atm, optical_thickness, gc
real(eb), intent(in) :: ptot, temp, omega, path_length_cm

real(eb), dimension(:, :), intent(inout) :: curtis_xstar, curtis_acollision, curtis_adoppler,
    optical_depth
real(eb) :: x_doppler, x_collision, xstar
real(eb) :: sdweak, a_collision, a_doppler
integer :: i_model ! model used for snb fitting: 1: goody, 2 malkmus, 3 elsasser
integer :: i

```

6.1.6 Function growth_doppler

GROWTH_DOPPLER

```
elemental function growth_doppler(xstar, a_doppler, i_model) result(x_doppler)
```

This function computes the Doppler curve of growth. Solves either Eq. 2.59 (if `i_model=1` or `3`) or Eq. 2.60 (for `i_model=2`).

Variables in:

- `xstar`: optical pathlength * mean absorption coefficient, $\bar{\kappa}U$
- `a_doppler`: Doppler fine structure parameter, γ_D/d
- `i_model`: model used for SNB fitting: 1: Goody, 2 Malkmus, 3 Elsasser

Variable out:

- `x_doppler`.

GROWTH_DOPPLER

```

real(eb), intent(in) :: xstar
real(eb), intent(in) :: a_doppler
integer, intent(in) :: i_model

real(eb) :: x_doppler

```

6.1.7 Function combined_lines

COMBINED_LINES

```
elemental function combined_lines(x_collision, x_doppler, xstar)
    result(optical_depth)
```

Computes the combined collision (Lorentz) and Doppler optical depths, and the optical depth based on Eqs. 2.61 and 2.62. See Section 2.4.1.

Variables in:

- x_collision: Lorentz curve of growth
- x_doppler: Doppler curve of growth
- xstar: optical pathlength * mean absorption coefficient

Variable out:

- optical_depth.

COMBINED_LINES

```
real(eb), intent(in) :: x_collision
real(eb), intent(in) :: x_doppler
real(eb), intent(in) :: xstar

real(eb) :: optical_depth
real(eb) :: y_doppler, y_collision, y_combined
```

6.1.8 Function Goody

GOODY

```
elemental function goody(xstar, a_collision) result(x_goody)
```

Function computes the equivalent line width over the average line spacing using the goody statistical model, as defined by Eq. 2.48.

Variables in:

- xstar: optical pathlength * mean absorption coefficient
- a_collision : fine structure parameter or overlap parameter β , see Eq. 2.39.

Returns `x_goody`.

GOODY

```
real(eb), intent(in) :: xstar
real(eb), intent(in) :: a_collision
real(eb) :: x_goody
```

6.1.9 Function Malkmus

MALKMUS

```
elemental function malkmus(xstar,a_collision) result(x_malkmus)
```

Function computes the equivalent line width over the average line spacing, using the Malkmus statistical model. See Eq. 2.52.

Variables in:

- `xstar`: optical pathlength * mean absorption coefficient
- `a_collision`: fine structure parameter or overlap parameter β , see Eq. 2.39

Returns `x_malkmus` (optical depth for a pure collision curve).

MALKMUS

```
real(eb), intent(in) :: xstar
real(eb), intent(in) :: a_collision
real(eb) :: x_malkmus
```

6.1.10 Function Elsasser

ELSASSER

```
elemental function elsasser(xstar,a_collision) result(x_elsasser)
```

This function computes the equivalent line width over the average line spacing using the Elsasser statistical model, see Eq. 2.42.

Variables in:

- `xstar`: optical pathlength * mean absorption coefficient
- `a_collision`: fine structure parameter or overlap parameter β , see Eq. 2.39

Returns `x_elsasser`.

ELSASSER

```
real(eb), intent(in) :: xstar
real(eb), intent(in) :: a_collision

real(eb) :: x_elsasser
real(eb) :: x_collision
```

6.1.11 Function `partition_function`

PARTITION_FUNCTION

```
pure function partition_function(transition_wn, degeneracy, temp)
```

This function calculates the partition function of a harmonic quantum oscillator knowing the different frequencies and degeneracies.

PARTITION_FUNCTION

```
real(eb), dimension(:), intent(in) :: transition_wn ! Wavenumber associated with
integer, dimension(:), intent(in) :: degeneracy ! Denegeracy of energy level
real(eb), intent(in) :: temp ! Temperature in Kelvin
real(eb) :: partition_function
real(eb), parameter :: q2 = 1.4388_eb ! speed of light*planck cns/boltzmann
real(eb) :: q2_over_T
integer :: n_mode
integer :: i_mode
```

6.1.12 Function `approx_vib_rot`

APPROX_VIB_ROT

```
pure subroutine approx_vib_rot(transition_matrix, line_strength, om, temp, omega,
& bcnt, be, gcl, gd, gdinv, gddinv, sdweak, line_spacing)
```

APPROX_VIB_ROT

```
integer , dimension(:, :, ), intent(in) :: transition_matrix ! Square matrix
real(eb), dimension(:), intent(in) :: bcnt ! Band center in wavenumbers (cm-1)
real(eb), dimension(:), intent(in) :: om
real(eb), dimension(:), intent(in) :: line_strength

real(eb), intent(in) :: omega ! Wavenumber of sought properties
real(eb), intent(in) :: be ! Rotational constant
real(eb), intent(in) :: temp ! Temperature in Kelvin
real(eb), intent(in) :: gc1
real(eb), intent(in) :: gd
real(eb), intent(in), optional :: line_spacing ! Optional

real(eb), intent(out) :: sdweak
real(eb), intent(out) :: gdinv
real(eb), intent(out) :: gddinv

real(eb), dimension(:), allocatable :: transition_wn, atot
real(eb), parameter :: q2 = 1.4388_eb ! speed of light*planck cns/boltzmann
real(eb), parameter :: t0 = 300._eb ! reference temperature, in kelvin

real(eb) :: t0ot
real(eb) :: q2ot
real(eb) :: dinv

integer :: n_transitions
integer :: n_vibrations
integer :: i_transition
```

6.1.13 Subroutine co2

CO2

```
elemental subroutine co2(omega,temp,gc1,sdweak,gdinv,gddinv,i_model)
```

Given `omega` (wavenumber in cm^{-1}), `temp` (temperature in K), and `gc1` (half width at half maximum for Lorentz line, in cm^{-1}), this subroutine returns the spectral properties of CO₂: spectral mean absorption coefficient (`sdweak`), the collision broadening fine structure parameter (`gdinv`), the Doppler broadening fine structure parameter (`gddinv`), and the narrow band model used (`i_model`).

CO2

```
real(eb), intent(in) :: omega ! wavenumber, units in cm-1
real(eb), intent(in) :: temp ! temperature, units in kelvin
real(eb), intent(in) :: gc1 ! half width at half maximum for lorentz line, units in cm-1

real(eb), intent(out):: sdweak ! narrow band mean absorption coefficient, units in cm-1
real(eb), intent(out):: gdinv ! line width to line spacing ration for lorentz lines
```

```

real(eb), intent(out):: gddinv ! line width to line spacing ration for doppler
integer, intent(out):: i_model ! model used for snb fitting: 1: goody, 2 malkmus, 3 elsasser

integer :: i,j,k,l

real(eb), parameter :: wm_co2 = 44._eb ! molecular weight (g/mol)
real(eb), parameter :: be      = 0.391635_eb ! rotational constant co2
real(eb), parameter :: q2      = 1.4388_eb ! speed of light*planck cns/boltzmann
real(eb), parameter :: t0      = 300._eb ! reference temperature, in kelvin

real(eb), parameter :: om1 = 1354.91_eb ! fundamental frequency for transition (000)->(100), units cm-1
real(eb), parameter :: om2 = 673.0_eb ! fundamental frequency for transition (000)->(010), units cm-1
real(eb), parameter :: om3 = 2396.49_eb ! fundamental frequency for transition (000)->(001), units cm-1

real(eb), dimension(3) :: atot, bcnt
real(eb), dimension(:, ), allocatable :: om, line_strength
integer, dimension(:, :, ), allocatable :: transition_matrix

real(eb) :: aa,bb,cc,qq,ff,gg,sminus,splus,sdstrg,gd,com1,com2,
com3,x13,x23,x33,xbar,oml2,alpha,omprim,v3.gam,omvv3,delta,v,omvbar,
f1,f2,unflo1,unflo2,unflo3,test,vbar1,oma,omb,ttemp,tt,
t1,tw,ww,temp1,temp2,temp3,dinv,a,b,d,g,w1,dinv1,dinv2,dinv3,q2ot,t0ot,q2ot0

```

6.1.14 Subroutine h2o

H₂O

```
elemental subroutine h2o(omega,temp,gc2,sdweak,gdinv,gddinv,i_model)
```

Given omega (wavenumber in cm⁻¹), temp (temperature in K), and gc2 (half width at half maximum for Lorentz line, in cm⁻¹), this subroutine returns the spectral properties of H₂O: spectral mean absorption coefficient (sdweak), the collision broadening fine structure parameter (gdinv), the Doppler broadening fine structure parameter (gddinv), and the narrow band model used (i_model).

H₂O

```

real(eb), intent(in) :: omega ! wavenumber, in cm-1
real(eb), intent(in) :: temp ! temperature, in kelvin
real(eb), intent(in) :: gc2 ! half width at half maximum, in cm-1

real(eb), intent(out) :: sdweak ! spectral mean absorption coefficient, in cm-1
real(eb), intent(out) :: gddinv ! line width to line spacing ration for doppler
real(eb), intent(out) :: gdinv ! line width to line spacing ratio for lorentz boradening
integer, intent(out) :: i_model ! model used for snb fitting: 1: goody, 2 malkmus, 3 elsasser

integer :: i,j
real(eb) :: w1, ww, t1, tt, tw, d, b, dinv, ttemp, gd
real(eb), parameter :: wm_h2o = 18._eb ! molecular weight (g/mol)

```

6.1.15 Subroutine co

CO SIGNATURE

```
subroutine co(omega,temp,gc4,sdweak,gdinv,gddinv,i_model)
```

Given omega (wavenumber in cm^{-1}), temp (temperature in K), and gc4 (half width at half maximum for Lorentz line, in cm^{-1}), this subroutine returns the spectral properties of CO: spectral mean absorption coefficient (sdweak), the collision broadening fine structure parameter (gdinv), the Doppler broadening fine structure parameter (gddinv), and the narrow band model used (i_model).

CO VARIABLES

```
integer j
real(eb) omega,temp,gc4,sdweak,gdinv,gddinv,aa,bb,cc,qq,
ee,ff,gg,sminus,splus,sdstrg,b,alpha,a,ome,wx,wy,omprim,
t0,q2,wm,gd,v,gam,omv,delta,d,omvbar,f1,f2,test,
dinv,q2ot,toaz

integer, intent(out) :: i_model
```

6.1.16 Subroutine pod

POD SIGNATURE

```
elemental subroutine pod(omega,soot_volume_frac,path_length_cm,temp,x_particle)
```

This subroutine calculates the particle optical depth, x_particle, of the soot particles present. Eq. 3.4 is used.

Argument in:

- omega: wavenumber, units: cm^{-1}
- soot_volume_frac: soot volume fraction. no units
- path_length_cm: physical path length. units in cm
- temp: temperature in Kelvin

Argument out:

- x_particle: optical depth due to the presence of soot particle. No units.

POD VARIABLES

```
real(eb), intent(in) :: omega, path_length_cm, temp, soot_volume_frac  
real(eb), intent(out) :: x_particle  
real(eb) :: abco, ff, lambda, rin, rik
```

6.1.17 Subroutine ch4_old

CH4_OLD SIGNATURE

```
subroutine ch4_old(omega,temp,pch4,ptot,gc3,sdweak,gdinv,gddinv,i_model)
```

Given `omega` (wavenumber in cm^{-1}), `temp` (temperature in K), and `gc3` (half width at half maximum for Lorentz line, in cm^{-1}), this subroutine returns the spectral properties of CH_4 using original RadCal data: spectral mean absorption coefficient (`sdweak`), the collision broadening fine structure parameter (`gdinv`), the Doppler broadening fine structure parameter (`gddinv`), and the narrow band model used (`i_model`).

CH4_OLD VARIABLES

```
integer i,j  
real(eb) omega,temp,pch4,ptot,gc3,sdweak,gdinv,gddinv,be,q2,wm,  
gd,om1,om2,om3,om4,com1,com2,com3,com4,dinv,pe,w1,sdb,sdc,q2ot,azot,toaz  
  
integer, intent(out) :: i_model  
  
real(eb), dimension(4) :: atot, bcnt
```

6.1.18 Subroutine ch4

CH4 SIGNATURE

```
subroutine ch4(omega,temp,pch4,ptot,gc3,sdweak,gdinv,gddinv,i_model)
```

Given:

- `omega`: wavenumber in cm^{-1} ,
- `temp`: temperature in K,
- `pch4`: methane partial pressure in atm,

- p_{tot} : total pressure in atm,
- $gc3$: collisional broadening half-width at half-maximum, units in cm^{-1} ,

this subroutine returns the spectral properties of CH_4 using new methane data:

- $sdweak$: spectral mean absorption coefficient, units in $\text{atm}^{-1} \cdot \text{cm}^{-1}$,
- $gdinv$: the collision broadening fine structure parameter, dimensionless,
- $gddinv$: the Doppler broadening fine structure parameter, dimensionless,
- i_model : the narrow band model used.

CH4 VARIABLES

```

real(eb), intent(in) :: omega, temp, pch4, ptot, gc3
real(eb), intent(out) :: sdweak, gdinv, gddinv

integer, intent(out) :: i_model

real(eb) :: gd, pressure_effective, q2ot, azot, toaz, fact1
real(eb) :: dinv_ch4

real(eb), parameter :: q2      = 1.4388_eb ! q2 = speed of light*planck cns/boltzmann
real(eb), parameter :: wm_ch4 = 16.0425_eb ! molecular weight (g/mol)

real(eb), parameter :: be_ch4 = 5.248_eb    ! rotational constants [cm-1]

real(eb), dimension(4), parameter :: om_ch4 = (/2914.2_eb, 1526.0_eb, 3020.3_eb, 1306.2_eb/),
com_ch4 = (/1526.0_eb+2._eb*1306.2_eb, 2914.2_eb+1306.2_eb, 3020.3_eb+1306.2_eb,
           1526.0_eb+3020.3_eb/),
s2_ch4  = (/0.64_eb, 17.6_eb, 14.8_eb, 5.04_eb/)

real(eb), dimension(4) :: atot

integer i

```

6.1.19 Subroutine c3h6

C3H6 SIGNATURE

```
subroutine c3h6(omega,temp,pc3h6,ptot,sdweak,gdinv,gddinv,i_model)
```

Given:

- ω : wavenumber in cm^{-1} ,
- temp : temperature in K,
- pc3h6 : propylene partial pressure in atm,

- p_{tot} : total pressure in atm,
- g_{c3} : collisional broadening half-width at half-maximum, units in cm^{-1} ,

this subroutine returns the spectral properties of propylene using new data:

- s_{dweak} : spectral mean absorption coefficient, units in $\text{atm}^{-1} \cdot \text{cm}^{-1}$,
- g_{dinv} : the collision broadening fine structure parameter, dimensionless,
- g_{ddinv} : the Doppler broadening fine structure parameter, dimensionless,
- i_model : the narrow band model used.

C3H6 VARIABLES

```
real(eb), intent(in) :: omega, temp, pc3h6, ptot
real(eb), intent(out) :: sdweak, gdinv, gddinv

integer, intent(out) :: i_model

real(eb) :: q2ot, azot, toaz
real(eb) :: gd, pressure_effective
real(eb) :: dinv_c3h6

real(eb), parameter :: q2          = 1.4388_eb ! q2 = speed of light*planck cns/boltzmann
real(eb), parameter :: wm_c3h6   = 42.0797_eb ! molecular weight (g/mol)

integer :: i_band, i

logical :: in_band ! true if omega is within some tabulated band, false otherwise
```

6.1.20 Subroutine c3h8

C3H8 SIGNATURE

```
subroutine c3h8(omega,temp,pc3h8,ptot,sdweak,gdinv,gddinv,i_model)
```

Given:

- ω : wavenumber in cm^{-1} ,
- T : temperature in K,
- p_{c3h8} : propane partial pressure in atm,
- p_{tot} : total pressure in atm,
- g_{c3} : collisional broadening half-width at half-maximum, units in cm^{-1} ,

this subroutine returns the spectral properties of propane using new data:

- `sdweak`: spectral mean absorption coefficient, units in $\text{atm}^{-1} \cdot \text{cm}^{-1}$,
- `gdinv`: the collision broadening fine structure parameter, dimensionless,
- `gddinv`: the Doppler broadening fine structure parameter, dimensionless,
- `i_model`: the narrow band model used.

C3H8 VARIABLES

```

real(eb), intent(in) :: omega, temp, pc3h8, ptot
real(eb), intent(out) :: sdweak, gdinv, gddinv

integer, intent(out) :: i_model

real(eb) :: q2ot, azot, toaz
real(eb) :: gd, pressure_effective
real(eb) :: dinv_c3h8

real(eb), parameter :: q2          = 1.4388_eb ! q2 = speed of light*planck cns/boltzmann
real(eb), parameter :: wm_c3h8   = 44.0956_eb ! molecular weight (g/mol)

integer :: i_band, i

logical :: in_band ! true if omega is within some tabulated band, false otherwise

```

6.1.21 Subroutine c7h16

C7H16 SIGNATURE

```
subroutine c7h16(omega,temp,pc7h16,ptot,sdweak,gdinv,gddinv,i_model)
```

Given:

- `omega`: wavenumber in cm^{-1} ,
- `temp`: temperature in K,
- `pc7h16`: heptane partial pressure in atm,
- `ptot`: total pressure in atm,
- `gc3`: collisional broadening half-width at half-maximum, units in cm^{-1} ,

this subroutine returns the spectral properties of heptane using new data:

- `sdweak`: spectral mean absorption coefficient, units in $\text{atm}^{-1} \cdot \text{cm}^{-1}$,
- `gdinv`: the collision broadening fine structure parameter, dimensionless,
- `gddinv`: the Doppler broadening fine structure parameter, dimensionless,

- `i_model`: the narrow band model used.

C7H16 VARIABLES

```

real(eb), intent(in) :: omega, temp, pc7h16, ptot
real(eb), intent(out) :: sdweak, gdinv, gddinv

integer, intent(out) :: i_model

real(eb) :: q2ot, azot, toaz
real(eb) :: gd, pressure_effective
real(eb) :: dinv_c7h16

real(eb), parameter :: q2          = 1.4388_eb ! q2 = speed of light*planck cns/boltzmann
real(eb), parameter :: wm_c7h16 = 100.2019_eb ! molecular weight (g/mol)

integer :: i_band, i

logical :: in_band ! true if omega is within some tabulated band, false otherwise

```

6.1.22 Subroutine c7h8

C7H8 SIGNATURE

```
subroutine c7h8(omega,temp,pc7h8,ptot,sdweak,gdinv,gddinv,i_model)
```

Given:

- `omega`: wavenumber in cm^{-1} ,
- `temp`: temperature in K,
- `pc7h8`: toluene partial pressure in atm,
- `ptot`: total pressure in atm,
- `gc3`: collisional broadening half-width at half-maximum, units in cm^{-1} ,

this subroutine returns the spectral properties of toluene using new data:

- `sdweak`: spectral mean absorption coefficient, units in $\text{atm}^{-1} \cdot \text{cm}^{-1}$,
- `gdinv`: the collision broadening fine structure parameter, dimensionless,
- `gddinv`: the Doppler broadening fine structure parameter, dimensionless,
- `i_model`: the narrow band model used.

C7H8 VARIABLES

```
real(eb), intent(in) :: omega, temp, pc7h8, ptot
real(eb), intent(out) :: sdweak, gdinv, gddinv

integer, intent(out) :: i_model

real(eb) :: q2ot, azot, toaz
real(eb) :: gd, pressure_effective
real(eb) :: dinv_c7h8

real(eb), parameter :: q2      = 1.4388_eb ! q2 = speed of light*planck cns/boltzmann
real(eb), parameter :: wm_c7h8 = 92.1384_eb ! molecular weight (g/mol)

integer :: i_band, i

logical :: in_band ! true if omega is within some tabulated band, false otherwise
```

6.1.23 Subroutine ch3oh

CH3OH SIGNATURE

```
subroutine ch3oh(omega,temp,pch3oh,ptot,sdweak,gdinv,gddinv,i_model)
```

Given:

- omega: wavenumber in cm^{-1} ,
- temp: temperature in K,
- pch3oh: methanol partial pressure in atm,
- ptot: total pressure in atm,
- gc3: collisional broadening half-width at half-maximum, units in cm^{-1} ,

this subroutine returns the spectral properties of methanol using new data:

- sdweak: spectral mean absorption coefficient, units in $\text{atm}^{-1} \cdot \text{cm}^{-1}$,
- gdinv: the collision broadening fine structure parameter, dimensionless,
- gddinv: the Doppler broadening fine structure parameter, dimensionless,
- i_model: the narrow band model used.

CH3OH VARIABLES

```
real(eb), intent(in) :: omega, temp, pch3oh, ptot
real(eb), intent(out) :: sdweak, gdinv, gddinv
```

```

integer , intent(out) :: i_model

real(eb) :: q2ot , azot , toaz
real(eb) :: gd, pressure_effective
real(eb) :: dinv_ch3oh

real(eb), parameter :: q2      = 1.4388_eb ! q2 = speed of light*planck cns/boltzmann
real(eb), parameter :: wm_ch3oh = 32.0419_eb ! molecular weight (g/mol)
integer :: i_band , i

logical :: in_band ! true if omega is within some tabulated band, false otherwise

```

6.1.24 Subroutine c5h8o2

C5H8O2 SIGNATURE

```
subroutine c5h8o2(omega,temp,pc5h8o2,ptot,sdweak,gdinv,gddinv,i_model)
```

Given:

- omega: wavenumber in cm^{-1} ,
- temp: temperature in K,
- pc5h8o2: MMA partial pressure in atm,
- ptot: total pressure in atm,
- gc3: collisional broadening half-width at half-maximum, units in cm^{-1} ,

this subroutine returns the spectral properties of MMA using new data:

- sdweak: spectral mean absorption coefficient, units in $\text{atm}^{-1} \cdot \text{cm}^{-1}$,
- gdinv: the collision broadening fine structure parameter, dimensionless,
- gddinv: the Doppler broadening fine structure parameter, dimensionless,
- i_model: the narrow band model used.

C5H8O2 VARIABLES

```

real(eb), intent(in) :: omega, temp, pc5h8o2, ptot
real(eb), intent(out) :: sdweak, gdinv, gddinv

integer , intent(out) :: i_model

real(eb) :: q2ot , azot , toaz
real(eb) :: gd, pressure_effective
real(eb) :: dinv_c5h8o2

```

```

real(eb), parameter :: q2      = 1.4388_eb    ! q2 = speed of light*planck cns/boltzmann
real(eb), parameter :: wm_c5h8o2 = 100.1158_eb ! molecular weight (g/mol)
integer :: i_band, i

logical :: in_band ! true if omega is within some tabulated band, false otherwise

```

6.1.25 Subroutine c2h6

C2H6 SIGNATURE

```
subroutine c2h6(omega,temp,pc2h6,ptot,sdweak,gdinv,gddinv,i_model)
```

Given:

- omega: wavenumber in cm^{-1} ,
- temp: temperature in K,
- pc2h6: ethane partial pressure in atm,
- ptot: total pressure in atm,
- gc3: collisional broadening half-width at half-maximum, units in cm^{-1} ,

this subroutine returns the spectral properties of ethane using new data:

- sdweak: spectral mean absorption coefficient, units in $\text{atm}^{-1} \cdot \text{cm}^{-1}$,
- gdinv: the collision broadening fine structure parameter, dimensionless,
- gddinv: the Doppler broadening fine structure parameter, dimensionless,
- i_model: the narrow band model used.

C2H6 VARIABLES

```

real(eb), intent(in) :: omega, temp, pc2h6, ptot
real(eb), intent(out) :: sdweak, gdinv, gddinv

integer, intent(out) :: i_model

real(eb) :: q2ot, azot, toaz
real(eb) :: gd, pressure_effective
real(eb) :: dinv_c2h6

real(eb), parameter :: q2      = 1.4388_eb    ! q2 = speed of light*planck cns/boltzmann
real(eb), parameter :: wm_c2h6 = 30.0690_eb ! nist webbook data
integer :: i_band, i

logical :: in_band ! true if omega is within some tabulated band, false otherwise

```

6.1.26 Subroutine c2h4

C2H4 SIGNATURE

```
subroutine c2h4(omega,temp,pc2h4,ptot,sdweak,gdinv,gddinv,i_model)
```

Given:

- omega: wavenumber in cm^{-1} ,
- temp: temperature in K,
- pc2h4: ethylene partial pressure in atm,
- ptot: total pressure in atm,
- gc3: collisional broadening half-width at half-maximum, units in cm^{-1} ,

this subroutine returns the spectral properties of ethylene using new data:

- sdweak: spectral mean absorption coefficient, units in $\text{atm}^{-1} \cdot \text{cm}^{-1}$,
- gdinv: the collision broadening fine structure parameter, dimensionless,
- gddinv: the Doppler broadening fine structure parameter, dimensionless,
- i_model: the narrow band model used.

C2H4 VARIABLES

```
real(eb), intent(in) :: omega, temp, pc2h4, ptot
real(eb), intent(out) :: sdweak, gdinv, gddinv

integer, intent(out) :: i_model

real(eb) :: q2ot, azot, toaz
real(eb) :: gd, pressure_effective
real(eb) :: dinv_c2h4

real(eb), parameter :: q2      = 1.4388_eb ! q2 = speed of light*planck cns/boltzmann
real(eb), parameter :: wm_c2h4 = 28.0532_eb ! nist webbook data
integer :: i_band, i

logical :: in_band ! true if omega is within some tabulated band, false otherwise
```

6.1.27 Function get_spectral_absorption

GET_SPECTRAL_ABSORPTION

```
pure real(eb) function
    get_spectral_absorption(omega,temp,sd_temp,bounds,absorption_data)
```

This function returns interpolated (in temperature and wavenumber) values of spectral absorption.

Variables in:

- omega : wavenumber, units in cm^{-1}
- temp : gas temperature, units in K
- sd_temp: vector of temperature measurements, units in K
- bounds : vector of wavenumber bounds and spacing for a given band, dimensions (3)
- absorption_data: array of species spectral measurements. Note: first dimension equals to dimension of sd_temp.

Action: Bilinear interpolation of absorption_data.

GET_SPECTRAL_ABSORPTION

```
real(eb), intent(in) :: omega
real(eb), intent(in) :: temp
real(eb), dimension(:), intent(in)    :: sd_temp, bounds
real(eb), dimension(:, :, ), intent(in) :: absorption_data

real(eb) :: delta_t
real(eb) :: delta_w
real(eb) :: w1
real(eb) :: omega_min, omega_max, delta_omega
real(eb) :: ttemp
real(eb) :: interpolated_value

integer :: n_temp, n_bounds, n_abs_data1, n_abs_data2
integer :: i_omega, i_temp, i_omegal, i_omega2

logical :: cross
```

6.1.28 Function planck

PLANCK

```
elemental real(eb) function planck(temp,lambda)
```

Computes blackbody distribution at wavelength lambda and at temperature temp. Values returned in units of $\text{W}/\text{m}^2/\text{str}/\text{cm}^{-1}$. Solves Eq. 2.21.

Variables in:

- `temp`: temperature, units in K
- `lambda`: wavelength, units in μm

PLANCK

```
real (eb), intent(in):: temp, lambda
real (eb), parameter :: q1 = 1.19088e8_eb ! q1 = 2*speed of light^2*planck_cnst
real (eb), parameter :: q2 = 14388._eb        ! q2 = speed of light*planck cns/boltzmann
real (eb) :: c      ! c = lambda * temp
```

6.1.29 Function `planck_wn`

PLANCK_WN

```
elemental real(eb) function planck_wn(temp, omega)
```

Computes blackbody distribution at wavenumber `omega` and at temperature `temp`. Values returned in units of $\text{W}/\text{m}^2/\text{str}/\text{cm}^{-1}$. Solves Eq. 2.21.

Variables in:

- `temp`: temperature, units in K
- `omega`: wavenumber, units in cm^{-1}

PLANCK_WN

```
real (eb), intent(in):: temp, omega
real (eb), parameter :: q1 = 1.19088e-8_eb ! q1 = 2*speed of light^2*planck_cnst
real (eb), parameter :: q2 = 1.4388_eb
real (eb) :: c      ! c = temp/omega
```

6.1.30 Function `integration`

INTEGRATION SIGNATURE

```
real(eb) function integration(x,y,io)
```

Performs numerical integration of the vector y over the range given by vector x . It does not assume any regularity of x . The integration is based on Simpson rule over non regular abscissa, uses Lagrangian interpolation using 3 points (quadratic interpolation). Note: io is the unit of output file, which is needed for printing error message.

INTEGRATION VARIABLES

```
real(eb), intent(in), dimension(:) :: x,y  
integer , intent(in) :: io  
  
real(eb) :: alpha, beta, gamma, b, a, segment_int  
integer :: i_point, n_points, i, j ,k
```

6.1.31 Subroutine ralloc

RCALLOC SIGNATURE

This subroutine allocates memory and assigns the variables containing the spectral properties of the species present in RadCal.

6.1.32 Subroutine populate_species

POPULATE_SPECIES SIGNATURE

```
subroutine populate_species(io)
```

This function populates the variable `species` that contains the RadCal name and the name of the species present in gas phase.

POPULATE_SPECIES VARIABLES

```
integer , intent(in) :: io
```

6.1.33 Function index_species

INDEX_SPECIES SIGNATURE

```
function index_species(molecule) result(i_molecule)
```

This function returns the index of the molecule presents in the variable species. i_molecule is such that:

molecule = species(i_molecule)%id or
molecule = species(i_molecule)%radcal_id.

INDEX_SPECIES VARIABLES

```
character(len=*) :: molecule  
integer :: i_molecule  
integer :: i_species  
logical :: found
```

6.1.34 Subroutine rcdealloc

RCDEALLOC SIGNATURE

```
subroutine rcdealloc
```

Deallocates arrays variables. Performed prior to RadCal exit.

6.1.35 Subroutine termination

TERMINATION SIGNATURE

```
subroutine termination(ierr,io)
```

Subroutine called when exceptions are raised. Terminates the program and writes error messages depending on the context.

Variables passed in:

- ierr : error message indice
- io : file unit number.

TERMINATION VARIABLES

```
integer , intent(in) :: ierr , io  
character(len=2056) :: message
```

6.1.36 Subroutine write_input

WRITE_INPUT SIGNATURE

```
subroutine write_input(io)
```

This subroutine writes a default RADCAL.in in the case that no RADCAL.in is provided. In particular, it writes the available species. This subroutine should only be called when RADCAL.in does not exist.

WRITE_INPUT VARIABLES

```
integer , intent(in) :: io  
  
integer , parameter :: i_input = 10  
integer :: ierr  
character(len=30) :: filename  
  
character(len=2048) :: header  
character(len=2048) :: line_text  
character :: character_line(80)  
  
logical :: file_exist  
  
integer :: i_species , i
```

6.1.37 Subroutine read_input

READ_INPUT SIGNATURE

```
subroutine read_input(io)
```

This subroutine reads the input file RADCAL.in (unit io).

READ_INPUT VARIABLES

```
integer , intent(in) :: io  
integer :: i_input , ierr
```

```

character(len=30) :: filename
logical           :: file_exist

```

6.1.38 Subroutine read_point

READ_POINT SIGNATURE

```
subroutine read_point(i_input,i_output)
```

This subroutine reads the input file RADCAL.in (unit i_input) and searches for the keyword path_segment. It counts the number of homogeneous segments that comprise a pathline, and assigns user defined values of species mole fractions or volume fraction (only for soot), temperature (assumed to be uniform along a given homogeneous segment of the pathline), length length, and pressure (in atm) to all the segments.

Units:

- T, temperature, in K
- LENGTH, homogeneous segment length, in m
- species data (x_{species}), in mole fraction
- pressure, in atm
- fv, soot volume fraction, dimensionless.

READ_POINT VARIABLES

```

integer , intent(in) :: i_input   ! unit of the input file. already opened
integer , intent(in) :: i_output  ! unit of the output file. already opened

type gas_phase
    real(kind=eb), pointer :: obj
    character(len=30)      :: name
end type gas_phase

type(gas_phase), allocatable, dimension(:) :: Mole_Fraction

real(kind=eb) :: sum_mole_fraction

real(kind=eb) :: t, length, pressure, fv

real(kind=eb), target :: xco2, xh2o, xco, xch4, xc2h4, xc2h6, xc3h8, xc3h6, xc7h8, xc7h16,
                      xch3oh, xmma, xn2, xch4_old, xo2

character(len=255) :: line

integer :: n_segment, i_segment, i_species, i_species_gas, status, i_fv

```

6.1.39 Subroutine read_band

READ_BAND SIGNATURE

```
subroutine read_band(i_input, i_output)
```

This subroutine reads the input file RADCAL.in (unit *i_input*) and searches for the keyword &BANDS. &BANDS defines the lower and upper bound of the spectrum to be computed, *ommin* and *ommax*, respectively. Both are given in cm⁻¹.

READ_BAND VARIABLES

```
integer , intent(in) :: i_input    ! unit of the input file. alreay opened
integer , intent(in) :: i_output   ! unit of the output file. alreay opened
integer :: io_err    ! error condition number
```

6.1.40 Subroutine read_wall

READ_WALL SIGNATURE

```
subroutine read_wall(i_input, i_output)
```

This subroutine reads the input file RADCAL.in (unit *i_input*) and searches for the keyword &WALL which defines the wall (or infinity) temperature: TWALL. In RadCal, the wall emits like a blackbody of temperature TWALL.

READ_WALL VARIABLES

```
integer , intent(in) :: i_input    ! unit of the input file. alreay opened
integer , intent(in) :: i_output   ! unit of the output file. alreay opened
integer :: io_err    ! catch the value of the error raised by output subroutine
```

6.1.41 Subroutine read_header

READ_HEADER SIGNATURE

```
subroutine read_header(i_input,i_output)
```

This subroutine reads the input file RADCAL.in (unit *i_input*) and searches for the keyword &HEADER. &HEADER defines the case id (CHID) used to generate the output Tecplot file and the case title (TITLE), which is to be printed in the output file.

READ_HEADER VARIABLES

```
integer , intent(in) :: i_input ! unit of the input file. already opened
integer , intent(in) :: i_output ! unit of the output file. already opened
integer :: io_err ! catch the value of the error raised by output subroutine
```

6.2 Driver (main) Program

6.2.1 Program driver

DRIVER MODULES USED

```
use radcal
```

This is the main program. It operates the different RadCal functions that read the input file, allocate the needed variables, solve the RTE, and print the results. Note: the type *real(exb)* is used for intrinsic timer routine *cpu_time*. The floating type *eb* is defined in the *radcal* module.

DRIVER VARIABLES

```
integer , parameter :: exb = selected_real_kind(16)
real(exb) , allocatable , dimension(:) :: transmissivity
real(exb) :: amean , planck_mean_absorption , flux , total_length_m , total_length_cm ,
total_transmissivity
integer :: io
character(len=255) :: filename
real(exb) :: time_init
real(exb) :: time_end
```

6.2.2 Subroutine tau_print

TAU_PRINT SIGNATURE

```
subroutine tau_print(case_id, pressure, path_length, transmissivity, wave_length)
```

This function prints, in ASCII format, the wavenumber in cm^{-1} , the transmissivity in %, and the incident radiance in $\text{W}/\text{m}^2/\text{str}/\text{cm}^{-1}$, in the file <case_id>.tec.

TAU_PRINT MODULES USED

```
use radcal, only : eb, incident_radiance
```

TAU_PRINT VARIABLES

```
real(eb), dimension(:), intent(in) :: wave_length      ! Wave length in micron
real(eb), dimension(:), intent(in) :: transmissivity   ! Transmissivity
real(eb), intent(in) :: pressure
real(eb), intent(in) :: path_length

character(len=255), intent(in) :: case_id

character(len=15)  :: pressure_atm
character(len=15)  :: path_length_m
character(len=255) :: filename
character(len=50)  :: format_output

integer :: n_max
integer :: i_tecfile, i
```

Chapter 7

Verification Tests

This chapter reports the results of the verification tests performed with the new fuel data, *i.e.* Ethylene (C_2H_4), Ethane (C_2H_6), Propylene (C_3H_6), Propane (C_3H_8), Toluene (C_7H_8), *n*-Heptane (C_7H_{16}), Methanol (CH_3OH), Methyl Methacrylate ($C_5H_8O_2$). Synthetic transmissivity spectrum were generated with RadCal and compared with all the experimental data they were extract from. The experimental data resolution was adjusted to match that of RadCal:

$$\begin{cases} 5 \text{ cm}^{-1}, & \omega \leq 1000\text{cm}^{-1} \\ 25 \text{ cm}^{-1}, & 5000 > \omega > 1000\text{cm}^{-1} \\ 50 \text{ cm}^{-1}, & \omega > 5000\text{cm}^{-1} \end{cases} \quad (7.1)$$

The relative error between the experimental and the RadCal-generated transmissivity, denoted $\varepsilon(\tau_\omega)$, was also quantified. The relative error between the experimental and the RadCal calculated transmissivities can also be quantified by a weighted average relative error ε over the entire experimental spectrum. A useful test function to perform the weighting is given by the spectral emissivity. Assuming Kirchhoff's law applies for each wavenumber over a narrow band, the spectral emissivity of a narrow band, denoted $\bar{\varepsilon}_\omega$, is given by:

$$\bar{\varepsilon}_\omega = 1 - \bar{\tau}_\omega. \quad (7.2)$$

The weighted average error is then defined by the following relation:

$$\langle \varepsilon(\bar{\tau}_\omega) \rangle = \frac{\int_{700}^{4000} \bar{\varepsilon}_\omega \varepsilon(\bar{\tau}_\omega) d\omega}{\int_{700}^{4000} \bar{\varepsilon}_\omega d\omega}. \quad (7.3)$$

Figure 7.1 plots the maximum relative error and the maximum integrated weighted error for all the new species. Note that the values given in these plot correspond to the maximum over the set of tested temperatures.

In the following sections below, for each species, detailed plots comparing the spectral experimental transmissivities with the synthetic ones calculated with RadCal are presented along with plots of the spectral relative error in transmissivity for each pressure-path and temperature tested. Very good agreement is overall found except in some well localized parts of the spectrum for the heaviest molecules and usually at elevated temperature. The reason behind it is that at elevated temperature, the experimental measurements were very close to the optically thin limit, *i.e.* $\tau \rightarrow 1$, and thus some of the measurements were affected by the FTIR sensitivity. Nevertheless, when comparing integrated quantities, *e.g.* the integrated weighted error, the match between experimental and predicted results is very good.

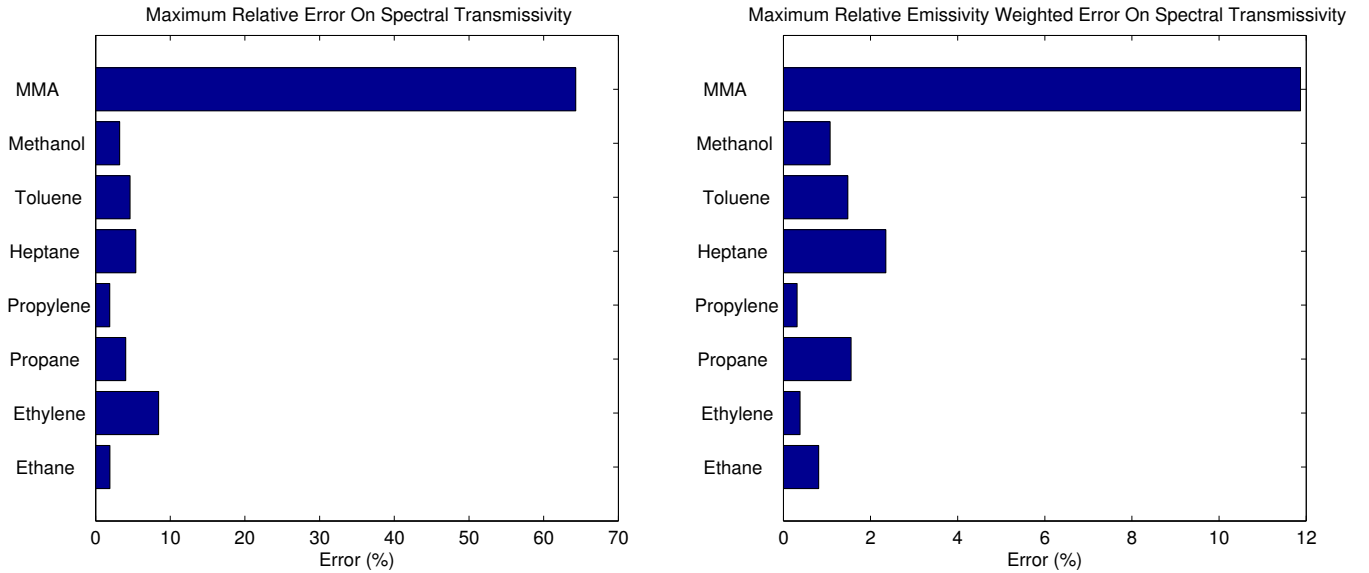


Figure 7.1: Left: Maximum relative error, in percent, across the whole spectrum and temperature for the new molecules implemented in RadCal. Right: Maximum integrated weighted error (across tested temperatures) calculated using Eq. 7.3.

7.1 Ethylene: C₂H₄

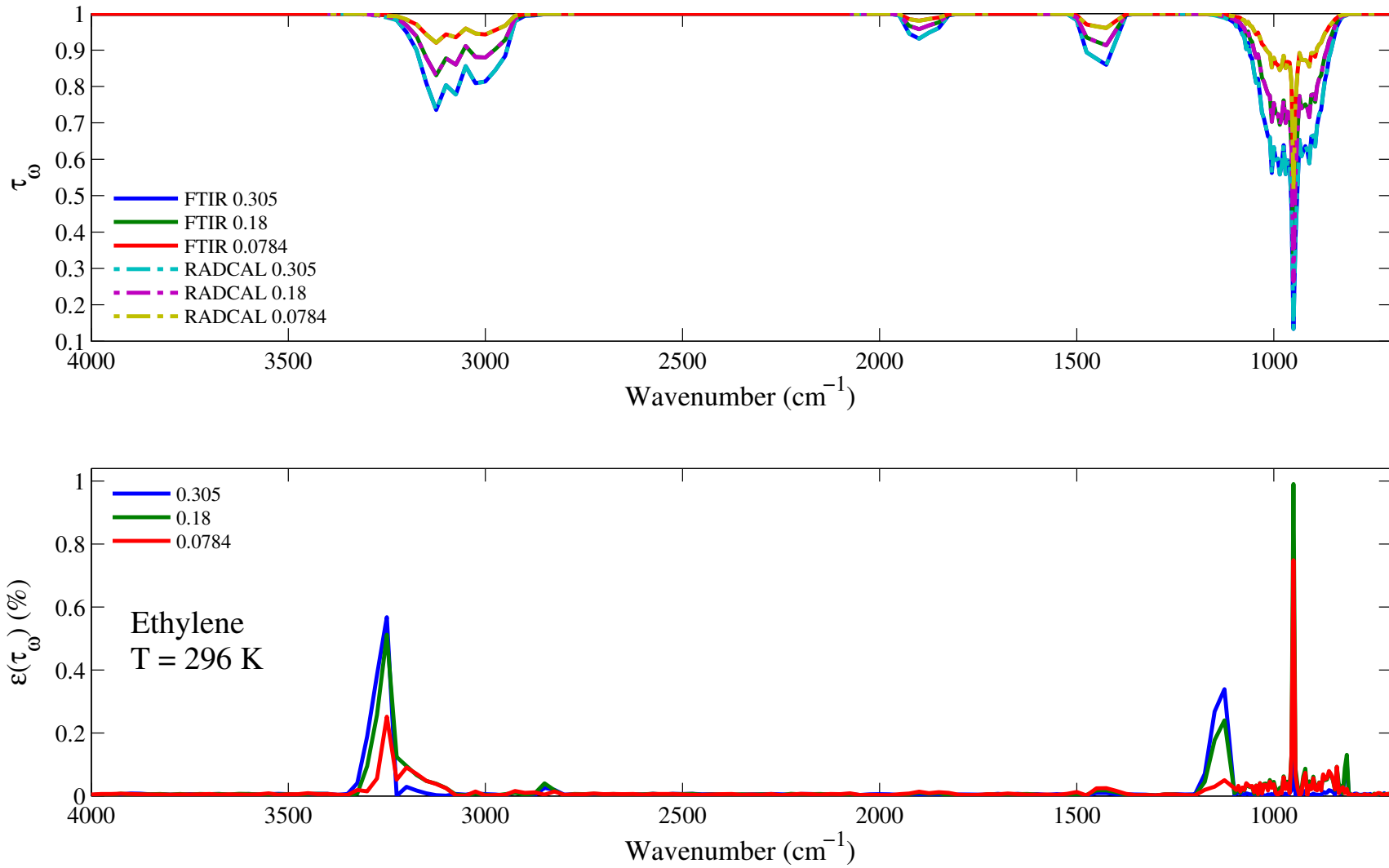


Figure 7.2: Top: comparison between the experimental (solid lines) and RadCal-generated synthetic (dashed lines) spectral transmissivity profiles, denoted τ_ω , of ethylene of an isothermal homogeneous column of ethylene. Bottom: relative transmissivity error, denoted $\varepsilon(\tau_\omega)$, between the experiment and the synthetic profiles presented on the top figure. Three different pressure path lengths are considered: 0.305, 0.18, and 0.0784 atm.cm. The gas temperature is set at 296 K and the total pressure is 101 kPa. Note: the experimental data resolution has been changed to match that of the narrow band model.

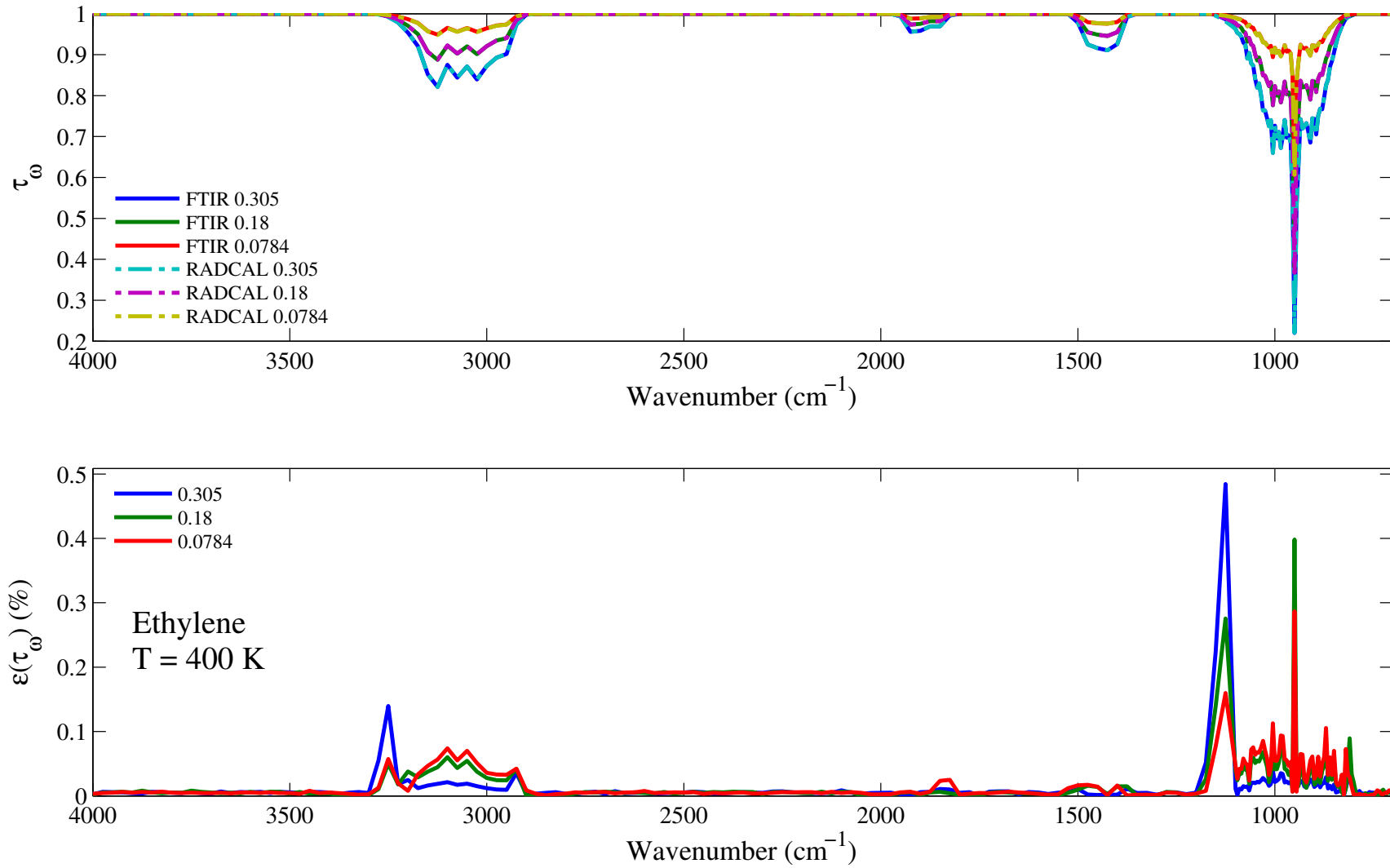


Figure 7.3: Top: comparison between the experimental (solid lines) and RadCal-generated synthetic (dashed lines) spectral transmissivity profiles, denoted τ_ω , of ethylene of an isothermal homogeneous column of ethylene. Bottom: relative transmissivity error, denoted $\varepsilon(\tau_\omega)$, between the experiment and the synthetic profiles presented on the top figure. Three different pressure path lengths are considered: 0.305, 0.18, and 0.0784 atm.cm. The gas temperature is set at 400 K and the total pressure is 101 kPa. Note: the experimental data resolution has been changed to match that of the narrow band model.

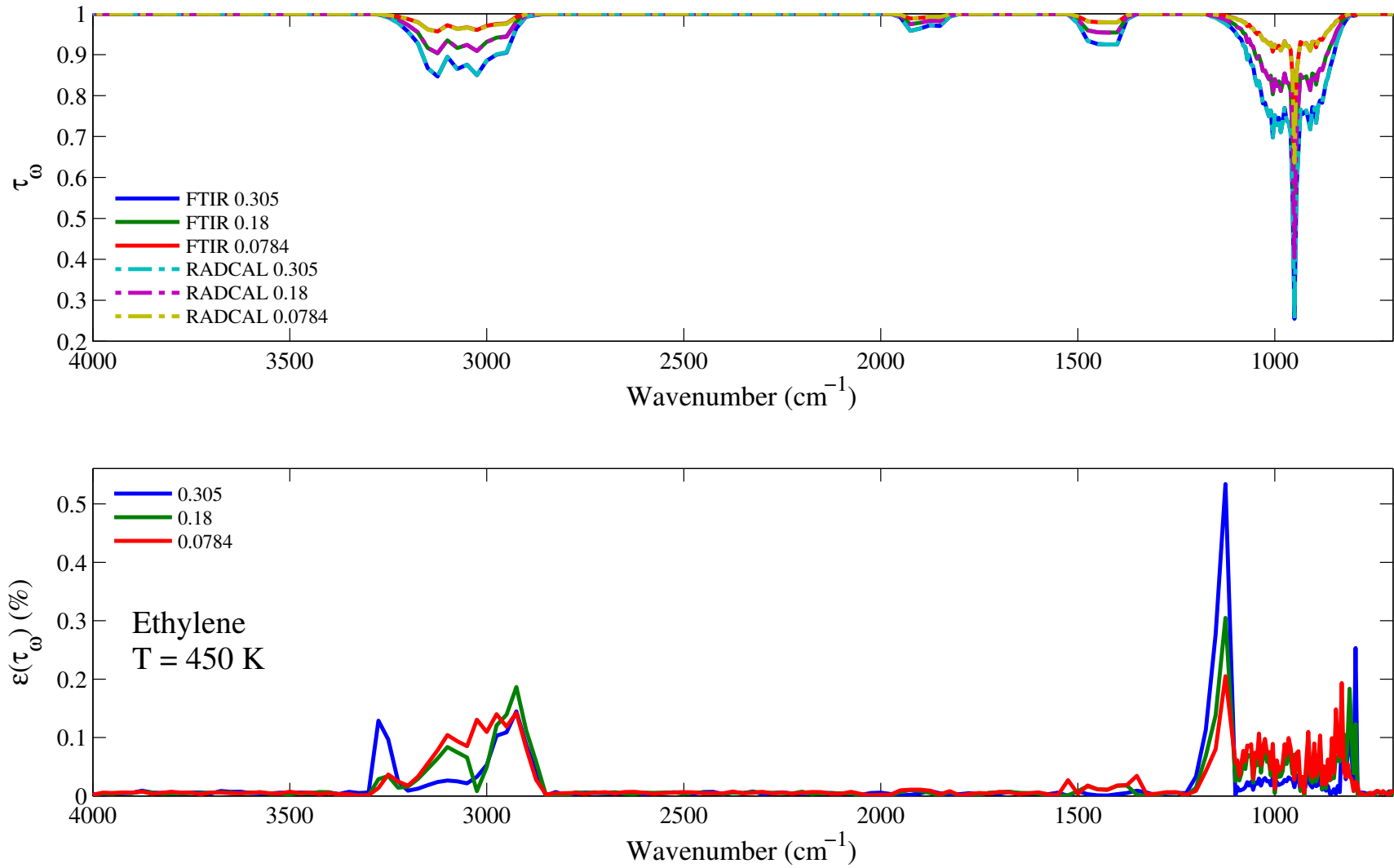


Figure 7.4: Top: comparison between the experimental (solid lines) and RadCal-generated synthetic (dashed lines) spectral transmissivity profiles, denoted τ_ω , of ethylene of an isothermal homogeneous column of ethylene. Bottom: relative transmissivity error, denoted $\varepsilon(\tau_\omega)$, between the experiment and the synthetic profiles presented on the top figure. Three different pressure path lengths are considered: 0.305, 0.18, and 0.0784 atm.cm. The gas temperature is set at 450 K and the total pressure is 101 kPa. Note: the experimental data resolution has been changed to match that of the narrow band model.

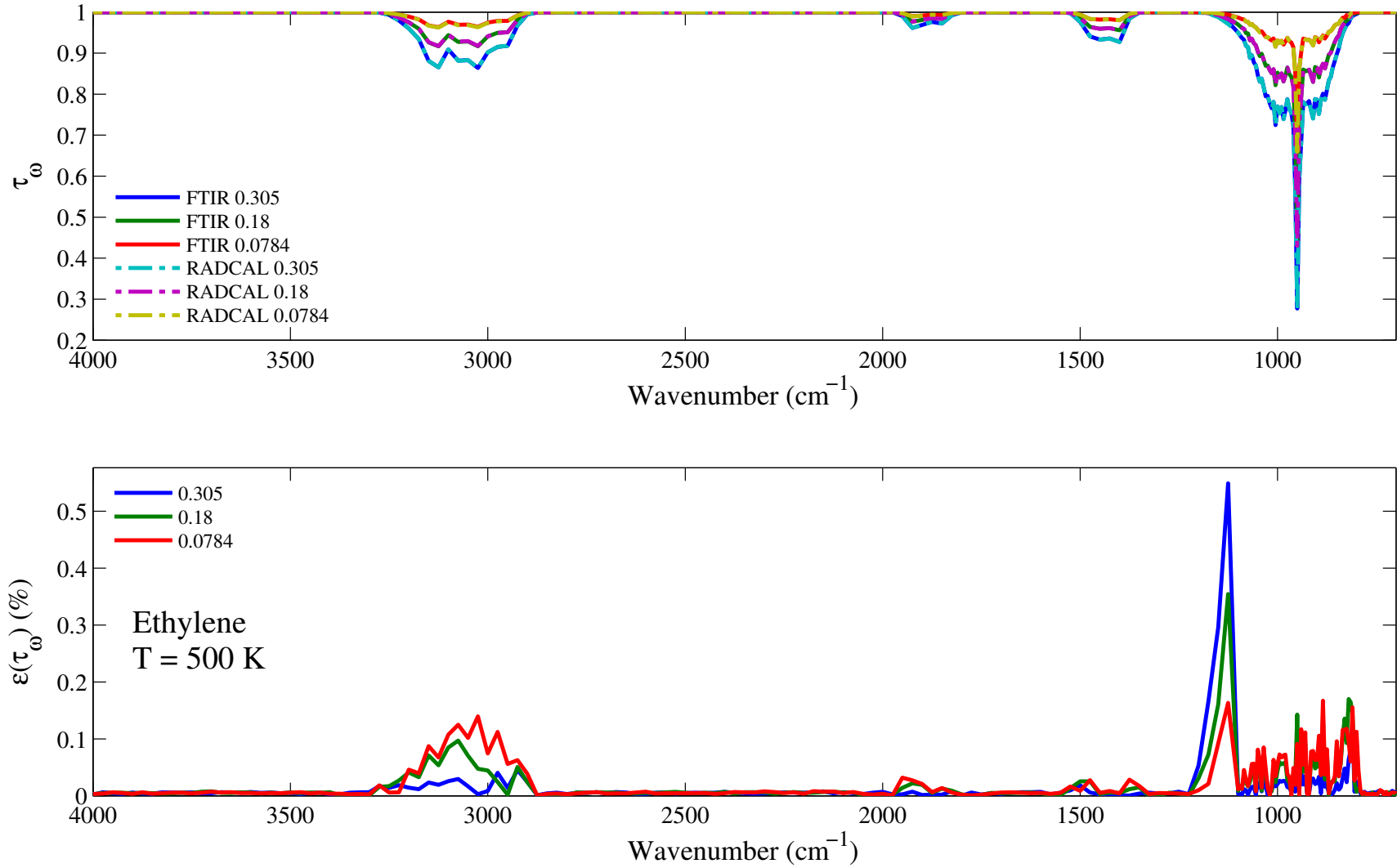


Figure 7.5: Top: comparison between the experimental (solid lines) and RadCal-generated synthetic (dashed lines) spectral transmissivity profiles, denoted τ_ω , of ethylene of an isothermal homogeneous column of ethylene. Bottom: relative transmissivity error, denoted $\varepsilon(\tau_\omega)$, between the experiment and the synthetic profiles presented on the top figure. Three different pressure path lengths are considered: 0.305, 0.18, and 0.0784 atm.cm. The gas temperature is set at 500 K and the total pressure is 101 kPa. Note: the experimental data resolution has been changed to match that of the narrow band model.

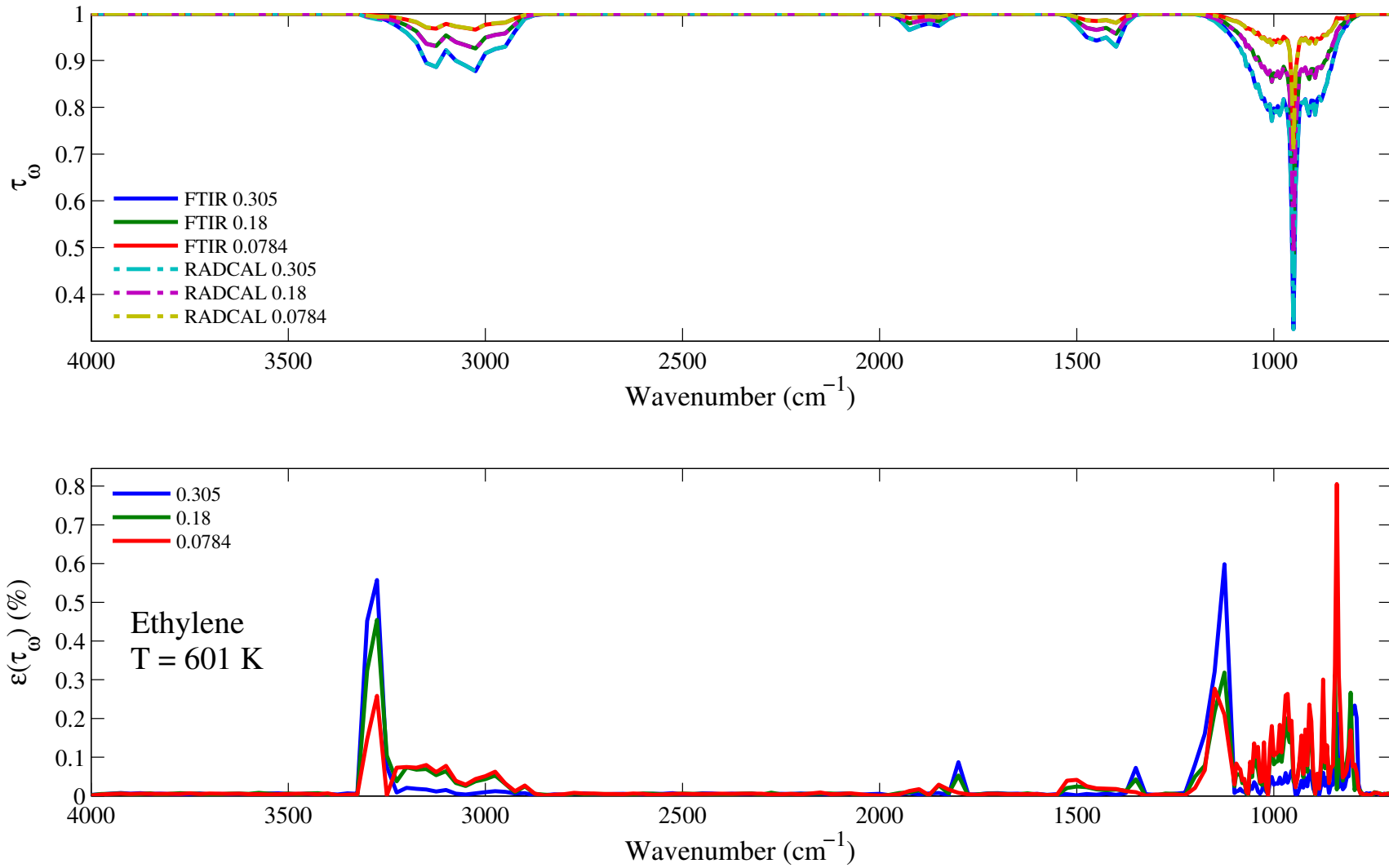


Figure 7.6: Top: comparison between the experimental (solid lines) and RadCal-generated synthetic (dashed lines) spectral transmissivity profiles, denoted τ_ω , of ethylene of an isothermal homogeneous column of ethylene. Bottom: relative transmissivity error, denoted $\varepsilon(\tau_\omega)$, between the experiment and the synthetic profiles presented on the top figure. Three different pressure path lengths are considered: 0.305, 0.18, and 0.0784 atm.cm. The gas temperature is set at 601 K and the total pressure is 101 kPa. Note: the experimental data resolution has been changed to match that of the narrow band model.

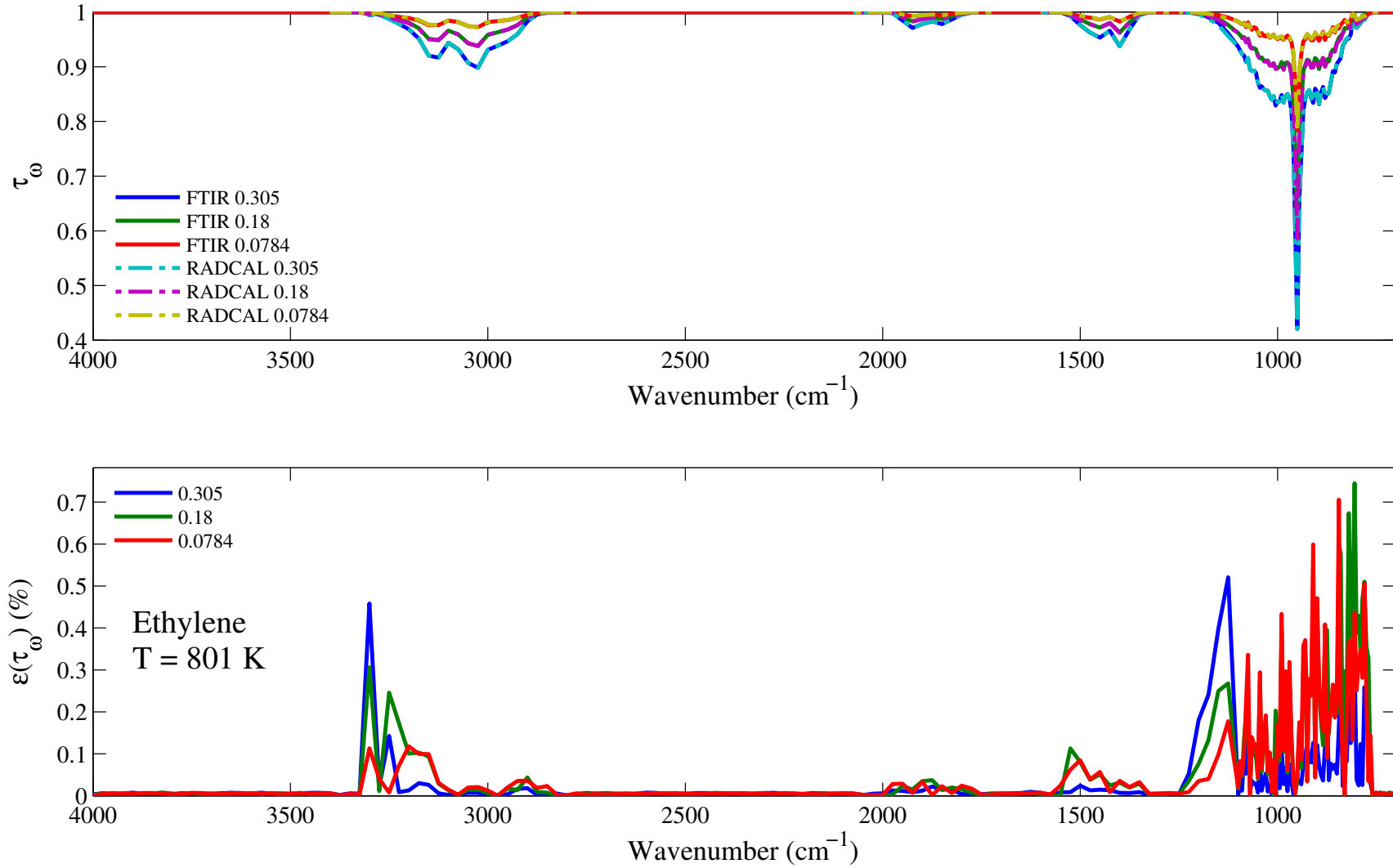


Figure 7.7: Top: comparison between the experimental (solid lines) and RadCal-generated synthetic (dashed lines) spectral transmissivity profiles, denoted τ_ω , of ethylene of an isothermal homogeneous column of ethylene. Bottom: relative transmissivity error, denoted $\varepsilon(\tau_\omega)$, between the experiment and the synthetic profiles presented on the top figure. Three different pressure path lengths are considered: 0.305, 0.18, and 0.0784 atm.cm. The gas temperature is set at 801 K and the total pressure is 101 kPa. Note: the experimental data resolution has been changed to match that of the narrow band model.

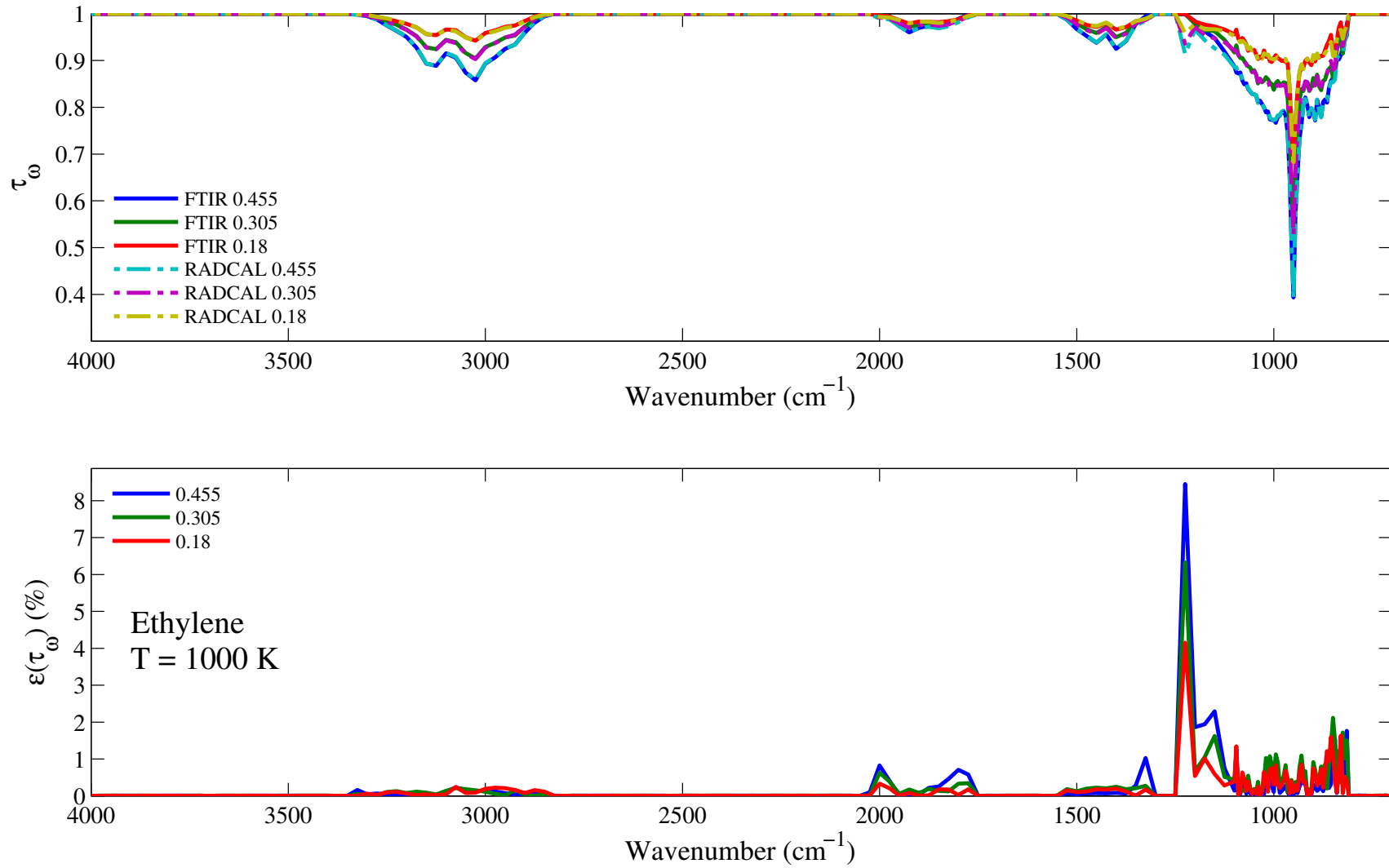


Figure 7.8: Top: comparison between the experimental (solid lines) and RadCal-generated synthetic (dashed lines) spectral transmissivity profiles, denoted τ_ω , of ethylene of an isothermal homogeneous column of ethylene. Bottom: relative transmissivity error, denoted $\varepsilon(\tau_\omega)$, between the experiment and the synthetic profiles presented on the top figure. Three different pressure path lengths are considered: 0.305, 0.18, and 0.0784 atm.cm. The gas temperature is set at 1000 K and the total pressure is 101 kPa. Note: the experimental data resolution has been changed to match that of the narrow band model.

7.2 Ethane: C₂H₆

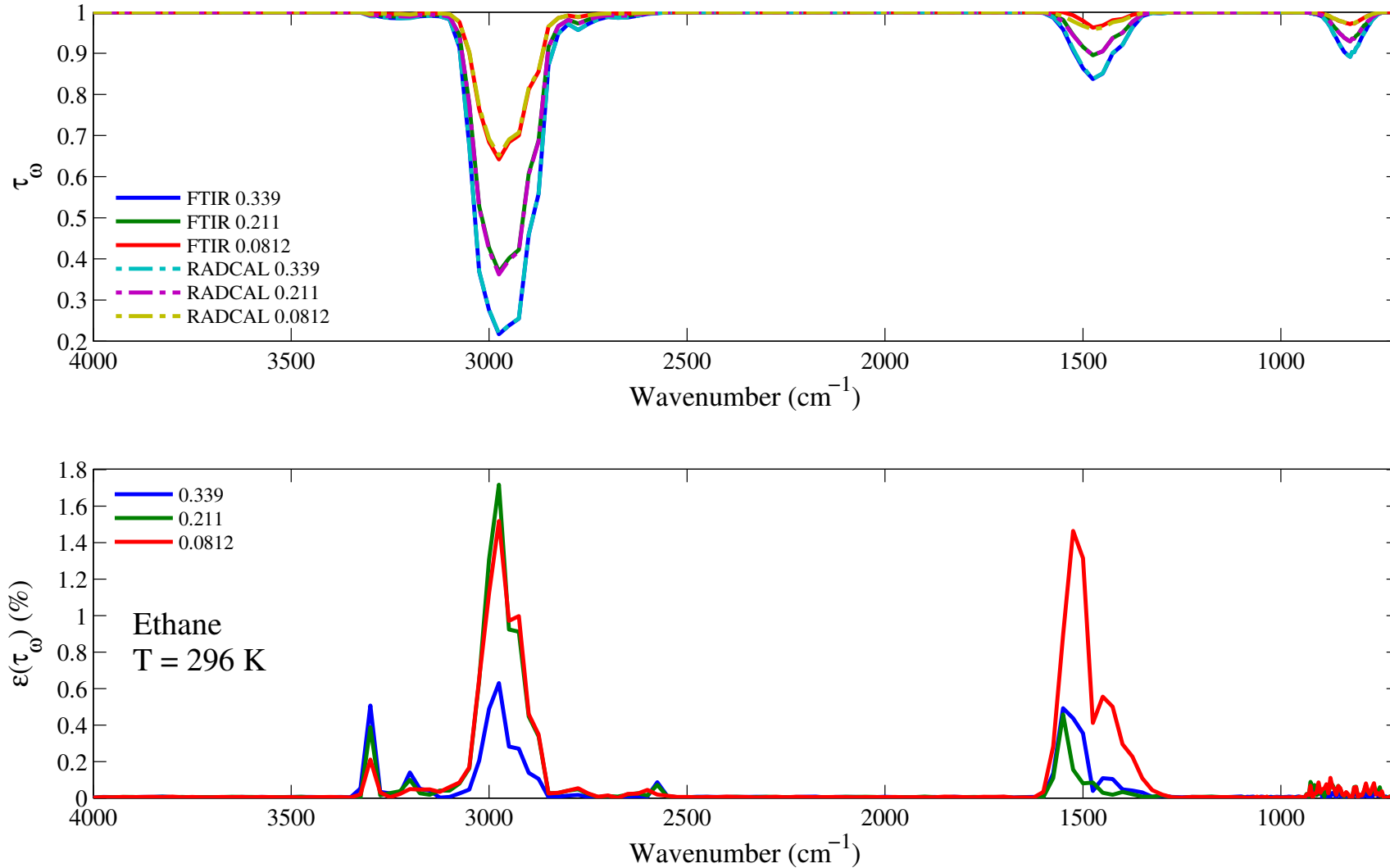


Figure 7.9: Top: comparison between the experimental (solid lines) and RadCal-generated synthetic (dashed lines) spectral transmissivity profiles, denoted τ_ω , of ethane of an isothermal homogeneous column of ethane. Bottom: relative transmissivity error, denoted $\varepsilon(\tau_\omega)$, between the experiment and the synthetic profiles presented on the top figure. Three different pressure path lengths are considered: 0.339, 0.211, and 0.0812 atm.cm. The gas temperature is set at 296 K and the total pressure is 101 kPa. Note: the experimental data resolution has been changed to match that of the narrow band model.

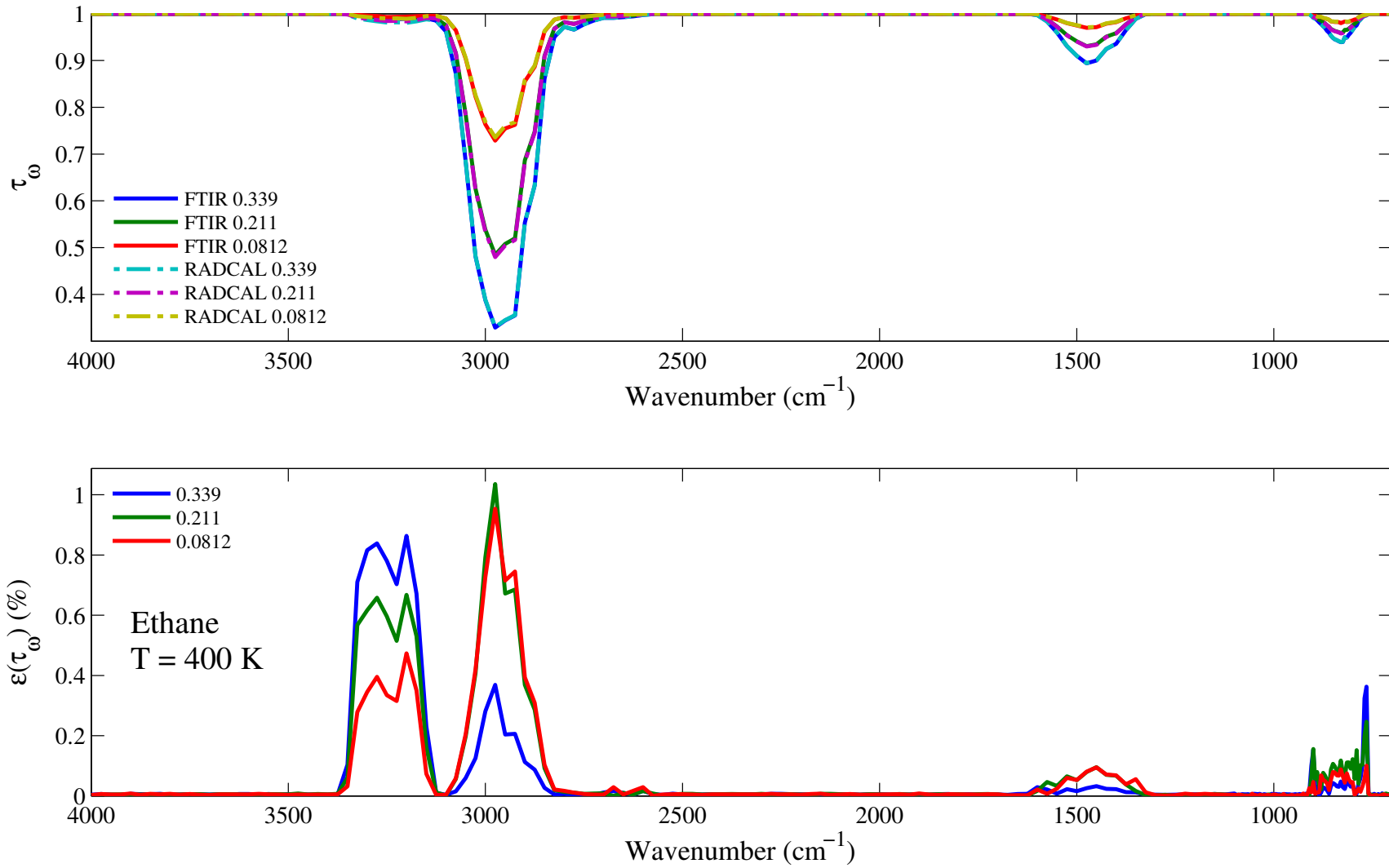


Figure 7.10: Top: comparison between the experimental (solid lines) and RadCal-generated synthetic (dashed lines) spectral transmissivity profiles, denoted τ_ω , of ethane of an isothermal homogeneous column of ethane. Bottom: relative transmissivity error, denoted $\varepsilon(\tau_\omega)$, between the experiment and the synthetic profiles presented on the top figure. Three different pressure path lengths are considered: 0.339, 0.211, and 0.0812 atm.cm. The gas temperature is set at 400 K and the total pressure is 101 kPa. Note: the experimental data resolution has been changed to match that of the narrow band model.

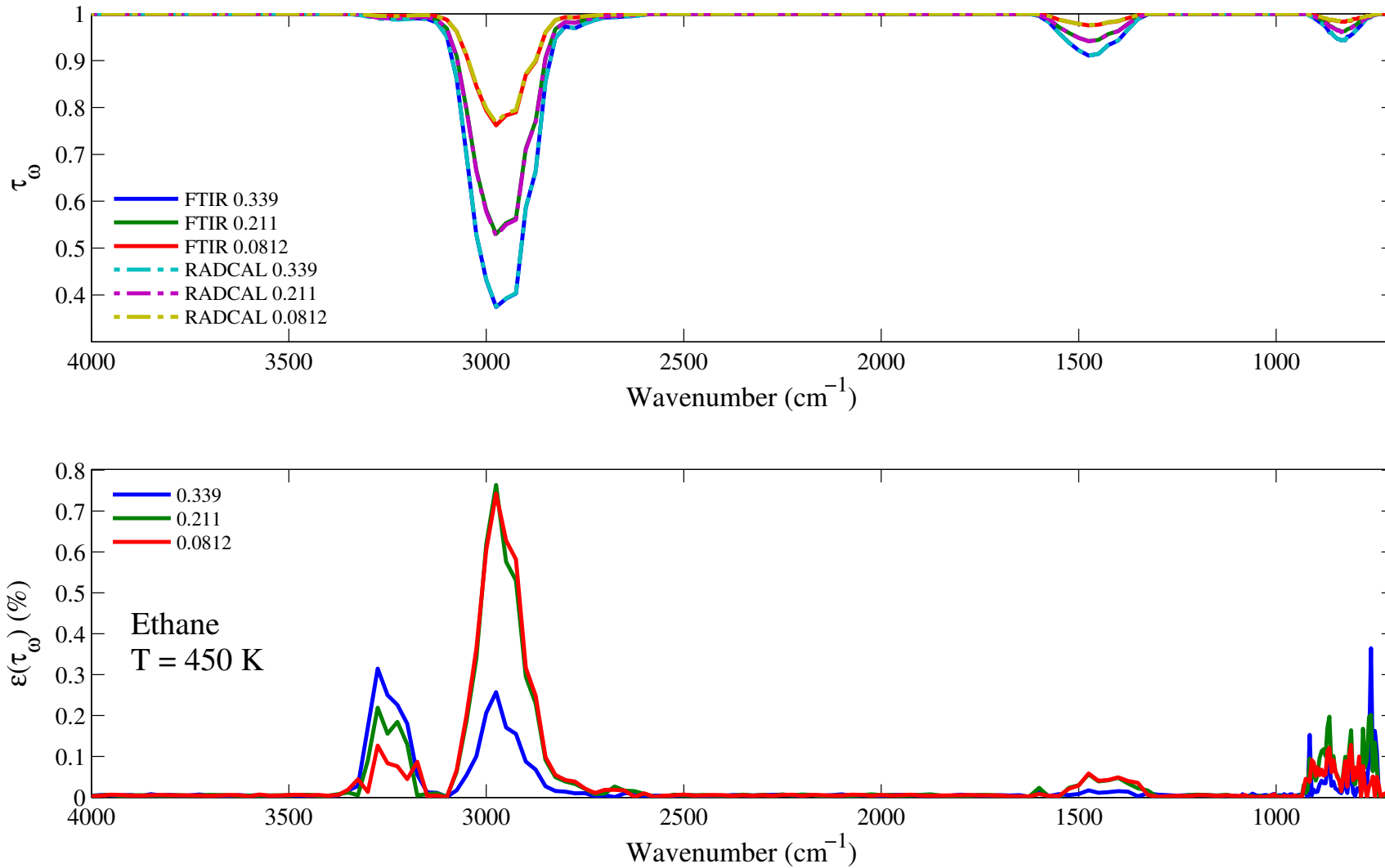


Figure 7.11: Top: comparison between the experimental (solid lines) and RadCal-generated synthetic (dashed lines) spectral transmissivity profiles, denoted τ_ω , of ethane of an isothermal homogeneous column of ethane. Bottom: relative transmissivity error, denoted $\varepsilon(\tau_\omega)$, between the experiment and the synthetic profiles presented on the top figure. Three different pressure path lengths are considered: 0.339, 0.211, and 0.0812 atm.cm. The gas temperature is set at 450 K and the total pressure is 101 kPa. Note: the experimental data resolution has been changed to match that of the narrow band model.

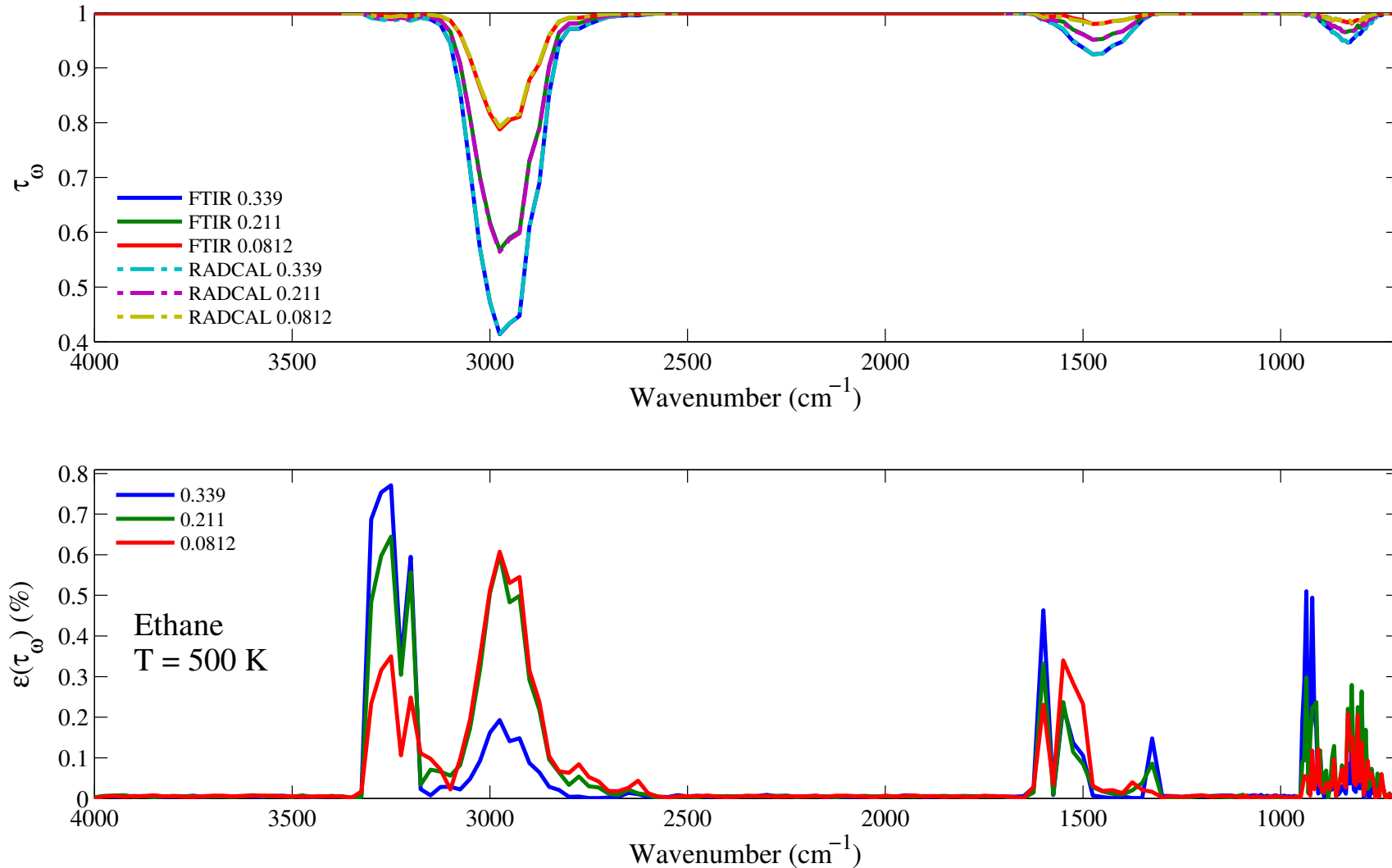


Figure 7.12: Top: comparison between the experimental (solid lines) and RadCal-generated synthetic (dashed lines) spectral transmissivity profiles, denoted τ_ω , of ethane of an isothermal homogeneous column of ethane. Bottom: relative transmissivity error, denoted $\varepsilon(\tau_\omega)$, between the experiment and the synthetic profiles presented on the top figure. Three different pressure path lengths are considered: 0.339, 0.211, and 0.0812 atm.cm. The gas temperature is set at 500 K and the total pressure is 101 kPa. Note: the experimental data resolution has been changed to match that of the narrow band model.

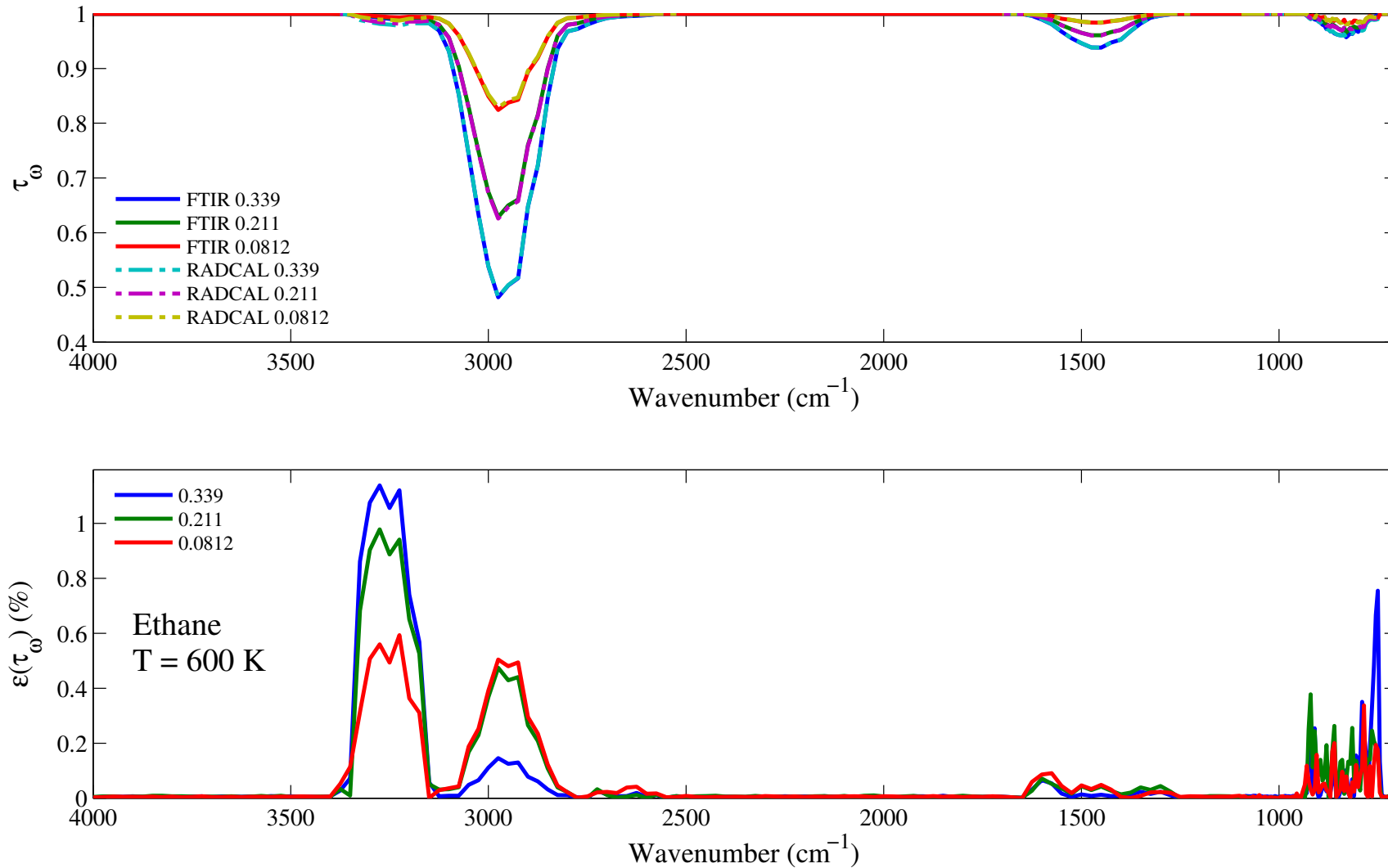


Figure 7.13: Top: comparison between the experimental (solid lines) and RadCal-generated synthetic (dashed lines) spectral transmissivity profiles, denoted τ_ω , of ethane of an isothermal homogeneous column of ethane. Bottom: relative transmissivity error, denoted $\varepsilon(\tau_\omega)$, between the experiment and the synthetic profiles presented on the top figure. Three different pressure path lengths are considered: 0.339, 0.211, and 0.0812 atm.cm. The gas temperature is set at 600 K and the total pressure is 101 kPa. Note: the experimental data resolution has been changed to match that of the narrow band model.

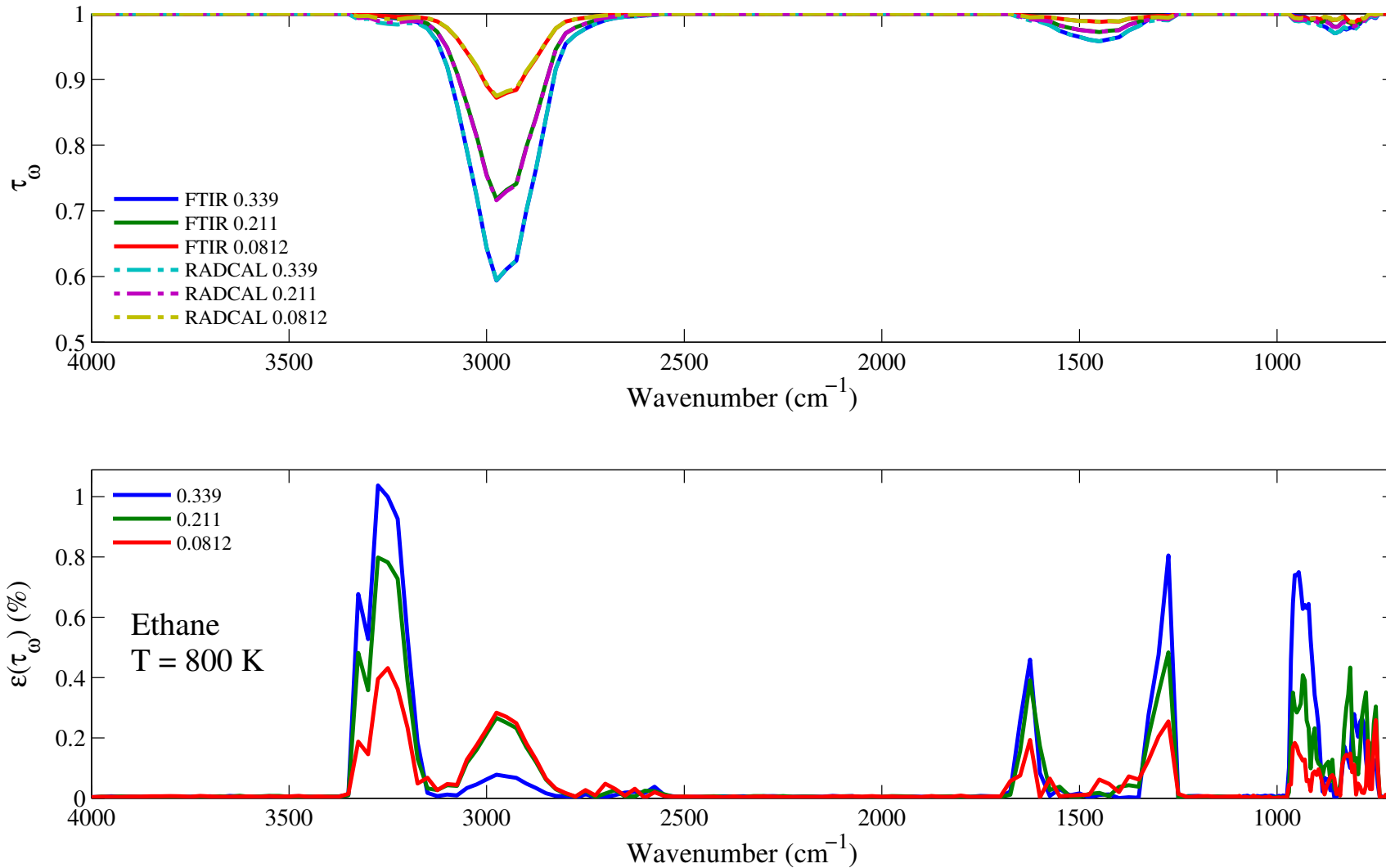


Figure 7.14: Top: comparison between the experimental (solid lines) and RadCal-generated synthetic (dashed lines) spectral transmissivity profiles, denoted τ_ω , of ethane of an isothermal homogeneous column of ethane. Bottom: relative transmissivity error, denoted $\varepsilon(\tau_\omega)$, between the experiment and the synthetic profiles presented on the top figure. Three different pressure path lengths are considered: 0.339, 0.211, and 0.0812 atm.cm. The gas temperature is set at 801 K and the total pressure is 101 kPa. Note: the experimental data resolution has been changed to match that of the narrow band model.

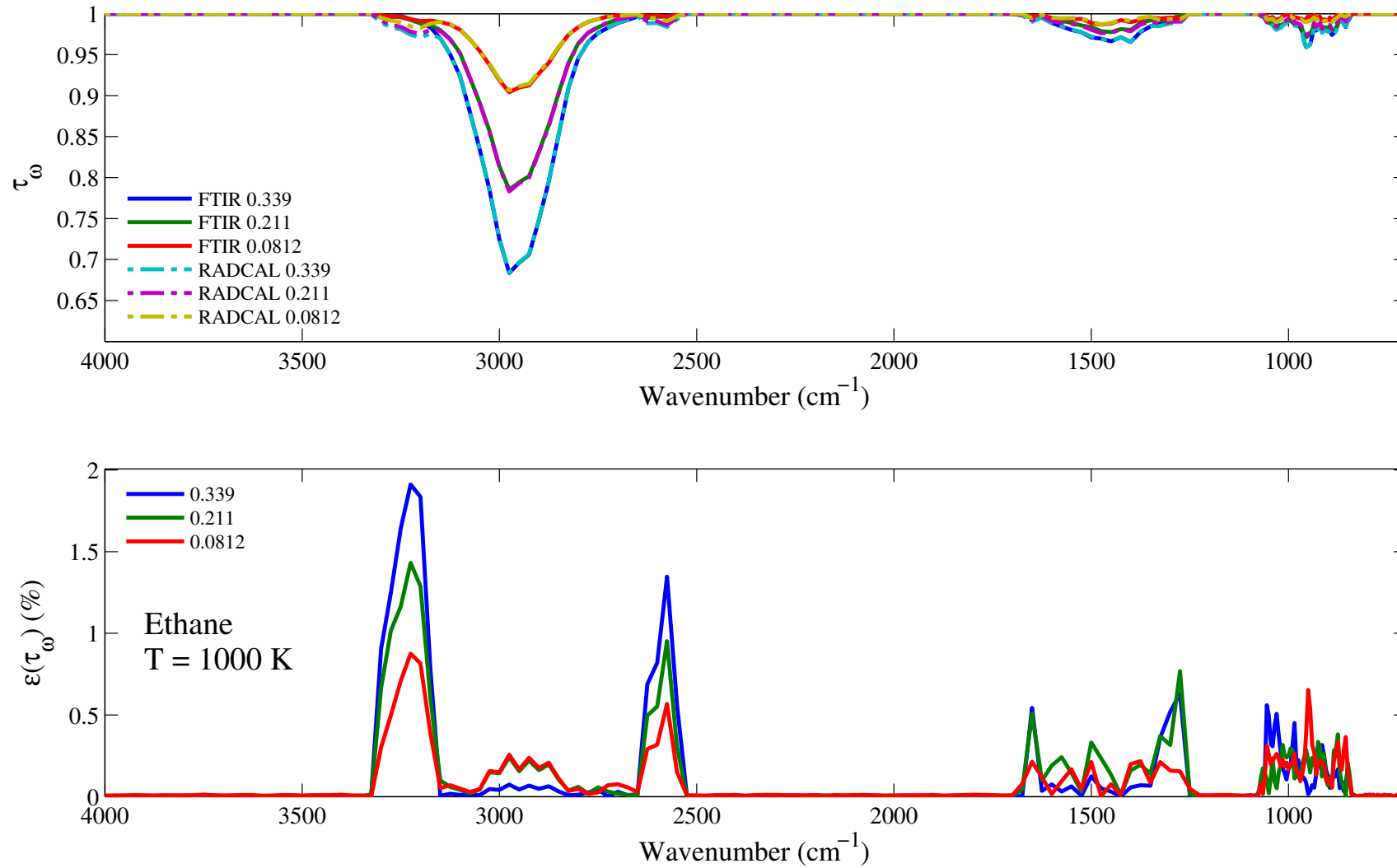


Figure 7.15: Top: comparison between the experimental (solid lines) and RadCal-generated synthetic (dashed lines) spectral transmissivity profiles, denoted τ_ω , of ethane of an isothermal homogeneous column of ethane. Bottom: relative transmissivity error, denoted $\varepsilon(\tau_\omega)$, between the experiment and the synthetic profiles presented on the top figure. Three different pressure path lengths are considered: 0.339, 0.211, and 0.0812 atm.cm. The gas temperature is set at 1000 K and the total pressure is 101 kPa. Note: the experimental data resolution has been changed to match that of the narrow band model.

7.3 Propylene: C₃H₆

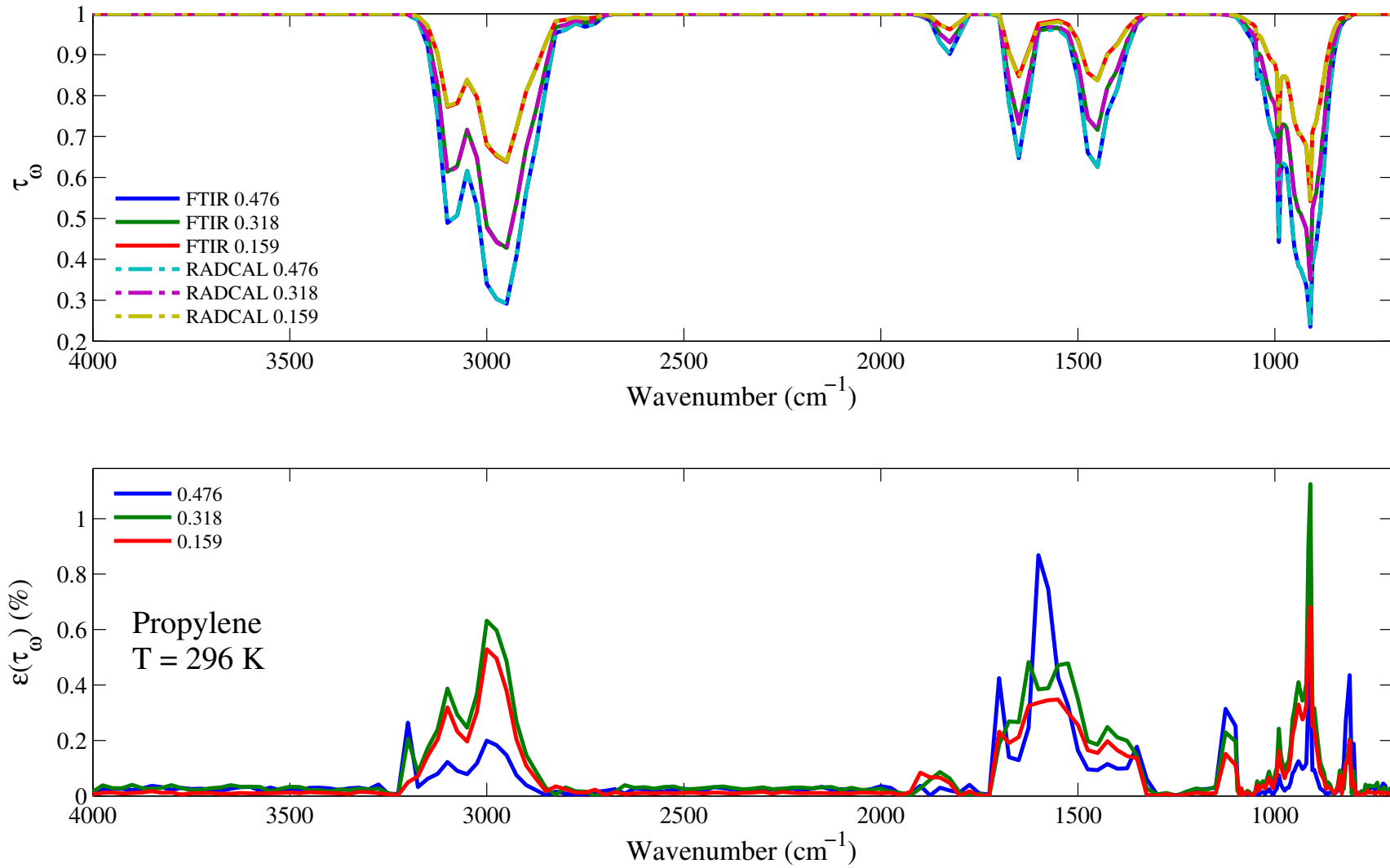


Figure 7.16: Top: comparison between the experimental (solid lines) and RadCal-generated synthetic (dashed lines) spectral transmissivity profiles, denoted τ_ω , of propylene of an isothermal homogeneous column of propylene. Bottom: relative transmissivity error, denoted $\varepsilon(\tau_\omega)$, between the experiment and the synthetic profiles presented on the top figure. Three different pressure path lengths are considered: 0.476, 0.318, and 0.159 atm.cm. The gas temperature is set at 296 K and the total pressure is 101 kPa. Note: the experimental data resolution has been changed to match that of the narrow band model.

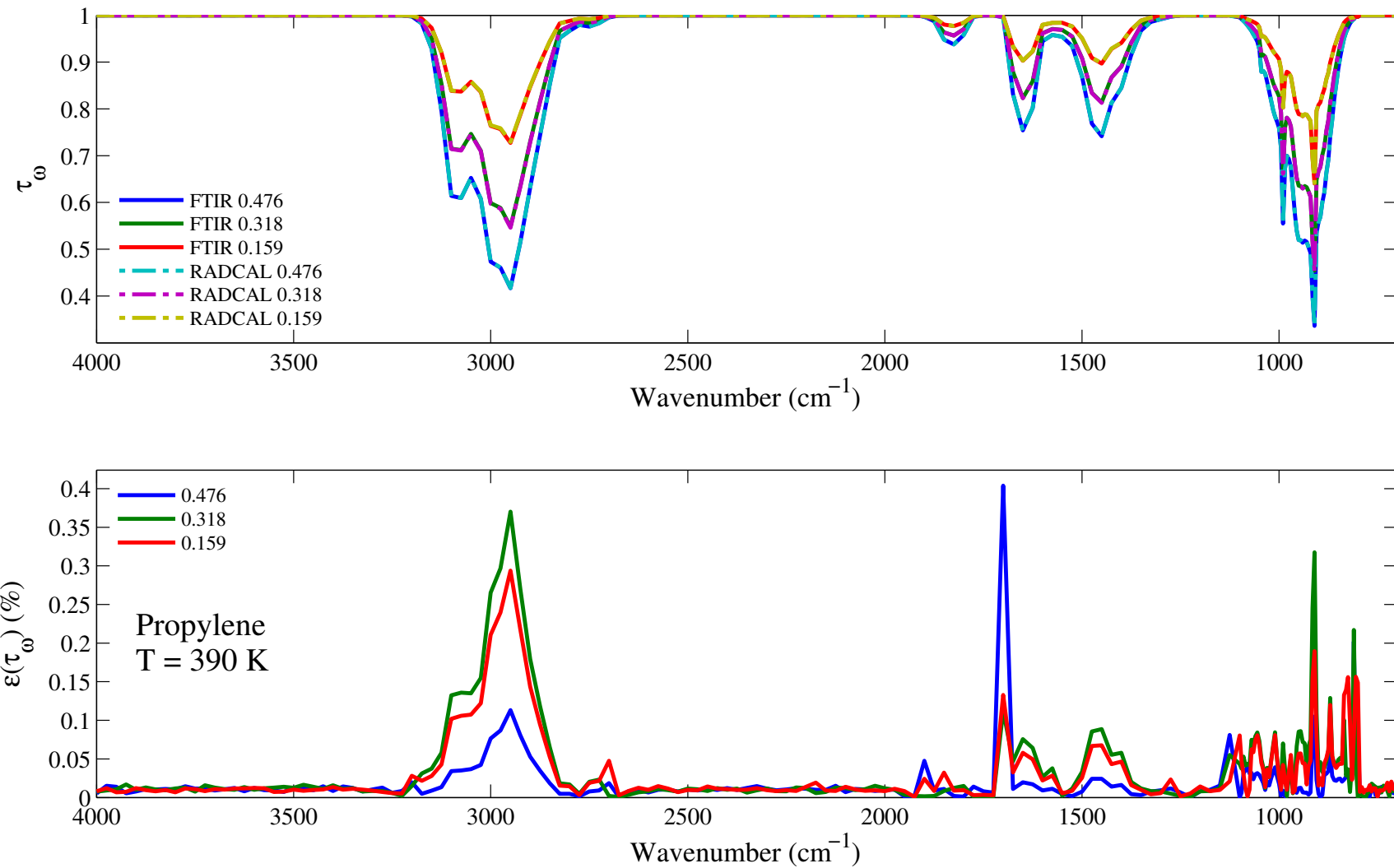


Figure 7.17: Top: comparison between the experimental (solid lines) and RadCal-generated synthetic (dashed lines) spectral transmissivity profiles, denoted τ_ω , of propylene of an isothermal homogeneous column of propylene. Bottom: relative transmissivity error, denoted $\varepsilon(\tau_\omega)$, between the experiment and the synthetic profiles presented on the top figure. Three different pressure path lengths are considered: 0.476, 0.318, and 0.159 atm.cm. The gas temperature is set at 390 K and the total pressure is 101 kPa. Note: the experimental data resolution has been changed to match that of the narrow band model.

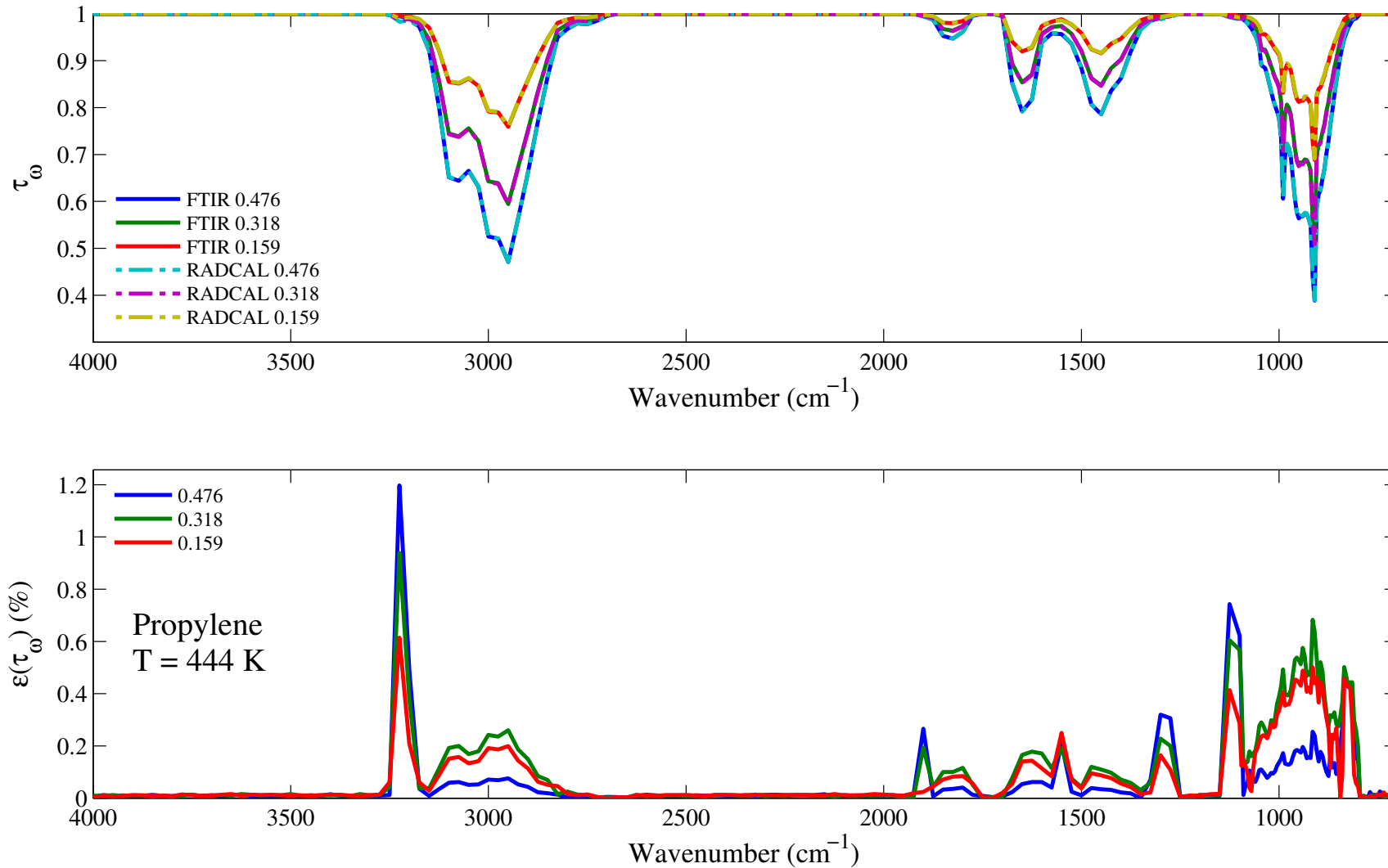


Figure 7.18: Top: comparison between the experimental (solid lines) and RadCal-generated synthetic (dashed lines) spectral transmissivity profiles, denoted τ_ω , of propylene of an isothermal homogeneous column of propylene. Bottom: relative transmissivity error, denoted $\varepsilon(\tau_\omega)$, between the experiment and the synthetic profiles presented on the top figure. Three different pressure path lengths are considered: 0.476, 0.318, and 0.159 atm.cm. The gas temperature is set at 444 K and the total pressure is 101 kPa. Note: the experimental data resolution has been changed to match that of the narrow band model.

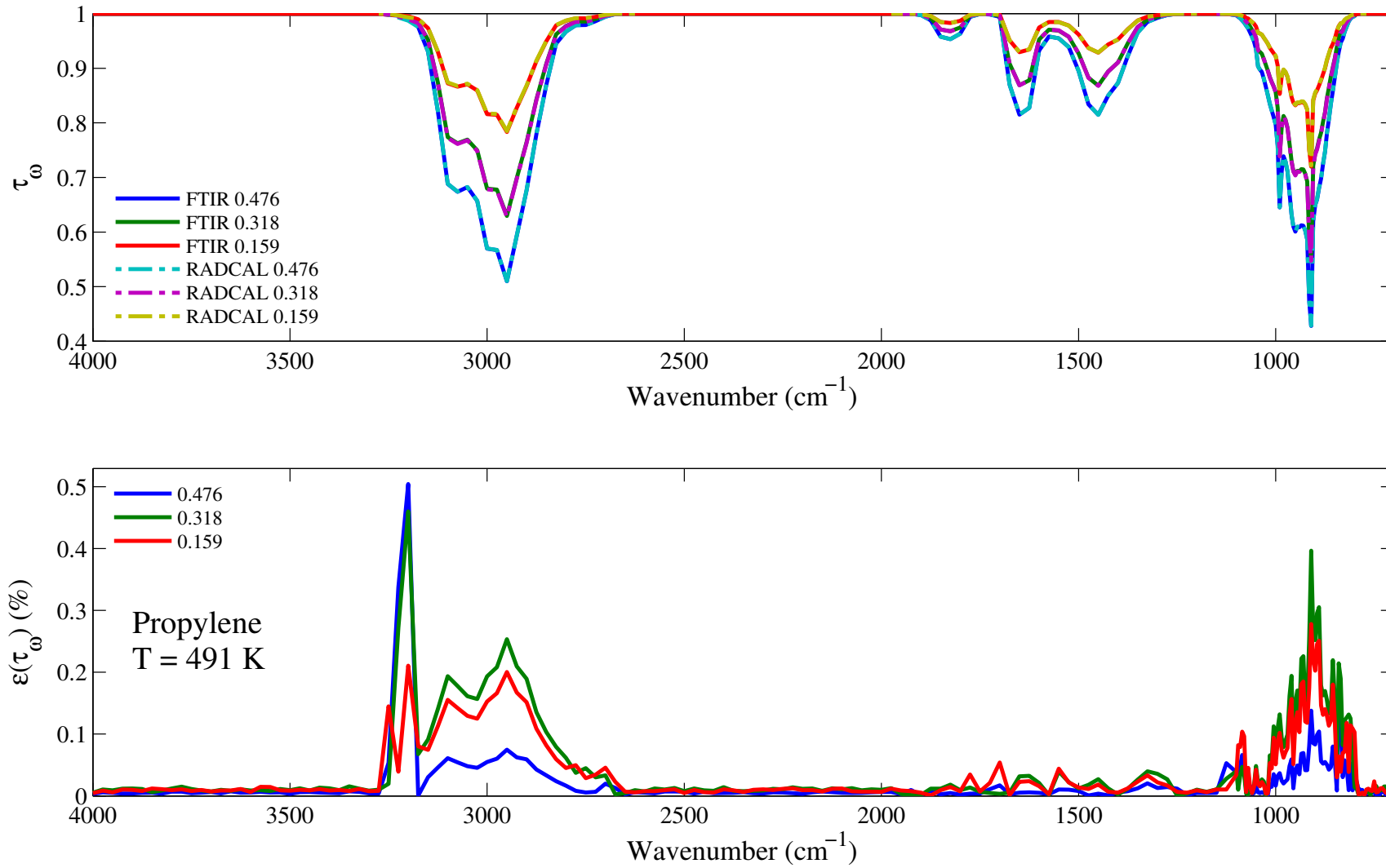


Figure 7.19: Top: comparison between the experimental (solid lines) and RadCal-generated synthetic (dashed lines) spectral transmissivity profiles, denoted τ_ω , of propylene of an isothermal homogeneous column of propylene. Bottom: relative transmissivity error, denoted $\varepsilon(\tau_\omega)$, between the experiment and the synthetic profiles presented on the top figure. Three different pressure path lengths are considered: 0.476, 0.318, and 0.159 atm.cm. The gas temperature is set at 491 K and the total pressure is 101 kPa. Note: the experimental data resolution has been changed to match that of the narrow band model.

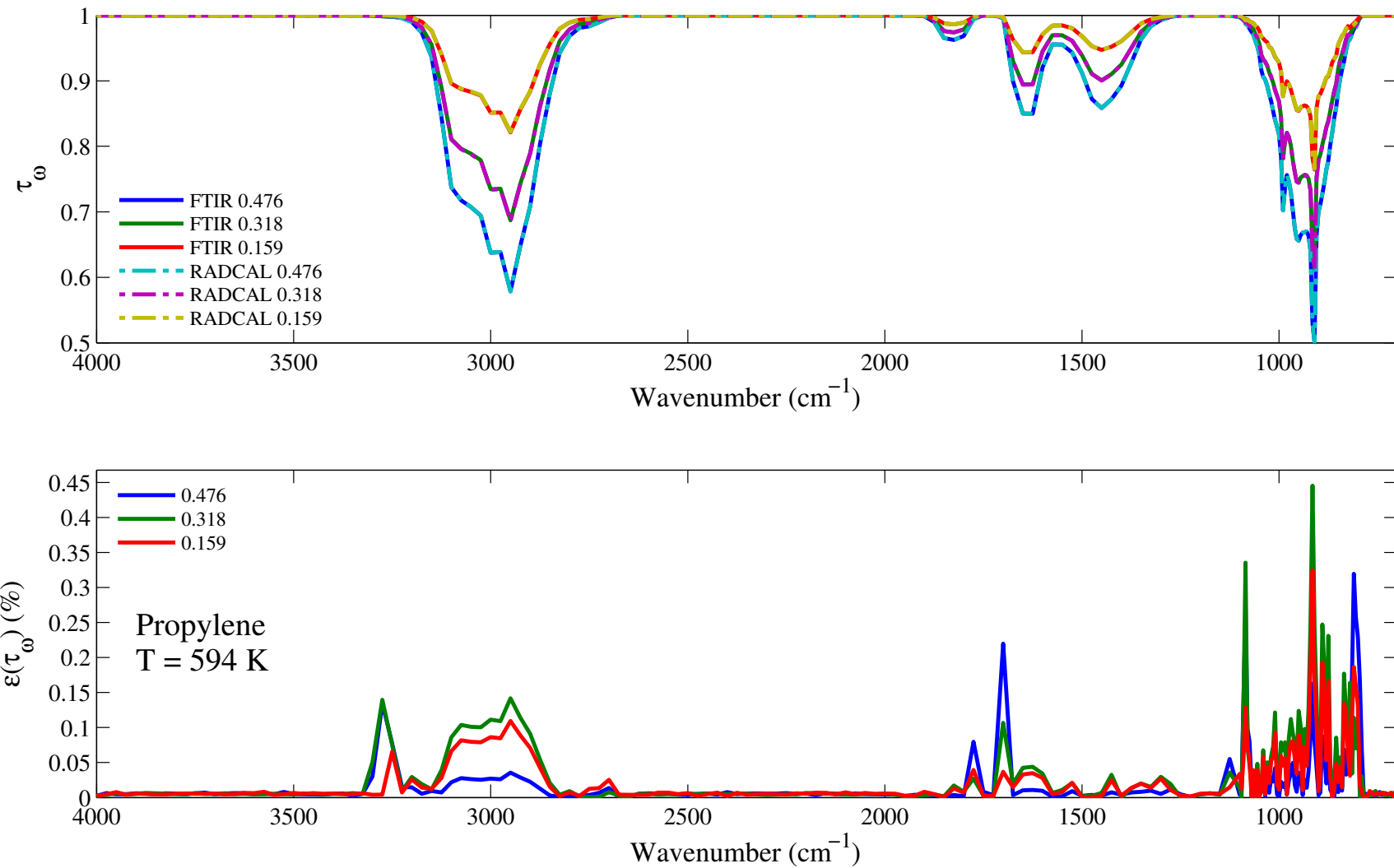


Figure 7.20: Top: comparison between the experimental (solid lines) and RadCal-generated synthetic (dashed lines) spectral transmissivity profiles, denoted τ_ω , of propylene of an isothermal homogeneous column of propylene. Bottom: relative transmissivity error, denoted $\varepsilon(\tau_\omega)$, between the experiment and the synthetic profiles presented on the top figure. Three different pressure path lengths are considered: 0.476, 0.318, and 0.159 atm.cm. The gas temperature is set at 594 K and the total pressure is 101 kPa. Note: the experimental data resolution has been changed to match that of the narrow band model.

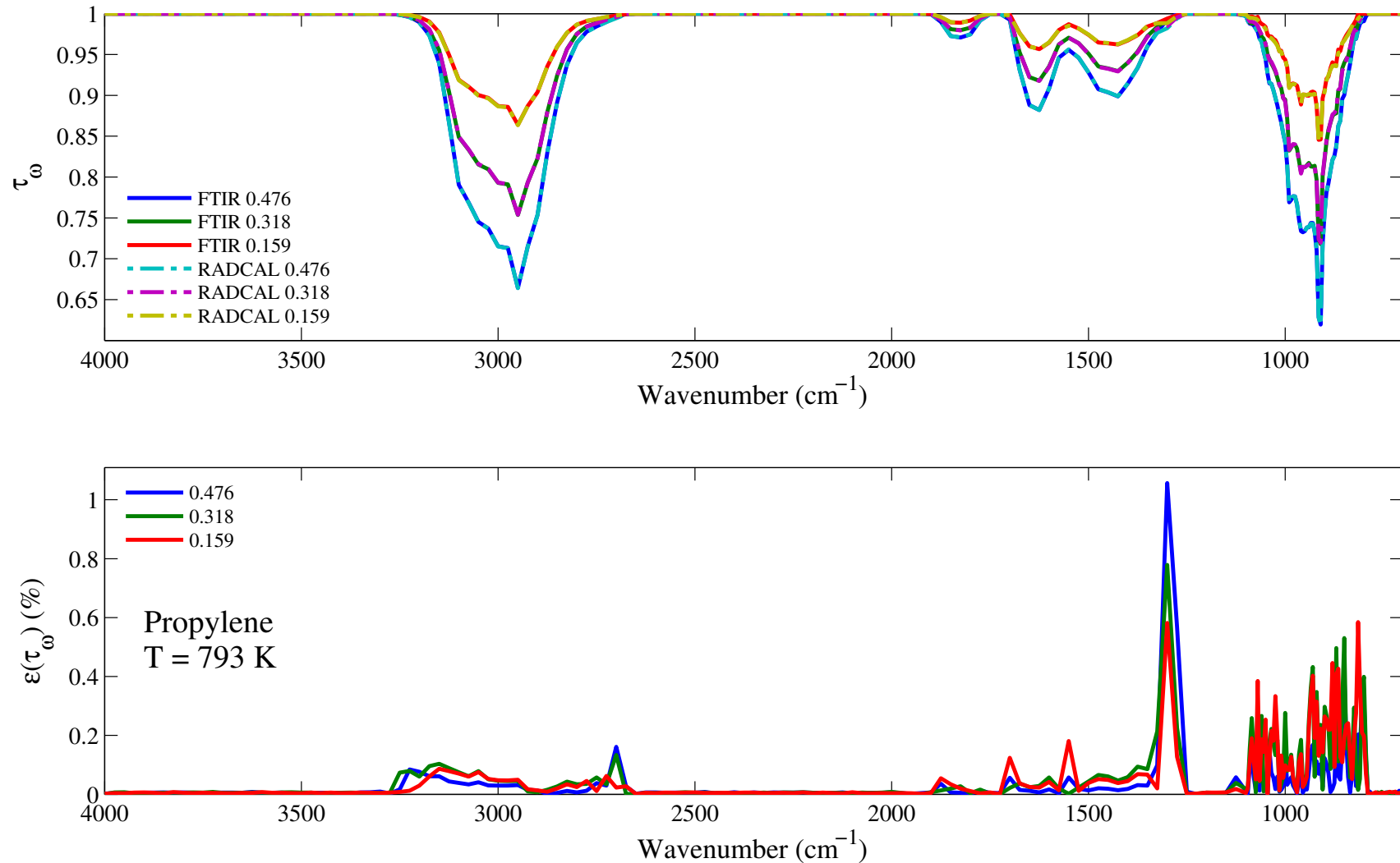


Figure 7.21: Top: comparison between the experimental (solid lines) and RadCal-generated synthetic (dashed lines) spectral transmissivity profiles, denoted τ_ω , of propylene of an isothermal homogeneous column of propylene. Bottom: relative transmissivity error, denoted $\varepsilon(\tau_\omega)$, between the experiment and the synthetic profiles presented on the top figure. Three different pressure path lengths are considered: 0.476, 0.318, and 0.159 atm.cm. The gas temperature is set at 793 K and the total pressure is 101 kPa. Note: the experimental data resolution has been changed to match that of the narrow band model.

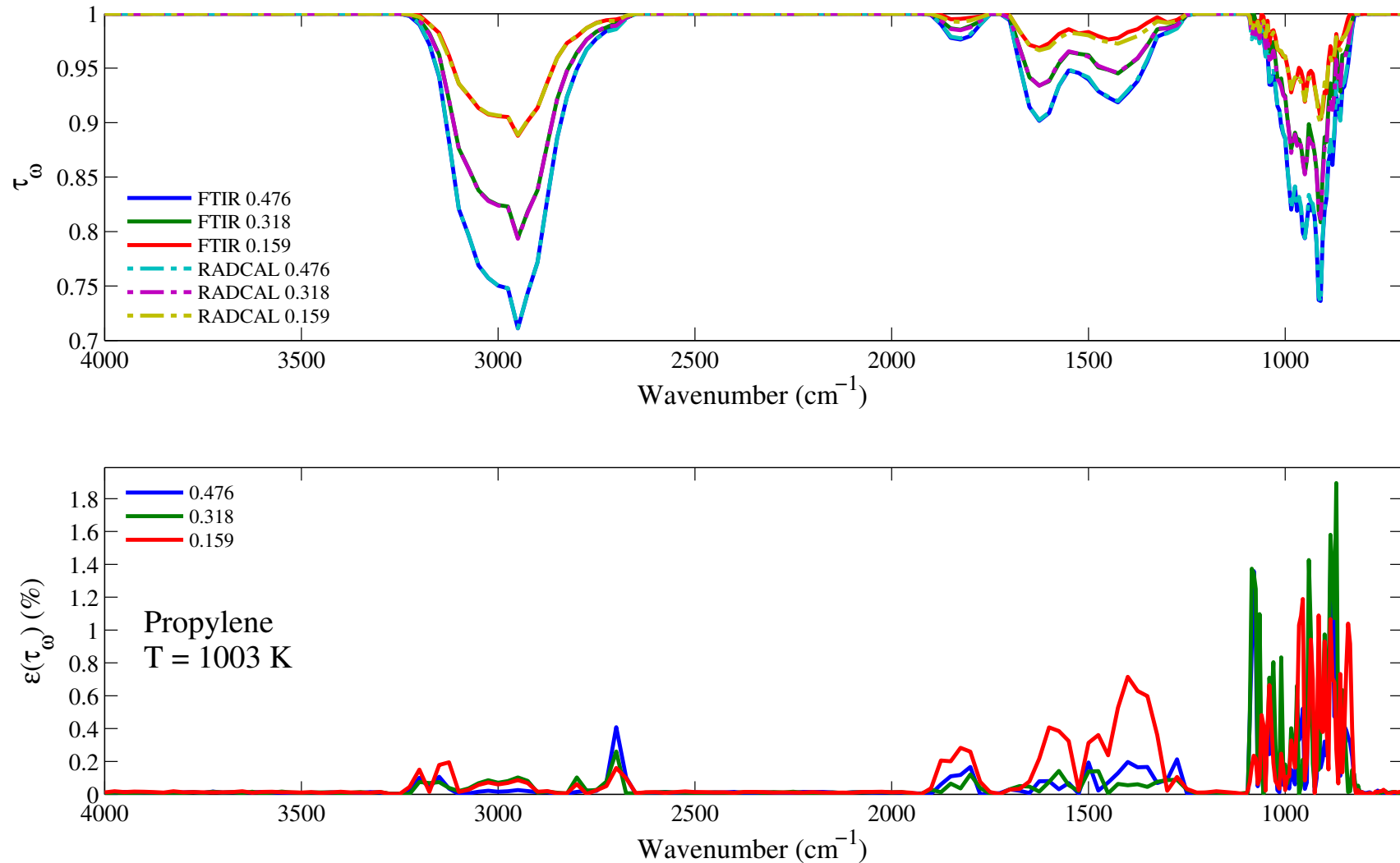


Figure 7.22: Top: comparison between the experimental (solid lines) and RadCal-generated synthetic (dashed lines) spectral transmissivity profiles, denoted τ_ω , of propylene of an isothermal homogeneous column of propylene. Bottom: relative transmissivity error, denoted $\varepsilon(\tau_\omega)$, between the experiment and the synthetic profiles presented on the top figure. Three different pressure path lengths are considered: 0.476, 0.318, and 0.159 atm.cm. The gas temperature is set at 1003 K and the total pressure is 101 kPa. Note: the experimental data resolution has been changed to match that of the narrow band model.

7.4 Propane: C₃H₈

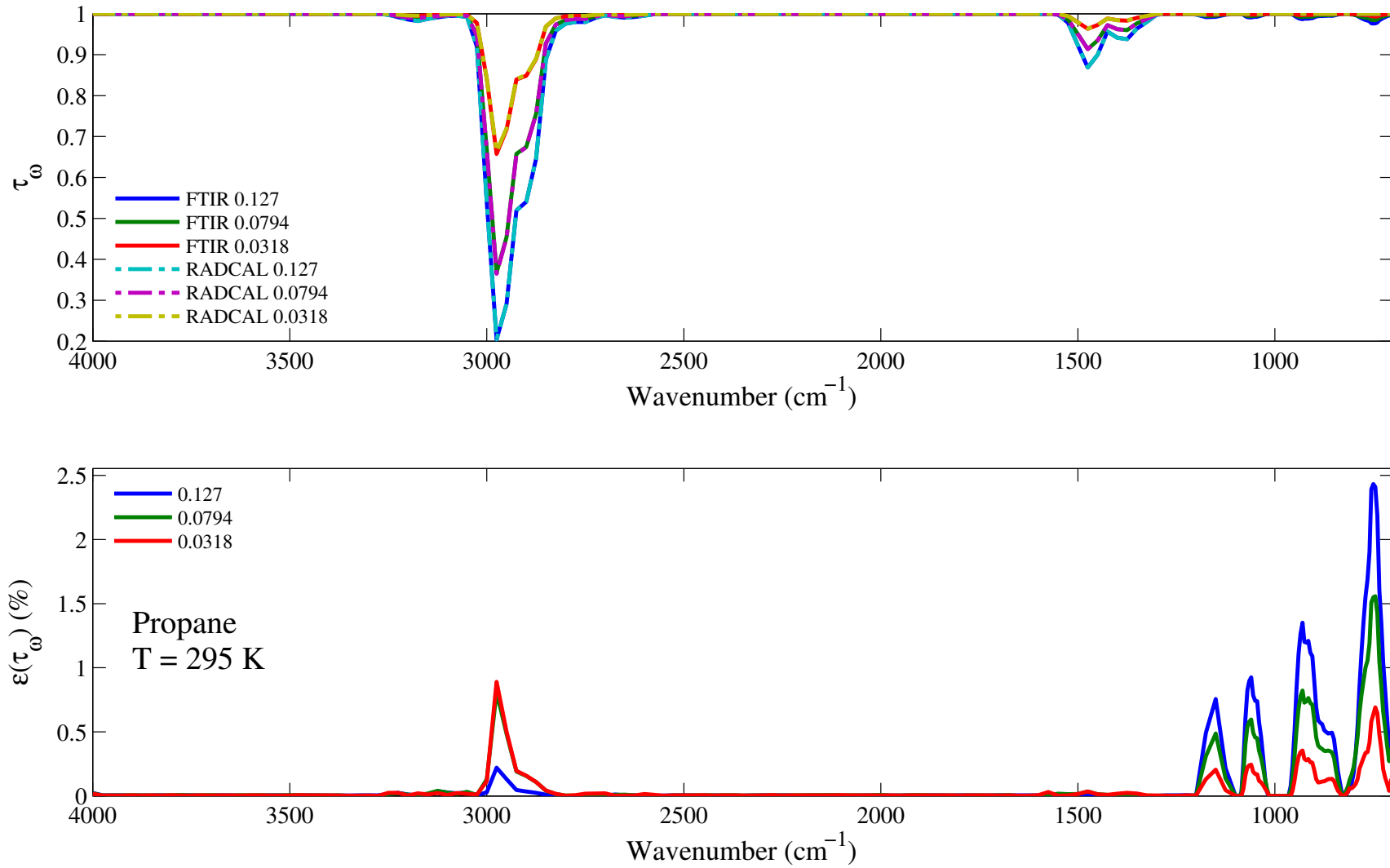


Figure 7.23: Top: comparison between the experimental (solid lines) and RadCal-generated synthetic (dashed lines) spectral transmissivity profiles, denoted τ_ω , of propane of an isothermal homogeneous column of propane. Bottom: relative transmissivity error, denoted $\varepsilon(\tau_\omega)$, between the experiment and the synthetic profiles presented on the top figure. Three different pressure path lengths are considered: 0.127, 0.0794, and 0.0318 atm.cm. The gas temperature is set at 295 K and the total pressure is 101 kPa. Note: the experimental data resolution has been changed to match that of the narrow band model.

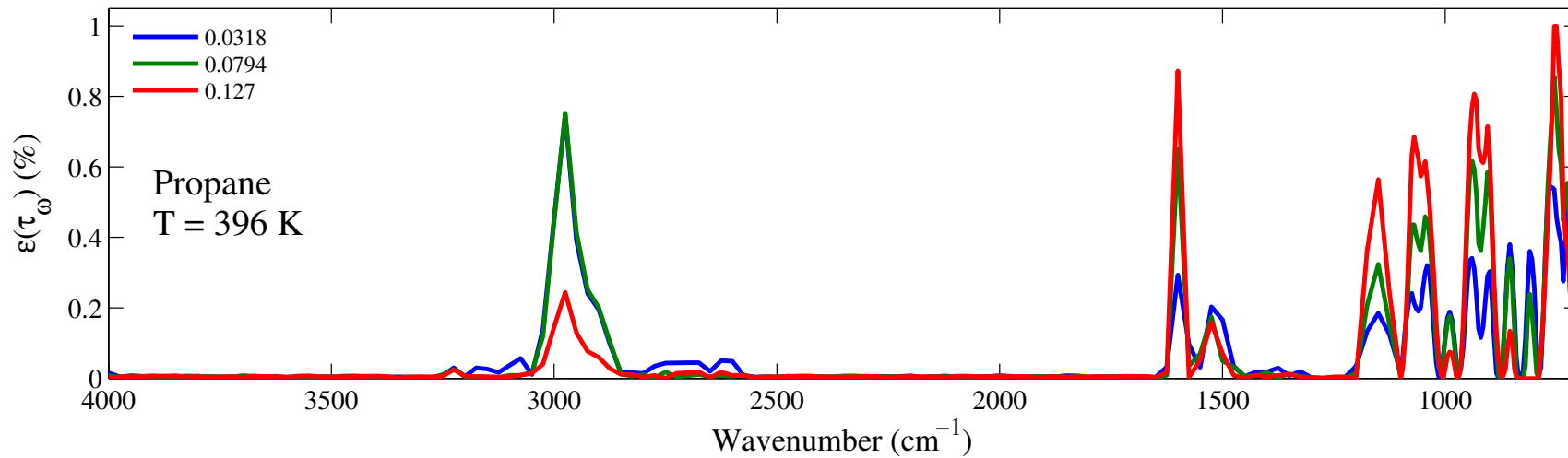
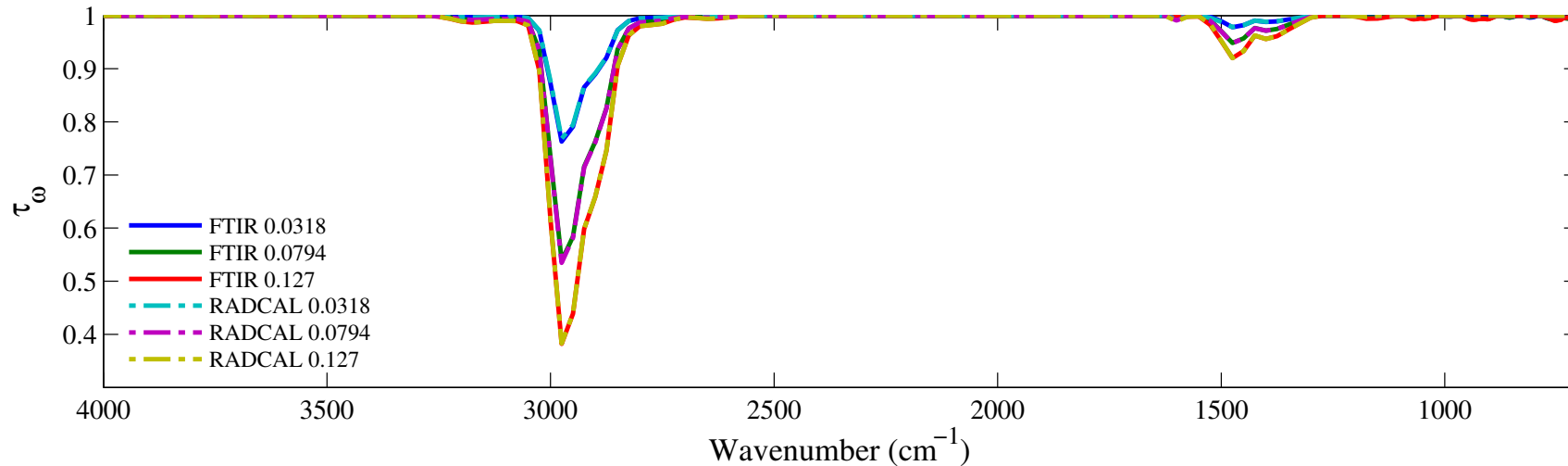


Figure 7.24: Top: comparison between the experimental (solid lines) and RadCal-generated synthetic (dashed lines) spectral transmissivity profiles, denoted τ_ω , of propane of an isothermal homogeneous column of propane. Bottom: relative transmissivity error, denoted $\varepsilon(\tau_\omega)$, between the experiment and the synthetic profiles presented on the top figure. Three different pressure path lengths are considered: 0.0318, 0.0794, and 0.127 atm.cm. The gas temperature is set at 396 K and the total pressure is 101 kPa. Note: the experimental data resolution has been changed to match that of the narrow band model.

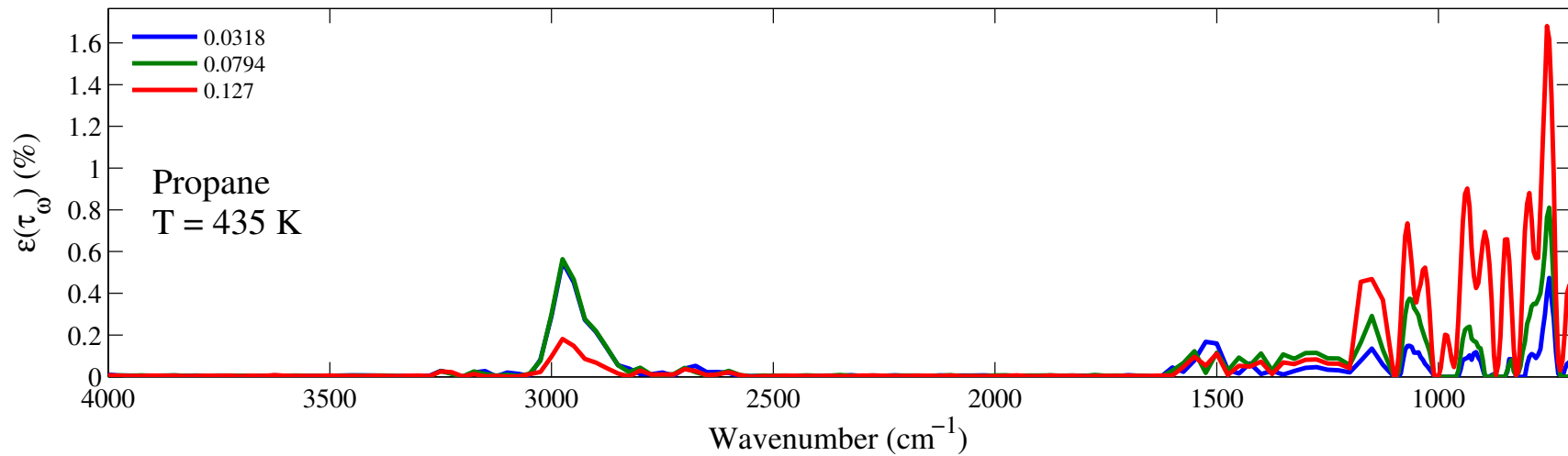
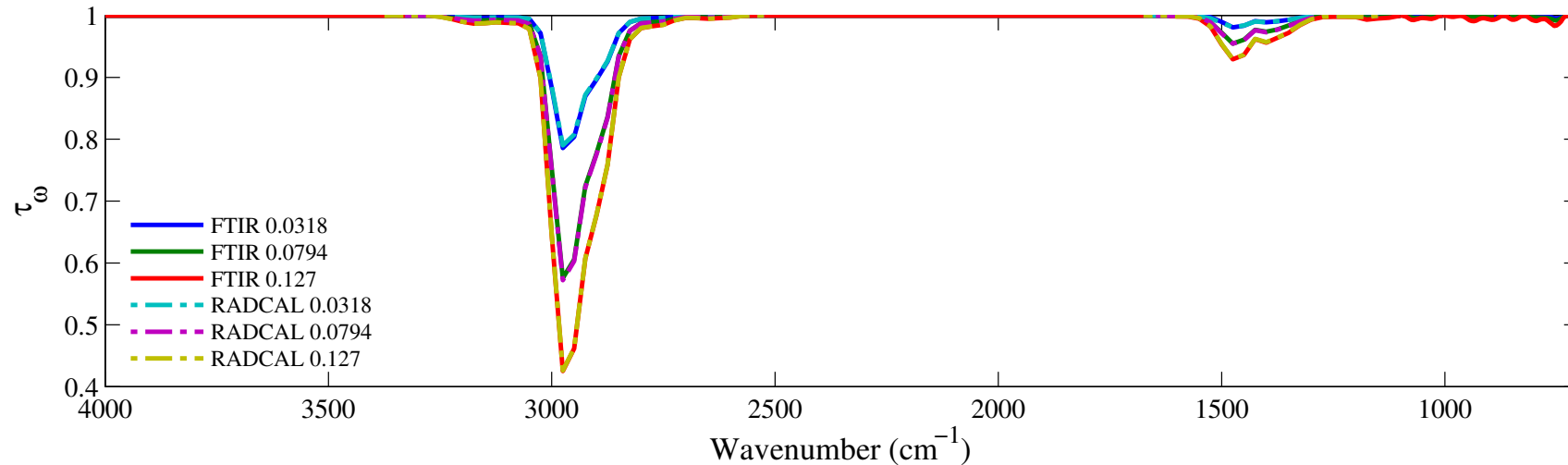


Figure 7.25: Top: comparison between the experimental (solid lines) and RadCal-generated synthetic (dashed lines) spectral transmissivity profiles, denoted τ_ω , of propane of an isothermal homogeneous column of propane. Bottom: relative transmissivity error, denoted $\varepsilon(\tau_\omega)$, between the experiment and the synthetic profiles presented on the top figure. Three different pressure path lengths are considered: 0.0318, 0.0794, and 0.127 atm.cm. The gas temperature is set at 435 K and the total pressure is 101 kPa. Note: the experimental data resolution has been changed to match that of the narrow band model.

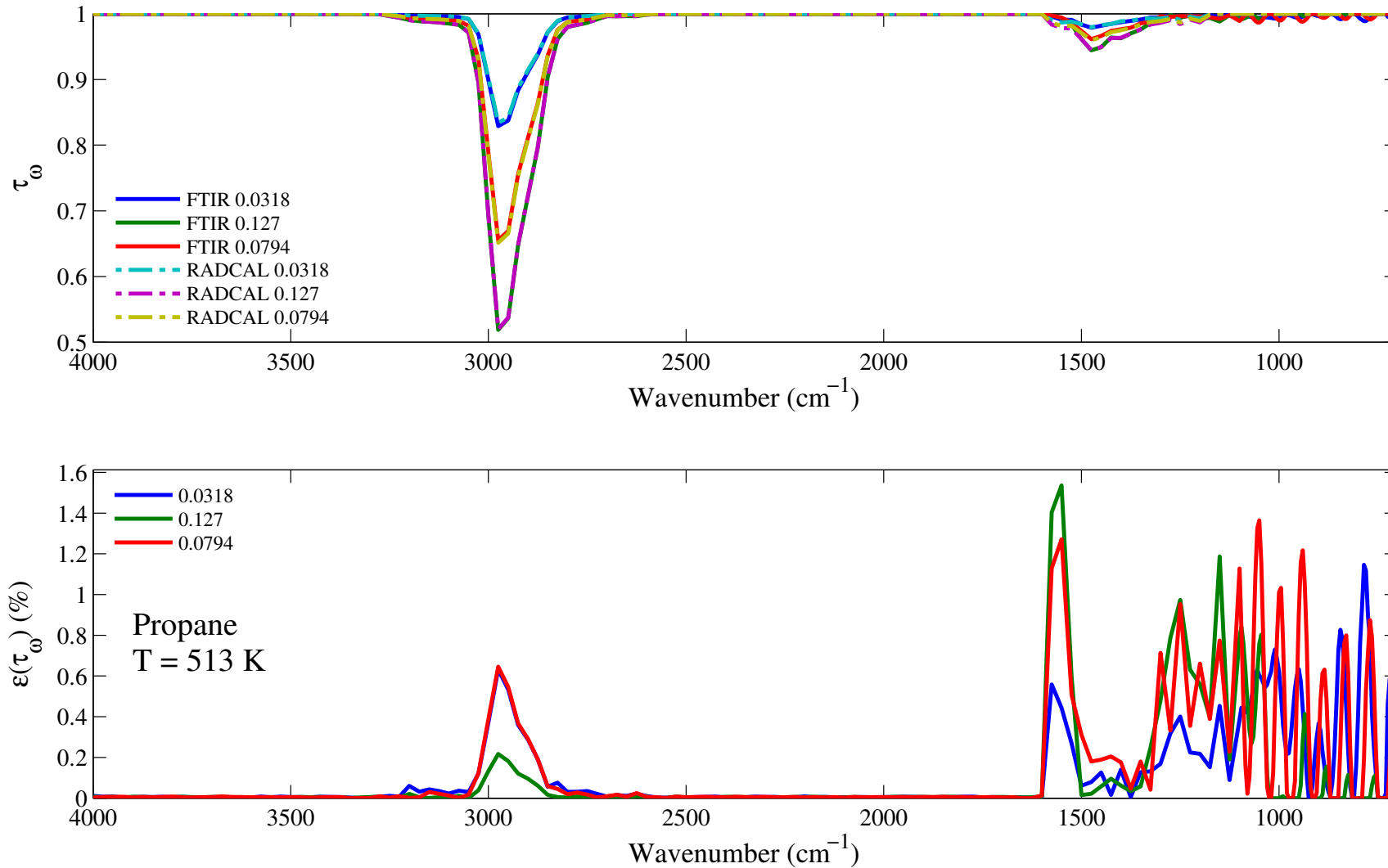


Figure 7.26: Top: comparison between the experimental (solid lines) and RadCal-generated synthetic (dashed lines) spectral transmissivity profiles, denoted τ_ω , of propane of an isothermal homogeneous column of propane. Bottom: relative transmissivity error, denoted $\varepsilon(\tau_\omega)$, between the experiment and the synthetic profiles presented on the top figure. Three different pressure path lengths are considered: 0.0318, 0.127, and 0.0794 atm.cm. The gas temperature is set at 513 K and the total pressure is 101 kPa. Note: the experimental data resolution has been changed to match that of the narrow band model.

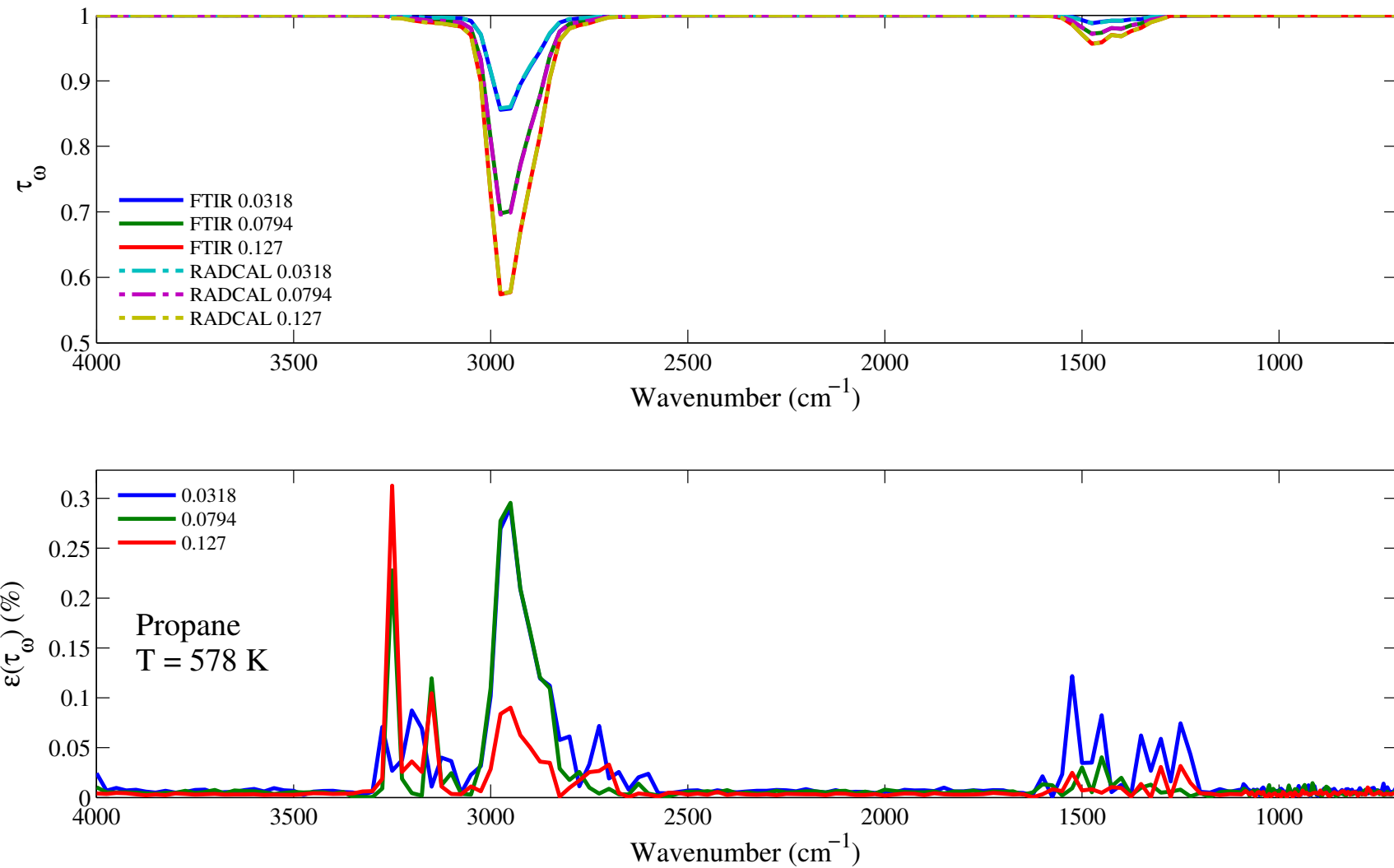


Figure 7.27: Top: comparison between the experimental (solid lines) and RadCal-generated synthetic (dashed lines) spectral transmissivity profiles, denoted τ_ω , of propane of an isothermal homogeneous column of propane. Bottom: relative transmissivity error, denoted $\varepsilon(\tau_\omega)$, between the experiment and the synthetic profiles presented on the top figure. Three different pressure path lengths are considered: 0.0318, 0.0794, and 0.127 atm.cm. The gas temperature is set at 578 K and the total pressure is 101 kPa. Note: the experimental data resolution has been changed to match that of the narrow band model.

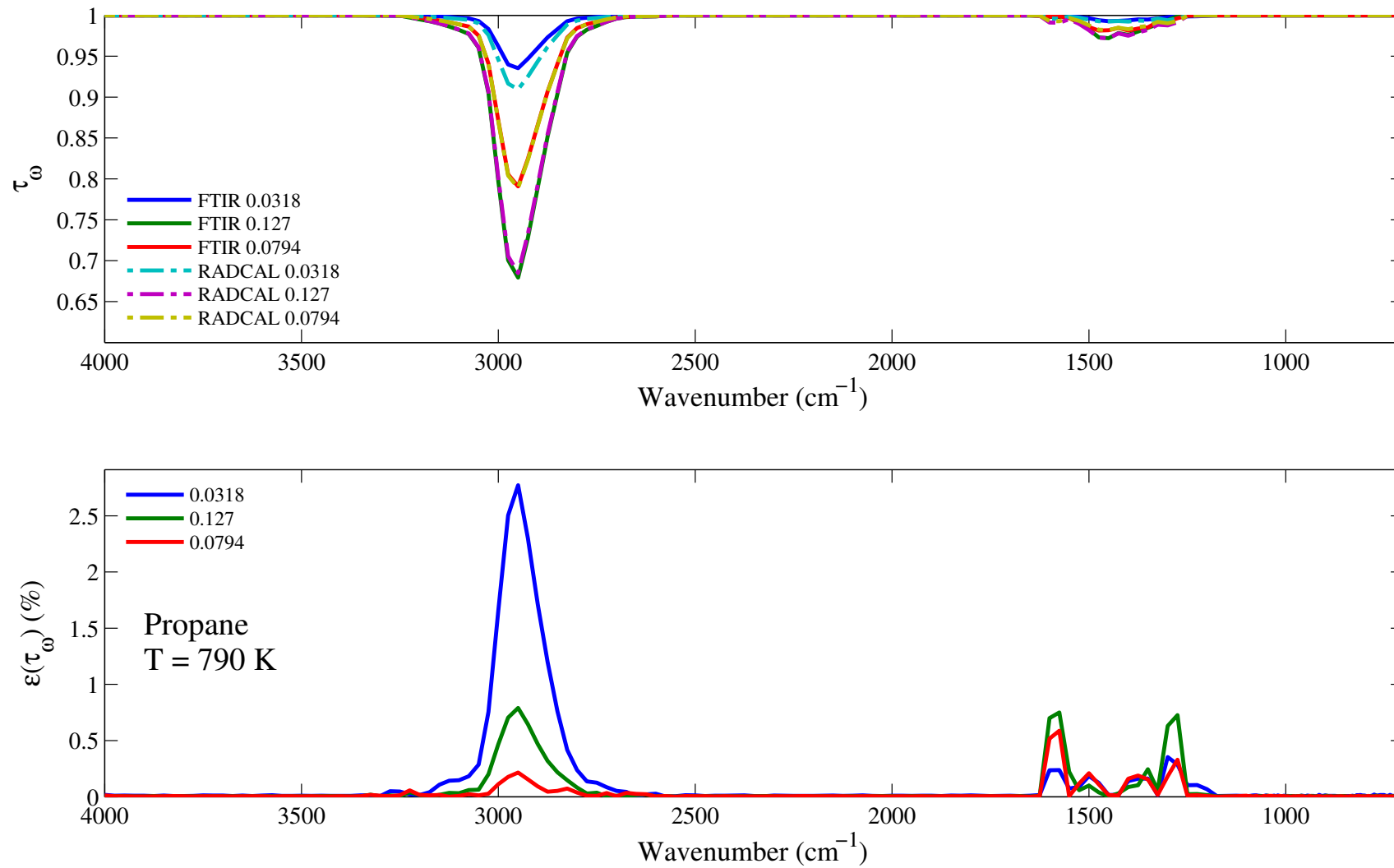


Figure 7.28: Top: comparison between the experimental (solid lines) and RadCal-generated synthetic (dashed lines) spectral transmissivity profiles, denoted τ_ω , of propane of an isothermal homogeneous column of propane. Bottom: relative transmissivity error, denoted $\varepsilon(\tau_\omega)$, between the experiment and the synthetic profiles presented on the top figure. Three different pressure path lengths are considered: 0.0318, 0.0794, and 0.127 atm.cm. The gas temperature is set at 790 K and the total pressure is 101 kPa. Note: the experimental data resolution has been changed to match that of the narrow band model.

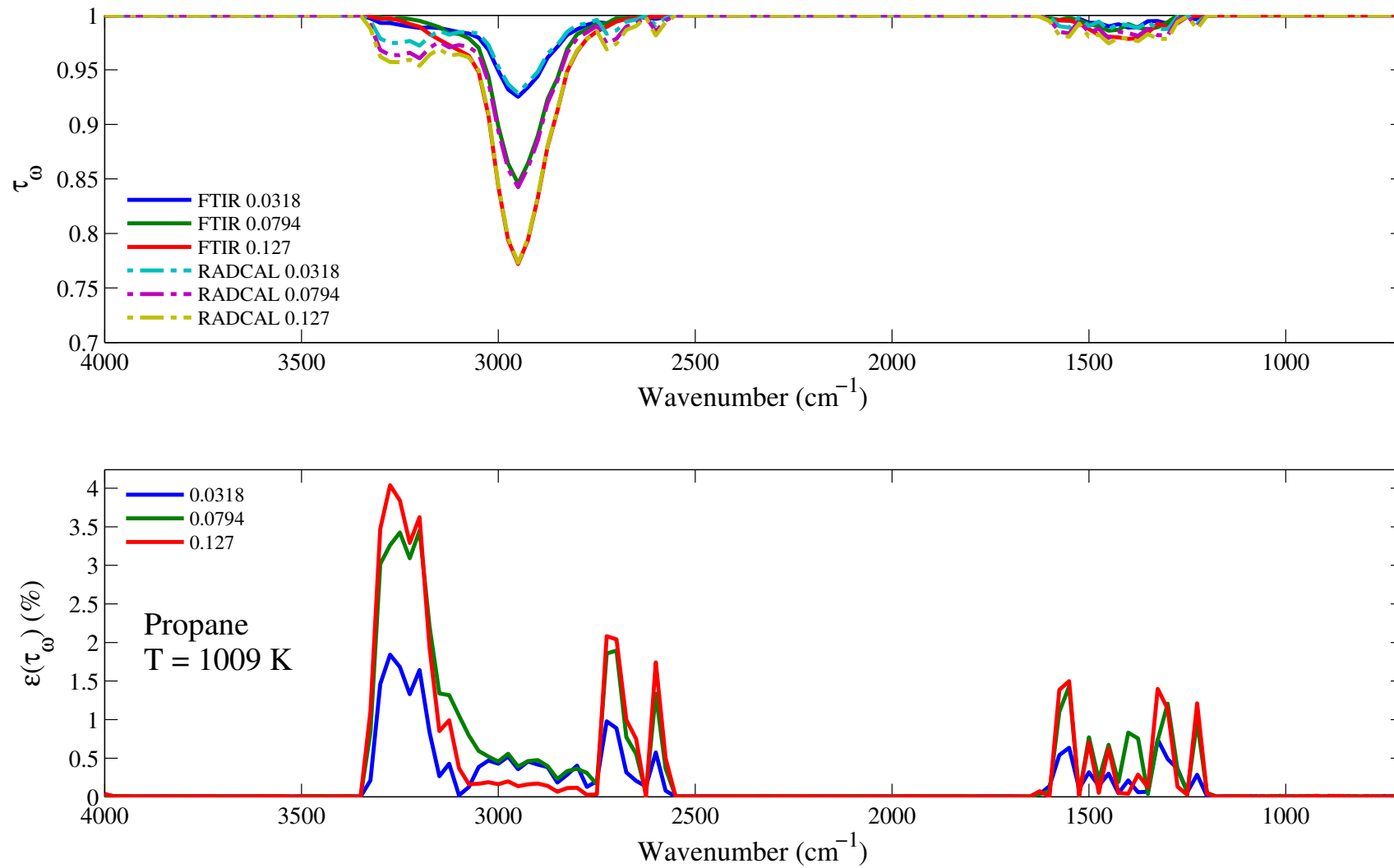


Figure 7.29: Top: comparison between the experimental (solid lines) and RadCal-generated synthetic (dashed lines) spectral transmissivity profiles, denoted τ_ω , of propane of an isothermal homogeneous column of propane. Bottom: relative transmissivity error, denoted $\varepsilon(\tau_\omega)$, between the experiment and the synthetic profiles presented on the top figure. Three different pressure path lengths are considered: 0.0318, 0.0794, and 0.127 atm.cm. The gas temperature is set at 1009 K and the total pressure is 101 kPa. Note: the experimental data resolution has been changed to match that of the narrow band model.

7.5 Toluene: C₇H₈

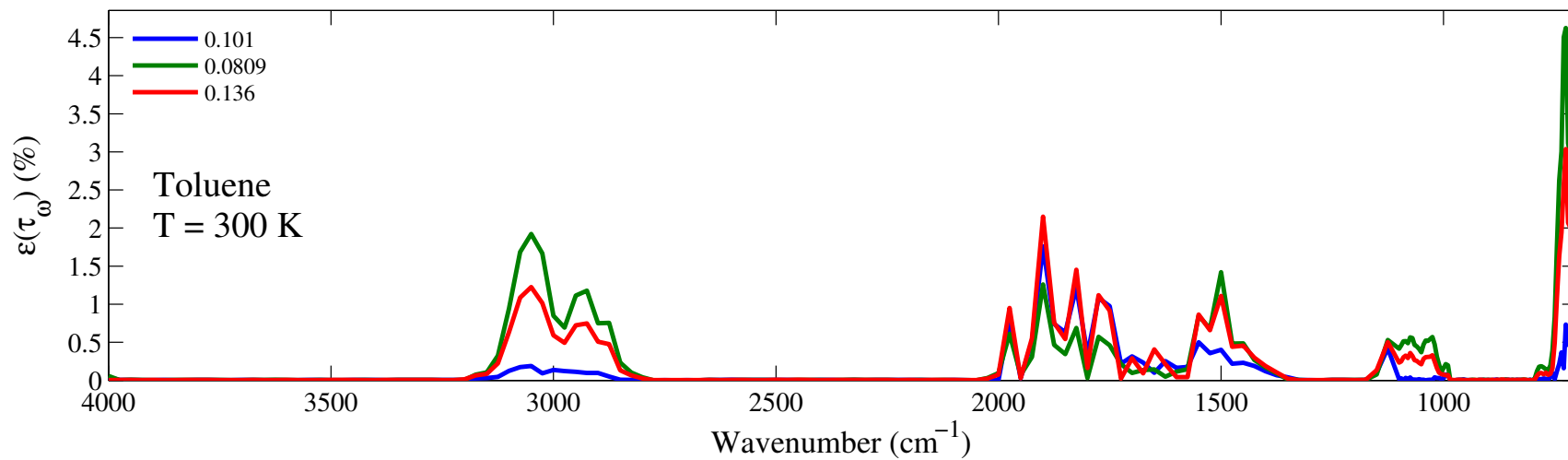
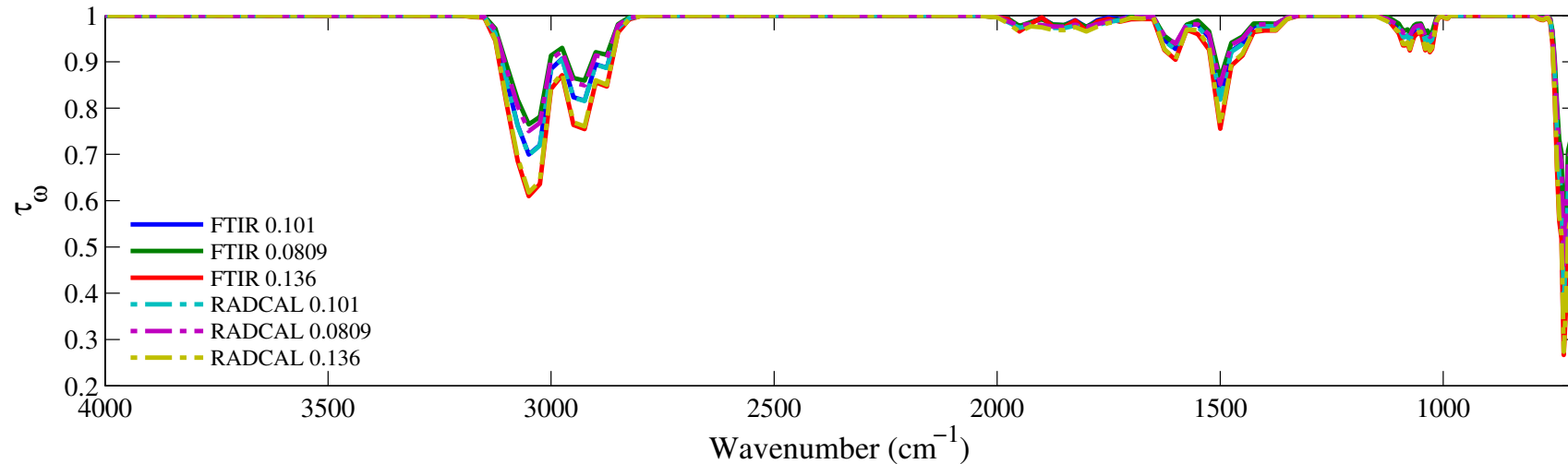


Figure 7.30: Top: comparison between the experimental (solid lines) and RadCal-generated synthetic (dashed lines) spectral transmissivity profiles, denoted τ_ω , of toluene of an isothermal homogeneous column of toluene. Bottom: relative transmissivity error, denoted $\varepsilon(\tau_\omega)$, between the experiment and the synthetic profiles presented on the top figure. Three different pressure path lengths are considered: 0.101, 0.0809, and 0.136 atm.cm. The gas temperature is set at 300 K and the total pressure is 101 kPa. Note: the experimental data resolution has been changed to match that of the narrow band model.

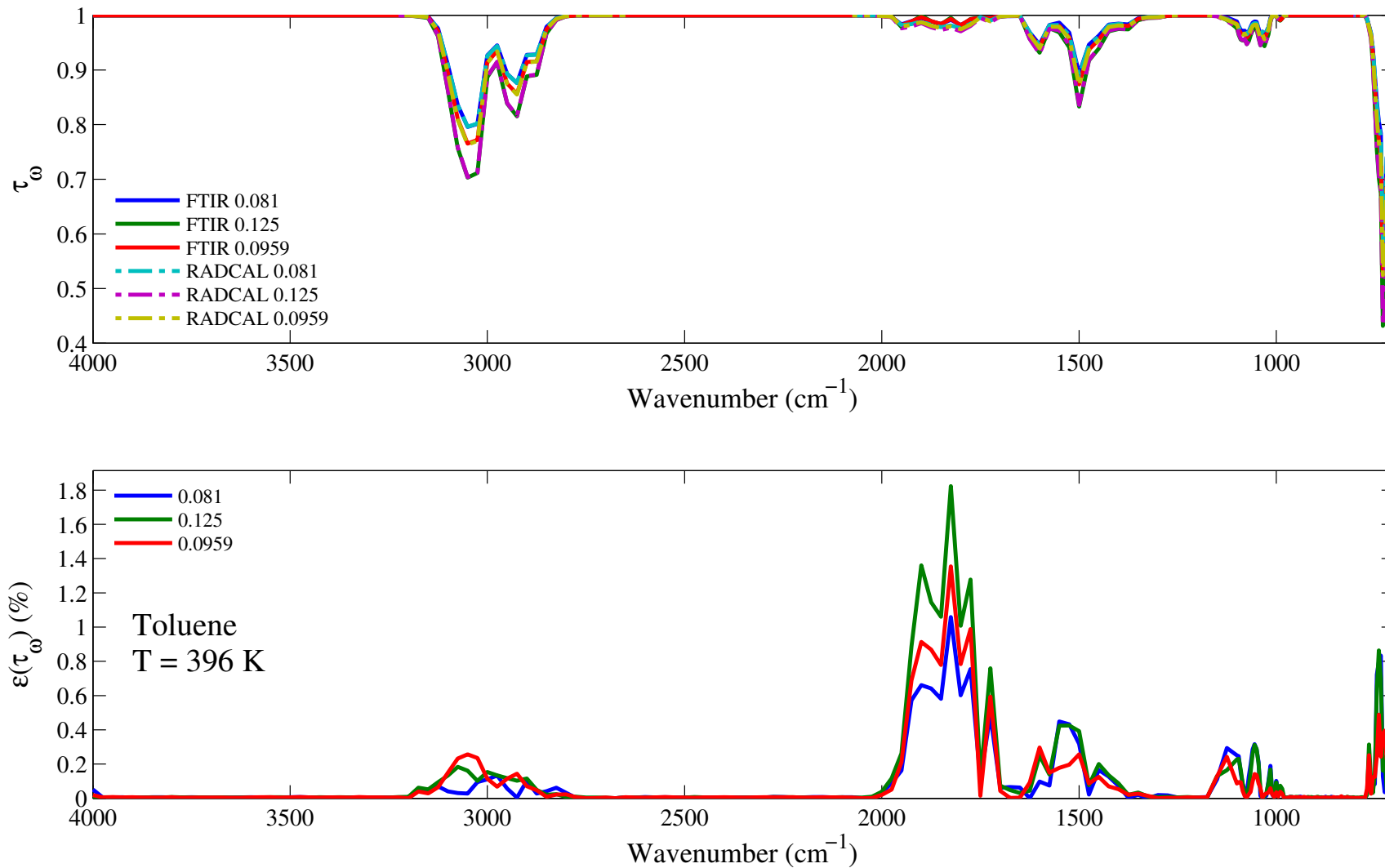


Figure 7.31: Top: comparison between the experimental (solid lines) and RadCal-generated synthetic (dashed lines) spectral transmissivity profiles, denoted τ_ω , of toluene of an isothermal homogeneous column of toluene. Bottom: relative transmissivity error, denoted $\varepsilon(\tau_\omega)$, between the experiment and the synthetic profiles presented on the top figure. Three different pressure path lengths are considered: 0.081, 0.125, and 0.0959 atm.cm. The gas temperature is set at 396 K and the total pressure is 101 kPa. Note: the experimental data resolution has been changed to match that of the narrow band model.

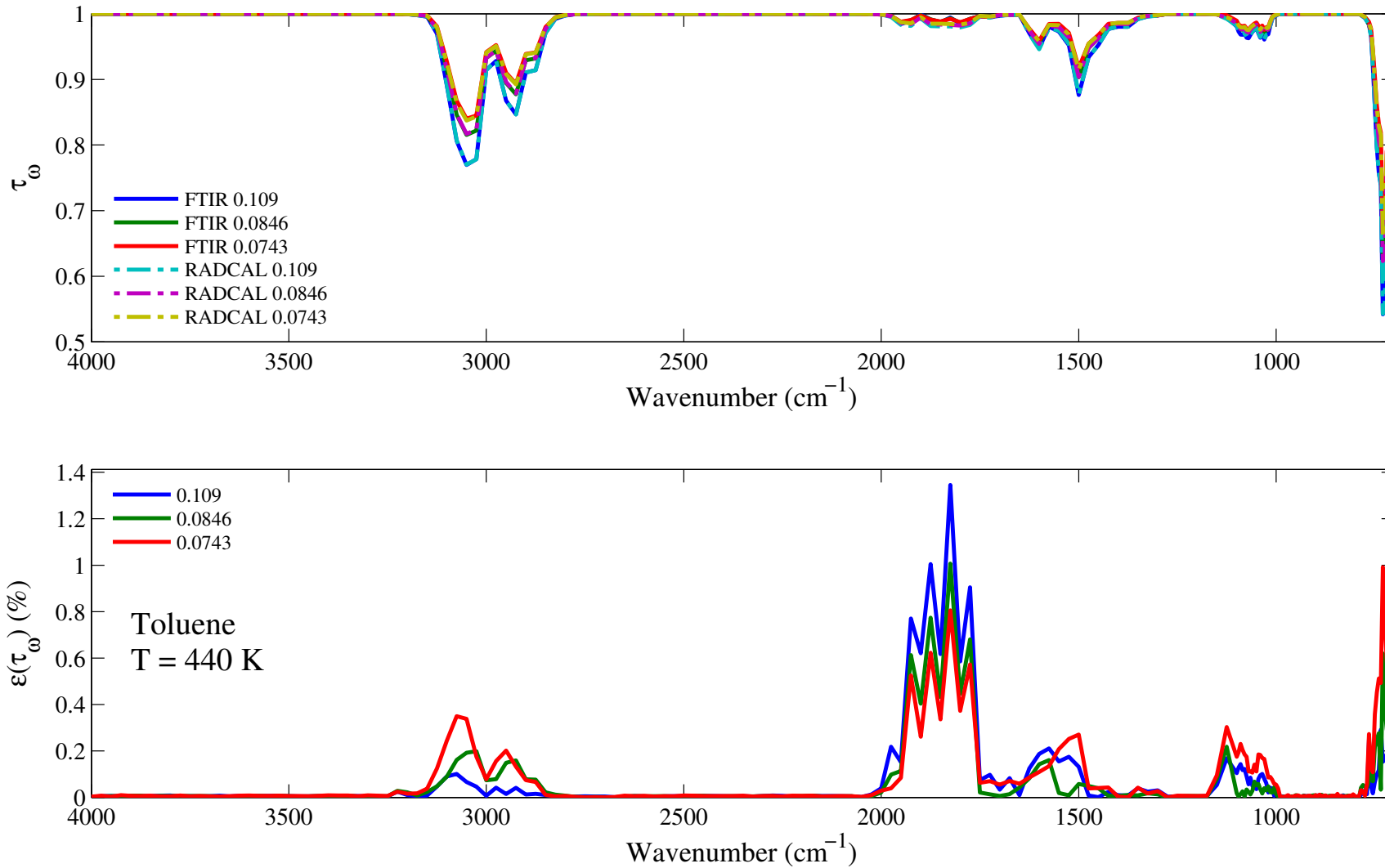


Figure 7.32: Top: comparison between the experimental (solid lines) and RadCal-generated synthetic (dashed lines) spectral transmissivity profiles, denoted τ_ω , of toluene of an isothermal homogeneous column of toluene. Bottom: relative transmissivity error, denoted $\varepsilon(\tau_\omega)$, between the experiment and the synthetic profiles presented on the top figure. Three different pressure path lengths are considered: 0.109, 0.0846, and 0.0743 atm.cm. The gas temperature is set at 440 K and the total pressure is 101 kPa. Note: the experimental data resolution has been changed to match that of the narrow band model.

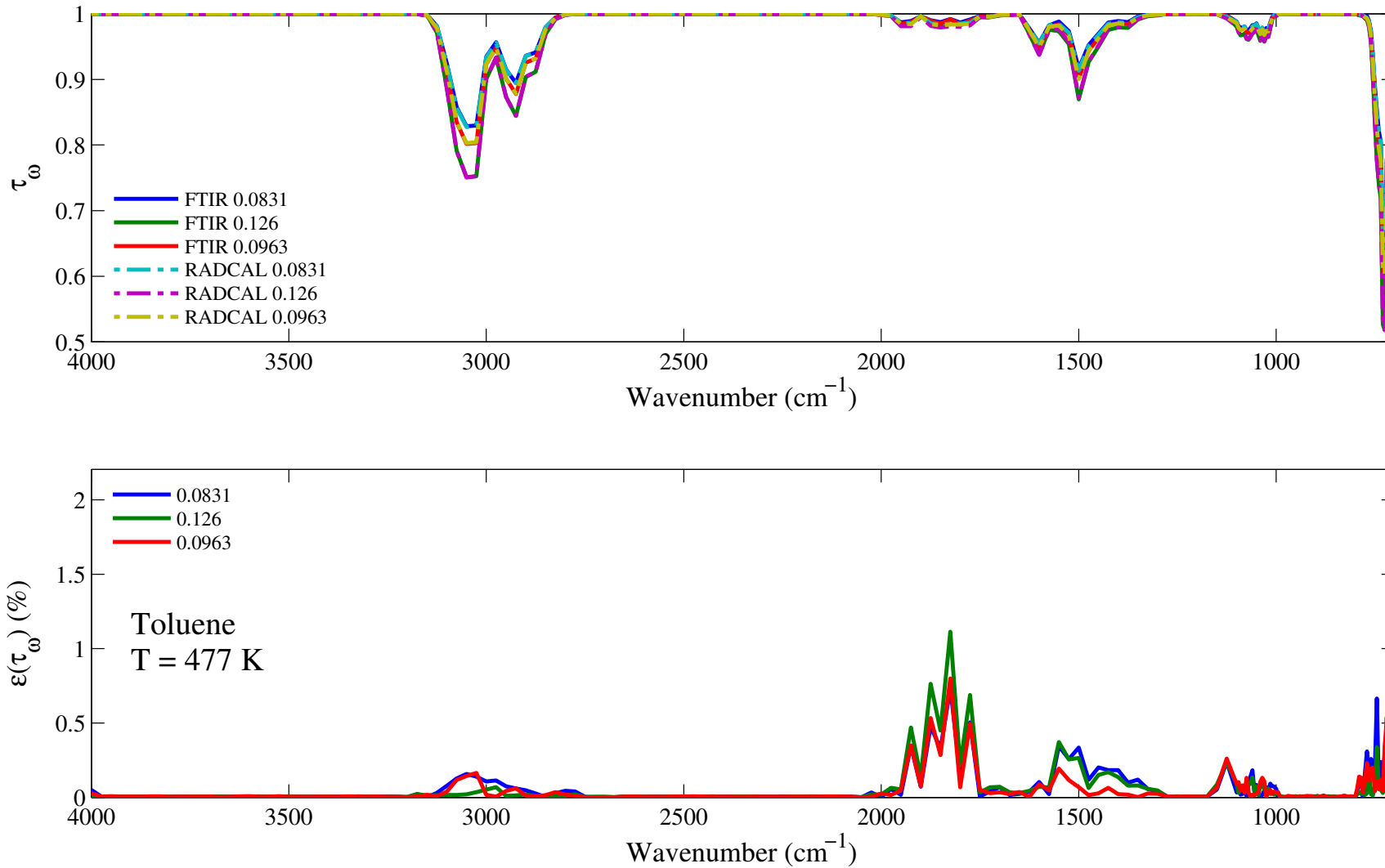


Figure 7.33: Top: comparison between the experimental (solid lines) and RadCal-generated synthetic (dashed lines) spectral transmissivity profiles, denoted τ_ω , of toluene of an isothermal homogeneous column of toluene. Bottom: relative transmissivity error, denoted $\varepsilon(\tau_\omega)$, between the experiment and the synthetic profiles presented on the top figure. Three different pressure path lengths are considered: 0.0831, 0.126, and 0.0963 atm.cm. The gas temperature is set at 477 K and the total pressure is 101 kPa. Note: the experimental data resolution has been changed to match that of the narrow band model.

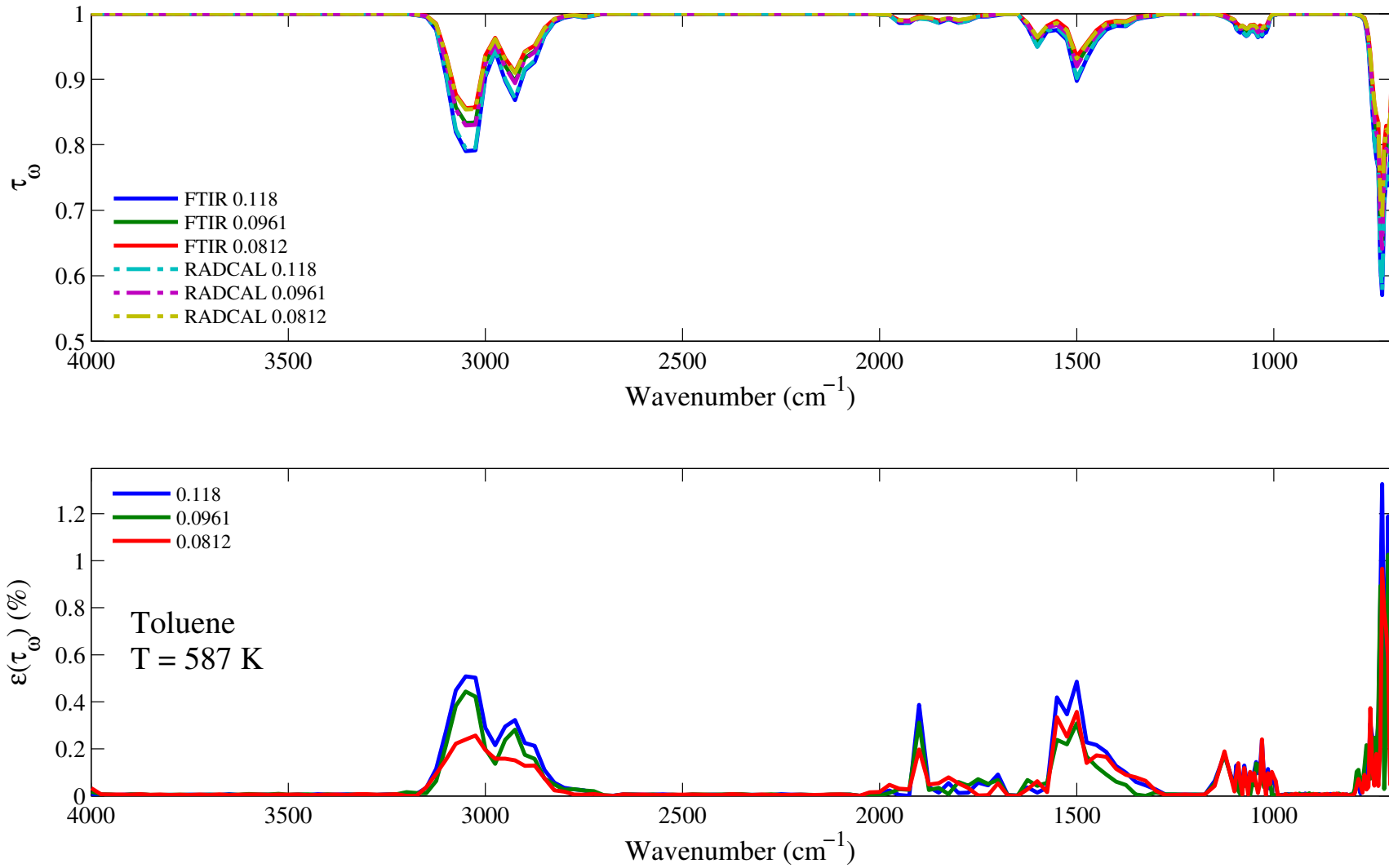


Figure 7.34: Top: comparison between the experimental (solid lines) and RadCal-generated synthetic (dashed lines) spectral transmissivity profiles, denoted τ_ω , of toluene of an isothermal homogeneous column of toluene. Bottom: relative transmissivity error, denoted $\varepsilon(\tau_\omega)$, between the experiment and the synthetic profiles presented on the top figure. Three different pressure path lengths are considered: 0.118, 0.0961, and 0.0812 atm.cm. The gas temperature is set at 587 K and the total pressure is 101 kPa. Note: the experimental data resolution has been changed to match that of the narrow band model.

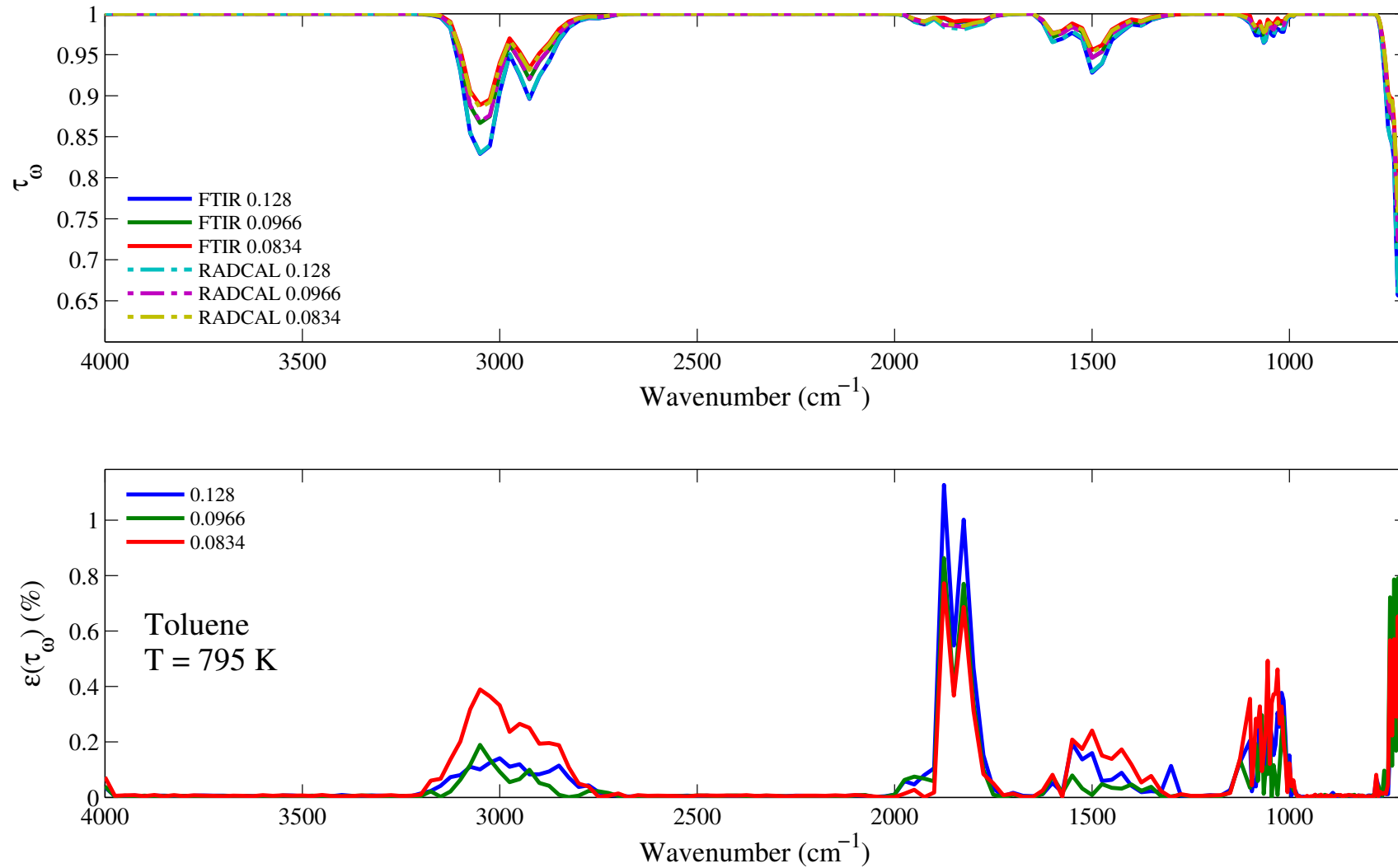


Figure 7.35: Top: comparison between the experimental (solid lines) and RadCal-generated synthetic (dashed lines) spectral transmissivity profiles, denoted τ_ω , of toluene of an isothermal homogeneous column of toluene. Bottom: relative transmissivity error, denoted $\varepsilon(\tau_\omega)$, between the experiment and the synthetic profiles presented on the top figure. Three different pressure path lengths are considered: 0.128, 0.0966, and 0.0834 atm.cm. The gas temperature is set at 795 K and the total pressure is 101 kPa. Note: the experimental data resolution has been changed to match that of the narrow band model.

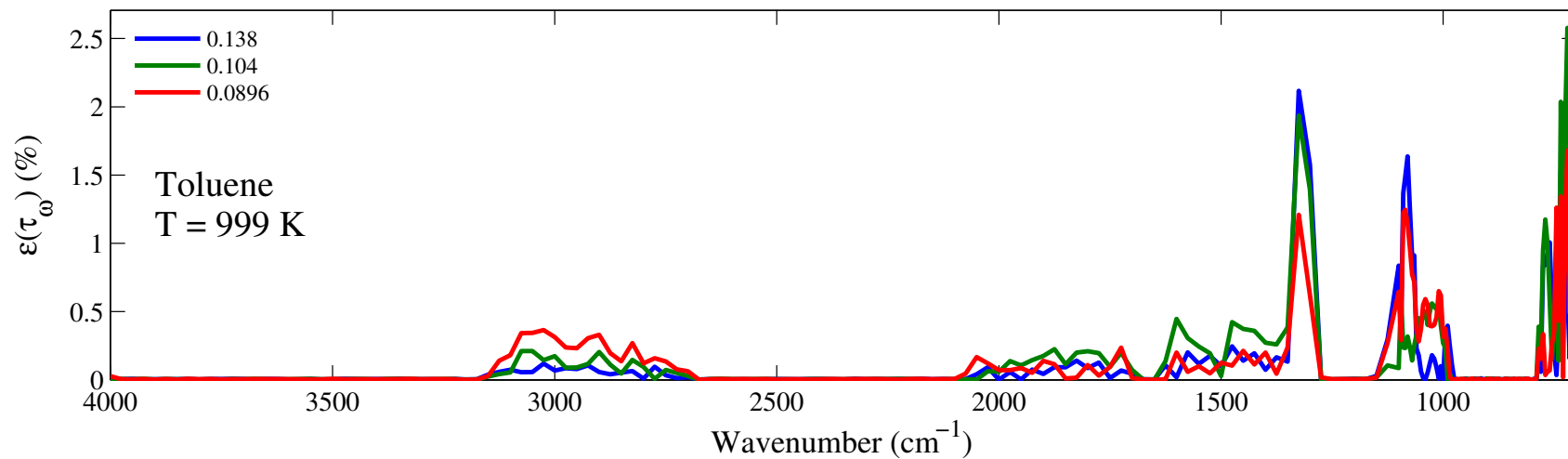
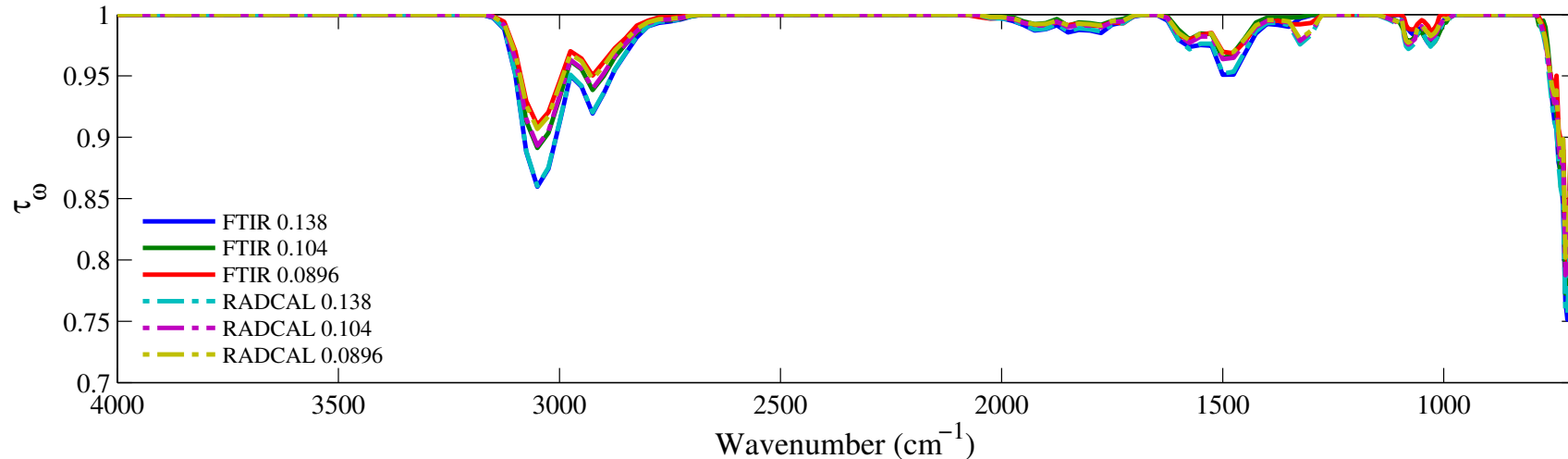


Figure 7.36: Top: comparison between the experimental (solid lines) and RadCal-generated synthetic (dashed lines) spectral transmissivity profiles, denoted τ_ω , of toluene of an isothermal homogeneous column of toluene. Bottom: relative transmissivity error, denoted $\varepsilon(\tau_\omega)$, between the experiment and the synthetic profiles presented on the top figure. Three different pressure path lengths are considered: 0.138, 0.104, and 0.0896 atm.cm. The gas temperature is set at 999 K and the total pressure is 101 kPa. Note: the experimental data resolution has been changed to match that of the narrow band model.

7.6 *n*-Heptane: C₇H₁₆

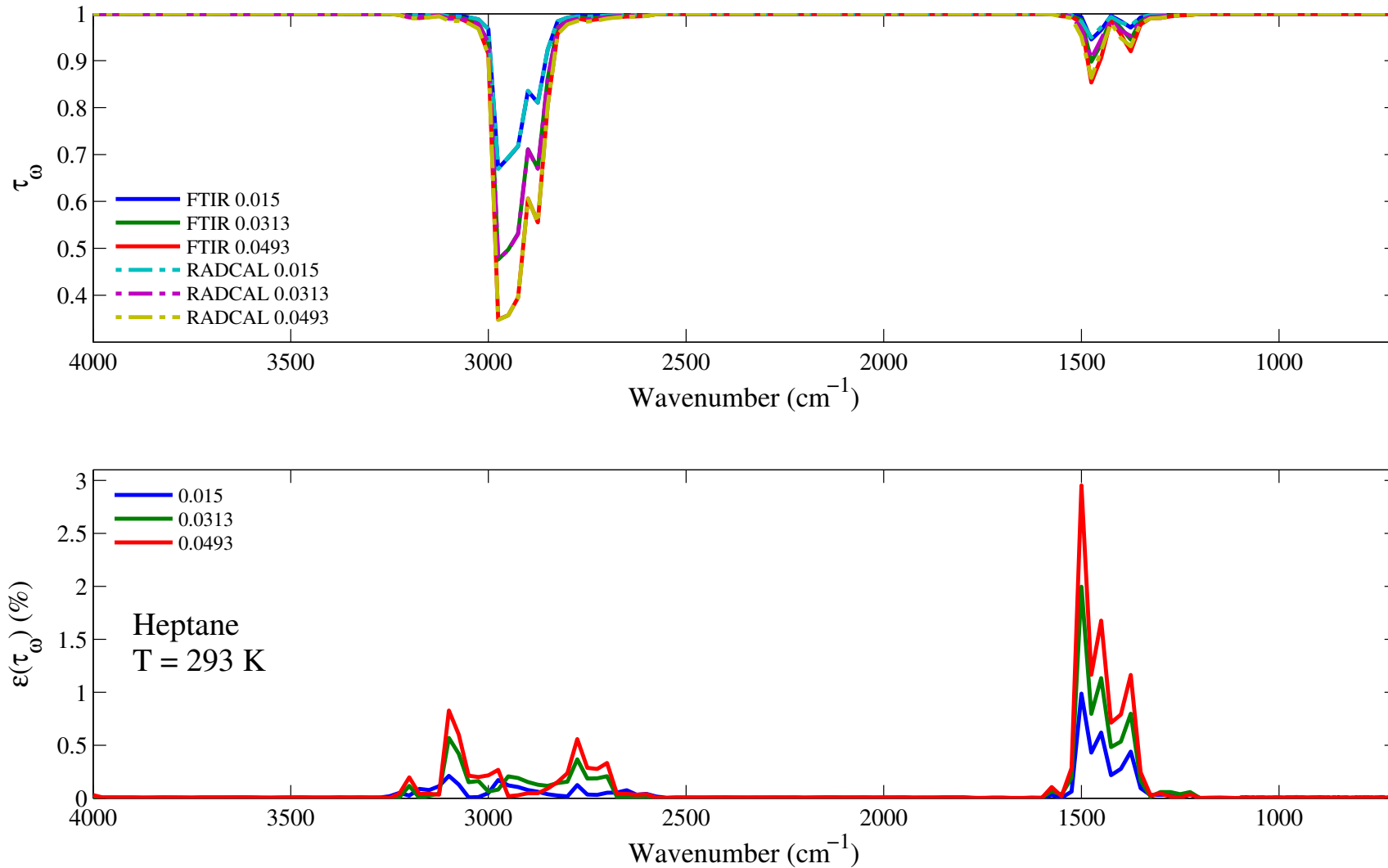


Figure 7.37: Top: comparison between the experimental (solid lines) and RadCal-generated synthetic (dashed lines) spectral transmissivity profiles, denoted τ_ω , of *n*-heptane of an isothermal homogeneous column of *n*-heptane. Bottom: relative transmissivity error, denoted $\varepsilon(\tau_\omega)$, between the experiment and the synthetic profiles presented on the top figure. Three different pressure path lengths are considered: 0.015, 0.0313, and 0.0493 atm.cm. The gas temperature is set at 293 K and the total pressure is 101 kPa. Note: the experimental data resolution has been changed to match that of the narrow band model.

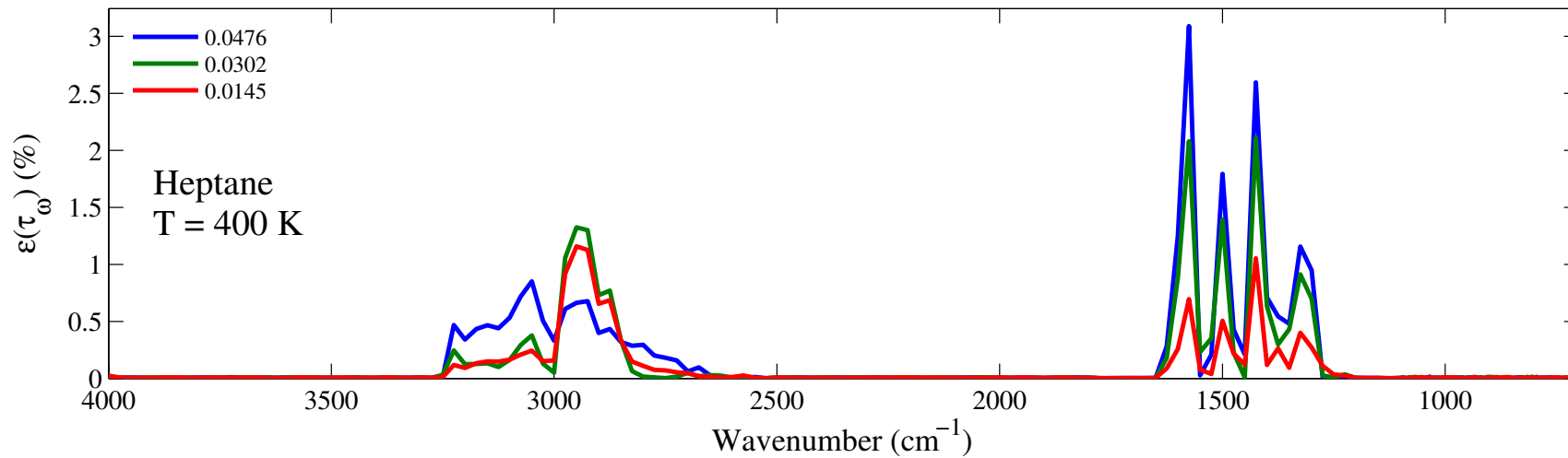
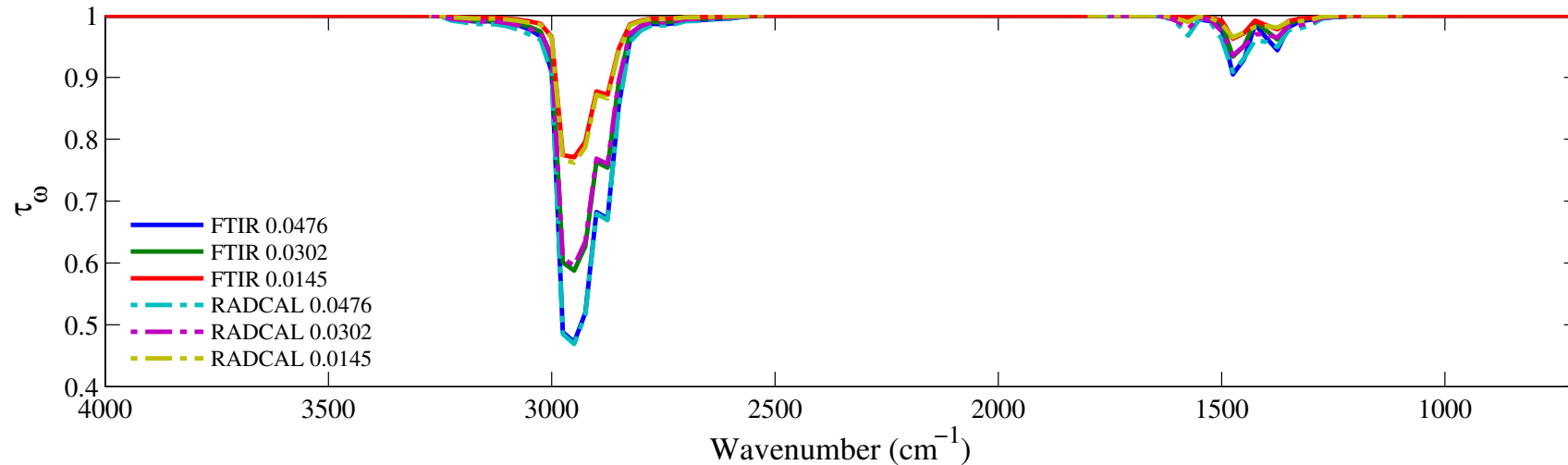


Figure 7.38: Top: comparison between the experimental (solid lines) and RadCal-generated synthetic (dashed lines) spectral transmissivity profiles, denoted τ_ω , of *n*-heptane of an isothermal homogeneous column of *n*-heptane. Bottom: relative transmissivity error, denoted $\varepsilon(\tau_\omega)$, between the experiment and the synthetic profiles presented on the top figure. Three different pressure path lengths are considered: 0.0476, 0.0302, and 0.0145 atm.cm. The gas temperature is set at 400 K and the total pressure is 101 kPa. Note: the experimental data resolution has been changed to match that of the narrow band model.

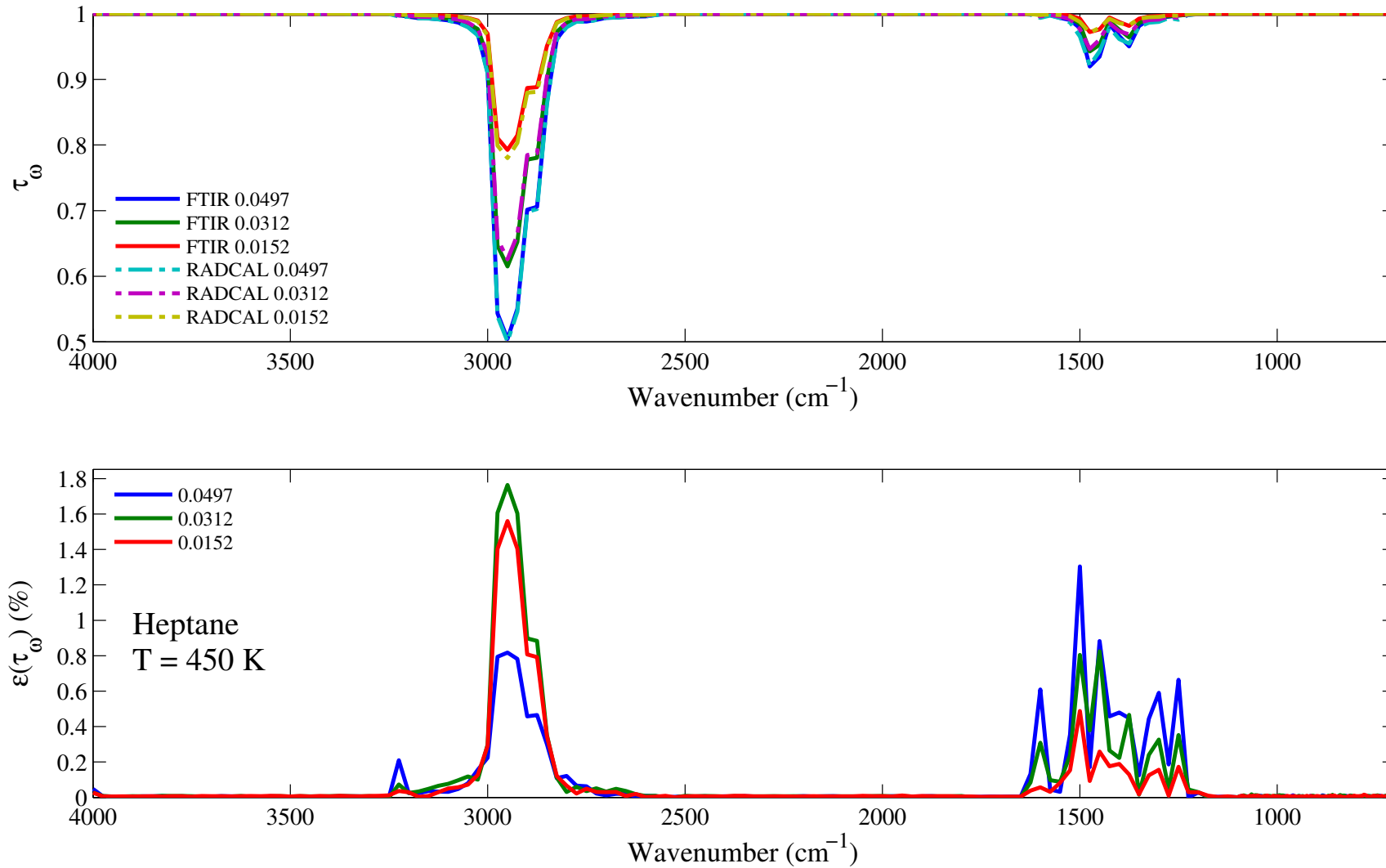


Figure 7.39: Top: comparison between the experimental (solid lines) and RadCal-generated synthetic (dashed lines) spectral transmissivity profiles, denoted τ_ω , of *n*-heptane of an isothermal homogeneous column of *n*-heptane. Bottom: relative transmissivity error, denoted $\varepsilon(\tau_\omega)$, between the experiment and the synthetic profiles presented on the top figure. Three different pressure path lengths are considered: 0.0497, 0.0312, and 0.0152 atm.cm. The gas temperature is set at 450 K and the total pressure is 101 kPa. Note: the experimental data resolution has been changed to match that of the narrow band model.

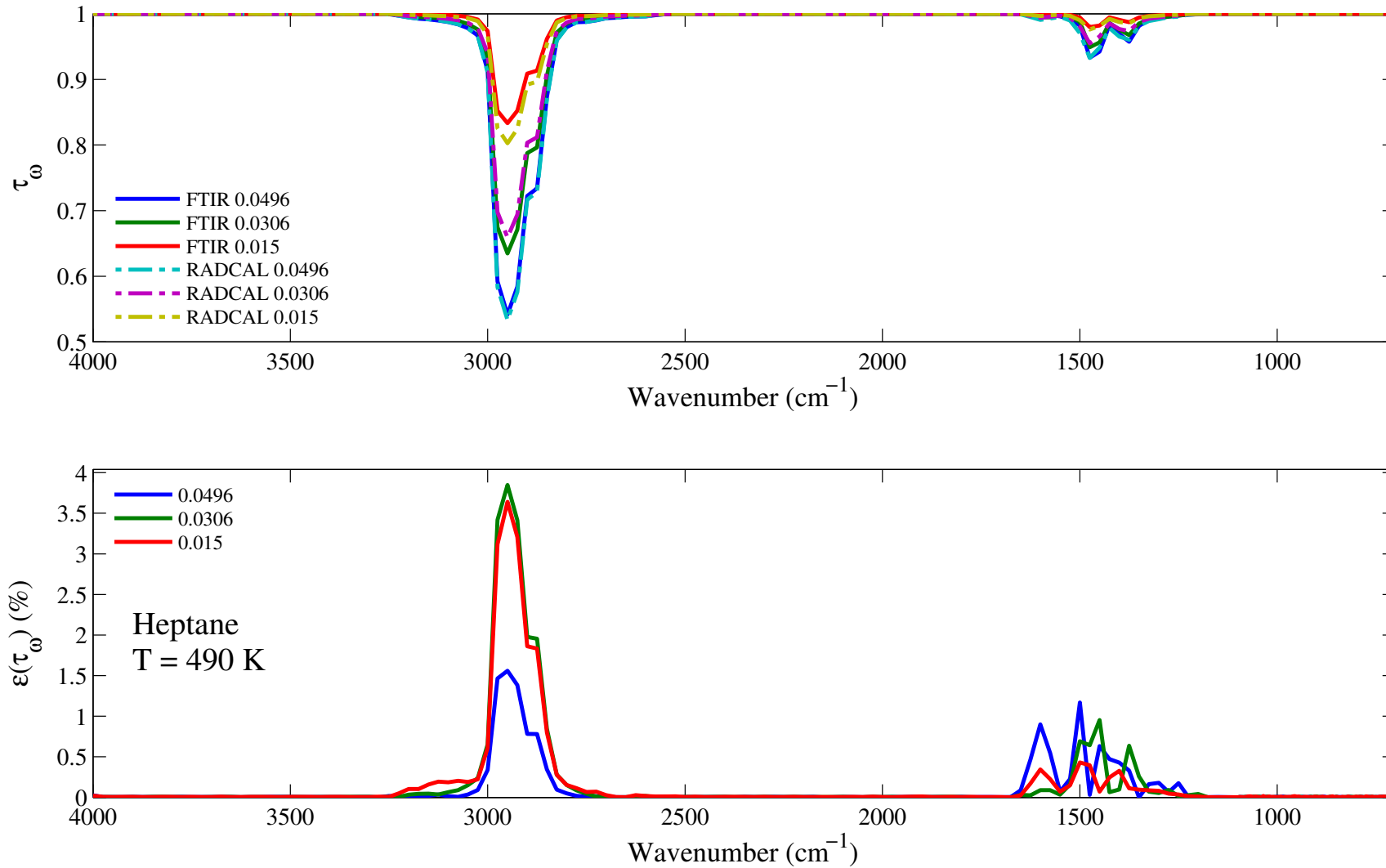


Figure 7.40: Top: comparison between the experimental (solid lines) and RadCal-generated synthetic (dashed lines) spectral transmissivity profiles, denoted τ_ω , of *n*-heptane of an isothermal homogeneous column of *n*-heptane. Bottom: relative transmissivity error, denoted $\varepsilon(\tau_\omega)$, between the experiment and the synthetic profiles presented on the top figure. Three different pressure path lengths are considered: 0.0496, 0.0306, and 0.015 atm.cm. The gas temperature is set at 490 K and the total pressure is 101 kPa. Note: the experimental data resolution has been changed to match that of the narrow band model.

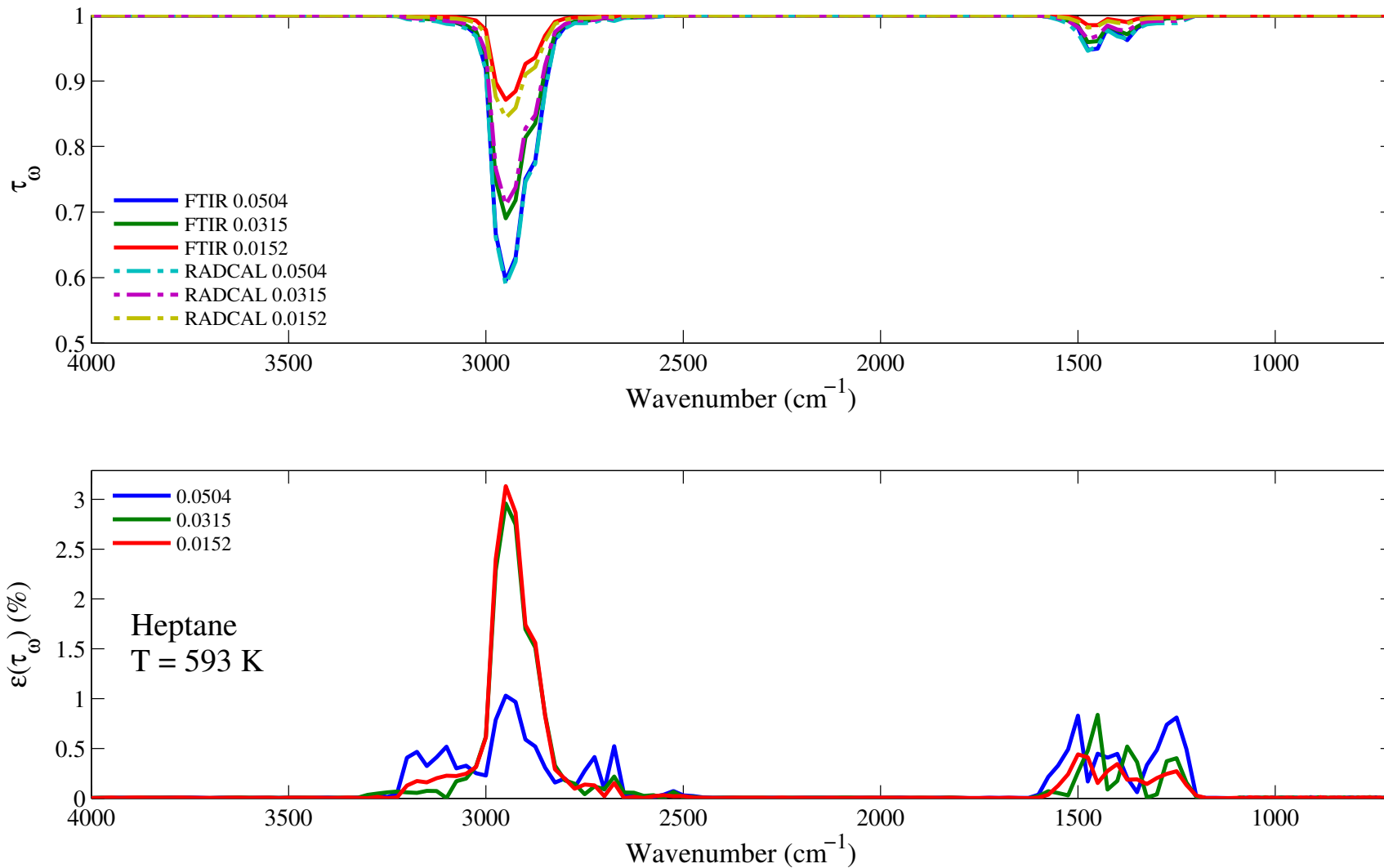


Figure 7.41: Top: comparison between the experimental (solid lines) and RadCal-generated synthetic (dashed lines) spectral transmissivity profiles, denoted τ_ω , of *n*-heptane of an isothermal homogeneous column of *n*-heptane. Bottom: relative transmissivity error, denoted $\varepsilon(\tau_\omega)$, between the experiment and the synthetic profiles presented on the top figure. Three different pressure path lengths are considered: 0.0504, 0.0315, and 0.0152 atm.cm. The gas temperature is set at 593 K and the total pressure is 101 kPa. Note: the experimental data resolution has been changed to match that of the narrow band model.

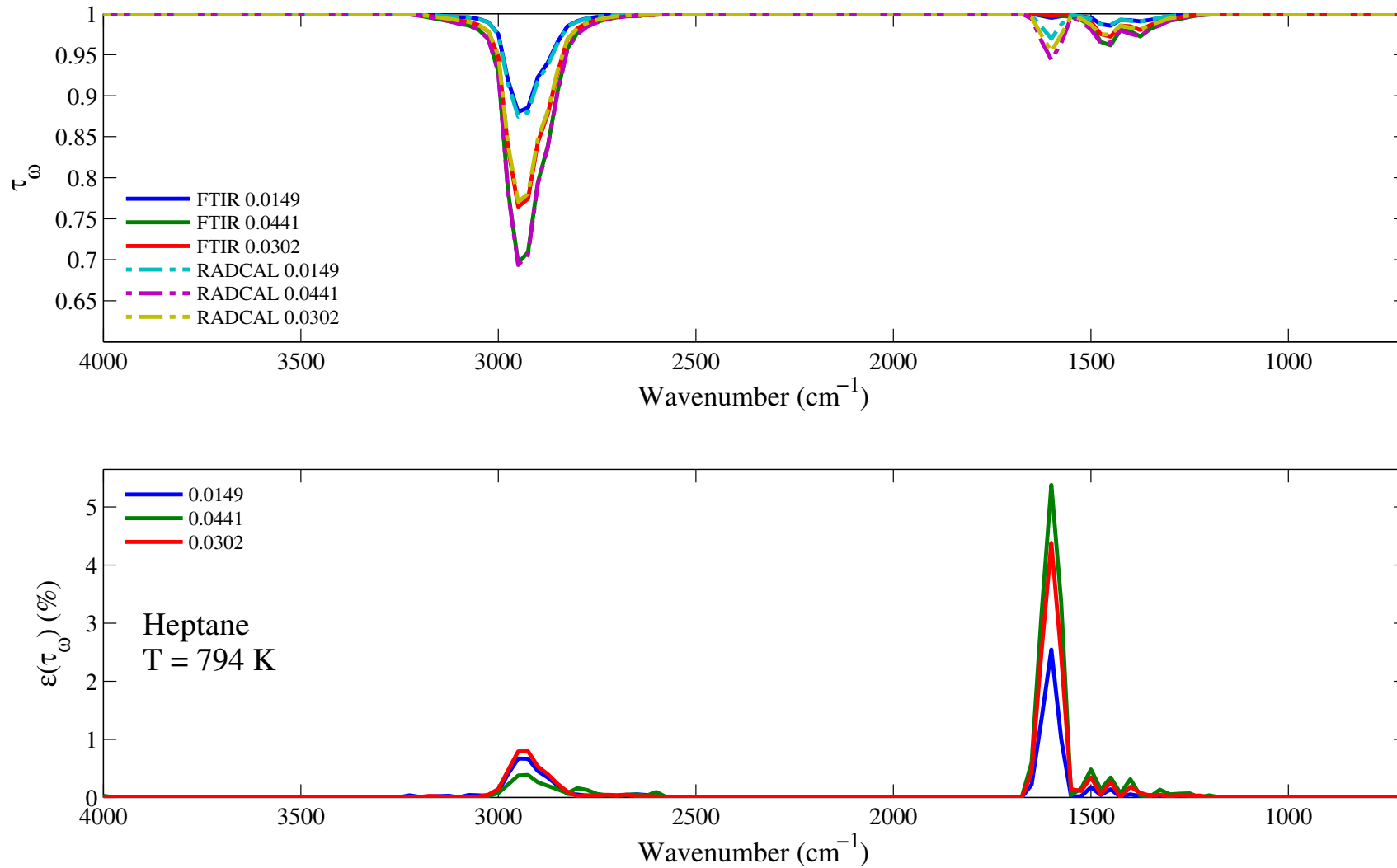


Figure 7.42: Top: comparison between the experimental (solid lines) and RadCal-generated synthetic (dashed lines) spectral transmissivity profiles, denoted τ_ω , of *n*-heptane of an isothermal homogeneous column of *n*-heptane. Bottom: relative transmissivity error, denoted $\varepsilon(\tau_\omega)$, between the experiment and the synthetic profiles presented on the top figure. Three different pressure path lengths are considered: 0.0149, 0.0441, and 0.0302 atm.cm. The gas temperature is set at 794 K and the total pressure is 101 kPa. Note: the experimental data resolution has been changed to match that of the narrow band model.

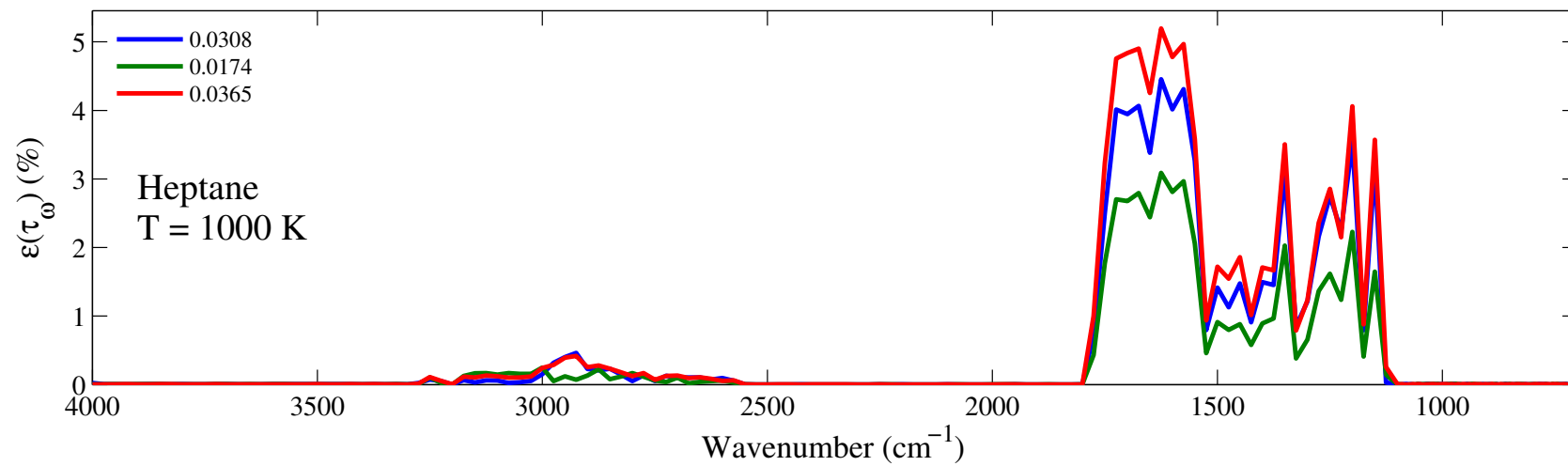
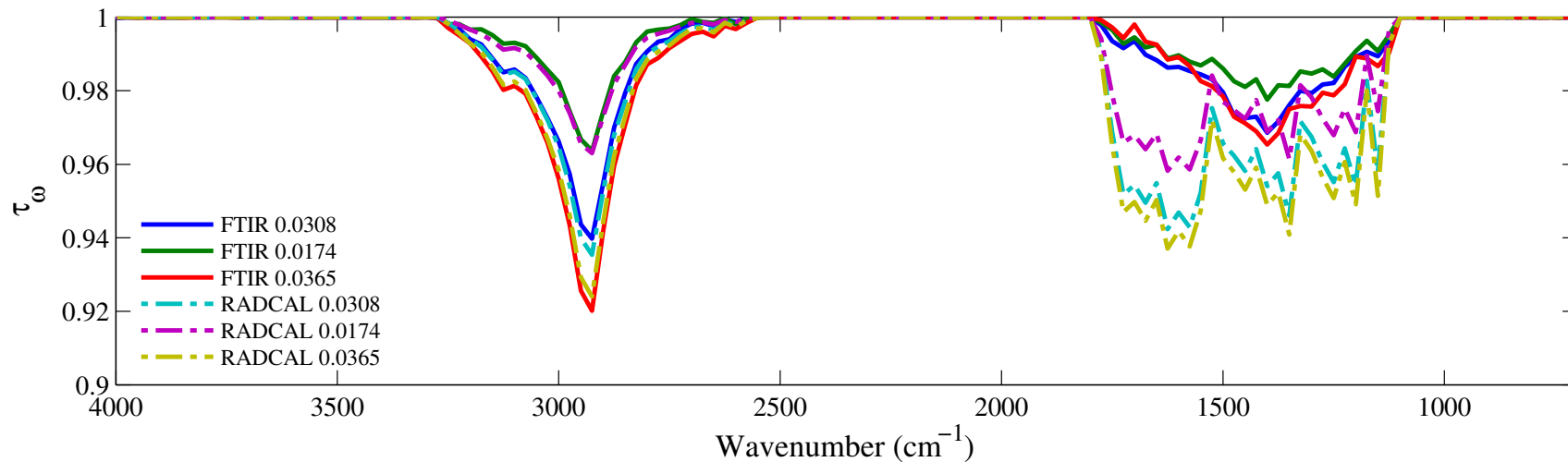


Figure 7.43: Top: comparison between the experimental (solid lines) and RadCal-generated synthetic (dashed lines) spectral transmissivity profiles, denoted τ_ω , of *n*-heptane of an isothermal homogeneous column of *n*-heptane. Bottom: relative transmissivity error, denoted $\varepsilon(\tau_\omega)$, between the experiment and the synthetic profiles presented on the top figure. Three different pressure path lengths are considered: 0.0308, 0.0174, and 0.0365 atm.cm. The gas temperature is set at 1000 K and the total pressure is 101 kPa. Note: the experimental data resolution has been changed to match that of the narrow band model.

7.7 Methanol: CH₃OH

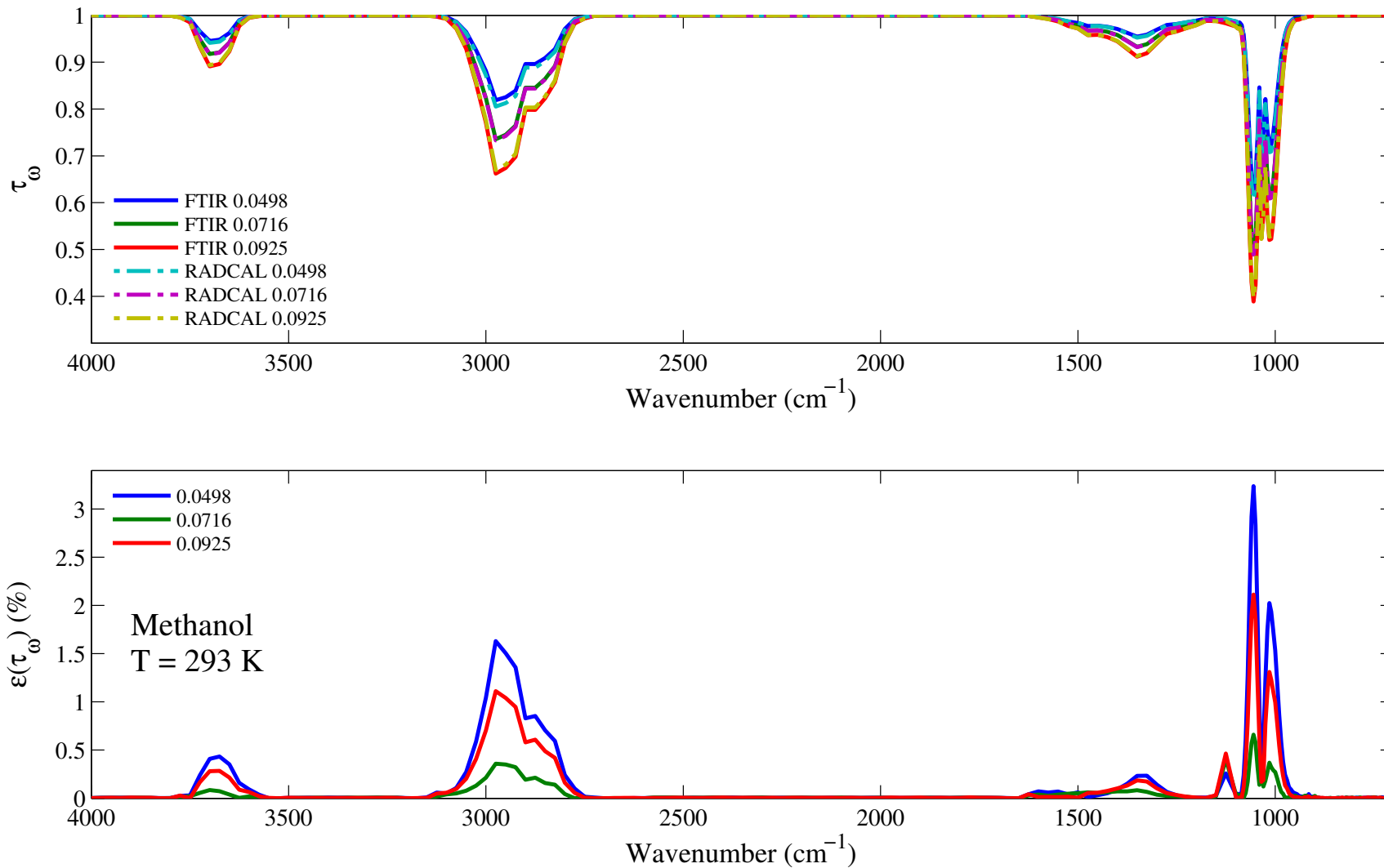


Figure 7.44: Top: comparison between the experimental (solid lines) and RadCal-generated synthetic (dashed lines) spectral transmissivity profiles, denoted τ_ω , of methanol of an isothermal homogeneous column of methanol. Bottom: relative transmissivity error, denoted $\varepsilon(\tau_\omega)$, between the experiment and the synthetic profiles presented on the top figure. Three different pressure path lengths are considered: 0.0498, 0.0716, and 0.0925 atm.cm. The gas temperature is set at 293 K and the total pressure is 101 kPa. Note: the experimental data resolution has been changed to match that of the narrow band model.

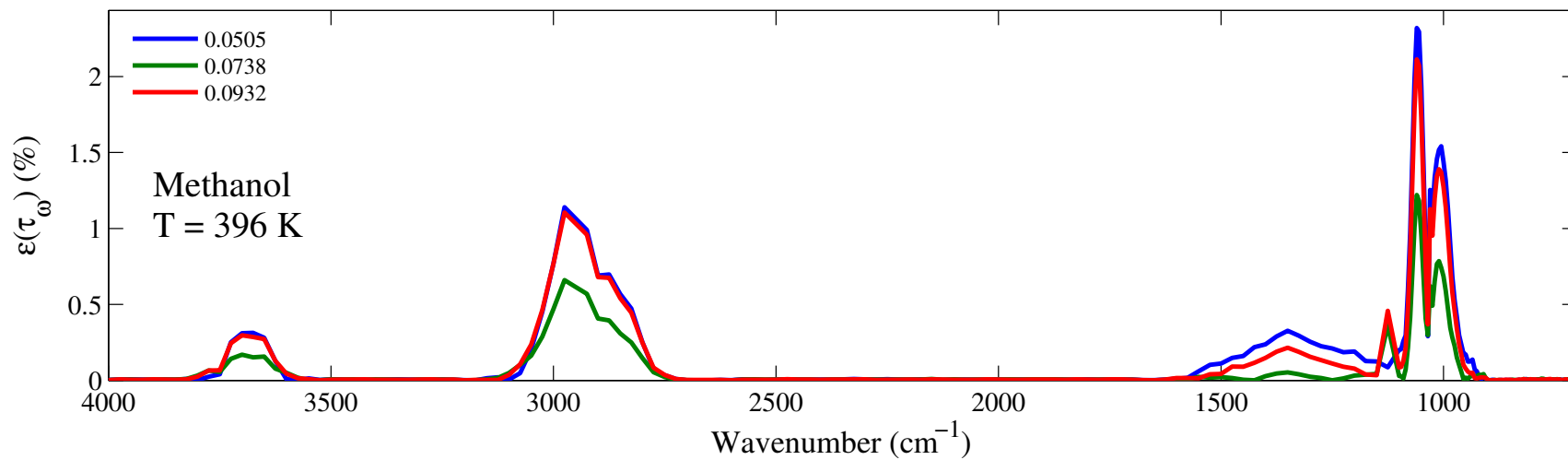
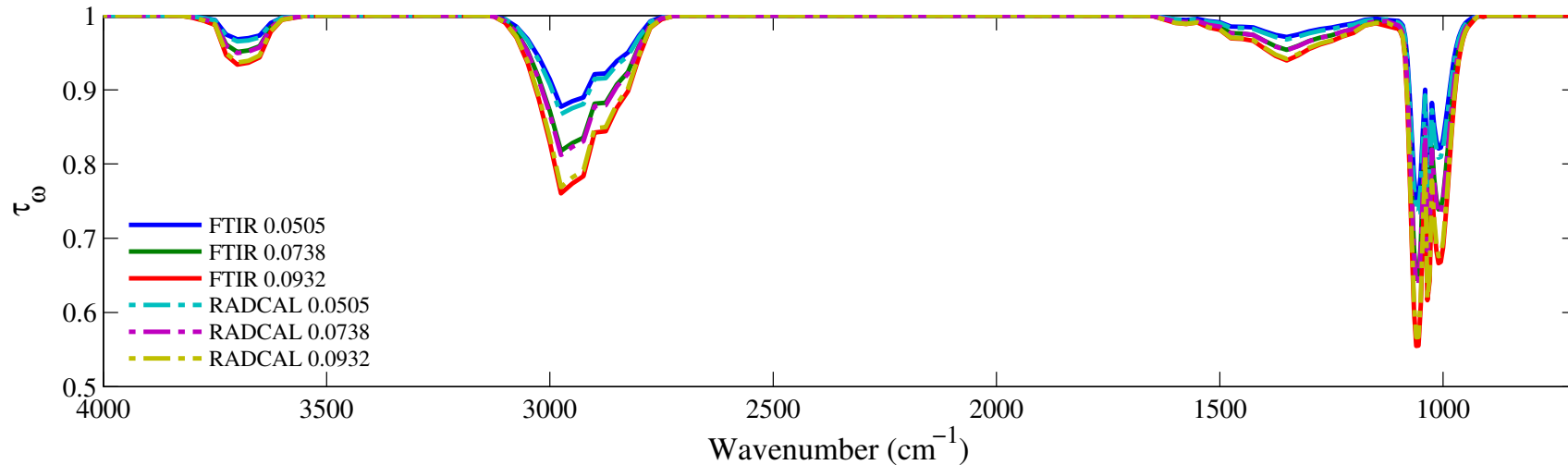


Figure 7.45: Top: comparison between the experimental (solid lines) and RadCal-generated synthetic (dashed lines) spectral transmissivity profiles, denoted τ_ω , of methanol of an isothermal homogeneous column of methanol. Bottom: relative transmissivity error, denoted $\varepsilon(\tau_\omega)$, between the experiment and the synthetic profiles presented on the top figure. Three different pressure path lengths are considered: 0.0505, 0.0738, and 0.0932 atm.cm. The gas temperature is set at 396 K and the total pressure is 101 kPa. Note: the experimental data resolution has been changed to match that of the narrow band model.

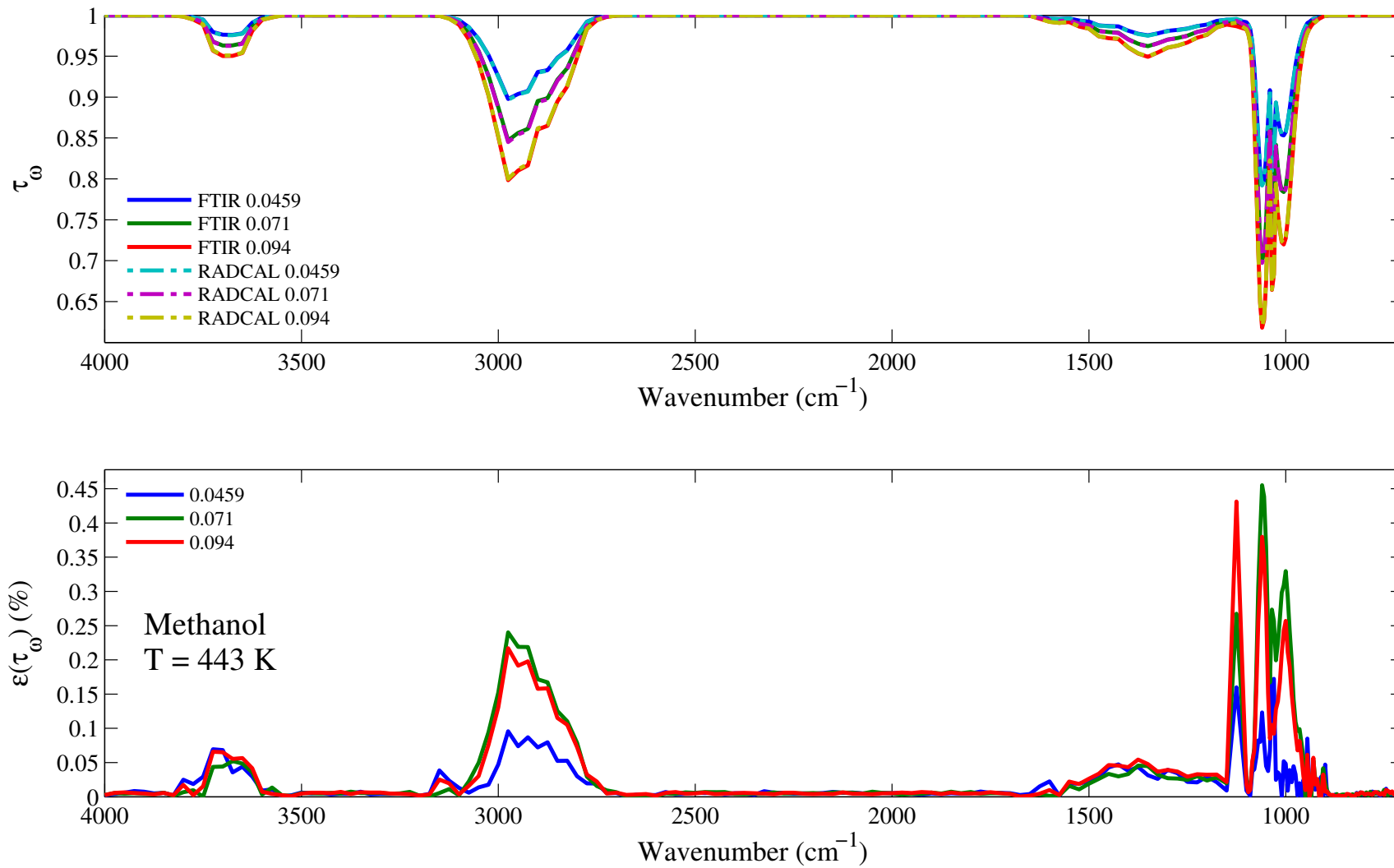


Figure 7.46: Top: comparison between the experimental (solid lines) and RadCal-generated synthetic (dashed lines) spectral transmissivity profiles, denoted τ_ω , of methanol of an isothermal homogeneous column of methanol. Bottom: relative transmissivity error, denoted $\varepsilon(\tau_\omega)$, between the experiment and the synthetic profiles presented on the top figure. Three different pressure path lengths are considered: 0.0459, 0.071, and 0.094 atm.cm. The gas temperature is set at 443 K and the total pressure is 101 kPa. Note: the experimental data resolution has been changed to match that of the narrow band model.

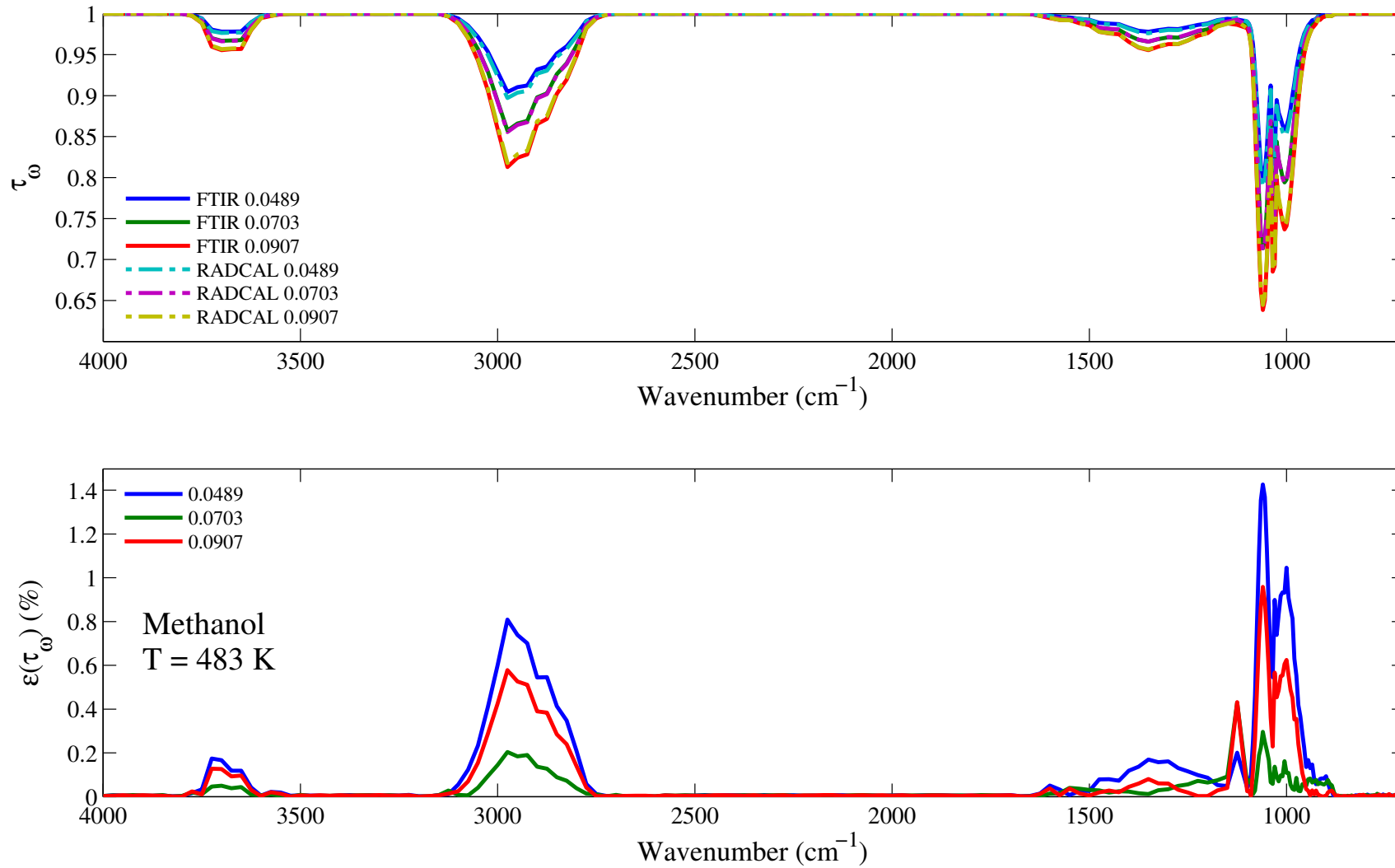


Figure 7.47: Top: comparison between the experimental (solid lines) and RadCal-generated synthetic (dashed lines) spectral transmissivity profiles, denoted τ_ω , of methanol of an isothermal homogeneous column of methanol. Bottom: relative transmissivity error, denoted $\varepsilon(\tau_\omega)$, between the experiment and the synthetic profiles presented on the top figure. Three different pressure path lengths are considered: 0.0489, 0.0703, and 0.0907 atm.cm. The gas temperature is set at 483 K and the total pressure is 101 kPa. Note: the experimental data resolution has been changed to match that of the narrow band model.

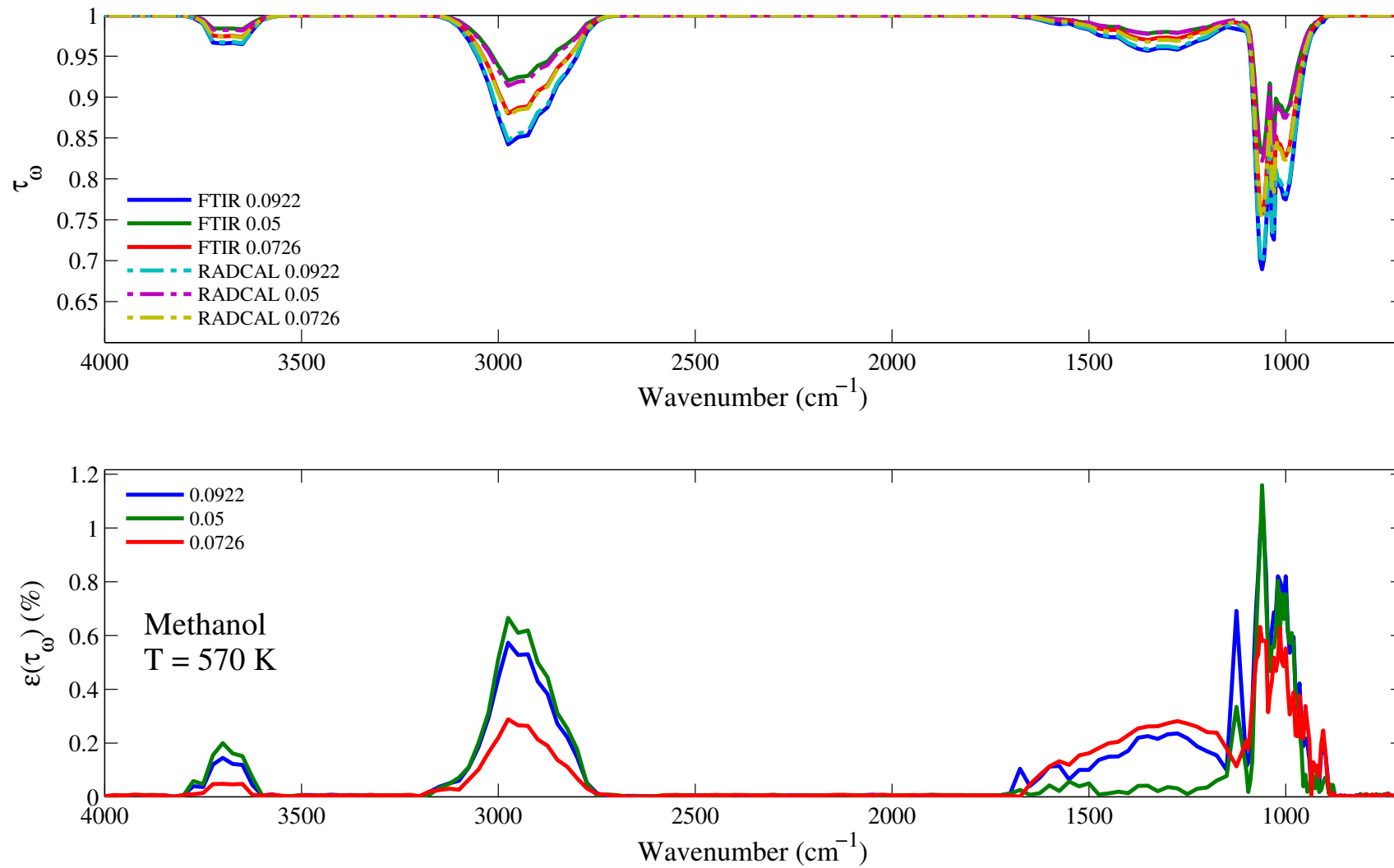


Figure 7.48: Top: comparison between the experimental (solid lines) and RadCal-generated synthetic (dashed lines) spectral transmissivity profiles, denoted τ_ω , of methanol of an isothermal homogeneous column of methanol. Bottom: relative transmissivity error, denoted $\varepsilon(\tau_\omega)$, between the experiment and the synthetic profiles presented on the top figure. Three different pressure path lengths are considered: 0.0922, 0.05, and 0.0726 atm.cm. The gas temperature is set at 570 K and the total pressure is 101 kPa. Note: the experimental data resolution has been changed to match that of the narrow band model.

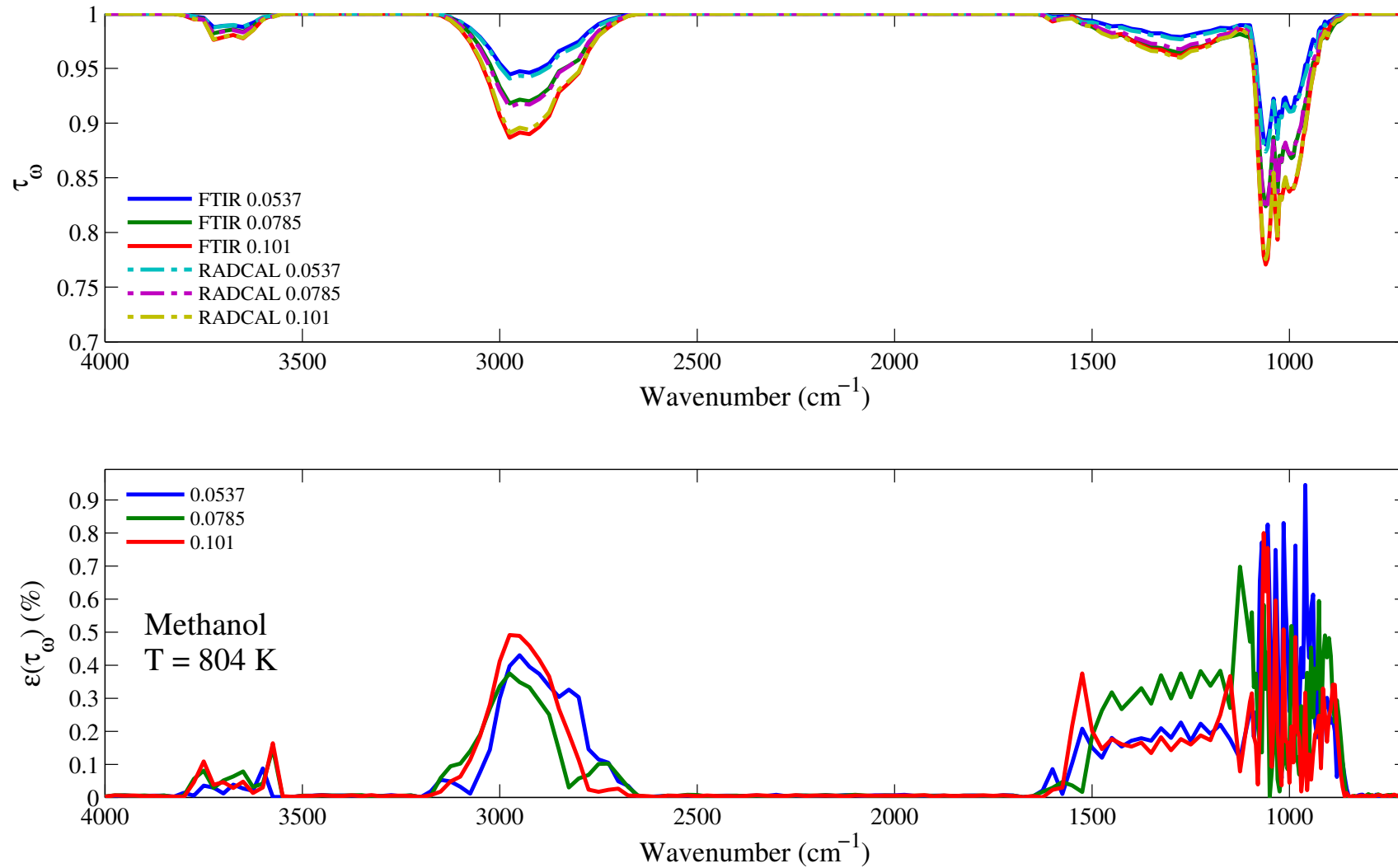


Figure 7.49: Top: comparison between the experimental (solid lines) and RadCal-generated synthetic (dashed lines) spectral transmissivity profiles, denoted τ_ω , of methanol of an isothermal homogeneous column of methanol. Bottom: relative transmissivity error, denoted $\varepsilon(\tau_\omega)$, between the experiment and the synthetic profiles presented on the top figure. Three different pressure path lengths are considered: 0.0537, 0.0785, and 0.101 atm.cm. The gas temperature is set at 804 K and the total pressure is 101 kPa. Note: the experimental data resolution has been changed to match that of the narrow band model.

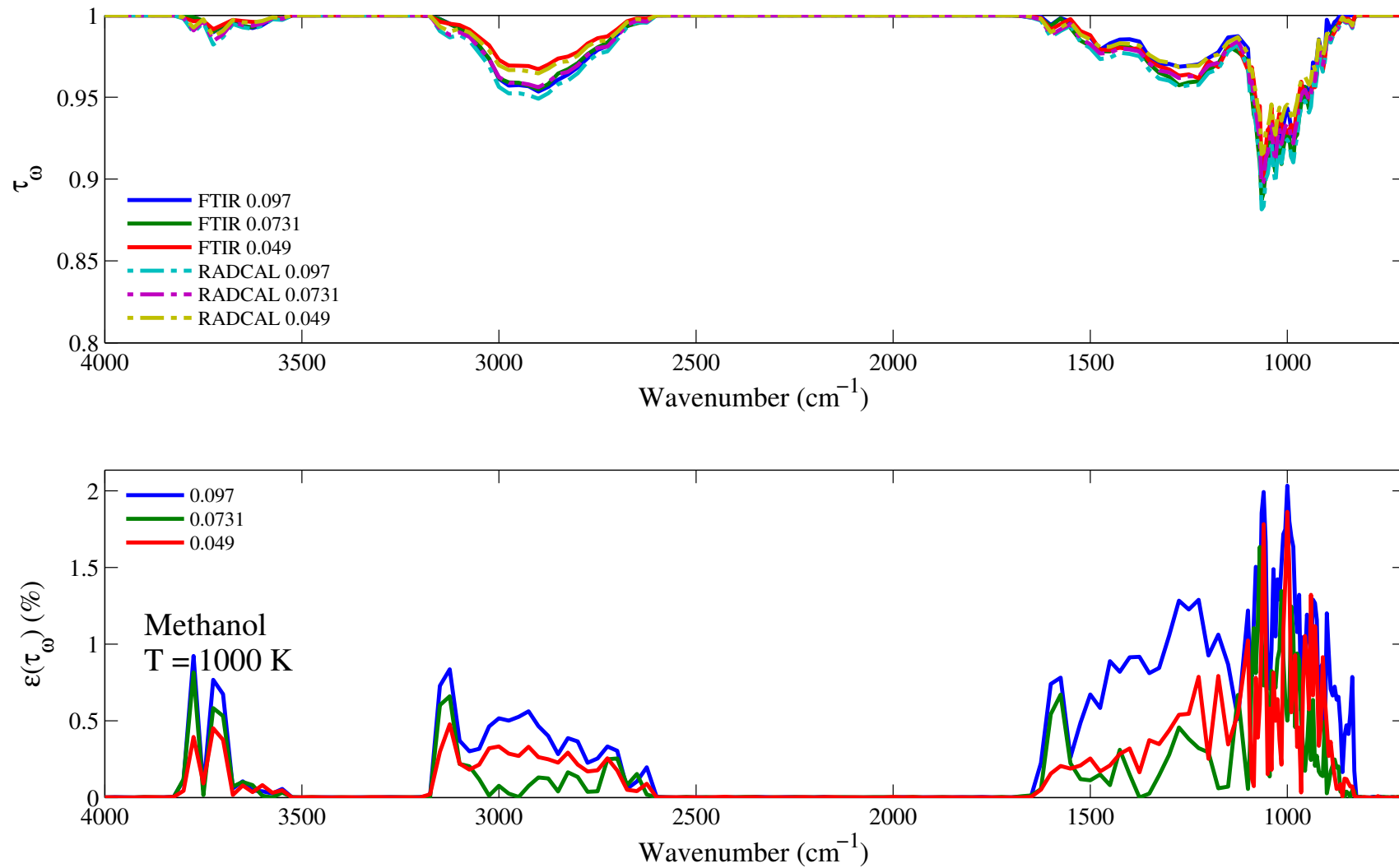


Figure 7.50: Top: comparison between the experimental (solid lines) and RadCal-generated synthetic (dashed lines) spectral transmissivity profiles, denoted τ_ω , of methanol of an isothermal homogeneous column of methanol. Bottom: relative transmissivity error, denoted $\varepsilon(\tau_\omega)$, between the experiment and the synthetic profiles presented on the top figure. Three different pressure path lengths are considered: 0.097, 0.0731, and 0.049 atm.cm. The gas temperature is set at 1000 K and the total pressure is 101 kPa. Note: the experimental data resolution has been changed to match that of the narrow band model.

7.8 Methyl Methacrylate: C₅H₈O₂

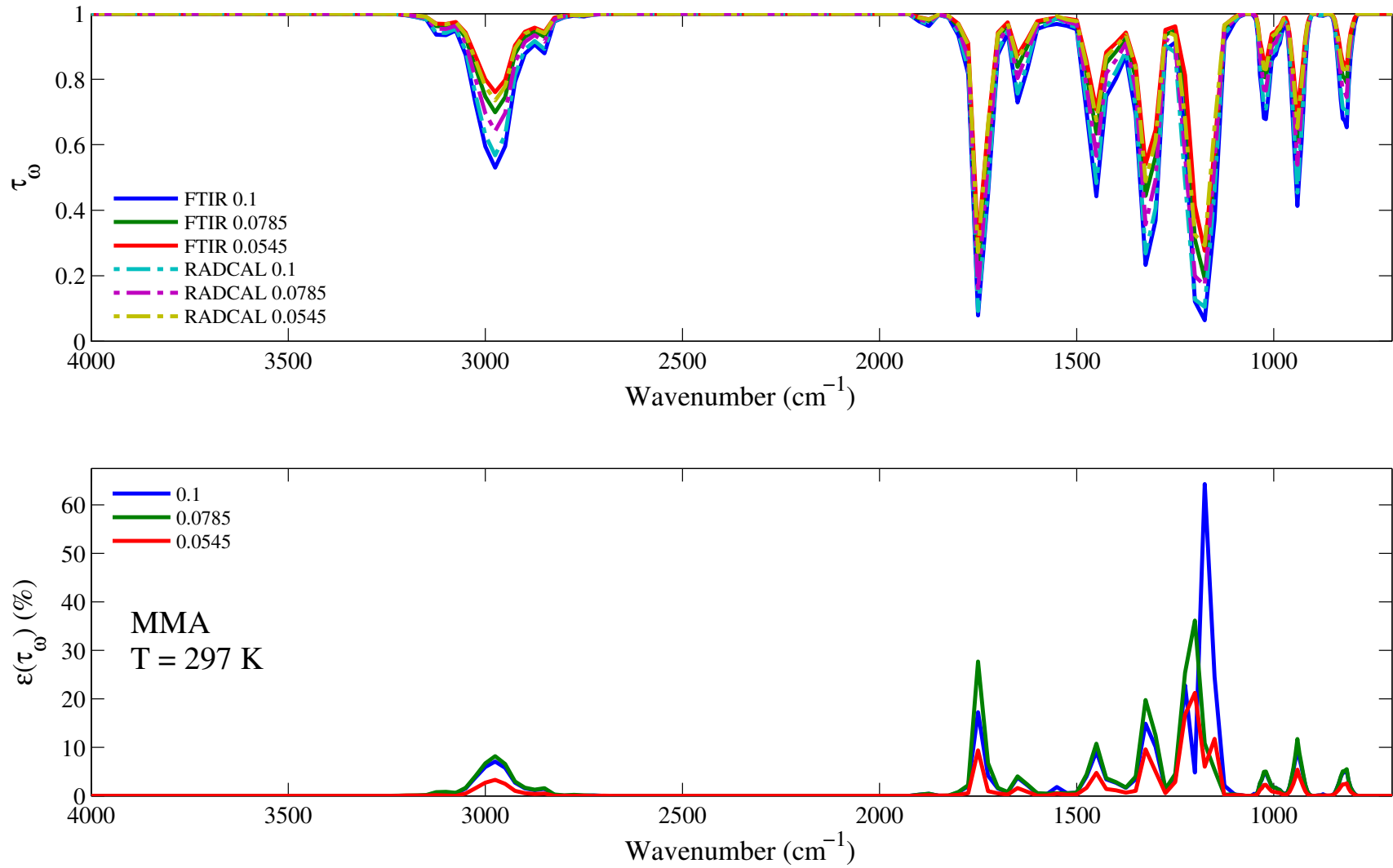


Figure 7.51: Top: comparison between the experimental (solid lines) and RadCal-generated synthetic (dashed lines) spectral transmissivity profiles, denoted τ_ω , of MMA of an isothermal homogeneous column of MMA. Bottom: relative transmissivity error, denoted $\varepsilon(\tau_\omega)$, between the experiment and the synthetic profiles presented on the top figure. Three different pressure path lengths are considered: 0.1, 0.0785, and 0.0545 atm.cm. The gas temperature is set at 297 K and the total pressure is 101 kPa. Note: the experimental data resolution has been changed to match that of the narrow band model.

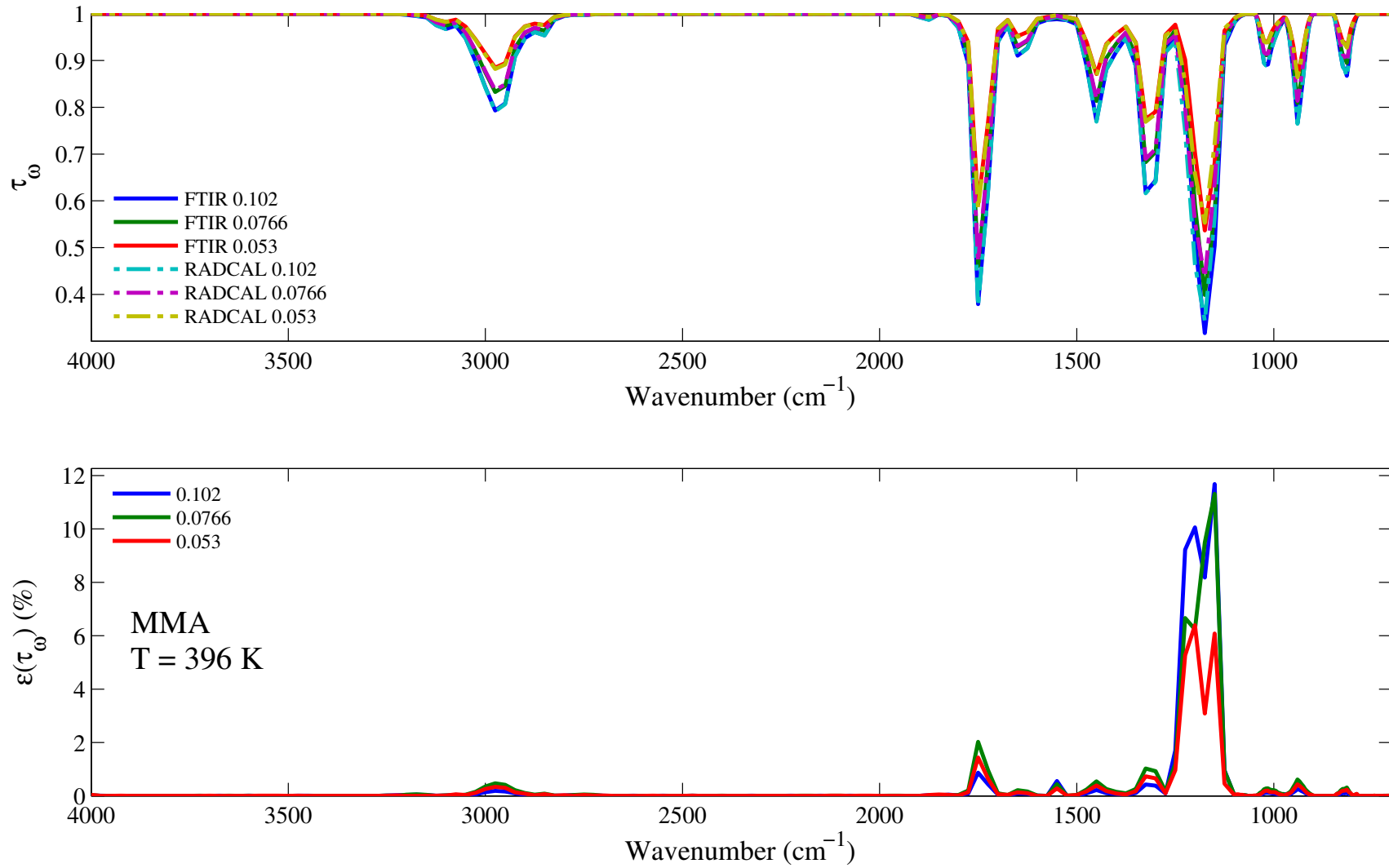


Figure 7.52: Top: comparison between the experimental (solid lines) and RadCal-generated synthetic (dashed lines) spectral transmissivity profiles, denoted τ_ω , of MMA of an isothermal homogeneous column of MMA. Bottom: relative transmissivity error, denoted $\varepsilon(\tau_\omega)$, between the experiment and the synthetic profiles presented on the top figure. Three different pressure path lengths are considered: 0.102, 0.179, and 0.0782 atm.cm. The gas temperature is set at 396 K and the total pressure is 101 kPa. Note: the experimental data resolution has been changed to match that of the narrow band model.

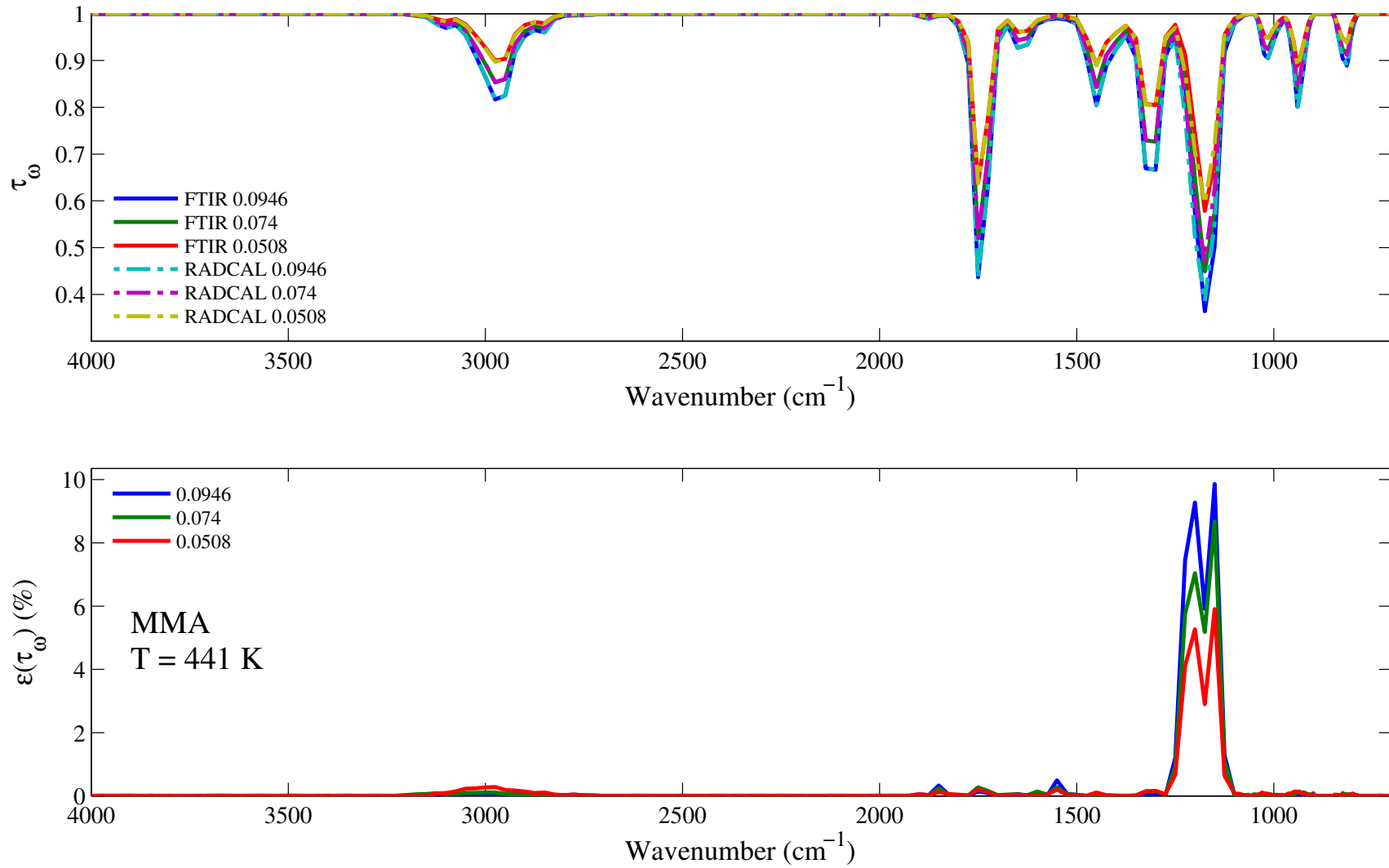


Figure 7.53: Top: comparison between the experimental (solid lines) and RadCal-generated synthetic (dashed lines) spectral transmissivity profiles, denoted τ_ω , of MMA of an isothermal homogeneous column of MMA. Bottom: relative transmissivity error, denoted $\varepsilon(\tau_\omega)$, between the experiment and the synthetic profiles presented on the top figure. Three different pressure path lengths are considered: 0.0946, 0.074, and 0.0508 atm.cm. The gas temperature is set at 441 K and the total pressure is 101 kPa. Note: the experimental data resolution has been changed to match that of the narrow band model.

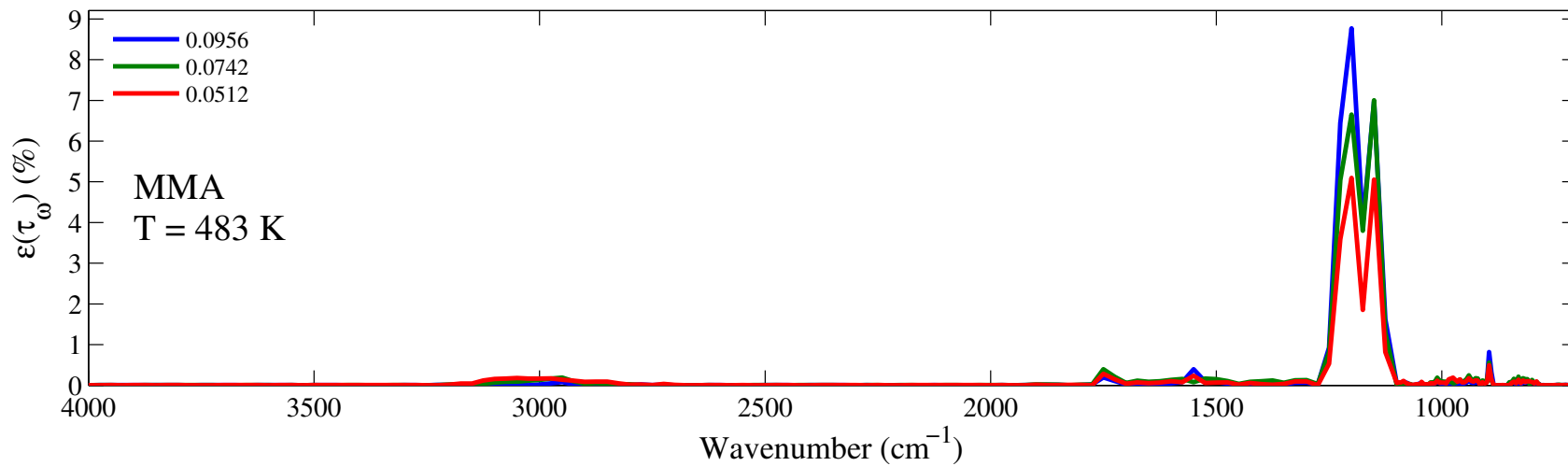
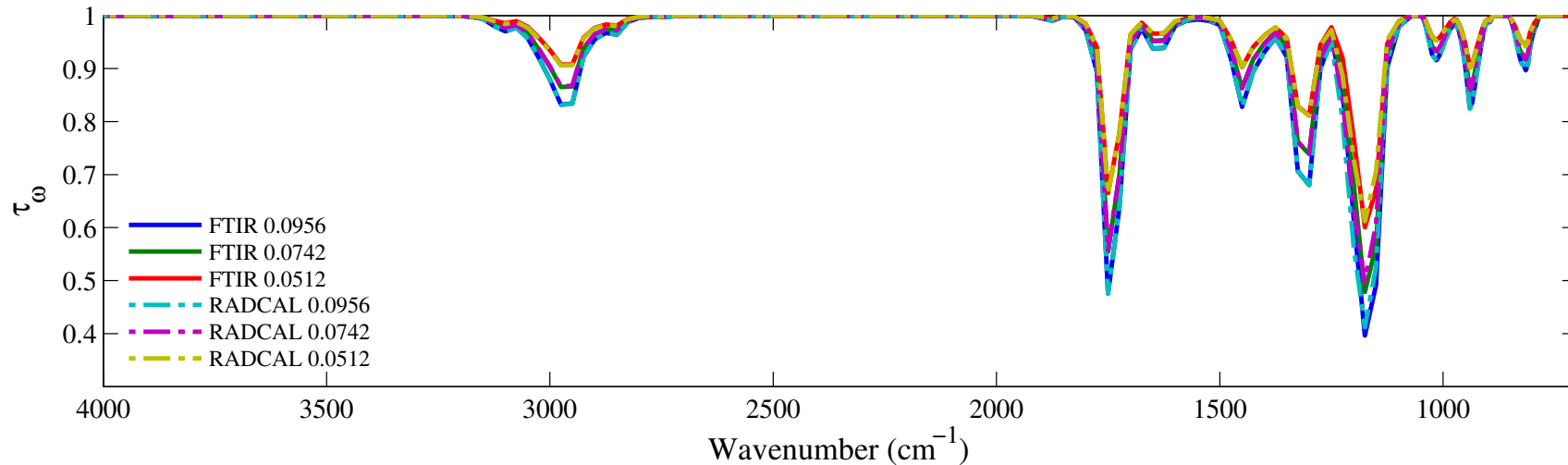


Figure 7.54: Top: comparison between the experimental (solid lines) and RadCal-generated synthetic (dashed lines) spectral transmissivity profiles, denoted τ_ω , of MMA of an isothermal homogeneous column of MMA. Bottom: relative transmissivity error, denoted $\varepsilon(\tau_\omega)$, between the experiment and the synthetic profiles presented on the top figure. Three different pressure path lengths are considered: 0.0956, 0.0742, and 0.0512 atm.cm. The gas temperature is set at 483 K and the total pressure is 101 kPa. Note: the experimental data resolution has been changed to match that of the narrow band model.

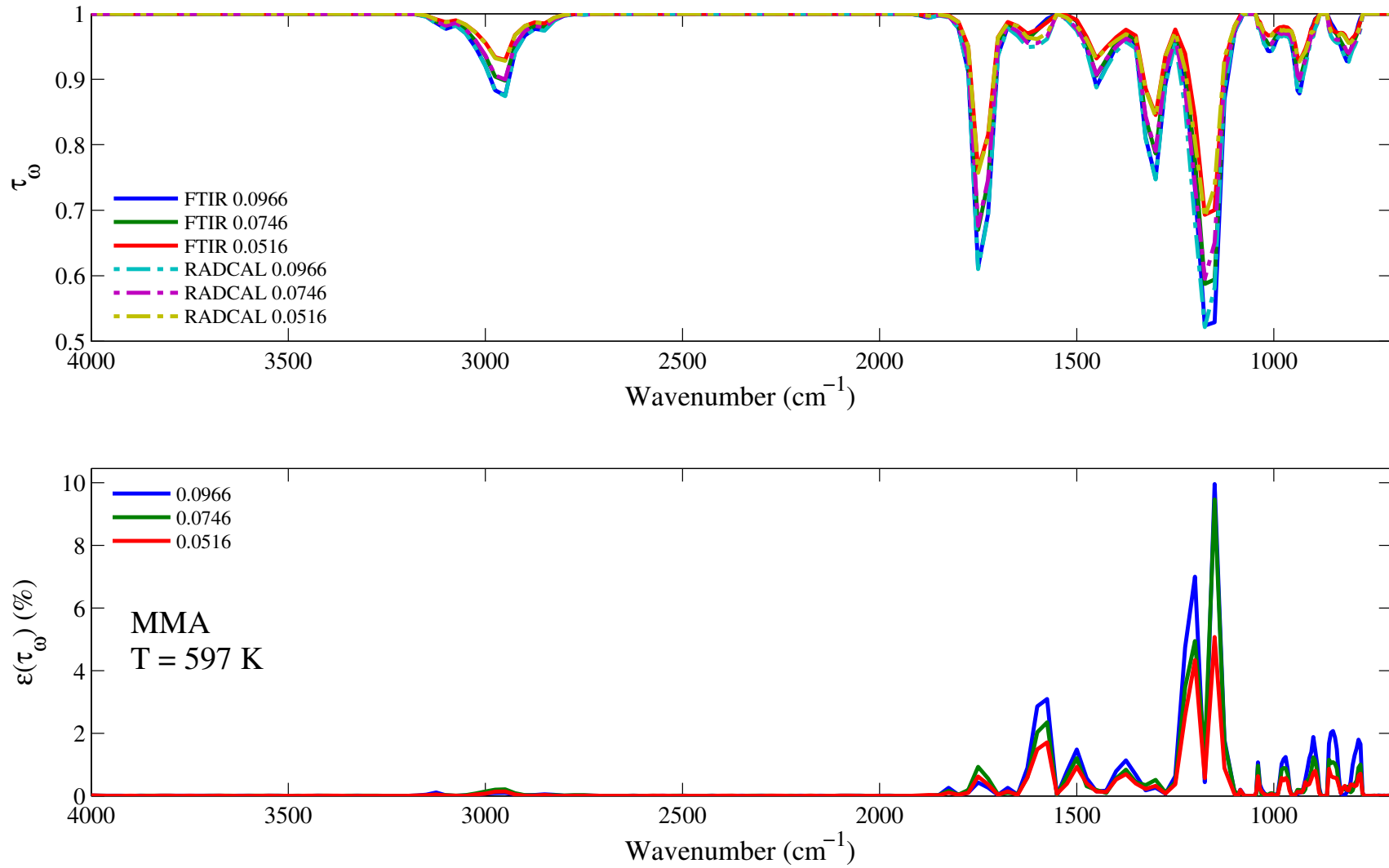


Figure 7.55: Top: comparison between the experimental (solid lines) and RadCal-generated synthetic (dashed lines) spectral transmissivity profiles, denoted τ_ω , of MMA of an isothermal homogeneous column of MMA. Bottom: relative transmissivity error, denoted $\varepsilon(\tau_\omega)$, between the experiment and the synthetic profiles presented on the top figure. Three different pressure path lengths are considered: 0.0966, 0.0746, and 0.0516 atm.cm. The gas temperature is set at 597 K and the total pressure is 101 kPa. Note: the experimental data resolution has been changed to match that of the narrow band model.

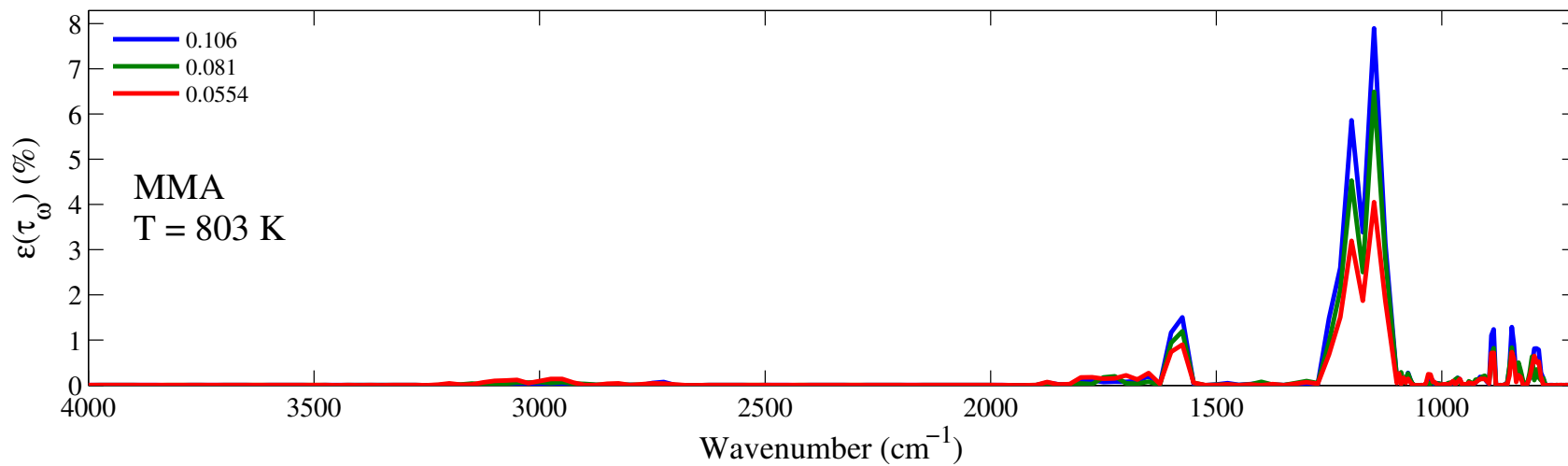
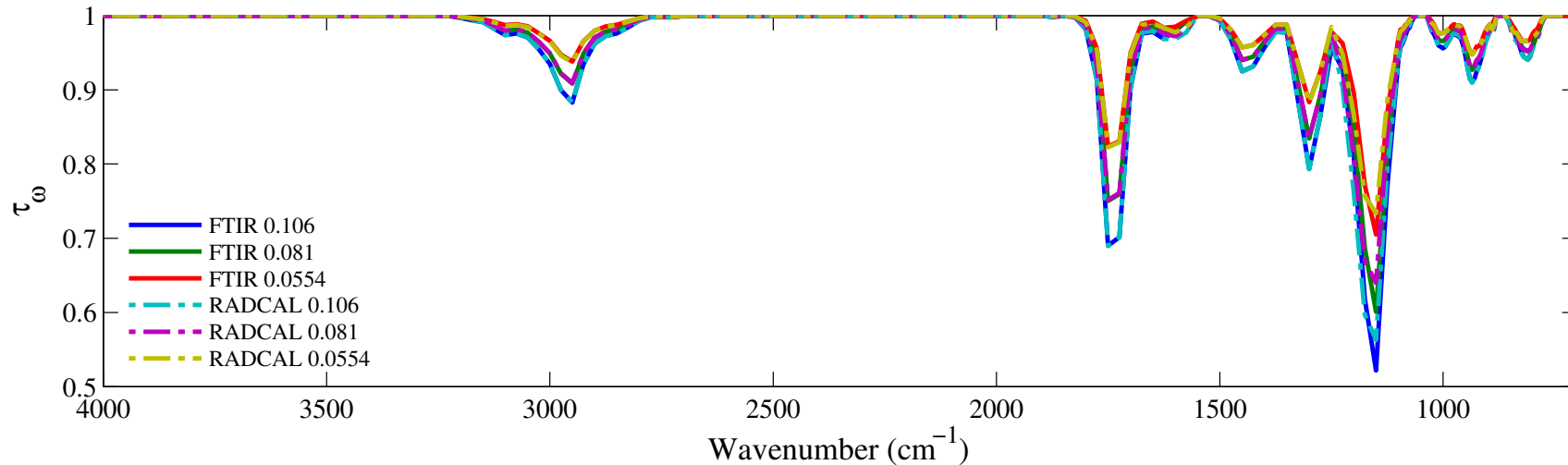


Figure 7.56: Top: comparison between the experimental (solid lines) and RadCal-generated synthetic (dashed lines) spectral transmissivity profiles, denoted τ_ω , of MMA of an isothermal homogeneous column of MMA. Bottom: relative transmissivity error, denoted $\varepsilon(\tau_\omega)$, between the experiment and the synthetic profiles presented on the top figure. Three different pressure path lengths are considered: 0.106, 0.081, and 0.0554 atm.cm. The gas temperature is set at 803 K and the total pressure is 101 kPa. Note: the experimental data resolution has been changed to match that of the narrow band model.

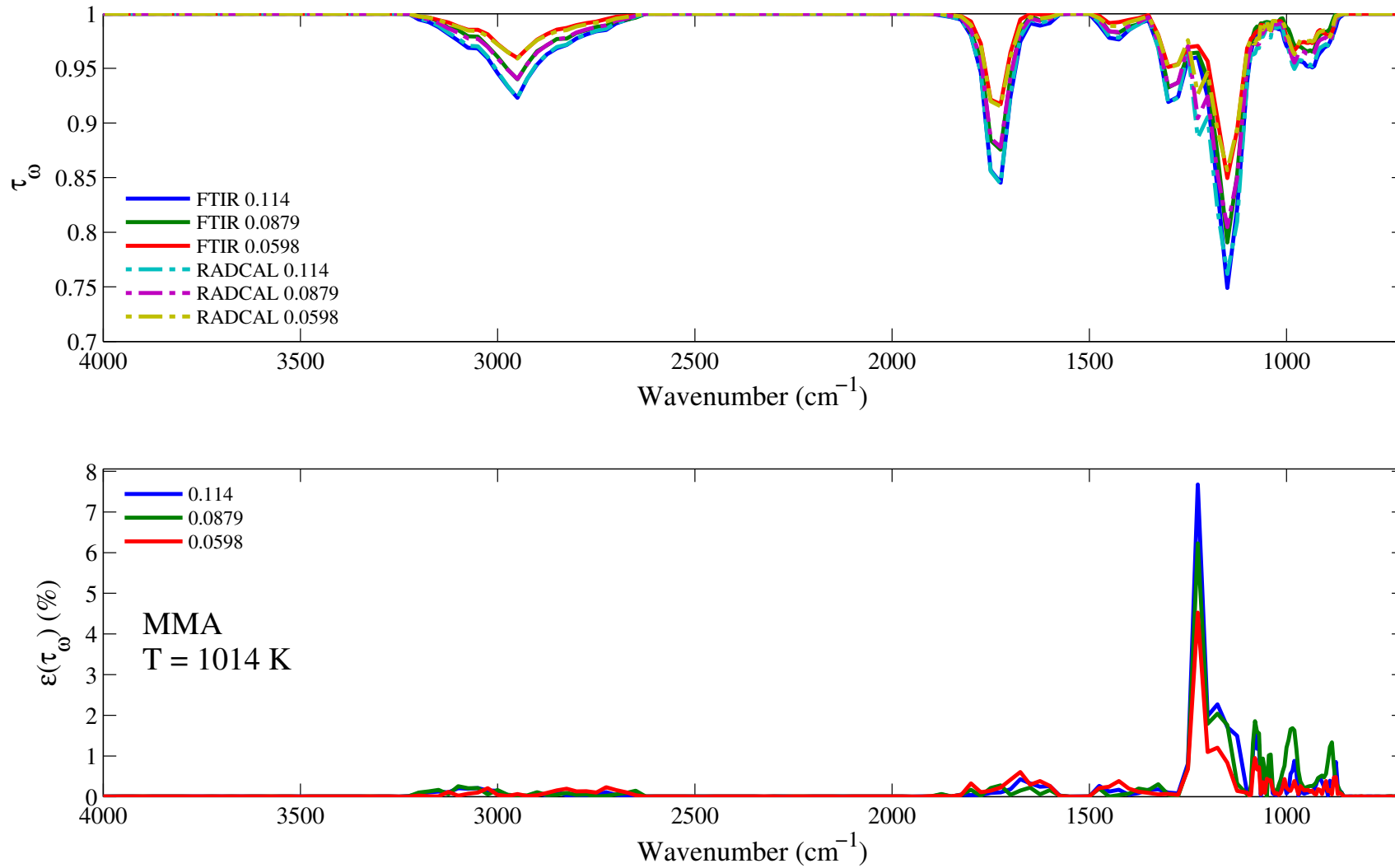


Figure 7.57: Top: comparison between the experimental (solid lines) and RadCal-generated synthetic (dashed lines) spectral transmissivity profiles, denoted τ_ω , of MMA of an isothermal homogeneous column of MMA. Bottom: relative transmissivity error, denoted $\varepsilon(\tau_\omega)$, between the experiment and the synthetic profiles presented on the top figure. Three different pressure path lengths are considered: 0.114, 0.0879, and 0.0598 atm.cm. The gas temperature is set at 1014 K and the total pressure is 101 kPa. Note: the experimental data resolution has been changed to match that of the narrow band model.

Chapter 8

Validations Tests

This chapter presents some validations tests that have been performed with the latest version of RadCal. The first six cases presented in this chapter are from the previous Grosshandler report [1]. For these tests, the numbering is similar to that of the aforementioned reference. In each test, predictions from the latest version of RadCal are compared with those obtained with the former version of RadCal. Test 1 compares values of CO₂ total emissivity at fixed temperature as function of pressure path-length. Test 2 compares values of CO₂ total emissivity at fixed pressure path-length as function of temperature. Test 3 compares values of H₂O total emissivity at fixed temperature as function of pressure path-length. Test 4 compares values of H₂O total emissivity at fixed pressure path-length as function of temperature. Test 5 compares the spectral intensity and transmittance profiles obtained from the simulation of a simplified pool fire. Test 6 compares the spectral transmittance and spectral incident radiance from a methane rich premixed flame. Test 7 is a new test included in this report. It simulates the spectral transmissivity and incident spectral intensity to the surface of a methanol 30 cm diameter pool fire. Experimental temperature and species mole fraction data were obtained experimentally by Aykut Yilmaz and were published in Ref. [10].

8.1 Test 1: isothermal CO₂

This test compares estimates of CO₂ of intensity and transmissivity obtained with the previous and latest version of RADCAL as a function of pressure-path length, P_iL . The previous version of RadCal is referred to as “Old RadCal” and the latest version as “New RadCal”. This test also compares at selected values the total emissivity as defined by Eq. 2.77 from the New RadCal with those published in the previous RadCal report [1]. These values are referred to as “TN1402”. Values extracted from the Hottel chart and presented in Ref. [1] are also reported under “Hottel”. Figure 8.1 plots the estimates from the New RadCal as a function of pressure path-length in the top figure. The bottom figure plots the integrated relative error in intensity, denoted ε_{rad} , and transmissivity, denoted ε_τ , between the two versions of RadCal as a function of pressure path-length. Values are given in percent. The relative error on transmissivity ε_τ was calculated as:

$$\varepsilon_\tau = \int_{50}^{10000} \frac{|\tau_{Old\ RadCal} - \tau_{New\ RadCal}|}{\tau_{Old\ RadCal}} d\omega. \quad (8.1)$$

Similar expression was applied to compute ε_{rad} . The total pressure was set to 1.0 atm, the temperature to 1500 K and CO₂ mole fraction to 5.0×10^{-3} . Air was mixed with CO₂. The total pressure and the amount of CO₂ were kept constant. The length of the homogeneous cell was varied to cover the desired range.

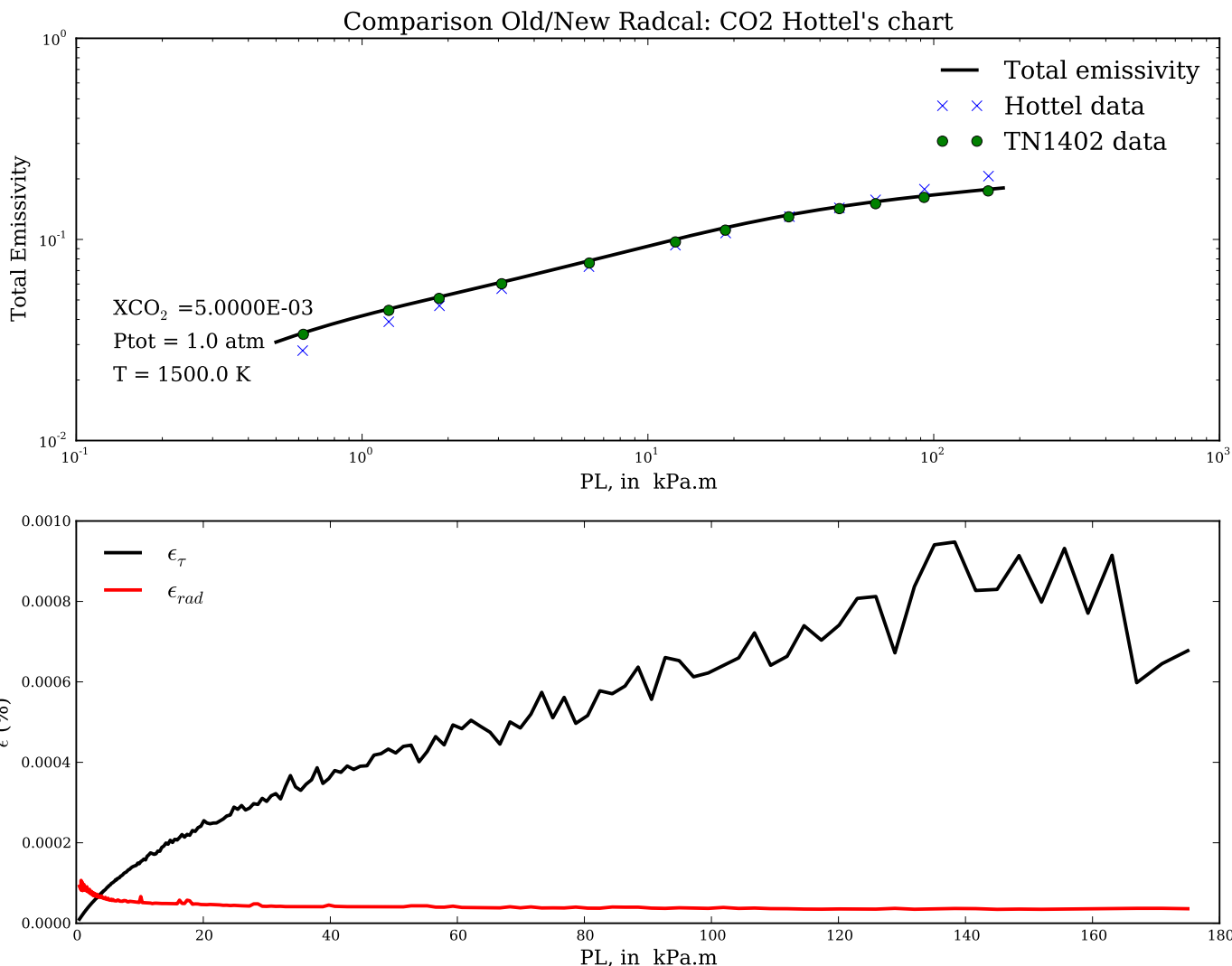


Figure 8.1: Top: total emissivity, as defined by Eq. 2.77, of isothermal, homogeneous CO₂/air mixtures as a function of the pressure path-length. Temperature was set at 1500 K, the mole fraction of CO₂ was set at 5.0×10^{-3} and the total pressure is set at 1 atm. Solid line indicates estimates obtained with the latest version of RadCal, the crossed symbols indicate Hottel data, and the filled circles are data extracted from Grosshandler [1]. Bottom: integrated relative error between the old RadCal and the new RadCal in spectral transmissivity, denoted ϵ_τ , and spectral intensity, denoted ϵ_{rad} , as defined by Eq. 8.1. Values are given in percentage.

The agreement between the two versions of RadCal for the simulations of a isothermal, homogeneous layer of CO₂, is very good. The new version of RadCal does not change the results of CO₂ simulations, which it should not as the CO₂ data have not been modified from the previous version.

8.2 Test 2: fixed pressure path-length CO₂

This second test compares the predictions of the two RadCal versions with the data from Hottel. In this test, CO₂ is mixed with air. The total pressure is set to 1 atm, and the mole fraction of CO₂ is set to 5×10^{-3} . The physical length is set to 36 m. The medium is assumed homogeneous and isothermal. The temperature of the mixture is varied between 300 K to 2800 K. Similarly to Test 1, the total emissivity as defined by Eq. 2.77 is reported on the top Fig. 8.2 and the integrated relative error between the old RadCal and the new RadCal in spectral transmissivity, denoted ε_τ , and spectral intensity, denoted ε_{rad} , as defined by Eq. 8.1, are reported on the bottom Fig. 8.2.

Overall very good agreement is obtained between the two RadCals and between RadCal and the Hottel data. Some discrepancies are observed between Hottel data and the RadCal predictions at low (around 300 K) and high temperatures (above 2000 K). A small discrepancy (<2 %) exists between the old and new versions of RadCal in the temperature range 1200–1500 K. This small discrepancy is attributed to a slightly better interpolation at this temperature range for the CO₂ Band 1 (between 500 – 800 cm⁻¹).

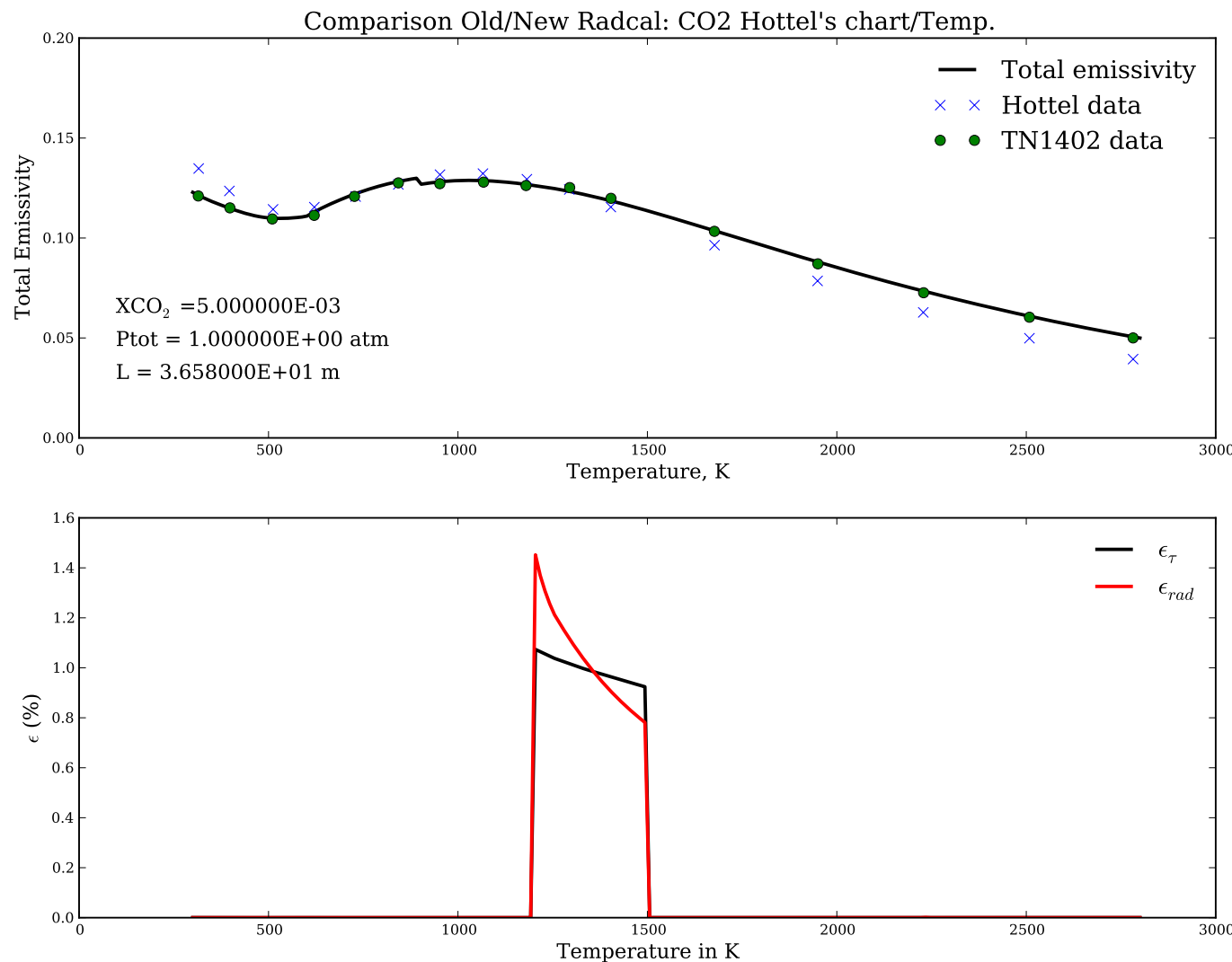


Figure 8.2: Top: total emissivity, as defined by Eq. 2.77, of homogeneous CO_2 /air mixtures as a function of the mixture temperature. The mole fraction of CO_2 was set at 5.0×10^{-3} , and the total pressure is set at 1 atm. Solid line indicates estimates obtained with the latest version of RadCal, crossed symbols are Hottel data, and filled circles are data extracted from Grosshandler [1]. Bottom: integrated relative error between the old RadCal and the new RadCal in spectral intensity, denoted ϵ_τ , and spectral intensity, denoted ϵ_{rad} . Values are given in percentage.

8.3 Test 3: isothermal H₂O

This test is almost identical to Test 1, the only difference lies in the choice of H₂O as the participating species. The configuration is that of a homogeneous column of H₂O mixed with air set at a pressure of 1 atm. The mole fraction of H₂O is set at 5×10^{-3} and the temperature is 1500 K. The physical length of the domain was varied between 1 m to 300 m.

This test compares at selected values the predicted total emissivity as defined by Eq. 2.77 from the New RadCal with those published in the previous RadCal report [1]. Results are plotted in Fig. 8.3. These values are referred to as “TN1402”. Values extracted from the Hottel chart and presented in Ref. [1] are also reported under “Hottel”. This test also compares the predicted values of the spectral intensity and transmissivity from the two RadCal versions. Very good agreement is obtained between the two versions of RadCal, and good agreement between the Hottel and RadCal data is obtained. It is noteworthy that this new version of RadCal does change the predictions when using H₂O.

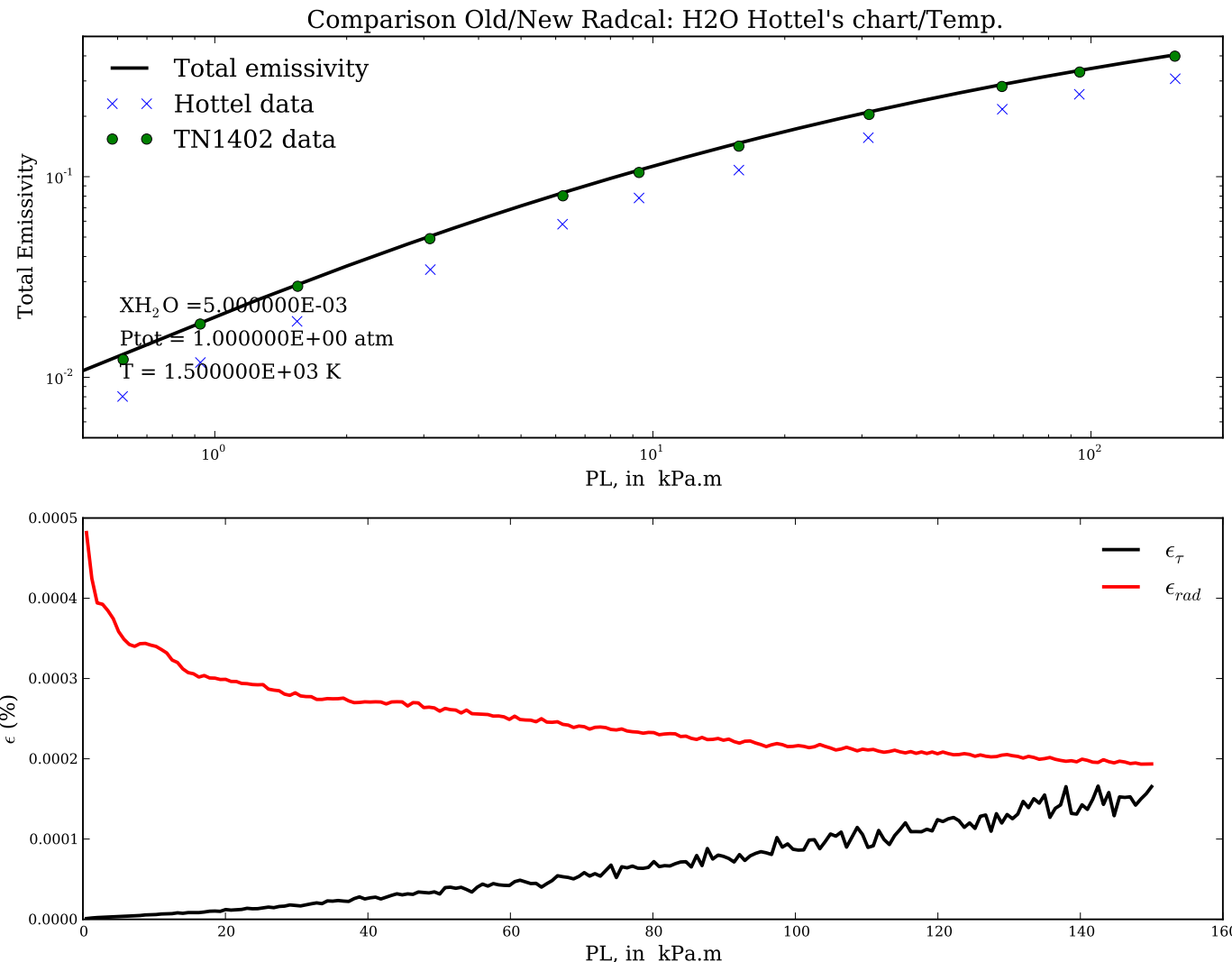


Figure 8.3: Top: total emissivity, as defined by Eq. 2.77, of isothermal, homogeneous H₂O/air mixtures as a function of the pressure path-length. Temperature was set at 1500 K, the mole fraction of H₂O was set at 5.0×10^{-3} , and the total pressure is set at 1 atm. Solid line indicates estimates obtained with the latest version of RadCal, crossed symbols are Hottel data, and filled circles are data extracted from Grosshandler [1]. Bottom: integrated relative error between the old RadCal and the new RadCal in spectral intensity, denoted ϵ_τ , and spectral intensity, denoted ϵ_{rad} . Values are given in percentage.

8.4 Test 4: fixed pressure path-length H₂O

This fourth test is very similar to Test 2, excepts that H₂O is used as participating species. Variations of the total emissivity of a homogeneous column of a H₂O-air mixture of 30.48 m length with the mixture temperature is plotted in Fig. 8.4 and compared with the previous data of Hottel and the previous RadCal prediction, referred to here as “TN1402”, as reported in Grosshandler [1]. Temperature is varied between 200 K and 2600 K. Evolution of the total emissivity as defined by Eq. 2.77 with temperature is reported in Fig. 8.4. Overall good agreement is reproduced between the old version of RadCal and the new one except near ambient temperature where some discrepancies exist. There are due to a small spurious spike that is present in the previous version of RadCal in the spectral range 500 – 800 cm⁻¹ which is not physical. This spurious spike disappears above 300 K. The new version of RadCal does not feature this spike. Similar discrepancies as those reported in Grosshandler [1] remain between Hottel data and RadCal in the total emissivity of H₂O, as plotted in Fig. 8.4. As Grosshandler wrote in Ref. [1]: “...Ludwig [15] pointed out that the earlier work by Hottel covered a more limited range of conditions and attempted to minimize the number of parameters for engineering estimates, and, thus, should not be expected to be as accurate as the narrow-band calculations.”

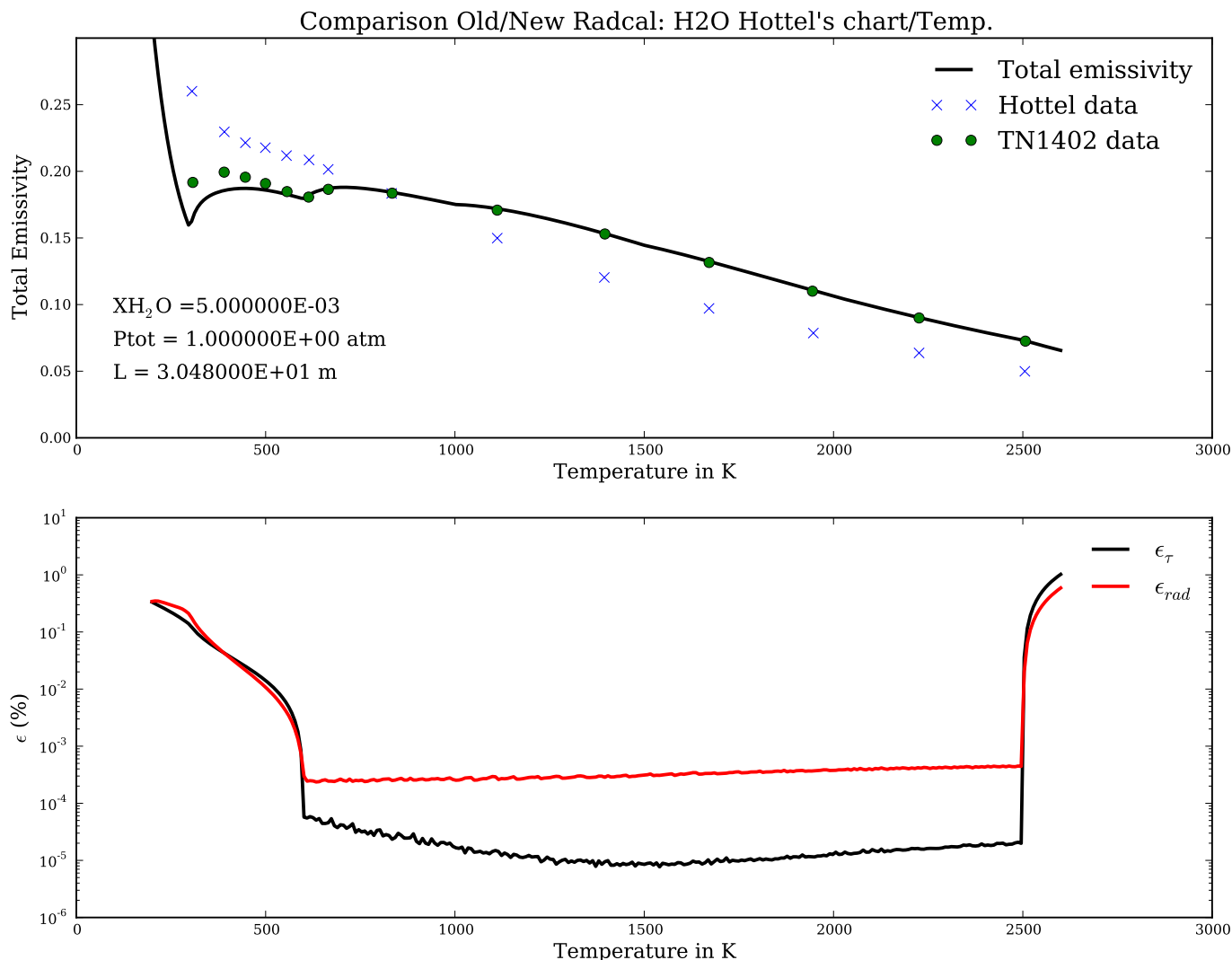


Figure 8.4: Top: total emissivity, as defined by Eq. 2.77, of homogeneous H₂O/air mixtures as a function of the temperature. The physical length is set to 30.48 m, the mole fraction of H₂O was set at 5.0×10^{-3} and the total pressure is set at 1 atm. The temperature was varied between 200 to 2800 K. Solid line indicates estimates obtained with the latest version of RadCal, crossed symbols are Hottel data, and filled circles are data extracted from Grosshandler [1]. Bottom: integrated relative error between the old RadCal and the new RadCal in spectral intensity, denoted ϵ_τ , and spectral intensity, denoted ϵ_{rad} . Values are given in percentage.

8.5 Test 5: simulated one meter diameter pool fire

This test compares the predictions from the old and new versions of RadCal from a simulated one meter diameter fire that contains CO₂, H₂O, and soot. Table 8.1 gives the temperature, species, and soot concentration as a function of the distance from the observer. Figure 8.5 plots the predicted spectral transmissivity (top) and the predicted spectral incident intensity from the old version of RadCal (given in red) and the new version of RadCal (given in black). Excellent agreement between the two versions is obtained. Table 8.2 reports the predicted received total intensities from the old and the new versions of RadCal. Excellent agreement is obtained between the two versions.

Table 8.1: Radial profile through simulated one meter diameter pool fire.

Distance (cm)	Temperature (K)	X _{CO2}	X _{H2O}	X _{N2}	f _v
5	899	0.070	0.070	0.860	5.55×10^{-8}
10	1158	0.099	0.099	0.802	5.55×10^{-8}
20	1438	0.130	0.130	0.741	5.55×10^{-8}
30	1637	0.152	0.152	0.695	5.55×10^{-8}
50	1770	0.167	0.167	0.665	5.55×10^{-8}
70	1637	0.152	0.152	0.695	5.55×10^{-8}
80	1438	0.130	0.130	0.741	5.55×10^{-8}
90	1158	0.099	0.099	0.802	5.55×10^{-8}
95	899	0.070	0.070	0.860	5.55×10^{-8}

Table 8.2: Predicted received intensity from the old and the new versions of RadCal for the simulated one meter diameter pool fire described in Table 8.1.

Quantity	Old Radcal	New RadCal
Received total intensity (W/m ⁻² /str)	33784.3	33746.9

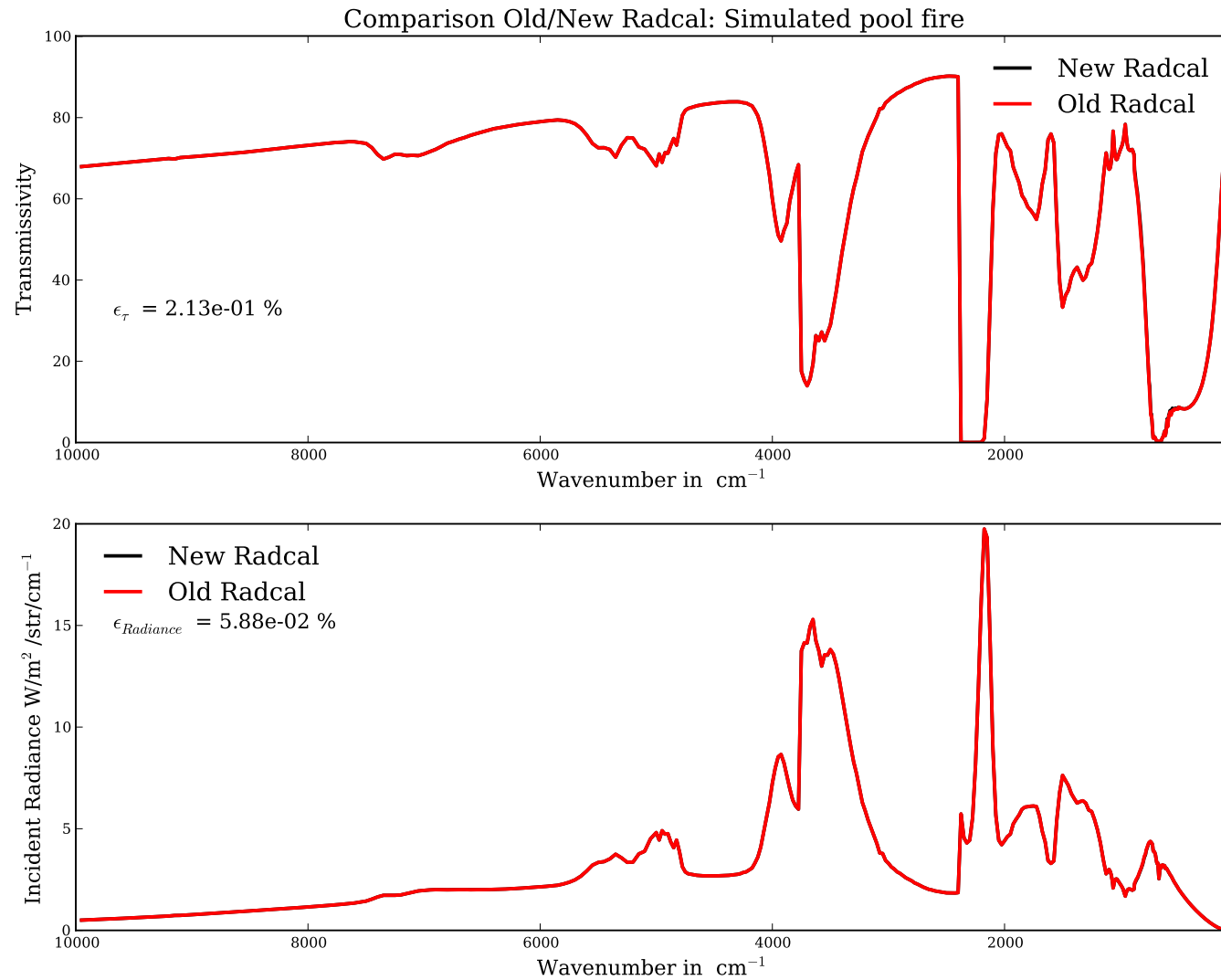


Figure 8.5: Top: Spectral transmissivity, $\bar{\tau}(\omega_0; 1000 \rightarrow 0)$, in %, for a simulated one meter diameter pool fire. Red line: predicted results using the previous version of RadCal. Black line: predicted profile using the new version of RadCal. Bottom: predicted incident spectral intensity, $I_{\omega_0}(0)$, given in $\text{W/m}^2/\text{str/cm}^{-1}$.

8.6 Test 6: methane premixed flame

Figure 8.6 represents the predicted spectral transmissivity and spectral incident intensity by the old and the new versions of RadCal for a 20 mm thick fuel rich premixed methane/N₂/O₂ flame at 606 kPa. Predictions with the new RadCal version were performed using the newest CH₄ data. The input file for the new version is given below:

```
&HEADER TITLE="Figure6_New_Radcal" CHID="Figure6_New_Radcal" /  
  
&BAND  
    OMMIN = 50.0  
    OMMAX = 10000.0 /  
&WALL TWALL = 0.0 /  
  
&Path_Segment ! Define a homogeneous segment  
    T      = 300.0      ! Temperature in Kelvin  
    LENGTH = 0.002      ! Length of the segment in meters  
    PRESSURE = 6.0      ! Pressure in atm  
    XCO2   = 0.0000E+000 ! Mole fraction of CO2  
    XH2O   = 0.0000E+000 ! Mole fraction of H2O  
    XCH4   = 2.0165E-001 ! Mole fraction of CH4  
    XCO    = 0.0000E+000 ! Mole fraction of CO  
    XO2    = 3.0660E-001 ! Mole fraction of O2  
    XN2    = 4.9175E-001 / ! Mole fraction of N2  
  
&Path_Segment ! Define a homogeneous segment  
    T      = 725.0      ! Temperature in Kelvin  
    LENGTH = 0.0020     ! Length of the segment in meters  
    PRESSURE = 6.0000E+000 ! Pressure in atm  
    XCO2   = 0.0000E+000 ! Mole fraction of CO2  
    XH2O   = 9.6700E-002 ! Mole fraction of H2O  
    XCH4   = 1.5330E-001 ! Mole fraction of CH4  
    XCO    = 4.8350E-002 ! Mole fraction of CO  
    XO2    = 2.3003E-001 ! Mole fraction of O2  
    XN2    = 4.7162E-001 / ! Mole fraction of N2  
  
&Path_Segment ! Define a homogeneous segment  
    T      = 1150.0      ! Temperature in Kelvin  
    LENGTH = 0.0020     ! Length of the segment in meters  
    PRESSURE = 6.0554E+000 ! Pressure in atm  
    XCO2   = 0.0000E+000 ! Mole fraction of CO2  
    XH2O   = 1.9163E-001 ! Mole fraction of H2O  
    XCH4   = 1.0235E-001 ! Mole fraction of CH4  
    XCO    = 9.7450E-002 ! Mole fraction of CO  
    XO2    = 1.5942E-001 ! Mole fraction of O2  
    XN2    = 4.4915E-001 / ! Mole fraction of N2  
  
&Path_Segment ! Define a homogeneous segment  
    T      = 1575.0      ! Temperature in Kelvin  
    LENGTH = 0.0020     ! Length of the segment in meters  
    PRESSURE = 6.1901E+000 ! Pressure in atm  
    XCO2   = 0.0000E+000 ! Mole fraction of CO2  
    XH2O   = 2.9079E-001 ! Mole fraction of H2O  
    XCH4   = 5.0065E-002 ! Mole fraction of CH4  
    XCO    = 1.5675E-001 ! Mole fraction of CO  
    XO2    = 7.9175E-002 ! Mole fraction of O2  
    XN2    = 4.2322E-001 / ! Mole fraction of N2
```

```

&Path_Segment ! Define a homogeneous segment
    T      = 2000.0      ! Temperature in Kelvin
    LENGTH = 0.0040      ! Length of the segment in meters
    PRESSURE = 6.1198E+000 ! Pressure in atm
    XCO2   = 8.0890E-003 ! Mole fraction of CO2
    XH2O   = 3.6272E-001 ! Mole fraction of H2O
    XCH4   = 1.6350E-002 ! Mole fraction of CH4
    XCO    = 1.7327E-001 ! Mole fraction of CO
    XO2    = 2.4591E-002 ! Mole fraction of O2
    XN2    = 4.1498E-001 / ! Mole fraction of N2

&Path_Segment ! Define a homogeneous segment
    T      = 2525.0      ! Temperature in Kelvin
    LENGTH = 0.0055      ! Length of the segment in meters
    PRESSURE = 6.1495E+000 ! Pressure in atm
    XCO2   = 8.0400E-003 ! Mole fraction of CO2
    XH2O   = 3.9350E-001 ! Mole fraction of H2O
    XCH4   = 0.0000E+000 ! Mole fraction of CH4
    XCO    = 1.8870E-001 ! Mole fraction of CO
    XO2    = 0.0000E+000 ! Mole fraction of O2
    XN2    = 4.0976E-001 / ! Mole fraction of N2
#-----

```

Very good agreement between the two versions is obtained. The main difference lies in the C–H stretch band of methane ($2700 - 3250 \text{ cm}^{-1}$). The new methane data present a better resolution than the old data. The new version of RadCal predicts a total incident intensity of $11.58 \text{ kW/m}^2/\text{str}$ while the previous version predicts a received total incident intensity of $11.84 \text{ kW/m}^2/\text{str}$.

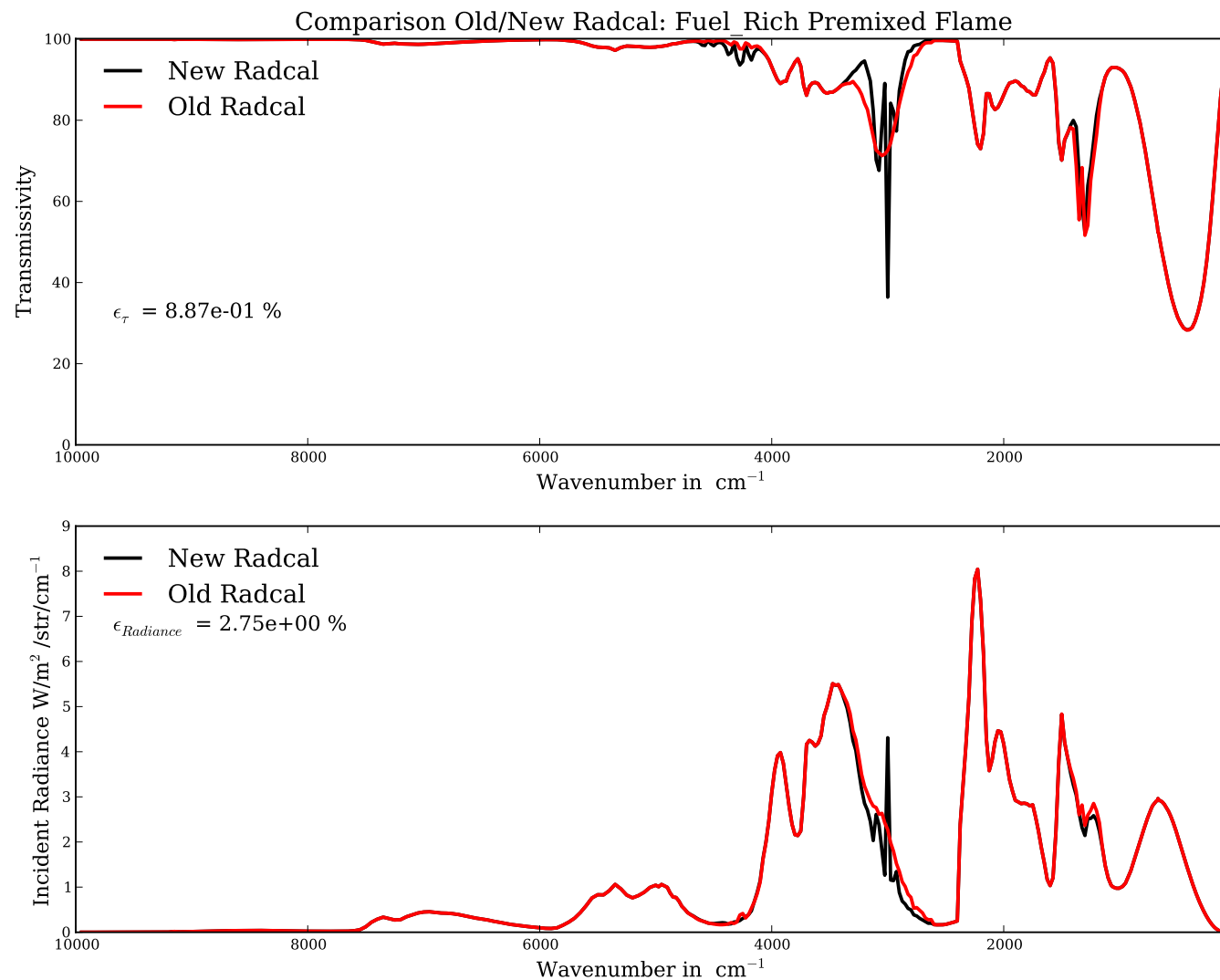


Figure 8.6: Top: spectral transmissivity, $\bar{\tau}(\omega_0; \infty \rightarrow 0)$ (the observer is in 0, in %, for a simulated 20 mm thick fuel rich premixed methane/ N_2/O_2 flame at 606 kPa. Red line: predicted results using the previous version of RadCal. Black line: predicted results using the new version of RadCal. Bottom: predicted incident spectral intensity, $I_{\omega_0}(0)$, given in $\text{W/m}^2/\text{str}/\text{cm}^{-1}$.

8.7 Test 7: methanol pool fire

In this section, predicted results for a 30 cm methanol pool fire are presented in this section. Measurements were made by Aykut Yilmaz, see Ref. [10]. Temperature data were averaged over three different tests using the same configuration. Species mole fraction were obtained by gas chromatography. Table 8.3 tabulates the experimental values used for this simulation.

Table 8.3: Measured temperature and species mole fraction as function of the height above the pool surface for a 30 cm diameter methanol pool fire. Data were obtained from Yilmaz, see Ref. [10].

X(cm)	Temp (K)	XH2	XO2	XN2	XCH4	XCO	XCO2	XC2H4	XC2H2	XH2O	XCH3OH
55	1101.2	5.91E-5	1.78E-1	7.61E-1	0.00E+0	0.00E+0	1.29E-2	0.00E+0	0.00E+0	7.62E-2	0.00E+0
40	1257.7	1.99E-3	1.54E-1	7.42E-1	0.00E+0	2.90E-3	2.18E-2	0.00E+0	0.00E+0	1.01E-1	3.27E-4
37.5	1267.1	2.97E-3	1.48E-1	7.36E-1	0.00E+0	4.20E-3	2.41E-2	0.00E+0	0.00E+0	1.12E-1	5.93E-4
30	1295	7.79E-3	1.25E-1	7.11E-1	0.00E+0	1.06E-2	3.10E-2	0.00E+0	0.00E+0	1.39E-1	2.64E-3
27.5	1284.4	5.62E-3	1.36E-1	7.19E-1	0.00E+0	6.94E-3	2.59E-2	0.00E+0	0.00E+0	1.35E-1	1.73E-3
20	1013.7	2.45E-2	8.35E-2	6.54E-1	0.00E+0	2.89E-2	3.98E-2	9.24E-6	3.05E-5	1.91E-1	1.25E-2
17.5	968.4	3.33E-2	7.96E-2	6.35E-1	0.00E+0	3.51E-2	3.75E-2	2.29E-5	3.07E-5	1.91E-1	1.81E-2
10	820.9	4.25E-2	5.80E-2	5.96E-1	4.43E-4	4.54E-2	4.11E-2	3.93E-5	7.17E-5	2.26E-1	4.87E-2
7.5	768.4	4.45E-2	5.24E-2	5.83E-1	5.31E-4	4.82E-2	4.17E-2	4.45E-5	8.31E-5	2.34E-1	6.36E-2
5	716	6.09E-2	3.39E-2	5.16E-1	1.16E-3	5.96E-2	3.92E-2	5.94E-5	1.05E-4	2.39E-1	1.44E-1
2.5	663.5	7.03E-2	1.93E-2	3.94E-1	1.38E-3	6.37E-2	3.25E-2	7.21E-5	1.29E-4	2.15E-1	3.72E-1
1.5	642.5	6.55E-2	1.18E-2	3.28E-1	1.27E-3	5.63E-2	3.00E-2	7.91E-5	1.30E-4	1.97E-1	5.57E-1

The RadCal input file is presented below:

```
&HEADER TITLE = "Methanol_Pool_Fire_30cm" CHID = "Methanol_Pool_Fire_30cm" /  
  
&BAND OMMIN = 50.0  
OMMAX = 10000.0/  
  
&WALL TWALL = 300.0 /  
&Path_Segment ! Define a homogeneous segment  
T = 642.5 ! Temperature in Kelvin  
LENGTH = 5.0000000000E-03 ! Length of the segment in meters  
PRESSURE = 1 ! Pressure in atm  
XO2 = 1.1819200000E-02 ! Mole fraction of O2  
XH2O = 1.9712830000E-01 ! Mole fraction of H2O  
XCO = 5.6268490000E-02 ! Mole fraction of CO  
XCO2 = 3.0011090000E-02 ! Mole fraction of CO2  
XC2H4 = 7.9050000000E-05 ! Mole fraction of C2H4  
XCH4 = 1.2657700000E-03 ! Mole fraction of CH4  
XC2H6 = 0.0000000000E+00 ! Mole fraction of C2H6  
XCH3OH = 5.5659982000E-01 ! Mole fraction of CH3OH  
XN2 = 1.4682828000E-01/ ! Mole fraction of N2  
  
&Path_Segment ! Define a homogeneous segment  
T = 663.5 ! Temperature in Kelvin  
LENGTH = 1.7500000000E-02 ! Length of the segment in meters  
PRESSURE = 1 ! Pressure in atm  
XO2 = 1.9288640000E-02 ! Mole fraction of O2  
XH2O = 2.1510620000E-01 ! Mole fraction of H2O  
XCO = 6.3724220000E-02 ! Mole fraction of CO  
XCO2 = 3.2544630000E-02 ! Mole fraction of CO2  
XC2H4 = 7.2090000000E-05 ! Mole fraction of C2H4  
XCH4 = 1.3836300000E-03 ! Mole fraction of CH4  
XC2H6 = 0.0000000000E+00 ! Mole fraction of C2H6  
XCH3OH = 3.7249435000E-01 ! Mole fraction of CH3OH  
XN2 = 2.9538624000E-01/ ! Mole fraction of N2  
  
&Path_Segment ! Define a homogeneous segment
```

```

T      = 716 ! Temperature in Kelvin
LENGTH = 2.5000000000E-02 ! Length of the segment in meters
PRESSURE = 1 ! Pressure in atm
XO2    = 3.3932530000E-02 ! Mole fraction of O2
XH2O   = 2.3930719000E-01 ! Mole fraction of H2O
XCO    = 5.9551970000E-02 ! Mole fraction of CO
XCO2   = 3.9167250000E-02 ! Mole fraction of CO2
XC2H4  = 5.9430000000E-05 ! Mole fraction of C2H4
XCH4   = 1.1647400000E-03 ! Mole fraction of CH4
XC2H6  = 0.0000000000E+00 ! Mole fraction of C2H6
XCH3OH = 1.4355283000E-01 ! Mole fraction of CH3OH
XN2    = 4.8326406000E-01/ ! Mole fraction of N2

&Path_Segment ! Define a homogeneous segment
T      = 768.4 ! Temperature in Kelvin
LENGTH = 2.5000000000E-02 ! Length of the segment in meters
PRESSURE = 1 ! Pressure in atm
XO2    = 5.2375440000E-02 ! Mole fraction of O2
XH2O   = 2.3403434000E-01 ! Mole fraction of H2O
XCO    = 4.8155710000E-02 ! Mole fraction of CO
XCO2   = 4.1740150000E-02 ! Mole fraction of CO2
XC2H4  = 4.4500000000E-05 ! Mole fraction of C2H4
XCH4   = 5.3133000000E-04 ! Mole fraction of CH4
XC2H6  = 0.0000000000E+00 ! Mole fraction of C2H6
XCH3OH = 6.3614460000E-02 ! Mole fraction of CH3OH
XN2    = 5.5950407000E-01/ ! Mole fraction of N2

&Path_Segment ! Define a homogeneous segment
T      = 820.9 ! Temperature in Kelvin
LENGTH = 5.0000000000E-02 ! Length of the segment in meters
PRESSURE = 1 ! Pressure in atm
XO2    = 5.8036420000E-02 ! Mole fraction of O2
XH2O   = 2.2611716000E-01 ! Mole fraction of H2O
XCO    = 4.5352720000E-02 ! Mole fraction of CO
XCO2   = 4.1128540000E-02 ! Mole fraction of CO2
XC2H4  = 3.9310000000E-05 ! Mole fraction of C2H4
XCH4   = 4.4256000000E-04 ! Mole fraction of CH4
XC2H6  = 0.0000000000E+00 ! Mole fraction of C2H6
XCH3OH = 4.8728810000E-02 ! Mole fraction of CH3OH
XN2    = 5.8015448000E-01/ ! Mole fraction of N2

&Path_Segment ! Define a homogeneous segment
T      = 968.4 ! Temperature in Kelvin
LENGTH = 5.0000000000E-02 ! Length of the segment in meters
PRESSURE = 1 ! Pressure in atm
XO2    = 7.9642260000E-02 ! Mole fraction of O2
XH2O   = 1.9075471000E-01 ! Mole fraction of H2O
XCO    = 3.5088720000E-02 ! Mole fraction of CO
XCO2   = 3.7473970000E-02 ! Mole fraction of CO2
XC2H4  = 2.2860000000E-05 ! Mole fraction of C2H4
XCH4   = 0.0000000000E+00 ! Mole fraction of CH4
XC2H6  = 0.0000000000E+00 ! Mole fraction of C2H6
XCH3OH = 1.8066990000E-02 ! Mole fraction of CH3OH
XN2    = 6.3895049000E-01/ ! Mole fraction of N2

&Path_Segment ! Define a homogeneous segment
T      = 1013.7 ! Temperature in Kelvin
LENGTH = 5.0000000000E-02 ! Length of the segment in meters
PRESSURE = 1 ! Pressure in atm

```

```

XO2      = 8.3520100000E-02 ! Mole fraction of O2
XH2O     = 1.9127008000E-01 ! Mole fraction of H2O
XCO      = 2.8887410000E-02 ! Mole fraction of CO
XCO2     = 3.9827410000E-02 ! Mole fraction of CO2
XC2H4    = 9.2300000000E-06 ! Mole fraction of C2H4
XCH4     = 0.0000000000E+00 ! Mole fraction of CH4
XC2H6    = 0.0000000000E+00 ! Mole fraction of C2H6
XCH3OH   = 1.2516090000E-02 ! Mole fraction of CH3OH
XN2      = 6.4396968000E-01/ ! Mole fraction of N2

&Path_Segment ! Define a homogeneous segment
T        = 1284.4      ! Temperature in Kelvin
LENGTH   = 5.0000000000E-02 ! Length of the segment in meters
PRESSURE = 1           ! Pressure in atm
XO2      = 1.3624232000E-01 ! Mole fraction of O2
XH2O     = 1.3468054000E-01 ! Mole fraction of H2O
XCO      = 6.9395300000E-03 ! Mole fraction of CO
XCO2     = 2.5908820000E-02 ! Mole fraction of CO2
XC2H4    = 0.0000000000E+00 ! Mole fraction of C2H4
XCH4     = 0.0000000000E+00 ! Mole fraction of CH4
XC2H6    = 0.0000000000E+00 ! Mole fraction of C2H6
XCH3OH   = 1.7271700000E-03 ! Mole fraction of CH3OH
XN2      = 6.9450162000E-01/ ! Mole fraction of N2

&Path_Segment ! Define a homogeneous segment
T        = 1295       ! Temperature in Kelvin
LENGTH   = 5.0000000000E-02 ! Length of the segment in meters
PRESSURE = 1           ! Pressure in atm
XO2      = 1.2502657000E-01 ! Mole fraction of O2
XH2O     = 1.3947277000E-01 ! Mole fraction of H2O
XCO      = 1.0584120000E-02 ! Mole fraction of CO
XCO2     = 3.0954850000E-02 ! Mole fraction of CO2
XC2H4    = 0.0000000000E+00 ! Mole fraction of C2H4
XCH4     = 0.0000000000E+00 ! Mole fraction of CH4
XC2H6    = 0.0000000000E+00 ! Mole fraction of C2H6
XCH3OH   = 2.6410300000E-03 ! Mole fraction of CH3OH
XN2      = 6.9132066000E-01/ ! Mole fraction of N2

&Path_Segment ! Define a homogeneous segment
T        = 1267.1      ! Temperature in Kelvin
LENGTH   = 5.0000000000E-02 ! Length of the segment in meters
PRESSURE = 1           ! Pressure in atm
XO2      = 1.4815693000E-01 ! Mole fraction of O2
XH2O     = 1.1201391000E-01 ! Mole fraction of H2O
XCO      = 4.1990100000E-03 ! Mole fraction of CO
XCO2     = 2.4057230000E-02 ! Mole fraction of CO2
XC2H4    = 0.0000000000E+00 ! Mole fraction of C2H4
XCH4     = 0.0000000000E+00 ! Mole fraction of CH4
XC2H6    = 0.0000000000E+00 ! Mole fraction of C2H6
XCH3OH   = 5.9345000000E-04 ! Mole fraction of CH3OH
XN2      = 7.1097947000E-01/ ! Mole fraction of N2

&Path_Segment ! Define a homogeneous segment
T        = 1257.7      ! Temperature in Kelvin
LENGTH   = 8.7500000000E-02 ! Length of the segment in meters
PRESSURE = 1           ! Pressure in atm
XO2      = 1.5356568000E-01 ! Mole fraction of O2
XH2O     = 1.0119799000E-01 ! Mole fraction of H2O
XCO      = 2.8958400000E-03 ! Mole fraction of CO

```

```

XCO2      = 2.1753130000E-02 ! Mole fraction of CO2
XC2H4     = 0.0000000000E+00 ! Mole fraction of C2H4
XCH4      = 0.0000000000E+00 ! Mole fraction of CH4
XC2H6     = 0.0000000000E+00 ! Mole fraction of C2H6
XCH3OH    = 3.2715000000E-04 ! Mole fraction of CH3OH
XN2       = 7.2026021000E-01 / ! Mole fraction of N2

&Path_Segment ! Define a homogeneous segment
T          = 1101.2      ! Temperature in Kelvin
LENGTH     = 7.5000000000E-02 ! Length of the segment in meters
PRESSURE   = 1           ! Pressure in atm
XO2        = 1.7842988000E-01 ! Mole fraction of O2
XH2O       = 7.6186860000E-02 ! Mole fraction of H2O
XCO        = 0.0000000000E+00 ! Mole fraction of CO
XCO2       = 1.2909800000E-02 ! Mole fraction of CO2
XC2H4     = 0.0000000000E+00 ! Mole fraction of C2H4
XCH4      = 0.0000000000E+00 ! Mole fraction of CH4
XC2H6     = 0.0000000000E+00 ! Mole fraction of C2H6
XCH3OH    = 0.0000000000E+00 ! Mole fraction of CH3OH
XN2       = 7.3247346000E-01 / ! Mole fraction of N2

```

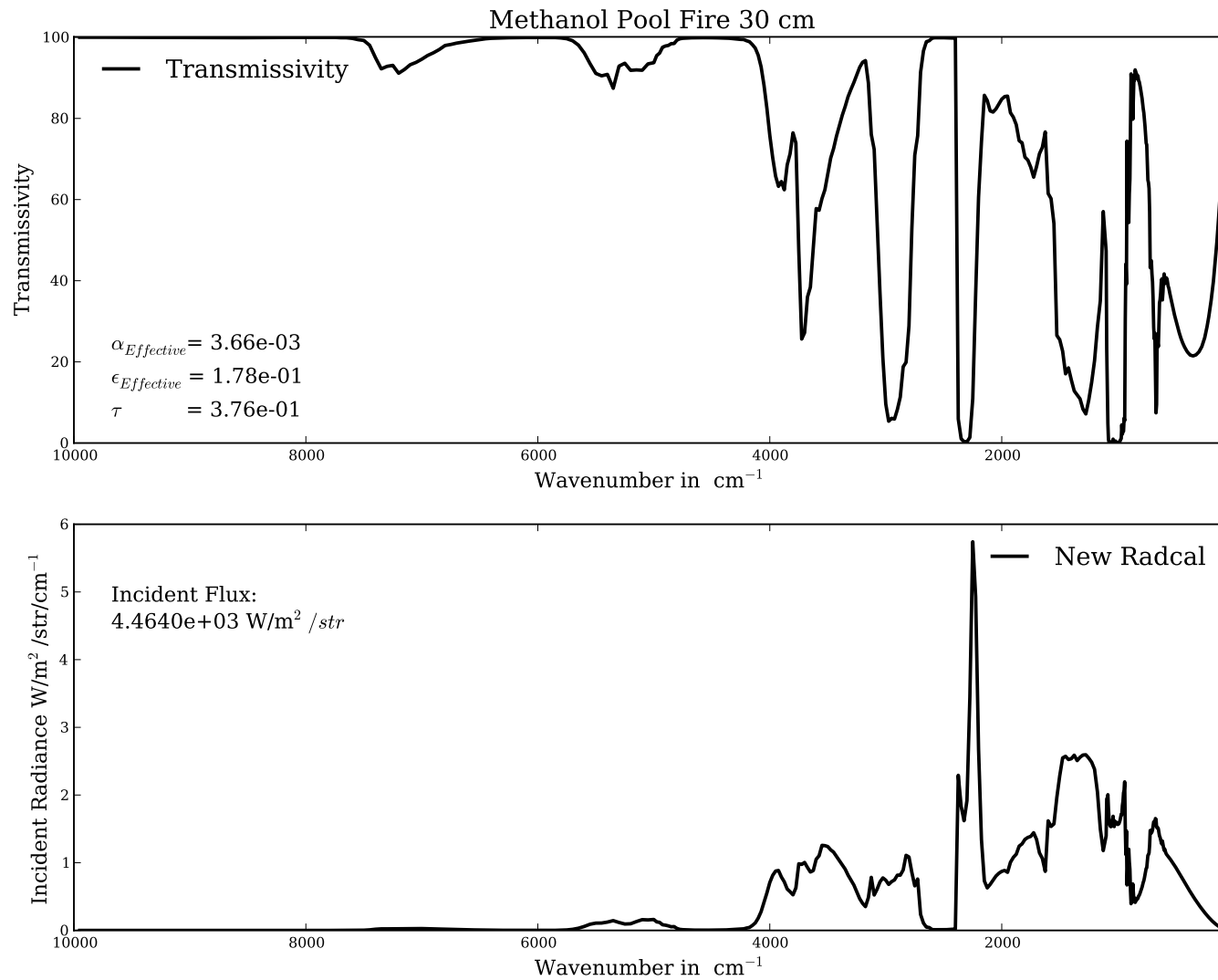


Figure 8.7: Top: Predicted spectral transmissivity for a 30 cm diameter methanol pool fire. The measured temperature and species mole fractions are tabulated in Table 8.3. Bottom: Predicted spectral incident radiative intensity to the surface of the pool fire. Emission by CO_2 is responsible for the main spike located between $2100\text{--}2500 \text{ cm}^{-1}$.

Bibliography

- [1] W. L. Grosshandler. RADCAL: A Narrow-Band Model for Radiation Calculations in a Combustion Environment. Technical report, NIST TN 1402, 1993. [1](#), [2](#), [141](#), [245](#), [246](#), [248](#), [249](#), [250](#), [251](#), [252](#)
- [2] William Grosshandler. *A Study of a Model Furnace Burning Methanol and a Methanol/Coal Slurry*. Phd thesis, University of California, Berkeley, 1976. [2](#)
- [3] William Grosshandler. Radiation From Nonhomogeneous Fires. Technical report, Factory Mutual Research Corporation FMRC J.I. 0A0E6.BU-4, 1979. [2](#)
- [4] H Hottel. *Heat Transmission*. McGraw-Hill, New York, 3rd edition, 1954. [2](#)
- [5] William Grosshandler and H Nguyen. Application of the Total Transmittance Nonhomogeneous Radiation Model to Methane Combustion. *Journal of Heat Transfer*, 107:445–450, 1985. [2](#)
- [6] M.A. Brosmer and C.L. Tien. Infrared Radiation Properties of Methane at Elevated Temperatures. *Journal of Quantitative Spectroscopy and Radiative Transfer*, 33:521–532, 1985. [2](#), [32](#)
- [7] R.H.C. Lee and J. Happel. Thermal radiation of methane gas. *Industrial & Engineering Chemical Fundamentals*, 3(2):167–&, 1964. [2](#)
- [8] K. Wakatsuki, S.P. Fuss, a. Hamins, and M.R. Nyden. A technique for extrapolating absorption coefficient measurements to high temperatures. *Proceedings of the Combustion Institute*, 30(1):1565–1573, January 2005. [2](#)
- [9] Kaoru Wakatsuki, Gregory S. Jackson, Jungho Kim, Anthony Hamins, Marc R. Nyden, and Stephen P. Fuss. Determination of Planck Mean Absorption Coefficients for Hydrocarbon Fuels. *Combustion Science and Technology*, 180(4):616–630, February 2008. [2](#), [38](#)
- [10] A. Yilmaz. *Radiation Transport Measurements in Methanol Pool Fires with Fourier Transform Infrared Spectroscopy*. PhD thesis, 2008. [2](#), [245](#), [258](#)
- [11] S.S. Penner. *Quantitative molecular spectroscopy and gas emissivities*. Addison-Wesley Publishing Company, Reading, Massachusetts, USA, 1959. [3](#), [8](#), [10](#), [12](#), [14](#), [38](#)
- [12] C.L. Tien. Thermal Radiation Properties of Gases. 5:253–324, 1968. [3](#), [8](#)
- [13] Michael F. Modest. *Radiative Heat Transfer, Third Edition*. Academic Press, 2013. [3](#), [8](#), [9](#), [10](#), [14](#), [16](#), [39](#)
- [14] R. Viskanta and M. P. Menguc. Radiation Heat Transfer in Combustion Systems. *Progress in Energy and Combustion Science*, 13:97–160, 1987. [3](#)

- [15] C.B. Ludwig, W. Malkmus, J.E. Reardon, and J.A.L. Thomson. Handbook of Infrared Radiation From Combustion Gases. Technical report, NASA SP-3080, 1973. [3](#), [12](#), [14](#), [15](#), [18](#), [19](#), [24](#), [27](#), [153](#), [251](#)
- [16] Allen Chu, Larry L Ggrdley, and Benjamin T Marshall. Linepak: algorithms for modeling spectral transmittance and radiance. *52(5):563–580*, 1994. [3](#)
- [17] L. S. Rothman, I. E. Gordon, Y. Babikov, A. Barbe, D. Chris Benner, P. F. Bernath, M. Birk, L. Bizzocchi, V. Boudon, L.R. Brown, A. Campargue, K. Chance, E. A. Cohen, L. H. Coudert, V. M. Devi, B. J. Drouin, A. Fayt, J. M. Flaud, R. R. Gamache, J. J. Harrison, J. M. Hartmann, C. Hill, J. T. Hodges, D. Jacquemart, A. Jolly, J. Lamouroux, R.J. Le Roy, G. Li, D. A. Long, O. M. Lyulin, C. J. Mackie, S. T. Massie, S. Mikhailenko, H. S. P. Müller, O. V. Naumenko, A. V. Nikitin, J. Orphal, V. Perevalov, A. Perrin, E. R. Polovtseva, C. Richard, M. A. H. Smith, E. Starikova, K. Sung, S. Tashkun, J. Tenneyson, G. A. Toon, Vl. G. Tyuterev, and G. Wagner. The HITRAN2012 molecular spectroscopic database. *Journal of Quantitative Spectroscopy and Radiative Transfer*, *130:4–50*, November 2013. [5](#)
- [18] Gerhard Herzberg. *Molecular Spectra and Molecular Structure: II, Infrared and Raman Spectra of Polyatomic Molecules*. D. Van Nostrand Company, Inc., New York, fourth printing edition, 1949. [8](#), [53](#), [65](#), [77](#), [88](#), [102](#), [113](#)
- [19] M. A. Brosmer and C. L. Tien. Infrared radiation properties of methane at elevated-temperatures. *Journal of Quantitative Spectroscopy & Radiative Transfer*, *33(5):521–532*, 1985. [13](#)
- [20] T. Kunitomo and M. Osumi. Narrow band model parameters for the CO₂ 4Å–3 μm band. *Journal of Quantitative Spectroscopy and Radiative Transfer*, *15(4):345–356*, April 1975. [13](#), [38](#)
- [21] Stephen J. Young. Nonisothermal Band Model Theory. *Journal of Quantitative Spectroscopy and Radiative Transfer*, *18(1):1–28*, 1977. [14](#), [15](#), [19](#)
- [22] W Malkmus. Random Lorentz Band Model with Exponential-Tailed S-1 Line-Intensity Distribution Function. *Journal of the Optical Society of America*, *57(3)*, 1967. [14](#), [15](#)
- [23] Russell D. Johnson. NIST Computational Chemistry Comparison and Benchmark Database. [23](#)
- [24] L.D. Gray and S.S. Penner. Approximate band absorption calculations for methane. *Journal of Quantitative Spectroscopy and Radiative Transfer*, *5(2):611–620*, 1965. [32](#)
- [25] K. Wakatsuki. *High Temperature Radiation Absorption of Fuel Molecules And An Evaluation of Its Influence on Pool Fire Modeling*. PhD thesis, 2005. [37](#), [39](#)
- [26] LA Lorne A. Matheson. The Intensity of Infrared Absorption Bands. *Physical Review*, *40(5):813–828*, June 1932. [37](#)
- [27] E. Bright Wilson and A. J. Wells. The Experimental Determination of the Intensities of Infra-Red Absorption Bands. *The Journal of Chemical Physics*, *14:578–580*, 1946. [38](#), [39](#)
- [28] A. M. Thorndike, A. J. Wells, and E. Bright Wilson. The Experimental Determination of the Intensities of Infra-Red Absorption Bands II. Measurements on Ethylene and Nitrous Oxide. *The Journal of Chemical Physics*, *15(4):157*, April 1947. [38](#), [39](#)
- [29] Lewis D. Kaplan and David F. Eggers. Intensity and Line-Width of the 15-Micron CO₂ Band, Determined by a Curve-of-Growth Method. *The Journal of Chemical Physics*, *25(5):876*, November 1956. [39](#)

- [30] V.R. Lecoustre, K. Wakatsuki, and G.S. Jackson. Fitting narrow-band models to temperature-dependent, spectral absorption coefficients of fuel vapors. *Journal of Quantitative Spectroscopy and Radiative Transfer*, 147:24–37, November 2014. [39](#)
- [31] J. D. Hunter. Matplotlib: A 2d graphics environment. *Computing In Science & Engineering*, 9(3):90–95, 2007. [145](#)